Royal Holloway, University of London

Architecture of distributive fluvial system deposits: quantitative characterisation and implications to reservoir modelling

Anna Kulikova

A thesis submitted for the degree of Doctor of Philosophy in Geology

2013

Declaration of authorship

I, Anna Kulikova, hereby declare that this thesis and the work presented in it is entirely my own. Where I have consulted the work of others, this is always clearly stated.

Signed:

Date: 17.05.2013

Acknowledgements

I would like to thank the Department of Earth Sciences and Royal Holloway College for providing the scholarship and the consortium members of the Fluvial Systems Research Group (FSRG) Project including BG Group, Chevron, ConocoPhillips and Total for funding my fieldwork.

I can hardly thank enough my supervisors Dr. Gary Nichols and Prof. Pete Burgess for their inspiration, guidance and support during the past years. Their contribution to this project and to the development of myself as a researcher could not be measured. Thanks also extend to Prof. Adrian Hartley, Prof. Gary Weissmann and Dr. Stephanie Davidson, members of the FSRG, for valuable discussions during fieldworks and research meetings that contributed to development of my ideas. I would also like to thank Chris Elders for all his support during my years in Royal Holloway.

I am very grateful for the help of Dr. Fred Peterson with the understanding of Colorado Plateau stratigraphy and with the outcrop reconnaissance in the USA. Many thanks also go to my field assistants Emiliano Peralta-Medina and Amanda Owen for all their help during fieldwork and for keeping me calm during stressful driving across Spain and USA.

Many thanks to my advisor Dr. Dan LeHeron for useful discussions and for providing field gamma-ray spectrometer used for studies of radioactivity of Huesca and Salt Wash fluvial sandstones. I very much appreciate help of Neil Holloway with thin section preparation, Dr. Dave Alderton with XRD analyses, Dr. Inga Sevastjanova with heavy mineral analyses and Dr. Martin Rittner with computer programming. I also appreciate the input of the discussions I had with Amanda Owen about the Salt Wash distributive fluvial system and with Guy Prince about numerical modelling. I am also extremely grateful to Frank Lehane for his help with my unlucky computers.

I would particularly like to thank my friends Alja Schmidt, Duncan Witts, Emi Bertoni and Inga Sevastjanova for their contribution to my research and support during these years. Many thanks also go to Naomi Griffiths, Basil Tulbah, Lydia Jagger, Amanda Owen, Jitmahantakul “Oo” Sukonmeth, Indra Gunawan, Ogechi Egbu, Francine Kurzawe, Karen Oud, Viola Warter and other PhD students and staff of the Department of Earth Sciences who made my time in the college enjoyable and unforgettable.

This thesis is dedicated to my parents for all their love, support and patience.

Abstract

Distributive fluvial systems (DFS) have been recently recognised to form a significant proportion of the deposits of modern sedimentary basins. The deposits of ancient DFSs can be preserved in the stratigraphic record and form hydrocarbon reservoirs. Few detailed studies of this type of fluvial systems have been made and facies models for DFSs are incomplete; furthermore sandstone body architecture, crucial for reservoir characterisation, and its controls are poorly understood.

This research provides detailed sedimentological and quantitative descriptions of the architecture of two outcrop examples of DFS successions: the Miocene Huesca DFS in Northern Spain and the Jurassic Salt Wash DFS in USA. A detailed fluvial architecture analysis has made it possible to develop unified facies and sandstone body classifications, and to quantify downstream trends in facies and sandstone body architecture. This quantitative outcrop data can potentially be used to characterise DFS deposits in the subsurface. Detailed sedimentological analysis of heterolithic overbank deposits of the Huesca DFS succession revealed that splay progradation was an important avulsion style, but statistical analysis showed no evidence of cyclicity in these deposits. Numerical object modelling was used to investigate controls on the sandstone body architecture. Implications of these studies to reservoir modelling are discussed.

Table of content

Declaration of authorship 2

Acknowledgements 3

Abstract 4

Table of content 5

List of tables 17

List of figures 19

1. Introduction 30

1.1. Introduction 30

1.2. Aims and objectives of the thesis 30

1.3. Why to study distributive fluvial systems? 31

1.4. DFS concept 32

1.5. Methods 34

1.6. Organisation of the thesis 35

1.7. Main findings 35

2. Geological background 37

2.1. Introduction 37

2.2. The Huesca DFS succession 37

2.2.1. Geographical setting 37

2.2.2. Stratigraphy 37

2.2.3. Tectonic setting 39

2.2.4. Depositional environment 39

2.2.5. Palaeoclimatic setting 41

2.2.6. Study area 41

2.3. The Salt Wash DFS succession 42

2.3.1. Geographical setting 42

2.3.2. Stratigraphy 42

2.3.3. Tectonic setting 45

2.3.4. Depositional environment 47

2.3.5. Palaeoclimatic setting 49

2.3.6. Study area 49

3. Field work techniques and data processing methodology 50

3.1. Introduction 50

3.2. Outcrop locations and quality of exposures 50

  3.2.1. The Huesca DFS succession 50

    Outcrop correlation 52

    Complimentary studies 52

    Exposure quality 52

  3.2.2. The Salt Wash DFS succession 53

    Outcrop correlation 55

    Complimentary studies 55

    Exposure quality 55

3.3. Outcrop documentation 55

  3.3.1. Use of photo mosaics 56

  3.3.2. Measurements of sandstone body dimensions 58

  3.3.3. Estimation of facies and sandstone body proportions 58

3.4. Sample Processing 58

  3.4.1. Grain size 59

  3.4.2. Thin sections and petrographic analyses 59

  3.4.3. X-ray diffraction 59

  3.4.4. Carbonate and heavy mineral concentrations 60

3.5. Gamma ray measurements 60

4. Facies analysis 62

4.1. Introduction 62

4.2. Facies description and interpretation 62

  4.2.1. Sandstone breccia (Sb) 62

  4.2.2. Sandstone with large-scale cross-bedding (Slc) 65

  4.2.3. Conglomerate and sandstone with medium and small-scale trough cross-bedding (St) 67

  4.2.4. Sandstone with horizontal or low-angle bedding (Sh) 70

  4.2.5. Sandstone with ripple cross-lamination (Sr) 71

  4.2.6. Sandstone with climbing ripple cross-lamination (Scr) 73

  4.2.7. Sandstone with inclined stratification (Sis) 73

  4.2.8. Heterolithic packages with inclined stratification (His) 76

4.2.9. Isolated lenses of coarse- to fine-grained sandstone (Sil) 79

4.2.10. Small-scale isolated lenses of fine- to very fine-grained sandstone (Sils) 81

4.2.11. Sheets of structureless sandstone with flat or erosional base (Ssh) 82

4.2.12. Heterolithic packages of interbedded sheets and lenses of sandstone, siltstone and mudstone (Hsh)............ 84

4.2.13. Heterolithic packages of interbedded sheets of mudstone and siltstone (Hm) 87

4.2.14. Limestone and wavy cross-laminated mudstone sheets............ 89

4.3. Facies associations 91

4.3.1. Channel fill facies association 92

Channel macroforms 92

Lateral accretion complexes 92

Isolated channel fill 93

4.3.2. Floodplain / Alluvial plain facies association 94

Proximal splay 94

Distal splay / Floodplain basin 94

Terminal splay 95

4.3.3. Lacustrine facies association 95

4.4. Conclusions............ 95

5. Sandstone body types 96

5.1. Introduction............ 96

5.2. Sandstone body types and interpretation of deposition processes 96

5.2.1. Type 1 97

5.2.2. Type 2 99

5.2.3. Type 3 101

5.2.4. Sandstone body dimensions 103

5.2.5. Interpretation summary 103

5.3. Sandstone body relationships and amalgamation complexes 105

5.3.1. Subtype 1/2 and subtype 3/2 amalgamation complex 105

5.3.2. Amalgamation complex of Type 3 sandstone bodies............ 107

5.3.3. Relationship of Type 1 and 2 sandstone bodies with Type 3 sandstone bodies............ 109

5.3.4. Large amalgamated sandstone body complexes 109
5.4. Avulsion - a mechanism of formation of sandstone bodies and their amalgamation complexes 111
5.5. Previous studies of the Huesca and Salt Wash DFS sandstone bodies .. 112
5.6. Limitation of the sandstone body classification 114
5.7. Discussion of applications of the sandstone body classification to DFS deposits formed in different climatic settings 115
5.7.1. Comparison with the Organ Rock Formation (dry climate) 115
5.7.2. Comparison with the Camargo Formation (semi-arid to relatively humid climate) 118
5.7.3. Comparison with the Fort Union Formation (humid climate) 120
5.8. Conclusions 122
6. The Huesca DFS succession 124
6.1. Introduction 124
6.2. Sandstones of the Huesca DFS succession 124
6.2.1. Composition 124
6.2.2. Grain size, roundness and sorting 127
6.2.3. Sediment source 127
6.3. Distribution of facies, architectural elements and facies associations 129
6.3.1. Main facies of the Huesca DFS successions 129
6.3.2. Downstream variations in facies distribution 130
6.4. Types and distribution of sandstone bodies 130
6.4.1. Sandstone body types of the Huesca DFS succession 130
6.4.2. Distribution of sandstone body types 133
Relatively proximal and medial outcrops (Monźon, Castelflorite) 133
Distal outcrop (Alcolea) 133
6.5. Downstream variations in sandstone body characteristics and sandstone body distribution 133
6.5.1. Overall proportion of sandstone bodies 136
6.5.2. Proportion of sandstone body types 136
6.5.3. Sandstone body dimensions 139
6.5.4. Grain size of sandstones 139
6.5.5. Summary of the downstream variations within the Huesca DFS deposits 140

7. The Salt Wash DFS succession 142

7.1. Introduction 142

7.2. Sandstones of the Salt Wash DFS succession 142

7.2.1. Composition 142

7.2.2. Grain size, roundness and sorting 144

7.2.3. Sediment source 144

7.3. Distribution of facies, architectural elements and facies associations 146

7.3.1. Main facies of the Salt Wash DFS successions 146

7.3.2. Downstream variations in facies distribution 147

7.4. Types and distribution of sandstone bodies 147

7.4.1. Sandstone body types of the Salt Wash DFS successions 147

7.4.2. Distribution of sandstone body types 150

Relatively proximal and medial outcrops (Bullfrog, Slick Rock) 150

Distal outcrop (Little Park) 150

7.5. Downstream variations in sandstone body characteristics and sandstone body distribution 153

7.5.1. Overall proportion of sandstone bodies 153

7.5.2. Proportion of sandstone body types 154

7.5.3. Sandstone body dimensions 156

7.5.4. Grain size of sandstones 157

7.5.5. Summary of the downstream variations within the Salt Wash DFS deposits 158

8. Discussion of possible controls on the downstream variations in facies distribution, sandstone body characteristics and their architecture 160

8.1. Introduction 160

8.2. Previous studies of the downstream variations in the architecture of the Huesca and Salt Wash deposits 160

8.3. Discussion of downstream trends in the DFS deposit architecture and their controls 162

8.3.1. Downstream trends in the gain size, sandstone body dimensions and sandstone body dimensions in the Huesca and Salt Wash successions 162

8.3.2. Decrease in transport capacity of the streams and decrease in grain size and sandstone body dimensions ... 163

Feeder channel ... 163

Evaporation ... 163

Infiltration ... 165

Bifurcation ... 165

8.3.3. Distributive discharge and increase in proportion of fine-grained deposits ... 167

8.3.4. Substrate cohesiveness and change in sandstone body type ... 167

8.3.5. Avulsion and change in sandstone body type ... 169

8.3.6. Termination of channels and change in sandstone body type ... 169

8.3.7. Lake level ... 170

8.3.8. Summary ... 171

8.4. Downstream variations in DFS characteristics and architecture of DFS deposits in documented modern and ancient DFSs ... 171

8.4.1. Downstream trends in the modern DFSs ... 172

8.4.2. Downstream trends in the ancient DFS deposits ... 174

8.5. Conclusions ... 176

9. Fine-grained deposits of the Huesca DFS succession and avulsion styles of the Huesca DFS ... 177

9.1. Introduction ... 177

9.2. Heterolithic deposits of the Huesca DFS succession ... 177

9.2.1. Heterolithic channel fill deposits ... 177

The heterolithic LA complexes ... 177

Channel scours filled with fine-grained heterolithic deposits ... 179

9.2.2. Heterolithic overbank deposits ... 179

Packages of closely-spaces sheet-like sandstone bodies ... 179

The heterolithic Hm facies ... 180

Small-scale scours filled with sand ... 180

“Heterolithic upper part” of LA complexes ... 180

9.3. Avulsion and avulsion deposits ... 184

9.4. Succession of avulsion deposits ... 185

9.5. Succession of avulsion deposits in the Huesca DFS succession ... 189

9.5.1. Apparent successions of avulsion deposits 189
9.5.2. Successions of avulsion deposits; are they real? 189
9.5.3. Vertical trends in avulsion successions; are they real?................. 195
9.6. Interpretation and discussion of the results.. 195
9.6.1. Splays of the Huesca DFS 195
9.6.2. Bank cohesiveness of the Huesca DFS.. 196
9.6.3. Avulsion styles of the Huesca DFS 197
Avulsion by splay progradation.. 197
Avulsion by re-occupation 197
9.6.4. Deposits of individual avulsion event or multiple avulsion events.. 198
9.6.5. Possible factors promoting avulsion on the Huesca DFS 199
9.7. Conclusions.. 201

10. Evidence for ordered facies and thickness successions in the DFS deposits 203

10.1. Introduction 203
10.2. Method 204
10.2.1. Order metric calculations 204
The Markov order metric (MOM) 204
Diagram explanation, part 1 204
The runs order metric (ROM) 206
The coarsening (shallowing) trend metric (CTM) 206
10.2.2. Comparison with synthetic models.. 208
The randomly shuffled same-data model 208
The randomly shuffled cycles model 208
The random model 209
The meaning of comparison between models and observations 209
Diagram explanation, part 2 211
10.3. Metric analysis results, their interpretation and discussion.................. 211
10.3.1. Preparation of stratigraphic sections.. 212
10.3.2. Metric values for the observed successions 212
System-scale Huesca and Salt Wash successions............................ 212
Floodplain succession of the Huesca DFS... 213

10.3.3. Comparison between MOM values of the observed successions and synthetic models 214

Comparison with randomly shuffled cycles and random models 214

Comparison with randomly shuffled same-data models 215

Comparison between system-scale and floodplain successions 217

Summary and interpretation 221

10.3.4. Comparison between ROM values of the observed successions and synthetic models 222

10.3.5. Comparison between CTM values of the Huesca floodplain successions and synthetic models 224

10.3.6. Comparison of a combination of CTM and MOM values of the observed successions with synthetic models 224

10.3.7. Variation in metric values with sample scale (section length) 225

Diagram explanation, part 3 227

Variations in MOM with scale 227

Variations in ROM with scale 228

Variations in CTM with scale 228

10.3.8. Comparison of test of significance with the method used in this research 241

10.4. Facies transitions and relationships within the DFS successions 241

10.4.1. The Huesca DFS succession 241

10.4.2. The Salt Wash DFS succession 243

10.4.3. Lateral variability in facies transitions and relationships 245

10.5. Conclusions 246

11. Heterogeneity of DFS deposits 249

11.1. Introduction 249

11.2. Heterogeneity of the Huesca and Salt Wash DFS deposits 249

11.2.1. Heterogeneity at pore scale 249

11.2.2. Heterogeneity at sedimentary structure scale 255

Mud drapes on lateral accretion surfaces 255

Variations in grain size 256

Type of sedimentary structures 257

11.2.3. Heterogeneity at sandstone body scale 258

11.2.4. Heterogeneity at succession scale 261

11.3. Net-to-gross ratio and sandstone body connectivity in the Huesca and Salt Wash DFS deposits 264
11.4. Conclusions 269

12. Two-dimensional geometric modelling of fluvial architecture.....271

12.1. Introduction 271
12.2. Elements and input parameters of the 2D model 272
12.2.1. Model dimensions, boundaries and grid 272
12.2.2. Initial floodplain topography 272
12.2.3. Subsidence 272
12.2.4. Channel element 273
12.2.5. Floodplain element 273
Uniform floodplain aggradation 275
Depth-dependent floodplain aggradation 275
Exponentially decreasing floodplain aggradation 275
Exponentially decreasing depth-dependent floodplain aggradation 276
12.2.6. Channel migration and avulsion 276
12.2.7. Input parameters 277
Time steps 277
Channel aggradation thickness 277
Channel erosion depth 277
Channel sandstone body width 277
Floodplain aggradation exponent 278
Avulsion frequency 279
Migration interval of channel element during local avulsion 279
12.3. Output parameters of the 2D model 280
12.3.1. Net-to-gross (NTG) ratio 280
12.3.2. Sandstone body connectivity 281
12.3.3. Distance between avulsion positions 283
12.3.4. Distance between channel centres 283
12.3.5. Calculation of spatial variability of sedimentation to subsidence ratio 283
12.4. Summary of model assumptions 286
12.5. Input parameters of the 2D model and physical processes 286

- 12.5.1. Channel/floodplain aggradation thickness 287
- 12.5.2. Erosion depth 287
- 12.5.3. Floodplain aggradation exponent 287
- 12.5.4. Channel sandstone body width 289

12.6. Modelling experiments 290

- 12.6.1. Variable input parameters 290
- 12.6.2. Variable channel avulsion algorithm 291
- 12.6.3. Variable floodplain algorithm 292
- 12.6.4. Variation in input parameters with time 292

12.7. Modelling successions of the Huesca and Salt Wash DFSs 292

- 12.7.1. The Huesca DFS succession 293
  - Relatively proximal succession (Monźon outcrop) 293
  - Medial succession (Castelflorite outcrop) 297
  - Distal succession (Alcolea outcrop) 300
- 12.7.2. The Salt Wash DFS succession 303
  - Relatively proximal succession (Bullfrog outcrop) 303
  - Medial succession (Slick Rock outcrop) 307
  - Distal succession (Little Park outcrop) 310
- 12.7.3. Summary of main results from the modelling of observed DFS strata 311

12.8. Sensitivity analysis: variable input parameters 313

- 12.8.1. Sensitivity of distance between channel sandstone bodies in the modelled strata to variation in input parameters 316
- 12.8.2. Effect of the floodplain aggradation parameters on the NTG ratio and sandstone body connectivity of the modelled strata 317
- 12.8.3. Effect of reworking parameters on the NTG ratio and sandstone body connectivity of the modelled strata 317
- 12.8.4. Sensitivity of the NTG ratio and sandstone body connectivity in the modelled strata to the width of sandstone bodies 318
- 12.8.5. Sensitivity of characteristics of strata with high and low channel sandstone body width to variations in input parameters 320
- 12.8.6. Artefacts within the models with compensational channel migration algorithm 324

12.9. Sensitivity analysis: variable avulsion mechanism 324

12.9.1. Sensitivity of NTG ratio and sandstone body connectivity in the modelled strata to channel avulsion mechanism 324

12.9.2. Sensitivity of the compensation thickness scale in the modelled strata to channel avulsion mechanism 329

Compensational avulsion mechanism 329

Random avulsion mechanism 329

Combined random and compensational avulsion mechanism 329

12.10. Sensitivity analysis: variable floodplain algorithm 333

12.10.1. Sensitivity of NTG ratio and sandstone body connectivity in the modelled strata to floodplain aggradation algorithm 333

Exponential depth-dependant and exponential floodplain aggradation 333

Depth-dependant and uniform floodplain aggradation 335

12.10.2. Sensitivity of the compensation thickness scale in the modelled strata to floodplain aggradation algorithm 335

12.11. Discussion of the results, limitations of the 2D model and recommendations for future work 337

12.11.1. Modelling of the Huesca and Salt Wash DFS strata................... 337

12.11.2. Non-unique controls on strata characteristics............................. 339

12.11.3. Sensitivity of NTG ratio and sandstone body connectivity in the modelled strata to variable input parameters of the model 340

12.11.4. Sensitivity of NTG ratio and sandstone body connectivity in the modelled strata to variable avulsion and floodplain aggradation mechanisms 341

12.11.5. Compensation thickness scale and its sensitivity to avulsion and floodplain aggradation algorithms 342

12.11.6. Regularity in channel distribution within the modelled strata: proposal for future work 343

12.12. Conclusions.. 347

13. Implications of the studies to reservoir modelling 350

13.1. Introduction.. 350

13.2. Use of modern and outcrop analogues in reservoir modelling 351

13.2.1. Outcrop analogues... 351

13.2.2. Modern analogues 352

13.3. Geometry of facies bodies as input for reservoir modelling 353
    13.3.1. Sandstone body geometry 353
    13.3.2. Measurements of sandstone body dimensions in outcrop and on photo panels 354
    13.3.3. Sandstone body correlation between wells 355
    13.3.4. Net-to-gross and sandstone body correlation between wells......... 361
13.4. Detailed sedimentological and petrographical studies 362
13.5. Sandstone body architecture and population of reservoir model 366
    13.5.1. Facies distribution, NTG ratio and outcrop analogues 366
    13.5.2. 3D seismic data for reservoir architecture predictions 368
    13.5.3. “Training images” and outcrop analogues for reservoir architecture predictions 370
13.6. Implications of process based / process-imitating modelling to modelling of reservoir architecture 371
    13.6.1. “Training images” and parameters for multiple-point geostatistics. 372
    13.6.2. Markov chain models 373
    13.6.3. NTG ratio, reservoir connectivity and reservoir architecture 374
        Sensitivity of NTG ratio to model input parameters 375
        Variations in NTG ratio in DFS deposits 376
        Sensitivity of sandstone body connectivity to rules of sandstone body distribution 378
        Compensation thickness scale and rules of sandstone body distribution 378
        Applications of the 2D model 379
    13.6.4. Future of the process-based / process-imitating modelling in reservoir modelling 379
13.7. Conclusions 381

14. Conclusions and recommendations for future research 383

14.1. Summary of the main conclusions 383
14.2. Recommendations for future work 389

Bibliography 392

Appendices 418

List of tables

Chapter 4. Facies analysis 62

Table 4.1 Summary table of facies classification for the Huesca and Salt Wash DFS successions. 63

Chapter 5. Sandstone body types 96

Table 5.1 Comparison of sandstone body dimensions in studied DFS succession and sandstone body dimensions in published descriptions of DFS successions formed in different climates 118

Chapter 6. The Huesca DFS succession... 124

Table 6.1 Comparison of percentage of sandstone body types out of all sandstone bodies estimated using interpreted 2D photo panels and 1D stratigraphic logs recorded in the Huesca DFS succession 137

Table 6.2 Percentage of sandstone bodies in the outcrops of the Huesca DFS succession that were studied in this research and in previous work of Hirst (1991) 138

Table 6.3 Maximum, minimum and average values of width and thickness for three sandstone body types in relatively proximal, medial and distal areas of the Huesca DFS 140

Table 6.4 Maximum, minimum and average values of the grain size (in φ) for three sandstone body types in relatively proximal, medial and distal outcrops of the Huesca DFS 141

Chapter 7. The Salt Wash DFS succession 142

Table 7.1 Comparison of percentage of sandstone body types out of all sandstone bodies estimated using interpreted 2D photo panels and 1D stratigraphic logs recorded in the Salt Wash DFS succession 155

Table 7.2 Percentage of sandstone bodies and their types in the Bullfrog outcrop of the Salt Wash DFS succession and comparison with the results of previous work by Kjemperud et al. (2008).. 156

Table 7.3 Maximum, minimum and average values of width and thickness for three sandstone body types in relatively proximal, medial and distal areas of the Salt Wash DFS 157

Table 7.4 Maximum, minimum and average values of the grain size (in φ) for three sandstone body types in relatively proximal, medial and distal outcrops of the Salt Wash DFS 159

Chapter 10. Evidence for ordered facies and thickness successions in the DFS deposits 203

Table 10.1 Metric values and parameters of the recorded system-scale sections of the Huesca and Salt Wash DFS successions 213

Table 10.2 Metric values and parameters of the recorded floodplain sections of the Huesca DFS succession 214

Table 10.3 Comparison of MOM values for synthetic models and recorded system-scale successions of the Huesca and Salt Wash DFS deposits and floodplain succession of the Huesca DFS deposits 220

Table 10.4 Comparison of ROM values for synthetic models and recorded system-scale successions of the Huesca DFS deposits 222

Chapter 11. Heterogeneity of DFS deposits 249

Table 11.1 Comparison between net-to-gross ratios estimated from 1D stratigraphic logs and from 2D photo panels 266

Chapter 12. Two-dimensional geometric modelling of fluvial architecture 271

Table 12.1 Abbreviations of input and output parameters 288

Table 12.2 Ranges of input parameters for model experiments 292

Table 12.3 Input parameters for the best-fit models of the Huesca outcrops 297

Table 12.4 Input parameters for the best-fit models of the Salt Wash outcrops 307

Table 12.5 Minimum and maximum NTG ratios for different channel sandstone body width 318

Table 12.6 Results of the sensitivity analysis for the Monźon and Bullfrog best-fit models and comparison of the effect of the input parameters on the modelled strata with high and low sandstone body widths 321

List of figures

Chapter 2. Geological background..37

2.1 Location of Ebro Basin and study area in Northern Spain 38

2.2 Geological map of the northern part of Ebro Basin showing outline of the Huesca DFS, palaeocurrent directions and study areas 38

2.3 Stratigraphy of the central Ebro Basin... 40

2.4 Schematic plan view of the Huesca DFS and palaeocurrent directions.......... 41

2.5 Location of the Colorado Plato and study area in Central USA 43

2.6 Topographic map of Utah and Colorado states showing outcrops of the Salt Wash DFS, palaeocurrent directions and study area outline for the 2011 fieldwork....... 43

2.7 Stratigraphy of the San Rafael Group and Morrison Formation...................... 44

2.8 Tectonic elements of the western North American continent in Jurassic........ 46

2.9 Palaeogeographic map of central USA in Middle Kimmeridgian, Jurassic...... 48

Chapter 3. Field work techniques and data processing methodology 50

3.1 Geological map of the central Ebro Basin showing study area outline for the 2010 and 2011 fieldwork and studied outcrop locations 51

3.2 Google Earth images of the main studied outcrops in Spain: Monźon, Castelflorite and Alcolea.. 51

3.3 Correlation of the outcrops based on their GPS elevation and geological cross section from NE to SW of Ebro Basin 53

3.4 Topographic map of Utah and Colorado states showing study area outline for the 2011 fieldwork and studied outcrop locations 54

3.5 Google Earth images of the main studied outcrops in USA: Bullfrog, Slick Rock and Little Park 54

3.6 Maps of GPS waypoints along the studied outcrops in Spain and USA showing outline of the outcrops and palaeocurrent rose diagrams for every location......... 57

3.7 Gamma ray spectrometer... 60

3.8 Methodology of GR measurements used during the fieldwork and size of the effective sample volume of the spectrometer.. 61

Chapter 4. Facies analysis 62

4.1 Facies Sb, sandstone breccia 65

4.2 Facies Slc, large scale cross-bedded sandstones 66

4.3 Facies St, trough cross-bedded sandstones 68

4.4 Facies Sh, horizontal and low-angle bedded sandstones 72

4.5 Facies Sr and Scr, ripple and climbing ripple cross laminated sandstones 72

4.6 Facies Sis, sandstones with inclined stratification.. 74

4.7 Schematic diagram showing lateral accretion on point bar resulting from the migration of meander loop... 75

4.8 Schematic cross section through a point bar showing internal architecture including lateral accretion surfaces at the bar top and through cross-bedded sandstones at the base of the bar formed by migration of dunes along the channel floor 75

4.9 Facies His, interbedded sandstones, siltstones and mudstones with inclined stratification 77

4.10 Facies Sil, isolated sandstone lenses 80

4.11 Facies Sils, small-scale isolated sandstone lenses...................................... 80

4.12 Facies Ssh, sandstone sheets 83

4.13 Facies Hsh, packages of sandstone, siltstone and mudstone sheets........... 85

4.14 Facies Hm, packages of interbedded siltstone and mudstone sheets 88

4.15 Facies Lm, interbedded limestones and wavy cross-laminated mudstones . 90

Chapter 5. Sandstone body types 96

5.1 Three subtypes of Type 1 sandstone bodies 98

5.2 Three subtypes of Type 2 sandstone bodies 100

5.3 Three subtypes of Type 3 sandstone bodies 102

5.4 Width and thickness relationships for the three sandstone body types and their subtypes 104

5.5 Relationships between sandstone bodies of subtype 3/2 and subtype 1/1 and 1/2 106

5.6. Evolution of the channel and formation of Type 1 sandstone body overlain by sheet-like sandstone body of Type 3/2 during avulsion by channel blockage 107

5.7 Amalgamated sandstone bodies of subtype 3/2 108

5.8 Relationships between sandstone bodies of Type 1 and 2 with sandstone bodies of Type 3 110

5.9 Large amalgamated sandstone body complexes... 111

5.10 Vertically stacked sandstone bodies with stepped edges 112

Chapter 6. The Huesca DFS succession..124

6.1 X-ray spectra for samples form the Huesca DFS succession showing main mineral constituents 126

6.2 Classification of the Huesca sandstones using Folk and Pettijohn triangle-classifications 126

6.3 Cumulative curves for weight percentage of grain size fractions of the Huesca sandstones used for estimation of mean grain size and sorting 126

6.4 Schematic geological map of the Pyrenees and adjacent Ebro Basin showing potential source areas for the Huesca DFS deposits... 128

6.5 Percentage of facies, architectural elements and facies associations in the deposits of the Huesca DFS 131

6.6 Downstream variations in percentage of facies, architectural elements and facies associations from the relatively proximal to medial and distal areas of the Huesca DFS 131

6.7 Sedimentary logs in the relatively proximal, medial and distal parts of the Huesca DFS deposits.. 132

6.8 Proportion of Type 1, 2 and 3 sandstone bodies and non-sandstone deposits in the Huesca DFS succession 134

6.9 Downstream variations in proportion of Type 1, 2 and 3 sandstone bodies and non-sandstone deposits from the relatively proximal to medial and distal areas of the Huesca DFS 134

6.10 Photo panels of relatively proximal, medial and distal outcrops of the Huesca DFS deposits 135

6.11 Downstream variations in overall sandstone body proportion relative to the finer-grained deposits in the Huesca DFS succession 136

6.12 Downstream variations in dominant sandstone body type in the Huesca DFS succession.. 137

6.13 Variations in maximum, minimum and average values of thickness and width for different sandstone body types in the Huesca DFS succession 139

6.14 Variations in minimum, mean and maximum grain size values for different sandstone body types in relatively proximal, medial and distal outcrops of the Huesca DFS 140

Chapter 7. The Salt Wash DFS succession 142

7.1 Classification of the Salt Wash sandstones using Folk and Pettijohn triangle-classifications 145

7.2 Cumulative curved for weight percentage of grain size fractions of the Salt Wash sandstones used for estimation of mean grain size and sorting 145

7.3 Percentage of facies, architectural elements and facies associations in the deposits of the Salt Wash DFS 148

7.4 Downstream variations in percentage of facies, architectural elements and facies associations from the relatively proximal to medial and distal areas of the Salt Wash DFS 148

7.5 Sedimentary logs in the relatively proximal, medial and distal parts of the Salt Wash DFS deposits 149

7.6 Proportion of Type 1, 2 and 3 sandstone bodies and non-sandstone deposits in the Salt Wash DFS succession 151

7.7 Downstream variations in proportion of Type 1, 2 and 3 sandstone bodies and non-sandstone deposits from the relatively proximal to medial and distal areas of the Salt Wash DFS 151

7.8 Photo panels of relatively proximal, medial and distal outcrops of the Salt Wash DFS deposits 152

7.9 Downstream variations in overall sandstone body proportion relative to the finer-grained deposits in the Salt Wash DFS succession 154

7.10 Downstream variations in dominant sandstone body type in the Salt Wash DFS succession 154

7.11 Variations in maximum, minimum and average values of thickness and width for different sandstone body types in the Salt Wash DFS succession 157

7.12 Variations in minimum, mean and maximum grain size values for different sandstone body types in relatively proximal, medial and distal outcrops of the Salt Wash DFS 158

Chapter 8. Discussion of possible controls on the downstream variations in facies distribution, sandstone body characteristics and their architecture..160

8.1 Previously proposed DFS models for the Huesca and Salt Wash DFSs 161

8.2 Examples of modern DFSs 164

8.3 Evidence of infiltration below major sandy braided channels.......................... 166

8.4 Examples of channel bifurcation 166

8.5 Diagram showing relationships between different factors affecting downstream variations in the DFS flow behaviour and resulted changes in DFS deposits....... 172

8.6 Geomorphic elements of three types of the DFS 173

8.7 Downstream decrease in gradient of Kosi DFS and change from channelized flow to unconfined flow downstream the avulsion lobe of the Taquari DFS 175

8.8 Coarsening-upward progradation succession in the Camargo Formation, Brazil and downstream variations in facies associations in the Organ Rock Formation and in sandstone body dimensions in 3D numerical model 175

Chapter 9. Fine-grained deposits of the Huesca DFS succession and avulsion styles of the Huesca DFS...177

9.1 Heterolithic channel-fill deposits.. 178

9.2 Floodplain elements 181

9.3 Relationship of floodplain deposits and Type 2 sandstone body in the Canal del Cinca outcrop 182

9.4 Photographs and sedimentary logs of the heterolithic deposits formed on relatively flat floodplain surface and in an abandoned channel fill....................................... 183

9.5 Proportion of avulsion deposits including Type 3 sandstone bodies and fine-grained overbank deposits in comparison to the proportion of channel sandstone bodies of Type 1 and 2 186

9.6 Model of avulsion by splay progradation by Smith et al. (1989)..................... 186

9.7 Stratigraphically transitional (A) and abrupt (B) types of avulsion successions and mechanisms of their formation suggested by Jones and Hajek (2007)................ 187

9.8 Apparent stratigraphically transitional (A) and abrupt (B) types of avulsion successions in the Huesca DFS succession... 190

9.9 Splay deposits truncated by subsequent channel sandstone bodies forming either stratigraphically transitional and abrupt types of avulsion successions 192

9.10 Possible scenarios of erosion and preservation of avulsion deposits 193

9.11 Vertically stacked packages of splay deposits in the Huesca DFS succession 194

9.12 Vertically connected two- and multi-storey subtype 1/1 and Type 2 sandstone bodies with stepped edges indicating avulsion by re-occupation/annexation 198

Chapter 10. Evidence for ordered facies and thickness successions in the DFS deposits 203

10.1 Three synthetic successions and results of their statistical analysis including facies frequency histogram, transition probability matrix, Markov order metric (MOM), runs thickness order metric (ROM) and coarsening trend order metric (CTM) 205

10.2 Effect of section length and number of different facies on the three order metrics 207

10.3 Variation in MOM and ROM of perfectly ordered cyclical succession with the number of shuffles for different number of facies 216

10.4 Variation in difference of MOM values for shuffled cycles model and recorded successions relative to MOM values for the recorded successions. Comparison between the Huesca and Salt Wash system-scale successions and Huesca floodplain successions 218

10.5 The MOM values for system-scale and floodplain succession relative to the MOM of the perfectly ordered cyclical succession presented on the background of the Fig.10.3 219

10.6 The ROM values for system-scale and floodplain succession relative to the runs order metric of the perfectly ordered cyclical succession presented on the background of the Fig.10.3 223

10.7 MOM and CTM analysis for synthetic coarsening-upward, random and dominant facies successions and Monźon 3 floodplain succession 226

10.8 The results of the metric analysis for the Alcolea 1&2 Log 1system-scale succession (Huesca DFS)... 229

10.9 The results of the metric analysis for the Castelflorite 4 Log1 system-scale succession (Huesca DFS)... 230

10.10 The results of the metric analysis for the Bullfrog 2 Log 125 system-scale succession (Salt Wash DFS) 231

10.11 The results of the metric analysis for the Bullfrog 3 Log 34 system-scale succession (Salt Wash DFS) 232

10.12 The results of the metric analysis for the Monźon 4 Log 1 system-scale succession (Huesca DFS) 233

10.13 The results of the metric analysis for the Little Park 3 Log 7 system-scale succession (Salt Wash DFS) 234

10.14 The results of the metric analysis for the Monźon 4 floodplain succession (Huesca DFS) 235

10.15 The results of the metric analysis for the Monte Aragón 4 floodplain succession (Huesca DFS) 236

10.16 The results of the metric analysis for the Bolea 2 floodplain succession (Huesca DFS) 237

10.17 The results of the metric analysis for the Castelflorite 1 floodplain succession (Huesca DFS) 238

10.18 The results of the metric analysis for the Monte Aragón 2 floodplain succession (Huesca DFS) 239

10.19 The results of the metric analysis for the Monźon 3 floodplain succession (Huesca DFS) 240

10.20 Facies transition diagrams for the Castelflorite 4 Log 1, Castelflorite 2&3 Log 2, Monźon 4 Log 1, Monźon 1 Log 12 and Alcolea 1&2 Log 1 successions of the Huesca DFS deposits 242

10.21 Facies transition diagrams for the Bullfrog 2 Log 125, Bullfrog 3 Log 34, Little Park 3 Log 7 and Little Park 1 Log 456 successions of the Salt Wash DFS deposits 245

Chapter 11. Heterogeneity of DFS deposits 249

11.1 Heterogeneity at pore scale and sedimentary structure scale 250

11.2 Examples of pore space in thin sections of the Huesca sandstones and siltstones used for porosity estimations 252

11.3 Examples of pore space in thin sections of the Salt Wash sandstones and siltstones used for porosity estimations 253

11.4 Variations in porosity between different facies and with grain size 254

11.5 Heterogeneity at the sandstone body scale and system scale 259

11.6 Outcrop photo panes showing potentially connected sandstone bodies in the Huesca and Salt Wash DFS successions 262

11.7 Correlation between net-to-gross ratio and 2D / 3D reservoir-to-well connectivity published by Larue and Hovadik (2006)... 265

Chapter 12. Two-dimensional geometric modelling of fluvial architecture 271

12.1 Geometric elements of the 2D model.. 274

12.2 Diagram explaining avulsion mechanism in the 2D model........................... 276

12.3 Graph explaining the choice of the value for the aggradation exponent 278

12.4 Examples of modelled strata with different frequencies of major avulsion.... 279

12.5 Definition of the sandstone body connectivity metric 281

12.6 Comparison of two gridding algorithms used for sandstone body connectivity calculations.. 282

12.7 Deposition by fluvial system in a basin and corresponding change in value and variability of aggradation to subsidence ratio across the basin with time............. 284

12.8 Main steps of calculation of variability of sedimentation to subsidence ratio 285

12.9 Examples of modelled strata with NTG ratio equal 30 % 294

12.10 Ranges of input parameters that can simulate strata with NTG ratios observed in the Huesca DFS successions 295

12.11 Best-fit model for the relatively proximal Monźon outcrop of the Huesca DFS deposits 296

12.12 Examples of modelled strata with NTG ratio equal 15 % 298

12.13 Best-fit model for the medial Castelflorite outcrop of the Huesca DFS deposits 299

12.14 Examples of modelled strata with NTG ratio equal 3 % 301

12.15 Best-fit model for the distal Alcolea outcrop of the Huesca DFS deposits .. 302

12.16 Examples of modelled strata with NTG ratio equal 85 % 304

12.17 Ranges of input parameters that can simulate strata with NTG ratios observed in the Salt Wash DFS successions 305

12.18 Best-fit model for the relatively proximal Bullfrog outcrop of the Salt Wash DFS deposits 306

12.19 Examples of modelled strata with NTG ratio equal 50 % 308

12.20 Best-fit model for the medial Slick Rock outcrop of the Salt Wash DFS deposits 309

12.21 Examples of modelled strata with NTG ratio equal 35 % 311

12.22 Best-fit model for the distal Little Park outcrop of the Salt Wash DFS deposits 312

12.23 Diagram illustrating non-uniqueness of the input parameters that control NTG ratio of the modelled strata 314

12.24 Sensitivity maps for the distance between avulsion locations, mean distance between channels and mean distance to the closest channel for the Monźon best-fit model 315

12.25 Variation in the NTG ratio and number of individual connected sandstone bodies with increase in channel sandstone body width 318

12.26 Sensitivity maps for the NTG ratio, number of individual sandstone bodies and strata thickness for the Monźon best-fit model 319

12.27 Sensitivity maps for the distance between avulsion locations, mean distance between channels and mean distance to the closest channel for the Bullfrog best-fit model 322

12.28 Sensitivity maps for the NTG ratio, number of individual sandstone bodies and strata thickness for the Bullfrog best-fit model 323

12.29 Comparison of variations in NTG ratio and number of individual sandstone bodies with increase in channel sandstone body width for the models with compensational and random channel avulsion mechanisms 325

12.30 Variation in NTG ratio and number of connected bodies in the Monźon best-fit model simulated with three different avulsion algorithms 326

12.31 Sensitivity maps for the NTG ratio, number of individual sandstone bodies and strata thickness for the Monźon best-fit model simulated with random avulsion mechanism 327

12.32 Sensitivity maps for the mean distance between channels and mean distance to the closest channel for the Monźon best-fit model simulated with random avulsion mechanism 328

12.33 Channel stacking for three different avulsion mechanisms 330

12.34 Compensation thickness scales for the Monźon best-fit model simulated with three different avulsion mechanisms 331

12.35 Compensation thickness scales for the Monźon best-fit model simulated with combined avulsion mechanisms and different avulsion frequency and migration distance 332

12.36 Variation in NTG and number of individual sandstone bodies in the modelled strata with different floodplain algorithms 334

12.37 Compensation thickness scales and channel distributions for the Monźon best-fit model simulated with four different floodplain mechanisms 336

12.38 Cross-section of the prototype of the 3D DFS model................................ 338

12.39 Modelled strata with apparently regular and not regular channel distribution 344

12.40 Sensitivity of the regularity metric to variable input parameters for the first example of modelled strata with high sandstone body width and low floodplain aggradation exponent.. 345

12.41 Sensitivity of the regularity metric to variable input parameters for the second example of modelled strata with low sandstone body width and high floodplain aggradation exponent.. 346

Chapter 13. Implication of the studies to reservoir modelling 350

13.1 Distinguishing individual sandstone bodies within amalgamated complexes in outcrops and from well log data 356

13.2 Lateral accretion complexes and preserved meander loops in the Caineville outcrop of the Salt Wash DFS succession 358

13.3 Character of base and top boundaries of sandstone bodies of the DFS sandstone bodies and well correlation based on different boundary types 360

13.4 Workflow of “pore-to-field” reservoir modelling approach............................. 363

13.5 Variation in heterogeneity and architecture of lateral accretion complexes .. 365

13.6 Downstream variations in the architecture of the Huesca and Salt Wash DFS deposits and sandstone body clustering in the Ferris DFS deposits, Wyoming, USA 367

13.7 Abundant thin sheet-like Type 3 sandstone bodies in the Huesca and Salt Wash DFS successions.. 369

13.8 “Training image” and transformations used in multiple-point geostatistical method 371

13.9 Downstream variations in DFS architecture modelled with 2D geometric model created in this project and 3D model of Karssenberg and Bridge, 2008 377

Appendices........418

Appendix 1. GPS coordinates for the studied locations, stratigraphic logs and outcrop maps........ 419

Appendix 2. Stratigraphic logs........ 427

Appendix 3. Tables of characteristics of the Huesca and Salt Wash sandstones. 448

Appendix 4. Thin section panels 461

Appendix 5. Outcrop photo panels (also see foldouts in the pocket at the back of the thesis)........ 469

Appendix 6. Results of order metric analysis for system-scale and floodplain successions........ 477

Appendix 7. Preliminary results of gamma ray survey 500

1. Introduction

1.1 Introduction

Distributive fluvial systems (DFS) form at margins of sedimentary basins where water enters the basin through a feeder channel, becomes unconfined and free to avulse or/and bifurcate, forming radial pattern of channel and floodplain deposits (Weissmann et al., 2010; Hartley et al., 2010(a)). It has been recognised that DFSs form a significant proportion of deposits in modern continental sedimentary basins, while tributary fluvial system deposits compose only a minor proportion of the basin fill (Weissmann et al., 2010). These relationships might have been preserved in facies distribution within the continental record (Weissmann et al., 2010). At present, the DFS concept is being actively discussed at various geological meetings and in published literature (Fielding et al., 2012; Sambrook Smith et al., 2010; Hartley et al., 2010(b)). Previous work has been mostly focused on the behaviour and geomorphological elements of modern DFSs (Wells and Dorr, 1987; Sinha, 1996; Singh et al., 1993; Chakraboty et al., 2010; Shukla et al., 1999, 2001; McCarthy et al., 1992; Assine, 2005; Buehler et al., 2011; Horton and DeCelles, 2001). Other workers characterised facies and sandstone body architecture of only limited areas of ancient DFS successions (Horton and DeCelles, 2001; Ayers et al., 1986, Kjemperud et al., 2008; Robinson and McCabe, 2008). However, despite the interest in the subject, there are still few detailed field-based descriptions of ancient DFS deposits available, particularly those focusing on sandstone body architecture and distribution of facies across the DFS (Hirst and Nichols, 1986; Nichols, 1987; Hirst, 1991; Cain and Mountney, 2009). This thesis focuses on the characterisation of facies trends across DFS deposits and documents the variations in sandstone body architecture by considering two ancient examples of DFS.

1.2 Aims and objectives of the thesis

In this thesis the sedimentology of ancient DFS deposits is discussed to provide an insight on the architecture of DFS deposits and DFS behaviour, and to better understand the main factors that control styles of sediment deposition during system development.

The primary objectives of the thesis are to:

- Document two ancient DFS successions, Huesca DFS (Miocene, Spain) and Salt Wash DFS (Jurassic, USA), and provide detailed classification of facies and sandstone bodies typical of DFSs;

- Quantify the characteristics of the DFS successions and their trends so that they could be used to characterise the architecture of analogous fluvial reservoirs;
- Investigate depositional record of channel avulsions in the Huesca DFS deposits to identify avulsion styles on the DFSs;
- Discuss main heterogeneities that occur in studied DFS strata;
- Identify factors that could have controlled the architecture of the two studied DFS successions; Create two-dimensional geometric model to complement outcrop data analysis with aim of providing a better understanding of the controls on large-scale reservoir qualities (net-to-gross ratio and sandstone body connectivity) of the DFS strata;
- Discuss the implication of the study to reservoir modelling.

1.3 Why to study distributive fluvial systems (DFS)?

Despite of a number of modern DFS examples that have been frequently studied in relation to flooding events influencing areas of human settlements (e.g. the Kosi DFS in India (Mookerjea, 1961; Gohain and Parkash, 1982; Singh et al., 1993) and the Taquari DFS in Brazil (Assine, 2005)), no significant attention have been given to the DFS deposits in geological record. Relatively few ancient DFS successions have been described in outcrops, for example, the Salt Wash DFS succession (Colorado Plato, USA, Craig et al., 1955; Mullens and Freeman, 1957), the Huesca and Luna DFS successions (Ebro Basin, Spain, Hirst and Nichols, 1986), the Camargo Formation (Eastern Cardillera, Horton and DeCelles, 2001), the Organ Rock Formation in the Paradox Basin, USA (Cain and Mountney, 2009) and in the subsurface, for example, the Tonger River Member of the Fort Union Formation, (Wyoming, USA, Ayers et al., 1986; Johnson and Pierce, 1990) and the Lower Clair Group (West of Shetland, Nichols, 2005). Deposits in non-aggrading rivers have relatively low preservation potential and should not be used as a basis for facies models that can be used to interpret the geological record (Bristow et al., 1999). Few conceptual facies models of distributive fluvial systems have been proposed (e.g. Kelly and Olsen, 1992; Stanistreet and McCarthy, 1993; Nichols and Fisher, 2007), and a comprehensive model considering all aspects of complex DFS behaviour does not exist (Cain and Mountney, 2009). The geomorphic elements of DFSs have been recognised using modern DFS examples by Davidson et al., 2013. This provides the first step towards a comprehensive facies model, but the link between modern geomorphic elements and preserved deposits has not yet been fully addressed. Thus, detailed outcrop studies of the DFS successions can contribute to understanding the link between modern DFS processes and preserved DFS deposits, and to the creation of DFS facies models.

As DFS deposits are likely to be preserved in geological record (Weissmann et al., 2010) they can form fluvial hydrocarbon reservoirs. The main challenge for petroleum geologists is to characterise the distribution of reservoir bodies and their connectivity using limited subsurface data. Outcrop analogues are widely used to compensate for the lack of 3D or 2D information about reservoirs (Alexander, 1993; Bridge and Tye, 2000). Robinson and McCabe (2008) demonstrated that fluvial outcrop studies could help to predict reservoir connectivity and compartmentalisation of sandstone bodies. As there are few well documented outcrop analogues for reservoirs in DFS strata, it is useful to study the deposits of DFS to provide such data sets.

Comparison of the architecture of DFS deposits formed in different sedimentary basins (Morrison and Ebro basins) can also provide an insight into factors that could have controlled the DFS deposition and resulted in differences in depositional architectures. This can help petroleum geologists choose suitable outcrop analogues for fluvial reservoirs.

1.4 The DFS concept

Distributive fluvial systems (DFS) form at margins of sedimentary basins where water that enters the basin through a feeder channel or valley becomes unconfined and free to avulse or/and bifurcate, forming radial channel pattern (Weissmann et al., 2010; Hartley et al., 2010(a)). However, DFS do not always have a fan-shape (Hartley et al., 2010(a)). It has been suggested that not all distributive channels on a DFS are active at the same time, however some can be (Weissmann et al., 2010; Hartley et al., 2010(a)). The profile of a DFS is concave-upward downstream and convex-upward across the fan (Weissmann et al., 2010). The deposits of DFSs are characterised by radial palaeocurrent patterns and downstream variations in facies distribution such as a decrease in sandstone-to-mudstone ratio and decrease in width of channel sandstone bodies (e.g. Craig et al., 1955; Hirst and Nichols, 1986; Hirst, 1991; Nichols and Fisher, 2007).

To investigate the DFS concept 700 modern sedimentary basins (Weissmann et al., 2010) and 415 large (> 30 km in radius) modern DFSs (Hartley et al., 2010(a)) have been studied using satellite images. It was shown that DFSs dominate amongst modern continental sedimentary basins (Weissmann et al., 2010) and are common in all climatic and tectonic settings (Hartley et al., 2010(a)). In contrast to the majority of modern "normal" tributary rivers, which form in degradational settings, modern DFSs form in aggradational sedimentary basins and their deposits are likely to be preserved in continental geological record (Weissmann et al., 2010). Therefore, deposits of ancient DFSs may dominate in continental geological record, while deposits of the majority of tributary rivers would not be preserved (Weissmann et al., 2010).

The dominance of the DFS deposits in continental geological record has been questioned by Sambrook Smith et al. (2010) and Fielding et al. (2012). The authors provided following arguments: 1) the DFS recognition criteria suggested by Weissmann et al. (2010) are ambiguous; 2) the large area occupied by some modern tributary river systems are greater than the areas occupied by modern DFSs; 3) thick sedimentary successions are preserved below large tributary rivers that could be formed by tributary fluvial systems.

The recognition criteria (radial channel pattern, decrease in channel size and grain size downstream a DFS), suggested by Weissmann et al. (2010), have been interpreted by Fielding et al. (2012) as product of bifurcation of contemporaneously flowing channels. However, the DFS definition has not been limited to bifurcating fluvial systems and includes fluvial systems where resulting radial channel pattern is formed by a combination of single channel avulsion and/or bifurcation (Fig. 12 in Hartley et al., 2010(a); Davidson et al., 2013). The term “distributive” has been chosen by Weissmann et al. (2010) instead of previously used term “distributary” (e.g. Nichols and Fisher, 2007) to exclude interpretations of coevally flowing channels. In addition, apart from bifurcation, a decrease in channel size downstream can also be controlled by a combination of factors such as variable rainfall and runoff in catchment, discharge loss through evapo-transpiration and infiltration, diversion of flow away from a main channel (bifurcation, anabranching and avulsion) and decrease in floodplain gradient (Davidson et al., 2013 and reference therein). The width of a main active channel on DFS can also remain constant from the apex to the toe (Davidson et al., 2013).

Fielding et al. (2012) have demonstrated that tributary drainage basins such as the Amazon or the Ob occupy much larger areas on continents than sedimentary basins with DFSs. Fielding et al. (2012) have also argued that tributary river deposits can be preserved and can comprise significant proportion of continental record even though for some period of time during their development they operate in degradational settings. This statement has been supported with examples of thick and extensive successions of tributary river deposits.

However, it has been emphasised by Weissmann et al. (2010) and Davidson et al. (2013) that the majority of large tributary fluvial systems form in degradational drainage basins where channel streams would transport sediment along their course and deposit them predominantly in marine or lacustrine basins where these rivers terminate (including the Amazon and the Ob). In addition, tributary rivers are confined to valleys. This limits proportions and preservation potential of tributary river deposits in sedimentary basins (Weissmann et al., 2010; Davidson et al., 2013). The DFS concept, however, does not ignore the importance of deposition by tributary rivers. The tributary rivers have been suggested to occur in axial positions within sedimentary basins, between two adjacent DFSs or incised into DFS (Weissmann et al., 2010). In these cases, tributary system deposits have a potential for being preserved together with DFS deposits. Therefore, the reaches of larger tributary fluvial systems could intersect sedimentary basins and their deposits can be preserved.

It is, therefore, clear that both distributive and tributary fluvial systems exist in modern sedimentary basins and their deposits could have been preserved in ancient continental successions. The published research discussed above is the first step towards understanding relative importance of tributary and distributive fluvial systems in modern and ancient sedimentary basins. This will require more studies of modern fluvial systems and ancient fluvial successions focusing on the differentiation criteria of deposits formed by two types of fluvial systems and distribution of their deposits in sedimentary basins.

This research does not directly address relative importance of distributive and tributary fluvial systems in formation of continental geological record, but recognises a necessity for additional studies of DFS and their deposits. Two ancient DFS successions, Salt Wash in USA and Huesca in Spain, are studied to improve the current knowledge of DFS deposit architecture and contributes towards an understanding of 1) DFS recognition criteria, 2) facies distribution within DFS deposits and 3) controls on DFS deposit architecture.

1.5 Methods

The data for this thesis are collected from two study areas: 1) Ebro Basin in Spain (Huesca DFS) and 2) Utah/Colorado in USA (Salt Wash DFS). The study areas have been chosen because the deposits have previously been interpreted as fluvial systems with radial channel pattern (Hirst and Nichols, 1986; Craig et al., 1955) and they are well-exposed, easily accessible and suitable for architecture studies.

Standard fieldwork techniques were used to document DFS outcrops and these are described in detail in Chapter 3. Statistical approaches, including Markov chain statistics, were used to quantitatively analyse new outcrop data and to recognise vertical and lateral trends in DFS characteristics within the successions. Numerical geometric modelling was used to explore the main controlling factors that affected the resulting architecture of the DFS deposits and their reservoir qualities.

1.6 Organisation of the thesis

The thesis contains 14 chapters and 7 graphical and table appendices. The introductory chapters 2 and 3 describe geological settings for the two study areas of the thesis and the methodology of data collection and data processing. The following two chapters, 4 and 5, present a classification of facies and sandstone body types typical for both DFS successions and discusses applicability of sandstone body classification for DFS strata formed in different climatic settings. These classifications are used to describe and quantify the characteristics of the Huesca and Salt Wash DFS successions, discussed in chapters 6 and 7. Chapter 8 utilises the descriptions presented in the previous two chapters in order to discuss downstream variations in facies and sandstone body types and their main controls. In Chapter 9 heterolithic fine-grained deposits of the Huesca DFS succession are described and interpreted addressing channel avulsion process on the DFS and the deposits related to avulsion. The degrees of order of facies and thickness successions within the DFS deposits are quantitatively analysed using a new statistical method and the results and applicability of the method are discussed in Chapter 10. Next Chapter 11 discusses heterogeneity of the DFS deposits at micro-to-macro scales in relation to the reservoir characterisation. The main factors controlling DFS architecture and reservoir quality of DFS strata are discussed in Chapter 12, where a geometric 2D model is used to explore the topic. Implications of the thesis studies to reservoir characterisation and reservoir modelling are discussed in Chapter 13. Chapter 14 finalises the work with the main conclusions of the thesis and recommendations for the future work. All appendices are presented in the end of the thesis.

1.7 Main findings

As a result of this research work, detailed sedimentological and quantitative descriptions of the architecture of two outcrop examples of DFS successions have been provided. Based on the detailed fluvial architecture analysis, a unified facies and sandstone body classification scheme has been developed and downstream trends in facies and sandstone body architecture has been quantified. This quantitative outcrop data can potentially be used to characterise DFS deposits in the subsurface.

As a result of the detailed sedimentological analysis of heterolithic overbank deposits in the Huesca DFS succession, avulsion through splay formation was recognised as an important avulsion style, but statistical analysis showed no evidence of previously recognised coarsing-upward trends in these deposits.

Numerical geometric modelling is used to investigate controls on the sandstone body architecture. Sensitivity analysis of the NTG ratio and sandstone body connectivity to variations in input parameters (proxies for external controls) has been carried out for the low net-to-gross Huesca succession and high net-to-gross Salt Wash succession.

The implications of the work, presented in this thesis, to reservoir modelling have been discussed to show the limitations and strengths of outcrop data, the results of their quantitative analysis and numerical modelling as a source of input information for reservoir modelling.

2. Geological background

2.1 Introduction

Two successions of distributive fluvial system (DFS) deposits have been studied for the purposes of this thesis. Geographical and geological setting of two study areas are described in this chapter to provide information about the stratigraphy of the successions, climatic and tectonic condition during their formation and location of the study areas. Sedimentological analysis of fluvial deposits of both successions is presented in the following chapters.

2.2 The Huesca DFS succession

The fluvial architecture of the Huesca fluvial system deposits is the main object of this thesis. The fluvial succession is well-exposed in outcrops of considerable length, making them suitable for large-scale sandstone body architecture observations.

Several authors have previously conducted their research on the Huesca fluvial deposits and have focused upon the individual aspects of the succession: point bar sandstones of sinuous channels (Donselaar and Overeem, 2007), overbank sheet-like sandstone bodies (Fisher et al., 2007(a), (b)) and palaeosols (Hamer et al., 2007(a), (b)). More comprehensive and large-scale architectural studies of the Huesca succession have been carried out by Hirst (1983, 1991); Hirst and Nichols (1986) and Nichols and Hirst (1998), who studied deposits of the main western part of the system.

2.2.1 Geographical setting

The Huesca DFS succession is exposed in the northern part of the Ebro Basin in Aragón province of Northern Spain (Fig. 2.1). The Ebro Basin is a foreland basin at the southern margin of Pyrenees where a thrust front limits the basin from the north, whereas the Iberian Ranges and Catalan Coastal Ranges frame the basin to the south and east, respectively (Riba et al., 1983; Arenas and Pardo, 1999; Alonso-Zarza et al., 2002). The Ebro Basin is drained by modern River Ebro that flows from west to east of the basin into the Mediterranean Sea (Evans and Arche, 2002) and incises into fluvial deposits of interest to this study.

2.2.2 Stratigraphy

Stratigraphically the Huesca fluvial succession corresponds to Sariñena Formation, which was deposited contemporaneously and intercalates with lacustrine deposits of the Alcubierre and Zaragoza Formations (Arenas and Pardo, 1999) in the central part of the basin (Fig. 2.2 and 2.3).

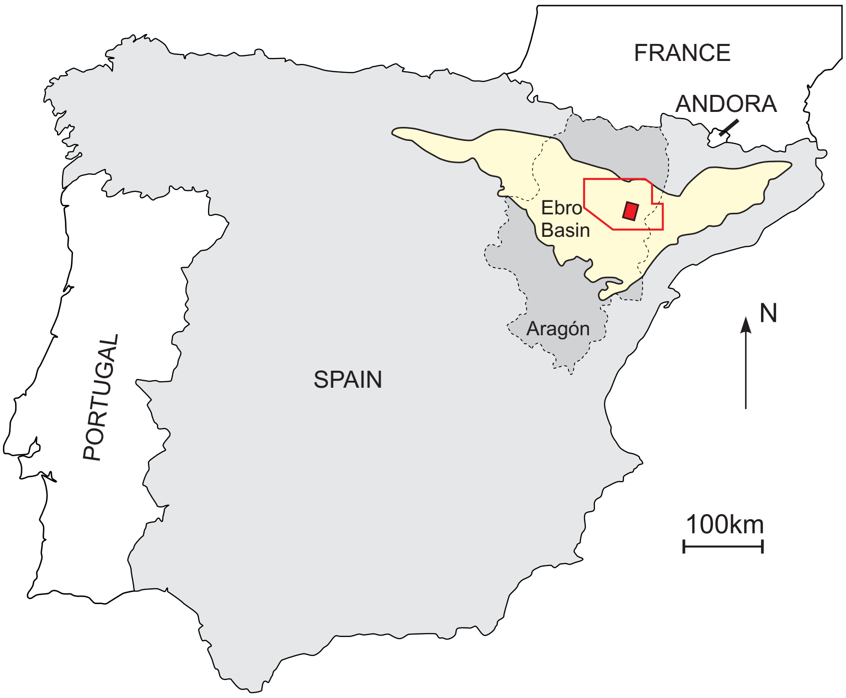

Figure 2.1. Location of the Ebro Basin and study area. Study area (red square) is located in the Aragón province of Northern Spain. The red polygon indicates the area of Figure 2.2. The Ebro Basin boundary is taken from Alonzo-Zaraza et al., 2002).

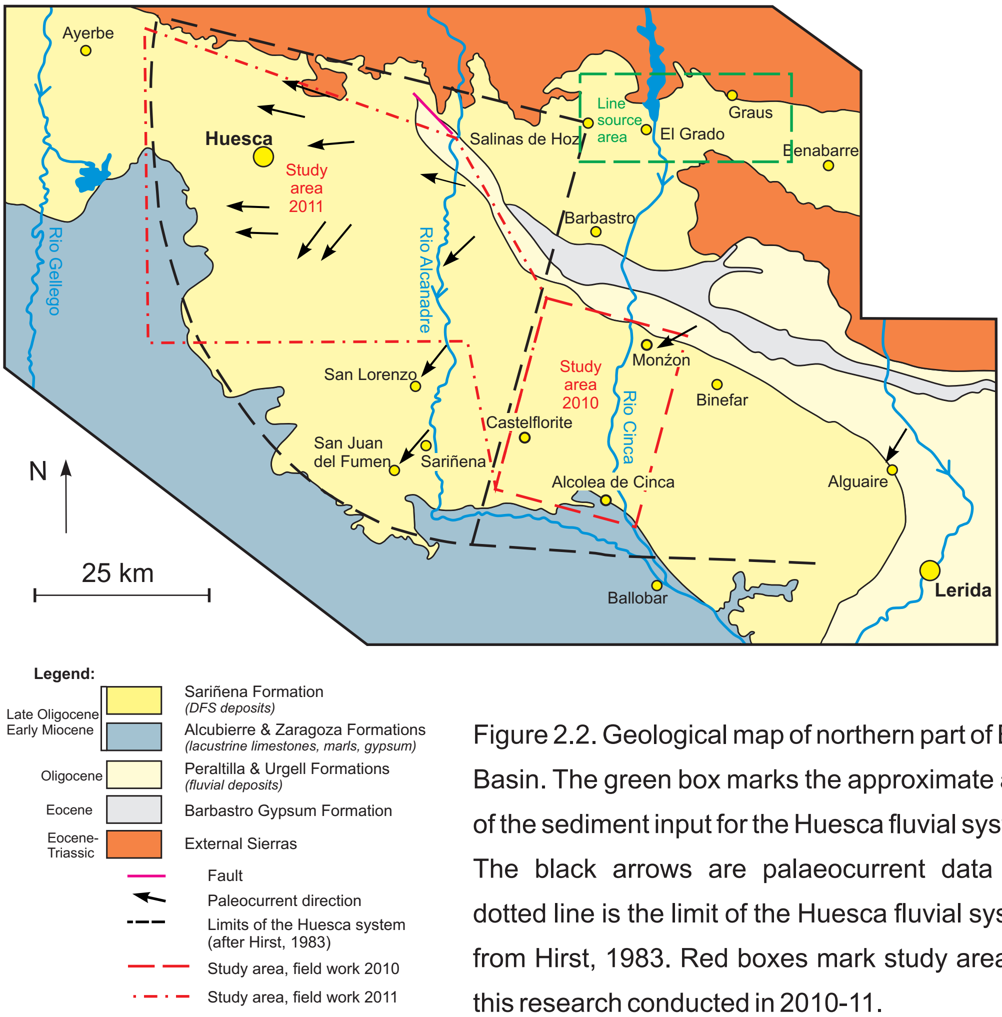

Figure 2.2. Geological map of northern part of Ebro Basin. The green box marks the approximate area of the sediment input for the Huesca fluvial system. The black arrows are palaeocurrent data and dotted line is the limit of the Huesca fluvial system from Hirst, 1983. Red boxes mark study areas of this research conducted in 2010-11.

The fluvial deposits of the Sariñena Formation correspond to late Oligocene - early Miocene tectosedimentary units T3, T4 and T5 (Alonso-Zarza et al., 2002). The ages are based on magentostratiraphic studies, correlation with dated marine analogues at the east of the basin and palynological and mammal biostratigraphic data (Perez-Rivares et al., 2004). Middle Tortonian (13.5 Ma) deposits are the youngest deposits of the Ebro Basin (Evans and Arche, 2002).

2.2.3 Tectonic setting

The late Oligocene – early Miocene sediment influx into the Ebro Basin has previously been related to emplacement of the Guara/Gavarnie/Cotiella-Monsec thrust units and folding and diapirism during the late Oligocene thrusting phases in the Southern Pyrenees (Hirst and Nichols, 1986; Alonso-Zarza et al., 2002; Arenas et al., 2001). Basin fill deposits attain a thickness up to 3 km in the basin centre (Coney et al., 1996) and increases up to 4 km towards the thrust front due to differential subsidence in foreland basin (Riba et al., 1984; Nichols, 1987).

Major tectonic activity in axial zone and southern margin of Pyrenees ceased in Late Oligocene (Teixell, 1998; Fisher and Nichols, 2013). Minor tectonic activity continued in Miocene after the major thrusting phase (Hirst, 1983; Hirst and Nichols, 1986; Alonso-Zarza et al., 2002). This was responsible for formation of Barbastro anticline that affected Huesca deposits exposed close to the southern margin of Pyrenees (Texiell, 1996). A combination of tectonic activity and climate variations is thought to determine the balance between sediment supply and subsidence and control fluvial and lacustrine deposition in the basin (Alonso-Zarza et al., 2002). Due to the post-depositional deformation in the proximal to the apex part of the Huesca DFS succession, this area has not been studied in this project.

2.2.4 Depositional environment

The Huesca fluvial system has been interpreted as a fan-shaped fluvial system characterised by a radius of 60 km, a south/south-western radial palaeocurrent pattern and source, located in structural lows of the thrust front with the most western point near the Salinas de Hoz (Fig. 2.2 and 2.4) (Hirst, 1983; Hirst and Nichols, 1986; Hirst, 1991; Nichols and Hirst, 1996). Statistical analysis of palaeocurrent data showed that source area was to the north from modern basin margin (Jupp et al., 1987; Hirst, 1983, 1991).

The Huesca fluvial system terminated in a shallow (10 – 15 m), low-gradient lacustrine zone in the middle of the Ebro Basin (Arenas and Pardo, 1999; Cabrera et al., 2002). The fan shape with a radial palaeocurrent pattern, the decrease in gradient downstream and evapo-transpiration of water resulted in facies and architecture

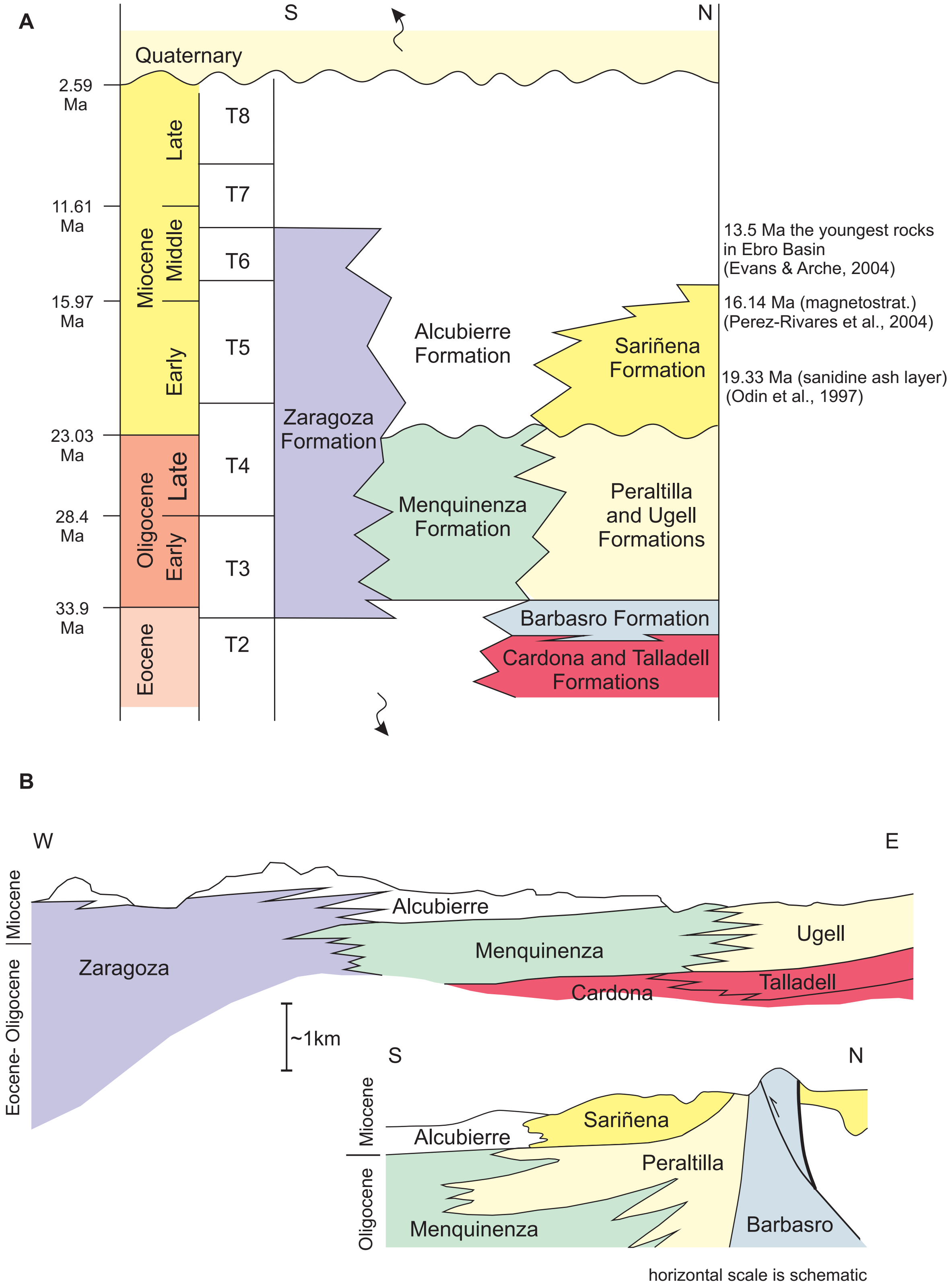

Figure 2.3. Startigraphy of the central Ebro Basin (modified after Hirst, 1983; Alonso-Zaraza et al., 2002; Pérez-Rivaréz et al., 2002). Geologic Time Scale is by Ogg et al., 2008. A – stratigraphic chart showing tectosedimentary units T2 - T8 of Alonso-Zaraza et al. (2002). B – lateral relationships between lithostratigraphic units in cross sections from west to east and north to south across Ebro Basin (modified from Hirst, 1983).

variations downstream across the system (Hirst, 1991; Nichols and Hirst, 1996). All characteristics of the Huesca fluvial system is consistent with the definition of a distributive fluvial system (DFS) (Weissmann et al., 2010; Hartley et al., 2010(a)) and it can therefore be referred as the Huesca DFS.

Ebro Basin was an endorheic aggradational basin during development of the Huesca DFS (Hirst and Nichols, 1986; Nichols, 1987; Fisher and Nichols, 2013). In the Late Miocene (middle Serravalian to middle Tortonian) the Rio Ebro started to drain from the Ebro Basin into the Mediterranean Sea and the area became degradational (Hirst and Nichols, 1986; Garcia-Castellanos et al., 2003; Evans and Arche, 2002).

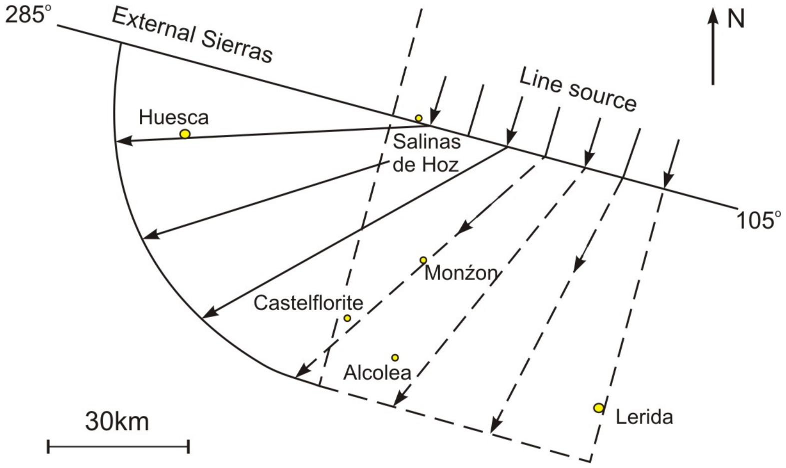

Figure 2.4. Schematic plan view of the Huesca DFS and general paleocurrent directions. (modified from Hirst, 1983).

2.2.5 Palaeoclimatic setting

Although global climate in late Oligocene – early Miocene was relatively constant, regional temperature and precipitation are considered to have been variable (Fig.5 in Hamer, 2007(a), (b)). Studies of palaeosols of the Huesca DFS have shown that the climate in Ebro Basin in Oligocene and Miocene was warm (MAT = 10 - 14^{0}C ± 4^{0}C) and humid (450 - 830 mm/yr ± 200 mm/yr) (Hamer et al., 2007(a)). Evaporation has been interpreted to be higher than the precipitation (Nichols, 1987; Nichols and Hirst, 1998). Plant fragments in palaeosol horizons of the fluvial deposits (Hamer et al., 2007(a)) and in lacustrine carbonates beyond the fluvial system (Cabrera et al., 2002) indicate that the surface of the Huesca DFS was characterized by abundant open woodland vegetation.

2.2.6 Study area

The main study area for this research lies on both sides of Rio Cinca between Monzón and Alcolea de Cinca towns. Supplementary data where also collected from several locations across the DFS (Fig. 2.2). The main study area of this research was not studied in detail during the previous research or was studied with the focus on the specific subjects (cf. Fisher et al. 2007(a)).

2.3 The Salt Wash DFS succession

The Salt Wash fluvial succession is the second example of the DFS deposits studied as part of this research. The Salt Wash succession is exposed in central USA, and is perfect for studies of sandstone body architecture due to easily assessable, large-scale and relatively uninterrupted outcrops.

The deposits of the Salt Wash fluvial system were previously studied with a focus on the uranium-vanadium ores associated with the Salt Wash sandstones (Craig et al., 1955; Mullens and Freeman, 1955; Tyler and Ethridge, 1983). Detailed sedimentological interpretation of Salt Wash depositional setting was provided by Tyler and Ethridge (1983), who focused their work in small study area in the Slick Rock district in Colorado. Peterson (1984) studied the effect of syn-depositional tectonic movements within the basin on sedimentation during development of the Salt Wash fluvial system. Later Peterson (1994) and Turner and Peterson (2004) described Salt Wash deposits in the context of regional palaeostratigraphy, papaeotectonics and palaeogeography. The first studies of sandstone body architecture of the succession with application to reservoir modelling were carried out by Robinson and McCabe (1997) and Kjemperud et al. (2008) for a limited area in the Henry Mountain region in Utah.

2.3.1 Geographical setting

The outcrops of the Salt Wash deposits occupy a large area of Utah and Colorado states of the USA. Additional outcrops are also located in the southern parts of Arizona and New Mexico (Mullens and Freeman, 1957; Tyler and Ethridge, 1983) (Fig. 2.5 and 2.6). Most of the outcrops are located within the Colorado Plateau which is bordered by the Basin and Range region to the south-west and the Rocky Mountains to the north-east (Peterson, 1994). The Colorado Plateau is incised by modern rivers that form canyons and provide outcrops of the fluvial deposits of the Salt Wash DFS.

2.3.2 Stratigraphy

In the regional lithostratigraphy, the fluvial succession belongs to the Salt Wash Member of the Late Jurassic Morrison Formation (Turner and Peterson, 2004) (Fig. 2.7). The Salt Wash Member is underlain conformably by the Tidwell Member, which is thought to overlay the Summerville Formation with a regional unconformity (the J5 unconformity, Pipiringos and O'Sullivan, 1978). Weissmann et al. (2013, in press)

Figure 2.5. Location of the Colorado Plateau and Salt Wash study area (Peterson, 1994). The study area (red filled polygon) is located in Utah and Colorado states of the USA. The red empty polygons indicate the area of Figure 2.6.

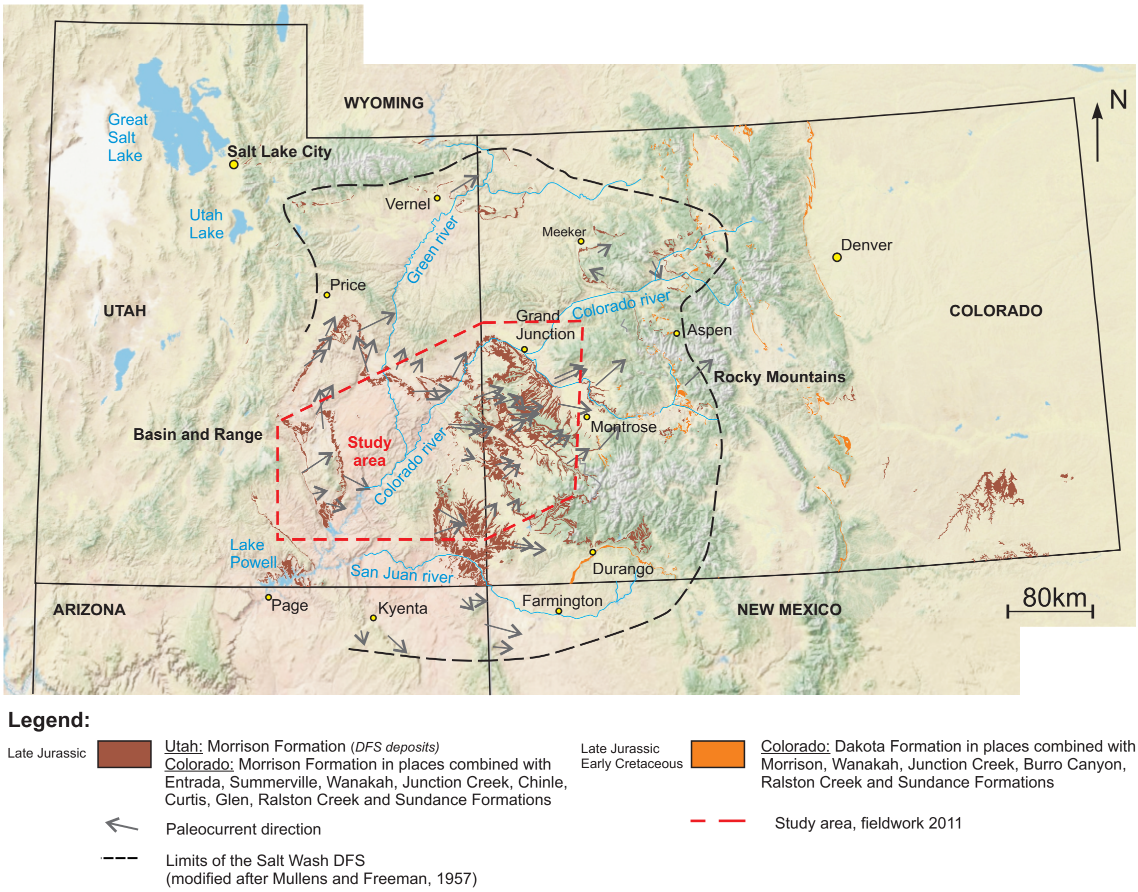

Figure 2.6. Topographic map of Utah and Colorado states of the USA with outcrops of Morrison Formation (dark brown and orange areas). The black arrows indicate palaeocurrent data (Craig et al., 1955) and the dotted line is a limit of the Salt Wash fluvial system (modified after Mullens and Freeman, 1957; Tyler and Ethridge, 1983). Red box marks study area of this research.

showed that Tidwell Formation represents distal deposits of the same fluvial system and Tidwell to Salt Wash transition is a signature of progradation of the fluvial system.

The boundary between the Salt Wash Member and overlaying Brushy Basin Member has previously been observed to occur along a red argillitic calcisol horizon and was considered to be a regional unconformity (Demko et al., 1996; Hatiotis et al., 1997). However, other studies of the Morrison Formation (Peterson, 1988; Kjemperud et al., 2008) suggest that transitions between Tidwell, Salt Wash and Brushy Basin Members are gradual or the members may interfinger.

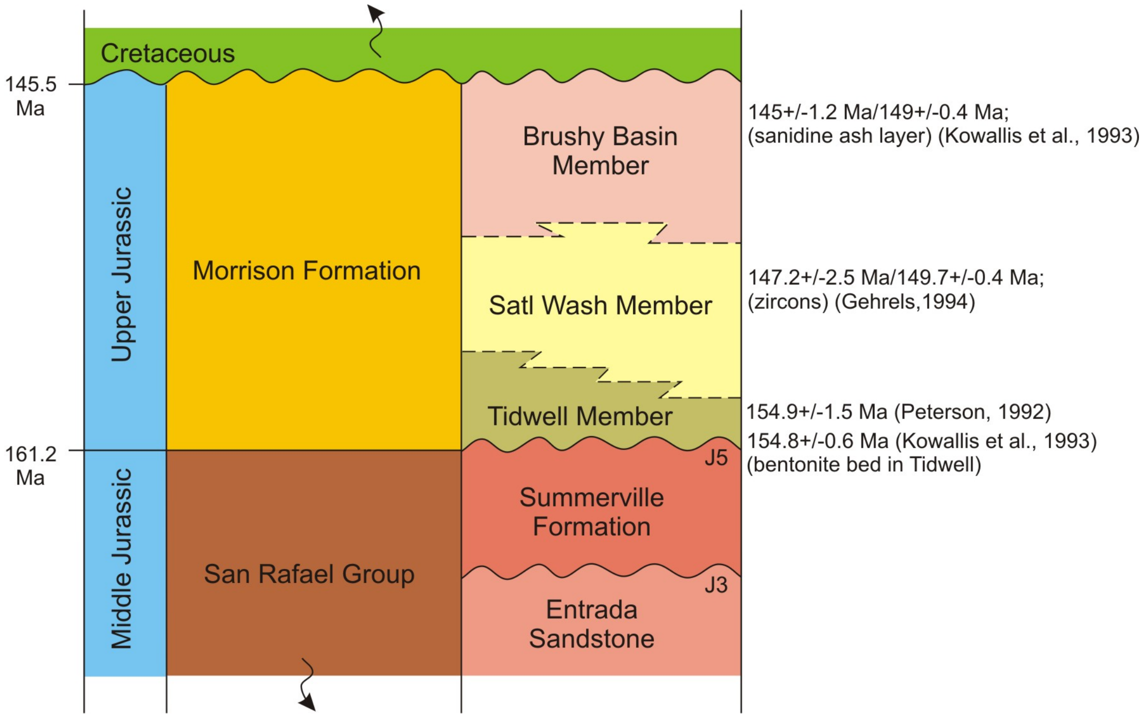

Figure 2.7. Stratigraphy of the Morrison Formation (after Kjemperud et al., 2008). Geologic Time Scale is by Ogg et al., 2008.

Aeolian sandstones, referred to in lithostratigraphic correlations as the Bluff Member of the Morrison Formation in southern Utah or as the Junction Creek Member in western Colorado, have been interpreted as being equivalent to and interfingering with the Salt Wash fluvial deposits (Turner and Peterson, 2004; Demko et al., 2004). In the eastern part of the basin the Salt Wash deposits pass into wetland and lacustrine deposits (Turner and Peterson, 2004) and ultimately onlap onto basement rocks outcropping in the Rocky Mountains (F. Peterson pers. com.). The continental succession of the Morrison Formation is equivalent to coastal marine deposits in Montana, USA and British Colombia, Canada that were formed in the Western Interior Seaway during the Late Jurassic (Turner and Peterson, 2004; Fig. 2.9).

The Kimmeridgian and Tithonian ages (scale of Gradstein et al., 2004; Ogg et al., 2008) for the entire Morrison Formation have been determined by isotopic and palaeontological methods (review in Turner and Peterson, 2004; Currie et al., 2010; Fig. 2.7). According to these ages, the Salt Wash fluvial deposits have been assigned to Middle Kimmeridgian. Palaeomagnetic studies have also been used to determine the age of the sedimentary succession, but produced ambiguous results (Turner and Peterson, 2004; Steiner et al., 1995).

2.3.3 Tectonic setting

The fluvial system transported sediments from the rift shoulders of a graben structure (the Mogollon Slope) into a broad, shallow asymmetric basin (Peterson, 1994). The rift formed in the middle of the continental-margin magmatic arc in the result of oblique subduction of Paleo-Pacific plate under the western margin of the North American continent in the Middle Triassic (Fig. 2.8) (Dickinson, 2001; Bilodeau, 1986, Saleeby & Busby-Spera, 1992; Dubiel, 1994; Busby-Spera, 1988; Dickinson, 2006; R. Blackey http://www2.nau.edu/rcb7/jur145seattle.html). The Western and Eastern Elko Highlands, also referred to as the Sevier Highlands (Peterson, 1988) (Fig. 2.8), formed during Middle Jurassic Elko Orogeny could have been additional sediment source for the Salt Wash fluvial system (Peterson, 1994; Turner and Peterson, 2004). Thrusting (the Luning - Fencemaker thrust system, Fig. 2.8) and back-arc magmatism were suggested to be causes of the uplift at the west margin of the basin (Dickinson, 2006 and reference therein; Currie et al., 2010; Thorman and Peterson, 2004; R. Blackey http://www2.nau.edu/rcb7/jur145seattle.html). Provenance studies of Salt Wash fluvial deposits can be related to some lithologies in the uplifted southern, south-western and western source areas (Peterson, 1994).

Although some authors noted lack of depositional patterns expected in a foreland basin - for example there is no western increase in deposit thickness (Heller et al., 1988; Thorman et al., 1992; Turner and Peterson, 2004) - others have considered the basin to be an “incipient foreland basin” (Robinson and McCabe, 1997; Currie et al., 2010). In contrast, Dickinson (2006) suggested formation of foreland basin occurred after the Jurassic and the Jurassic deposition was thought to occur in a back-arc region.

Local uplifts within the basin occurred during early stages of Salt Wash deposition as indicated by lateral facies distribution and thickness of the succession (Peterson, 1984). However, there is no evidence to suggest that the uplifted areas contributed sediment to the basin (Peterson, 1984, 1988; Turner and Peterson, 2004). Previously structural movements were interpreted to be a result of salt diapirs developing during Summerville and early Salt Wash deposition (Mullens and Freeman, 1957) or/and differential subsidence within the basin (Cadigan, 1967). However, Peterson (1984) stated that they were not related to the Pennsylvanian salt flows but were related to reactivated basement structures during Laramide and younger orogenic events. The

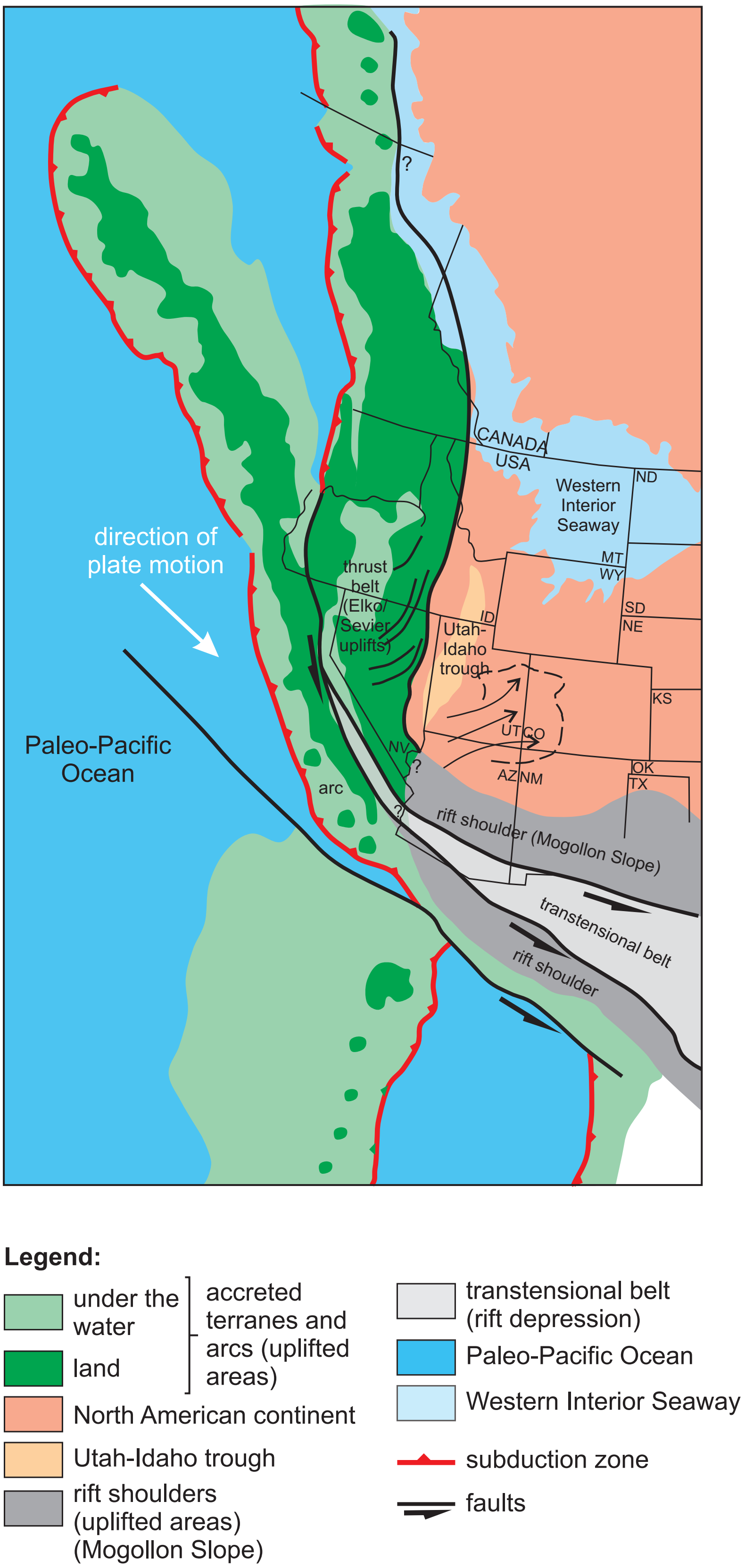

Figure 2.8. Tectonic elements of the western North American continent in Middle Jurassic, modified from Peterson, 1994; Saleeby and Busby-Spera, 1992; Turner and Peterson, 2004; Dickinson, 2006; R. Blackey (http://www2.nau.edu/rcb7/jur145seattle.html).

variation in facies and thickness (0 - 155 m) due to local tectonics adds complexity to the general downstream facies trends.

Post-sedimentary deformation in Late Jurassic, Cretaceous and Cenozoic times was not significant and in general strata are sub-horizontal (dip 0.5^{o} - 2^{o}) although in monoclines in Capitol Reef National Park and Colorado National Monument and at the flanks of Tertiary intrusions in Henry Basin beds dip at 20^{o} or more (Peterson, 1984, 1988). These post-depositional deformations did not significantly affect studied outcrops.

2.3.4 Depositional environment

The Salt Wash fluvial system has been interpreted as aggrading fan-shaped distributary fluvial system with the apex at the south-western margin of the basin (SE Utah and NE Arizona) (Fig. 2.6 and 2.9) (Craig et al., 1955; Mullens and Freeman, 1957). The apical area of the fluvial system in the southwest is now absent due to uplift and erosion prior to the deposition of Cretaceous Dakota Formation. Consequently, it could not be identified more precisely. The radius of the Salt Wash system is estimated to be approximately 200-300 km (Fig. 2.6 and 2.9). The fluvial system was thought to have formed on a nearly flat surface with some irregularities related to local syn-depositional tectonics (Mullens and Freeman, 1957, Peterson, 1984).

Water was thought to be transported into the basin by surface and ground water streams through Paleozoic and Lower Mesozoic aquifers (Sanford, 1994; Turner and Peterson, 2004). The streams on the surface of the fluvial system were determined to be mostly intermittent and rarely perennial (Turner and Peterson, 2004). Ground water travelled through aquifers and fed wetlands and lakes in low areas of eastern part of the basin where Salt Wash fluvial system terminated (Fig. 2.9). The wetlands were interpreted to be hydrologically open (Turner and Peterson, 2004) due to lack of evaporates (Carrol and Bohacs, 1999).

The fluvial complex has previously been characterised as vertically and laterally amalgamated channel-fill sandstones forming sheet-like sandstone bodies with a small proportion of floodplain deposits (Craig et al., 1995; Mullens and Freeman, 1957; Tyler and Ethridge, 1983; Robinson and McCabe, 1998; Kjemperud et al., 2008). In addition, these authors have demonstrated that the Salt Wash deposits show downstream SW-NE trends, such as a decrease in grain size, a decrease in sandstone-mudstone ratio, a change from fluvial to wetland/lacustrine facies and a change in channel planform from braided to meandering. The characteristics of the Salt Wash fluvial system are therefore consistent with the definition of a DFS (Weissmann et al., 2010; Hartley et al., 2010(a)) and the fluvial system is referred to as Salt Wash DFS in the text hereafter.

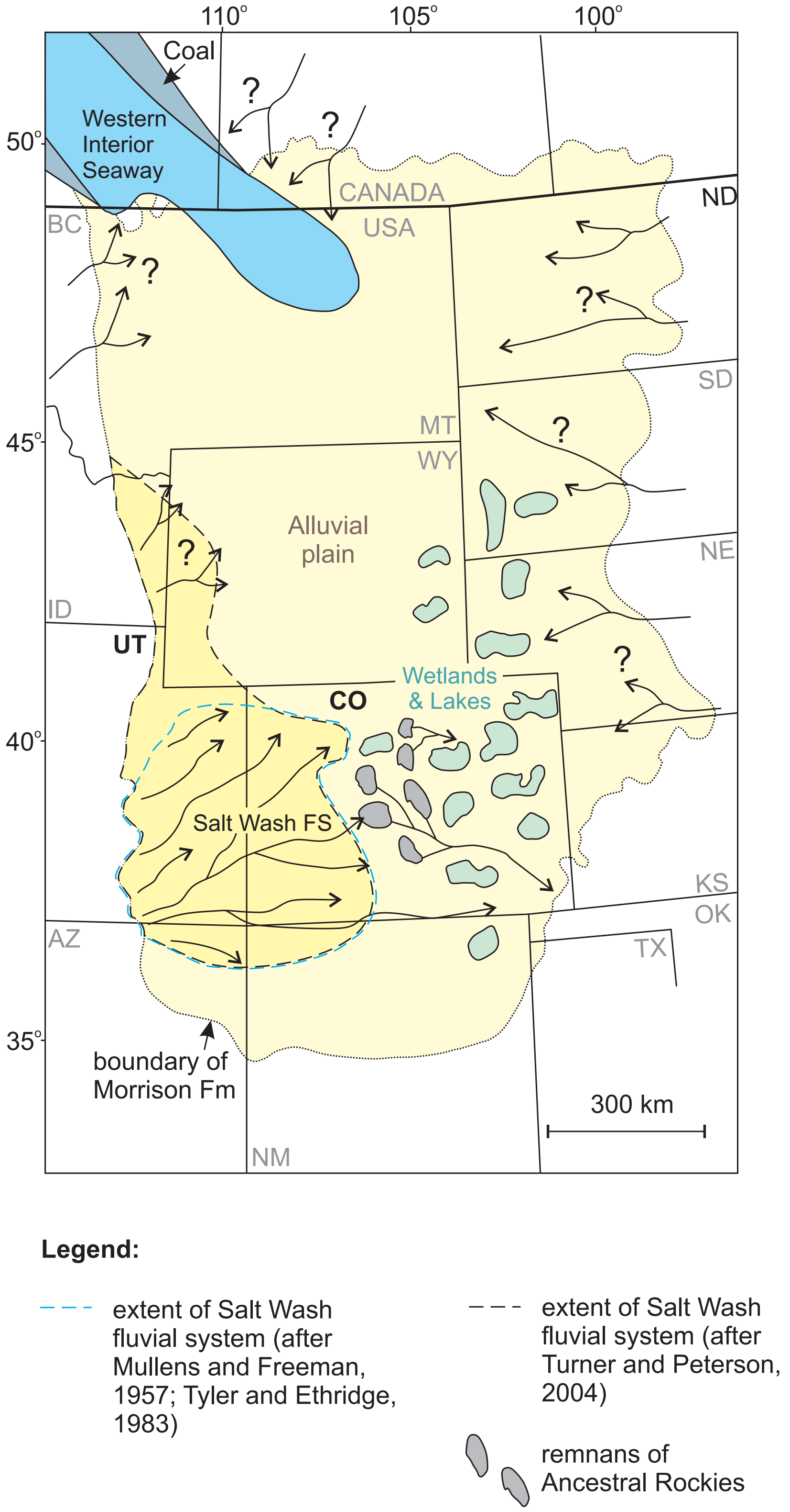

Figure 2.9. Palaeogeographic map of Middle Kimmeridgian (modified from Turner and Peterson, 2004).

2.3.5 Palaeoclimatic setting

The climate in the depositional basin during the Late Jurassic has been determined to be warm and dry on the basis of palaeomagnetic reconstructions, palaeontological data, geological evidence and climate modelling. It is generally accepted that the Salt Wash depositional basin was at approximately 30 - 35° N palaeolatitude and was moving northward (Robinson and McCabe, 1997; Parrish and Peterson, 1988), although other higher palaeolatitudes have also been suggested (e.g. Van Fossen and Kent, 1992; Steiner and Helsley, 1975). The palaeolatitude suggests that the climate in the basin in Late Jurassic was warmer than today (Turner and Peterson, 2004). Globally a CO_2 content four times higher than today has been proposed by (Ekart et al., 1999). When these values are used in climate modelling, they indicated high mean winter and summer temperatures of 20° and 40 – 45° C, respectively, and evaporation rates higher than precipitation rate (< 500 mm) (Moore et al., 1992). Modelling with modern-day CO_2 concentration showed lower winter and summer temperatures, 8° and 24-28° C, respectively (Valdes and Sellwood, 1992).

The occurrence of evaporites (gypsum in Tidwell Member), lacustrine carbonates, aeolian deposits and red palaeosols and palaeontological data (Cheirolepids) indicate a semi-arid, warm and dry climate (Robinson and McCabe, 1997; Turner and Peterson, 2004). Although seasonality in basin temperature and precipitation was inferred from studies of fresh water lacustrine unionid bivalves from Brushy Basin Member (Good, 2004), it is not thought that the climate changed significantly during the Late Jurassic (Parrish et al., 2004). Evaporation rate has been interpreted to be high (Demko et al., 2004; Turner and Peterson, 2004). Overall the area of deposition has been interpreted to resemble a savannah (Parrish et al., 2004).

The possibility of different climates within the catchment and depositional areas of the basin (Davidson and North, 2009) could explain the availability of water and formation of large river system in a dry depositional basin. Surface and ground waters are thought to have entered the basin from the western and south-western uplifted drainage areas fed by precipitation of moisture carried from Paleo-Pacific Ocean by easterly winds (Turner and Peterson, 2004, Fig. 2.9).

2.3.6 Study area

During this study the deposits of the Salt Wash DFS were investigated in five outcrops located in the Four Corners area of the Colorado Plato, in south-eastern Utah and south-western Colorado, USA (Fig. 2.6).

Outcrop locations, fieldwork techniques and data processing methodologies for the Huesca and Salt Wash DFS successions are discussed in the following chapter.

3. Field work techniques and data processing methodology

3.1 Introduction

Outcrops of the Huesca and Salt Wash DFS successions are well suited for architecture studies in terms of their excellent exposure and accessibility across the entire DFSs. This has made it possible to conduct a detailed study of fluvial sandstone body architecture. Standard fieldwork techniques were used to document outcrops of both successions including sedimentary logging, outcrop mapping, outcrop photo panels and sample collection. In addition, gamma ray logs were recorded to provide a link between the sandstone body architecture and subsurface data (Appendix 7). Sedimentary logs (Appendix 2), data measured from outcrops (chapters 4 to 7) and outcrop photo mosaics (Appendix 5) were used to analyse facies and architecture of the DFS deposits. Rock samples were processed with standard methods to determine composition, grain size and sorting of DFS sandstones (Appendix 3). The shortcomings and limitations of the obtained data were assessed.

3.2 Outcrop locations and quality of exposures

The location of the apex, the extent of the DFS and the radial paleocurrent pattern have been previously suggested for the Huesca DFS by Hirst (1983) and Jupp et al. (1987) and for the Salt Wash DFS by Craig et al. (1955), Mullens and Freeman (1957) and Tyler and Ethridge (1983) (Fig. 2.2 and 2.6). For the architecture analysis three outcrops were chosen in each study area during reconnaissance studies. The outcrops represent relatively proximal, medial and distal parts of the Huesca and Salt Wash DFSs (Appendix 5, Fig 3.6).

3.2.1 The Huesca DFS succession

The area of the investigation is located in the poorly documented eastern part of the Huesca DFS along the Rio Cinca (Fig. 3.1), where sandstone body architecture could be observed in outcrops of 1 - 2.5 km long. Three outcrops near Monźon, Castelflorite and Alcolea de Cinca towns were documented in proximal to distal transect during fieldwork in spring of 2010 (Fig. 3.1 and 3.2):

- Monźon outcrop (UTM WGS-84: 31T zone, 267055E/4642825N);
- Castelflorite outcrop (UTM WGS-84: 30T zone, 748852E/4633034N);
- Alcolea outcrop (UTM WGS-84: 31T zone, 261714E/4619921N).

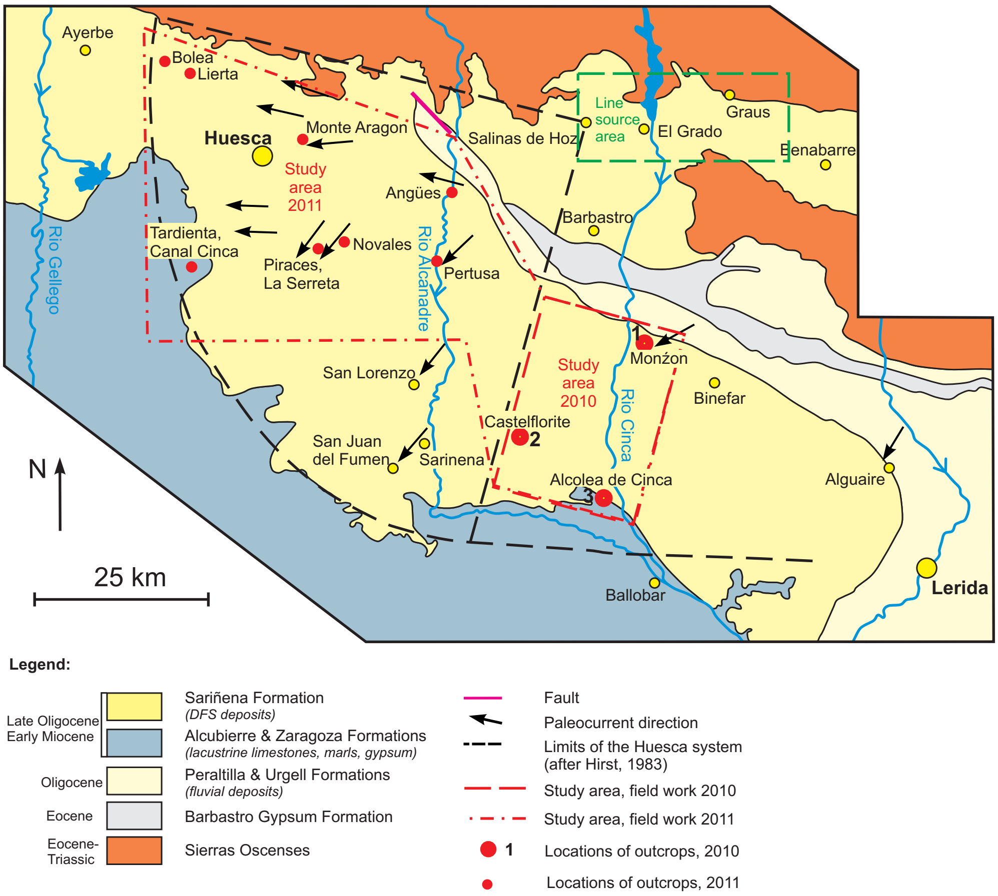

Figure 3.1. Geological map of the northern part of the Ebro Basin. Red boxes and dots mark study areas and outcrop locations studied during fieldwork in 2010 and 2011. Large red dots indicate main large-scale outcrops studied in 2010, smaller red dots show location of sedimentary logs recorded in floodplain deposits in 2011.

Figure 3.2. Google Earth images of the three studied outcrops near Monźon, Castelflorite and Alcolea towns (from left to right). Outcrop cliff surfaces are marked by white lines.

The distance between studied locations along the radius of the Huesca DFS is approximately 15 km between Monźon and Castelflorite outcrops and about 5 km between Castelflorite and Alcolea outcrops (Fig. 3.3).

Outcrop correlation

The absence of regional markers makes correlation of the outcrops difficult. Deformation of the studied Huesca DFS deposits after their deposition was considered insignificant with regional dip between 0.5 and 2.5 degrees towards south/south-west (Hirst, 1983). The relative ages of the outcrops could be demonstrated by comparison of outcrop elevations considering general south/south-western dip (Fig. 3.3).

The elevation comparison revealed that Huesca DFS deposits exposed in the Castelflorite outcrop could be considered contemporaneous with the deposits of the Alcolea outcrop, whereas the Monźon outcrop exposes relatively older deposits. Inaccuracy of the altitude measurements with hand-held GPS has been frequently emphasised in literature especially when measuring near outcrop cliffs (McCaffrey et al., 2005; Pringle et al., 2006) and could have affected the results. In addition, Coney et al., (1992) emphasised that the uplift history of the DFS source area in the post late Miocene period is not constrained. Thus, elevation difference should be used with caution. Although outcrops could not be correlated with confidence, it is believed that they represent relatively proximal, medial and distal part of the system because no evidence has been found for significant progradation or retrogradation of the DFS (Fisher and Nichols, 2013).

Complimentary studies

Fine-grained floodplain deposits were the subject of specific study of avulsion deposits during fieldwork in summer of 2011. For this study 32 detailed stratigraphic logs of fine-grained overbank deposit intervals were recorded in 10 locations across the northern part of the Ebro Basin (Fig. 3.1 and Appendix 1) including locations at Monźon, Castelflorite, Pertusa, intersection of Rio Alcanadre and road A22 (near Angües), Piracés, Monte Aragón, Novales, Bolea and Lierta (log examples are presented in Appendices 2.13-18). Log intervals were chosen between two major channel sandstone bodies to represent floodplain deposit accumulated between periods when the channel occupied this particular location.

Exposure quality

Protruding sandstone bodies are easily distinguished from overbank fine-grain deposits on the exposure surface. Due to high proportion of fine-grained deposits preserved in the succession almost every sandstone body could be accessed on the outcrop slope.

The quality of the exposure decreases with distance from the DFS apical area due to an increase in proportion of fine-grained deposits. In general, the poorly consolidated fluvial deposits are highly weathered and sedimentary structures are mostly not visible.

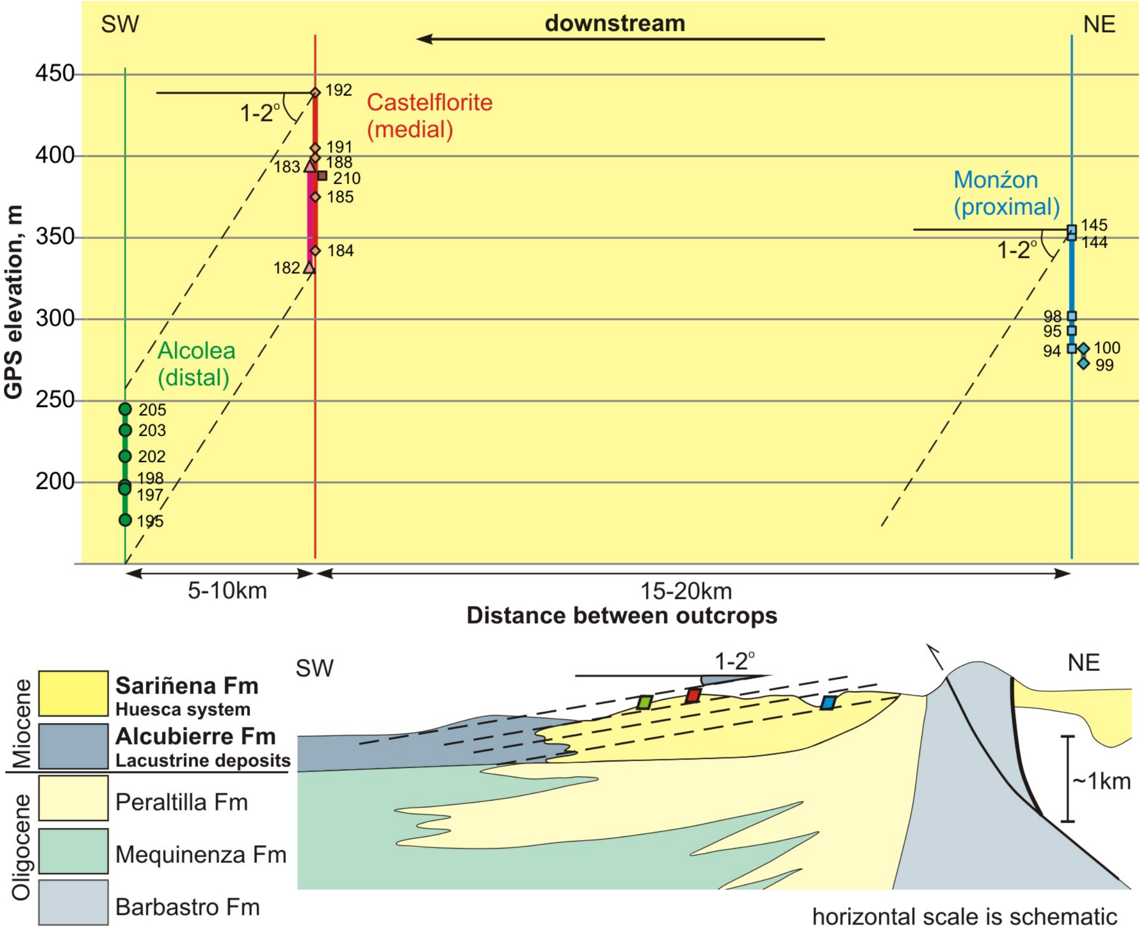

Figure. 3.3. Correlation of the outcrops based on their GPS elevation (top). Waypoints are shown along the sedimentary logs. Schematic geological cross section from NE to SW (bottom) (modified from Hirst, 1983). See stratigraphic logs used for the correlation in Appendix 2.

3.2.2 The Salt Wash succession

The Salt Wash DFS succession was studied in the same way as the Huesca DFS succession. Three outcrops were chosen in proximal to distal transect downstream the DFS (Fig. 3.4 and 3.5):

- Bullfrog outcrop (UTM WGS-84: 12S zone, 532989E/4224426N);
- Slick Rock outcrop (UTM WGS-84: 12S zone, 706540E/4321660N);
- Little Park outcrop (UTM WGS-84: 12S zone, 680562E/4208848N);

The distances between the Bullfrog, Slick Rock and Little Park outcrops along the DFS radius are approximately 120 km and 70 km, respectively. The length of the studied outcrop is similar to the length of the Huesca outcrops (0.5 – 2 km). Note that relatively

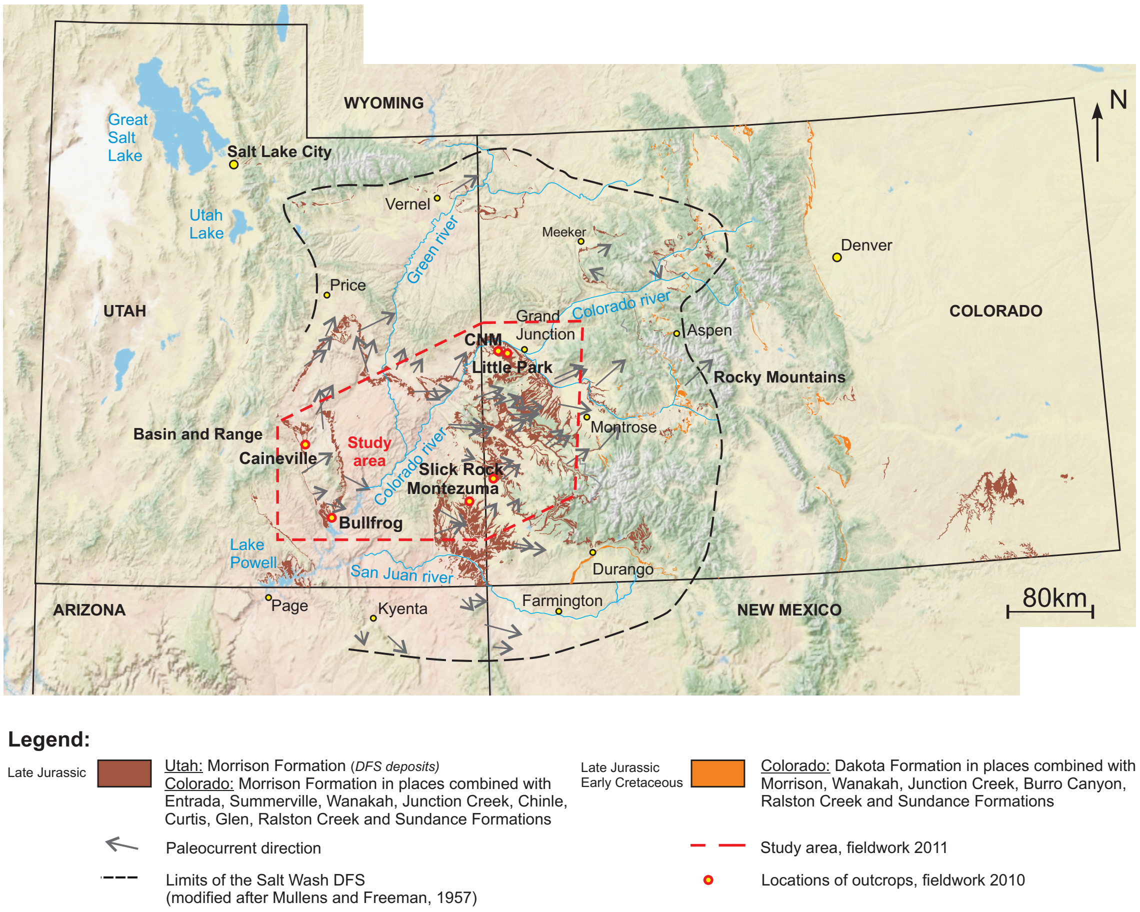

Figure 3.4. Topographic map of Utah and Colorado states of the USA with outcrops of the Morrison Formation. Black arrows indicate paleocurrent data (Craig et al., 1955) and the dotted line is a limit of the Salt Wash DFS (modified after Mulllens and Freeman, 1957; Tyler and Ethridge, 1983). The red box and red dots show the study area and outcrop locations.

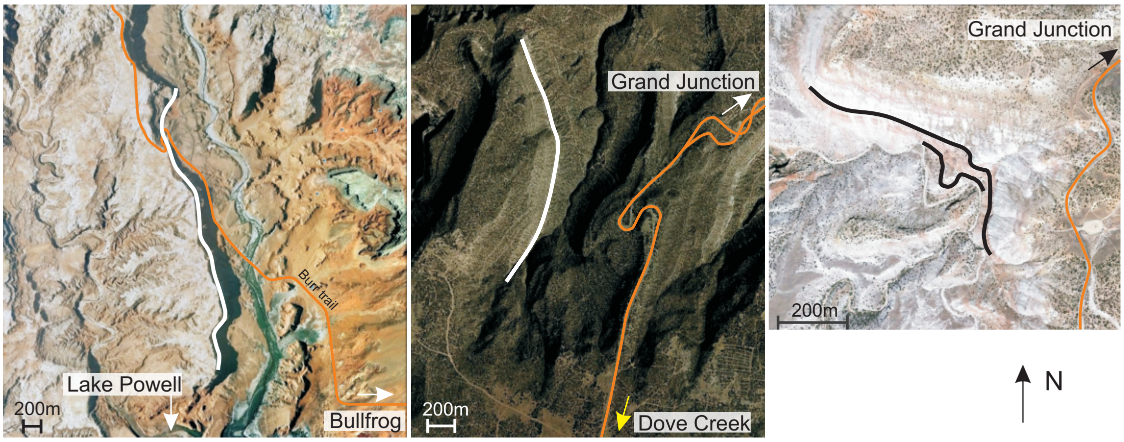

Figure 3.5. Google Earth images of the three studied outcrops, Bullfrog, Slick Rock, Little Park (from left to right). Outcrop cliff surfaces are marked by white lines. Orange lines mark the closest roads.

proximal Monźon outcrop of the Huesca DFS succession is relatively further away from the apex than the Bullfrog outcrop of the Salt Wash DFS succession (Fig. 3.1 and 3.4).

Outcrop correlation

As for the Huesca DFS succession, there are no well-studied, correlated regional markers in the Salt Wash succession. The Salt Wash deposits in the Bullfrog and Slick Rock outcrops are dipping at no more than 2^0. The deposits in the Little Park outcrop are dipping at approx. 10^0 towards north-east. Although in general the dip of the strata in the studied area does not exceed 0.5^0 – 2^0, regional tectonics of the area involved folding and uplift of some areas in the basin creating dip angles that are locally up to 20^o (Peterson, 1984). Consequently, correlation of the Salt Wash DFS outcrops is uncertain. However, underlying Tidwell Member and Summerville Formation and overlying Brushy Basin Member and Cretaceous Formation could be confidently used to constrain the position of the Salt Wash DFS succession in outcrops (Fig. 2.7). Thus it is possible to be confident that the studied outcrops represent relatively proximal, medial and distal system successions.

Complimentary studies

Complementary data were collected in Caineville (relatively proximal), Montezuma (medial) and Colorado National Monument (distal) outcrops (Fig. 3.4 and Appendix 1). Collected data where used for the analysis of facies and characteristics of the Salt Wash sandstones.

Exposure quality

Exposure of Salt Wash sandstones is better than the exposure in Spain and structures are easy to recognise. However, the high degree of sandstone body amalgamation in the proximal and medial outcrops makes observation of dimensions, type and shape of individual sandstone bodies difficult. Steep, vertical cliffs formed by thick sandstone bodies in the succession restrict outcrop access in some areas and where only photo panels were used.

3.3 Outcrop documentation

Large-scale outcrops of both DFS successions were studied using the same methodology. The six outcrops were photographed to create photo mosaics. The main features of different sandstone body types and the architecture of the succession were documented during the fieldwork. Recorded data were further processed and analysed in the office using Hugin software for photograph stitching and Corel Draw software for architecture interpretation. Photo mosaics and interpretation panels were also subsequently used to document the sandstone body characteristics and their architecture. Outcrop panels are presented in the Appendix 5.

Two or three sedimentary logs were recorded in 1:100 scale for every outcrop for the purposes of facies analysis and scaling of the photo mosaics. Sedimentary logs were converted into text table form and processed in SedLog and Corel Draw software. Rock samples were collected from a range of facies and sandstone body types along one of the sedimentary logs in each of the outcrops. The recorded sedimentary logs showing the sample locations are presented in the Appendix 2.

Figure 3.6 shows maps of outcrop outlines with GPS point and sedimentary log locations. Outcrops are divided into sections representing the positions of the studied photo panels as they are presented in the Appendix 5. Paleocurrent rose diagrams shown on the Figure 3.6 are constructed based on measurements of dip directions in trough cross-bedding of the Huesca and Salt Wash sandstones which were collected during the fieldwork. The outcrops have been chosen so that they are, where possible, at the sharp angle to the paleocurrent direction.

3.3.1 Use of photo mosaics

The use of photo mosaics for architecture studies is argued in literature. Although this method has several disadvantages it was chosen for these studies because of the low cost, fast acquisition time, fast processing and sufficient accuracy (~ 0.2 m) (McCaffrey et al., 2005; Pringle et al., 2006). The main drawbacks emphasised in the published literature are a distortion due to the photo not being parallel to the outcrop plane and distortions at the image edges (Wizevich, 1993; Bridge, 2003; Pringle et al., 2006). Recommendations given by the authors to reduce these distortions were taken into account, where possible, when collecting the data. The distortions of images were minimized by taking photos from similar distance along an outcrop and, where possible, from a point elevated in front of the outcrop. Sufficient overlap of one photo to another (50 %) was applied to reduce edge distortion.

Nevertheless most of the photos have significant distortion due to the inclined outcrop plane (upper part is further from the location of photographer than lower part) and lateral irregularities. This problem was overcome by recording detailed sedimentary logs and by measuring actual sandstone body thicknesses during outcrop mapping. The logs and measurements were used to specify the scale of the outcrop areas which appear distorted (Appendix 5).

Comparison of bed thicknesses from the outcrop photo and sedimentary logs in the same scale shows variation in difference between thicknesses across the outcrop panel without any particular trends. The range of difference is between 6 and 12 %.

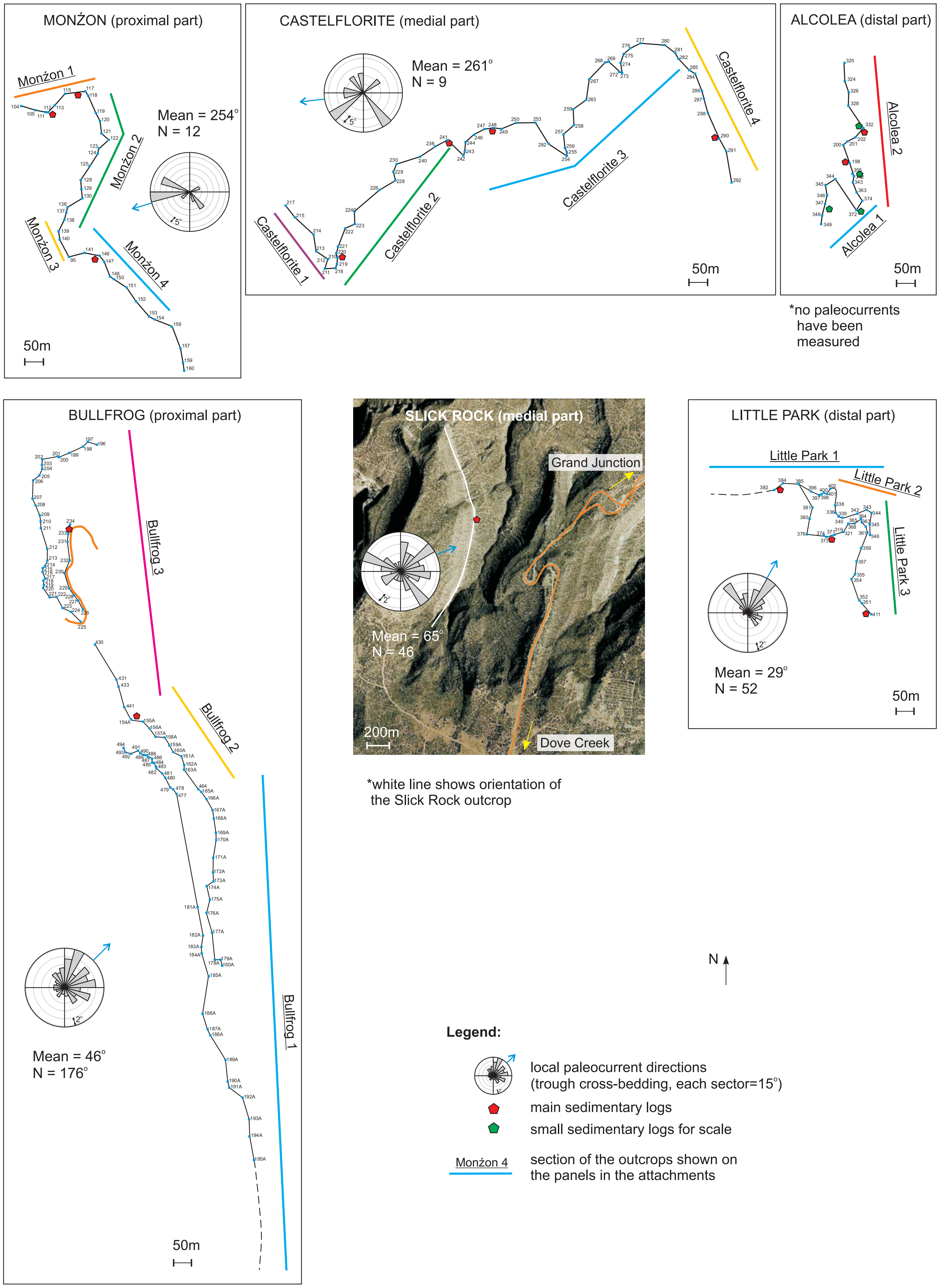

Figure 3.6. GPS waypoint maps along studied outcrops of the Huesca DFS succession (Monźon, Castelflorite and Alcolea) and the Salt Wash DFS succession (Bullfrog, Slick Rock and Little Park). There is no suitable cross bedding to measure paleocurrents at the Alcolea outcrop. GPS map was not created for the Slick Rock outcrop and its orientation relative to the palaeocurrent directions is shown on the satellite Google Earth image. Coloured sections indicate sections of the outcrops representing interpretation panels in the Appendix 5. The list of GPS points is presented in the Appendix 1.

Main causes of this inaccuracy are distortion of the photo images themselves, distortion as a result of mosaic stitching or inaccurate positioning of sedimentary logs on the outcrop photo.

An alternative method of outcrop data acquisition is very accurate laser scanning or ground-based LIDAR (5 mm resolution). LIDAR data processing and visualisation, however, is time consuming and requires powerful computers (Pringle et al., 2006). The authors of the paper also emphasised that interpretation of outcrop photo mosaics would be satisfactory for the purposes of metre scale resolution studies. Thus, the error of 6 – 12 % in thickness differences is considered to be acceptable for the metre scale studies of this research.

3.3.2 Measurements of sandstone body dimensions

Width measurements of sandstone bodies were taken from outcrop sections that are perpendicular or only slightly oblique to the average paleocurrent at the particular location of a DFS. Width measurements represent actual width or minimum width limited by outcrop exposure length or quality. In contrast, thickness was measured in the thickest parts of sandstone bodies and therefore represents maximum thickness.

3.3.3 Estimation of facies and sandstone body proportions

The proportions of facies and sandstone bodies were calculated from thicknesses recorded in 1D stratigraphic logs. To reduce effect of lateral variations in facies distribution and proportion two or three logs for each outcrop have been used and results were averaged between logs (except Alcolea and Slick Rock outcrops where only one log was recorded). Separately interpreted 2D photo panels were used to calculate 2D percentage of sandstone bodies and their types by pixel counting in Corel Photo-Paint software. Large covered areas were cut out from interpreted outcrop image to minimise the effect of variable exposure quality. Percentage of number of pixels which belongs to particular sandstone body type was found out of a number of pixels in whole image of the outcrop. In the process of the interpretation of the photo panels, it was not always possible to resolve all sandstone bodies, small and thin ones in particular, that together with exposure quality could have affected the estimates of the proportions.

3.4 Sample processing

Samples were collected from sandstone bodies of different facies and types and rarer from fine-grained overbank deposits (Appendix 2). A selection of these samples was used to conduct grain size and petrographical analyses that are summarised Appendix 3 Table 1.

3.4.1 Grain size

Grain size was estimated in the field visually and in the laboratory by sieving of poorly consolidated sandstones. Eighteen Huesca sandstones and twenty-two Salt Wash samples were sieved using standard phi sieves and weighed to obtain the percentage of each grain size fraction (Appendix 3 Table 2). Samples of 100 to 380 grams were used for sieving analysis, which is considered to be more than sufficient for this type of grain size analysis (50 - 100 g is suggested by Pettijohn et al., 1987). Histograms and cumulative frequency curves were used to estimate maximum, minimum and mean grain size and sorting. The latter was calculated using the graphical formula from Folk and Ward (1957):

$S = (\phi 84 - \phi 16)/4 + (\phi 95 - \phi 5)/6.6$

where $\phi 84$, $\phi 16$, $\phi 95$, $\phi 5$ – grain size (phi) percentiles taken from the cumulative frequency curves for each sample (Fig. 6.3, 7.2 and Appendix 3 Table 2).

3.4.2 Thin sections and petrographic analyses

Twenty-one thin sections were cut from rock samples selected to represent all facies and grain sizes of each DFS succession (Appendix 3 Table 1). Samples were impregnated with blue resin before cutting which made it possible to estimate porosity of the sandstones. The thin section photographs were processed with pixel counting in Corel Photo-Paint software to determine two-dimensional estimate of porosity (Appendix 3 Table 8).

Only visual analysis of Salt Wash samples in thin sections has been conducted, while point counting, XRD and heavy mineral separation have been carried out for the Huesca samples. For each of selected fifteen thin sections from the Huesca DFS succession 300 points were counted with 0.25 mm vertical and horizontal lag. Counting of 200-500 points were considered sufficient for estimation of percentage of grains which comprise more than 1% of the sample (Pettijohn et al., 1987). The lag between counted points was chosen according to the average grain size of sandstones, which was 0.25 mm (fine/medium).

3.4.3 X-ray diffraction

X-ray diffraction was conducted for the Huesca samples on the diffractometer “Philips PW 1830”, and obtained data were processed using TRACES 6.7.25 software to support visual analysis of the main mineral constituents of the Huesca sandstone samples. In addition Rietveld modelling was applied to determine an approximate percentage of main minerals (Appendix 3 Table 5) (Dr. D. Alderton pers.com., Rietveld, 1969; Young, 1993).

3.4.4 Carbonate and heavy mineral concentrations

Eight samples of the Huesca sandstones were subjected to acetic acid dissolution as they were prepared for standard heavy mineral separation (using SPT heavy liquid). The dissolution allowed determination of carbonate concentration in the sandstones (Appendix 3 Table 6). The heavy mineral separation and slides are done for four of the samples (Appendix 3 Tables 1 and 7). Visual recognition of heavy minerals have been conducted.

3.5 Gamma ray measurements

In addition to sedimentological data, the concentration of Potassium (%), Thorium (ppm), Uranium (ppm) (spectral GR) and total gamma radioactivity (total GR) were measured with gamma ray spectrometer (Bismuth germanate scintillation crystal detector) (Fig. 3.7).

Figure 3.7. Gamma ray spectrometer with Bismuth Germanate Scintillation Crystal Detector, GF Instruments (photo is taken from GF Instruments website: http://www.gfinstruments.cz).

Measurements were conducted, where possible, according to the requirements and procedure described by Myers and Wignall (1987) and with some assumptions:

- Studied rocks are Miocene age that satisfies requirement of the radioactive equilibrium for Uranium (older than 1 Ma).
- Moisture content is assumed constant.
- Spectrometer was hold for 3 - 4 minutes (4 - 10 min, provide ± 10 % precision (Myers and Wignall, 1987), while 3 - 4 minutes would give less precision).

- Two other criteria, a low degree of weathering and an availability of a three-metre square area for measurements could not always be maintained.

The spectrometer was located against a side or on top of a chosen bed (Fig. 3.8) along some of the recorded sedimentary logs for all of the outcrops (Appendix 7). Beds were chosen according to the variation of lithology and facies along the succession. One to three measurements for a bed were taken depending on the thickness of the bed.

The effective volume of the spectrometer measurement is defined as a volume with 80 cm radius, 14 cm depth and 49 kg mass (Lovborg, 1971) (Fig. 3.8). Therefore, measurements in a cliff section would give an averaged signal from several vertically stacked thin beds (less than 80 cm beds). The main sandstones bodies, the amalgamated complexes or heterolithic overbank packages, however, are thicker than 80 cm and therefore, give clear measurement.

Although bed surfaces were cleaned from a mud-wash layer before applying the spectrometer, some measurements could be affected by the mud and should be used with caution. Mud layers on the cliff surfaces may be leached and this will affect the measurements of Potassium (Hampson et al., 2005) and Uranium (Levinson and Coetzee, 1978; Myers and Widnall, 1987) concentrations. Unfortunately, gamma ray data could not be interpreted in the time frames of this project and the GR curves and preliminary results are presented in the Appendix 7.

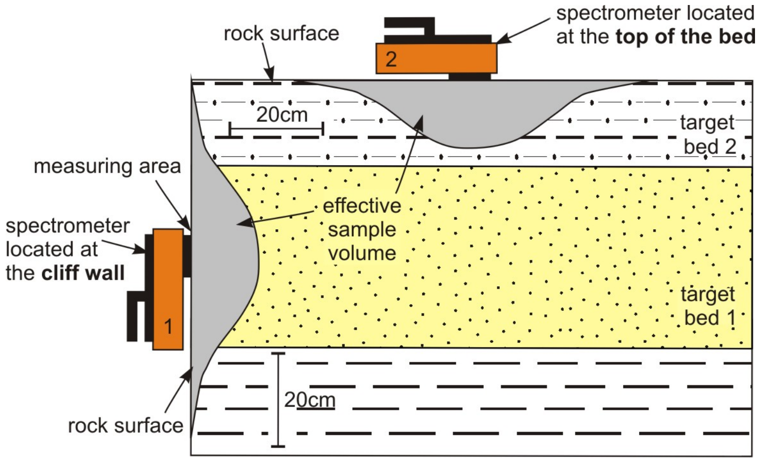

Figure 3.8. Placing of gamma ray spectrometer during field measurements 1) against the cliff surface and 2) on the top of a bed (modified from Mayers and Wignall, 1987). The grey area demonstrates effective sample volume.

The data collected and processed in the field and lab will be described and interpreted in the following chapters. The methodology of statistical analysis of the recorded successions and 2D geometrical modelling of DFS architecture are described in the relevant chapters 10 and 12.

4. Facies analysis

4.1. Introduction

Facies classification is based on the analysis of lithology, sedimentary structures, shape and dimensions of sedimentary bodies recorded in the field and can be interpreted in terms of characteristic depositional processes (Anderton, 1985) occurring during the formation of a DFS.

A combination of data from recorded logs (Appendix 2), outcrop panels (Appendix 5) and field measurements for the Huesca and Salt Wash DFS successions was used for the facies analysis. Thickness ranges given in the text are sometimes different from ones presented on the sedimentary logs because they may include data from other locations.

Fourteen facies have been distinguished according to their sedimentological characteristics and relationships between each other. In general the facies were interpreted to have formed in fluvial and lacustrine depositional environments. Three main depositional settings have been recognised, namely deposition by channelised flow, by unconfined flow and deposition in standing body of water. The facies have been grouped into six facies associations including channel macroforms, lateral accretion complexes, isolated channel fill, proximal overbank splay, distal overbank splay and lacustrine. The facies and their relationships are described and interpreted in the following sections, and have been summarised in Table 4.1 and are shown on sedimentary logs in Appendix 2.

4.2. Facies description and interpretation

The coding system used for each facies is as followers: The first letter of each facies code is assigned as either S (sandstone/conglomerate), H (heterolithic interbedding of sandstone, siltstone and mudstone) or L (limestone). Small letters, which follow, indicate sedimentary structures or other distinctive characteristics such as shape, relative dimensions or lithology. The facies described below were observed in both studied successions unless otherwise stated.

4.2.1. Sandstone breccia (Sb)

Description

Facies Sb occurs as 15 - 30 cm thick continuous beds of breccia composed of laminated angular sandstone fragments of different sizes (2 – 20 mm) enclosed in fine- to medium-grained sand matrix (Fig. 4.1). Upper and top boundaries are irregular.

				Huesca			Salt Wash		
Code	**Name of facies**	**Facies Description**	**Process interpretation**	**Monzon**	**Castel-florite**	**Alcolea**	**Bullfrog**	**Slick Rock**	**Little Park**
Sb	**Sandstone breccia**	Angular fragments (2-20 mm) of laminated sandstone with sand-size matrix. Bed is 15-30 cm bed with irregular base and sharp top.	Collapse of lithified sandy channel banks triggered by erosion of the banks by a subsequent channel flow.				▨		
Slc	**Sandstone with large-scale cross-bedding**	Coarse- to medium-grained sandstone wih large-scale cross-bedding. Cross sets are 1-3.5 thick. Width of the lenses exceeds 20 m. Cross beds are irregular or concave up and become subparallel to the the base. Mudclasts are common. Bases and tops are erosional.	Downstream or oblique accretion of the large-scale bedforms.	▨			▨		▨
St	**Conglomerate and sandstone with medium and small-scale trough cross-bedding**	Conglomerate and very coarse- to fine-grained sandstone with medium and small scale trough cross-bedding. Cross sets thickness is 0.1-1.2 m, sometimes decreases upwards to 0.8-0.1 m. Width of lenses varies from 7 m to greater than 300 m. Granules, small pebbles (up to 3 cm) and mudclasts are clustered at the toesets of cross beds. Occasionally show folding and bioturbation. Base and tops are erosional.	Migration of curved-crested dunes on the channel floor. Recumbent folds indicate rapid deposition and transitional to the upper plane bed flow regime.	▨	▨	▨	▨	▨	▨
Sh	**Sandstone with horizontal or low-angle bedding**	Coarse- to fine-grained sandstone with apparent horizontal or low-angle bedding forming lenses of 0.3-2 m in thickness and 7 to more than 300 m width. Bases are commonly flat and tops are erosional.	Transitional or upper plane bed flow regime under the high deposition rate condition which prevent formation of dunes.				▨	▨	▨
Sr	**Sandstone with ripple cross-lamination**	Very fine to fine-grained sandstones with current ripple cross-lamination. Lenses are several meters wide and 5-30 cm thick. Gradational or sharp bases and tops.	Migration of current ripples on the channel floor at a flow regime weaker than required for dune formation.	?	?	?	▨	▨	▨
Scr	**Sandstone with climbing ripple cross-lamination**	Very fine- to fine-grained sandstone lenses with climbing ripple cross-lamination of similar dimensions and geometry to the facies Sr.	Migration of current ripples on the channel floor or overbank under condition of high deposition rate at lower flow regime.						▨
Sis	**Sandstone with inclined stratfication**	Coarse to fine-grained sandstones low-angle inclined surfaces draped by millimetre-scale mudstone layers. Stratification either crosses sandstone lense from top to bottom or partly at its top part. Lenses are 1-3 m thick and 20 - > 60 m wide. Bases are erosional, Tops are gradational or sharp, follow one of the inclined surfaces.	Lateral accretion of sediment on the bar during lateral migration of sinuous channel. Thin mud drapes were deposited from suspension at periods of low flow.	▨	▨				▨
His	**Heterolithic packages with inclined stratification**	**Subfacies His1** - Series of interbedded horizontal or inclined medium to very fine-grained sandstone (> 60 %) and mudstone in beds of 3 – 50 cm thick. Individual layers can be either structureless or cross-bedded and show undulating bounding surfaces. Abundant grey root traces and borrows. The thickness heterolithic packages is 0.4 - 1.8 m.	“Heterolitic inclined strata” (IHS) representing lateral accretion complexes in channel meander loop. The internal organisation of IHS units is related to a variation of flow regime 1) at the point bar top and adjacent floodplain (subfacies His1); 2) in the channel as point bar (subfacies His2).	▨	▨	▨			▨
		Subfacies His2 - Lenses of gently inclined alternating structureless medium to very fine-grained sandstone and mudstone. Thickness and width of the lenses ranges as 0.8 - 1.5 m and 1.5 - 3 m, respectively for sandstones and mudstones. Geometry is similar to facies Sis. Roots and verticall borrows are common.		▨	▨	▨			▨
		Subfacies His3 - Small scale lenses of gently inclined fine to very fine-grained sandstone, siltstone and mudstone beds without sedimentary structures. Thickness is < 0.5 m and width ranges between 1 and 3 m.	Lateral accretion in small-scale ephemeral channels on a floodplain.		▨	▨			

Table 4.1. Facies classification for the Huesca and Salt Wash DFS deposits, summary (table continues at the next page). Right six columns indicate presence of the facies in studied outcrops (shaded cells indicate presence)

				Huesca			Salt Wash		
Code	**Name of facies**	**Facies Description**	**Process interpretation**	**Monzon**	**Castel-florite**	**Alcolea**	**Bullfrog**	**Slick Rock**	**Little Park**
Sil	**Isolated lenses of coarse- to fine-grained sanstone**	Coarse to very fine-grained sandstone in lenses with scoured concave-up bases and flat tops. Thickness and width are 1.5 – 2 m and 7 - 11 m, respectively. Internal sedimentary structures are represented commonly by medium or small-scale trough cross-bedding, "concentric" bedding parallel to the base of the lens or less often by inclined stratification.	Deposition by flow confined in laterally stable channel enclosed into fine-grained cohesive sediment with abundant vegetation resistant to channel bank erosion. Variable flow discharge. Chute channels on the bar top and splay feeder channels.		▨	▨	▨		▨
Sils	**Small isolated lenses of fine- to very fine-grained sandstone**	Fine- to very fine-grained sandstones form small, 0.5 - 5 m wide, lenses with maximum thickness of 0.6 -1.5 m. Sandstones are mostly structureless or characterised by "concentric" bedding parallel to the base of the sandstone lens and occasionally show small-scale trough cross-bedding.	Deposition by flow confined in stable channels enclosed into fine-grained cohesive sediment with abundant vegetation resistant to channel bank erosion. Ephemeral streams on lateral splay which discharge is controlled by periodic flooding events.		▨	▨		?	▨
Ssh	**Sheets of structureless sandstone with flat or erosional base**	Medium- to fine-grained sandstones form 0.2 to 2 m thick continuous beds with width higher than 25 -150 m. The sheets are structureless or occasionally ripple laminated and bounded by sharp flat or slightly scoured base and commonly flat sharp or in places convex-upward top. Beds commonly thin and pinch out laterally, or split and pass into finer-grained facies.	Rapid deposition by poorly-confined or unconfined flow. 1) Final stage of channel fill by an unconfined flow which expands over the top of a bankfull filled channel; 2) on proximal part of overbank lateral or terminal splays.	?	▨	▨	▨	▨	▨
Hsh	**Heterolithic packages of interbedded sheets and lenses of sandstone, siltstone and mudstone**	Interbedded in variaous proportions continuous sheets of fine- to very fine-grained sandstones/siltstones and mudstones with thicknesses of 5 – 50 cm and 3 – 15 cm, respectively. Undulating or flat bases and tops which are flat or gradational to finer deposits. Both structureless and ripple cross-laminated sandstone sheets are common. Burrows, root traces, dinoturbation and soft sediment folding and loading structures are common. Packages of up to 1.5 m thick continues for more than 100 m.	Deposition on a competent surface by unconfined flow with frequent variation in flow strength due to initiation and waning of repetitive flood flow on overbank lateral or terminal splays.	▨	▨	▨	▨	▨	▨
Hm	**Heterolithic packages of interbedded mudstone and siltstone sheets**	Structureless mudstone sheets with some minor proportion of structureless or occasionally horizontal or ripple laminated siltstone sheets. Thicknesses of the packages could reach 2 m, but typically is 0.5 - 1 m. The packages could be traced for a distance more than 400 m. Iintensive mottling, abundant root traces, plant remains and verticall borrows are common for the Huesca succession. Vertical borrows are the most common characteristic of the predominantly one-coloured facies Hm in the Salt Wash succession.	Deposition in areas on the floodplain distal from the channel where fine-grained sediment is transported in suspension by decelerated thin unconfined flow. Distal overbank splays. Pedogenically altered.	▨	▨	▨	▨	▨	▨
Lm	**Limestone and wavy cross-laminated mudstone sheets**	Very continuous bluish-grey hard structureless limestone sheets are characterised by thickness from 5 to 50 cm and sharp flat or undulating base and top. Bioturbation, gastropods, ostracods, charophytes and rhizoliths as well as gypferous limestones and stromatolites were recorded previously (Arenas and Pardo, 1999; Fisher et al., 2007(a)). In places limestone beds are interbedded with wavy cross-laminated soft grey mudstone (and/or marls) sheets of similar thicknesses.	Deposition in low energy conditions of standing body of water. Biogenic $CaCO3$ precipitation in shallow lake. Deposition of the mudstones/marls due to periodic input of sediment with fresh water by unconfined flows generated in the distal area of the DFSs.			▨			

Table 4.1.(continues) Facies classification for the Huesca and Salt Wash DFS deposits, summary. Right six columns indicate presence of the facies in studied outcrops (shaded cells indicate presence)

Sandstone fragments are represented by sandstones of surrounding facies with the same colour and texture. No sorting or grading is observed. This facies was only observed along major scoured surfaces in the large-scale sandbodies at the Bullfrog outcrop in the Salt Wash succession.

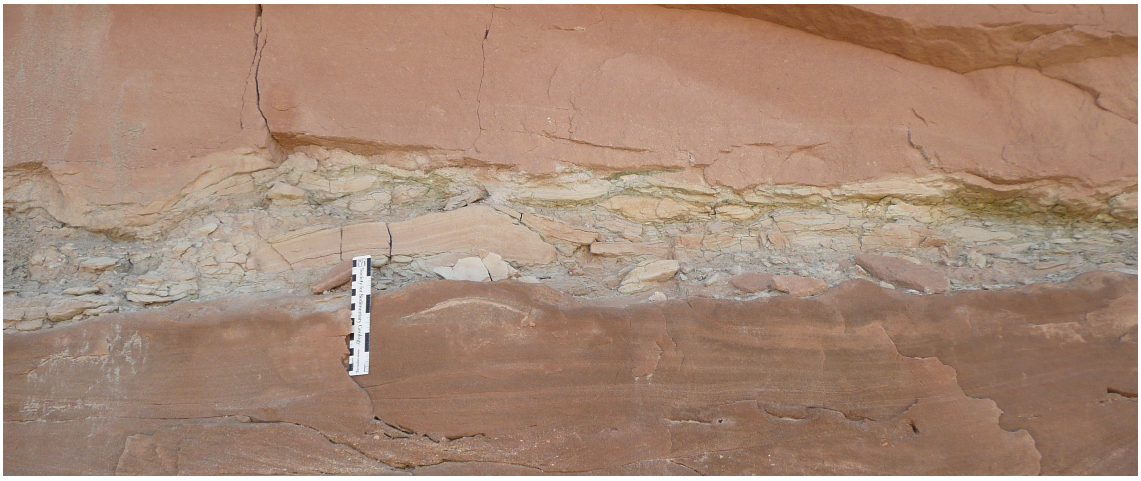

Figure 4.1. Examples of facies Sb in the Bullfrog outcrop of the Salt Wash DFS succession, Utah, USA (scale bar is 15cm).

Interpretation

Hard, lithified, intraformational sandstone fragments in the breccia indicate extended non-deposition and non-flow period between the channel-fill event and subsequent scouring of a new channel that allowed enough time for partial lithification and fracturing of the sandstone. Angular fragments suggest only a small degree of reworking and deposition close to the source as it has been demonstrated for mudstone intraclasts by Smith (1972). This is likely the case for sandstone intraclasts. Based on the above analogy with interpretation of the origin of mudclasts, the sandstone breccia of this facies was possibly formed by collapse of a channel bank composed of dry, lithified sandstone, perhaps an old channel bed, and its subsequent erosion (Plint, 1986). The area would probably have been abandoned by channel flow for a relatively long period before one of the following avulsions diverted channel flow back to the same place.

4.2.2. Sandstone with large-scale cross-bedding (Slc)

Description

Large-scale cross sets of very coarse to medium-grained sandstone represent facies Slc (Fig. 4.2, A-G). The cross-bed sets range between 1 - 3.5 m thick but are always truncated at their top by overriding set or by beds of facies St. Therefore, original cross-bed thickness could not be estimated. The width of the facies Slc can be seen to exceed 20 m but its real value is difficult to determine due to limitations of the

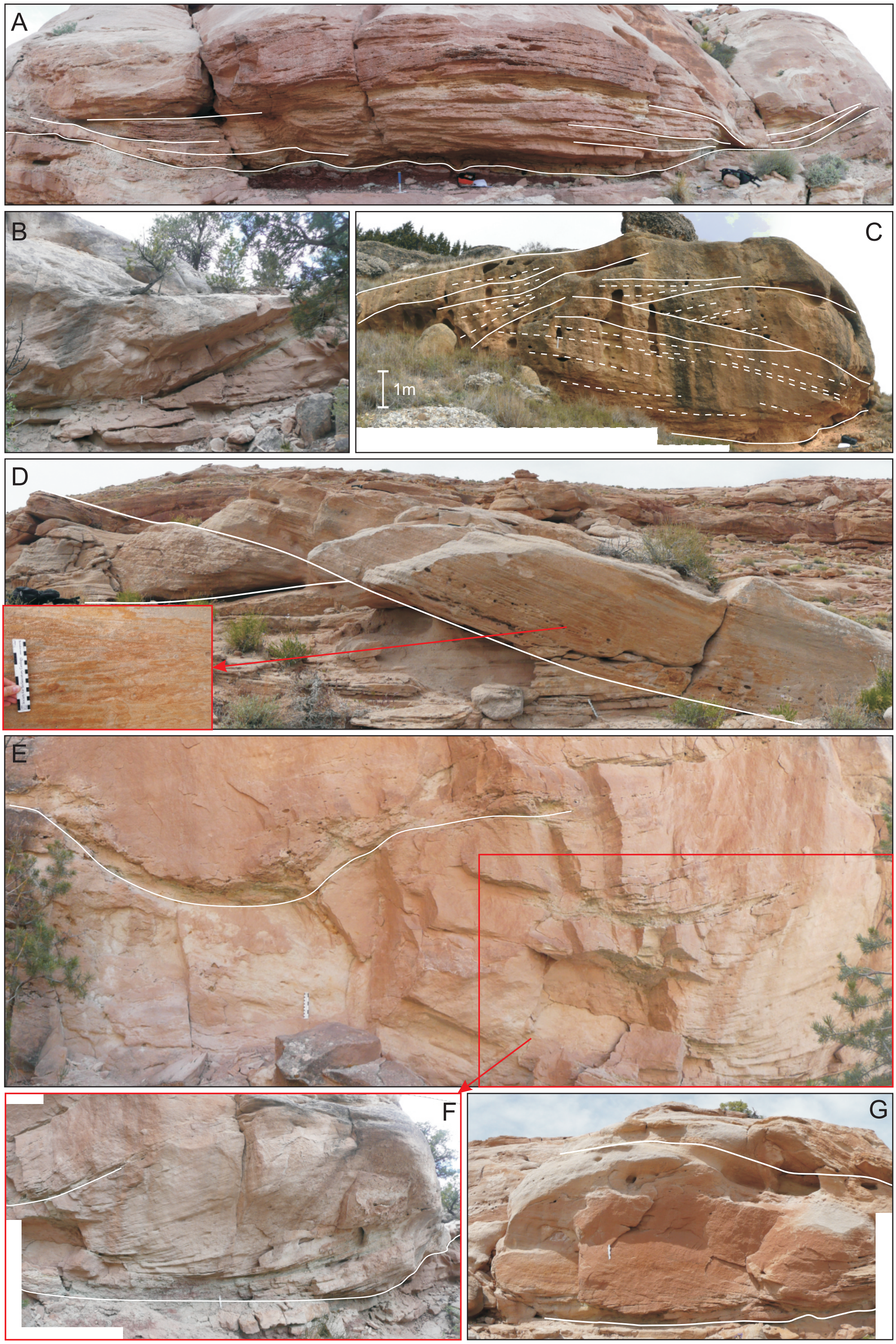

Figure 4.2. Examples of facies Slc, large-scale cross-bedded sandstones from Bullfrog (A, D, G) and Little Park (B, E, F) outcrops of Salt Wash DFS succession and Monźon outcrop (C) of the Huesca DFS succession (white scale bar is 15cm).

exposure. Previously Tyler and Ethridge (1983) reported 6m thick and 60m wide large-scale cross sets in the Salt Wash system succession.

The sandstones usually, but not always, overlie a major erosive irregular surfaces of large sandstone bodies (Fig. 4.2, C). The facies is characterised by concave-upward or inclined at 10 - 25° base truncating underlying beds. Bedding within sandstones is often subparallel to the base surface (Fig. 4.2, B, D). Flat or concave-up foresets of facies Slc display dipping surfaces that are inclined close to the average paleoflow direction. Concave-up foresets are contorted in places and more often flatten along the base into horizontal bedding (Fig. 4.2, A, F). Mudstone rip-up clasts are common along the foresets near the set base. If several large-scale sets are observed, they truncate each other along steep, sharp surfaces (up to 20°) where foresets of the upper cross set are parallel to this surface (Fig. 4.2, B, D). In places, ripple cross-lamination was found within individual beds of the set (Fig. 4.2, D). This facies occurs in all outcrops of both studied DFS successions with the exception of the Alcolea outcrop in the distal portion of the Huesca succession.

Interpretation

The irregular or concave-upward basal surface, coarse grade of the sandstones and abundant mudclasts indicate an erosional event at the channel base (McCabe, 1977) as a result of channel avulsion (Tyler and Ethridge, 1983). The large-scale foresets which dip steeply in the direction of average paleocurrent denote downstream and oblique sediment accretion on a slip face of large-scale, in-channel bedforms during their migration (McCabe, 1977; Best et al., 2003). These bedforms were interpreted to be alternate bars (McCabe, 1977), mid-channel or bank-attached transverse or linguoid bars (Collinson, 1996), giant ripples (Singh and Kumar, 1974; Tyler and Ethridge, 1983), bars (Best et al., 2003) or large-scale dunes and sand waves (Coleman, 1969). The collective term “macroform” (Crowley, 1983; Miall, 1985) can be used for these large-scale bedforms which were accreting downstream.

4.2.3. Conglomerate and sandstone with medium and small-scale trough cross-bedding (St)

Description

The St facies is represented by a range of lithologies, from conglomerates to fine-grained sandstones, all with trough cross-bedding (Fig. 4.3, A–I). The cross sets of 0.1 - 1.2 m thickness with scoop-shaped bases are stacked vertically and laterally to form continuous lenses or sheets with an average thickness of 3 m (range 1.5 – 6 m).

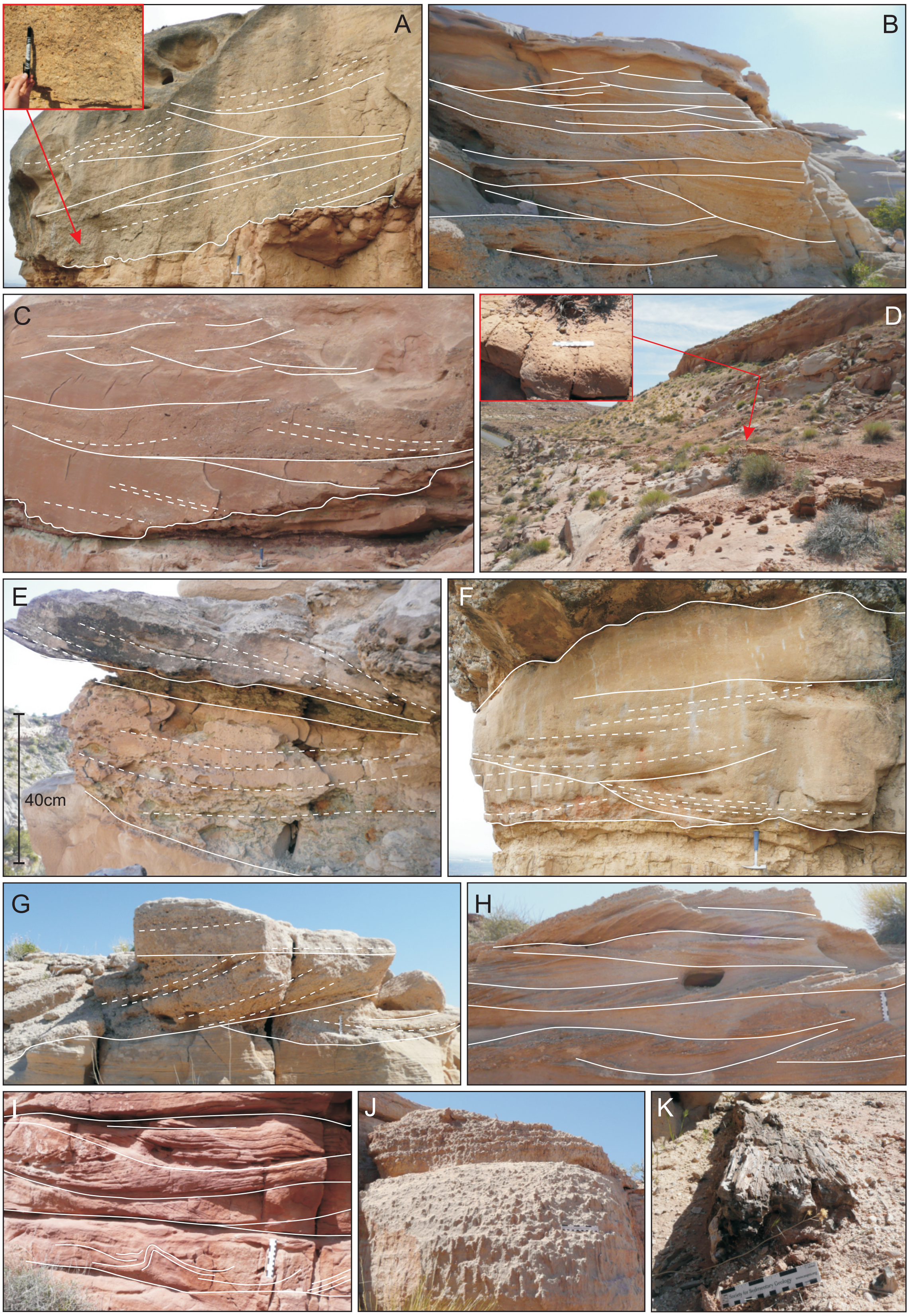

Figure 4.3. Examples of facies St, trough cross-bedded sandstones from Monźon outcrop (A, F) of the Huesca DFS succession and Bullfrog (B, C, D, G, H, J, K), Slick Rock (I) and Little Park (E) outcrops of Salt Wash DFS succession. D – brown bioturbated sandstone body top, E – mudclasts, I – soft sediment deformation, J – bioturbation, K – silicified tree log (white scale bar is 15cm).

The St complexes either overlie a very irregular or sharp, flat base of a sandbody or are characterised by convex-upward base following the base of the trough cross beds truncating underlying deposits. The tops of the complexes are flat, sharp or irregular when truncated by subsequent facies St or beneath a major irregular surface at the base of the overlying sandbody. The minimum width of the stacked complexes is estimated to be 7 – 80 m for the Huesca succession and be more than 300 m for the Salt Wash succession. Within single sandstone bodies in the Salt Wash succession the thickness of cross sets decreases upwards from 0.8 m to 0.1 m (Fig. 4.3, B, C, H).

The grain size varies between different cross sets and between lamina in the sets. Granules, small pebbles (up to 3 cm) and mudclasts were observed clustered at the toesets of cross beds, spread along the foresets or scattered randomly across the set (Fig. 4.3, A, B, C, E, F, G, H). In some St lenses, the cross sets at the base are made of finer-grained deposits than the ones in the middle or upper part, for others the granule and pebble concentration increases upward. In addition, cross sets with abundant pebbles and mudclasts were often found in the middle of the stacked complex rather than at the bottom. Sets with variable grain size are a characteristic of the more proximal Monźon and Bullfrog outcrops while St sandstones in the more medial Castelflorite and SlickRock outcrops are more homogeneous and finer-grained. The mudclasts are represented by light green or dark purple mudstones in the Salt Wash succession and by predominantly pink mudstones in the Huesca system succession.

Occasionally, foresets of St facies were observed to be deformed into small, 15 cm - high, folds (Fig. 4.3, I). Bioturbation, including roots and vertical borrows, may occur in individual cross sets of the facies (Fig. 4.3, J) or at the top of the stacked complexes. Those bioturbated tops are dark brown, cemented and could be traced across the outcrop at the Bullfrog location of the Salt Wash succession (Fig. 4.3, D). Small plant fragments are common for the St sandstones and a tree log ~ 20 - 25 cm in diameter and ~ 50 cm long was found in the Bullfrog outcrop at the top of Salt Wash succession (Fig. 4.3, K). The facies St is abundant in both studied DFS successions.

Interpretation

Trough cross-bedded conglomerates and sandstones are interpreted to form as the result of the migration of curved-crested dunes on the channel floor (Allen, 1963; Miall, 1978; Collinson, 1996; Bridge, 2003). The formation of dunes requires a sediment size greater than 0.1 mm and conditions which are hydraulically transitional from plane bed and rough flow regime in a channel (Bridge, 2003).

The deformation observed in facies St represents penecontemporaneous overtuning of foresets soon after the deposition (recumbent folds) due to shear stress in the direction of the paleocurrent, hence current drag (Hendry and Stauffer, 1977; Owen, 1999).

Rapid deposition during transitional flow regime to the upper plane bed has been stated as a cause of the deformation (Collinson, 1996).

The arrangement of coarse material along and closer to the toe of the foresets is controlled by sediment sorting during periodic grain flows on the lee slope of the dune during periods of relatively low sediment input and transport rates (Allen, 1963; Hunter, 1985; Bridge, 2003; Kleinhans, 2004). Frequent change of grain size of sandstone cross set through the facies St and the occurrence of coarse-grained cross sets, mudclasts and pebbles in the middle of the facies indicate periods of high flow capable of transporting larger clasts and eroding muddy channel banks to produce mudclasts (Robinson and McCabe, 1997). Tree logs also indicate the occurrence of high-energy events. In contrast, bioturbation and the brown oxidised sandstone body tops observed in sandstones of facies St supports the interpretation of periodic low flow or no-flow conditions inferred for the breccia beds (facies Sb). Thus, it can be concluded that flow regime in the DFS channels was variable. The facies St is therefore interpreted to represent the deposits of curved-crested dunes in a channel with variable flow regime.

4.2.4. Sandstone with horizontal or low-angle bedding (Sh)

Description

Coarse- to fine-grained sandstones with apparent horizontal or low-angle bedding form lenses averaging 1.5 m in thickness (range 0.3 – 2 m). The lenses usually overly the facies below along flat, almost horizontal surfaces and are eroded by subsequent facies along irregular, undulating surfaces (Fig. 4.4, A-D). Facies Sh is common only in the Salt Wash DFS succession.

Interpretation

Although horizontal bedding in fluvial channel deposits have not received significant attention in published literature, several examples have been found. Allen (1983) has distinguished “plane bedded simple bars” consisting entirely of horizontal / low-angle bedded sandstones in the deposits of low-sinuosity sand-bed river in the Brownstones of Welsh borders. Smith (1970) related the formation of horizontal bedding to coarse poorly-sorted sediments of upper flow longitudinal bars in proximal reaches of braided Platte River in North-Central Appalachians. Abundant horizontal bedding was observed in shallow (4.7 m), braided-to-meandering (sinuosity 1.5) Cimarron River in Oklahoma which is characterised by dominance of low-flow regime (Shelton and Noble, 1974). In the sandstones of facies Sh, however, both fine and coarse-grained sandstones were observed. Kjemperud et al. (2008) also suggested that the horizontally bedded sandstone in the Salt Wash succession were formed at the top of the bar in braided streams where flow is expected to be slower than in the channel thalweg. The low energy flow, however, would not be able to transport the coarse fraction observed in the facies Sh.

The Trentishoe Formation in SW England is dominated by parallel bedded, fine to medium-grained sandstone that has been interpreted as high energy flood deposits in a semi-arid climate formed either in channels with variable or ephemeral discharge or from unconfined overbank flow (Tunbridge, 1981; McKee et al., 1967; Frostick et al., 1988). The high energy flow regime is consistent with the observations of erosional bases, tree logs, abundant mudclasts and relatively coarse to fine grade of the sandstones of facies Sh observed in this study. Low-angle or horizontal bedding is usually interpreted to indicate transitional or upper plane bed flow conditions which prevent formation of dunes and ripples by decreasing turbulence due to high sediment concentration near the flow bed (Allen, 1982, 1983(a); Leeder, 1983; Reid and Frostick, 1994). High sediment concentration and high deposition rate during high energy flow, therefore, could prevent formation of bedforms and sediment is deposited in parallel or low-angle dipping beds. Therefore, the facies Sh is interpreted to represent low-relief bedforms which formed on the channel floor under high sediment concentration and high deposition rate conditions at high energy dune or transitional to upper plane bed flow regime.

4.2.5. Sandstone with ripple cross-lamination (Sr)

Description

Facies Sr is represented by lenses several meters wide of very fine to fine-grained sandstones with current ripple cross-lamination. The lenses are thin, not more than 30 cm thick (range 5 – 30 cm). Lower boundaries of this facies are either gradational or sharp. At the upper boundaries the facies is either truncated by subsequent facies or overlain by finer-grained deposits along sharp, undulating surface (Fig. 4.5, A, C). Ripple cross-laminated sandstones were not observed in the Huesca DFS succession.

Interpretation

Ripple cross-laminated sandstones of facies Sr were formed in the result of a migration of ripple bedforms at a flow regime lower than required for dune formation (Allen, 1963; Allen, 1982; Harms et al., 1963; Smith, 1970; Tunbridge, 1981). Therefore, the facies Sr could be related to decelerating flow in the channel that makes formation and

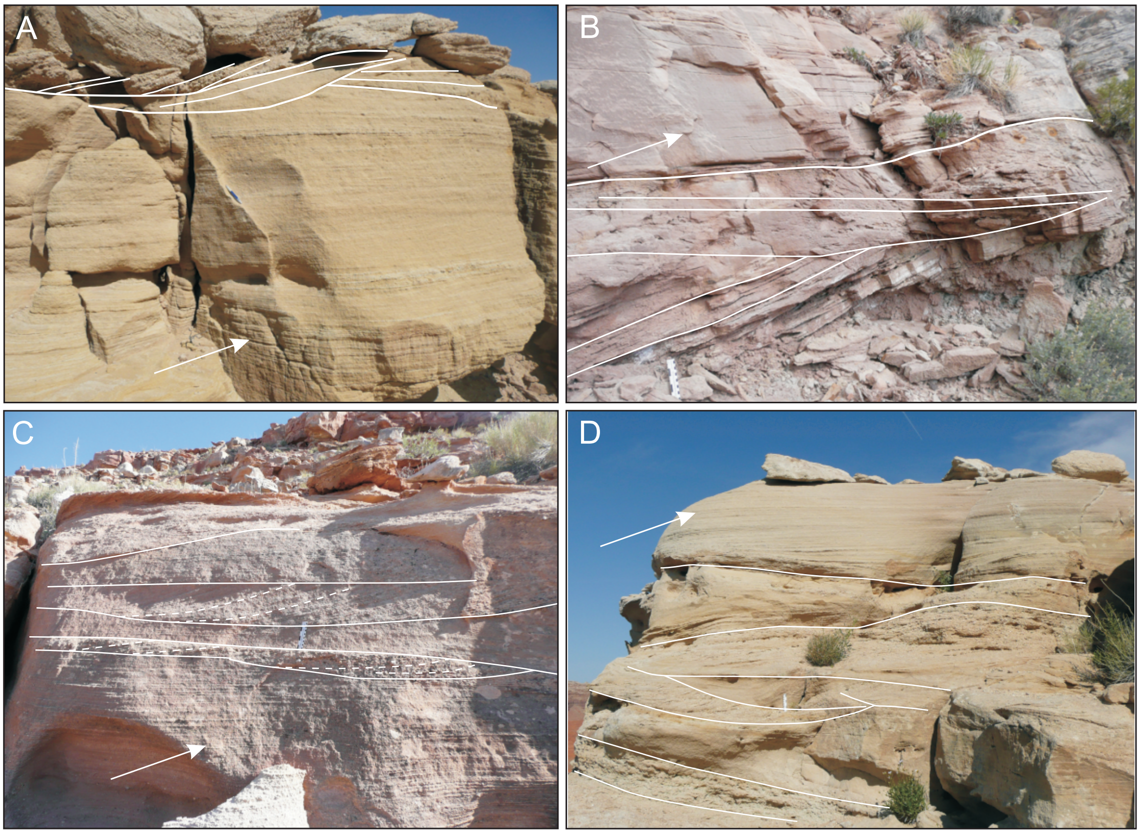

Figure 4.4. Examples of facies Sh, horizontal or low-angle bedded sandstones from Bullfrog (A, D), Slick Rock (C) and Little Park (B) outcrops of the Salt Wash DFS succession (white scale bar and pen are 15cm).

Figure 4.5. Examples of facies Sr (A, C) and Scr (B, D), sandstones with ripple cross-lamination and sandstones with and climbing ripple cross-lamination from Little Park outcrops of Salt Wash DFS succession (white scale bar and pen are 15cm).

preservation of ripples, superimposed on dune or bar surfaces, possible (Smith, 1970; Shelton and Noble, 1974; Mial, 1985).

4.2.6. Sandstone with climbing ripple cross-lamination (Scr)

Description

This facies consists of very fine- to fine-grained sandstone lenses with climbing ripple trough cross-lamination of similar dimensions and geometry to the facies Sr. These sandstones usually overly sandstone facies below with gradational transition and are overlain by either fine-grained deposits transitionally or truncated by subsequent sandstone facies (Fig. 4.5, B, D). Facies Scr was observed only at the Little Park outcrop in the Salt Wash DFS succession.

Interpretation

Climbing ripple cross-lamination is formed by ripple migration processes similar to facies Sr, but under conditions of rapid sediment deposition under low flow regime. For example, in rapidly waning unconfined flow during a flooding event (Hunter, 1977; McKee et al., 1967; Tunebridge, 1981) or superimposed on a channel bar or dune in channel at high sediment deposition rates. Climbing ripples were also described as a characteristic of flood deposits by Williams (1971) in Central Australia. Flume experiments have demonstrated that climbing ripple cross-lamination similar to those observed in facies Scr is produced under conditions of high sediment aggradation rate and low ripple migration rate (Type B ripples, Ashley et al., 1982). Therefore, the facies Scr could be interpreted to represent deposits of flood-triggered unconfined flow which carries sediment out of the channel, decelerates and deposits them next to it on the floodplain. Alternatively facies Scr can be deposited in a channel where flow conditions are similar to facies Sr but sediment aggradation rate is higher.

4.2.7. Sandstone with inclined stratification (Sis)

Description

Wedge-shaped sandstone bodies of facies Sis comprise lenses of predominantly coarse to fine-grained sandstones and exceptionally very coarse-grained sandstones with granules. Lenses are characterised by low angle inclined stratification (5-20^{o}) draped by millimetre-scale mudstone layers that maybe continuous and cross the lens from top to bottom (Fig. 4.6, A, D, E, J) or may extend only through the top part of the lens (Fig. 4.6, B, C, F, H). In places where the latter occurs the lower part of the lense is characterised by trough cross-bedding. Lenses of Sis facies are characterised by flat, locally irregular, sharp bases and flat sharp or inclined parallel to the internal

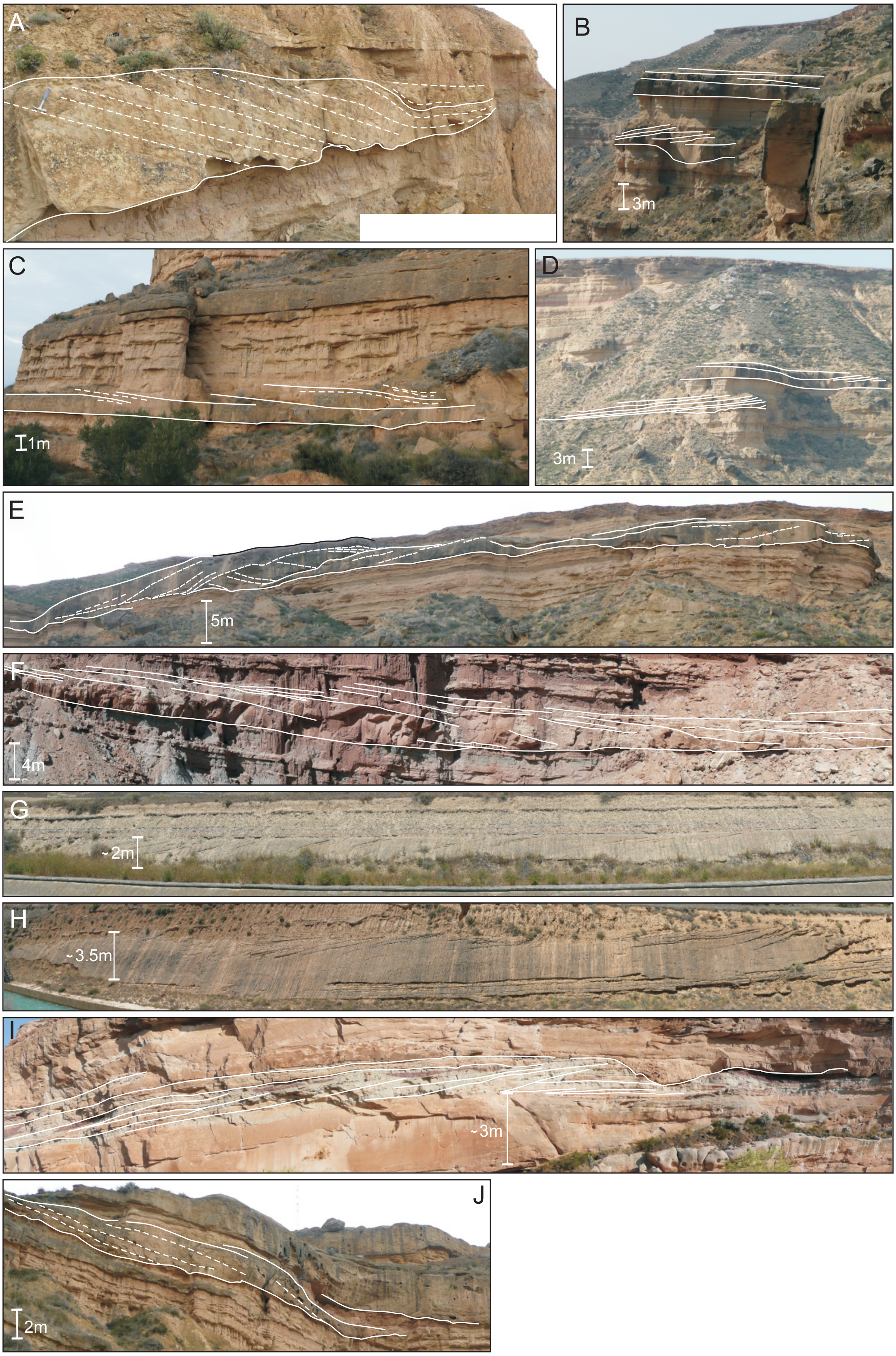

Figure 4.6. Examples of facies Sis, sandstones with inclined stratification from Monźon (C, J), Castelflorite (A, C, D, E) and Canal del Cinca (G, H) outcrops of the Huesca DFS succession and Caineville (I) and Little Park (F) outcrops of the Salt Wash DFS succession.

stratification tops. Centimetre-scale mudclasts were found along the inclined surfaces close to the base and in some trough cross-bed sets.

The individual lenses of this facies can reach 1 – 3 m in thickness and are between 20 m to more than 60 m wide. The width could not be determined more precisely due to erosion by subsequent lenses and oblique orientation of the lenses relative to the paleocurrent direction. The lenses are usually stacked laterally forming 3 – 6 m thick sheet-like complexes in which individual lenses are separated by larger-scale inclined surfaces. Individual lenses in the complex occasionally show slightly different orientation and angle of inclined stratification. The stacked complexes were estimated to continue laterally for a minimum 60 m and may extend for more than 400 m, although the dimension estimates are limited by the length of the exposure. The facies Sis is common for both the Huesca DFS succession and was observed less often in the Salt Wash DFS succession.

Interpretation

The flat, sharp, occasionally scoured base and coarse grade of sandstones of facies Sis indicate deposition in high-energy, in-channel environment. Inclined stratification dipping perpendicular to the paleocurrent direction, the wedge shape of the lens and the absence of deep scouring indicate lateral accretion of sediment on the bar during lateral migration of a sinuous channel (Moody-Stuart, 1966; Allen, 1965; 1982; Puidefabregas, 1973; Miall, 1985). Thin mud drapes on the inclined beds were deposited from suspension during low flow periods.

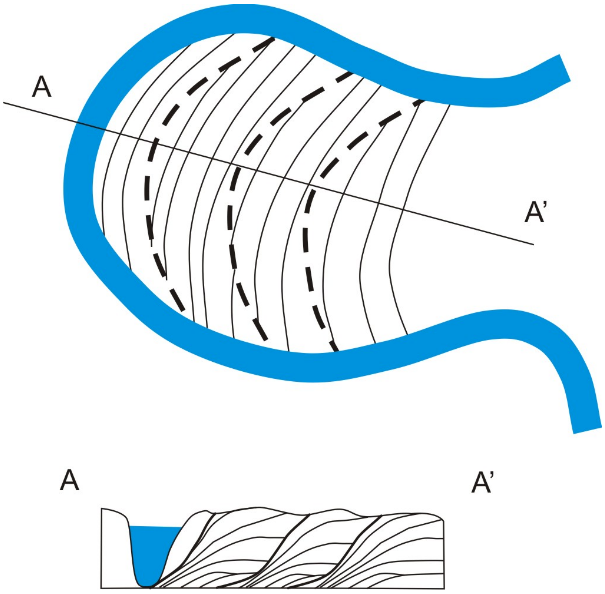

Figure 4.7. Lateral accretion surfaces resulting from migration of meander loop. Erosion surfaces are formed during major flood events. Steps or benches in the point par deposits form due to accretion at the lower flow regime (A - A') (compiled from Thomas et al., 1987 and Hirst, 1983).

Sheet-like stacked complexes were most likely formed by channels migrating freely across the floodplain. Larger-scale internal surfaces separating accretion wedges of facies Sis are a result of erosional major flood events during gradual migration of the meander loop (Fig. 4.7, Thomas et al., 1987). Previously Hirst (1983) has described stepped profiles of laterally stacked lateral accretion complexes that suggests lateral accretion at the different flow levels (Hirst, 1983) (Fig. 4.7, A-A') and this is consistent with previously inferred variation in flow discharge in DFS channels. Well-developed lateral accretion complexes suggest relatively long active period of channel migration between avulsions (e.g. "long-living channels" of Horton and DeCelles, 2001).

The trough cross-bedded sandstones at the base of some sandstone lenses represent development and migration of dunes on the channel floor simultaneously with lateral accretion on the point bar (Donselaar and Overeem, 2008) (Fig. 4.8).

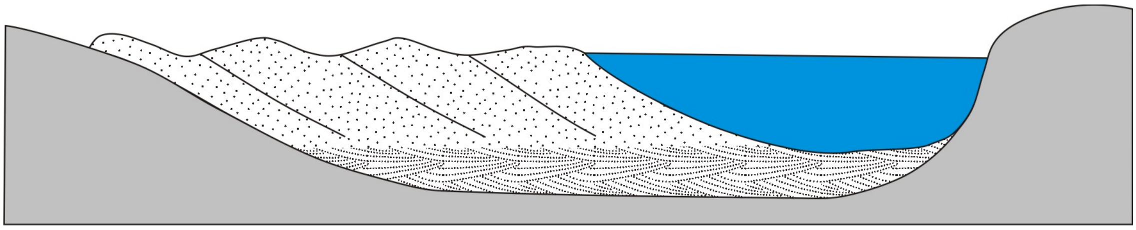

Figure 4.8. Schematic cross section through a point bar with lateral accretion surfaces at the bar top and through cross-bedded sandstones at the base of the bar formed by migration of dunes along the channel floor (modified from Donselaar and Overeem, 2008) (Appendix 5.1, B).

4.2.8. Heterolithic packages with inclined stratification (His)

Heterolithic packages (subfacies His1) are represented by a series of interbedded horizontal or inclined medium to very fine-grained sandstone (> 60 %) and mudstone in beds of 3 – 50 cm thick (Fig. 4.9, A-E). Individual sandstone layers can be either structureless or cross-bedded, including small-scale trough cross-bedding and ripple cross-lamination, while mudstones are always structureless. The coarser beds are bounded by undulating scoured or sharp flat bases, and flat or undulating tops (Fig. 4.9, C-E). The sandstone to mudstone transition is usually sharp or, less often, gradational. The thickness of entire heterolithic packages varies from 0.4 m to 1.8 m.

A separate subfacies His2 has been distinguished to describe heterolithic wedge-shaped lenses stacked laterally with the same organisation as their sandier analogues in facies Sis (Fig. 4.9, F, G). Lenses consist of gently inclined alternating, structureless, medium to very fine-grained sandstones and mudstones with sharp or uneven transition between them. Thickness and width of the lenses ranges between 0.8 and 1.5 m and between 1.5 and 3 m, respectively. The heterolithic complexes of the Huesca DFS succession can contain abundant grey root traces and burrows.

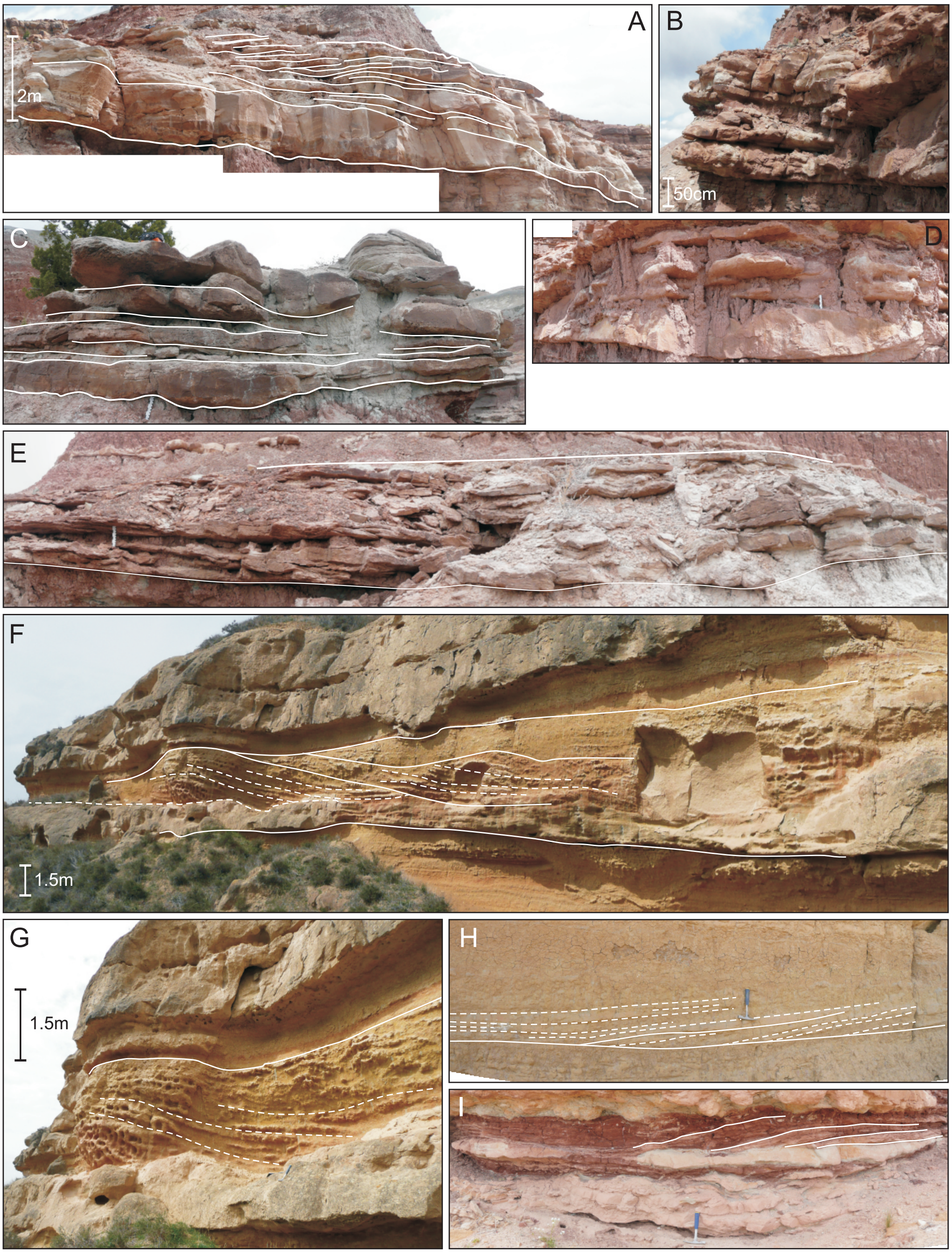

Figure 4.9. Examples of facies His, interbedded sandstones, sitstones and mudstones with inclined stratification from Monźon (F, G) and Castelflorite (H) outcrops of the Huesca DFS succession and Little Park (A, B, C, D, E) and Bullfrog (I) outcrops of the Salt Wash DFS succession (white scale bar is 15cm).

Smaller-scale inclined heterolithic complexes (subfacies His3) were occasionally observed enclosed in finer-grained floodplain deposits (Fig. 4.9, H, I). They are represented by gently inclined fine to very fine-grained sandstone, siltstone and mudstone beds without sedimentary structures. The facies thickness does not exceed 0.5 m and width ranges between 1 and 3 m. All subfacies of the facies His are observed in both studied DFS successions.

Interpretation

Similar strata to ones of subfacies His1 and His2 were previously recognized as “inclined heterolitic strata” (IHS). The majority of the observed IHS represent lateral accretion complexes in channel meander loops (Thomas et al., 1987). The internal organisation of IHS units has been related to a variation of flow regime at the point bar top and adjacent floodplain where erosion occurs and coarse sediment is deposited during high flow stage, whereas suspended finer-grained sediment is deposited during the low flow or flow quiescence (Thomas et al., 1987; Donselaar and Overeem, 2008; González - Bonorino et al., 2010). Bioturbation and root traces in subfacies His1 and His2 support long periods of low flow and probably exposure of the bar top.

Small-scale cross-bedding and ripple cross-lamination in sandstone beds of IHS (His1) indicate flow on the top of the bar, with sufficient energy to scour the underlying deposits and form small-scale dunes and ripples. The sharp contacts between coarse and fine-grained lithologies in heterolithic strata suggests quite rapid deposition of coarse sediment from waning flow that separates coarse-grained bedload sediment from suspended finer-grained sediment (Ghosh et al., 2006, Thomas et al., 1987).

The heterolithic lateral accretion complexes of subfacies His2 indicate a variable and overall low flow regime in the channel itself. The absence of structures in the beds also indicates rapid deposition of sediment due to frequent variation of flow regime (Ghosh et al., 2006). Alternatively, formation of the complexes could be caused by a change in the grain size of the supplied sediment. However, lenses of subfacies His2 have comparable dimensions and closely associate with or are enclosed by more sandy complexes of subfacies His1 and facies Sis (Fig. 4.9, F; Appendix 5.1). This suggests smaller-scale changes in channel flow regime rather than large-scale variation in type of supplied sediment.

Small-scale lenses of subfacies His3 are interpreted to represent lateral accretion complexes of small ephemeral channels on the floodplain.

4.2.9. Isolated lenses of coarse- to fine-grained sandstone (Sil)

Description

Facies Sil consists of lenses with scoured concave-up bases and flat or convex-up tops made up of medium to very fine-grained sandstones. Thickness and width varies between 1.5 – 2 m and 7 - 11 m, respectively. Internal sedimentary structures are represented commonly by medium or small-scale trough cross bedding, “concentric” bedding (Hirst, 1983) parallel to the base of the lens or less often by inclined stratification. The lenses are commonly enclosed by fine-grained deposits or cut into underlying deposits of other facies (Fig. 4.10, A-C). In contrast to the Huesca succession, sandstone lenses of this facies are uncommon in the studied outcrops in the Salt Wash DFS succession.

Interpretation

The channel-like geometry indicates high-energy confined flow which was able to erode underlying deposits to a depth up to 3 m. The lenses with concentric layering could indicate periodic or ephemeral channel discharge when sediment is deposited rapidly without bedform development (Martínez et al., 2010; Allen et. al., 1983). Similar deposits have been referred to as “ribbon sandbodies” by González - Bonorino et al. (2010). Downstream migration of bedforms and lateral migration of the point bar were also interpreted as channel fill processes for “ribbon sandbodies” of the Guadalope-Matarranya fluvial fan in the southern Ebro Basin (González-Bonorino et al., 2010; Martínez et al., 2010) that could produce inclined bedding observed in the outcrops of this study.

The relatively small width of the sandstone lenses (W / T < 15), their channel-like cross section geometry and rarely observed inclined stratification (lateral accretion surfaces) indicate limited lateral migration of the channels (Hirst and Nichols, 1986; Hirst, 1983, 1991; Slingerland and Smith, 2004; Gibling, 2006; Cain and Mountney, 2009). This was likely controlled by a bank strength (Allen et al., 1983) which is determined by the cohesive character of floodplain deposits and vegetation (Hirst and Nichols, 1986; Hirst, 1983; Nadon, 1994). The possibility of anabranching or anastomosing nature of these channels was discussed for the Willwood Formation, Wyoming (Nadon, 1994; Kraus, 1996) and for the Organ Rock Formation (Cain and Mountney, 2009). Anastomosing low sinuosity channels were also described for the modern Okavango Fan (Stainstreet and McCarthy, 1993). However, as was noted by (Martínez et al., 2010), 2D exposure of the facies is not sufficient to infer the planform pattern of the channels network and whether they were active at the same time or not.

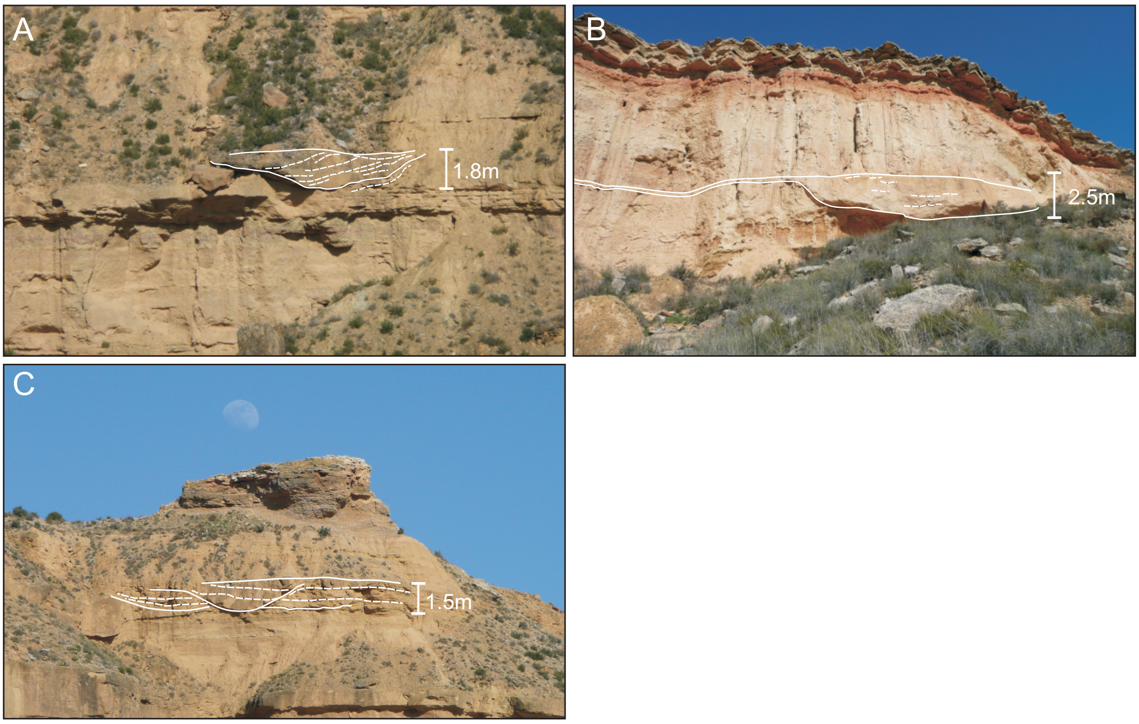

Figure 4.10. Examples of facies Sil, isolated sandstone lenses in Castelflorite (A, C) and Alcolea (B) outcrops of the Huesca DFS succession.

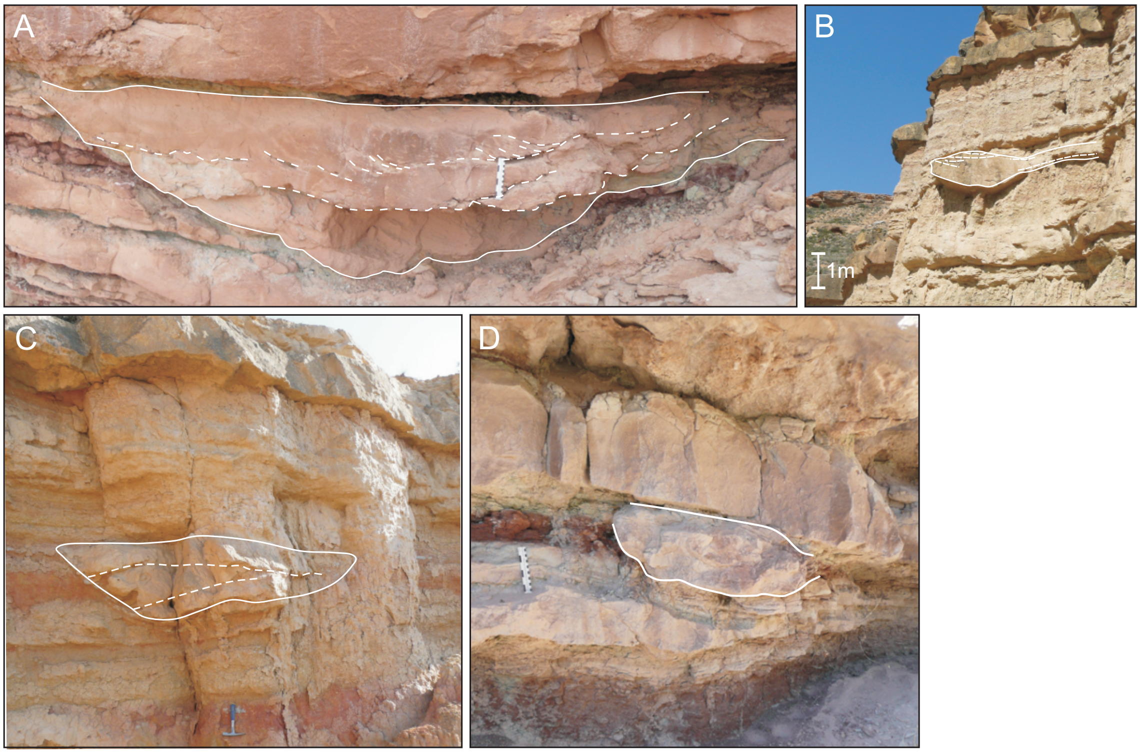

Figure 4.11. Examples of facies Sils, small-scale isolated lenses of sandstones in Monźon (C) and Castelflorite (B) outcrops of the Huesca DFS succession and Bullfrog (A) and Little park (D) outcrops of the Salt Wash DFS succession (white scale bar is 15cm).

The lenses can also represent chute channels on the top of the point bars (Constantine et al., 2010) that requires the facies Sil to be incised into bar sandstone body or facies Sis or His (Fig. 4.10, C). Alternatively, the lenses of the facies Sil can be formed as a feeder channels to the lateral or terminal splays (Martínez et al., 2010) which in this case would be enclosed by fine-grained overbank deposits (Fig. 4.10, A-B). Therefore, facies Sil is interpreted to represent deposits of laterally stable channels with variable flow discharge that could be formed as isolated laterally stable channels, chute channels on a bar top or as splay feeding channels on a floodplain.

4.2.10. Small-scale isolated lenses of fine- to very fine-grained sandstone (Sils)

Description

The facies Sils has a similar geometry to the Sil facies but is characterised by much smaller dimensions. The fine- to very fine-grained sandstones of the facies Sils form small lenses with width ranging from 0.5 to 5 m and thickness ranging from 0.6 to 2 m. Sandstones are mostly structureless or characterised by “concentric” bedding (Hirst, 1983) parallel to the base of the sandstone lens or occasionally contain small-scale trough cross-bedding (Fig. 4.11, A-D). This description is similar to the "small ribbons" described by Kraus (1996). The facies Sils was observed predominantly in the Huesca DFS succession (Fig. 4.11, B-D), but a few lenses were also recorded in the Salt Wash DFS succession (Fig. 4.11, A).

Interpretation

Similarly to the previous facies, the scoured base and channel-like geometry of the facies Sils also indicate deposition by confined flow in laterally stable channels enclosed into vegetated, cohesive sediment resistant to channel bank erosion (Hirst, 1983; Nadon, 1994). The absence of sedimentary structures and the presence of concentric layering indicate rapid sand deposition due to possibly frequent variation in flow regime. For instance, such sedimentary characteristics could develop in ephemeral streams associated with lateral splays in which discharge is controlled by periodic flooding events (Nandon, 1994; Smith et al., 1989). Occasionally, small-scale bedforms could have been formed on the channel floor during a relatively extended period of high flow energy.

Sandstone lenses of similar size were observed in the St. Mary River Formation in Canada (Nadon, 1994) and in modern deposits of the Saskatchewan River (Smith et al, 1989) and were interpreted as shallow distributary channels forming anastomosing network on lateral splays. Numerous small channels forming anastomosing (Assine, 2005) or anabranching (Buehler et al., 2011) pattern were also observed on overbank splays of the modern Taquari DFS. In contrast to modern DFS observations, planform characteristics of sandbodies in the outcrops could not be determined and therefore whether the channels were anastomosing remains uncertain. The facies Sils is, therefore, interpreted to form in small, ephemeral, laterally stable channels on lateral or terminal splays.

4.2.11. Sheets of structureless sandstone with flat or erosional base (Ssh)

Description

Medium- to fine-grained sandstones form laterally continuous beds with thicknesses between 0.2 and 2 m and widths greater than 25 -150 m. The sheets are structureless and bounded by very sharp flat or slightly scoured bases and commonly sharp, flat or in places convex-upward top. Ripple cross-lamination was observed in places but is uncommon. In some sandstone sheets horizontal layers draped by very thin mudstone layers were observed (Fig. 4.12, C). Beds of the facies Ssh are either pinch out laterally (Fig. 4.12, A, B, E-G), or split and pass into finer-grained facies (Fig. 4.12, H). In addition the grain size of the sandstones decreases from the thickest part of the sheet to its edges. Limited exposure length has restricted observation of lateral variation in characteristics of the facies Ssh. Facies Ssh have been observed in both the Huesca and Salt Wash DFS successions.

Interpretation

Absence of structures, sheet-like geometry and lateral fining, thinning and pinching out of the sandstones indicate rapid sediment deposition from an unconfined flow due to rapid reduction of the flow strength as it expands radially with distance from the source (Ghosh et al., 2006; Fisher et al., 2007(a), 2008; Bristow et al., 1999). Such a scenario could have initiated from an active channel during a flooding event.

The unconfined flow of such events has been suggested to be strong enough to transport sand as coarse as 0.25 - 0.5 mm (medium sand) for a considerable distance up to 1.1 km (Fisher et al., 2007(b)). Bedload sediment is deposited in the proximal or central part of the flow that changes to deposition of suspended load towards flow periphery (Fisher et al., 2007(a), 2008). The sandstone sheets with a slightly erosional base in their middle part (Fig. 4.12, A-B) are interpreted to record sediment deposition from poorly confined flow (“sheetflood deposits” of Kasse et al., 2003) strong enough to erode the substrate but not enough to create a channel scour. Sharp or even slightly erosional base and medium grain size of sandstones indicate proximal position to the source of the unconfined flow (North and Davidson, 2012).

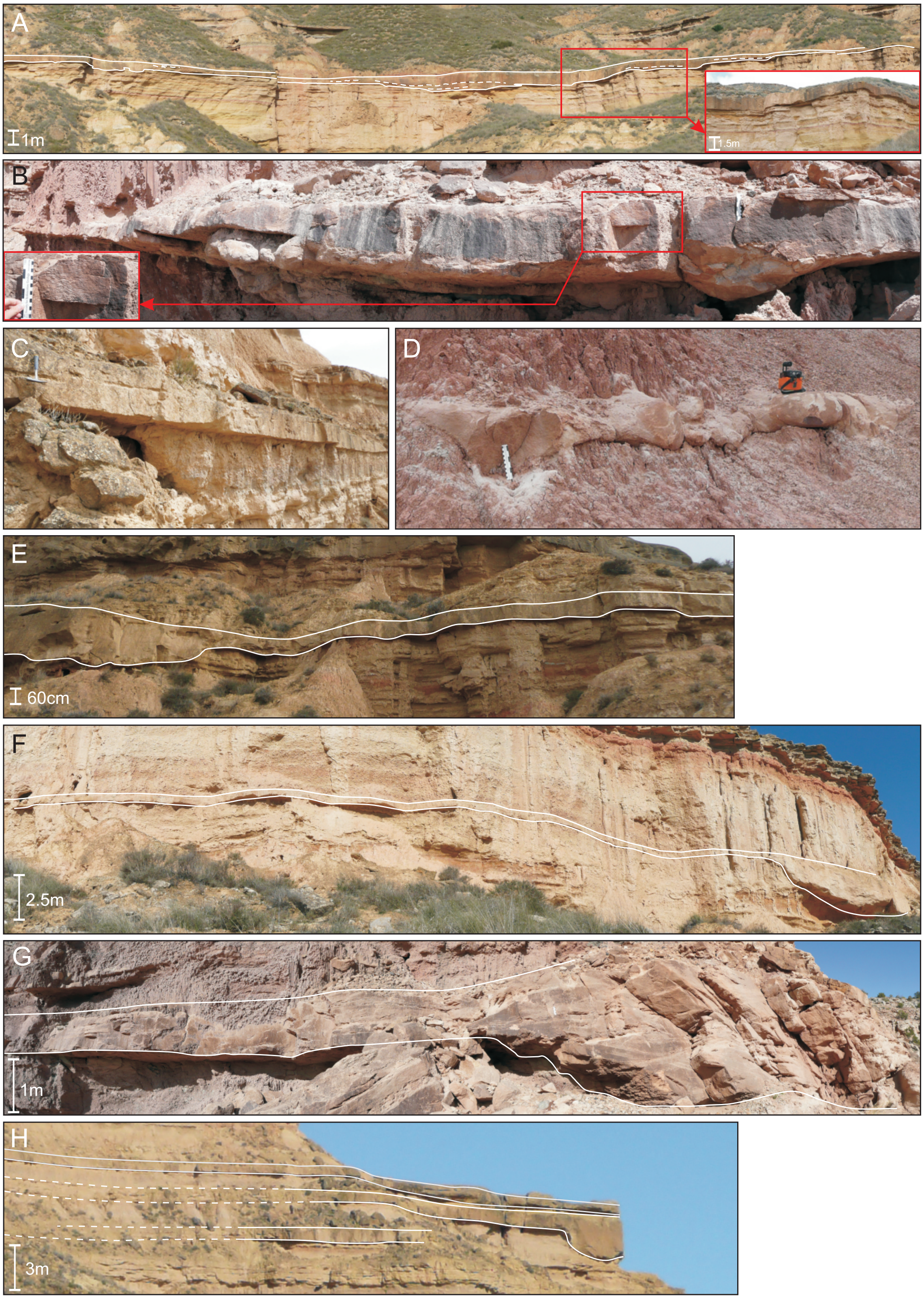

Figure 4.12. Examples of facies Ssh, sandstone sheets in Monźon (E), Castelflorite (C, H) and Alcolea (A, F) outcrops of the Huesca DFS succession and Little Park (B, D, G) outcrop of the Salt Wash DFS succession (white scale bar is 15cm).

Similar facies were interpreted previously as levee deposits for the Scala Dei Group, Spain by Allen et al. (1983), for the Huesca system, Spain by Hirst (1983, 1991), and for St. Mary River Formation, Canada by Nadon (1994). Characteristic relationships of levee with channel deposits were not observed in the successions of this study. Laboratory experiments conducted by Sheets et al. (2007) showed that thin sandstone sheets also form at a final stage of channel fill by an unconfined flow which expands over the top of a bankfull filled channel. The geometry of such sandstone sheets would probably be similar to those observed in studied DFS successions.

It is possible that facies Ssh also represents terminal splay sandstones, similar to those observed in the distal areas of the Guadalope-Matarranya fluvial fan in Spain (Martínez et al., 2010), in addition to those of ephemeral rivers in Central Australia ("floodouts" of Tooth, 2000, 2005) and in Lake Eyre in Central Australia (Fisher et al., 2008). In order to differentiate between interpretations presented here facies associations need to be considered.

In summary, the facies Ssh is interpreted to be deposited in overbank splays which were formed either lateral to the channel by poorly confined or unconfined flow during flooding events or downstream from the channel in terminal splays. The facies represents proximal part of the splays.

4.2.12. Heterolithic packages of interbedded sheets and lenses of sandstone, siltstone and mudstone (Hsh)

Description

Facies Hsh comprises interbedded continuous sheets of fine- to very fine-grained sandstones, siltstones and mudstones. The thickness of sandstone and siltstones vary between 5 and 50 cm while the thickness of mudstone sheets ranges from 3 to 15 cm (Fig. 4.13, A-I). The lateral extent of packages usually exceeds 100 m and is limited by the exposure length. The sandstone sheets are typically characterised by undulating or flat bases and tops which are flat or gradational with finer deposits. In places the bases of individual sandstone beds are slightly scoured. Siltstone and mudstone beds are commonly structureless while both structureless and ripple cross-laminated sandstone sheets (Fig. 4.13, G-H) are common in both study areas.

Burrows and root traces were also recorded in this facies in both studied successions. A few load structures at the base of sandstone sheets were found in the Huesca succession. Dinoturbation (bioturbation resulting from dinosaur walking traces) and soft sediment folding are common in this facies in the Salt Wash succession.

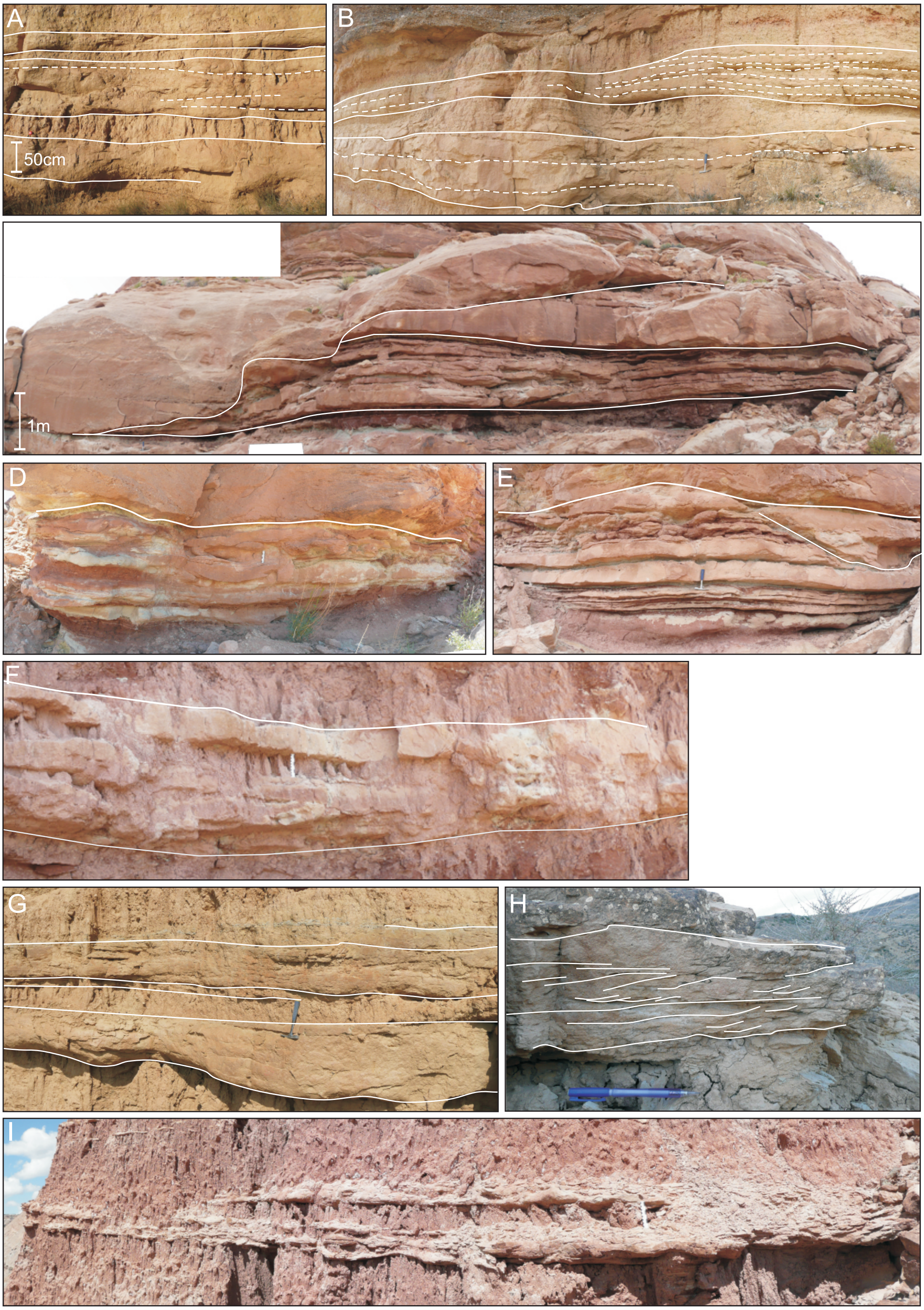

Figure 4.13. Examples of facies Hsh, packages of interbedded sandstone, siltstone and mudstone sheets in Castelflorite (A, B, G, H) outcrop of the Huesca DFS succession and Bullfrog (C, D, E) and Little Park (F, I) outcrops of the Salt Wash DFS succession (white scale bar and pen are 15cm).

The sandstone to mudstone ratio varies between packages and laterally within the packages creating a continuum between entirely sandy units of amalgamated sandstone sheets to heterolithic units with a mudstone content up to 60%. Accordingly, sandstone sheets in the package may amalgamate laterally into sandstone beds up to 1.5 - 2 m thick (Fig. 4.13, A, B). These may thin and eventually split into isolated sheets and lenses (Fig. 4.13, I). In addition, thickness of an entire heterolithic package may decrease laterally. For a few sandbodies, a decrease in sandstone grain size from the thickest part of the sandbody towards its thinner edges was observed. The facies Hsh is abundant in studied outcrops of both DFS successions.

Interpretation

The sheet-like geometry of this facies, overall fine grain size and absence of significant souring at the base indicate deposition on a competent surface by unconfined flow (Fisher et al., 2007(a); Bristow et al., 1999) which could have been initiated from an active channel during a flooding event or from the channel mouth due to change in the surface gradient (North and Davidson, 2012) or decrease in flow strength. The heterolithic character of the packages indicates frequent variation in flow strength due to initiation and waning of repetitive flood flow when deceleration of the flow results in bedload deposition followed by deposition of suspended load (Bridge, 1984; Bristow et al., 1999; Tooth, 2005; Fisher et al., 2007(a); North and Davidson, 2012). It has been previously noted that individual sandstone sheets often consist of amalgamated smaller lenses (facies Ss_a in Fisher et al., 2007(a)) which indicate that splay deposits are formed by multiple smaller-scale unconfined flows (see also North and Davidson, 2012). Ripple cross lamination in sandstone sheets denotes bedload transport as an initial sediment transport mechanism (Fisher et al., 2007(a)). In contrast structureless sandstone sheets suggest rapid waning of the flow and rapid deposition of coarse sediment suppressing bedform formation (Ghosh et al., 2006; North and Davidson, 2012). Observed bioturbation and root traces typically suggests relatively low energy flow or standing water conditions such as between flood events.

Such processes could have formed lateral splays at a side of a channel or terminal splays at a mouth of a channel. Slingerland and Smith (2004) also considered that sandstone sheets and heterolithic packages represent amalgamated lateral splay lenses and mouth-bar lenses at the front edge of a lateral splay. Terminal splays, however, could also produce the same type of deposits which could not be distinguished without full analysis of facies associations and their distribution across a DFS.

Rapid deceleration of the unconfined flow away from the initiation point (Fisher et.al., 2007(b)) would explain the thinning of the heterolithic packages and sandstone sheets and lateral increase in sandstone to mudstone ratio within the packages. For instance, packages of amalgamated sandstone sheets with a lower mudstone proportion represent more proximal part of the splay that is laterally replaced by its heterolithic counterpart. Consequently, the sandstone proportion in the package, sheet thickness and change in sedimentary structures could qualitatively indicate the distance from the channel. The facies Ssh described previously could also represent the most proximal equivalent of the heterolithic packages.

4.2.13. Heterolithic packages of interbedded sheets of mudstone and siltstone (Hm)

Description

Facies Hm is represented dominantly by sheets of structureless mudstone interbedded with a minor proportion of structureless or occasionally horizontal or ripple laminated siltstone sheets (Fig. 4.14, A-G). A few beds of pure claystone and occasional lenses or sheets of very fine-grained sandstone were also recorded (Fig. 4.14, A). The heterolithic packages of the facies Hm can reach thicknesses of more than 2 m, but typically are between 0.5 m and 1 m. The top and bottom boundaries of individual sheets in the packages are sharp, undulating, flat or less often gradational. Packages could be traced laterally across entire outcrops for a distance more than 400 m if not truncated by coarser-grained facies. Soft sediment deformation features (S-shaped folds) were observed in some of the heterolithic packages of the Salt Wash DFS succession (Fig. 4.14, H).

The facies Hm is a component of both studied DFS successions. This facies in the Huesca succession is characterised by pale yellow, red, orange, purple, white/pink or grey colour and intensive mottling (Fig 4.14, A-D). The packages contain abundant root traces and less abundant vertical borrows. Plant remains were recorded in some of the Huesca beds (Fig. 4.14, C). The colour of facies Hm in the Salt Wash DFS succession is more uniform and predominantly red/purple with light green fractures and root traces or, less often, entirely light green (Fig. 4.14, E-H). The latter is usually observed immediately below the major sandstone bodies. Verticall burrowing is the most abundant structure in mudstones and siltstones of this facies in the Salt Wash DFS succession.

Interpretation

The small grain size, absence of structures, pedogenic features and presence of

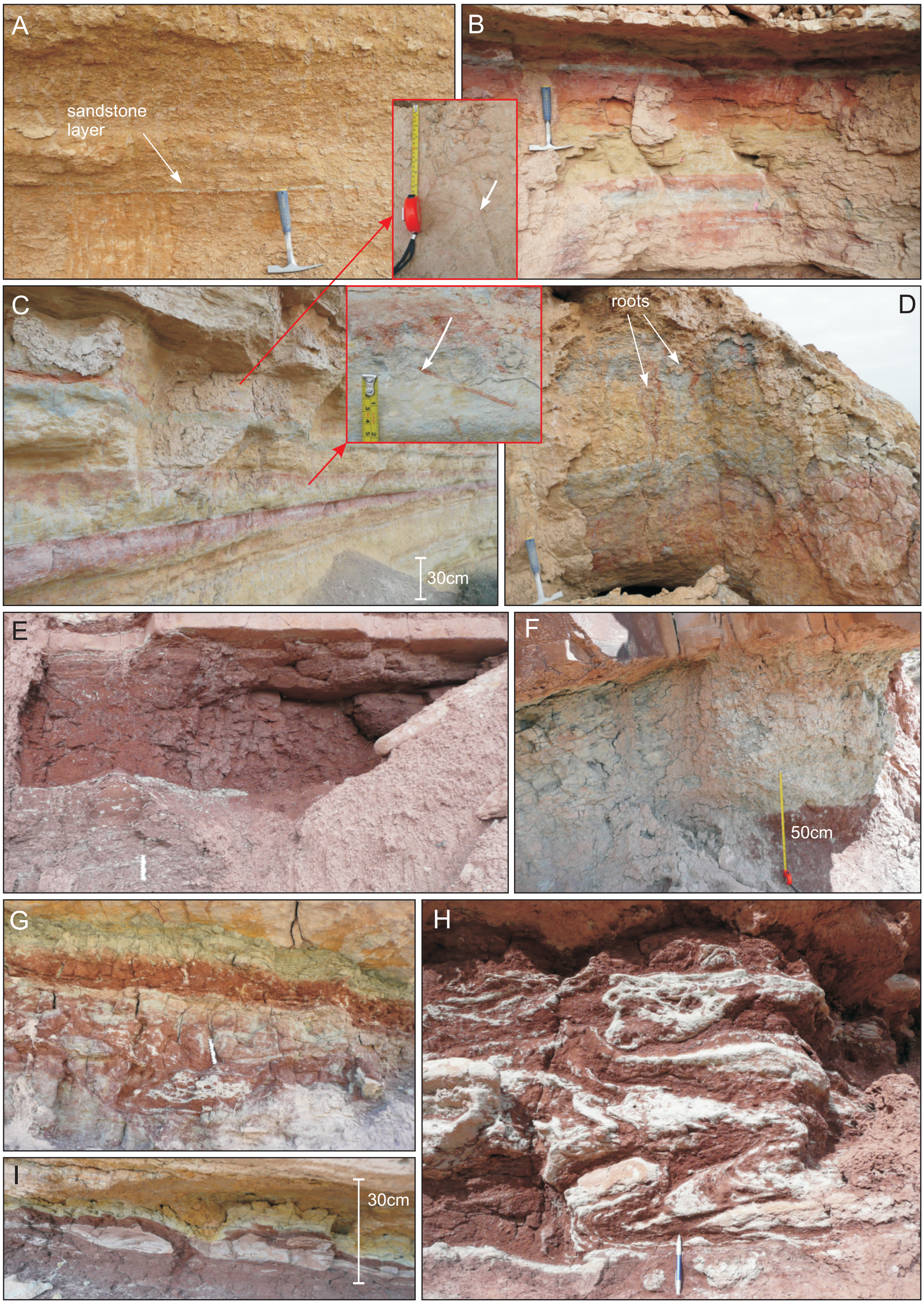

Figure 4.14. Examples of facies Hm, interbedded siltstone and mudstone sheets in Monźon (A) and Alcolea (B, C, D) outcrops of the Huesca DFS succession and Bullfrog (I) and Little Park (E, F, G, H) outcrops of the Salt Wash DFS succession. G, I - bioturbation, C - plant fragments, D - roots and G, I, H - soft sediment deformations (white scale bar and pen are 15cm).

abundant burrows and root traces indicate deposition in very low energy environment and breaks in deposition (Bristow et al., 1999). The siltstones with horizontal bedding may also indicate shallow water deposition (Kasse et al., 2003). Fine-grained sediment could have been transported by decelerating unconfined flow of splays and deposited in floodplain ponds (see also Bristow et al., 1999; North and Davidson, 2012). The fine-grain size of the facies and great thickness of the packages of this facies could suggest that it represents deposits of lateral or terminal splay distal to the channel area.

The bright colours, mottling and abundant root traces of facies Hm in the Huesca system deposits indicate relatively extensive periods of low energy or non-deposition conditions that allowed pedogenic alteration. Reed-like monocotyledons, small trees, low stature plants and herbaceous vegetation have been identified to be present in paleosols in the Huesca succession (Hamer et. al., 2007(a)). The majority of the Huesca paleosols were interpreted by the authors to be well-drained (Inceptisols, Alfisols and Entisols). These paleosols were suggested to be characteristic of different DFS areas and were interpreted to be controlled by similar climate, degree of water drainage and small fluctuations of basin lake level (Hamer, 2007). Grey colouring around the root traces and at the tops of a few channel sandbodies has been previously attributed to the leaching of clay minerals or lithic clasts (Hirst, 1983).

A more homogeneous red/purple colour is typical for facies Hm in the Salt Wash DFS succession and is interpreted to indicate oxidation in a well-drained floodplain environment (Tyler and Ethridge, 1983). The absence of structures in the mudstones has also been related to soil-forming processes (Kjemperud et al., 2008), particularly to bioturbation, which is relatively intensive in this area. Light green beds underlying erosional bases of sandstone facies were possibly formed in reducing conditions or leaching under the channel or splay deposit. Generally paleosols in the Salt Wash DFS succession have previously been classified as argillic Calcisols (Demko et al., 2004). Folds in the facies Hm were formed by deformation of water-logged sediment soon after its deposition by gravitational slumping or bed shear by current drag (Owen, 1999).

Thus, the facies Hm are interpreted here to record the most distal and finest product of lateral or terminal splays and flooding events which were subjected to pedogenesis in oxidising and reducing conditions in a low energy environment.

4.2.14. Limestone and wavy cross-laminated mudstone sheets (Lm)

Description

The facies Lm comprises beds of structureless limestone (carbonate mudstone) and wavy cross-laminated clasitc mudstone beds (Fig. 4.15, A-F). Bluish-grey hard

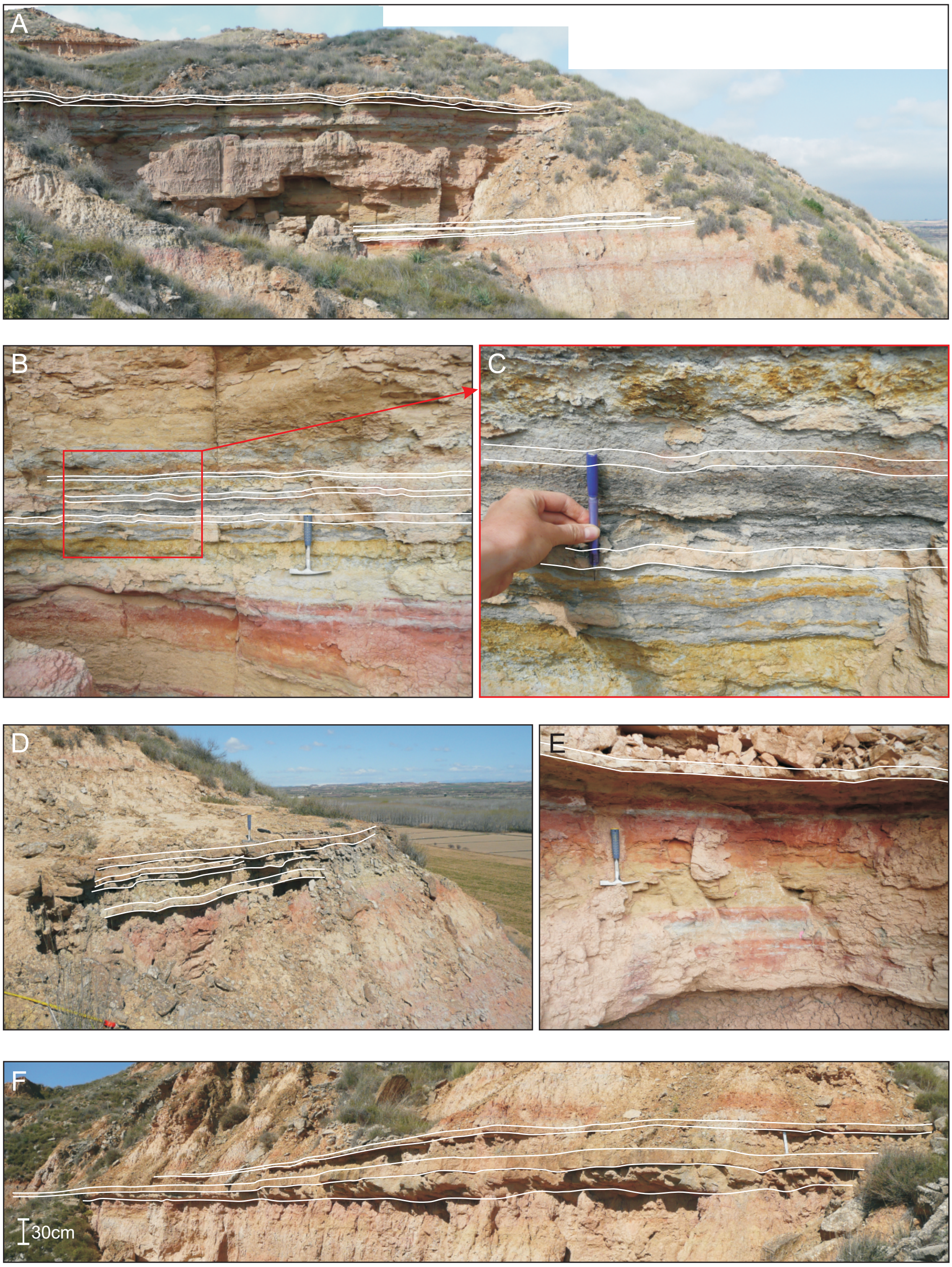

Figure 4.15. Examples of facies Lm, interbedded grey limestones and wavy-laminated grey mudstone from Alcolea outcrop in the Huesca DFS succession (white scale bar is 15cm).

limestone layers range in thicknesses from 5 to 50 cm. Bases and tops of the beds are sharp and either flat or undulating. According to the classification of Dunham (1962) the limestone beds of this facies are mudstones. Although no biogenic fragments or bioturbation were recorded during the fieldwork in the study area, heavy bioturbation, gastropods, ostracods, charophytes and rhizoliths as well as gypferous limestones and stromatolites have previously been recorded in other outcrops representing the more distal parts of the Huesca DFS (Arenas and Pardo, 1999; Fisher et. al, 2007(a)).

Continuous beds of facies Lm could be traced laterally across the entire outcrop and were found armouring the tops of hills around the study area at various levels. In places limestone beds are interbedded with wavy cross-laminated soft grey mudstones (and/or marls) of similar thickness. The facies Lm was observed only in the Alcolea outcrop in the Huesca DFS succession.

Interpretation

Structureless limestones were formed by biogenic $CaCO_3$ precipitation in a shallow lake setting with high biogenic productivity under periods of constant water influx during high lake levels (see facies Lm and Fig. 6 in Arenas and Pardo, 1999). The flat or undulating bases of the limestone beds, conformable relationships with underlying deposits and wavy cross-laminated mudstones suggest deposition in low energy conditions in shallow standing body of water. Deposition of the mudstones/marls associated with limestones indicates periodic input of sediment by fresh water into lakes by intermittent unconfined flows generated in the distal area of a DFS (Arenas and Pardo, 1999; Fisher et al., 2007a).

High values of Uranium concentration for the intervals of interbedded limestones and grey mudstones have been recorded with spectral GR surveyor during this study. The high Uranium concentration usually indicates deposition in relatively anoxic conditions with the presence of organic matter (Myers and Wignall, 1987; Rider, 2001). The unusual light grey colour of the organic-rich mudstone beds could be possibly explained by high $CaCO_3$ content which possibly dilutes the effect of darker organic matter. Evaporites, bioturbation and stromatolites described by previous workers were interpreted to record periodic shallowing of the lake waters and a transition to more saline conditions (Arenas and Pardo, 1999).

4.3. Facies associations

Facies associations have been distinguished on the basis of facies distributions and relationships between each other. They are described as a complete set of facies, but in reality some facies may be not present. Six facies associations have been distinguish and grouped into channel fill, floodplain and lacustrine major association.

4.3.1. Channel fill facies association

The channel fill facies association includes three sub-associations distinguished by their geometry, dimensions and set of facies that composes them.

Channel macroforms

The channel macroform association includes facies Sb (sandstone breccia), Slc (sandstones with large-scale cross bedding), St (sandstones with medium and small-scale trough cross bedding) and/or Sh (sandstones with horizontal/low-angle bedding), and Sr (sandstones with ripple cross lamination) which could occur in succession up-section. A decrease in cross set thickness from large-scale to ripple lamination is recognised in deposits of in-channel macroforms due to decrease in flow depth on the bar tops (e.g. bar margin succession Fig. 9 in Best et al., 2003). The rare presence of Sh facies among St sets may indicate periods when the rate of deposition was high that prevented the formation of bedforms. The channel macroforms association was observed predominantly in the Salt Wash DFS succession and less often in relatively proximal Monźon outcrop of the Huesca DFS succession.

Lateral accretion complexes (LA complexes)

Wedge-shaped LA complexes include facies Sis (sandstones with inclined stratification), His1 and His2 (heterolithic complexes with inclined stratification), St (trough cross bedded sandstones) and Sil (small scale scours filled with sand). According to the interpretation of the Sis and His facies, the association was formed on laterally accreting bars in channels with variable flow regime. The facies Sis usually passes laterally and vertically into facies His1 (Fig. 4.6) which represents the “heterolithic upper part” of a laterally accreting bar (Donselaar and Overeem, 2008). The decrease in sandstone grain size, scale of sedimentary structures and transition to the IHS units indicate decrease in flow velocity and bed shear stress along the inclined depositional surface from channel floor to the bar top in a sinuous channel (Allen, 1965, 1982). Occasionally facies St was observed at the bases of the lateral accretion channel fills and records dune formation on the channel floor at the toe of the point bar (Donselaar and Overeem, 2008). Small-scale channel-shape lenses of facies Sil cut into the Sis and His1 facies representing chute channels formed on the top of the point bars (Fig. 4.6, I; Fig. 4.10, C). Small-scale channel-shaped scours filled by facies Hm and Hsh are commonly observed associated with LA complex, and are interpreted to represent abandoned channel scours (see also Hirst, 1991, Donselaar and Overeem,

2008) filled by fine-grained sediment supplied by splays from an adjacent active channel. Completely heterolithic lateral accretion complexes (His2) were observed as a part of such amalgamated complexes (Fig. 4.6, F; Appendix 5.1) indicating low flow periods in the channels and in general variable flow regime.

If lateral accretion complexes occur in vertically amalgamated sandbody complexes, the heterolithic top part (facies His1) could be eroded. In addition, large amounts of trough cross-bedded sandstones could obscure lateral accretion surfaces (Miall, 1985). The IHS complexes could be weathered and form intervals of non-exposure or could be taken for floodplain deposits. For example, the LA complexes have not been observed in the relatively proximal Bullfrog and medial Slick Rock outcrops of the Salt Wash DFS succession where sandstone bodies are amalgamated and are represented mainly by St facies. However, LA complex deposits were seen in the relatively proximal Caineville outcrop of the Salt Wash DFS succession (Fig. 4.6, I). Therefore, LA complexes are present in the relatively proximal and medial outcrops of the Salt Wash DFS succession but inclined surfaces and heterolithic upper part are either eroded by subsequent channel flow or perhaps the LA surfaces are very large and gently dipping, and obscured by other smaller-scale sedimentary structures. The LA channel fill association is common in both the Huesca and Salt Wash successions.

Isolated channel fill

The isolated channel fill association includes facies Sil (isolated sandstone lenses) associated with the facies Ssh or Hsh (sandstone sheets) which forms channel “wings” (Friend et al., 1997). The isolated channel fill represents bankfull–filled, laterally stable channels which before abandonment were plugged and overtopped with sheet of sand (Sheets et al., 2007). Positive topography can be formed as the result of the final stage of channel filling by unconfined flow (Fig. 5.6; Sheets et al., 2007). Occasionally observed positive topography of the facies Sil in the studied outcrops supports the idea of filling of the channel following blockage and flow avulsion (Kelly and Olsen, 1992; Jones and Schumm, 1999; Bridge, 2003; Sheets et al., 2007; Martínez et al., 2010).

The isolated channel lenses could also possibly represent plains-fed / groundwater-fed channels which are frequently observed in modern DFS (Sinha and Friend, 1994; Gohan and Parkash, 1990). This type of channel forms where unconfined flow, ground flow or several small streams on the alluvial plain are confined into one channel somewhere downstream. Similar facies were interpreted as “on-fan” channels for the Organ Rock Formation, USA (Cain and Mountney, 2009). In addition as it was shown above the isolated channel fill also forms as chute channels on the point bars (Fig. 4.10, C; Fig. 4.6, I). Alternatively these confined channels could be a result of decrease in water discharge and increae in substrate cohesiveness (Hirst and Nichols, 1986;

Hirst, 1983, 1991) that transformed large laterally unstable channels into laterally confined channels. These channels in turn could represent feeder channels for lateral and terminal splays (Martínez et al., 2010). Characteristics which could be used to distinguish these possible origins, however, are unclear. The isolated channel fill association was observed only in relatively medial and distal areas of the Huesca DFS succession and in distal part of the Salt Wash DFS succession.

4.3.2. Floodplain / Alluvial plain

The floodplain/alluvial plain facies association consists of facies Ssh (sandstone sheets), Hsh (heterolithic packages of interbedded sandstone, siltstone and mudstone sheets), Sils (small-scale isolated channel-shaped lenses of sandstone) and Hm (heterolithic packages of fine-grained deposits). Two sub-associations are distinguished; proximal and distal splays which are common in both the Huesca and Salt Wash DFS successions.

The lateral transition from facies Ssh into facies Hsh and ultimately into Hm is interpreted to represent decelerating / waning unconfined flow on lateral or terminal splays. The channel-shaped lenses of the facies Sils cut through the sheets of facies Hsh, suggesting the presence of small channels on the splays. Often splay associations can be traced laterally directly into the channel fill facies indicating their origin from an unconfined flow generated from an active channel. Proximal and distal (with respect to the channel) parts of the splays could possibly be qualitatively distinguished on the basis of relative proportion of sandstone and finer-grained sheets and the degree of their amalgamation. These are discussed below.

Proximal splay

The proximal, with respect to the channel, part of the splay is characterised by relatively high flow energy and high concentration of sandy material in the flow. The deposits of this association consist of facies Ssh, Sil and facies Hsh where sandstone sheets represent more than 60 % of the package.

Distal splay / Floodplain basin

Distal areas of a splay are characterised by thinner sandstone sheets and a relatively higher proportion of mudstone and siltstone interbeds or by sandstone and siltstone lenses enclosed by mudstone (Fig. 4.13, I). The facies Sils was rarely observed. The fine-grained facies Hm is interpreted to have been deposited in the most distal from the channel floodplain area, where unconfined flow terminates in floodplain ponds or on alluvial plane.

Terminal splay

The same two splay associations, proximal and distal splays, may also form deposits of terminal splays originated from a channel mouth on the low gradient alluvial plain in the distal area of a DFS. Lateral and terminal splay deposits cannot be confidently distinguished unless associations of facies are considered for the entire area of a DFS and a distal setting is recognised.

4.3.3. Lacustrine facies association

The facies Lm represents lacustrine deposits which were observed only in the distal Alcolea outcrop of the Huesca DFS succession. For detailed interpretation see description of the facies Lm above. Intercalation of fluvial and lacustrine deposits in the Alcolea outcrop indicates fluctuations in the lake level that was also recognised during detailed studies of lacustrine deposits and paleosols of the Ebro Basin by Arenas and Pardo (1999) and Hamer (2007). The change in the lake level has been related to the climatic changes based on the results of mineralogical and isotopic analysis (Arenas et al., 1993(a), 1997).

Facies and facies association distribution within the Huesca and Salt Wash DFS succession are discussed separately in the following chapters 6 and 7.

4.4. Conclusions

Fourteen fluvial and lacustrine facies, representing processes occurring in-channels, and on the floodplain / alluvial plain, were recognised based on the data collected from both the Huesca and Salt Wash DFS successions. The main characteristics used for facies recognition are geometry of the sedimentary body, combination of lithologies and sedimentary structures. Detailed analysis of facies relationships make it possible to distinguish six main facies associations which can be combined into three major facies associations: channel fill, floodplain and lacustrine. Most of distinguished facies and facies associations can be observed in both studied DFS successions.

The proportions and relationships of facies and facies associations in the Huesca and Salt Wash DFS successions are discussed in the following chapters where this classification is used to describe, quantify and compare characteristics of the successions and their lateral and vertical variations. The depositional processes interpreted in the result of the facies analysis are utilised when interpreting behaviour of the DFSs. The following Chapter 5 describes characteristic sandstone body types within the DFS succession where facies interpretation is used to distinguish the processes responsible for the formation of particular sandstone body type.

5. Sandstone body types

5.1. Introduction

In addition to the facies associations sandstone body geometries and sandstone body relationships have been studied with the aim being to distinguish types of sandstone bodies and amalgamation complexes that are typical in studied DFS successions. The definition of these parameters has important implications for reservoir modelling where the geometry and dimensions of individual sandstone bodies together with their lateral relationships are the main input parameters. Determination of these parameters for fluvial successions in the subsurface is usually difficult because of the heterogeneity of fluvial deposits and the lack of spatial data. Interpretation is also complicated by a lack of understanding of the relationship between the geometry of individual channels and the final preserved sandstone body geometry that is determined by channel lateral stability, aggradation rate and avulsion characteristics (Miall, 1985). Therefore, data from the geological record (outcrops) are needed to provide qualitative and quantitative data for input into the reservoir models.

Sandstone bodies were studied in six locations representing relatively proximal, medial and distal areas of both the Huesca and Salt Wash DFSs respectively. The sandstone bodies are easily distinguishable in the outcrops of the study areas making it possible to use photo mosaics in addition to the field observations which in some places are limited by outcrop accessibility. The geometries of all sandstone bodies have been studied including those formed in channel and in overbank settings. Significant attention has also been given to the relationships between sandstone bodies and distinguishing characteristic sandstone body amalgamation styles. The results of the sandstone body analysis provide information on the dimensions and shape of the sandstone bodies in these DFS successions and also provide an insight into the main depositional processes that are responsible for sandstone body formation on DFSs.

5.2. Sandstone body types and interpretation of deposition processes

For the DFS deposits of both the Huesca and Salt Wash systems three main types of sandstone bodies were distinguished based on their dimensions, shape, facies associations and interpretation of depositional processes. Sandstone body dimensions were measured in the outcrop sections perpendicular or slightly oblique to the average trend of paleocurrents: south-westerly for the Huesca DFS (Hirst, 1983) and north-easterly for the Salt Wash DFS (Craig et al., 1955). The width to thickness ratio (W / T ratio) for sandstone bodies was calculated using maximum thickness and actual or minimum width limited by outcrop length or exposure quality (Chapter 3).

5.2.1. Type 1

The measured W / T ratio for Type 1 sandstone bodies varies between 3 and 12, which corresponds to the "ribbon sandstone body" defined by Friend et al. (1979) and is frequently used to describe isolated sandstone bodies (e.g. Miall, 1985; Kraus, 1996; Martínez et al., 2010). The third dimension of the sandstone bodies, however, was not observed and therefore the word "ribbon" would not be used in this classification.

Sandstone bodies of Type 1 are characterised by a scoured base (up to 5 m) and a flat or slightly convex-upward top (Fig. 5.1). A range of facies, including St, Slc, Sil and Sils, comprises the Type 1 sandstone bodies. On the basis of their dimensions and internal characteristics sandstone bodies of Type1 could be subdivided into 3 subtypes which are distributed in different environments within a DFS and have different relationships with other sandstone body types (Section 5.3).

Subtype 1/1 sandstone bodies are made up of facies St and Slc and have the largest thicknesses and widths, 3 - 9 m and 25 – 80 m, respectively. These sandstone bodies are interpreted to be formed by high-energy flow in relatively stable major channels. The flow eroded the underlying deposits forming the scour that was subsequently filled with coarse sediment through the mechanism of curve-crested dune migration and bar accretion. According to the facies analysis and paleocurrent directions the bars were migrating downstream or slightly oblique to the paleoflow (Chapter 4).

Subtype 1/2 sandstone bodies are represented by lenses of facies Sil. The dimensions vary between the two DFS successions. The sandstone bodies of the Huesca DFS succession are characterised by thicknesses from 1.5 to 2 m and widths from 7 to 11 m, while the sandstone bodies of the Salt Wash DFS succession are wider, from 10 to 23 m, and thicker, from 1.3 to 3.5 m. Following the facies interpretation, these sandstone bodies were formed in laterally stable channels with variable flow regime. Such channels eroded into the cohesive substrate in the middle and distal parts of the systems. For example, the stable channels could represent chute channels on the heterolithic top of the channel bar, "on-fan" channel formed from unconfined flows or distal reaches of the main channel flowing along more cohesive and vegetated substrate (Chapter 4).

Subtype 1/3 sandstone bodies are represented by lenses of facies Sils which are thinner (0.4 – 2 m) and not as wide (0.5 – 5 m) as sandstone bodies of subtype 1/2. These sandstone bodies were formed in channels or scours on overbank splays. For detailed description refer to the Chapter 4.

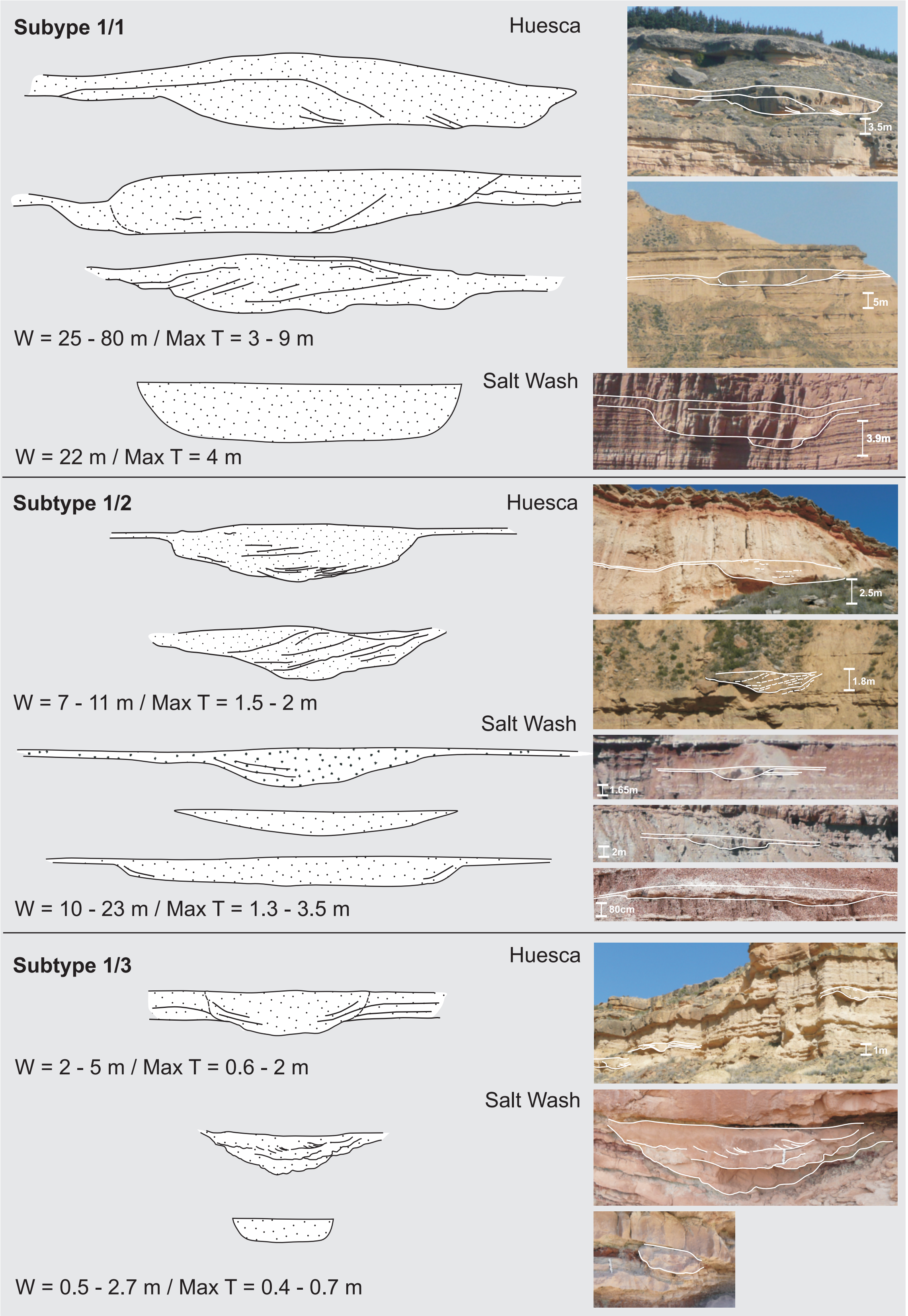

Figure 5.1. Examples of the three subtypes of Type 1 sandstone bodies in the Huesca and Salt Wash DFS successions. Actual width and maximum thickness ranges have been measured in the field and from photo mosaics. Schematic sandstone body representation is not to scale (white scale bar is 15 cm).

5.2.2. Type 2

Sandstone bodies of Type 2 consist of St, Sh, Sis, His and Slc facies, and were deposited by laterally unstable channels with variable flow regime through the mechanism of downstream and lateral accretion of bars on the channel flow (Moody-Stuart, 1966; Allen, 1965, 1982; Puidefabregas, 1973; Miall, 1985). The W / T ratio of Type 2 sandstone bodies varies between 20 and 320, where top value is usually limited by outcrop length. The thickness of the sandstone bodies is greater than 2 m. The sandstone bodies are characterised by scoured or flat bases and flat or gradational tops (Fig. 5.2). Three subtypes were distinguished on the basis of variations in shape and dimensions.

Subtype 2/1 sandstone bodies have flat bases and gradational or flat tops and consist of facies St, Sis and His and are characterised by inclined accretion surfaces. The sandstone bodies have thicknesses from 2 - 4.5 m and widths from 60 – 350 m. Subtype 2/1 was interpreted to be formed by lateral migration of bars in laterally migrating channels (Moody-Stuart, 1966; Allen, 1965, 1982; Puidefabregas, 1973; Miall, 1985). The flat bases of the sandstone bodies indicate an absence of incision after initial scour has been formed; only lateral erosion of the channel bank occurred.

Subtype 2/2 sandstone bodies are characterised by flat tops and scoured bases which have thick middle parts and thin laterally in steps. The thickness and width of the sandstone bodies ranges from 2 to 10.5 m and from 120 to 900 m, respectively. Outcrops length limits the maximum values of the width, whereas erosion within the amalgamated sandstone body complexes makes it difficult to measure the original thicknesses of single bodies. The sandstone bodies of subtype 2/2 do not show obvious LA surfaces and are mainly made up of Slc, St, Sh and Sr facies. However, large-scale LA surfaces could be present but obscured by smaller-scale sedimentary structures (Chapter 4). The exception is the sandstone bodies of the Little Park outcrop of the Salt Wash succession which consist of facies St, Sis and His and are characterised by clear LA surfaces (Fig 4.6, F).

Similarly to the subtype 2/1, subtype 2/2 sandstone bodies are also interpreted to be formed in laterally unstable channels by downstream and lateral accretion of bars. It appears, however, that channel flow was initially confined and became more laterally unstable with time. This is based on the observation that thickness of the sandstone body changes from its middle part to its edges.

Subtype 2/3 sandstone bodies are characterised by thicknesses similar to subtype 2/1 (2 - 4.5 m), but smaller widths (30 – 60 m). The main facies comprising the sandstone bodies are Sis and His facies which are enclosed by finer-grained floodplain facies. The sandstone bodies have scoured bases and flat or gradational tops. They are also

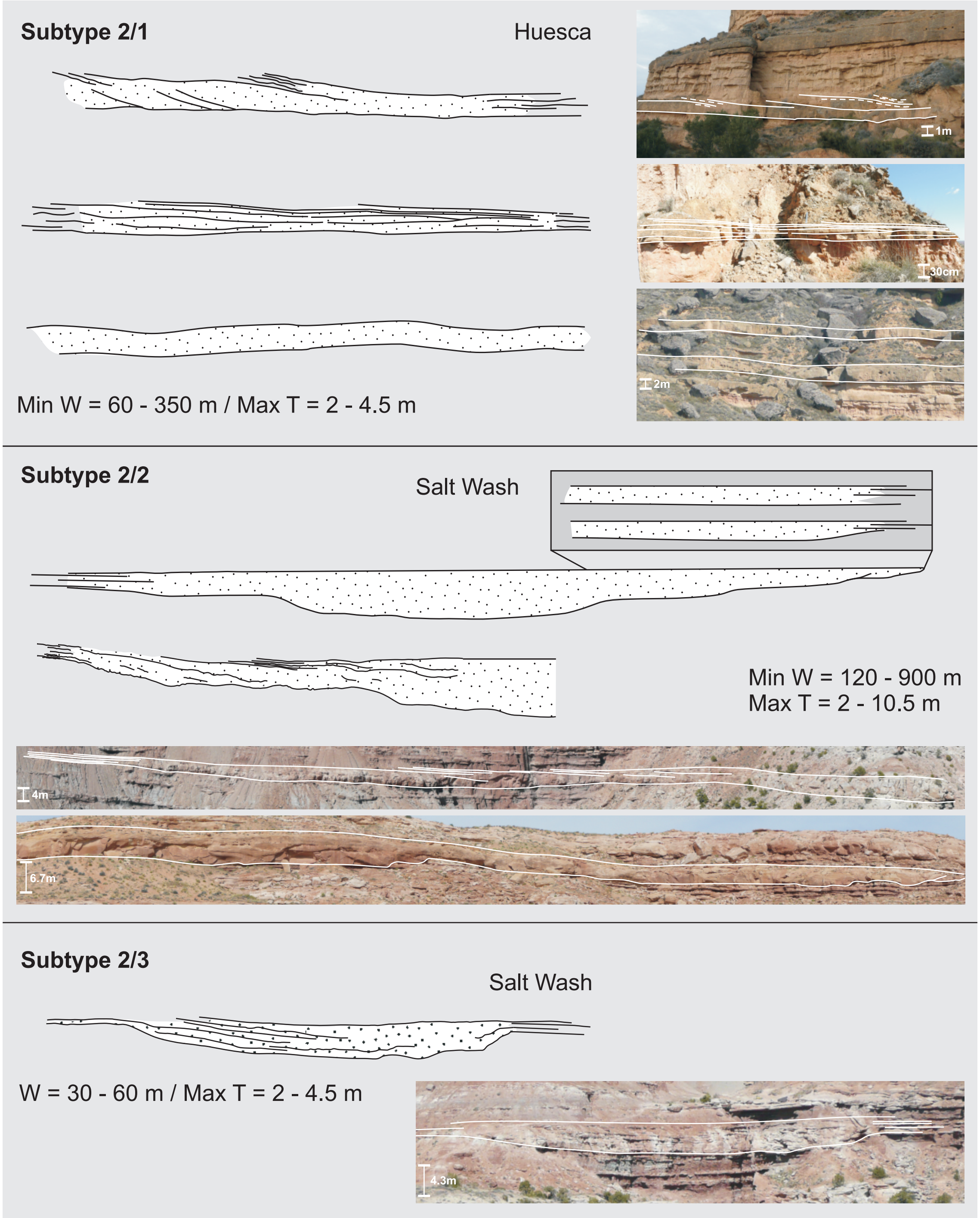

Figure 5.2. Examples of sandstone bodies of Type 2 in the Huesca and Salt Wash DFS successions. Actual and minimum width and maximum thickness ranges have been measured in the field and from photo mosaics. The schematic sandstone body representation is not to scale.

the product of lateral migration of bars within a channel as LA surfaces were observed (Chapter 4). The smaller width of the sandstone bodies indicates that they were formed in more laterally stable channels than channels forming sandstone bodies of subtype 2/1 and 2/2 that could be due to formation in a more cohesive substrate (Hirst and Nichols, 1986; Hirst, 1983; Nadon, 1994).

5.2.3. Type 3

The third sandstone body type is made up of facies Ssh and Hsh and is interpreted to be a product of the poorly confined and unconfined flow either on the floodplain next to a channel, or on top of a bankfull filled channel, or at the channel mouth where flow becomes unconfined on a low gradient plain (Ghosh et al., 2006; Fisher et al., 2007(a), 2008; Bristow et al., 1999; Sheets et al., 2007). In the response to these processes lateral or terminal splays are formed (North and Davidson, 2012). The difference between the width and thickness of the sandstone bodies is large giving W / T ratios between 30 and 1300. The ratios could be affected by lack of exposure and limited outcrop width. In contrast to the Type 2, thickness of the majority of the Type 3 sandstone bodies is less than 2 m (Fig. 5.3). Three subtypes could be distinguished based on the sandstone bodies shape and characteristics.

Subtype 3/1 sandstone bodies have wide shallow scours at the base, flat tops and are 0.7 – 2 m thick and 40 – 300 m wide. They are represented by facies Ssh. These sandstone bodies were formed by poorly confined flow in proximal to the channel part of lateral or terminal splays where flow was still strong enough to erode underlying deposits (Ghosh et al., 2006; Fisher et al., 2007(a), 2008; Bristow et al., 1999; Sheets et al., 2007).

Subtype 3/2 sandstone bodies incorporate facies Ssh and sandy beds within facies Hsh. These sandbodies have smaller thickness than subtype 3/1, which is between 0.1 - 1.3 m, but could be traced laterally for up to 500 m. Some of the sandstone bodies show localised scours at their base and all of them thin laterally. The subtype 3/2 sandstone bodies are interpreted to be formed by unconfined flow on a competent floodplain surface (Fisher et al., 2007(a); Bristow et al., 1999). Their smaller thicknesses, finer grain size and mostly flat bases suggest a relatively more distal location from a channel than has been interpreted for the subtype 3/1.

Subtype 3/3 sandstone bodies have convex-up tops and flat bases. Their widths and thicknesses vary between 20 and 480 m and 0.5 and 1.9 m, respectively. Some sandstone bodies of subtype 3/3 have two convex-up parts next to each other (Fig. 5.3). The convex-up sandstone bodies could either be deposited by unconfined flow in splays (Cloyd and Cemicco et al., 1990) or represent small-scale point bars formed in

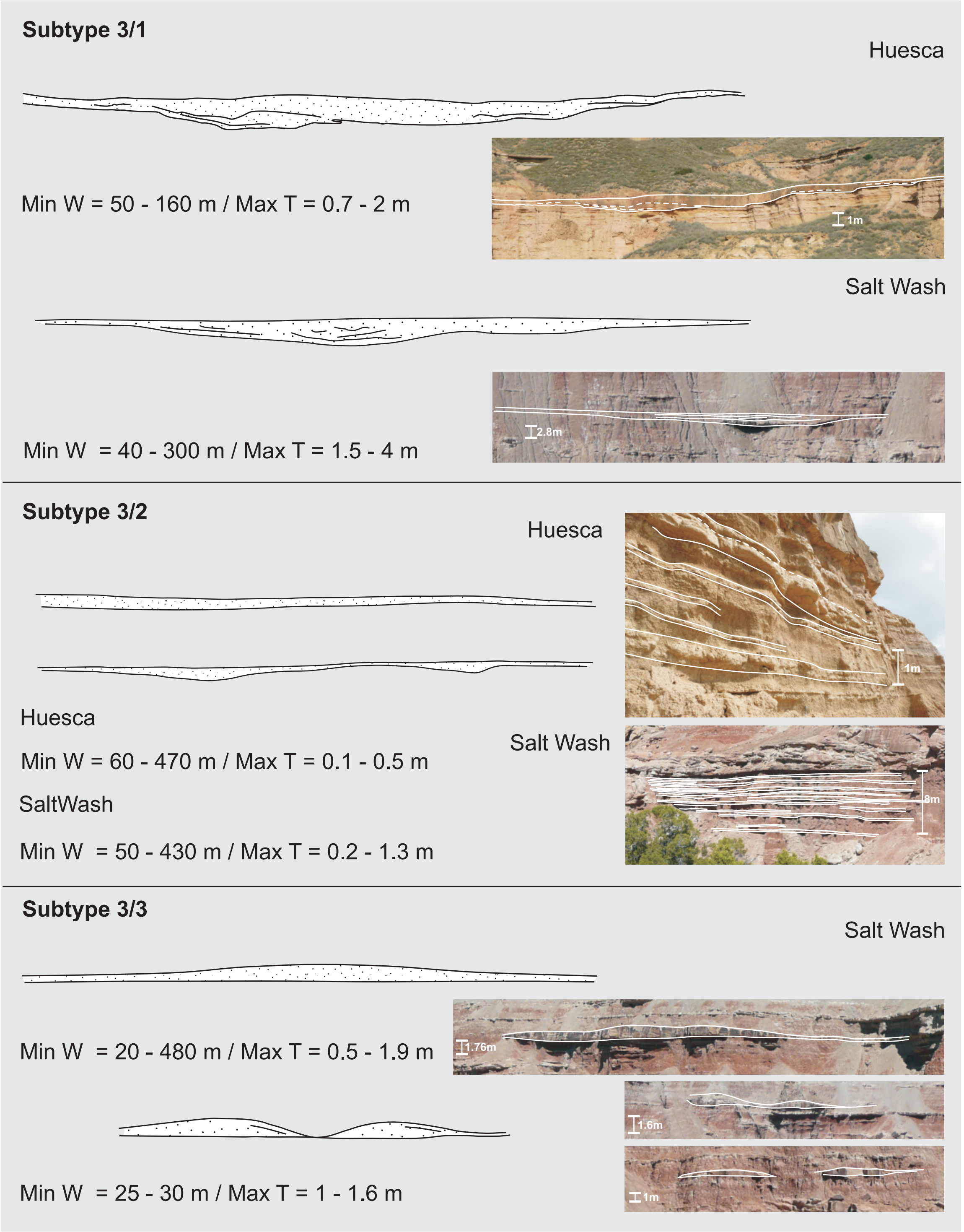

Figure 5.3. Examples of two subtypes of Type 3 sandstone bodies in the Huesca and Salt Wash DFS successions. Minimum width and maximum thickness ranges have been measured in the field and from photo mosaics. The schematic sandstone body representation is not to scale.

wide sinuous ephemeral channels on the floodplain or alluvial plain. In places the bars consist of heterolithic deposits of subfacies His3 where LA surfaces have been observed (Fig. 4.9, I). The bars retain their convex-up shape because the channel scour next to them is filled with fine-grained deposits of the facies Hm (Donselaar and Overeem, 2008). The preservation of the scour is defined by the frequent abandonment of such channels which is controlled by flooding events.

5.2.4. Sandstone body dimensions

The dimensions for three sandstone body types can be represented on width to thickness plots. Although the sandstone body types appear to form distinct fields that differentiate them (Fig. 5.4, A-C), there are two intermediate subtypes that lie in overlapping fields: subtype 2/3 with widths less than 100 m and subtype 3/1 with thicknesses > 1 m and < 4 m (Fig. 5.4, C). These two subtypes are transitional members between Type 1 to Type 2 and Type 2 to Type 3, respectively. Although the sandstone body type division is based on both geometrical and process-based parameters they may show intermediate forms between types (Hirst, 1991), such as subtype 3/1 and 2/3 (Fig. 5.4).

5.2.5. Interpretation summary

The three types of sandstone bodies can be grouped into two categories: sandstone bodies formed in channels (Type 1 and 2) and sandstone bodies formed in an overbank setting (Type 3). The exception to this are the few sandstone bodies of subtype 3/3 which could have formed in shallow, small-scale channels on the floodplain/alluvial plain.

Type 1 sandstone bodies were formed in laterally stable channels with stable channel banks. In this case flow was confined within the banks and the scour was almost or entirely filled with sand. Subtypes 1/1 and 1/2 were formed in major DFS channels while subtype 1/3 was deposited in small channels or scours on overbank splays. Sandstone bodies of Type 1 have been observed in both DFS systems.

Type 2 sandstone bodies, in contrast, are a product of relatively laterally unstable channels. Lateral accretion surfaces observed in some of the sandstone bodies indicate lateral accretion on the point bars while their absence in others shows dominance of downstream accretion of in-channel bedforms and bar forms. Subtype 2/2 differs from the subtype 2/1 by its thicker middle part that could indicate expansion of the channel belt with time, as there are no erosional surfaces in the middle, deeper part, indicating later incision. Subtype 2/2 is characteristic of the Salt Wash DFS succession, while Subtype 2/1 is more common in the Huesca DFS successions.

A. The Huesca DFS succession

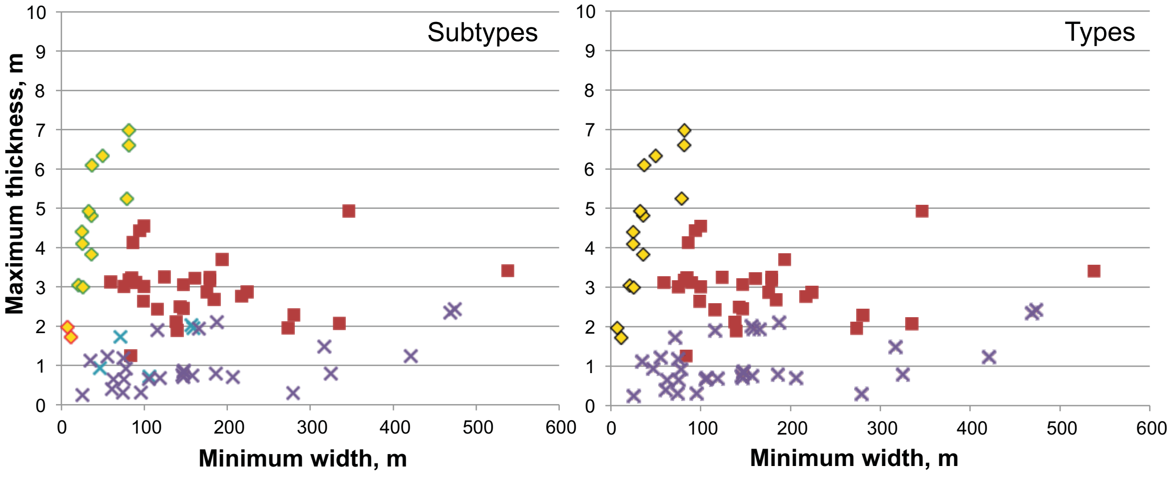

B. The Salt Wash DFS succession

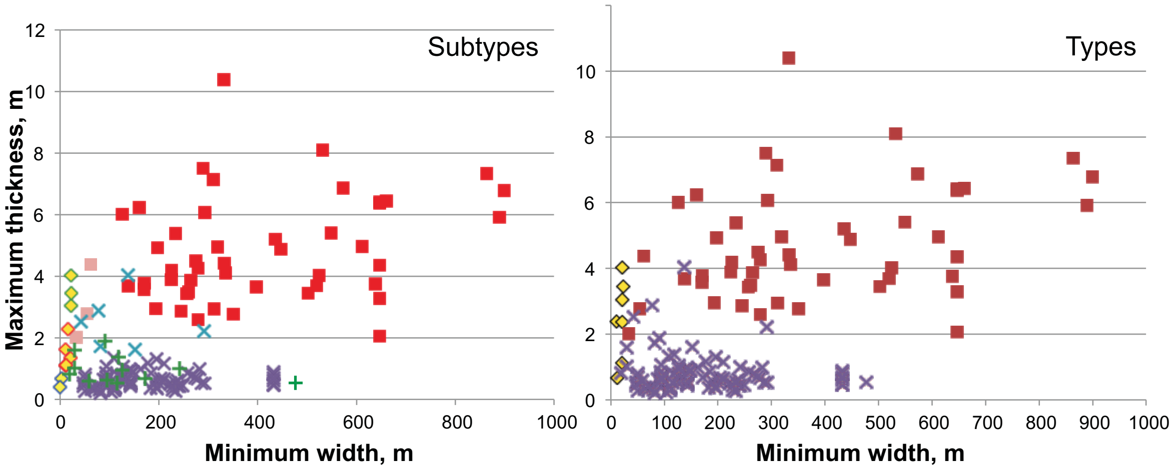

C. The Huesca and Salt Wash DFS successions

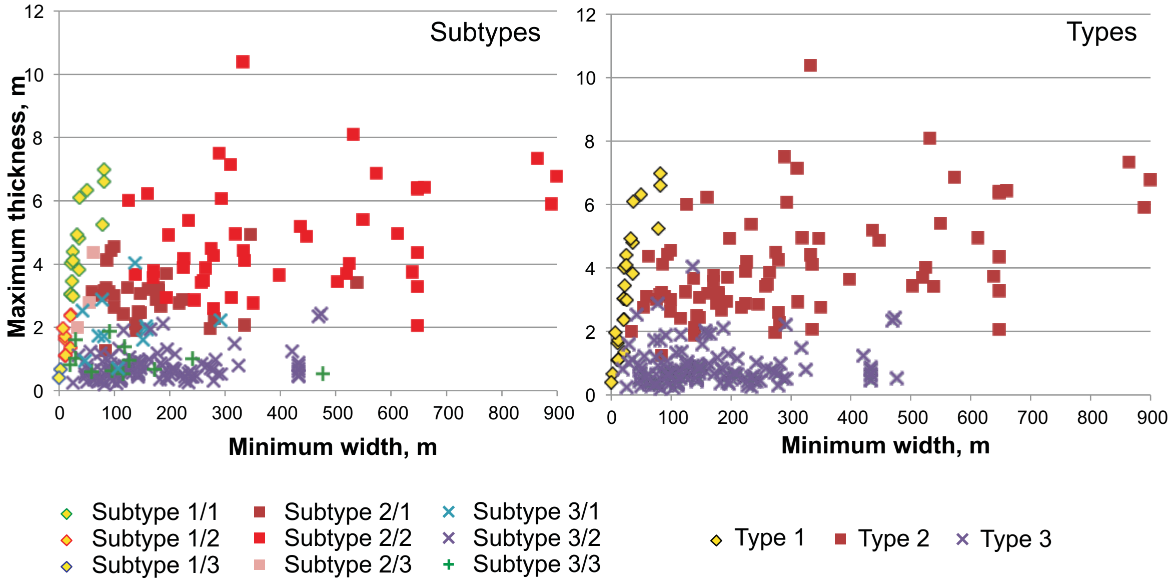

Figure 5.4. Width to thickness plots for sandstone body types and subtypes in the Huesca and Salt Wash DFS successions. A – the Huesca DFS successions; B – the Salt Wash DFS succession; C – combined data from the Huesca and Salt Wash DFS successions.

The smaller width of subtype 2/3 bodies shows that they were formed in more stable channels that were still migrating laterally, as indicated by the presence of LA surfaces. The stability of these channels may have been controlled by more cohesive substrate in the area where they were formed. These sandstone bodies have been observed only in the distal part of the Salt Wash DFS succession which is dominated by fine-grained deposits that is consistent with this interpretation.

Type 3 sandstone bodies were formed in an overbank setting by poorly confined or unconfined flow including lateral and terminal splays (subtype 3/1, 3/2 and 3/3) and wide poorly confined channels with thin, wide point bars (subtype 3/3). Poorly confined forms of sandstone sheets (subtype 3/1) represent the most proximal splays where flow is still capable of eroding the underlying deposits. Thinner sheets (subtype 3/2) formed further from the channel or were the result of less powerful floods.

5.3. Sandstone body relationships and amalgamation complexes

The sandstone bodies of different types and subtypes represent the simple elements of the DFS architecture and are also found to be organised into various sandstone body amalgamation complexes.

5.3.1. Subtype 1/2 and Subtype 3/2 amalgamation complex

Subtype 3/2 sandstone bodies were observed overlying sandstone bodies of subtype 1/1 or 1/2 forming a continuous top cap to the isolated sandstone lens (Fig. 5.5, A-E). Some of these sandstone body complexes are characterised by a convex-upward top (Fig. 5.5, C).

Type1 - Type 3 amalgamation complexes were formed as the result of aggradation of the channel to its bankfull level followed by unconfined flow across the channel scour resulting in deposition of a sand sheet on top of the filled scour (Sheets et al., 2007) (Fig. 5.6). Subsequent flow is diverted (avulses) away from the positive topography to create new channel on the floodplain (Fig. 5.6, C-C’).

Channel blocking with sediment has been described as one of the main causes of bifurcation and subsequent avulsion (Kelly and Olsen, 1992; Slingerland and Smith, 1998; Jones and Schumm, 1999; Field, 2001; Bridge, 2003; Smith et al., 1989; Morozova and Smith, 2000; Stouthamer and Berendsen, 2001). Accretion on the channel floor leading to its fill to the bankfull level and subsequent flow avulsion was interpreted as the main cause of the development of “ribbon sandstone bodies” of similar dimensions from the Casper Formation of Guadalupe-Matarranya fluvial system (Martínez et al., 2010).

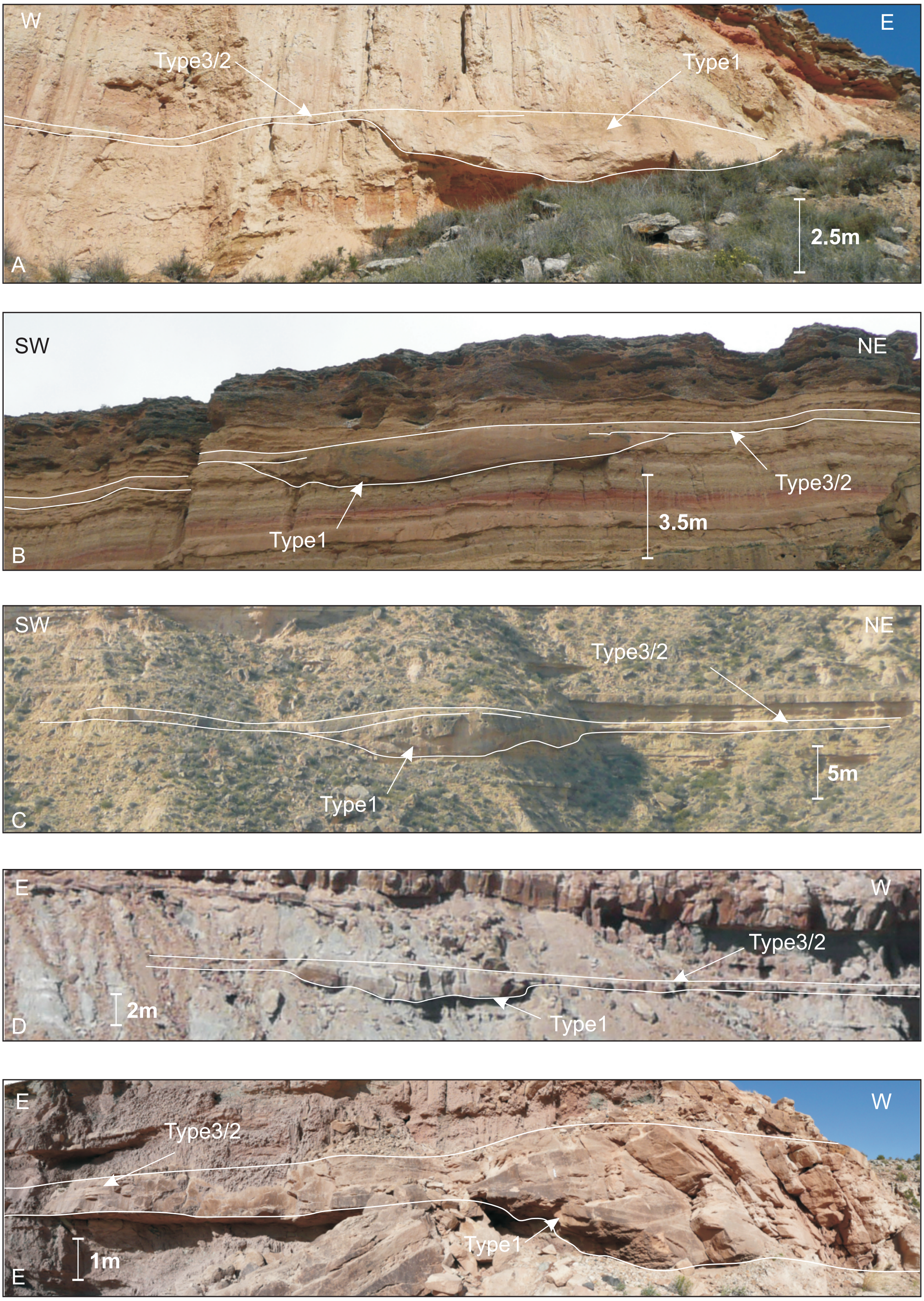

Figure 5.5. Examples of relationships between sandstone bodies of subtype 3/2 and subtype 1/1 and 1/2. A - Alcolea and B, C - Castelflorite outcrops of the Huesca DFS succession; D, E – Little Park outcrop of the Salt Wash DFS succession.

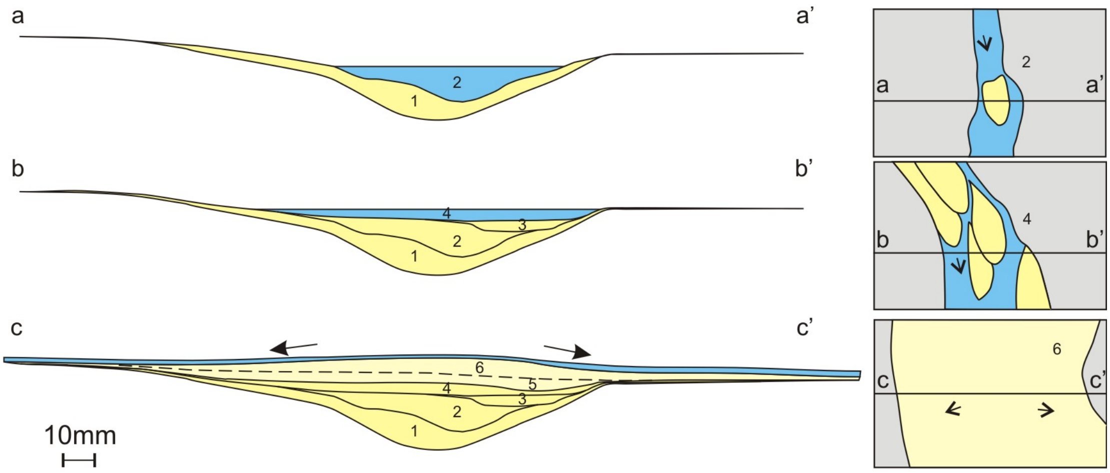

Figure 5.6. Evolution of the channel and formation of Type 1 sandstone body overtopped by sheet-like sandstone body of subtype 3/2. In-channel aggradation follows by channel blockage and spread of unconfined flow depositing sand sheet on top of the bankfull-filled channel scour. The resulting convex-up topography will divert the flow away to another location (modified after Sheets et al., 2007).

5.3.2. Amalgamation complex of Type 3 sandstone bodies

Intervals of the overbank deposits (up to 2 m thick) include abundant sandstone bodies of subtype 3/2 which all have similar dimensions and grain size and are considered to represent similar splay events. Individual sandstone bodies can be amalgamated in up to 1.5 m thick packages. These packages are characterised by variable mudstone to sandstone proportions (Fig. 5.7, A-E). Amalgamation complex may include scour-like sandstone bodies of subtype 1/3 cutting into a sandstone body package (Fig. 4.13, E) and small heterolithic point bars (Fig. 4.9, I). The proportion of mudstone sheets in the packages and the thicknesses of the packages varies laterally, as individual sandstone sheets pinch out (Fig. 5.7, C).

Amalgamated packages of sandstone bodies of subtype 3/2 were formed on overbank splays by multiple unconfined flows triggered by flooding events. Unconfined flow in splays concentrates into small-scale channel networks (Smith et al., 1989) which when filled with sand form sandstone bodies of subtype 1/3. A decrease in the proportion of sandstone bodies and an increase in mudstone interbeds were caused by deceleration of the flow and qualitatively indicate distance from the channel (Bristow et al., 1999; Fisher et al., 2007(a)).

These very continuous packages together with paleosol intervals of facies Hm are similar to the deposits described as “simple paleosol” packages in the Willwood formation in Wyoming, USA (paleosols, sheet-like sandstones and small lenses of sandstones formed in small channels). These deposits were interpreted as “avulsion deposits” formed on the floodplain during channel avulsion process (Kraus, 1996;

Kraus and Wells, 1999). Avulsion style in this case is called “avulsion by splay progradation” (Mohrig et al., 2000; Slingerland and Smith, 2004; Smith et al., 1989).

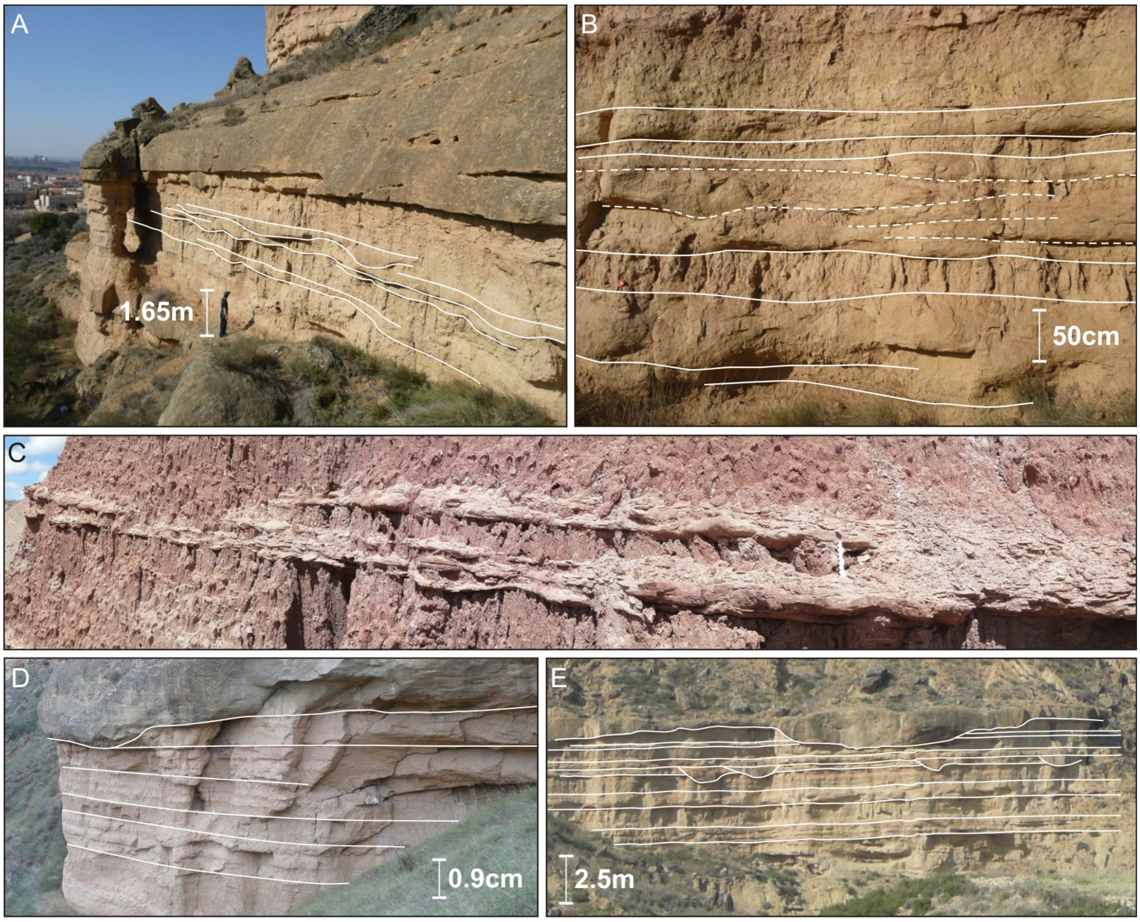

Figure 5.7. Examples of amalgamated sandstone bodies of subtype 3/2. A, B, D – Monźon outcrop of the Huesca DFS succession, C – Little Park outcrop of the Salt Wash succession, E – Castelflorite outcrop of the Huesca DFS succession (note four small sandstone bodies of subtype 1/3 cutting into the sandstone body package) (white scale bar is 15 cm).

Slingerland and Smith (2004) emphasised that only a small proportion of the floodplain deposits is represented by deposits formed during short flooding events and only thin very fine suspended sediment is preserved (Gomez et al., 1995). Dominance of the deposits generated by overbank events, including crevasse splays and avulsions, which fill depressions on the floodplain, over deposits accumulated during floods was observed in the overbank deposits of the Mississippi River by Aslan and Autin (1999). Kraus and Wells (1999) stated that up to 50 % of floodplain deposits are formed during avulsion events. Although this is possibly true, it is quite difficult to distinguish between deposits either formed by single flood or deposits formed by splay which did not lead to avulsion or deposits of avulsion splays, because even avulsion splays are formed by multiple flooding and splaying events. Furthermore, levee deposits have not been observed in the studied successions that could suggest different mechanism of splay formation, not crevassing. In this thesis these deposits would be referred as splay deposits. This subject will be discussed in detail in Chapter 9 where floodplain deposits of the Huesca DFS succession are studied in relation to avulsion process.

5.3.3. Relationship of Type 1 and 2 sandstone bodies with Type 3 sandstone bodies

Subtypes 1/1 and 1/2 and Type 2 sandstone bodies may truncate or pass laterally into the sandstone bodies of Type 3 or into amalgamation complexes of sandstone bodies of Type 3 (Fig. 5.8, A-J). The cross-cutting relationships show incision of channel flow into the floodplain deposits, while the gradational relationships indicate that sandstone bodies of Type 3 were formed by unconfined flow initiated from a channel bank during flooding and/or avulsion events.

5.3.4. Large amalgamated sandstone body complexes

The sandstone bodies of Type 2 are usually organised in large amalgamated sandstone body complexes, which might also include sandstone bodies of Type 1 and Type 3. Laterally amalgamated sandstone bodies may split into individual sandstone bodies separated by lenses of heterolithic lateral accretion complexes (facies His), remains of fine-grained overbank deposits of facies Hm and Hsh and lenses filled with fine-grained deposits of facies Hm and Hsh (“clay plugs”) (Fig. 5.9, A-D). The individual sandstone bodies and their types within amalgamated complexes are difficult to distinguish because younger sandstone bodies are incised into older sandstone body complexes. Sandstone bodies in the studied successions are amalgamated both laterally and vertically.

Amalgamated sandstone body complexes are indicators of multiple channel avulsion events that resulted in reworking of pre-existing deposits by a new channel flow. Lenses of floodplain deposits and clay plugs are the remnants of overbank deposition during periods of channel abandonment between periods of channel activity.

In places, two-storey Type 1 sandstone bodies (Fig. 5.10, A) and vertically stacked sandstone bodies of Type 2 with stepped edges (Fig. 5.10, B-C) can be distinguished. Amalgamated sandstone bodies with stepped edges have been previously described to be an evidence of avulsion by re-occupation of pre-existing channel by Mohrig et al. (2000) or avulsion by incision or annexation by Slingerland and Smith (2004) and Martínez et al. (2010). In this process, flow reoccupies existing abandoned channel scour as it forms a depression on the floodplain. For example, such abandoned channels have been observed on the modern Kosi DFS (Chakraboty et al., 2010). The new flow may incise into the existing channel scour and preserved sandstone bodies (annexation, Slingerland and Smith, 2004). Finally, new sand bars are accumulated in the new channel forming second story sandstone bodies.

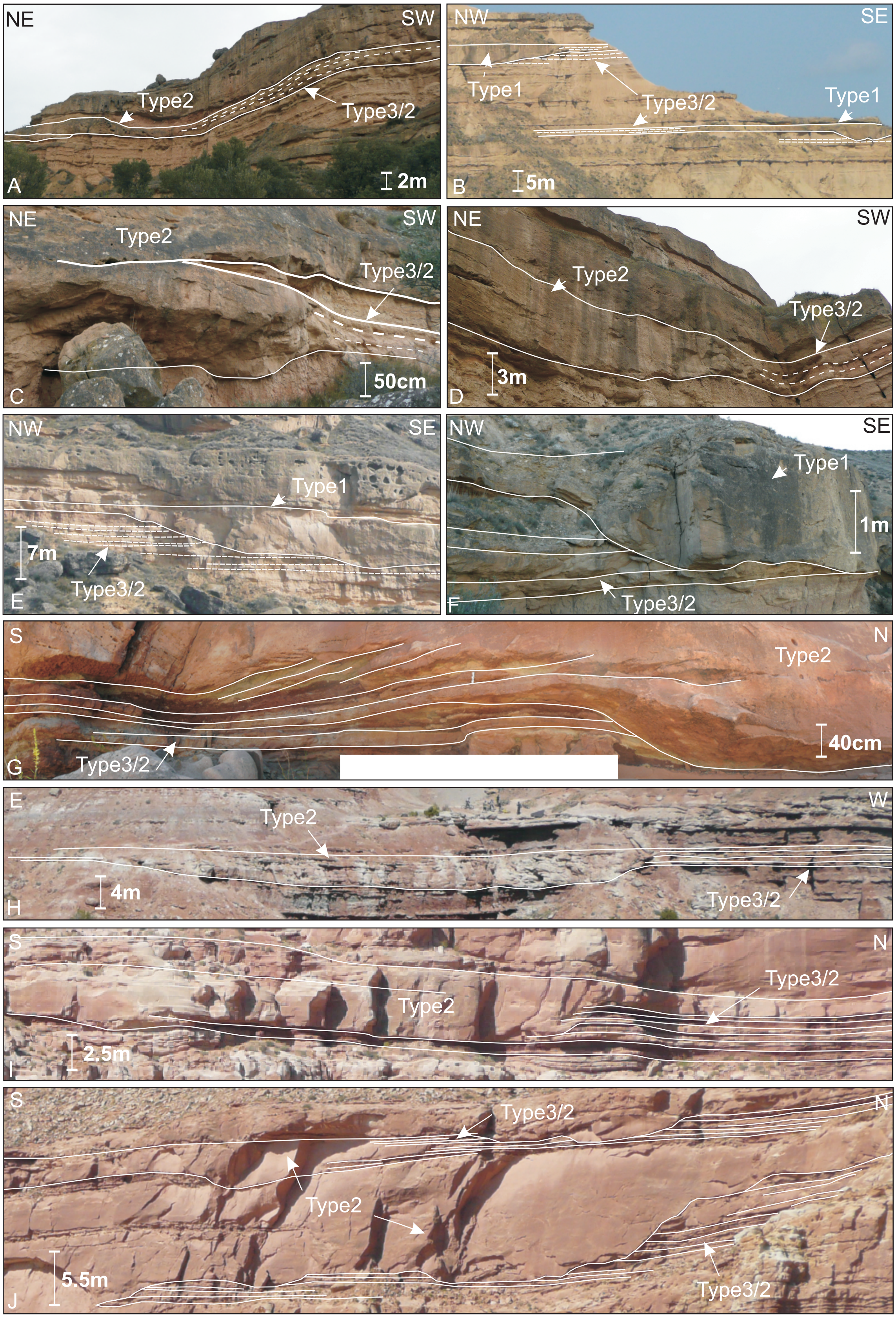

Figure 5.8. Examples of the relationship between channel sandstone bodies of Type 1 and 2 and sandstone bodies of Type 3 and their amalgamation complexes: A, B, C, D, G, H, I - gradational; E, F, J – truncational. A, C, D, E – Monźon and B, F – Castelflorite outcrops of the Huesca DFS succession. G – Little Park and I, J – Bullfrog outcrops of the Salt Wash DFS succession.

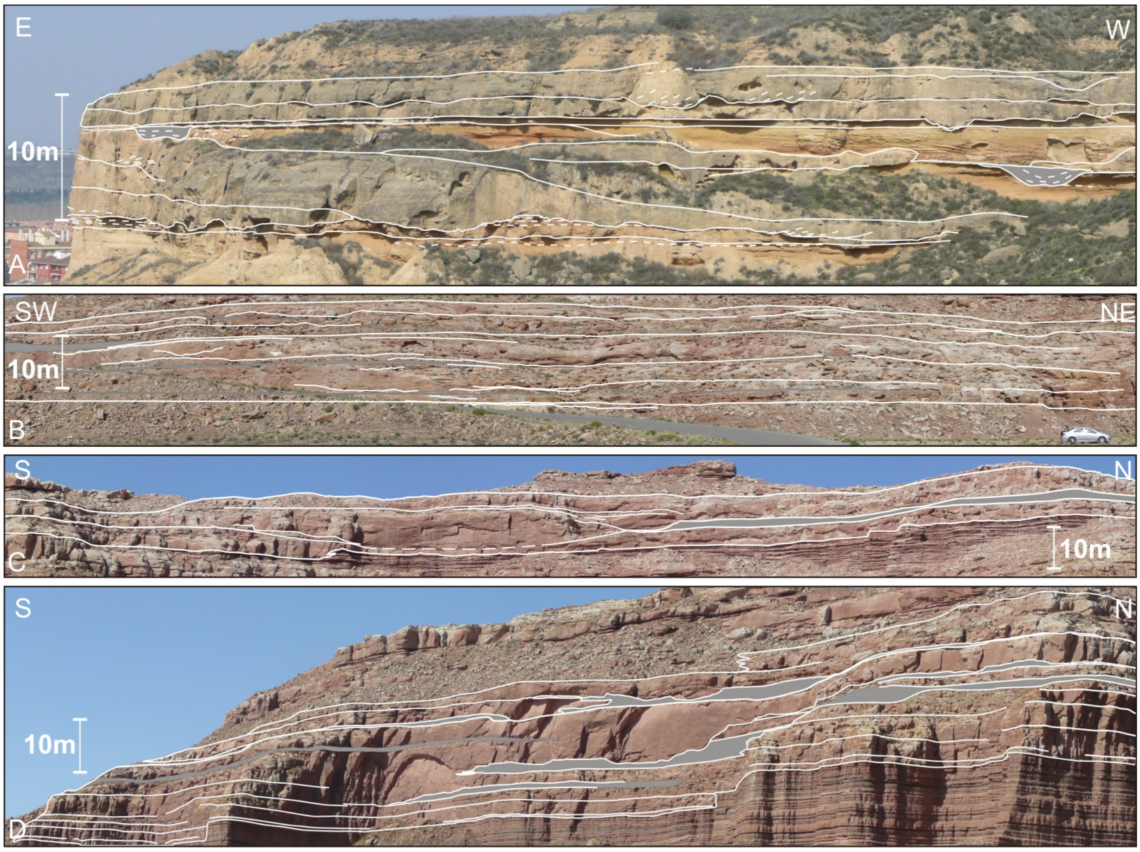

Figure 5.9. Examples of amalgamated sandstone body complexes: A – Monźon outcrop of the Huesca DFS succession and B, C, D – Bullfrog outcrop of the Salt Wash DFS succession. Grey lenses represent lenses of facies Hm and Hsh formed in abandoned channels or in overbank splays.

5.4. Avulsion – a mechanism of formation of sandstone bodies and their amalgamation complexes

Channel avulsion appears to be one of the major processes responsible for the formation of individual sandstone bodies and their amalgamation complexes. All amalgamated packages of sandstone bodies discussed above are formed as a result of channel avulsions. Avulsion events of different scales and styles control channel migration and therefore sediment distribution, erosion, transport and deposition, across a DFS. This process is recorded in sandstone body relationships between each other, and with fine-grained floodplain deposits.

For example, amalgamated sandstone body complexes and individual sandstone bodies intercalate with packages of floodplain deposits (Appendix 5) indicating that flow periodically avulsed to a new position on the floodplain and in-channel deposition was replaced by overbank deposition and vice versa. Multiple channel avulsions formed large amalgamated sandstone body complexes that are common in the relatively proximal outcrops of the studied DFS successions. “Clay plugs” associated with the sandstone bodies of Type 1 and 2 are another distinctive form of evidence for channel avulsion in the geological record: the scours represent abandoned channels left by the flow and subsequently filled with overbank fine-grained sediment (Donselaar and Overeem, 2008). Amalgamated packages of the sandstone bodies of subtype 3/2 that were observed attached to the channel sandstone body edge also partly originated from the channel during avulsion. The bankfull filled scours (subtype 1/2) overlain by sandstone sheets (subtype 3/1) in the studied DFS successions are the result of the continuous depositional process leading to the channel blockage and flow avulsion.

Avulsion is in turn governed by a set of climatic and tectonic factors. Avulsion styles and its controls will be discussed in the next chapters in general and considering specific geological setting of the Huesca and Salt Wash DFS successions.

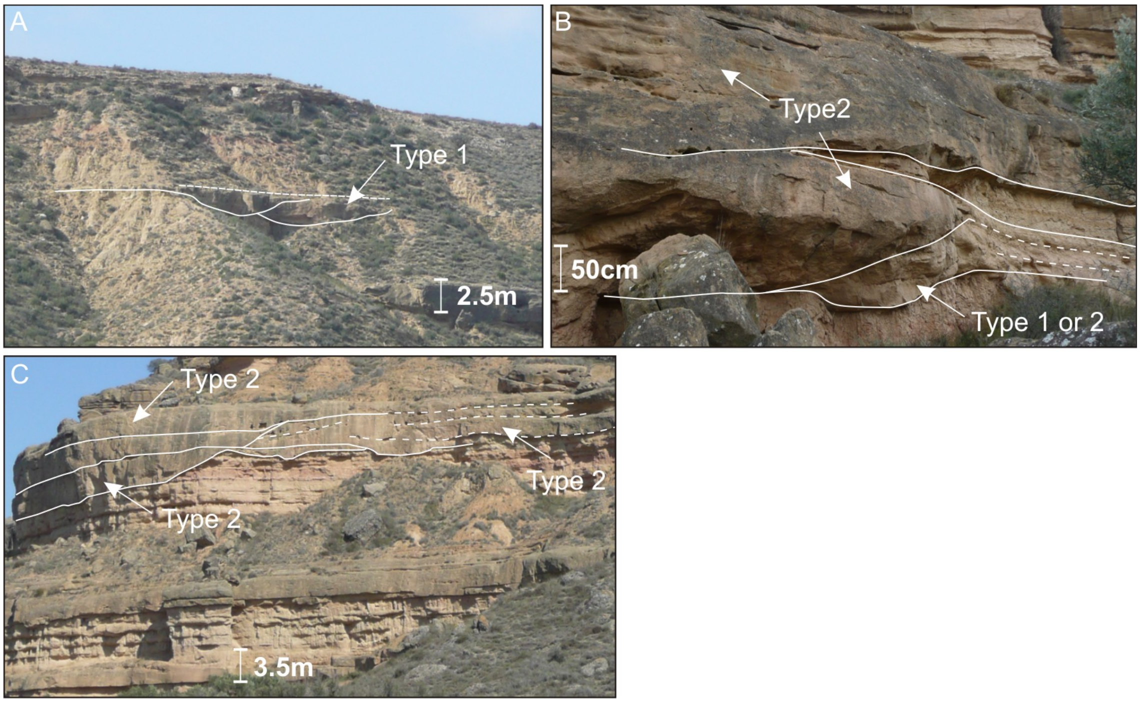

Figure 5.10. Examples of stacked sandstone bodies with stepped edges. A – Castelflorite and B, C – Monźon outcrops of the Huesca DFS succession.

5.5. Previous studies of the Huesca and Salt Wash DFS sandstone bodies

Detailed studies of sandstone body geometries and architecture have been carried out for the Huesca succession by Hirst (1983, 1991). Two sandstone body types have been distinguished based on their width to thickness ratio (classification by Friend et al., 1979) and type of depositional process; they are ribbon and sheet sandstone bodies. Three subtypes formed by channelised, poorly confined and unconfined flow have been differentiated within the second type. Simple, multi-storey/multilateral and amalgamated sandstone bodies have been also recognised. The classification is similar to the proposed classification in this research.

Studies of the Salt Wash sandstone body architecture have been focused on the Henry Mountain area that represents a relatively proximal part of the DFS (Robinson and McCabe, 1997; Kjemperud et al., 2008). Robinson and McCabe (1997) have distinguished single-storey and multi-storey sandstone bodies, where the latter include lenses of abandoned channel fill deposits (“clay plugs”) and intercalate with heterolithic overbank packages. Dimensions of individual sandstone bodies (W / T = 53 - 59) are comparable with the dimensions of Type 2 sheet-like sandstone bodies in the classification presented in this thesis. Channel sandstone bodies of Type 1 have not been recognised and overbank sandstone bodies were not studied by the authors. The width and thickness of entire heterolithic overbank complexes have been determined instead, and they vary from 10 to 1500 m and from 1 to 13 m, respectively.

Continuous outcrops of the relatively proximal Salt Wash DFS succession along the Water Pocket fold (near the Bullfrog outcrop) were studied in detail by Kjemperud et al. (2008). Four sandstone body types have been distinguished including steerhead distributary channels, crevasse channels, laterally amalgamated braided channels, and vertically aggradational braided channels. The first type was mainly observed in the Tidwell Member of the Morrison Formation and rarely in the Salt Wash succession and this is consistent with observations made in this study: the Type 1 was rarely observed in the Salt Wash DFS succession during this research. Sandstone bodies formed in crevasses splays and crevasse channels have been characterised and have similar dimensions to ones distinguished in the classification presented here. In the studies by Kjemperud et al. (2008) the large-scale braided channel sandstone bodies have been described as amalgamated complexes without distinguishing individual sandstone bodies.

The sandstone body classification and architecture studies by Hirst (1983, 1991), Robinson and McCabe (1997) and Kjemperud et al. (2008) have been based on the data from one DFS example. In this study two data sets from both the Huesca and Salt Wash DFS successions have been incorporated. Although the studies of the proximal portion of the Salt Wash DFS succession by Robinson and McCabe (1997) and Kjemperud et al. (2008) are detailed, they do not take into account downstream variations in sandstone body types and their relationships. In contrast, in this research three outcrops have been documented in apex to distal transect downstream the DFSs and consider sandstone bodies formed in different parts of the DFSs. In addition, significant attention is given to the relationships between sandstone bodies and their causes that have been discussed in detail above.

Although sandstone body types are generally similar to the ones determined by Hirst (1983, 1991) in the Huesca DFS succession, the classification divides three subtypes within each type and these individual subtypes indicate specific depositional processes. More importantly, individual subtypes are characterised by specific relationships with other subtypes and by characteristic distributions within the DFS and this is shown in the following two chapters.

This type of study has direct implication for reservoir architecture characterisation where shape, dimensions and distribution of sandstone bodies have to be predicted from limited subsurface data.

5.6. Limitations of the sandstone body classification

Despite the detailed analysis of data from two DFS successions, this study has its limitations. Firstly, although three outcrops have been studied in a downstream transect along both of the DFSs, lengths of the outcrops are small relative to the system scale and therefore there is a possibility that some sandstone body subtypes might have been missed, especially in the Salt Wash DFS succession. For example, continuous sandstone bodies of aeolian origin within the Salt Wash DFS succession (Bluff Member of Morrison Formation, Turner and Peterson, 2004) are not exposed in the studied outcrops and have not been included into the classification. Fluvial sandstone bodies interfingering with the contemporaneous aeolian sandstones (Turner and Peterson, 2004) could form large-scale good quality reservoir bodies. Additional studies of the aeolian sandstone bodies within a DFS setting are required.

Although the most proximal outcrops also have not been included in the study area due to lack of exposure and accessibility (Salt Wash DFS) and difficulty in establishing stratigraphic equivalent due to deformation (Huesca DFS), it is predicted that these areas would consist of Type 2 sheet-like sandstone bodies composed of coarser grain size (pebbly sandstones and conglomerates) than those in the relatively proximal Bullfrog and Monźon outcrops (cf. Peterson, 1994).

In addition, small-scale sandstone bodies (e.g. subtype 1/3) could have been missed due to the resolution of the photo mosaics. Small-scale sandstone bodies, however, do not contribute much to a reservoir volume and could be omitted for the purposes of large-scale studies. On the other hand they provide important sedimentological information about depositional processes on the DFS floodplain.

Secondly, exposure quality and outcrop length affect the measurements of sandstone body dimensions. Continuous sandstone bodies such as Type 2 and Type 3 are often longer than the outcrops or partly covered with scree or vegetation and therefore only a minimum width can be measured. In spite of this limitation, the difference in W / T ratios between sandstone body types is large enough to form a basis for distinguishing between them.

Furthermore, the high degree of sandstone body amalgamation, such as observed in the Bullfrog and Slick Rock outcrops of the Salt Wash DFS successions, makes study of geometries and dimensions of individual sandstone bodies difficult. To overcome this limitation, sandstone bodies, which could be relatively confidently recognised within the amalgamated complexes, have been used. These problems were previously pointed out in the discussion by Alexander (1993) where outcrops are considered to be reservoir analogues, and emphasised by Robinson and McCabe, 1997 in their sandstone body outcrop studies of the Salt Wash DFS deposits.

Thirdly, the classification is based on the Jurassic and Miocene DFS successions, when vegetation was abundant. Kelly and Olsen (1993) have pointed out that behaviour of channels and therefore geometries of sandstone bodies could have been different in DFSs formed before Devonian, where vegetation did not stabilise the banks. Thus, studies of older DFS successions are required to test the classification.

Finally, this research investigates sandstone body types and their relationships in two DFS successions which were deposited in slightly different climatic setting. The Huesca DFS was formed in a temperate climate (Hamer et al., 2007(a), (b)), in an internally drained foreland basin (Nichols, 2011), while the Salt Wash DFS was developed in semi-arid climate (Demko et al., 2004) in shallow, large, open “incipient foreland basin” (Robinson and McCabe, 2008). Although the classification of sandstone bodies was found applicable to both studied DFS successions, it requires additional testing on other ancient examples of DFS deposits formed in geological settings contrasting to the settings in these study areas.

5.7. Discussion of applications of the sandstone body classification to DFS deposits formed in different climatic settings

In this section the applicability of the classification to deposits of DFS formed in different climatic settings is considered. The sandstone body types are compared to the architectural elements of DFS successions previously described in the literature. The Organ Rock Formation, SE Utah, USA, the Camargo Formation in central Andes, Southern Bolivia and the Fort Union Formation, Wyoming, USA were chosen to represent examples of DFS deposits formed in the dry to humid climate range.

5.7.1. Comparison with the Organ Rock Formation (dry climate)

The Permian Organ Rock Formation represents deposits of a terminal distributary fluvial system (“terminal fan”, Friend, 1977) which developed under an arid climate in the Paradox foreland basin (“dryland fluvial system”, Cain and Mountney, 2009, 2011). The extent of the fluvial deposits of the formation is comparable with the dimensions of the Salt Wash DFS (200 - 300 km in radius, Chapter 2). Cain and Mountney (2009) provided a detailed analysis of the proximal to distal architecture of fluvial-aeolian deposits that can be used to test the proposed sandstone body classification. Nine architectural elements have been distinguished in the deposits of the Organ Rock Formation including six elements formed by fluvial processes (F1-6) and three by aeolian processes (A1-3). Only fluvial sandstone elements F1 to F5 are discussed here.

Individual sandstone bodies within amalgamated channel-fill element (F1) have similar facies associations and sedimentary structures to the sheet-like sandstone bodies of Type 2 (subtype 2/2). Similarity of structures suggests that the same depositional processes occurred in the channels. The dimensions of individual bodies are not provided in the paper because sandstone bodies are truncated by overlying sandstones within amalgamated complexes. However, from the scaled figures provided (Fig. 5 in Cain and Mountney, 2009) the minimum width of the individual sandstone bodies is similar to the width of the Type 2 sandstone bodies (~ > 250 m), whereas their thickness is at the lower boundary of the Type 2 sandstone bodies (~ 2 - 2.5 m). Low-angle LA surfaces within the sandstone bodies of the F1 element indicate lateral migration of bars within channels. Lateral accretion surfaces are also observed in the Type 2 (subtype 2/2), but they are not as pronounced. The amalgamated channel-fill element of Cain and Mountney (2009) in turn corresponds to large amalgamated sandstone body complexes of the Salt Wash DFS succession which were formed due to multiple channel avulsions and reworking (Section 5.3). Process interpretation given for the F1 element is identical to one for the Type 2 sandstone bodies and their amalgamation complexes.

The second element is ribbon channel-fill element (F2) consisting of horizontally or low-angle cross-bedded fine-grained sandstones. The thicknesses and widths of the element is 7 - 8 m and ~ 200 m, respectively. The closest sandstone body type is Type 1 (subtype 1/1) which has a similar shape, depth of erosion and thickness. These characteristics indicate that erosion processes during formation of the channel scour in both cases were similar. Initial high-energy event incised into underlying deposits, usually floodplain facies, forming the characteristic scour shape, subsequently channel banks remained stable or partially widened during the channel fill stage. The facies association in the F2 element, however, differs from the facies of the subtype 1/1 sandstone bodies (trough cross-bedding of facies St) and matches facies of subtype 1/2 sandstone bodies (concentric layering, facies Sil). The ribbon channel-fill element of the Organ Rock Formation was interpreted to represent deposits laterally stable channel filled to its bankfull level before avulsion. This interpretation is similar to the interpretation in this study of the facies Sil representing sandstone bodies of subtype 1/2.

The width of the F2 element is twice as high as the width of subtype 1/1 sandstone bodies and ten times wider than subtype 1/2 sandstone bodies observed in the Huesca and Salt Wash DFS successions. The higher width of the subtype 1/2 sandstones could be possibly related to lack of vegetation due to dry conditions in the Paradox Basin and therefore less cohesive substrate where channel could incise more easily. In contrast, Salt Wash and Huesca DFS have been interpreted to be formed in vegetated and possibly relatively more humid environment, where banks in the distal area of the system could have been more cohesive.

Packages of amalgamated sandstone bodies of Type 3 (subtype 3/1 and 3/2) described in this research are comparable with fluvial sheetflood sandstone element F5, represented by alternating horizontally laminated and ripple cross-laminated and massive sandstones and massive and horizontally laminated siltstones and mudstones. The dimensions of the element correspond well to the sheet-like geometry of Type 3 sandstone bodies: 1 to 3 m thick and more than 300 m wide. The sheetflood sandstone element was interpreted to form on the relatively flat floodplain surface or as a fill of abandoned scours (element F5 and F4, respectively) on a floodplain. The sediment was carried by an unconfined overbank flow from the side of a channel or from its termination. This interpretation provided in the paper is analogous to the interpretation given in this work for the sandstone bodies of subtype 3/1 and 3/2.

The intraformational granule-stone channel-fill element (F3), comprising 2 to 3 m thick and more than 50 m wide scours filled with massive very fine-grained mudclast-rich sandstone, was not observed in the Huesca and Salt Wash successions. The closest by shape and dimensions is the sandstone bodies of Type 2 (subtype 2/3) observed only in the distal part of the Salt Wash DFS succession and which represent deposits of relatively laterally stable channels.

Abundant mudclasts have been also observed in the sandstone bodies of subtype 2/2 and 2/3 in the distal part of the Salt Wash succession but they occur only in some cross sets within sandstone body and concentration of the mudclasts appear to be lower than in the F3 element. The high cohesiveness of the banks in the distal areas of the Salt Wash DFS could also prevent formation of channel fill deposits made up of intraformational granules and pebbles such as in the Organ Rock Formation.

In summary, all three types distinguished in the classification have their analogues in the Organ Rock Formation (Table 5.1). Depositional processes responsible for the formation of each element and sandstone body type corresponding to it are similar, including 1) bar migration in laterally unstable channels (Type 2 (2/2) and F1 element), 2) laterally stable channels representing bankfull channel fill (Type 1 (1/2) and element F2) and unconfined flow on the floodplain or alluvial plain (Type 3 (3/1, 3/2) and elements F4 and F5). Some differences, however, have been found in width and thickness ranges of the sandstone body types (widths in particular). The subtype 1/2 sandstone bodies could be wider than ones observed in the Huesca and Salt Wash DFS successions. The F3 element resembles sandstone bodies of subtype 2/3 by its dimensions but differs by composition and internal structures. Therefore alternative internal characteristics could be added to the subtype 2/3 and width range of the subtype 1/2 could be increased. These conclusions demonstrate that more studies of DFS strata formed in different settings are required to complete the classification.

Type	**Subtype**	**Sandstone body classification**	**Organ Rock Formation (Cain and Mountney, 2009)**	**Camargo Formation (Horton and DeCelles, 2001)**	**Fort Union Formation (Ayers et.al, 1986; Johnson and Pierce, 1990)**
Type 1	Subtype 1/1	W = 22 - 80 m, T = 3 - 9 m	W ~ 200 m, T = 7 - 8 m		W = 10 - 100 m, T = 1 -10 m
	Subtype 1/2	W = 7 - 23 m, T = 1.3 - 3.5 m			
	Subtype 1/3	W = 0.5 - 5 m, T = 0.4 - 2 m			
Type 2	Subtype 2/1	W = 60 - 350 m, T = 2 - 4.5 m			
	Subtype 2/2	W = 120 - 900 m, T = 2 - 10.5 m	W ~ > 200 m, T ~ 2 - 2.5 m	W ~ 200-500 m, T = 0.5 - 10 m	?
	Subtype 2/3	W = 30 - 60 m, T = 2 - 4.5 m			
Type 3	Subtype 3/1	W = 40 - 300 m, T = 0.7 - 4 m	W = > 300 m, T = 1 - 3 m		
	Subtype 3/2	W = 50 - 470 m, T = 0.1 - 1.3 m		W ~ 10s/100s m, T = 0.2 - 0.8 m	W ~ 500 m, T = 0.3 - 2 m
	Subtype 3/3	W = 20 - 480 m, T = 0.5 - 1.9 m			

Table 5.1. Comparison of sandstone body types and dimensions. Thickness represents maximum thickness of a sandstone body, while width is actual or minimum measured width of a sandstone body.

5.7.2. Comparison with the Camargo Formation (semi-arid to relatively humid climate)

The Cenozoic (Late Eocene – Miocene?) Camargo Formation was interpreted to have been formed in a wet, perennial fluvial depositional system (megafan) in the foredeep of the foreland basin at the eastern side of the Central Andes (Horton and DeCelles, 2001). A change from arid to humid climate has been reported in the late Miocene (Strecker et al., 2007 and references therein). The formation extent was approximately compared to the plan-view dimensions of modern megafans of the Chaco Plain (~ 150

- 250 km in radius) (Horton and DeCelles, 2001) that is similar to the Salt Wash DFS (200 – 300 km, Chapter 2). The authors have described five sedimentary facies of the proximal part of the fan which include three sandstone/conglomerate facies (facies 3, 4 and 5). The facies description, however, is not as detailed as for the Organ Rock Formation.

Facies of medium- to coarse-grained sandstones and sandy conglomerates (facies 4 and 5) compose continuous (~ 200 – 500 m) and thick (0.5 – 10 m) bodies which are comparable with the dimensions and composition of the Type 2 sandstone bodies. Both facies 4 and 5 and Type 2 (subtype 2/2) sandstone bodies are characterised by an erosional base, the presence of mudclasts, a similar grain size and sedimentary structures (trough cross-bedding, horizontal bedding and ripple cross-lamination), hence similar facies associations. Amalgamated Type 2 sandstone bodies were also observed in the Camargo Formation. The facies have been interpreted to represent a process of dune, bars and gravel sheet migration within large channels that is analogous to processes that have been interpreted for subtype 2/2 sandstone bodies, excluding gravel sheet migration, that could have occurred in the most proximal areas of the studied DFSs.

In contrast to the Salt Wash, Huesca and Organ Rock sandstone bodies of this type, LA surfaces have not been observed in the sandstone bodies of the Camargo Formation. As only the most proximal part of the DFS succession has been described by Horton and DeCelles (2001), sandstone bodies are highly amalgamated and LA surfaces can be obscured by other sedimentary structures such as trough cross-bedding or destroyed by subsequent reworking (Miall, 1985). In the relatively proximal part of the Salt Wash DFS succession amalgamated sandstone bodies lack LA surfaces as well as in the Camargo Formation. Inclined stratification, however, has been observed in relatively proximal Caineville outcrop (Fig. 4.6, I) that demonstrates that lateral accretion has occurred in channels of the Salt Wash DFS but evidences are obscured in the amalgamated sandstone bodies.

Conglomerate bodies of comparable geometry to facies 5 have been described in the most proximal Salt Wash DFS succession (Peterson, 1994) that could be analogues for the proximal conglomerates of the Camargo Formation. They can also be common for the most proximal part of the Huesca DFS successions. The proximal areas of the Salt Wash and Huesca successions, however, have not been studied in this research (chapters 2 and 3), but follow the logic above LA surfaces in the most proximal conglomerates have even higher chance to be reworked or obscured due to high degree of amalgamation and coarser grain size of the deposits, or did not form in coarse-grained sediment.

Thin (0.2 - 0.8 m) beds of fine to medium sandstones (facies 3) in the Camargo Formation were observed extending for tens to hundreds of metres. Flat bounding surfaces and horizontal and ripple lamination are characteristic of these sandstone bodies. The description resembles Type 3 sandstone bodies (subtype 3/2). Furthermore, sandstone bodies of facies 3 were found interbedded with siltstones forming packages similar to facies Hsh in the study areas considered here. Thin, continuous sandstone bodies of the Camargo Formation and Type 3 sandstone bodies of the classification presented in this study have been both interpreted to represent splay deposits formed by unconfined flow on the floodplain.

To sum up, both sandstone body types observe in the Camargo Formation could be described using the proposed classification (Table 5.1). The only difference that has been found is the absence of the LA surfaces in the facies 4 and 5 that could have been destroyed by a later reworking or obscured by other sedimentary structures and coarse grain size of the proximal deposits.

5.7.3. Comparison with the Fort Union Formation (humid climate)

Late Paleocene Fort Union Formation includes the coal-bearing Tongue River Member that was formed by fan-shaped fluvial systems on the flanks of the Powder River foreland basin in Wyoming / Montana, USA (Ayers et al., 1986). The fluvial systems were thought to have fed large perennial lakes in the middle of the basin (Ayers et al., 1986) or join an axial trunk river (Johnson and Pierce, 1990). The climate in the basin was interpreted to be humid, temperate to subtropical (Trotter, 1963; Hickey, 1980) where areas between channels were poorly drained due to a high water table (Johnson and Pierce, 1990). Jonson and Pierce (1990) distinguished five depositional facies within the distal succession of the fan which included three sandstone facies (Type A, B and C). The facies description for the Camargo Formation is less detailed that for the Organ Rock Formation.

Type A very fine- to fine-grained sandstones form lenticular, 1 to 10 m thick and 10 - 100 m wide bodies. Trough cross-bedding, ripple cross-lamination, mudclasts and plant debris are the main characteristics of the facies. The geometry of the sandstone bodies is close to the geometry of the Type 1 sandstone bodies (subtype 1/1 and 1/2). Similarly to Type 1, the sandstone bodies of the Fort Union Formation were interpreted to be formed in isolated channels encased in overbank deposits, in this case in a wetland setting. The channels were interpreted to change their position on the floodplain by avulsion. Absence of LA surfaces or associated “clay plugs” observed by Jonson and Pierce (1990) could indicate that channel scours in Powder River Basin have been almost filled to their bankfull level that facilitated avulsion. Stability of the channel banks and filling by vertical aggradation rather than lateral migration was probably controlled by the cohesiveness of deposits formed in poorly-drained and vegetated floodplain areas (Ayers et al., 1986) dominating the landscape in the basin ("grey mudrock facies" in Jonson and Pierce, 1990). Thick coal beds support the interpretation of channels' stability (Ayers et al., 1986). Sandstone bodies of Type 1 distinguished in this study were also formed in stable channels with similar behaviour. In addition, "wings", sheet-like thin sandstone bodies attached to the top edge of a channel sandstone body, were observed in the Fort Union Formation that supports the comparison of Type A with Type 1 sandstone bodies which show the same relationships with Type 3 sandstone bodies.

Type B silty, very fine- to fine-grained sandstones were described as thin, continuous sandstone bodies which intercalate with mudstones forming packages up to 5.8 m thick. Type C very fine- to fine-grained sandstones were reported to form tabular bodies of 0.3 to 2 m in thickness and up to 500 m in width. Both sandstones were characterised by small-scale trough cross-bedding, parallel bedding and ripple cross-lamination or more often are structureless (Johnson and Pierce, 1990). Type B and C sandstones were interpreted to represent levee and splay deposits on the floodplain. The characteristics of the sandstone bodies and interpretation correspond well to the description of Type 3 sandstone bodies (subtype 3/2) in the classification presented in this study. Type B sandstone packages can be compared to packages of interbedded mudstone and Type 3 sandstone bodies (facies Hsh).

Jonson and Pierce (1990) also observed amalgamated trough cross-bedded sandstone sheets with flat bases, but did not describe individual sandstone bodies within them. A concave-up base was the only characteristic mentioned in the description. The amalgamated complexes were interpreted to be the deposits of laterally migrating braided streams (Johnson and Pierce, 1990) and could perhaps represent amalgamated sandstone bodies of subtype 2/2; however, there is not enough information to support this suggestion.

To sum up, Type 1 and Type 3 sandstone bodies describe well three sandstone facies observed in the Fort Union Formation (Table 5.1). Amalgamation complexes of sandstone bodies in the fluvial deposits of the Powder River Basin depict exactly the same types of amalgamations observed in the Huesca and Salt Wash DFS successions; they are an amalgamation complex of Type 1 and Type 3 sandstone bodies ("wings") and an amalgamation of Type 3 sandstone bodies into packages.

The comparison of the DFS sandstone body types using published literature is limited by: 1) different areas of study relatively to the apex of a DFS (proximal part - Camargo Formations and distal part - Fort Union Formation), 2) different degree of detail of facies description provided by different authors, 3) inability to assess a quality of the exposure that differs between study areas and 4) limited possibility to compare sandstone bodies visually. Fieldwork would be preferable for such comparison.

In conclusion, Hartley et al. (2010(a)) showed that channel planform type in modern DFSs is not controlled by the climate in the basin and therefore sandstone body types may not necessarily be strongly controlled by climate. The results of the comparison show that this statement is more or less valid for the discussed DFS successions which all can be described using the proposed classification. However, few discrepancies have been found. More studies of DFS strata formed in different climatic settings are needed to investigate this further. In addition, although sandstone body types, which have been discussed in this chapter, are similar in DFS successions formed in different climatic settings, proportion of different types and their distribution along a DFS (from the apex to the basin) could vary.

5.8. Conclusions

In this chapter the classification of sandstone bodies in DFS successions and the processes of their formation has been introduced. Three sandstone body types are distinguished based on their dimensions, shape, facies associations and depositional processes. Several common amalgamation complexes of sandstone bodies are described and represent the products of the principle depositional processes, such as channel avulsion, which controls both formation of sandstone body in a channel and sandstone body distribution and relationships. In contrast to previous descriptions of DFS deposits, the proposed classification compiles data sets from two DFS successions representing relatively proximal to distal DFS areas and includes detailed descriptions and dimensions of every sandstone body type and its subtypes.

The limitations of the classification are mainly related to outcrop size relatively to DFS extent, outcrop position relatively to DFS apex, quality of exposure and degree of sandstone body amalgamation. In addition, studies of DFS deposits that were formed earlier than the Devonian should consider sandstone bodies formed in a non-vegetated environment.

This classification could be used, with some limitations and additions, for DFS successions formed in dry to humid climatic setting that was demonstrated on the examples of ancient DFS successions formed in different climates. Thus, the sandstone body classification, in general, summarises a set of depositional processes occurring on DFSs independent on the climatic settings; they are 1) downstream and lateral bedform and bar form accretion in laterally unstable major channels, 2) vertical aggradation and bedform accretion in laterally stable channels, and 3) deposition from poorly confined and unconfined flow on the floodplain and alluvial plain. Internal structure of the sandstone bodies, however, could vary. Importantly, a combination of sandstone body types, types of amalgamation complexes and proportions of each type within a DFS succession might vary and could be controlled by climatic and tectonics external factors.

Extensive studies of DFS successions formed in different geologic settings are required to account for all details of the architecture of DFS deposits, but classification presented here is the step towards development of unified detailed facies model and description of sandstone body architecture of DFS deposits. The ultimate sandstone body classification would provide data for prediction of possible sandstone body subtypes for reservoir modelling based on particular geologic settings of DFS strata. The current classification contributes to the database of outcrop analogues for DFS reservoirs.

The proportion of different sandstone body types and trends in their distribution within the Huesca and Salt Wash successions are discussed in the following three chapters.

6. The Huesca DFS succession

6.1. Introduction

This chapter summarises the main features of the Huesca DFS succession using a proposed facies and sandstone body classifications (chapters 4 and 5), and describes their variations laterally through the system. Interpretation of all the characteristics of the succession architecture and their variations make it possible to consider depositional processes on the Huesca DFS that will be discussed in Chapter 8. Previous work and geological setting for the Huesca DFS have been covered in Chapter 2. The locations of studied outcrops and field techniques have been described in Chapter 3.

6.2. Sandstones of the Huesca DFS succession

Sample locations, numbers and methods used for the analysis of the Huesca sandstones are presented in Appendix 2 and Appendix 3 Table 1.

6.2.1. Composition

On the basis of petrographic analysis of the sandstones the main grain types in the sandstones were recognised; and they include lithic fragments of mica-quartz schist, gneiss, igneous plutonic rocks, clastic sedimentary rocks and limestones, plus mineral grains of quartz, feldspar, mica (biotite, white mica, chlorite) and minor amounts of Fe oxides and heavy minerals (zircon, apatite, garnet, tourmaline, rutile, epidote, orthopyroxene(?), staurolite and kyanite(?)). Similar main mineral components were determined by X-ray diffraction; they are quartz, calcite, chlorite, muscovite or Illite, feldspars (orthoclase and albite), kaolinite and gypsum (Fig. 6.1; Appendix 3 Table 5).

For point counting purposes quartz grains were additionally divided into unstrained (Qm), strained (Qs) and polycrystalline quartz with sutured and polygonised contacts (Qp) (Appendix 4 Panel 1, A-C). Chert and quartzite (Appendix 4 Panel 2, D-E) were also counted separately from sedimentary rocks and polycrystalline quartz because of their different use in different sandstone classifications.

Plutonic rock fragments are thought to be fine-grained granodiorites (Appendix 4 Panel 3, E) which could be a source for grains of chloritised biotite (Hirst, 1983) (Appendix 4 Panel 3, A), feldspar and some of the quartz present. Feldspar grains are commonly altered to sericite but may show clear twinning characteristic of plagioclase (Appendix 4 Panel 1, D).

Schist fragments are characterised by a great variability of quartz and mica proportion between different grains (Appendix 4 Panel 2, B). A mica concentration threshold of either 10 % or 0 % was used to differentiate between lithic polycrystalline quartz fragments and clear polycrystalline quartz by Ingersol (1984). The second threshold was found by the author to be more satisfactory when describing the origin of fragments and sediment provenance (Ingersol, 1984). Accordingly the polycrystalline quartz with even small amounts of mica was counted in this study as lithic fragments. It is possible that the white mica, polycrystalline quartz and some of the strained quartz are the product of rock fragment breakage during transport.

Sandstones with clay, carbonate or Fe oxide cements represent clastic sedimentary rock fragments in the Huesca sandstones (Appendix 4 Panel 2, C). Detrital and crystalline limestones (Appendix 4 Panel 2, A) are also very abundant as lithic clasts of carbonate sedimentary rocks and together with the carbonate cement commonly comprise 20 – 40 % of the sandstone (Appendix 3 Table 6). Fossil fragments could be seen in some of detrital limestone fragments (Appendix 4 Panel 2, A, sample 2-21) which were interpreted to be fragments of foraminifera by (Hirst, 1983).

Oxidisation rims were observed around limestone grains (Appendix 4 Panel 3, D) and these rims make it possible to distinguish between limestone grains and calcite overgrowth cements (Appendix 4 Panel 4, C). Calcite cement was mostly found in places around limestone grains and grains next to them and this results in a non-uniform distribution of the cemented and porous areas (Appendix 4 Panel 4, B-D). However, one of analysed sandstone samples is entirely cemented with calcite (Appendix 4 Panel 4, E, sample 2-3) indicating an irregular distribution of porosity in the Huesca sandstones where one bed or part of the bed is more cemented than others (Appendix 4 Panel 4, D-F). Sample 3-2 is cemented by gypsum (Appendix 4 Panel 4, A) that is also supported by the XRD data from this sample (Appendix 3 Table 5). Oxides are present in form of cement in sandstone lithic fragments, as whole grains, and rims of grains (Appendix 4 Panel 3, D).

The proportion of heavy minerals as determined by counting was found to be 0.3 - 2.3 % (Appendix 4 Panel 3, B) whereas separation by heavy liquids indicates that 1 – 2 % of grains are heavy minerals (Appendix 3 Table 7). The latter concentration is higher due to mica and Fe oxides which separates together with heavy minerals.

A low matrix proportion was noted for the sandstones by (Hirst, 1983), however this study shows that up to 15 % matrix could be present. Matrix is mostly represented by very fine-grained schist fragments and mica which are squashed and crushed between harder grains (Appendix 4 Panel 4, G).

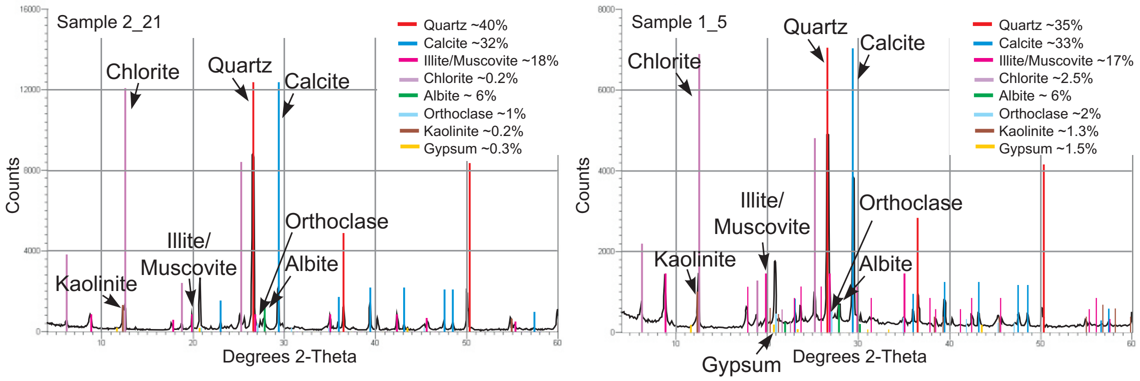

Figure 6.1. X-ray spectra for the sample 2-21 (coarse- to medium–grained sandstone) and sample 1-5 (siltstone) showing main mineral constituents of the Huesca DFS deposits.

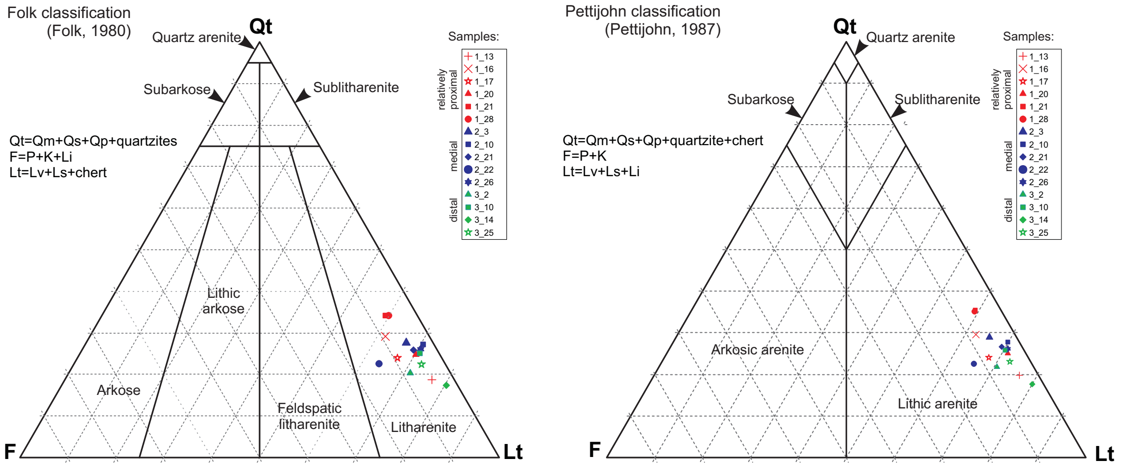

Figure 6.2. Classification of Huesca DFS sandstones using Folk and Pettijohn classification triangles (modified from Folk, 1980 and Pettijohn et al., 1987).

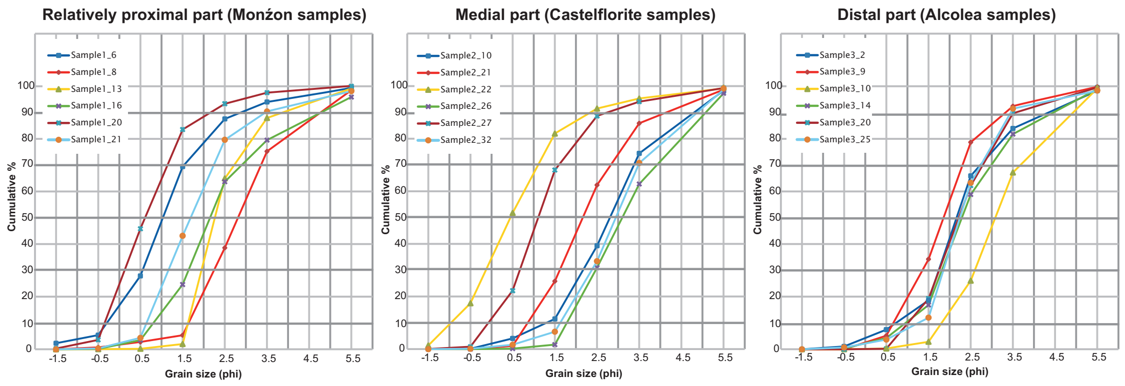

Figure 6.3. Cumulative curves for weight percentage of grain size fractions of the Huesca sandstones. A graphic method was used to estimate mean grain size value and sorting (Appendix 3 Table 2 and 3).

The percentages of the main grain classes obtained from the results of the point counting are presented in the Appendix 3 Table 4. Using the percentage of different grain types and the estimated matrix proportion sandstones were classified as lithic arenites using the (Folk, 1980) and (Pettijohn et al., 1987) classifications (Fig. 6.2). Following Pettijohn's classification, matrix-rich sandstones were classified as transitional class between lithic arenite and lithic wacke.

6.2.2. Grain size, roundness and sorting

Sandstones of the Huesca DFS are represented by a full range of sand grades which would have been determined by transport processes (facies), type of supplied sediment and distance from the DFS apex (source). The average grain size for the sandstone is 2 - 3 φ (0.25 - 0.125 mm) (Appendix 3 Table 3).

Quartz and feldspar grains are very angular and have square (Fsp), triangular or needle (Q) shape with sharp edges (Appendix 4 Panel 1, A, D), while schist/gneiss and limestone fragments are rounded or subrounded due to their lower resistance to mechanical breakage (Appendix 4 Panel 2, A-B).

Graphical analysis of grain size cumulative curves which are created based on sandstone sieving results (Fig. 6.3; Appendix 3 Table 2) showed that sandstones are mostly poorly sorted (STD = 1 - 2) to rarely moderately well sorted (STD = 0.5 - 0.71) (Appendix 3 Table 3).

6.2.3. Sediment source

The drainage area of the Huesca system was about 10^4 - 10^5 km^2 (Donselaar and Overeem, 2008) and separated from the drainage area of the adjacent Luna fluvial system to the west by the Boltaña anticline (Fig. 9 in Hirst and Nichols, 1986; Table 2 in Nichols and Hirst, 1998). Sediment was transported from Ainsa and Tremp-Graus basins and axial zone of Pyrenees (Fig. 6.4). A compilation of data from the geological map (Insituto Technlógico Geominero de España, 1994), the PhD thesis of (Hirst, 1983), papers by (Hirst and Nichols, 1986; Nichols and Hirst, 1998) and a summary of geology of Spain (Gibbons and Moreno, 2002) make it possible to determine potential source rocks for the different grain types of the Huesca sandstones.

Abundant limestone clasts could have been formed in the result of erosion of deposits of Late Triassic – Early Jurassic carbonate platforms within Pyrenees formed during tectonically quiet stage following extension and rifting. Inverted limestones of Upper Cretaceous carbonate platforms could have also provided a source of some of the clasts (Martin-Chivelet et al., 2002).

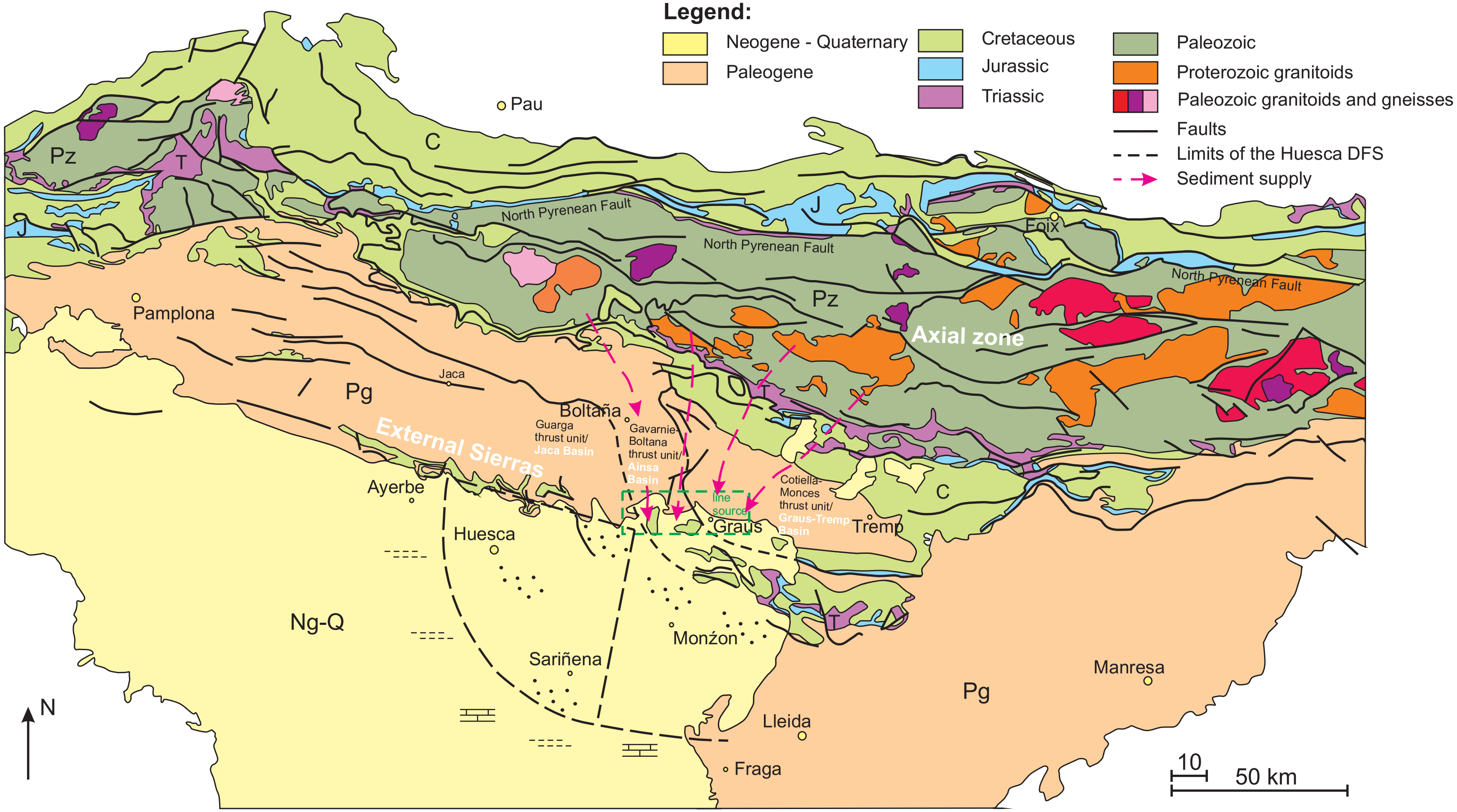

Figure 6.4. Schematic geological map of the Pyrenees and adjacent Ebro Basin showing potential source for the Huesca deposits. Dotted lines show limits of the Huesca DFS (Hirst, 1983). Pink arrows indicate sediment supply from the axial zone of Pyrenees, Ainsa and Tremp-Grause basin deposits (modified from Mapa gelógico Peninsular Ibérica, Baleares y Canarias, Insituto Technlógico Geominero de España, 1994).

Plutonic rock fragments and, formed from them grains of monocrystalline quartz, feldspar and chloritised biotite could have been sourced from Late Paleozoic (Variscan) intrusive rocks, granitoids and gneisses, in the axial zone of Pyrenees (Castro et al., 2002; Hirst and Nichols, 1986). Fragments of metamorphic schist/gneiss, strained quartz, muscovite and quartzites could have been derived from Precambrian (Valladares et al., 2002) metamorphic rocks in the axial zone of Pyrenees.

Fragments of shale and siltstone could have had very diverse source from terrestrial rocks of Carboniferous (Colmenero et al., 2002) and Permian-Triassic (Lopez-Gomez et al., 2002), and siliciclatic shallow and deep marine rocks of Cambrian-Ordovician (Gutierrez-Marco et al., 2002), Devonian (Garcia-Alcalde et al., 2002; Insituto Technlógico Geominero de España, 1994) and Cretaceous (Martin-Chivelet et al., 2002) within the axial zone of Pyrenees.

The assemblage of heavy minerals supports the interpretation of the source areas. Abundant zircon and apatite and sparser orthopyroxene grains indicate acidic and intermediate igneous rock source in the axial zone of Pyrenees (see also Hirst and Nichols, 1986). The angular shape of the apatite grains shows that they were transported only a short distance and represent first cycle deposits. Abundant amounts of garnet, tourmaline, rutile and epidote, and sparser staurolite and kyanite were possibly sourced by medium to high-grade metamorphic rocks such as mica schists, gneisses or phyllites (Mange and Maurer, 1986) exposed in the axial zone.

In contrast, zircon grains are mostly rounded indicating multiple reworking and, therefore, can be sourced from sedimentary rocks of older basins. Sedimentary rocks of Paleogene Ainsa and Tremp-Graus basins, located within the drainage area of the Huesca DFS, undoubtedly contributed to the sediment load of the Huesca DFS (Fig. 6.4). Grains in the Huesa sandstones could, therefore, represent reworked material of the Paleogene rocks rather than fragments of rocks in the axial zone of Pyrenees (Hirst and Nichols, 1986).

The interpretation of potential source rocks is not precise and direct petrographical and geochemical comparison between grains of Huesca sandstones and basement rocks is needed to determine the exact source rocks for every grain type.

6.3. Distribution of facies and facies associations

6.3.1. Main facies of the Huesca DFS succession

The Huesca succession includes facies St, Sis, His, Sil, Sils, Ssh, Hsh, Hm and Lm. Facies Hm and Hsh (floodplain fine-grained depostis and overbank sandstone sheets) dominate and comprise 69.7 % of the succession. Channel fill facies Sis, His and St represent 25.3 % of the succession whereas other facies (Sil, Sils, Ssh and Lm) are sparse (4.8 % all together) (Fig. 6.5, A). The channel fill facies association of the Huesca succession is in turn dominated by lateral accretion association (16.2 %) with minor occurrence of the channel macroform association (9.1 %) (Fig. 6.5, B, C).

6.3.2. Downstream variations in facies distribution

The facies distribution shows a distinctive trend through the successions from relatively proximal to distal part of the DFSs (Fig. 6.6 and 6.7). Channel fill facies association comprises a significant proportion of the relatively proximal and medial successions (38.8 % and 25.4 %, respectively) but is almost absent in the distal succession (8 %). In contrast, the distal part is dominated by the fine-grained floodplain / alluvial plain facies association (86.8 %).

The proportion of channel macroform and lateral accretion associations decreases from the relatively proximal to the distal outcrops from 14.2 % to 3 % and from 24.6 % to 4 %, respectively, while the isolated channel fill association was observed only in the distal successions (1.6 %). A decrease in the splay association proportion from 27.2 % to 12 % is correlated with the decrease in the proportion of channel fill facies. However splay proportion increases relatively to proportion channel fill facies.

Lacustrine facies (Lm) contribute only 5 % to the distal succession where the fluvial system was influenced by lake. Clastic lacustrine deposits are difficult to distinguish from distal fine-grained facies of the Huesca succession, and therefore their actual proportion could be higher. Specific facies associations of the distal DFS area can be distinguished and predominantly includes facies Hm, Hsh, Lm, Ssh and Sil and a very small proportion of facies St, Sis, and His (Fig. 6.7).

6.4. Types and distribution of sandstone bodies

6.4.1. Sandstone body types of the Huesca DFS succession

All three types of sandstone body are present in the Huesca DFS succession in proportions as follows: Type 1, 9.6 %, Type 2, 16.2 % and Type 3, 18.7 % (Fig. 6.8). Sandstone body types of the Huesca succession include 1/1, 1/2 and 1/3 subtypes of Type 1, subtype 2/1 of Type 2 and subtypes 3/1 and 3/2 of Type 3. All sandstone body amalgamations described in Chapter 5 are observed in the Huesca DFS succession.

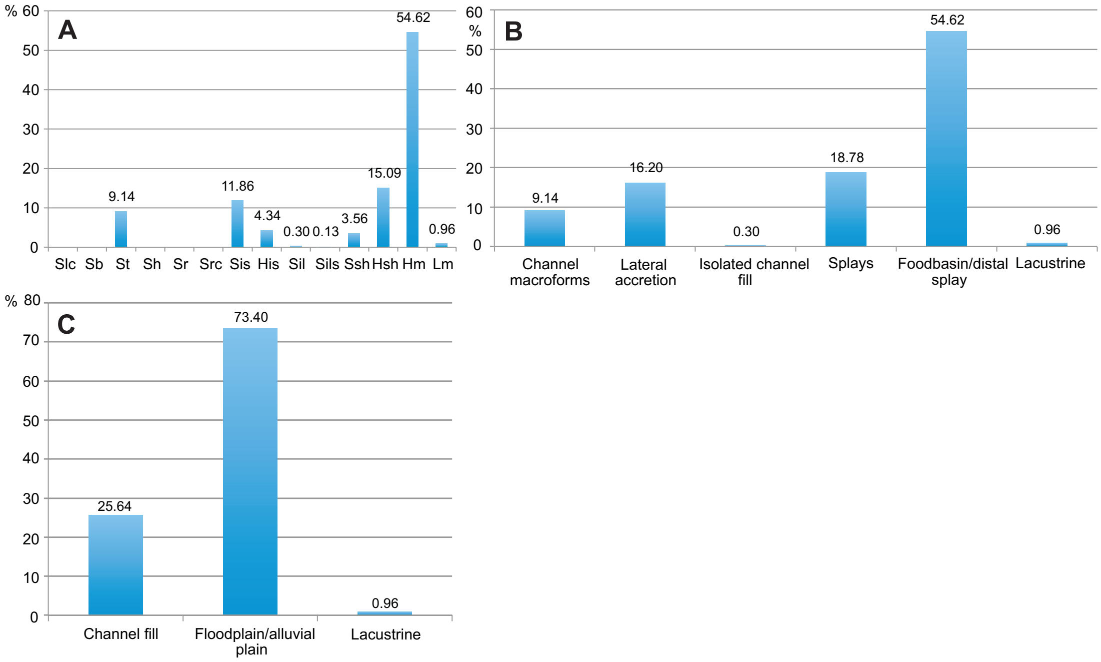

Figure 6.5. Percentage of facies (A), facies associations (B) and major facies associations (C) in the Huesca DFS succession.

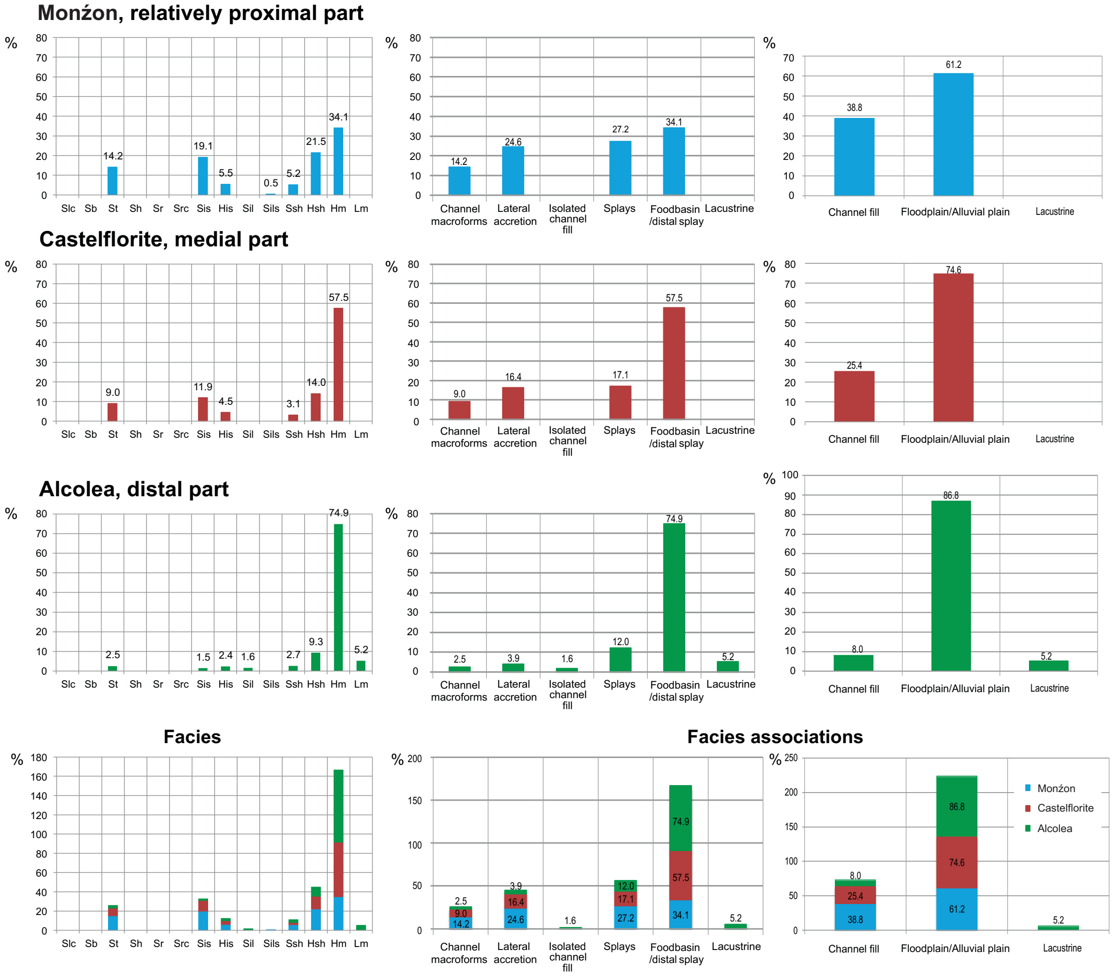

Figure 6.6. Downstream variation in proportion of facies (left) and facies associations (middle and right) in the Huesca DFS succession. Comparison between relatively proximal, medial and distal areas corresponding to Monźon, Castelflorite and Alcolea outcrops.

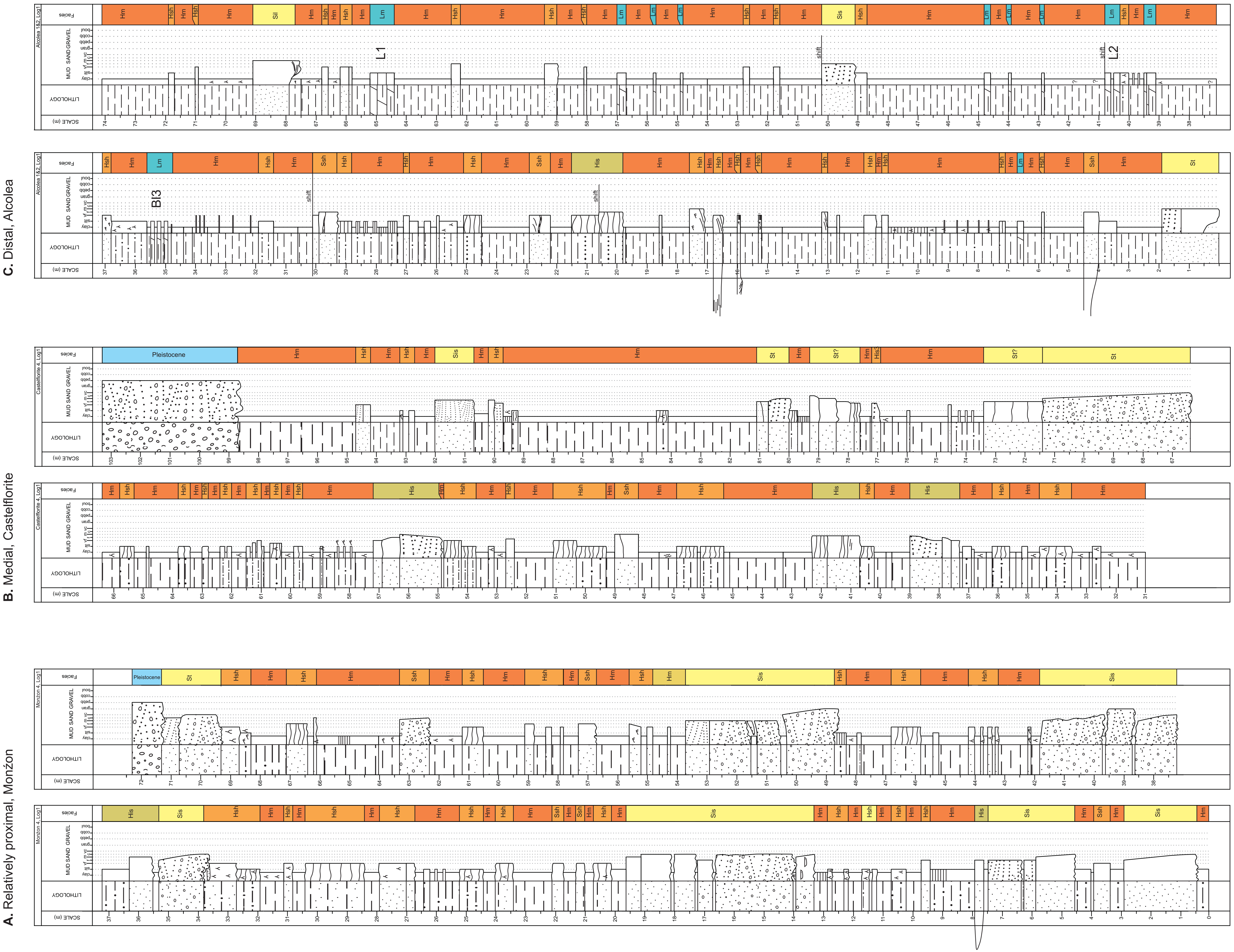

Figure 6.7. Sedimentary logs of the relatively proximal (A), medial (B) and distal (C) successions of the Huesca DFS. Note decrease in channel fill facies (yellow and green) relatively to floodplain facies (orange and brown). All detailed sedimentary logs for the Huesca DFS succession and legend for sedimentary structures see in Appendix 2.

6.4.2. Distribution of sandstone body types

Relatively proximal and medial outcrops (Monźon, Castelflorite)

Monźon and Castelflorite outcrops represent relatively proximal and medial parts of the Huesca DFS succession. Sandstone bodies of subtype 1/1 and 2/1 coexist in the relatively proximal and medial parts (Fig. 6.9 and 6.10). In the Castelflorite outcrop these two sandstone body types are commonly found separately at different levels of the succession (Fig. 6.10; appendices 5.1-3). Subtype 1/1 sandstone bodies in Monźon outcrop are 35 - 80 m wide and 6 – 9 m thick and in the Castelflorite outcrop they reach only 20 – 50 m in width and 3 – 6 m in thickness. The width of sybtype 2/1 sandstone bodies is 60 – 350 m in the Monźon outcrop and 75 - 180m in Castelflorite outcrop while thickness varies in a similar range of 2 - 4.5 m.

Large amalgamated sandstone body complexes in the Monźon outcrop are up to 10 m thick and 100 m wide. The Castelflorite outcrop is characterised by sparse, smaller, up to 4 m thick and 100 m wide, amalgamated complexes (Fig. 6.10).

Both Monźon and Castelflorite outcrops show abundant sandstone bodies of Type 3/2 with similar thicknesses and widths, which are enclosed into fine-grained overbank deposits (Fig. 6.9 and 6.10). The Castelflorite outcrop is characterised by the presence of a small proportion of subtype 1/2 and of subtype 3/1 sandstone bodies which were not seen in the Monźon outcrop. A small number of subtype 1/3 sandstone bodies were also observed in both outcrops.

Distal outcrop (Alcolea)

The Alcolea outcrop represents the distal part of the Huesca DFS succession. The succession observed here significantly differs from successions exposed in the Monźon and Castelflorite outcrops (Fig. 6.9 and 6.10). Subtype 2/1 channel sandstone bodies are almost absent in the distal succession, while subtype1/2 isolated sandstone bodies are more common and do not reach widths and thicknesses greater than 7 to 11 m and 2 m, respectively. Channel sandstone bodies are generally sparse and together represent only 8 % of the distal succession while dominant sandstone body types are subtype 3/1 and 3/2 sandstone bodies (11.5 %) (Fig. 6.10).

6.5. Downstream variations in sandstone body characteristics and sandstone body distribution

Comparison of sandstone body architecture in relatively proximal, medial and distal outcrops of the Huesca DFS succession revealed distinctive downstream trends in sandstone body proportions, dominant type, grain size and dimensions. The thickness

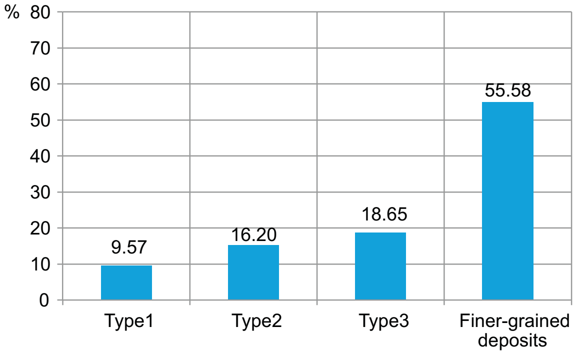

Figure 6.8. Proportions for Type 1, 2 and 3 sandstone bodies and non-sandstone deposits (including lacustrine beds) within the Huesca DFS succession.

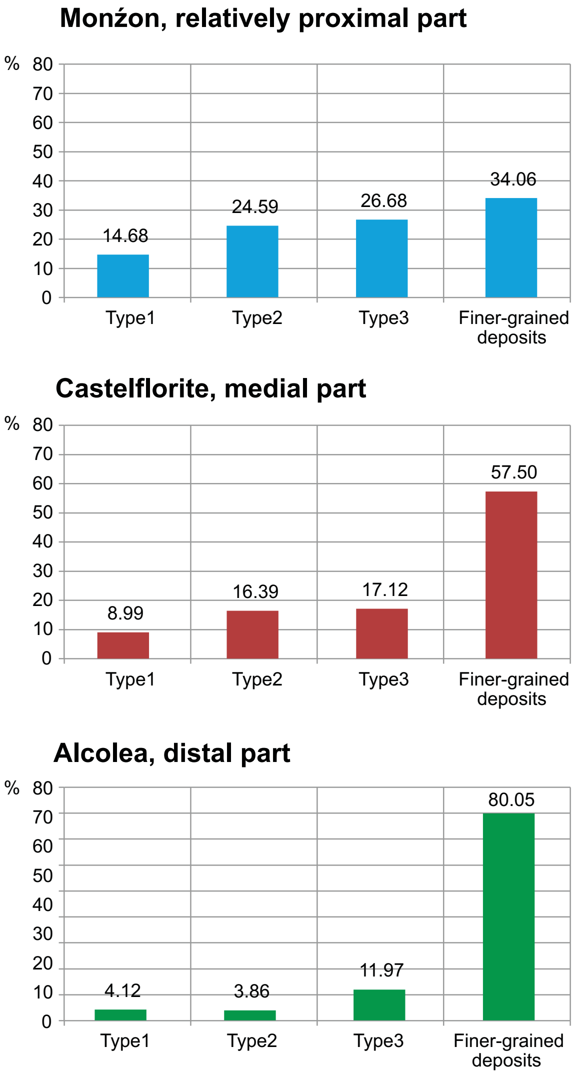

Figure 6.9. Downstream variations in proportion of sandstone body types and non-sandstone deposits (including lacustrine beds) within The Huesca DFS succession.

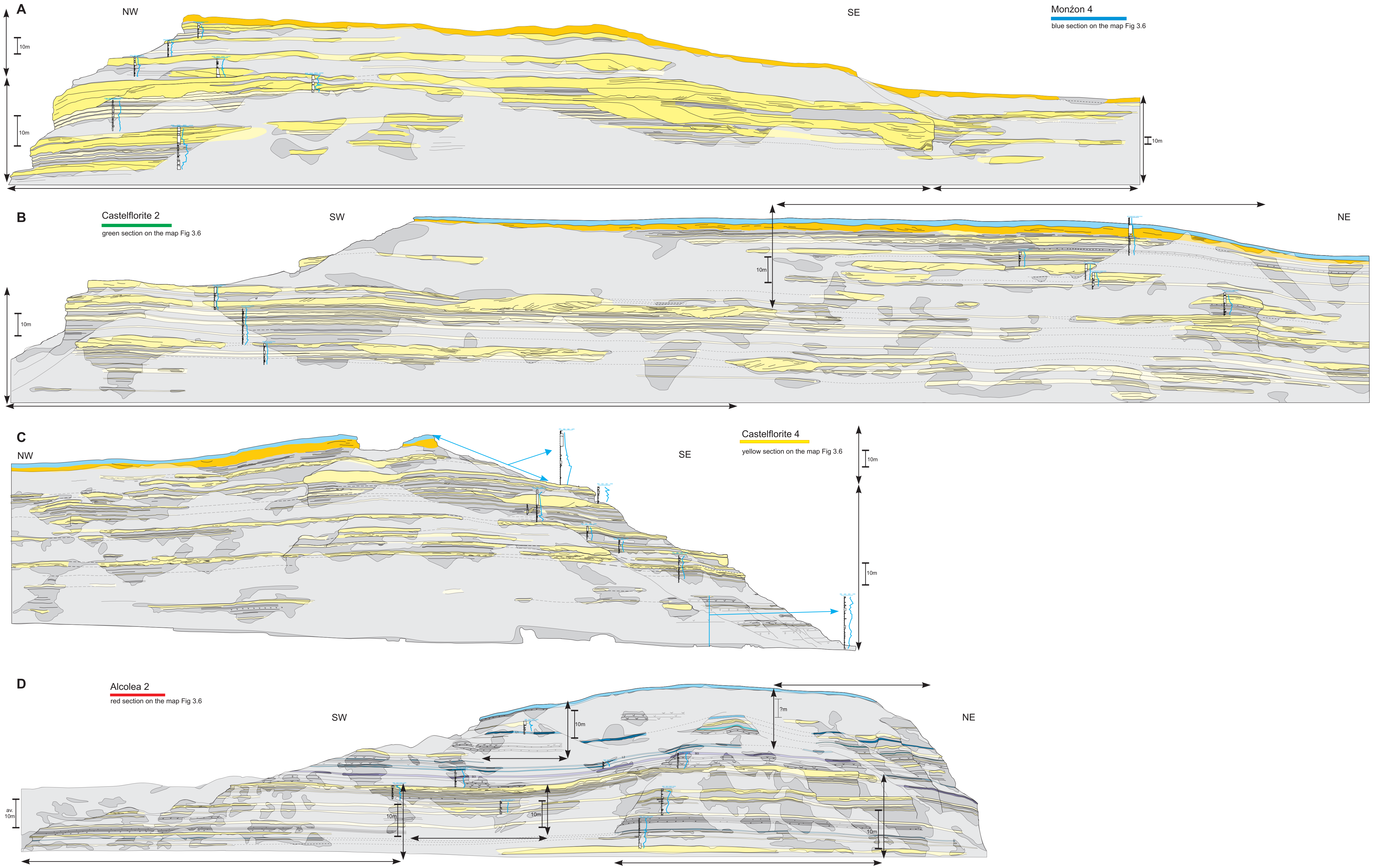

Figure 6.10. Interpreted outcrop panels of the Huesca DFS succession: A - relatively proximal Monźon outcrop, B, C - medial Castelflorite outcrop , D - distal Alcolea outcrop. Note downstream decrease in sandstone body proportion and in sandstone body dimensions and change in dominant sandstone body type from Type 2 and 1 in the relatively proximal outcrop, to more abundant Type 1 in the medial outcrop and to Type 3 in distal outcrop. Light grey areas on the outcrop mark areas of poor exposure, sandstone bodies are drawn in yellow and lacustrine limestones shown in shades of blue and green. For detailed large-scale Huesca outcrop panels, their location and legend see Appendix 5.1-3.

of sandstone body types and fine-grained deposits recorded in the stratigraphic logs (Appendix 2) was used to estimate their proportion. Separately the proportion of different sandstone body types was estimated on 2D photo panels (Chapter 3). The dimensions of the sandstone bodies were measured in the field and on photo panels (appendices 5.1-3). Grain size was recorded in sedimentary logs and determined by sieving of Huesca sandstones (Section 6.2). Interpretation of controls on downstream variations in architecture of the Huesca DFS deposits, described in this section, will be discussed in Chapter 8.

6.5.1. Overall proportion of sandstone bodies

Firstly, fine-grained deposits clearly dominate the Huesca succession. Secondly, The overall proportion of sandstone bodies of all types decrease downstream from 66 % to 20 % relative to the proportion of fine-grained deposits including facies Hm, His and Lm (Fig. 6.11). That corresponds to the NTG ratios ranging from 0.6 to 0.2.

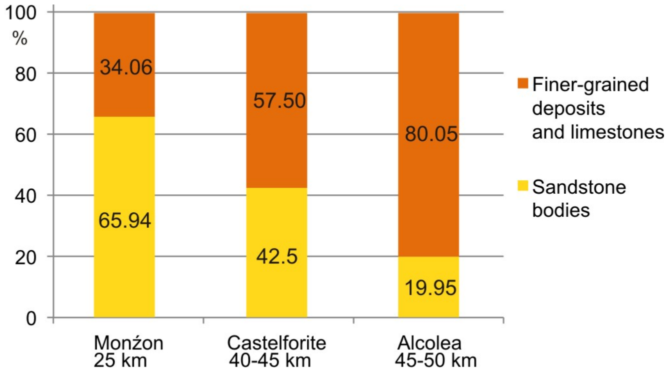

Figure 6.11. Downstream variation of the overall sandstone body proportion relative to the finer - grained deposits including lacustrine limestones.

The degree of sandstone body amalgamation decreases downstream together with sandstone body proportion. Sandstone bodies in the medial outcrop are already vertically isolated while in the proximal outcrop they show vertical connections in places (compare outcrops in Fig. 6.10 and in appendices 5.1 and 5.2).

6.5.2. Proportion of sandstone body types

The dominant type of sandstone bodies also changes down-system (Fig. 6.12). The percentage of sandstone bodies of Type 2 and 1 decreases moderately from relatively proximal to medial locations but their proportion dramatically decreases from the medial to distal areas to only 3.8 % and 4.1 %, respectively. Type 2 dominates over Type 1 sandstone bodies for both the Monźon and Castelflorite outcrops.

The proportions of Type 3 sandstone bodies, which are formed by flooding events, gradually decreases downstream, and this correlates with the decrease in number of channel sandstone bodies. The proportion of Type 3 sandstone bodies relative to other types gradually increases from relatively proximal to distal part, and Type 3 sandstone bodies become dominant over other types.

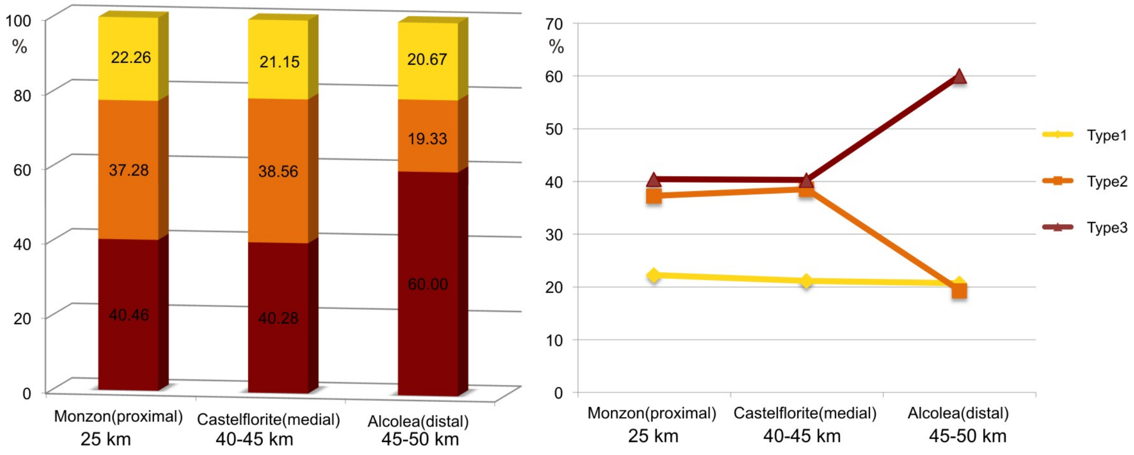

Figure 6.12. Downstream variation in dominant sandstone body type shown on histogram and plot for three outcrops. The percentage of sandstone body types was calculated using data recorded in sedimentary logs.

			2D			1D	
Outcrop	**Section**	**Type 1, %**	**Type2, %**	**Type3, %**	**Type 1, %**	**Type2, %**	**Type3, %**
Monźon	1	0.00	89.17	10.83			
	2	0.00	77.90	22.10			
	3	21.17	65.87	12.96			
	Range	**0 - 21**	**77 - 89.2**	**12 - 22.1**	**22.26**	**37.29**	**40.45**
	Average	**7.06**	**77.65**	**15.30**			
Castelflorite	1	1.13	52.94	45.93			
	2	11.86	33.73	54.41			
	3	9.61	42.72	47.67			
	4	13.33	63.15	23.53			
	Range	**1 - 13.3**	**33 - 63.2**	**23 - 54.4**	**21.15**	**38.56**	**40.28**
	Average	**8.98**	**48.13**	**42.88**			
Alcolea	1	1.26	16.69	82.05			
	2	0.14	0.00	99.86			
	Range	**0.1 - 1.3**	**0 - 17**	**82 - 100**	**20.65**	**19.35**	**60.00**
	Average	**0.70**	**8.35**	**90.96**			

Table 6.1. Comparison of the percentage of sandstone body types out of all sandstone bodies estimated using interpreted 2D photo mosaics and 1D stratigraphic logs.

The proportion of sandstone body types estimated from two-dimensional (2D) photo images shows similar trends as proportions estimated from one-dimensional (1D) logs (Table 6.1). The percentages of sandstone bodies of Type 1 and 3 differ in their absolute values measured in 1D and 2D: the percentage of Type 3 sandstone bodies from 2D panels is underestimated because the sandstone bodies are often partly covered with debris and vegetation and are not always resolved from the photo images. In contrast, percentage of Type 1 sandstone bodies from 1D logs is overestimated, because thick Type 1 sandstone bodies were preferentially logged to collect data for the full range of channel fill facies present.

The sandstone body proportion estimated from 2D photo panels could be compared to in-channel component estimated by (Hirst, 1991) (Table 6.2). In this study the percentage of in-channel sandstones has been estimated while Hirst (1991) estimated percentage of sandstones and finer-grained deposits formed in channels together. Nevertheless the values could still be compared because the proportion of fine-grained in-channel deposits in the succession is quite small (for instance, His facies represent only 4 %). The Monźon outcrop is located at the same radius distance from the apex as the Angües outcrop (Hirst, 1991) and shows similar values for Type 1 sandstone bodies but higher values for in-channel sandstone bodies as a whole. The Castelflorite outcrop is characterised by similar values to the equivalent Pertusa and La Serreta (Piraces) outcrops of Hirst (1991). The Alcolea outcrop is located at the same radial distance as Monte Aragón outcrop (Hirst ,1991) and is characterised by similar sandstone body proportion but much lower Type 1 sandstone body proportion. The difference in percentage could be a result of irregular clustered sandstone body distribution but could also be biased by different outcrop size and exposure quality.

This research				**Hirst, 1991**						
	Monźon	**Castel-florite**	**Alcolea**		**Angües**	**Pertusa**	**La Serreta**	**Monte Aragon**	**Rio Flumen**	**Galo cha**
Distance from the apex, km	25	39	48		25	32	45	45	48	57
Sandstone bodies, %	**35.63**	**23.93**	**11.69**		-	-	-	-	-	-
Overbank Type 3 SB, %	15.3	42.88	90.96		-	-	-	-	-	-
Channel Type 1 & 2 SB, %	84.7	57.12	9.04	**In-channel deposits %**	62	55	37	15	13	<5
Type 1 SB out of channel SB, %	8.33	15.72	7.7	**Ribbon SB, %**	10	21	21	85	94	70

Table 6.2. Percentage of sandstone bodies in the outcrops of the Huesca succession; Proportion of channel Type 1 and 2 sandstone bodies, Type 1 sandstone bodies and overbank Type 3 sandstone bodies out of all sandstone bodies. The percentage is estimated from 2D photomontages and compared to in-channel component and ribbon sandstone body percentage estimated in (Hirst, 1991).

6.5.3. Sandstone body dimensions

The variation in sandstone body dimensions (width and thickness) can be also seen between the Monźon and Alcolea outcrops (Fig. 6.10; 6.13 and Table 6.3). Type 1 sandstone bodies dramatically reduce their average dimensions downstream mostly due to substitution of subtype 1/1 by subtype 1/2. Type 2 sandstone bodies show an insignificant decrease in thickness and increase in their width. The latter is most likely due to smaller outcrop length of Monźon outcrop in comparison with the Castelflorite outcrop. The dimensions of the Type 2 sandstone bodies decrease significantly from medial to distal outcrops. In addition the sandstone bodies of Type 2 become more heterolithic (facies Sis is substituted by facies His). There is no consistent downstream trend in dimensions of the Type 3 sandstone bodies.

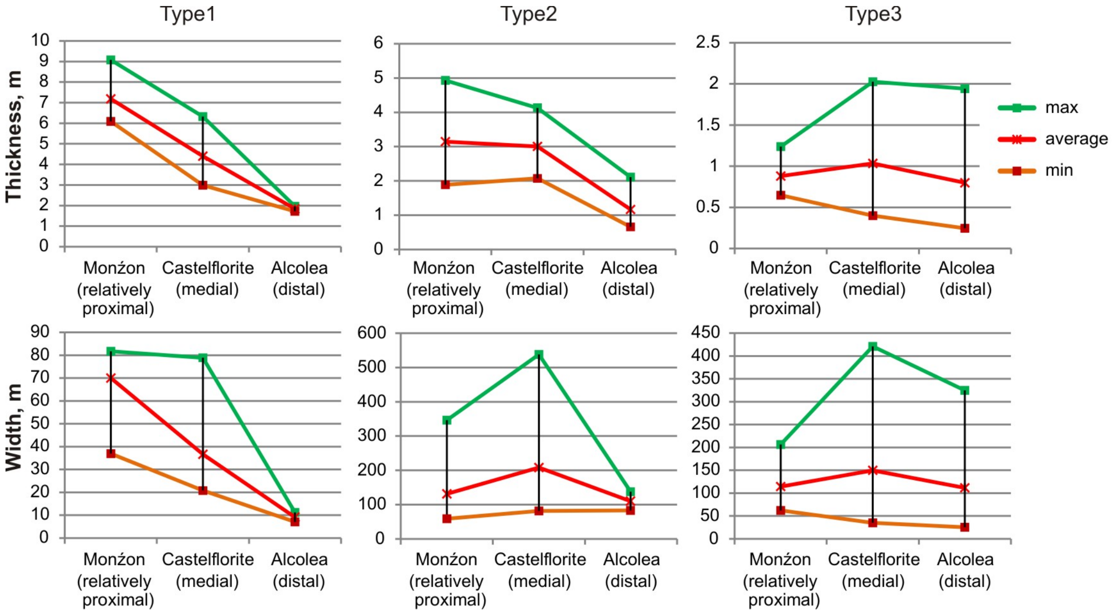

Figure 6.13. Variations in maximum, minimum and average values of thickness and width for three different sandstone body types in the Huesca DFS succession. Width represents actual or maximum observed width of a sandstone body, while thickness is maximum observed thickness of a sandstone body. Note that only two sandstone bodies of Type 1 were logged in the Alcolea outcrop. See Table 6.3 for number of measured sandstone bodies.

6.5.4. Grain size of sandstones

The grain size of sandstone comprising the sandstone bodies is another parameter which shows variation downstream (Fig. 6.14 and Table 6.4). Grain size decreases from relatively proximal to distal parts for sandstones of Type 1 and 2 sandstone bodies. The coarse fraction decreases significantly from relatively proximal to medial part and is almost absent in the sandstones of distal outcrop. Sandstones of Type 3 sandstone bodies do not show a significant change in their grain size, but there is a slight decrease in maximum grain size.

In comparison to other parameters, downstream variations in composition, sorting (Appendix 3 Table 3 and 4) and porosity (Appendix 3 Table 8; Chapter 11; Fig. 11.2 - 11.4) of the sandstones of all sandstone body types are not significant. A radial decrease in the carbonate proportion of Huesca sandstones was previously noted by (Hirst, 1983). Higher mean values of total gamma ray and K, Th and U concentrations are observed in the distal deposits of the Huesca DFS (Appendix 7).

		Width, m			**Thickness, m**		
Sandstone body type		**Monźon (relatively proximal)**	**Castelflorite (medial)**	**Alcolea (distal)**	**Monźon (relatively proximal)**	**Castelflorite (medial)**	**Alcolea (distal)**
Type 1	max	81.77	78.95	11.25	9.08	6.33	1.97
	min	37.00	20.84	7.15	6.10	2.99	1.72
	average	**70.06**	**36.71**	**9.20**	**7.19**	**4.41**	**1.85**
	counts	4	9	2	4	9	2
Type 2	max	346.42	538.07	138.26	4.93	4.13	2.11
	min	59.38	81.75	83.60	1.89	2.08	0.65
	average	**131.72**	**208.55**	110.93	**3.15**	**3.01**	1.17
	counts	14	15	2	14	15	5
Type 3	max	206.40	421.18	324.86	1.24	2.03	1.94
	min	62.37	35.12	25.48	0.65	0.40	0.25
	average	**114.54**	**149.98**	**111.80**	**0.88**	**1.04**	**0.80**
	counts	3	15	14	6	15	11

Table 6.3. Maximum, minimum and average values of width and thickness for three sandstone body types in relatively proximal, medial and distal areas of the Huesca DFS succession. Counts represent the number of measured sandstone bodies.

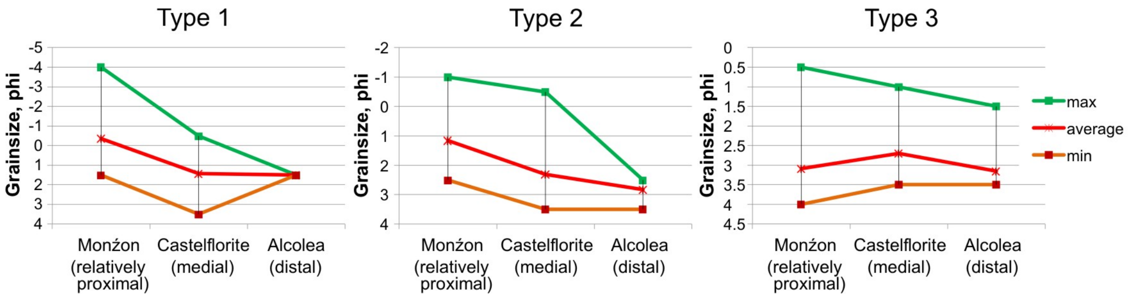

Figure 6.14. Maximum, minimum and average grain size values for different sandstone body Types in relatively proximal, medial and distal outcrops of the Huesca DFS. Grain size recorded in 1D stratigraphic logs is used in the analysis. Note that only one sandstone body of Type 1 was logged in the Alcolea outcrop. See Table 6.4 for number of measurements.

6.5.5. Summary of the downstream variations within the Huesca DFS deposits

- Overall increase in the non-sandstone, fine-grained deposit proportion;
- Decrease in the degree of sandstone body amalgamation;
- Decrease in Type 1 and Type 2 sandstone body dimensions;

- Decrease in the sandstone grain size of Type 1 and Type 2 sandstone bodies;
- Increase in the proportion of isolated subtype 1/1 and 1/2 sandstone bodies in medial and distal outcrops over Type 2 and amalgamated sandstone bodies in relatively proximal outcrop;
- Dominance of Type 3 sandstone bodies over other types in the distal outcrop;
- Exclusive occurrence of lacustrine mudstones and limestones in the distal outcrop

		Grain size, φ		
Sandstone body type		**Monźon (relatively proximal)**	**Castelflorite (medial)**	**Alcolea (distal)**
Type 1	max	-4.00	-0.50	1.50
	min	1.50	3.50	1.50
	average	**-0.36**	**1.43**	**1.50**
	counts	11	14	2
Type 2	max	-1.00	-0.50	2.50
	min	2.50	3.50	3.50
	average	**1.17**	**2.31**	**2.83**
	counts	30	29	3
Type 3	max	0.50	1.00	1.50
	min	4.00	3.50	3.50
	average	**3.08**	**2.70**	**3.15**
	counts	53	35	23

Table 6.4. Maximum, minimum and average values of the grain size (in φ) for three sandstone body types in relatively proximal, medial and distal outcrops of the Huesca DFS succession. Counts represent a number of measurements.

7. The Salt Wash DFS succession

7.1. Introduction

The sandstone composition, facies and sandstone body distribution within the Salt Wash DFS succession will be discussed in this chapter in the same manner as for the Huesca DFS succession to make comparison of two DFS successions easier. Such description allows interpretation of depositional processes on the Salt Wash DFS that will be discussed in Chapter 8. The tectonic and climatic settings of the Salt Wash DFS are summarised in Chapter 2, whereas Chapter 3 describes the locations studied and the data collection techniques.

7.2. Sandstones of the Salt Wash DFS succession

The description of the Salt Wash sandstones is based on visual analysis of thin sections and lab analysis of grain size distributions. The methods of sample processing are described in Chapter 3 and summarised in Appendix 3 Table 1.

7.2.1. Composition

The thin section description showed that sandstones of the Salt Wash DFS succession mainly consist of fragments of clear and strained quartz (~ 70 – 95 %), feldspar (~ 4 – 20 %) and lithic fragments (~ 1 – 10 %) (see also Meunier et al., 1990; Brady, 1969). Among them, the lithic grains are mainly represented by metamorphic polycrystalline quartz (quartzite) consisting of medium- to micro-size crystals with sutured or polygonized contacts and small amount of white mica (Appendix 4 Panel 5, C). Some of microcrystalline quartz fragments have been identified to be fragments of chert. Other rock fragments include minor amounts sedimentary rocks, metamorphic quartz-mica schists and igneous rocks (Appendix 4 Panel 6, A, E, F, G). Igneous rock fragments consist of quartz and feldspar crystals and have previously been determined to be fragments of acid igneous rocks (Brady, 1969). Sedimentary rock grains include siltstone, mudstone and limestone fragments. The limestone grains are aggregates of small calcite crystals. Coarser grained sandstone samples contain more lithic fragments than fine-grained ones, in which they are probably disintegrated into smaller mineral fragments (Appendix 4 Panel 6, G, sample 8-4). The feldspar grains are often altered to clay minerals or sericite/muscovite, but in places grains may show distinct plagioclase or microcline twinning (Appendix 4 Panel 5, D).

Minor components of the sandstones, comprising less than 1 % of the rock, are represented by fragments of mica (biotite and muscovite) (Appendix 4 Panel 5, D), heavy minerals (Appendix 4 Panel 5, A, D), and iron oxide (Appendix 4 Panel 7, C). The hematite was found to be the main iron oxide in all sandstones of the Morrison Formation (Brady, 1969). Less than 0.25 weight % of heavy minerals has been determined by Cadigan (1967). Heavy minerals observed in thin sections are represented by zircons, rutile and tourmaline (Appendix 4 Panel 6, A-C and Panel 5, D). Other heavy minerals could also be present, but cannot be recognised in the thin sections without heavy mineral separation. For example, hornblende was identified by Brady (1969) and garnet, staurolite, epidote and apatite have been found by Cadigan (1967).

The sandstones are predominantly cemented by poikilotopic calcite and quartz overgrowth cements (Appendix 4 Panel 7, A, B, D) (see also Cadigan, 1967; Brady, 1969; Meunier et al., 1988). Other cement types such as microcrystalline quartz, poikilotopic gypsum (sample 7-4), and microcrystalline calcite cements were also observed in minor amounts (Appendix 4 Panel 7, C, E, G). Some grains are found partially or completely replaced by calcite crystals. Calcite also occurs in rhomboid crystals with zonation marked by iron oxide in a pore space of the sandstones (Appendix 4 Panel 7, E). The hematite cement was observed in Salt Wash samples by (Brady, 1969) that has been interpreted to be the third phase of cementation after quartz and calcite cements. Some metamorphic polycrystalline quartz fragments are overgrown by chlorite fibrous crystals forming roses (Appendix 4 Panel 7, G).

The matrix is rarely seen and was observed only in four samples (Appendix 4 samples 4-7, 5-12, 7-5 and 7-6). The matrix in the very fine-grained sandstone contains large amounts of secondary mica and chlorite and fills all pore space (Appendix 4 Panel 7, F, sample 4-7). Originally the matrix could have been represented by clay minerals. Brady (1969) determined that matrix content in the sandstones does not reach 10 %. The results of XRD analysis conducted by Brady (1969), illite was found to be the most abundant clay mineral in the Salt Wash succession: this is the same as was found in the XRD data for the Huesca succession (Chapter 6).

The Salt Wash sandstones have been previously identified by point counting to be mainly quartz arenites and subarkoses by Cadigan (1967) and Brady (1969). The estimated percentage of grain types and matrix in this study defines the sandstones of Salt Wash succession as subarkoses and sublitharenites according to the classification of (Folk, 1980) and as quartz arenites, subarkoses and sublitharenites following the classification of (Pettijohn et al., 1987) (Fig. 7.1). The coarse- and granule-grained sandstones could be classified as sublitharenites due to higher percentage of lithic and feldspar fragments preserved. Rare, matrix dominated sandstones can be classified as arkosic wacke (Pettijohn et al., 1987).

7.2.2. Grain size, roundness and sorting

Very fine-grained to granule-grained sandstones are present in the succession (Appendix 2). The average grain size of the Salt Wash sandstones is 1 - 2 φ (0.5 - 0.25 mm) (Appendix 3 Table 3; see also Meunier et al., 1990; Brady, 1969) and this is coarser than the Huesca sandstones (2 - 3 φ).

Quartz and feldspar grains in the sandstones are generally well rounded to subrounded (Appendix 4 Panel 5, B, D), while some grains of clear and strained quartz are angular (Appendix 4 Panel 5, A). Lithic fragments are mostly subrounded or subangular excluding limestone fragments which are rounded due to their lower resistance to abrasion.

On the basis of the graphic analysis of the grain size cumulative curves (Fig. 7.2), which were created using sieving results (Appendix 3 Table 2), sorting of the Salt Wash sandstones is determined to be between 0.5 and 2 corresponding to moderately to poorly sorted sandstones (see also Meunier et al., 1990) that is similar to the Huesca DFS sandstones.

7.2.3. Sediment source

The Salt Wash sandstones have been interpreted to originate from multiple sources in areas to the south-west, west and north-west of the Colorado Plato (Turner and Peterson, 2004; Cadigan, 1967). Cadigan (1967) determined main source area lithologies based on the dominant minerals or absence of specific minerals in certain areas and dominant directions of sediment transport. For the south-western source area the author suggested the following source rocks: granitic igneous rocks or arkoses, rhyolitic extrusive rocks (tuffs), metaquartzites and sedimentary quartzitic rocks. The western and north-western source areas were considered to consist of silicified limestones, metaquartzites, fresh and altered sodic granitic, rhyolitic igneous rocks and sedimentary quartzitic rocks.

Polycrystalline quartz found in the sandstones could have been sourced from metamorphic, metasedimentary or sedimentary quartz-rich rocks. The presence of staurolite, garnet, tourmaline and rutile (Cadigan, 1967) support a metamorphic origin (Mange and Maurer, 1986). Some clear quartz grains are angular and therefore could be a result of breakage of metamorphic polycrystalline quartzose rocks and acid igneous rocks. Feldspar was also probably sourced from the igneous rocks.

Rounded and subrounded quartz grains indicate multiple reworking cycles and an origin in older mature sedimentary rocks. Abundant illite in the Salt Wash DFS

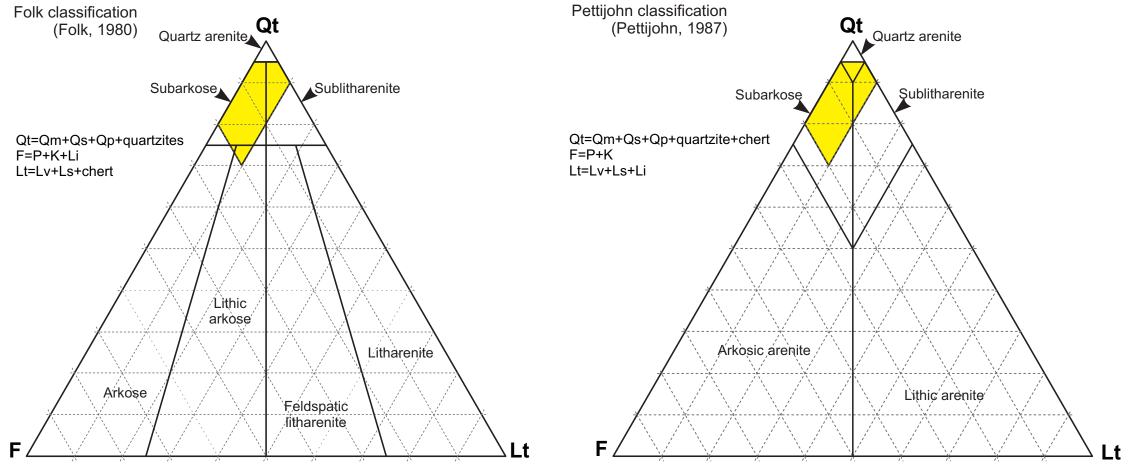

Figure 7.1. Classification of Salt Wash sandstones using Folk and Pettijohn classification triangles (modified from Folk, 1980; Pettijohn et al., 1987).

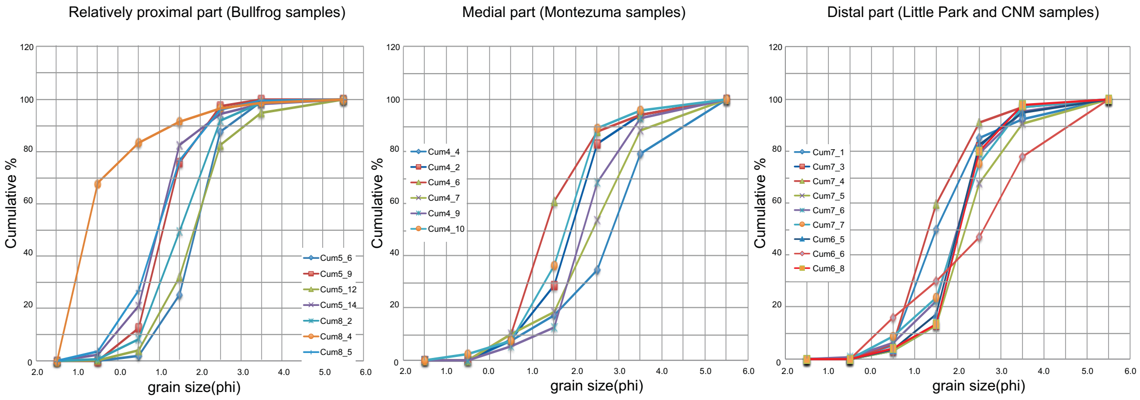

Figure 7.2. Cumulative curves for weight percentage of grain size fractions of the Salt Wash sandstones. A graphic method was used to estimate mean grain size value and sorting (Appendix 3 Table 2 and 3).

succession has also been previously described derived from sedimentary rocks (Keller, 1962, Brady, 1969). According to the experiments that showed that mechanical abrasion is negligible in river transport (Kuenen, 1959; Brady, 1969), internal reworking can be excluded as a possible cause of roundness. Many sedimentary rock fragments observed in the Salt Wash sandstones support presence of sedimentary source.

The sedimentary San Rafael Group was suggested as one of the sources (Cadigan, 1967) an area that was uplifted in the Middle Jurassic by forces of thrusting and volcanism in the source area (Thorman and Peterson, 2004; Dickinson, 2006). The volcanic rock fragments, therefore, could have been also supplied from these areas. Older Mezosoic formations have been also suggested as sources for the Salt Wash fluvial system by Peterson (1988). In addition Middle to Late Paleozoic fossils were found in chert pebbles in the Salt Wash deposits (Craig et.al, 1955). Paleozoic formations have been reported to be currently well preserved in the source area of the Salt Wash fluvial system (Peterson, 1988).

The possible source areas that contributed sediment to the Morrison depositional basin have been suggested to be Basin and Range province, Sierra Nevada and Peninsula Ranges (Cadigan, 1967). The exact rocks that could have been source rocks for the Salt Wash sediment are not identified here and could be an objective of future research.

7.3. Distribution of facies and facies associations

7.3.1. Main facies of the Salt Wash DFS succession

In contrast to the Huesca succession, channel fill facies (Slc, St, Sh) dominate the Salt Wash succession and compose 55.2 % of the succession, and St facies is the most dominant facies among them (46.5 %) (Fig. 7.3, A, C). Floodplain facies Hm and Hsh represent the second most abundant facies (34.5 %) within which facies Hm contributes 27.7 % to the succession (Fig. 7.3, A). Facies Sils, Sis, His, Sr, Scr, and Sb are rare and together represent 8.5 % of the succession, while the lake facies association is missing from the studied sections (Fig. 7.3, A).

Channel macroform association occurs much more often (56 %) than LA complexes (6.6 %) (Fig. 7.3, B) which is in contrast to the Huesca succession where the latter is the dominant channel fill facies association. This could be related to the high degree of amalgamation where evidences of LA accretion are reworked.

7.3.2. Downstream variations in facies distribution

The comparison of facies proportions between relatively proximal, medial and distal outcrops shows downstream changes in facies distribution (Fig. 7.4 and 7.5). Similarly to the Huesca DFS succession, the proportion of channel fill facies association relative to the floodplain/alluvial plain facies association decreases from 77.3 % to 48.3 % from relatively proximal to distal outcrop. The proportion of floodplain facies association in turn increases from 27.7 % to 51.69 %. The estimation of proportion of facies from floodplain/alluvial plain association in the Slick Rock outcrop should be interpreted with caution due to poor quality of the exposure (Fig. 7.4).

The isolated channel fill association was observed only in the distal outcrop (Little Park) where the floodplain facies association makes up a significant part of the succession (51.7 %) (Fig. 7.4). The channel fill association in the distal outcrop includes both LA complexes and channel macroform associations (17.8 % and 30 %, respectively), while channel macroforms dominate proximal and medial parts of the succession (76.7 % and 56.1 %, respectively). The splay association is observed to increase from proximal to distal outcrop from 9.9 % to 13.6 %.

The distal facies association in the Salt Wash DFS deposits is represented by almost all facies, except facies Sb and Lm, and dominated by facies Hm, Hsh, Sis, His, St and Sh.

7.4. Type and distribution of sandstone bodies

7.4.1. Sandstone body types of the Salt Wash DFS succession

All three types of sandstone bodies described in Chapter 5 were observed in the Salt Wash outcrops. Sandstone bodies of Type 1 are quite rare and represent only 1.2 % of the succession, while Type 2 dominates the succession and comprises 62.6 % of it (Fig. 7.6). In contrast to the Huesca DFS succession, sandstone bodies of Type 3 and fine-grained overbank deposits are minor constituents of the Salt Wash succession (8.5 % and 27.7 %, respectively).

Large amalgamated sandstone bodies of Type 2 are the most common sandstone amalgamation style observed in the Salt Wash succession (Chapter 5). The amalgamated bodies were found truncating or passing into packages of sandstone bodies of Type 3. The same relationships were seen in the Huesca DFS outcrops. Other amalgamations such as amalgamation of Type 1 and Type 3 sandstone bodies were not observed, because sandstone bodies of Type 1 were not often recorded in the Salt Wash succession.

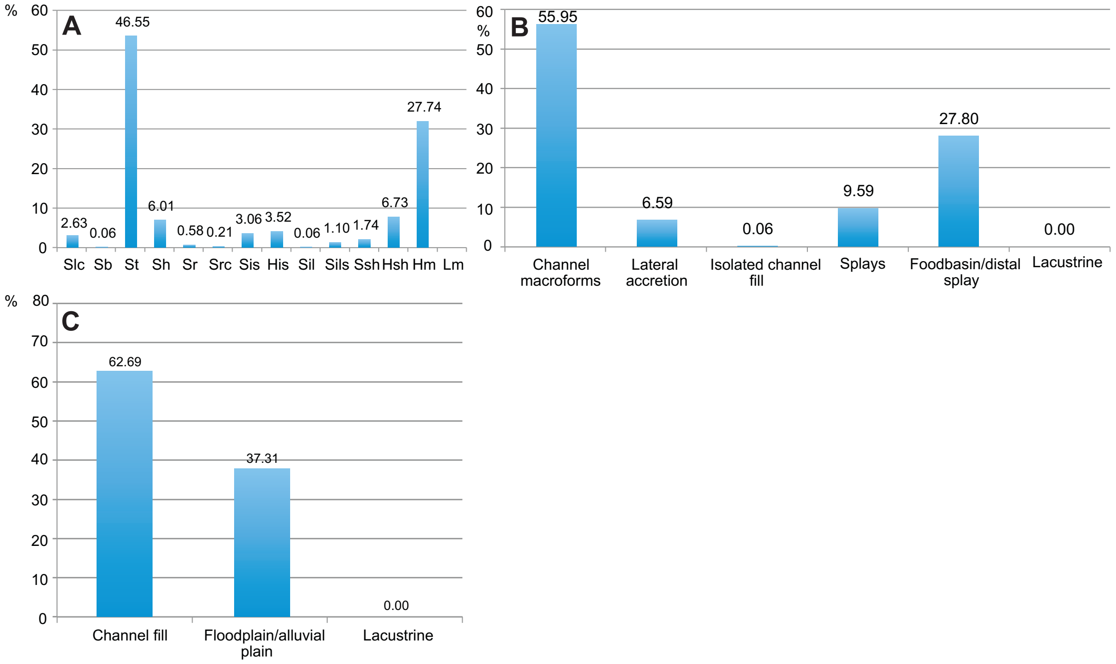

Figure 7.3. Percentage of facies (A), facies associations (B) and major facies associations (C) in the Salt Wash DFS succession.

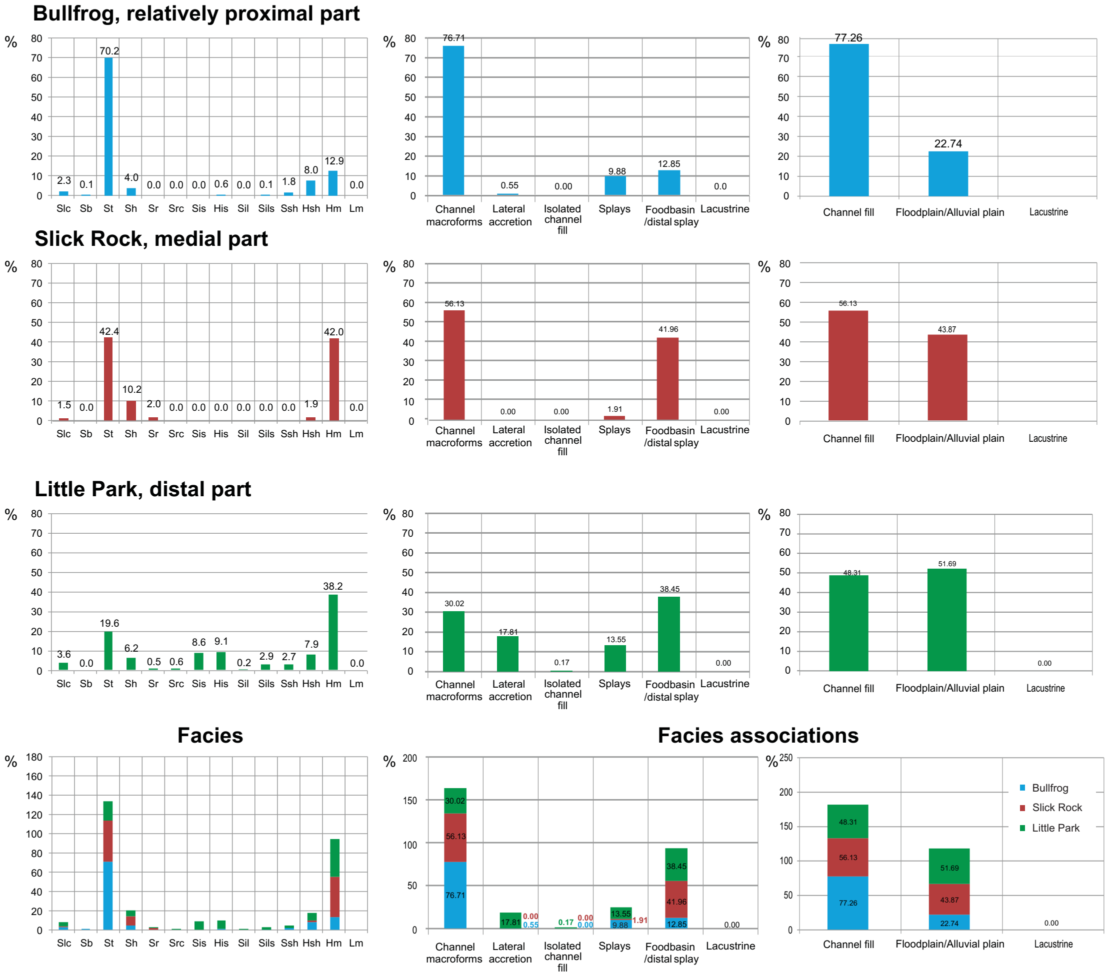

Figure 7.4. Downstream variation in proportion of facies (left) and facies associations (middle, right) in the Salt Wash DFS succession. Comparison between relatively proximal, medial and distal areas corresponding to Bullfrog, Slick Rock and Little Park outcrops.

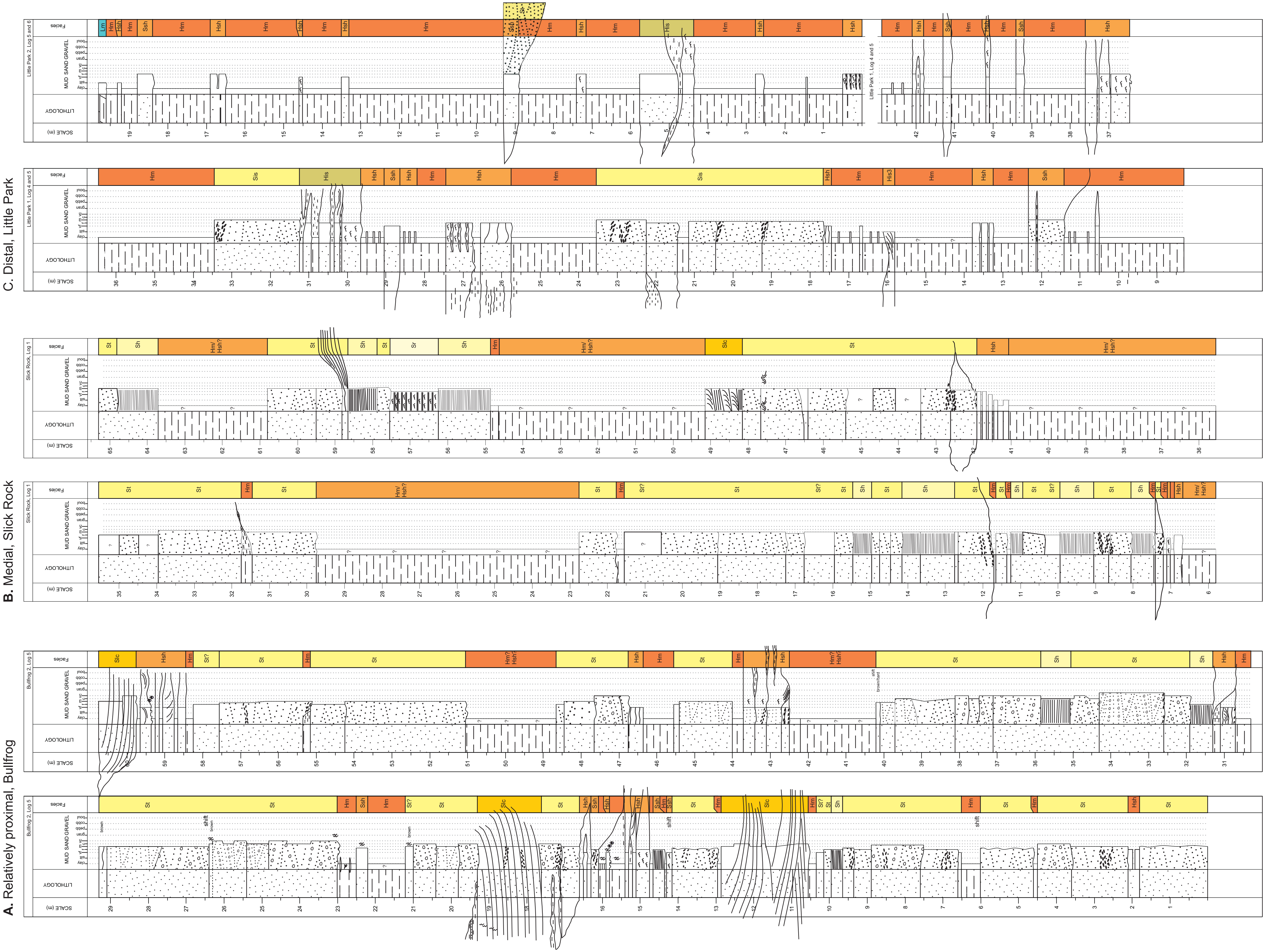

Figure 7.5. Sedimentary logs of the realtively proximal (A), medial (B) and distal (C) successions of the Salt Wash DFS. Note decrease in channel fill facies (yellow / green) relatively to floodplain facies (orange / brown). Detailed sedimentary logs of the Salt Wash DFS succession and legend for sedimentary structures see in Appendix 2.

7.4.2. Distribution of sandstone body types

Relatively proximal and medial outcrops (Bullfrog, Slick Rock)

The Bullfrog and Slick Rock outcrops represent relatively proximal and medial parts of the Salt Wash DFS succession. Both outcrops are dominated by sandstone bodies of subtype 2/2, while subtype 1/1 is observed very rarely (0 – 0.2 %) (Fig. 7.7 and 7.8).

The Type 2 sandstone bodies are amalgamated into large, up to 25 m thick and minimum 2.5 km wide (limited by outcrop length), sandstone body complexes in both outcrops. Although individual sandstone bodies are difficult to distinguish within the amalgamated complexes, it is possible to estimate variations in thickness and width of Type 2 sandstone bodies from relatively proximal to medial areas. The thickness of the sandstone bodies in the Bullfrog outcrop varies between 2 m and 10 m, while maximum thickness of the sandstone bodies in the Slick Rock outcrop reaches only 6 m (Table 7.3). The average width of the sandstone bodies decreases from 470 m to 320 m, although this may be determined by the length of the outcrop and the quality of the outcrop exposure.

Although the n Type 3/2 and Type 1/3 sandstone bodies have been observed in both outcrops, their proportion can not be estimated due to poor exposure of fine-grained deposits, particularly in the Slick Rock outcrop. The difference in the architecture of the Salt Wash DFS succession from relatively proximal to medial areas is not as pronounced as in the Huesca DFS succession.

Distal outcrop (Little Park)

The Little Park outcrop is the most distal among studied outcrops of the Salt Wash succession. The difference in architecture between this outcrop and two outcrops described above is clearly seen (Fig. 7.8).

Type 2 sandstone bodies are less abundant in the distal outcrop, whereas fine-grained deposits and Type 3 sandstone bodies become much more common (Fig. 7.7 and 7.8). The Type 2 sandstone bodies become more confined and subtype 2/3 can be observed. The maximum measured width of the Type 2 sandstone bodies decreases from relatively proximal (900 m) to distal outcrops (650 m). The thickness of the Type 2 sandstone bodies in the distal succession is slightly smaller.

Sandstone bodies in the distal succession are commonly vertically isolated with finer-grained deposits, but the two largest sandstone bodies of Type 2 in the Little Park outcrop amalgamate in their middle part creating a thick sandstone body complex (Appendix 5.6).

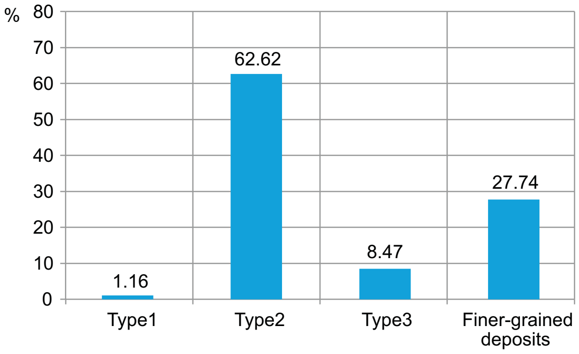

Figure 7.6. Proportions for Type 1, 2 and 3 sandstone bodies and non-sandstone deposits within the Salt Wash DFS succession.

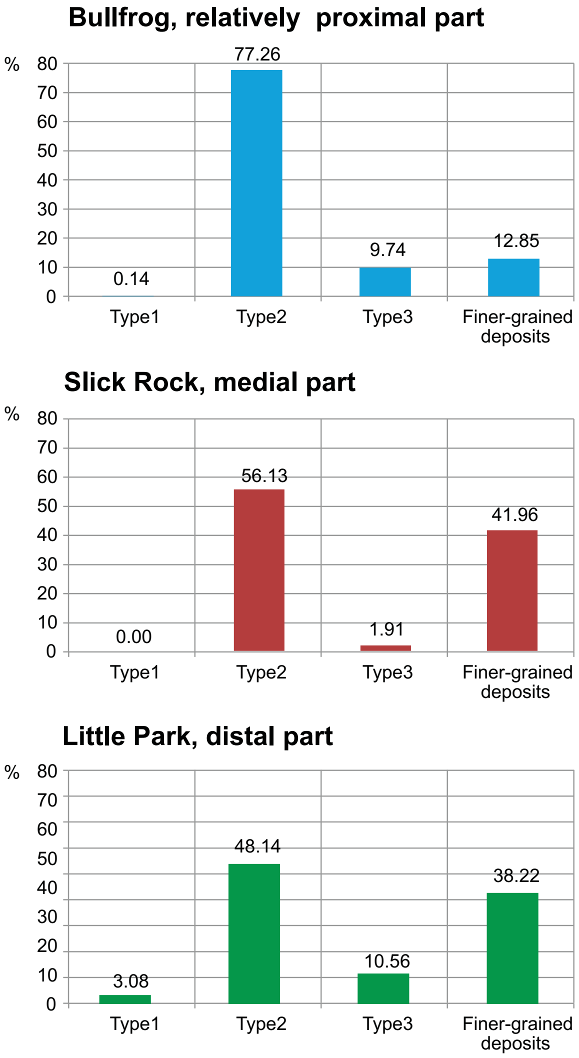

Figure 7.7. Downstream variations in proportion of sandstone body types within the Salt Wash DFS succession.

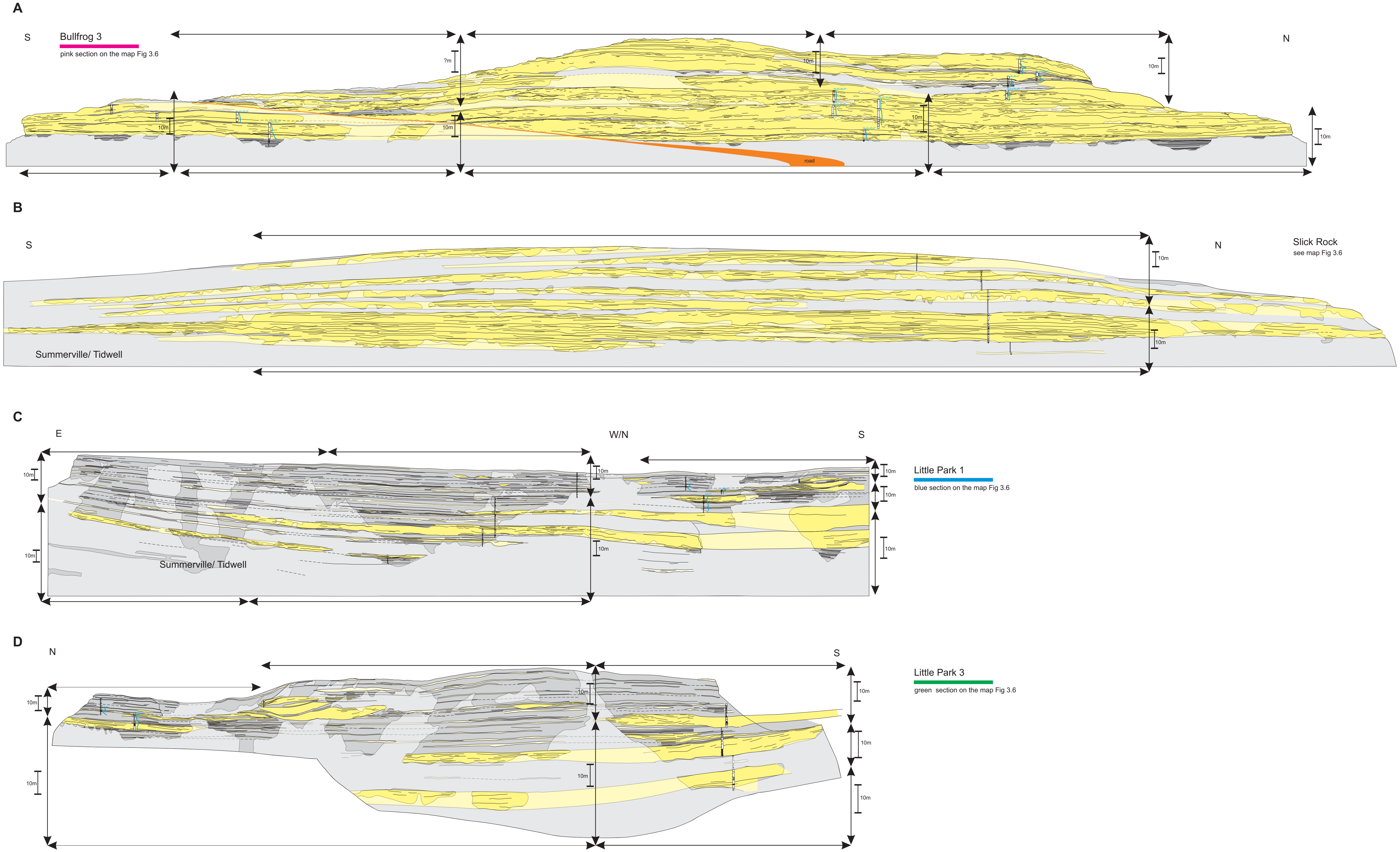

Figure 7.8. Interpreted outcrop panels: A - relatively proximal Bullfrog outcrop , B - medial Slick Rock outcrop , C and D - distal Little Park outcrop. Note downstream decrease in sandstone body proportion and in sandstone body dimensions. Light grey areas on the outcrop mark areas of poor exposure, sandstone bodies are drawn in yellow. For detailed large-scale outcrop panels of the Salt Wash DFS succession, their locations and legend see Appendix 5.4-6.

In comparison to the relatively proximal and medial outcrops, some of the Type 3 sandstone bodies in the Little Park outcrop are quite thick (up to 3 – 4 m). This is defined by the presence of subtype 3/1 and 3/3 (terminal splays) which were not observed in the other outcrops.

The distal outcrop of the Salt Wash DFS succession differs significantly from the distal outcrop of the Huesca DFS succession by higher proportion of sandstone bodies and by a different set of sandstone body subtypes.

7.5. Downstream variations in sandstone body characteristics and sandstone body distribution

Downstream trends in sandstone body proportion, dimensions and grain size of the sandstones were observed in the Salt Wash outcrops. Sandstone body dimensions and grain size were estimated and described quantitatively in the same manner as for the Huesca DFS (Chapter 6). Interpretation of controls on downstream variations in architecture of the Salt Wash DFS deposits, described in this section, will be discussed in Chapter 8.

7.5.1. Overall proportion of sandstone bodies

The Salt Wash DFS succession is dominated by sandstone bodies, in contrast to the Huesca DFS succession which is dominated by fine-grained floodplain deposits. The downstream decrease in sandstone body proportion (by ~ 25 %) (Fig. 7.9) is not as great as for the Huesca succession (by ~ 46 %). The Slick Rock outcrop data are standing out from the trend due to the presence of large intervals of non-exposure. The intervals were assumed to represent fine-grained overbank deposits that skewered the resulting proportions towards the finer-grained deposits. However, these intervals might also contain small-scale sandstone bodies of Type 3 and subtypes 1/2 and 1/3 that are usually observed within intervals of floodplain deposits. Covered areas may also contain parts of Type 2 sandstone bodies.

The degree of amalgamation of sandstone body complexes decreases along with the sandstone body proportion. The degree of sandstone body amalgamation within the complexes remains the same from relatively proximal to medial outcrop (appendices 5.4-6). In the distal outcrop sandstone bodies are mostly vertically isolated and only the two largest sandstone bodies are amalgamated in the middle part of the outcrop (Appendix 5.6).

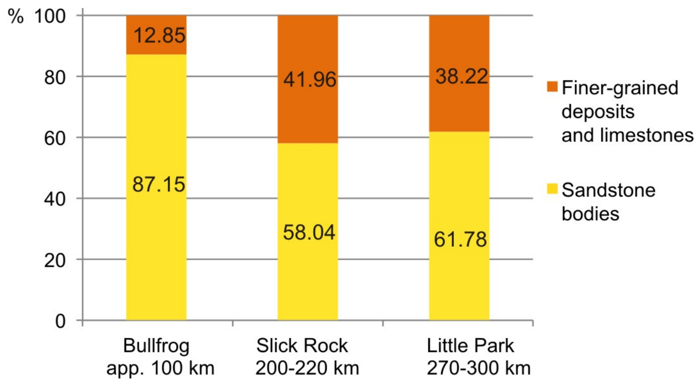

Figure 7.9. Downstream variation of the overall sandstone body proportion relative to the fine-grained deposits.

7.5.2. Proportion of sandstone body types

The variations in the proportion of different sandstone body types are not as pronounced as for the Huesca DFS, because the succession is dominated by the sandstone bodies of Type 2 in all outcrops. Their proportion, however, significantly decreases downstream from 77 % to 48 % (Fig. 7.10). Excluding the biased Slick Rock outcrop data, the proportion of Type 1 sandstone bodies maintains the same and comprises approximately 10 % of the succession. The percentage of the Type 3 sandstone bodies is very small and represents 3 % of the distal succession in the Little Park outcrop and much less in the relatively proximal Bullfrog outcrop (Fig. 7.10).

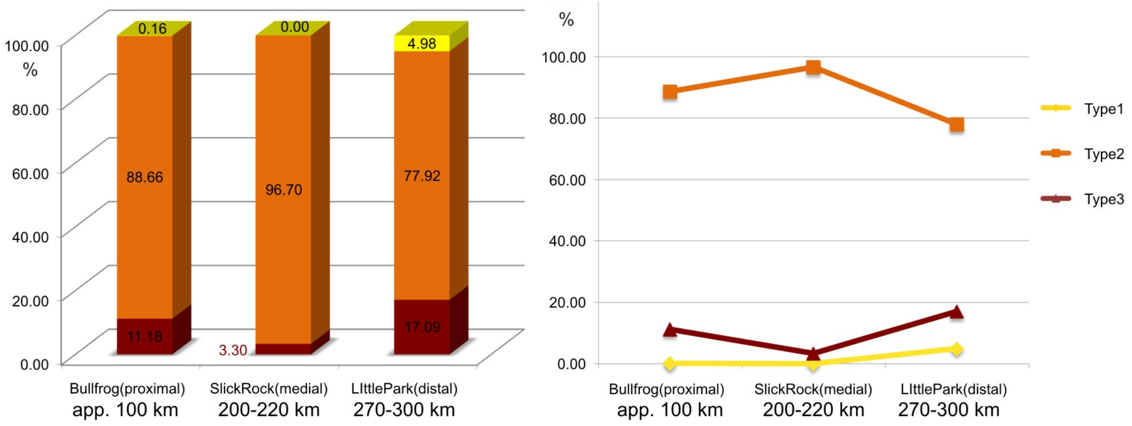

Figure 7.10. Downstream variation in dominant sandstone body type in the Salt Wash DFS succession shown on histogram and line plots for all three outcrops. The percentage of sandstone bodies was calculated using data recorded in sedimentary logs (Appendix 2).

The difference between outcrops is better seen in the variation in subtypes of the sandstone bodies and facies. The sandstone bodies of subtype 2/3 are present only in the distal succession (Little Park outcrop). Furthermore, Type 2 sandstone bodies in the Little Park outcrop are more heterolithic and are characterised by lateral accretion surfaces (LA complex) which were not observed in other outcrops (Fig.7.8; Appendix 5.6).

The estimation of proportions of sandstone body types from two-dimensional (2D) photo mosaics and one-dimensional (1D) sedimentary logs shows similar results (Table 7.1). The percentages of Type 2 sandstone bodies are very similar because the sandstone bodies of this type dominate the succession and can be easily recorded in both stratigraphic logs and on the photo panels. A good match is seen between 1D and 2D estimates for Type 1 sandstone bodies. The difference in the percentage of Type 3 sandstone bodies between two estimates is about 5 units of a percent that is due to the presence of small-scale sandstone bodies of this type, which could not be seen on the large-scale photo mosaics, but were recorded in detailed stratigraphic logs. Small differences also occur between two estimates due to lateral variation in sandstone body distribution which can not be recorded in 1D sedimentary logs.

		2D			**1D**		
Outcrop	**Section**	**Type 1, %**	**Type2, %**	**Type3, %**	**Type 1, %**	**Type2, %**	**Type3, %**
Bullfrog	1	0.21	94.21	5.58			
	2	0.00	97.65	2.35			
	3	0.00	97.96	2.04			
	Range	**0 - 0.21**	**94 - 98**	**2 - 5.6**	**0.16**	**88.71**	**11.13**
	Average	0.07	96.61	3.32			
Slick Rock	1	0.00	100.00	0.00			
	Range	**0.00**	**100.00**	**0.00**	**0.00**	**96.72**	**3.28**
	Average	0.00	100.00	0.00			
Little Park	1	4.02	71.96	24.01			
	2	0.00	91.73	8.27			
	3	5.04	77.37	17.59			
	Range	**0 - 5.1**	**71 - 91.7**	**8.2 - 24.1**	**5.02**	**77.83**	**17.15**
	Average	3.02	80.35	16.62			

Table 7.1. Comparison of the percentages of sandstone body types out of the sandstone bodies in the Salt Wash DFS succession estimated using interpreted 2D photo mosaics and 1D stratigraphic logs.

The 2D estimation of the Type 2 sandstone body proportion in the Bullfrog outcrop can be compared with the areal percentage determined for the sandstone bodies of similar geometry and characteristics in the Waterpocket fold outcrop by (Kjemperud et al., 2008). Regionally the outcrop is also located in relatively proximal area of the Salt Wash DFS. The thick sheet-like sandstone bodies, so-called “braided channel sandstones”, were determined to represent 93 % of the channel sandstones of the Waterpocket fold outcrop (Kjemperud et al., 2008): this is consistent with the percentage of equivalent Type 2 sandstone bodies estimated in the Bullfrog outcrop (95 – 97 %, Table 7.2).

		% of succession	% of sandstone bodies		
	Measured section	**sandstone bodies**	**Type1**	**Type2**	**Type3**
Bullfrog	1	77.60	0.21	94.21	5.58
	2	86.31	0.00	97.65	2.35
	3	84.27	0.00	97.96	2.04
Waterpocket fold outcrop (Kjemperud et al., 2008)				93.00	

Table 7.2. Percentage of sandstone body types calculated from overall sandstone body proportion in the Bullfrog outcrop of the Salt Wash DFS succession. Percentage is estimated from 2D photo mosaics and compared to the areal percentage of thick sheet-like “braided channel sandstones” in the Waterpocket outcrop estimated by Kjemperud et al. (2008).

7.5.3. Sandstone body dimensions

Downstream changes can be seen in the thickness and width of all sandstone body types (Fig. 7.11, Table 7.3). The average thickness of Type 1 sandstone bodies very slightly decreases from the Bullfrog to Little Park outcrop by 0.5 m, while their width increases by 2 m. However, the number of measurements of Type 1 sandstone bodies is low (four to seven bodies) and, therefore, may not be representative.

The average thickness of sandstone bodies of Type 2 is relatively constant throughout the succession but the maximum observed values significantly decrease downstream. The difference between Slick Rock and Little Park values (Fig. 7.11) could be perhaps explained by the difficulty in distinguishing individual sandstone bodies within amalgamated sandstone complexes. The width of this type of sandstone bodies dramatically decreases from relatively proximal to distal outcrop by about 200 m. Width measurements, however, are likely to be biased by the length of the outcrop and therefore should be interpreted with caution. The subtype 2/3 sandstone bodies which are characterised by smaller widths have been observed only in the distal outcrop, and this supports the decrease in the width of Type 2 sandstone bodies distally.

The sandstone bodies of Type 3 are characterised by much smaller thicknesses in the relatively proximal Bullfrog outcrop than sandstone bodies of Type 3 in the distal Little Park outcrop. This is, as mentioned before, due to the presence of different subtype set. For example, subtype 3/1 and some sandstone bodies of subtype 3/3 are up to 3.5 m thick (Chapter 5). The width of the Type 3 in the Bullfrog outcrop is based on small number of measurements due to small amounts of deposits of floodplain association preserved and could be higher (appendices 5.4-6).

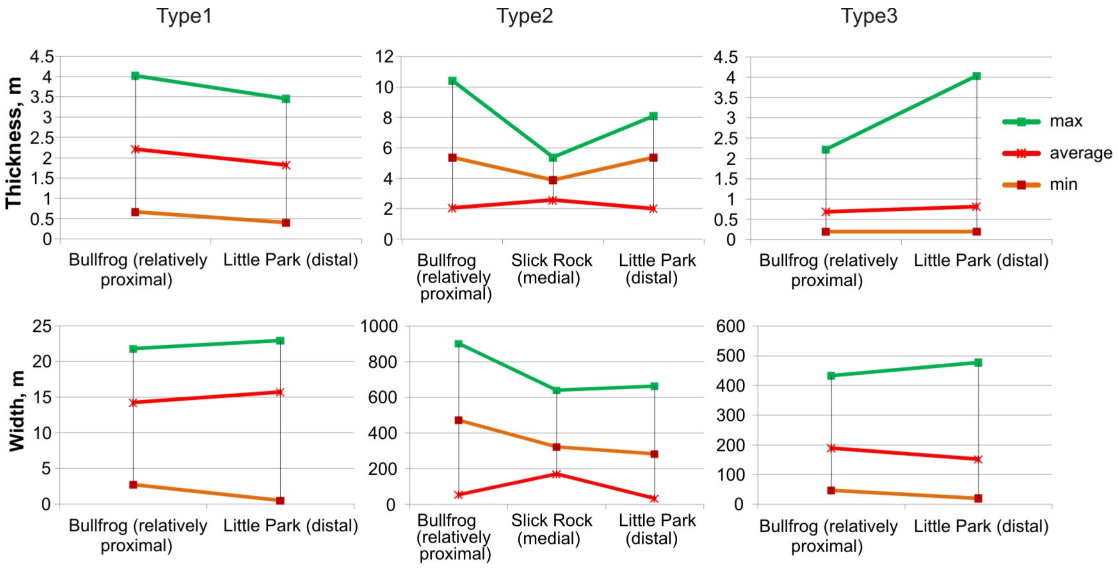

Figure 7.11. Variations in maximum, minimum and average values of thickness and width for different sandstone body types in the Salt Wash DFS succession. Width represents minimum or observed width of a sandstone body, while thickness represents maximum observed thickness of a sandstone body. See Table 7.3 for number of measured sandstone bodies.

		Width, m			**Thickness, m**		
Sandstone body type		**Bullfrog (relatively proximal)**	**Slick Rock (medial)**	**Little Park (distal)**	**Bullfrog (relatively proximal)**	**Slick Rock (medial)**	**Little Park (distal)**
Type1	max	21.79	-	22.92	4.02	-	3.45
	min	2.70	-	0.50	0.67	-	0.40
	average	**14.24**	**-**	**15.72**	**2.21**	**-**	**1.82**
	counts	4		7	4		7
Type2	max	899.36	637.96	660.32	10.39	5.39	8.10
	min	54.46	170.14	33.20	2.06	2.59	2.01
	average	**471.33**	**321.28**	**282.51**	**5.37**	**3.88**	**5.39**
	counts	23	21	5	23	21	5
Type3	max	432.71	-	476.71	2.22	-	4.04
	min	47.42	-	19.47	0.20	-	0.20
	average	**189.68**	**-**	**151.90**	**0.68**	**-**	**0.81**
	counts	40		54	47		56

Table 7.3. Maximum, minimum and average values of width and thickness for three sandstone body types in relatively proximal, medial and distal areas of the Salt Wash DFS succession. Counts represent the number of measurements for every type.

7.5.4. Grain size of sandstones

A downstream decrease in grain size of the sandstones is observed for Type 1 and Type 2 sandstone bodies (Fig. 7.12, Table 7.4). Coarse grains already disappear from sandstones of the Type 2 sandstone bodies in the medial outcrop and the average grain size steadily decreases from coarse/medium to medium/fine. Conglomerates have been described by (Peterson, 1994) in the most proximal outcrop of the Salt Wash succession (south-west of the Bullfrog location, Fifty-mile Point, Fig. 7 in Peterson, 1994) that are already substituted by gravelly sandstones in the Bullfrog outcrop. In contrast the average grain size of Type 3 sandstone bodies shows a slight increase, while its maximum value varies without any consistent trend. The increase in grain size can be explained by occurrence of different subtypes in the distal outcrop. The grain size variations for the sandstones of Type 1 are based on small number of records (Table 7.4) and therefore will not be interpreted.

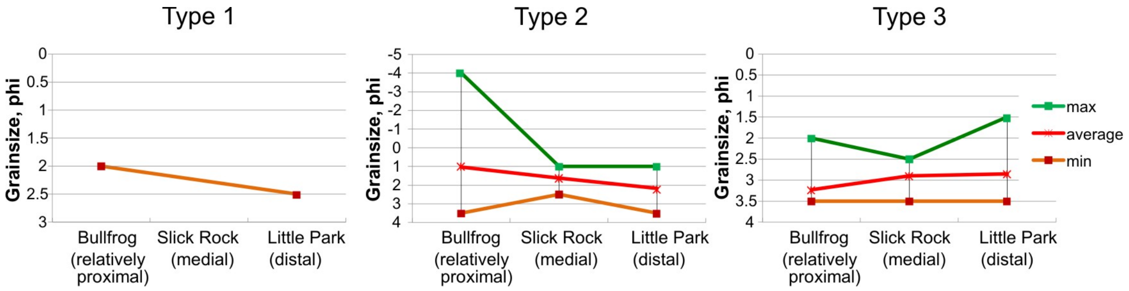

Figure 7.12. Maximum, minimum and average grain size values for different sandstone body types in relatively proximal, medial and distal outcrops of the Salt Wash DFS succession. The grain size recorded in 1D stratigraphic logs is used in the analysis. Note that only three sandstone bodies of Type 1 were logged in the Bullfrog 1 and Little Park 2 outcrops. See Table 7.4 for the number of measurements.

Evident downstream variations in sandstone composition, sorting (Appendix 3 Table 2) and porosity (Appendix 3 Table 8; Chapter 11; Fig. 11.2 - 11.4) have not been found. Higher mean values of total gamma ray and K, Th and U concentrations are observed in the distal deposits of the Salt Wash DFS (Appendix 7).

7.5.5. Summary of the downstream variations within the Salt Wash DFS deposits

- Overall increase in the non-sandstone, fine-grained deposit proportion;
- Decrease in the degree of amalgamation of sandstone body complexes;
- Decrease in width and thickness of Type 2 sandstone bodies;
- Increase in thickness of some of Type 3 sandstone bodies;
- Decrease in sandstone grain size of Type 2 (possibly Type 1) and increase in grain size of some Type 3 sandstone bodies;
- Increase in the proportion of Type 1 sandstone bodies in the distal outcrop;

- Change from channel macroform association to LA complexes association in Type 2 sandstone bodies;
- Change in subtypes of Type 3 and Type 2 sandstone bodies (occurrence of subtype 2/3, 3/1, 3/3 in the distal outcrop).

		Grain size , φ		
Sandstone body Type		**Bullfrog (relatively proximal)**	**Slick Rock (medial)**	**Little Park (distal)**
Type 1	max	2.00	-	2.50
	min	2.00	-	2.50
	average	**2.00**	**-**	**2.50**
	counts	1	-	2
Type 2	max	-4.00	1.00	1.00
	min	3.50	2.50	3.50
	average	**1.03**	**1.63**	**2.17**
	counts	122	47	63
Type 3	max	2.00	2.50	1.50
	min	3.50	3.50	3.50
	average	**3.23**	**2.90**	**2.85**
	counts	35	5	40

Table 7.4. Maximum, minimum and average values of the grain size (in φ) for three sandstone body types in relatively proximal, medial and distal outcrops of the Salt Wash DFS succession.

8. Discussion of possible controls on the downstream variations in facies distribution, sandstone body characteristics and their architecture

8.1 Introduction

Distinctive downstream trends in facies distribution, sandstone body characteristics and their architecture have been observed in the Huesca and Salt Wash DFS successions. The variations in sandstone body proportions, degree of their amalgamation, sandstone grain size, dominant sandstone body types and facies associations from relatively proximal to distal outcrops have been described in chapters 6 and 7. This chapter discusses possible causes of the downstream variations in depositional architecture within DFS successions considering data from these study areas and previous work.

8.2 Previous studies of the downstream variations in the architecture of the Huesca and Salt Wash DFS deposits

A downstream decrease in grain size, average channel body dimensions and proportion of channel-fill deposits has been described previously for the deposits of the western part of the Huesca DFS (Hirst, 1991; Nichols and Hirst, 1998). These changes were interpreted to be the result of downstream decrease in stream power due to evapo-transpiration of water and channel bifurcation. Downstream change in dominant sandstone body type from sheet-like to confined scoured (Type 2 to Type 1) were also noted (Hirst and Nichols, 1986; Hirst, 1991; Nichols and Hirst, 1998) and related to the increase in channel stability due to decrease in gradient, lower flow velocities, an ephemeral flow regime, cohesive overbank deposits and more frequent channel avulsions in the distal area of the Huesca DFS (Hirst and Nichols, 1986; Hirst, 1991; Nichols and Hirst, 1998). The distributive radial drainage of the DFS was also recognised to be one of the causes of the downstream changes in architecture of the deposits (Fig. 8.1, A; Nichols and Fisher, 2007).

Previous workers on the Salt Wash DFS deposits have also noted a downstream decrease in grain size of the DFS sandstones (Cadigan, 1967), a decrease in sandstone proportion (Fig. 8.1, B; Craig et al., 1955; Mullens and Freeman, 1957; Tyler and Ethridge, 1983), a change in channel type from braided (sheet-like Type 2 sandstone bodies) to more confined straight channels (isolated scoured Type 1 sandstone bodies) (Turner and Peterson, 2004), changes in paleosol types from dry to wet (vertic Calcisols to palustrine Protosols and argillic Calcisols) (Demko et al., 2004)

A. The Huesca DFS

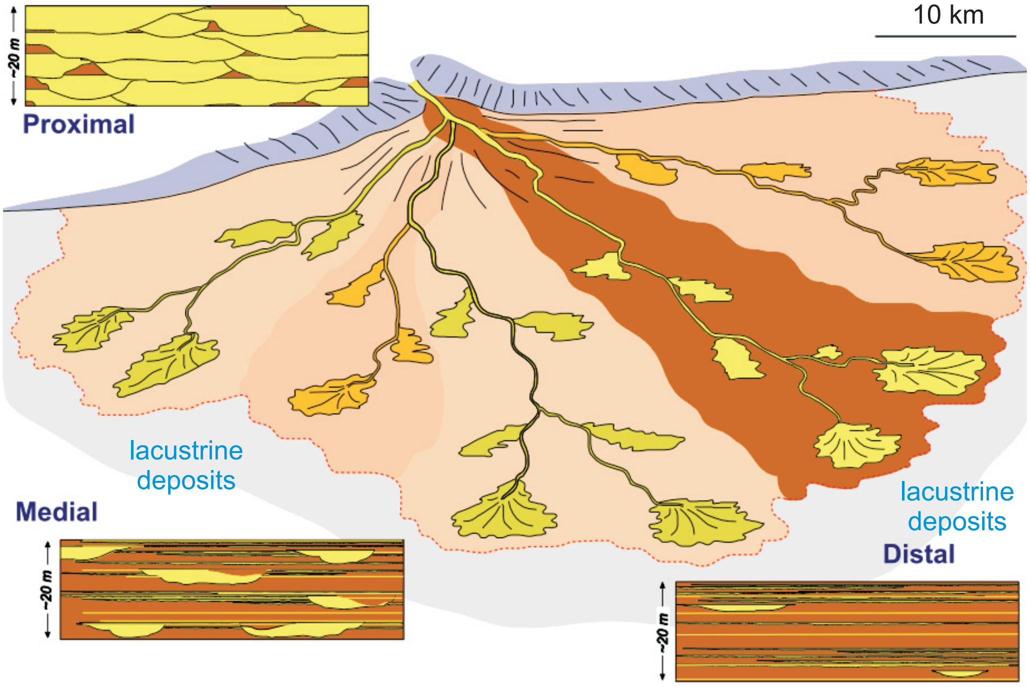

B. The Salt Wash DFS

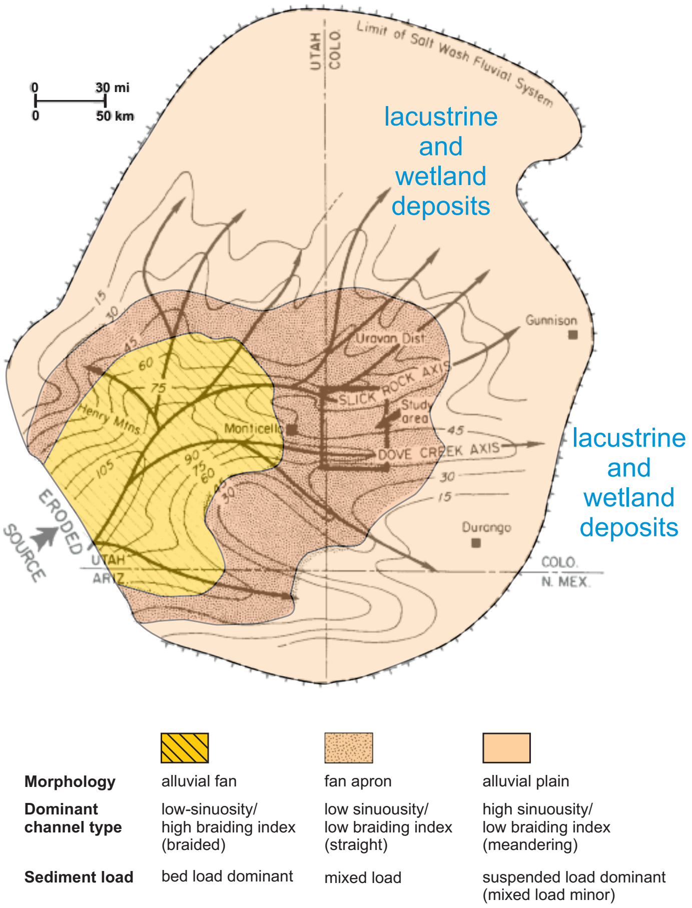

Figure 8.1. Previously proposed models showing downstream variations in the Huesca DFS (modified from Nichols and Fisher, 2007) (A) and Salt Wash DFS (modified from Tyler and Ethridge, 1983) (B).

and, finally, transition of fluvial deposits to wetland / lacustrine facies in the eastern part of the basin (Fig. 3.9 and 8.1, B; Turner and Peterson, 2004). Previously a change in channel planform from braided to meandering was recognised by Peterson (1977, 1986). Although recognised, the downstream variation in succession characteristics were not interpreted in detail and have mainly been described as a list of observations; however, few explanations have been provided. For example, the downstream decrease in channel deposit proportion was related to distributive radial drainage by Mullens and Freeman (1957). An intermittent water discharge was thought to be a cause of the change in channel type downstream (braided to more isolated straight) (Turner and Peterson, 2004). The dominance of wetland/lacustrine deposits in the distal area and downstream change from dry to wet paleosols were interpreted to be a result of higher water table in the distal area due to ground water and spring discharge (Turner and Peterson, 2004; Demko et al., 2004). Furthermore, some local changes in succession characteristics were related to local syn-depositional tectonic movements that locally affected the gradient of the DFS surface and therefore flow regime (Peterson, 1984).

In summary, the main previously suggested causes of downstream changes in deposit characteristics of the Huesca and Salt Wash DFS successions are: 1) distributive drainage pattern, 2) decrease in flow power downstream due to evaporation and infiltration of water and bifurcation of the streams and 3) intermittent discharge, more cohesive substrate and more frequent avulsions in the distal areas. These and other controls are discussed in the next sections.

8.3 Discussion of downstream trends in the DFS deposit architecture and their controls

8.3.1 Downstream trends in the grain size, sandstone body proportion and sandstone body dimensions in the Huesca and Salt Wash DFS successions

The grain size of sandstones of channel sandstone bodies (Types 1 and 2) becomes increasingly finer downstream in both DFS successions (chapters 6 and 7). The pebble size fraction present in proximal areas is noted to be absent in the medial outcrops and overall fine-grained deposits dominate the distal outcrops.

In the Huesca system the sediment was sorted by its grain size along a quite short transport distance of approximately 60 km which suggests a relatively rapid deposition rate. Coarse sandstone is definitely not present in the area beyond 40 - 45 km downstream of the apex of the Huesca DFS (there are no very coarse sandstones in the Castelflorite outcrop, Fig. 3.1). However, this distance should be regarded as a maximum and could be smaller as gaps in the downstream transect require more grain size data to be collected.

The Salt Wash DFS has a much larger radius of approximately 350 km and the coarse fraction disappears by approximately 220 km from the apex (e.g. very coarse sandstones are absent in the Slick Rock outcrop, Fig. 3.4). These data also require additional grain size study along downstream transects.

Both DFS successions studied in this research are also characterised by a decrease in sandstone body proportion from relatively proximal to distal outcrops (chapters 6 and 7). The sandstone body proportion decreases by 46 % in the Huesca succession and by 25 % in the Salt Wash succession. The difference in the magnitude of the decrease could be related to the overall dominance of the fine-grained sediment in the sediment load of the Huesca DFS compared to the Salt Wash DFS. Decrease in sandstone body dimensions has been also observed for Types 1 and 2 sandstone bodies (chapters 6 and 7).

8.3.2 Decrease in transport capacity of the streams and decrease in grain size and sandstone body dimensions

The decrease in the percentage of the coarse fraction and overall downstream decrease in the grain size in an aggradational setting is thought to be a result of a selective deposition during the sediment transport (Kuenen, 1959; Paola et al., 1992). The selective deposition is controlled mainly by grain entrainment velocity, and hence by flow strength (Kuenen, 1959; Paola et al. 1992). The observations of the decrease in grain size and channel sandstone body dimensions downstream in each study area imply that the transport capacity of the DFS streams decreases downstream and this reduces transport capacity of the channels (hence grain size of the sediment being transported) and reduces channel belt size (hence resulted sandstone body dimensions).

Feeder channel

The DFS feeding stream experiences energy loss when it becomes unconfined as it enters the basin (Fig. 8.2, A-E) due to increase in friction, reduction in flow velocity and shallowing of the flow (Weissmann et al., 2013 in press). This promotes deposition of the coarsest fraction of its sediment load (Weissmann et al., 2013 in press). Therefore, only finer grained sediment remains to be transported further downstream.

Evaporation

Further down the DFS the flow strength could be additionally reduced by water evaporation (Tooth, 2000; Nichols, 2005, Nichols and Fisher, 2007; Donselaar et al.,

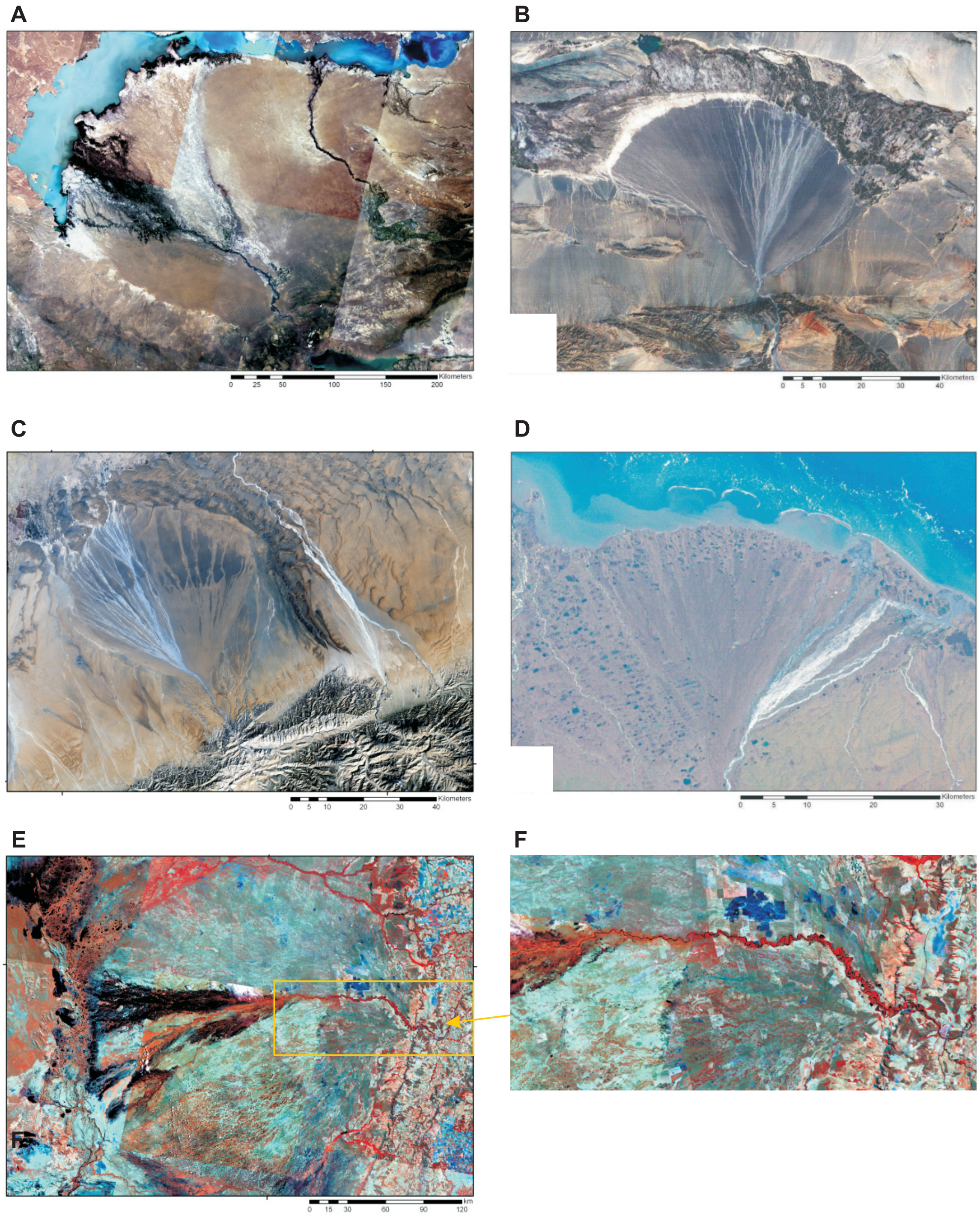

Figure 8.2. Examples of distributive fluvial systems showing that feeder channel becomes free to bifurcate and avulse when enter the basin. A - Ili DFS in Kazakhstan, B - DFS in China, C - DFS in Tarim Basin, China, D - DFS in Alaska, E - Taquari DFS in Brazil (all pictures are from Fig. 4, 5, 9 in Hartley et al., 2010). F - downstream narrowing and shallowing of the main channel of the Taquari DFS (Fig.1 in Assine, 2005). North is to the top in all images.

2012). Although the climate in the Miocene Ebro Basin was interpreted as temperate (Hamer et al., 2007(a)), it was characterised by a high evaporation to precipitation ratio (Nichols and Hirst, 1998). High evaporation to precipitation ratio was also chosen by Garcia-Castellanos et al. (2003) to model an endorheic, closed Miocene Ebro lake. Lower evaporation rates and higher precipitation (more humid climate) in the model resulted in the lake level rise and opening of the basin that is not consistent with the endorheic nature of the basin during Miocene. The Salt Wash DFS probably formed in a semi-arid, warm climate with high precipitation to evaporation ratio that is indicated by the presence of evaporites, pedogenic carbonates and aeolian deposits (Turner and Peterson, 2004; Demko et al., 2004). Thus evaporation could have reduced flow strength in both DFSs.

Infiltration

Decrease in flow discharge downstream has also been previously interpreted to be partially controlled by infiltration of water in dry Australian rivers by Tooth (2000) and in the dryland Rio Colorado in Bolivia (Donselaar et al., 2012). Turner and Peterson (2004) have also interpreted “losing” channels in the upper part of the Salt Wash DFS due to seepage of water through the sandy substrate deposits that spring in distal wetlands. Using electrical conductivity survey Massuel et al. (2006) showed that infiltration occurs below sandy channels on semiarid Niger fan (Fig. 8.3, A-B). Amalgamated sandstone bodies in the proximal area of a DFS could provide a suitable high permeability substrate for the infiltration of water (Weissmann et al., 2013 in press, Massuel et al., 2006; Blainey and Pelletrier, 2008). Both DFS successions are characterised by sandy / gravelly proximal deposits where infiltration could have occurred. The proximal to medial Salt Wash DFS deposits are dominated by amalgamated sandstone bodies that could have created continuous substrate suitable for the infiltration. In the Huesca DFS sandy channel deposits are enclosed in finer-grained floodplain deposits and perhaps less infiltration could have occurred.

Bifurcation

Bifurcation has been stated to be common in the medial and distal area of the modern DFSs (Fig. 8.6, A-C) (Davidson et al., 2013; Weissmann et al., 2013 in press). The bifurcation occurs due to in-channel deposition caused by reduction in flow strength downstream. The bifurcation in turn additionally reduces stream discharge and size by partitioning between two smaller channels according to their current capacities (Slingerland and Smith, 2004). This would reduce channel dimensions and possibly resulting sandstone body dimensions (Fig. 8.4, A-B). The reduction in water discharge downstream in a DFS due to infiltration, evaporation and stream bifurcation have been also stated to reduce channel belt dimensions by Weissmann et al. (2013 in press).

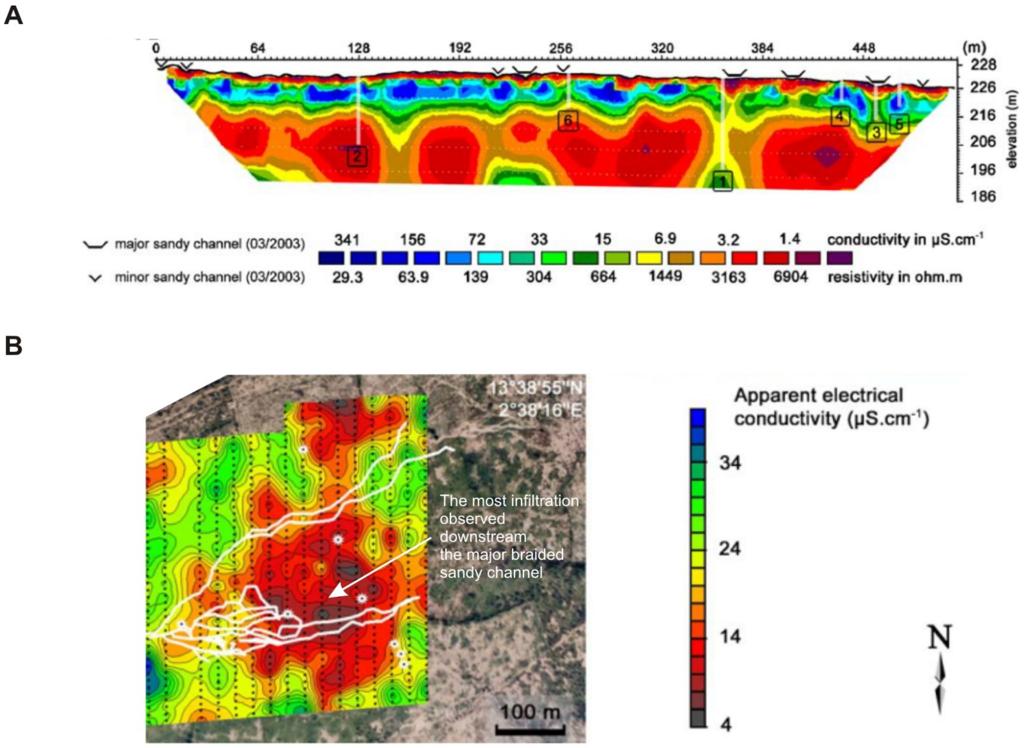

Figure 8.3. Electrical conductivity survey cross section and maps for Niger alluvial fan, NIamey, Africa (from Massuel et al., 2006). A – Cross section showing high conductivity layer between 5 and 10 m depth. This layer is disrupted by low conductivity anomalies below sandy channels that are cause by infiltrated water. B – Conductivity map showing low conductivity downstream the major braided stream on the fan.

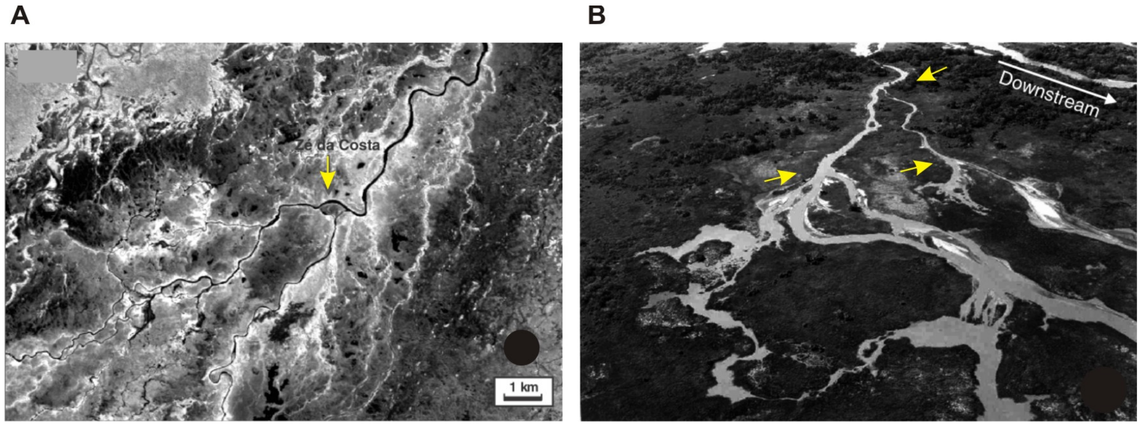

Figure 8.4. Bifurcation of channels on the Taquari DFS (from Assine, 2005). A – narrower bifurcated channels leading to future avulsion, B – bifurcation on the crevasse splay; note narrower channels immediately downstream from bifurcation point and transformation of channels into poorly-confined flow downstream due to subsequent bifurcations.

8.3.3 Distributive discharge and increase in proportion of fine-grained deposits

Channels on the DFS avulse and bifurcate forming a radial distributive facies pattern (Fig. 8.2; Weissmann et al., 2010, 2013 in press, Hartley et al., 2010(a)). The proportion of sandstone bodies can be related to the radial drainage of a DFS (Nichols and Fisher, 2007; Weissmann et al., 2013 in press). In the proximal part of the system channel migration is limited to a smaller area and channels are forced to rework previous deposits and especially finer-grained material transporting it further downstream (Nichols and Fisher, 2007; Davidson et al., 2013; Weissmann et al., 2013 in press). In addition, the flow power in the proximal part could be still high and that will prevent deposition of the fine-grained sediment (Weissmann et al., 2013 in press). Due to energy loss of the feeder stream in the proximal part of the DFS the accommodation is filled faster resulting in progradation of the DFS that in turn results in incision, reworking and bypass of the sediment in the proximal part and more reworking in the medial area (Weissmann et al., 2013 in press). Fine-grained deposits in these areas are reworked and transported downstream. This could create amalgamated sandstone bodies observed in relatively proximal successions of the studied DFSs, especially in the Salt Wash DFS.

The DFS occupies a larger area in the medial and distal parts where channels are smaller and can be located farther from each other (Fig. 8.1-2) (Nichols and Fisher, 2007; Weissmann et al., 2013 in press). Davidson et al. (2013) noted that channel to floodplain ratio in modern DFSs decreases downstream when floodplain area increases. Less coarse sediment is available in these areas because it was mostly deposited in the proximal part. Therefore in these areas channel sandstone bodies are separated by thicker and wider floodplain deposits. The same architecture has been observed in the distal Huesca and Salt Wash DFS successions (chapters 6 and 7). Weissmann et al. (2013 in press) stated that accommodation space in the distal areas of a DFS is relatively high and reworking is low resulting in preservation of floodplain deposits unless progradation of the DFS occurs and floodplain deposits are reworked.

8.3.4 Substrate cohesiveness and change in sandstone body type

The downstream increase in proportion of fine-grained deposits caused by selective deposition from decelerating flow and decrease in degree of reworking leads to the formation of a cohesive substrate in the distal part of the DFS. Fine-grained deposits in the distal parts of the Huesca and Salt Wash DFS successions represent 83 % and 38 %, respectively (chapters 6 and 7). A cohesive substrate together with low flow strength and low gradient in the distal area reduces the ability of flow to incise (Wohl and Ikeda, 1997) and, consequently, migrate laterally. Changes in the depth of channel scours was also related to the cohesiveness of the substrate on the floodplain of the

Rhine-Meuse delta by Makaske (2007). This could result in formation of Type 1 sandstone bodies of limited width and depth that were mainly observed in the medial and distal areas of the Huesca DFS succession and in the distal part of the Salt Wash DFS succession.

Vegetated channel banks indicated by abundant roots in the floodplain deposits in both studied fluvial systems (Chapter 4) could also have strengthened the bank resistance to erosion (Tooth, 2000). For example, channels confined by vegetation have been observed on the Okavango fan (McCarthy et al., 1992). Alfisols and Entisols (USDA classifcation, Soil Survey Staff, 1992; Argillisols and Protosols in Mack et al.,1993) were interpreted to form on the floodplain deposits of the Huesca DFS in areas furthest from channels and the source (Hamer et al., 2007(a)). These areas were described to be covered by herbaceous vegetation, reed-like monocotyledons, low stature plants and small open woodland trees (Hamer et al., 2007(a)). The paleosols of the Salt Wash system have also been described as forming a lateral catena from poorly-developed Protosols near the channel or in proximal area of the DFS to better-developed, wetter Calcisols (Mack et al., 1993; Aridisols or Molisols, Alfisols and Inceptisols in USDA classification, Soil Survey Staff, 1992) furthest from the channel or closest to the lake margin areas (Demko et al., 2004). The areas close to the channel were the areas of riparian vegetation (coniferous shrubs and trees and smaller plants including ginkgophytes, cycades, tree ferns, horsetails and variety of ferns) while herbaceous vegetation cover was characteristic of the floodplain that was more distal to the channels (Turner and Peterson, 2004). The herbaceous vegetation cover was stated to prevent significant erosion of floodplain deposits by Turner and Peterson (2004). Thus the vegetation could have contributed to the cohesiveness of the channel banks in both DFSs.

Flume experiments by Wohl and Ikeda (1997) and Shepherd and Schumm (1974) and field studies by Wohl and Achyuthan (2002) showed that anastomosing, narrow and deep channels form with increasing of substrate resistance. Although the experimental flume model cannot be scaled to the real conditions, the low / moderate gradient case of the model resulting in small, slightly anatomising grooves could explain the presence of sandstone bodies of stable channels (subtypes 1/2 and 2/3) in the distal area of the Huesca and Salt Wash DFS successions. The sandstone bodies of subtype 1/2 are consistent with the model results, but they are not very deep (up to 2 m) that could be explained by a reduced ability of flow to incise (Wohl and Ikeda, 1997) due to a low flow discharge and cohesive substrate. The authors of the model emphasised that, in addition to substrate type, variation in other external factors such as water and sediment discharges, together with variations in base level may influence incision.

8.3.5 Avulsion and change in sandstone body type

In addition, a downstream decrease in flow strength also causes an increase in deposition. Sedimentation in turn results in alluviation of a channel and finally blockage of the channel with sediment that promotes avulsion (Bridge, 2003; Jones and Schumm, 1999; Sheets et al. 2007). The channel, therefore, has no time to migrate laterally and create laterally continuous sandstone bodies, instead it leaves small lenses of sand (subtype 1/2 or subtype 2/3) representing bankfull-filled channel scours. Avulsion by capacity reduction was described for many modern narrow anastomosing channel networks (Martínez et al., 2010). Frequent avulsion on the Chaco Plain DFSs was also interpreted as a cause of limited lateral migration of channels (Horton and DeCelles, 2001). Whether narrow sandstone bodies observed in the Huesca and Salt Wash DFS succession represent anastomosing channel network or not is difficult to justify in 2D outcrops, but frequent avulsion could have been a control on their size because evidence of avulsion by channel blockage have been observed (Chapter 5).

Alternatively, occasional subtype 1/2 sandstone bodies could have formed as “on-fan” channels (Cain and Mountney, 2009) that originated from unconfined flow generated in the medial/distal part of a DFS that converged into a single channel downstream. Evidences supporting this interpretation are impossible to observe in the outcrops.

Another possible explanation for the formation of laterally stable channels in the distal areas is occasional strong flows that reach the distal area during high water discharge periods. For example, progradation and retrogradation of a coarse sediment front within alluvial fans on the margin of the foreland basin model have been related to high discharge phases by Clevis et al. (2003).

In summary, the reduced flow strength in vegetated distal part of a DFS leads to more frequent channel avulsions and formation of finer-grained and cohesive substrate. These factors in turn could result in the formation of more laterally stable and less incised channels resulting in a decrease in width and thickness of channel sandstone bodies. The change from sheet-like Type 2 sandstone bodies to narrower subtype 1/2, 1/3 and 2/3 sandstone bodies have been observed within the studied DFS successions.

8.3.6 Termination of channels and change in sandstone body type

The downstream change in characteristics of a DFS, in particular the decrease in flow strength and increase in substrate cohesiveness, can affect the ability of flow to form scours. Channels become shallower or even poorly confined downstream and consequently form thinner sandstone bodies of subtype 3/1 observed in the studied successions. Shallow, poorly confined channels in the distal area are more affected by floods which gradually smooth channel boundaries and transform them into unconfined flows (floodout zones of Tooth, 2000). Poorly confined and unconfined flows form fan-shape terminal splays which terminate in mudflows (Kelly and Olsen, 1993). Spreading of water in splays in the distal area adds to the reduction of water flow discharge through transmission loss (Tooth, 2000) that in turn could cause termination of the flow or its accumulation in lake(s) or wetlands.

Terminal splays form sheet-like sandstone bodies of sybtypes 3/1, 3/2 and 3/3. The first two sandstone body types dominate distal outcrops of the Huesca succession and all three types are abundant in the distal outcrop of the Salt Wash succession. Lacustrine limestones and wetland deposits observed in the distal outcrops of the studied DFSs are consistent with this model.

In contrast to the observed downstream decrease in grain size and dimensions of Type 1 and 2 sandstone bodies, sandstone bodies of subtype 3/2 are characterised by similar grain size and dimensions in all parts of the DFS successions (chapters 6 and 7). This could be explained by their similar origin from “low energy unconfined flow” (Fisher et al. 2007(a)) both on the floodplain next to a channel and on the distal alluvial plain in terminal splays. Sandstone bodies of subtypes 3/1 and 3/3, however, are an exception and are represented by thicker and in places coarser sandstones (Chapter 7). These sandstone bodies were formed by poorly-confined flow or in poorly-confined sinuous channels, respectively, where flow has relatively higher energy (Chapter 5) and is capable of transporting coarser material. However, it remains uncertain why some flows in the distal DFS area are incised, forming channel scours and others are less confined. One of the explanations of this could be that these variations in flow behaviour are related to fluctuations in discharge such that an increased discharge will force flows to incise.

8.3.7 Lake level

Lake and wetland level fluctuations probably had little effect on the fluvial channels due to the low surface gradient of the distal areas of the studied DFSs (Schumm, 1993; Posamentier et al., 1992; Shanley and McCabe, 1994). These conditions correspond to the case described by Posamentier et al. (1992) when channel gradient adjustments, either erosion or deposition, do not occur. The lake level fall, in this case, would not cause a change in river profile but would extend its length in which case there is no requirement for the channel to adjust. That is in contrast to the conditions when the lake slope is steeper or shallower resulting in acceleration or deceleration of a channel flow promoting erosion or deposition, respectively. It has also been shown that a change in base level does not affect the upstream reaches of a fluvial system with a low gradient at their termination or distal from the source area (Posamentier et al., 1992; Holbrook et al., 2006).

Lakes in the centre of the Ebro Basin have been previously described as ephemeral lakes and changed their extent according to small variations in climate (Nichols and Fisher, 2007; Hamer et al., 2007(a), (b)). The architecture of the distal succession of the Huesca DFS records only minor meter-scale variations caused by lake level fluctuations (Fisher and Nichols, 2012). In this work, field observations in the distal outcrops of the Huesca succession do not show any significant change in the amount of erosion beneath sandstone bodies either adjacent to, interbedded with or more distant from lacustrine limestones. The distal succession interbedded with the limestones is dominated throughout by sheet-like sandstone bodies formed by terminal splays, with only occasional scoured channel sandstone bodies, indicating relatively constant stream power overall (Chapter 6, Fig. 6.10).

The distal environment of the Salt Wash DFS is poorly studied due to poor exposure of the succession in central Colorado but it is generally considered to represent hydrologically open wetlands and small lakes (Turner and Peterson, 2004). Thus fluctuation in base level could have occurred. The Salt Wash DFS has also been determined to flow over an almost flat surface with small, localised irregularities (Mullens and Freeman, 1957; Peterson, 1984). The base level effect on the deposits exposed in the Salt Wash outcrops studied in this research is considered minor due to the low surface gradient and large distance from the basin centre to the upstream study areas. Thus, it could be concluded that lake level fluctuations did not significantly affect channel behaviour and resulted architecture in the Huesca and Salt Wash DFSs.

8.3.8 Summary

The complex relationships between different factors affecting downstream variations are presented in diagrammatic way in Figure 8.5. The ultimate result of the combination of all factors is a downstream decrease in the degree of sandstone body amalgamation and connectivity.

8.4 Downstream variations in DFS characteristics and architecture of DFS deposits in documented modern and ancient DFSs

Distributive fluvial systems have been rarely recognised in the geological record, while their modern analogues have received greater attention (e.g. Assine, 2005; Weissmann et al., 2010; Hartley et al., 2010(a); Chakraboty et al., 2010; Buehler et al., 2011; Davidson et al., 2013). Downstream variations that have been mainly recognised from the modern DFS and then observed in the ancient DFS deposits are exemplified in this section.

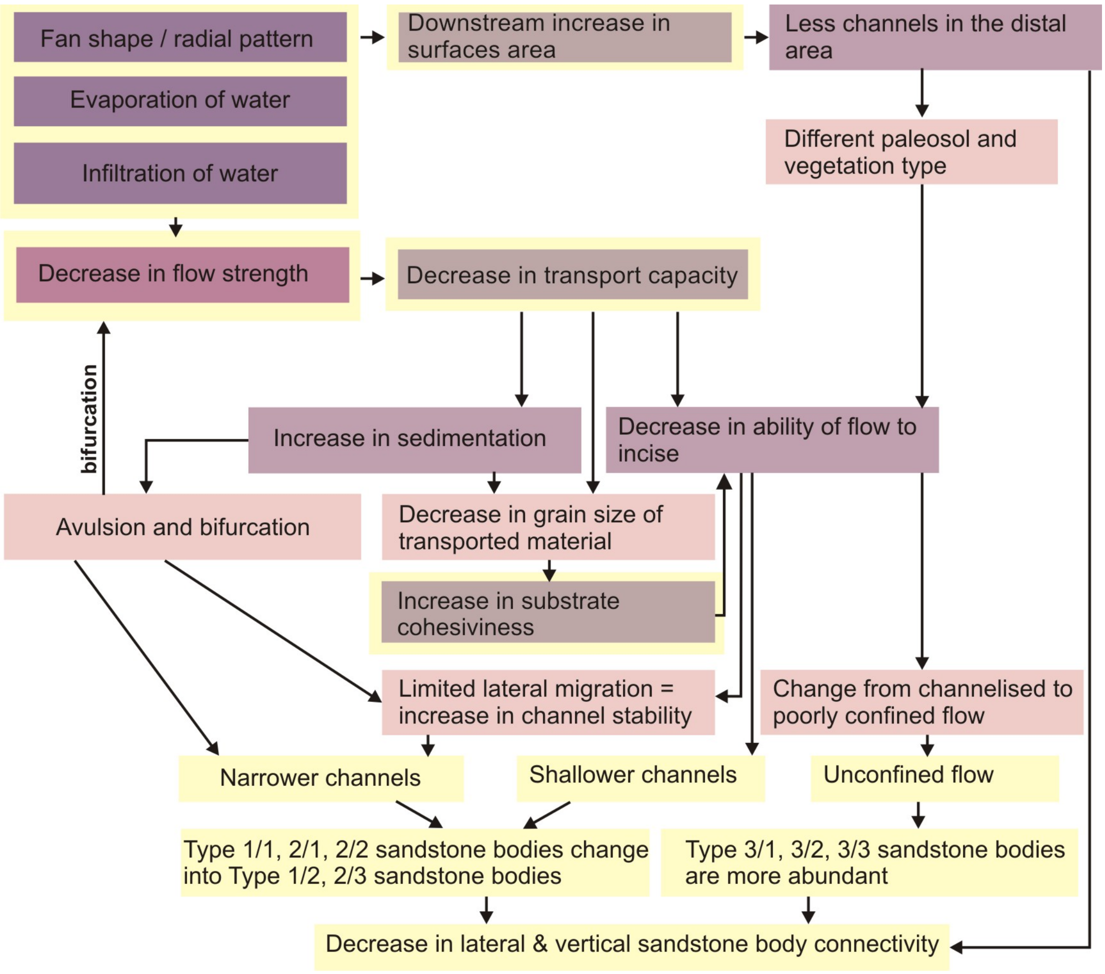

Figure 8.5. Downstream variation in the DFS flow behaviour and resulted changes in DFS deposit architecture.

8.4.1 Downstream trends in the modern DFSs

Four main DFS zones from apex to the distal areas have been distinguished by Davidson et al. (2013) based on the studies of satellite images of modern DFSs (Fig. 8.6, A-C). Davidson et al. (2013) recognised following downstream changes through the zones: 1) decrease in discharge and stream power; 2) decrease in grain size of material being transported; 3) decrease in channel width and depth; 3) increase in avulsion and bifurcation of the channels, 4) increase in channel sinuosity. Decrease in stream power and gradient downstream, causing change in channel types and dimensions, and more frequent avulsions have been recognised for a number of modern examples. Narrower, incised and more sinuous channels have been observed in the distal part of the Kosi fan and were related to decrease in the gradient of the system (Fig. 8.7, A-B; Wells and Dorr, 1987; Singh et al., 1993; Chakraborty et al. 2010). Decrease in discharge and surface gradient downstream causing narrowing and

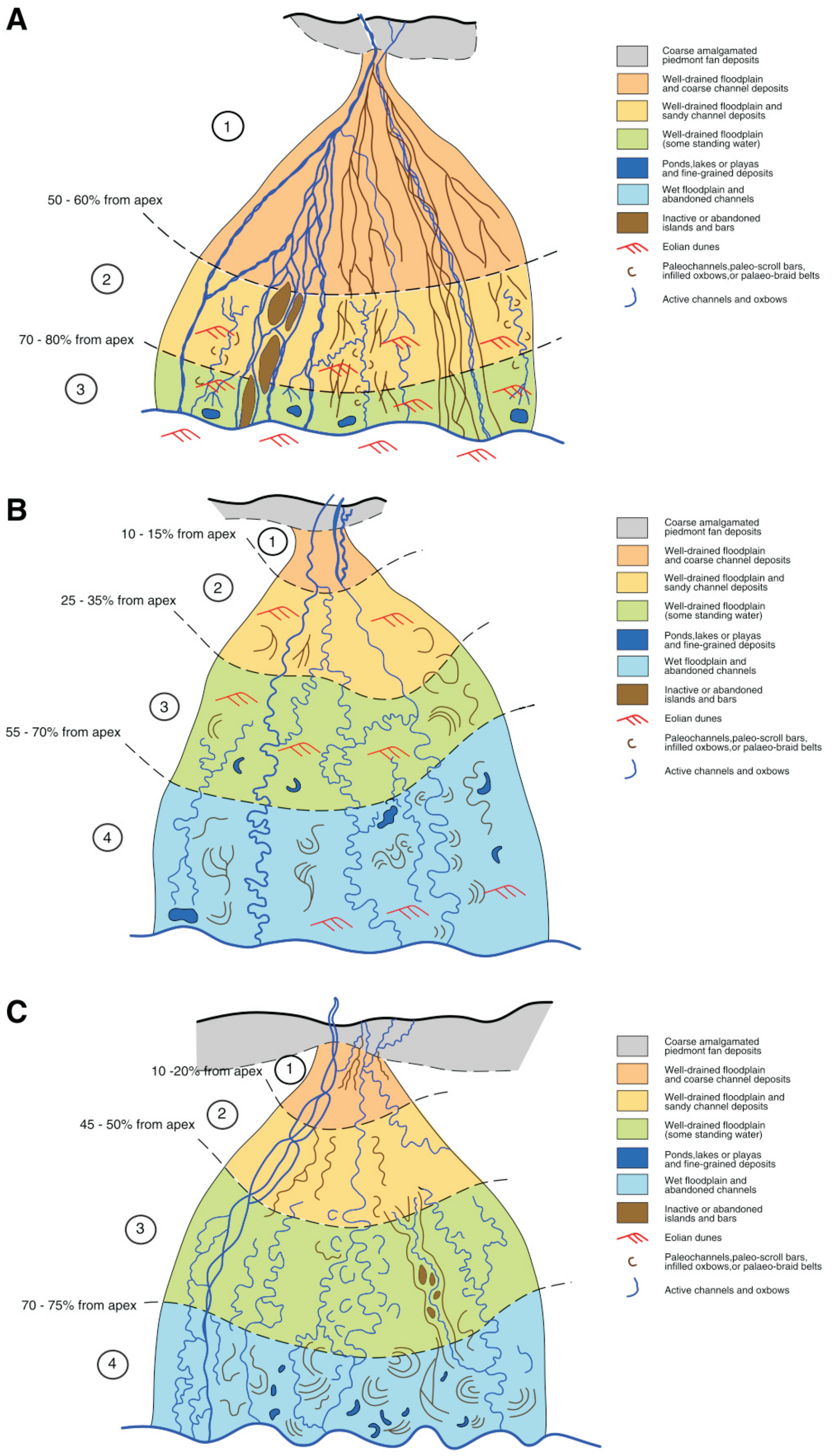

Figure 8.6. Schematic models of the geomorphic elements for three types of DFSs: A - braided bifurcating, B - single-thred sinuous (meandering) anabranching, C - multi-thread (braided) anabranching. Note bifurcation in the medial area (from Davidson et al., 2012).

shallowing of the Taquari River was described for the modern Taquari DFS of the Pantanal wetland, Brazil (Fig. 8.2, E-F; Assine, 2005). Anastomosing channels within an avulsion lobe of the Taquari DFS change to unconfined flow downstream and spread into wetlands (Fig. 8.7, C; Buehler et al., 2011). Channel avulsions caused by downstream decrease in flow velocity were also observed on the Okavango DFS in Botswana that are cause by rapid aggradation and blockage of the channels (MaCarthy et al., 1992).

8.4.2 Downstream trends in the ancient DFS deposits

Proximal to distal trends in proportion of sandstones, sandstone grain size and width and thickness of sandstone bodies have been described for the Cenozoic Camargo Formation exposed in the Eastern Cordillera, Bolivia (Fig. 8.8, A) (Horton and DeCelles, 2001). The authors have pointed out that downslope reduction in grain size and water discharge is characteristic for distributive fluvial systems (fans), while “normal” tributary rivers in contrast increase their channel size and discharge downstream. The Camargo succession was compared to modern fluvial megafans of the Chaco Plain which show similar downstream trends in grain size and channel size. In addition, large main channels in the proximal area of these modern systems were observed bifurcating into smaller distributive channels downstream and ultimately changing into unconfined flow in its distal part where they terminate in swamps. Such downstream changes were also interpreted to be associated with downstream decrease in water discharge.

Proximal to distal variations in sedimentary style have been observed for the fluvial deposits of the Permian Organ Rock Formation, Utah, USA (Cain and Mountney, 2009, Fig. 8.8, B); they are a decrease in degree of sandstone body amalgamation, overall sandstone body proportion, grain size, change from sandstone bodies formed in major channels to thin sheet-like sandstone bodies (~ Type 3) and ribbon channel elements (~ Type 1) formed by unconfined flow and in minor channels, respectively. These changes in deposit characteristics were also stated to be controlled by a downstream decrease in discharge, increase in cohesiveness of channel banks, decrease in channel capacity due to frequent flooding events, evapo-transpiration of water and infrequent discharge regime.

Krassenberg and Bridge (2008) created a 3D model of a distributive fluvial system based on the data from Rhine-Meuse delta that showed a downstream decrease in width, thickness and connectivity of channel deposits governed by downstream decrease in water discharge, longevity of channel belts (avulsion frequency) and aggradation rate (Fig. 8.8, C).

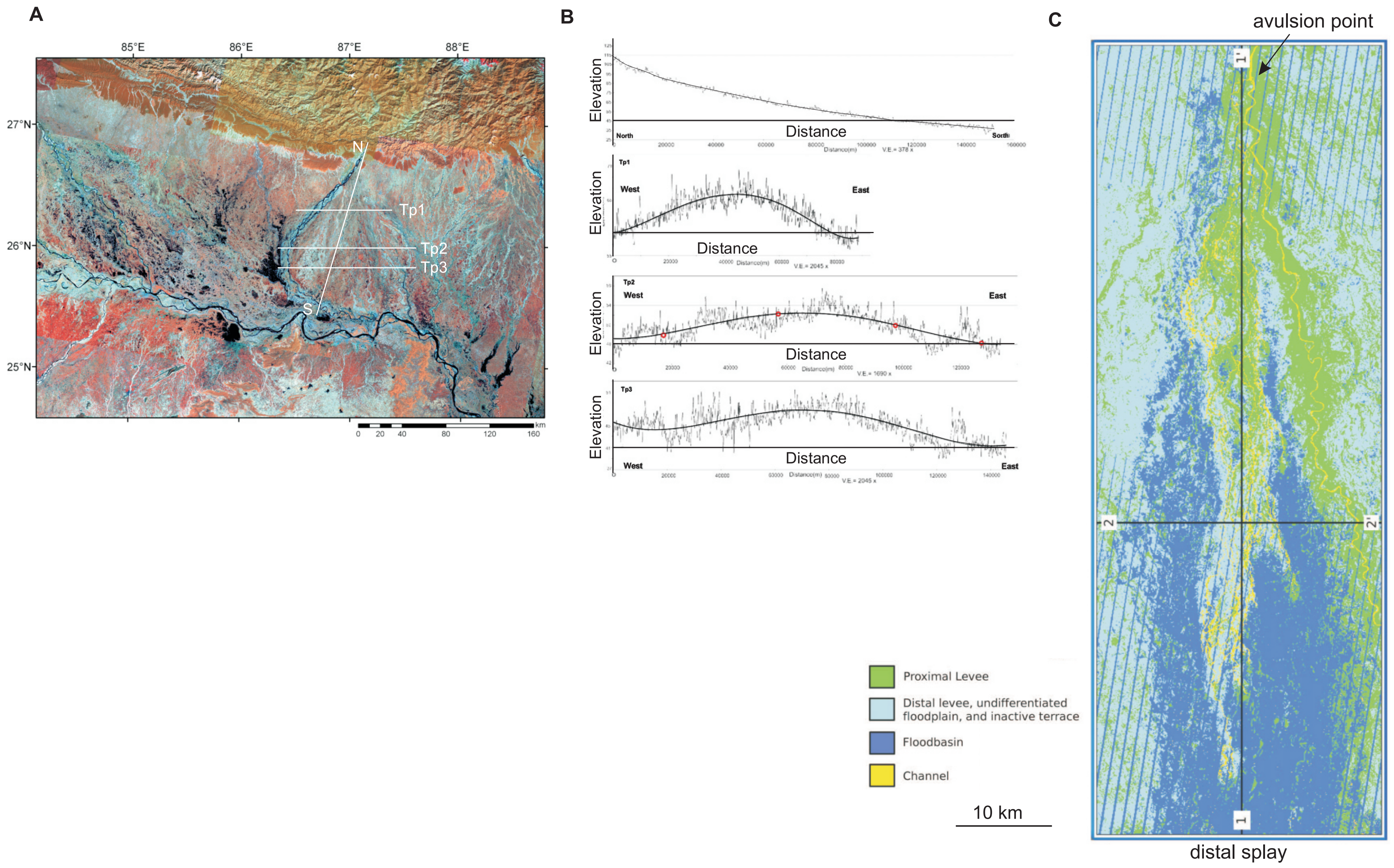

Figure 8.7. A - Kosi DFS in the Himalayan Basin (from Fig. 2 in Weissmann et al., 2010). White lines mark cross section shown in the figure B. B - downstream and cross slopes of the Kosi DFS (from Fig .5 in Chakraboty et al., 2010). Note decrease in gradient downstream. C - Map of avulsion splay on the Taquari DFS showing transition from the environment dominated by channel-levee facies to the area downstream that dominates by floodbasin facies (modified from Fig.11 in Buehler et al., 2011).

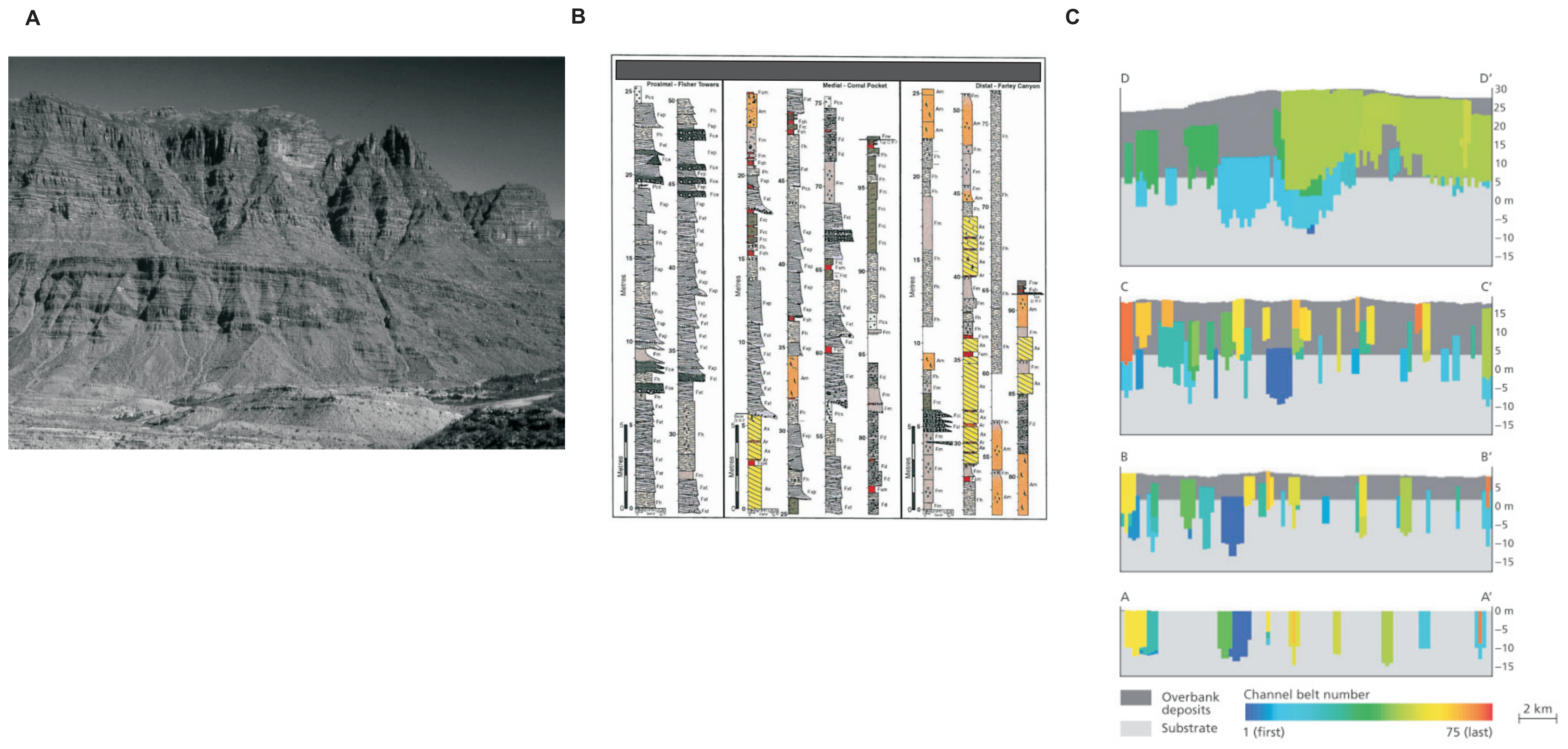

Figure 8.8. A - coarsening-upward succession of Camargo Formation formed due to progradation of proximal, medial and distal zones of the DFS (from Fig. 7 in Horton and DeCelles, 2001), B - sedimentary logs of Organ Rock Formation representing proximal, medial and distal DFS successions (from Fig. 4 in Cain and Mountney, 2009). Note downstream decrease in proportion of channel sandstone bodies relatively to fine-grained deposits of the alluvial plain and aeolian deposits (yellow), C - cross section across the 3D numerical model of DFS showing modelled decrease in channel size downstream (from top to bottom) (from Fig.14 in Karssenberg and Bridge, 2008).

Previously observed downstream trends within modern and ancient DFS deposits and interpretation of their controls are consistent with the discussion presented in this thesis.

8.5 Conclusions

In the last three chapters the main facies associations, sandstone body types and their variations downstream the Huesca and Salt Wash DFSs have been described. Distinctive proximal to distal trends are recognised in facies associations, sandstone grain size, sandstone body proportion, their types and dimensions, and architecture within both DFS successions. The comparison with other ancient DFS examples shows that downstream trends are common for DFS deposits in general. The DFS parameters appear to vary downstream in a specific way that is controlled mainly by downstream decrease in water discharge. The flow strength is in turn controlled by distributive nature of the discharge and infiltration and evaporation of water. The same factors have been observed controlling modern DFSs behaviour.

Hartley et al. (2010(b)) emphasised a lack of basin-scale studies of variations in deposit architecture within fluvial system successions. This research documents and interprets such variations within two DFS successions. The description of downstream trends in DFS deposit characteristics makes it possible to predict the main depositional elements and their distribution in proximal, media or distal parts of a DFS and this has important implications for reservoir characterisation and modelling (see discussion in chapters 11 and 13).

9. Heterolithic fine-grained deposits of the Huesca DFS succession and avulsion styles

9.1 Introduction

A study of the fine-grained, heterolithic elements of DFS deposits architecture has been undertaken to compliment the analysis of DFS sandstone bodies and investigate avulsion styles of the Huesca DFS. The Huesca DFS succession has been chosen for this study because it is dominated by fine-grained deposits which are well exposed. For the purposes of this study a number of sedimentary logs have been recorded in floodplain intervals (Chapter 3; appendices 2.13-18). Heterolithic architectural elements within channel-fill and floodplain intervals will be discussed in this chapter and the role of avulsion processes in the formation of floodplain deposits together with interpretation of the main avulsion styles of the Huesca DFS will be considered.

9.2 Heterolithic deposits of the Huesca DFS succession

Two main categories of heterolithic deposits in the Huesca DFS succession can be distinguished: channel fill and overbank heterolithic deposits. The characteristics of heterolithic deposits and the interpretation of their origin are discussed in detail in Chapter 4 and are briefly summarised in this section.

9.2.1 Heterolithic channel fill deposits

Heterolithic channel fill deposits include large- and small-scale heterolithic lateral accretion (LA) complexes (facies His2 and His3) and channel scours filled with heterolithic overbank facies Hsh and Hm.

The heterolithic LA complexes

The heterolithic LA complexes are a product of accretion of sand grade and finer sediment on a point bar in laterally unstable major and minor channels (Fig. 9.1, A, C, G, H, I; Chapter 4). In general the heterolithic nature of large-scale LA complexes (facies Sis and His1) has been related previously to changes in the flow regime in a channel (Thomas et al., 1987; Donselaar and Overeem, 2008; González-Bonorino, 2010). The occurrence of large-scale fine-grained heterolithic LA complexes (subfacies His2, Fig. 9.1, A, C) is considered to be the result of an overall low flow regime in the major channels in comparison to a high flow regime associated with sandy deposition within the channel (facies Sis and His1). Smaller-scale and finer-grained heterolithic LA complexes (subfacies His3, Fig. 9.1, G-I) may have formed in minor channels on the

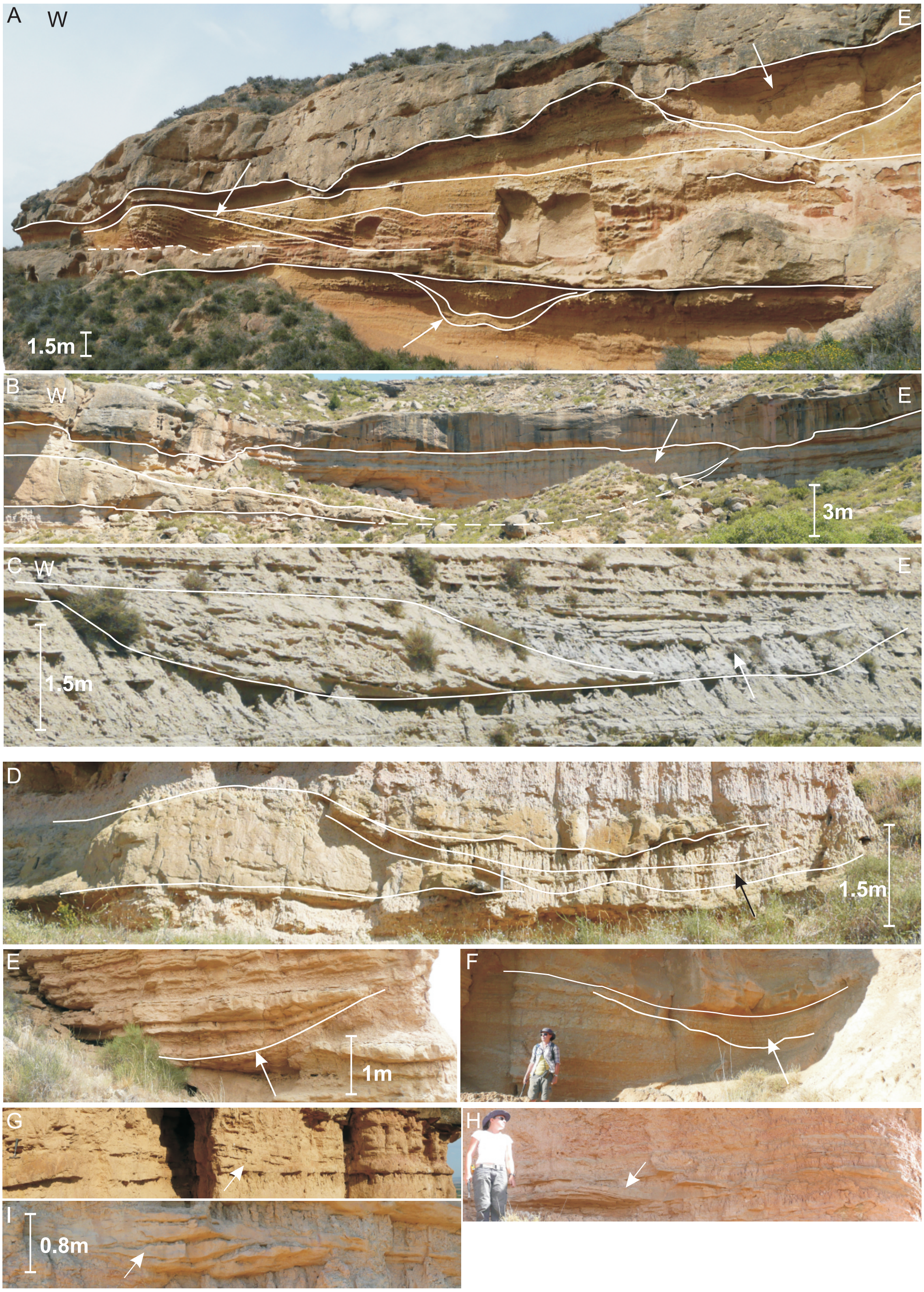

Figure 9.1. Examples of heterolithic channel fill deposits. A - large-scale heterolithic LA complex and isolated channel scours filled with fine-grained deposits (Monźon outcrop); B, C, D – “clay plugs” associated with Type 2 sandstone bodies (Piracés and Canal del Cinca near Piracés outcrops); E, F - isolated channel scours filled with heterolithic fine-grained deposits (Pertusa and Monźon outcrops); G, H, I - small-scale LA complexes and associated “clay plugs” (Piracés, Castelflorite and Bolea outcrops). Locations of the outcrops see in the Fig. 3.1.

floodplain where the flow regime would have been also variable but weaker than in the major channels. The small-scale heterolithic point bars are observed isolated and enclosed by finer-grained floodplain deposits (facies Hm, Fig. 9.1, G, I) or within packages of closely-spaced Type 3 sandstone bodies (facies Hsh, Fig. 9.1, H).

Channel scours filled with fine-grained heterolithic deposits

Channel scours filled with fine-grained heterolithic deposits of facies Hsh and Hm are usually found associated with Type 2 channel sandstone bodies (Fig. 9.1, B-D) (more rarely with Type 1) and with heterolithic LA complexes (His2 and His3 facies). The scours may have a scour depth similar to the thickness of the associated sandstone body or less and occur within the top part of the sandstone body. They are considered to represent abandoned channel scours (Hirst, 1991, Donselaar and Overeem, 2008; Mohrig et al., 2000).

Some abandoned channel scours were observed to be isolated and encased within finer-grained overbank deposits (Fig. 9.1, A, E-F). The isolated scours could represent channels abandoned before in-channel sand deposition occurred.

The deposits filling both types of abandoned scours are represented by the same interbedded facies Hsh and Hm. Abandoned scours of both types created depressions on the floodplain that were filled with overbank sediments derived from adjacent active channels (cf. Kraus, 1996; Mohrig et al., 2000). The presence of abandoned scours is indicative of channel avulsion.

9.2.2 Heterolithic overbank deposits

The heterolithic overbank deposits include sheet-like sandstone packages, consisting of amalgamated lenses intercalated with mudstone interlayers (facies Ssh and Hsh), isolated scours filled with sand (facies Sils), and packages of interbedded siltstone and mudstone sheets (facies Hm) (Fig. 9.2, A-G). All deposits are pedogenically altered and bioturbated (Fig. 9.2, H, I). In terms of the sandstone body classification presented in Chapter 5, the heterolithic overbank deposits include sandstone bodies of subtypes 3/1, 3/2 and 1/3, but mainly sandstone bodies of subtype 3/2.

Packages of closely-spaced sheet-like sandstone bodies

Packages of closely-spaced sheet-like sandstone bodies (subtype 3/2) interbedded with thin mudstone layers (Fig. 9.2, A-C) and occasionally cut by small-scale scours (Type 1/3) (Fig. 9.2, D-E) show less pedogenic alteration than the packages of finer facies Hm separating them (Fig. 9.2, F-G). As interpreted in Chapter 4, the deposits of the packages are considered to have accumulated on a lateral splay in a position that was relatively proximal to the main channel axis, or in a terminal splay proximal to the channel mouth in the distal part of the Huesca DFS.

The heterolithic Hm facies

The heterolithic finer-grained Hm facies (Fig. 9.2, F, G) are represented by bioturbated and pedogenically altered packages of interbedded siltstones and mudstones sheets. The packages are interpreted to be deposits which were distal to the channel in lateral or terminal splays (Chapter 4).

Small-scale scours filled with sand

Small sours filled with structureless very fine- to fine-grained sandstone (Fig. 9.2, D, E) could have been formed as a result of scouring at the base of unconfined flow or by channelised flow on splays. The scours are often associated with the sandstone sheet packages of proximal splays.

“Heterolithic upper part” of LA complexes

In places where there is continuous, good quality exposure, some packages of interbedded subtype 3/2 sandstone bodies and mudstone layers were observed to be laterally equivalent to the “heterolithic upper part” of LA complexes of a Type 2 sandstone body (Fig. 9.3). They consist of similar deposits as proximal splay facies and it is difficult to differentiate them in cases of limited exposure quality unless the available outcrop exposes the “heterolithic upper part” facies and related channel sandstone body.

In summary, channel fill deposits of major channels in the Huesca DFS succession include heterolithic deposits in addition to sandstones, indicating that rivers on the Huesca DFS had variable discharge. The floodplain intervals of the Huesca DFS are also characterised by more complex architecture than just a simple succession of interbedded sandstone, siltstone and mudstone sheets of facies Ssh, Hsh and Hm. The floodplain succession usually consists of fine-grained heterolithic deposits of lateral splays formed both proximal and distal to the channel, deposits formed towards the upper part of point bars, heterolithic point bar deposits in minor channels, and minor and major abandoned scours filled with heterolithic deposits (appendices 2.13-18). The floodplain architecture of the Huesca DFS was therefore defined by a combination of unconfined and channelised water/sediment transport processes operating at different distances relative to the major channel. The architecture was also governed by floodplain topography at the time of deposition, e.g. abandoned channel scours were filled with heterolithic floodplain deposits.

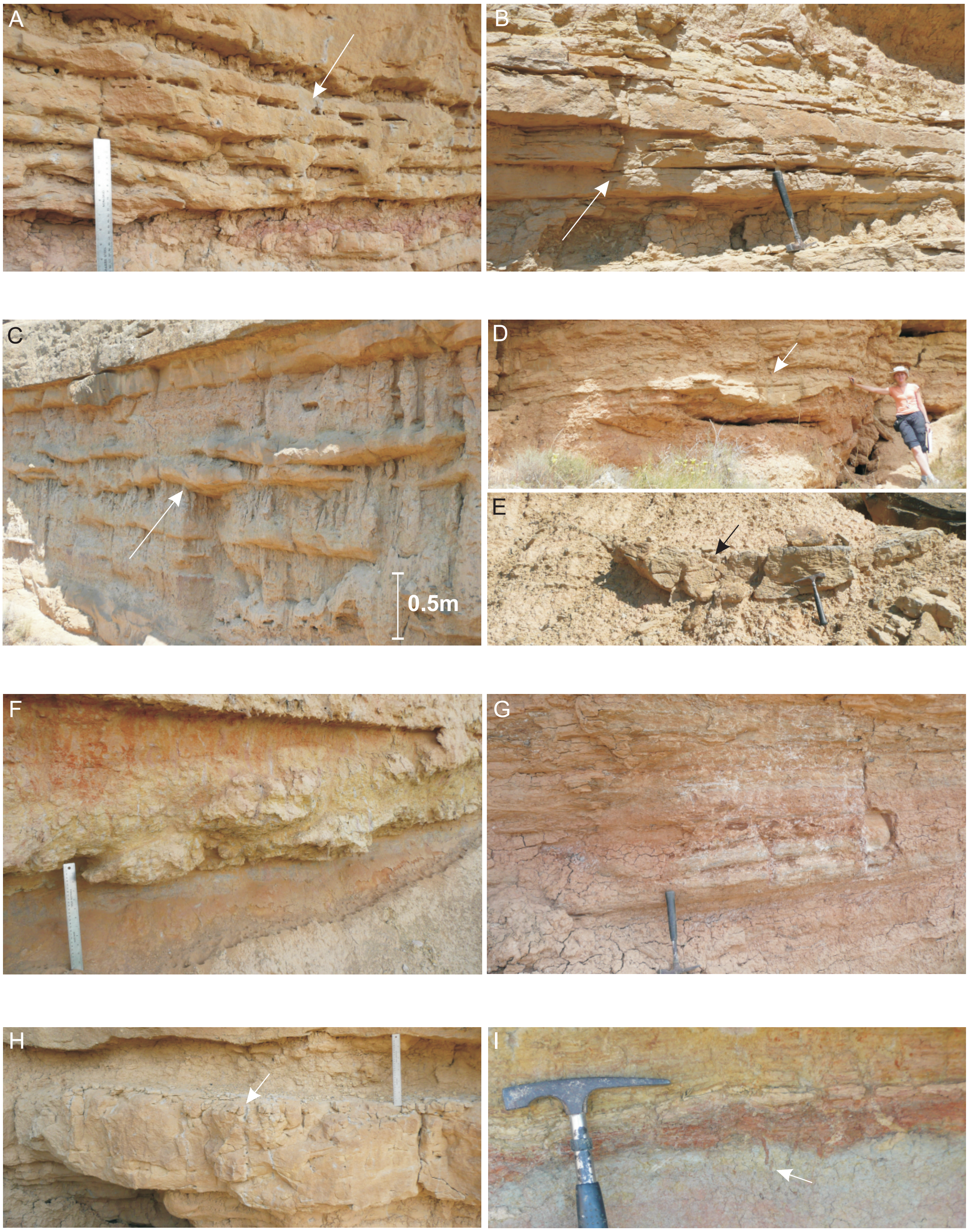

Figure 9.2. Examples of floodplain elements: A, B – packages of interbedded Type 3 sandstone bodies and mudstone layers from Pertusa and Castelflorite outcrops; C – Type 3 sandstone bodies with scoured bases from Monźon outcrop; D, E - small-scale scours filled with sand (Type 1/3 sandstone body) from Pertusa and Monte Aragón outcrops; F, G – fine-grained heterolithic overbank deposits from Novales and Bolea outcrops; H – bioturbation in sandstone body of subtype 3/2 from Pertusa outcrop and I – bioturbation in overbank siltstones from Piracés outcrop. Locations of the outcrops see in Fig. 3.1.

The large-scale heterolithic LA complexes may be distinguished from floodplain deposits if inclined stratification can be identified and it is possible to establish their association with sandstone bodies of Type 2 and abandoned scours ("clay plug"). In contrast, the deposits filling abandoned scours are similar to the overbank heterolithic deposits and could not be easily differentiated unless an onlapping relationship with the margin of the channel scour can be observed (Fig. 9.4). Less developed paleosols were observed within abandoned scours, especially in their lower part, in comparison with surrounding paleosols in the floodplain deposits in the Willwood Formation in Wyoming, USA (Bown and Kraus, 1987): the deposits within the scour are younger and were deposited at higher aggradation rate and therefore are less mature. The degree of paleosol maturity within abandoned channel scours was not recorded during this research, but could help to differentiate these deposits in future work. The heterolithic channel fill and overbank deposits are probably indistinguishable in core, on low-resolution photo mosaics and often in an outcrop if viewed from a distance.

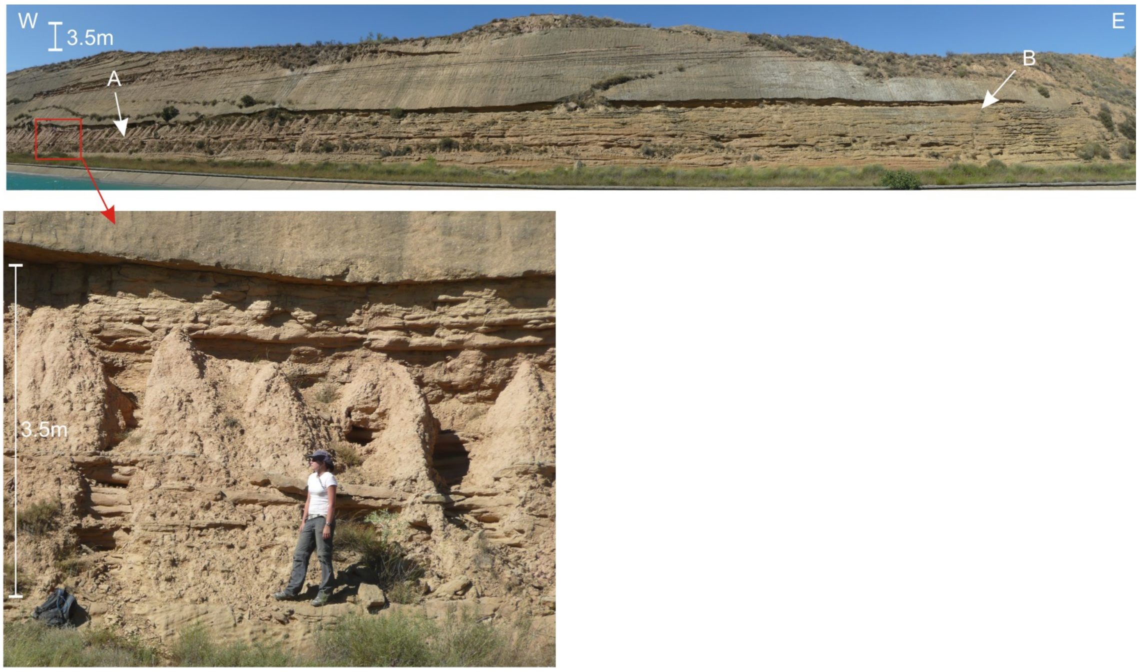

Figure 9.3. Relationship of floodplain deposits and Type 2 sandstone body in the Canal del Cinca outcrop (for location see Fig. 3.1). Heterolithic package of subtype 3/2 sandstone bodies and mudstone layers (A) passes laterally into more sandy "heterolithic top part" of point bar (B) and, further to the right, into Type 2 sandstone body.

The overall high proportion of heterolithic channel fill and overbank deposits (40-83% of the whole succession) indicate that the Huesca DFS had large amounts of fine-grained sediment in its sediment load (mixed bedload and suspended load). Most of the fine-grained sediment accumulated in the distal area of the Huesca DFS (83% of the distal Alcolea outcrop, Appendix 5.3). The high proportion of very fine- to medium-

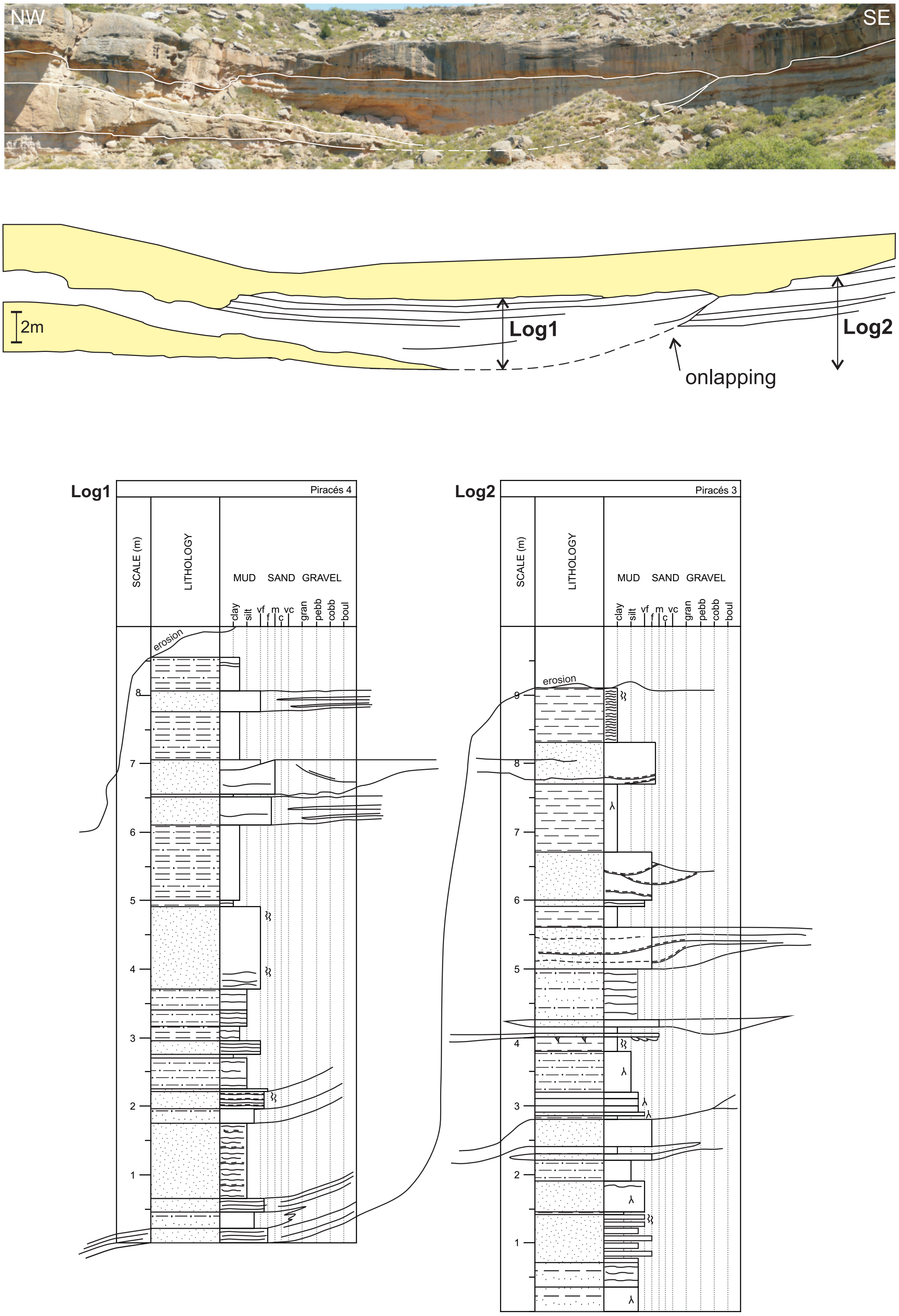

Figure 9.4. Comparison of heterolithic deposits formed on relatively flat floodplain surface (Log2) and in abandoned channel fill deposits (“clay plug”, Log1), Piracés outcrop (location of the outcrop see in Fig. 3.1). Legend for sedimentary logs see in Appendix 2.

grained sandstones and siltstones in the floodplain deposits of the relatively proximal and medial parts of the succession suggests that the Huesca DFS had large amounts of sand and silt in its suspended load when overbank flow has occurred and splays formed (e.g. Willwood Formation, Jones and Hajek, 2007).

9.3 Avulsion and avulsion deposits

It has been suggested frequently that most of the heterolithic overbank deposits are formed during channel avulsion when water flow carries sediment out of the channel onto the floodplain (Kraus and Wells, 1999; Aslan and Autin, 1999; Morozova and Smith, 2000; Stouthamer, 2001; Makaske et al., 2007; Slingerland and Smith, 2004; Jones and Hajek, 2007). For example, large amounts of fine-grained sediment were supplied by splays during avulsion on the floodplain of modern Taquari DFS in Brazil (Assine, 2005), the Rhine-Meuse delta in Netherlands (Stouthamer, 2001) and the Saskatchewan River in Canada (Morozova and Smith, 2000). In contrast, much less sediment was reported to be accumulated during regular flooding events (Aslan and Autin, 1999; Slingerland and Smith, 2004).

Avulsion is thought to have been a common process on the Huesca DFS and it would have controlled sediment distribution and resulting sandstone body relationships (Chapter 5). The occurrence of avulsion is indicated by lateral and vertical intercalation of channel sandstone bodies with intervals of fine-grained heterolithic overbank deposits (appendices 5.1-3) (Jones and Hajek, 2007). Other indicators of avulsion include the presence of abandoned channel scours filled with fine-grained overbank deposits, large amalgamated sandstone body complexes and amalgamations of Type 1 and Type 3 (“channel wings”) sandstone bodies (Fig. 5.6, Chapter 5). Another indirect indication of avulsion occurrence is maturity of paleosols (Slingerland and Smith, 2004): the paleosols in the Huesca DFS succession are in general poorly developed indicating frequent overbank water flow and sediment deposition (Hamer et al., 2007(a)) that could be a result of frequent splay formation related to avulsions. In general, fan shaped fluvial systems are considered to be prone to avulsions (Slingerland and Smith, 2004).

Three styles of avulsion are usually recognised: avulsion by splay-progradation (aggradational), avulsion by re-occupation/annexation of pre-existing channel scours and avulsion by incision (Smith et al., 1989; Aslan and Blum, 1999; Mohrig et al., 2000; Slingerland and Smith, 2004; Burhler et al., 2011). The last two types could be combined (Mohrig et al., 2000), because they both involve incision process and are distinguished on the basis of presence or absence of pre-existing topographic feature on a floodplain.

Mohrig et al. (2000) suggested that topography, surface gradient, vegetation cover, water table and substrate type on the floodplain define the deposition style during avulsion. Poorly drained, low gradient, vegetated floodplains, for instance, would promote sediment deposition and splay formation, while sediment is deposited only locally on a well-drained, high gradient floodplain and incision/re-occupation would occur more frequently (Mohrig et al., 2000). Deposition during avulsion by incision/re-occupation has been described as being insignificant (Morozova and Smith, 2000; Stouthamer, 2001) and mostly confined to the channel scour (Slingerland and Smith, 2004). Therefore, avulsion by splay progradation possibly contributes the most sediment to the floodplain aggradation. However, Mohrig et al. (2000) stated that avulsion by incision could also include several depositional episodes contributing sediment to overbank areas.

It is likely that all avulsion styles contribute sediment to the floodplain because the process involves outflow of water and sediment on to the floodplain where flow decelerates immediately due to flow expansion and increased friction promoting deposition of transported sediment. This statement is true unless the avulsing flow is captured immediately by an abandoned channel scour close to the avulsion site (Stouthamer, 2001). In general, independent of avulsion style, the amount of sediment contributed to the floodplain by avulsion is controlled by the amount of suspended sediment in the upper portion of the channel flow (Jones and Hajek, 2007). The grain size of the suspended sediment is also important. The thickness of avulsion deposits is also thought to be controlled by the relative elevation of the channel bank above the floodplain and the aggradation rate of the fluvial system (Slingerland and Smith, 2004).

9.4 Succession of avulsion deposits

Extensive heterolithic overbank deposits observed in the relatively proximal and medial outcrops of the Huesca DFS succession resemble the successions of avulsion deposits recognised by Kraus (1996) and Kraus and Wells (1999) in the Willwood Formation, Wyoming, USA. The overbank deposits consist of packages of sandstone bodies of subtype 3/2 which are interbedded with heterolithic facies Hm and cut by small-scale sand-fill channel scours (facies Sils). These deposits make up a large portion of the Huesca DFS succession (Fig. 9.5) and are consistent with the definition of avulsion deposits of Kraus and Wells (1999).

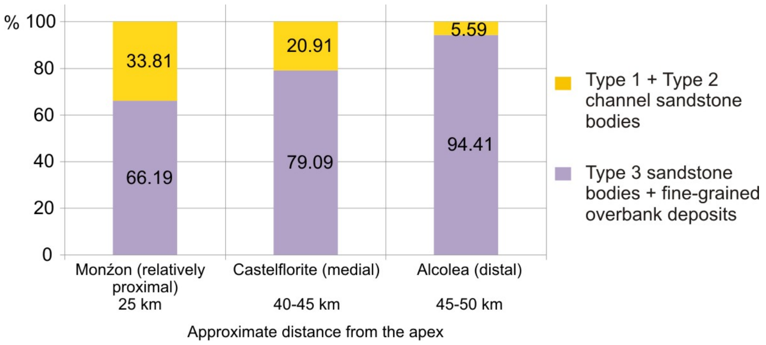

Figure 9.5. The proportion of avulsion deposits including Type 3 sandstone bodies and fine-grained overbank deposits in comparison to the proportion of channel sandstone bodies of Type 1 and 2. In the distal outcrop (Alcolea) the avulsion deposits include terminal splay deposits.

Avulsion deposits are commonly described to form coarsening-upward successions (Kraus, 1996; Perez-Arlucea and Smith, 1999; Horton and DeCelles, 2001; Morozova and Smith, 2000) that are overlain by sandstone bodies formed by the major channels (Kraus and Wells, 1999). These successions were interpreted to be formed during avulsion by splay progradation where a new channel is gradually established over heterolithic deposits of prograding splay (Kraus, 1996; Smith et al., 1989; Slingerland and Smith, 2004) (Fig. 9.6).

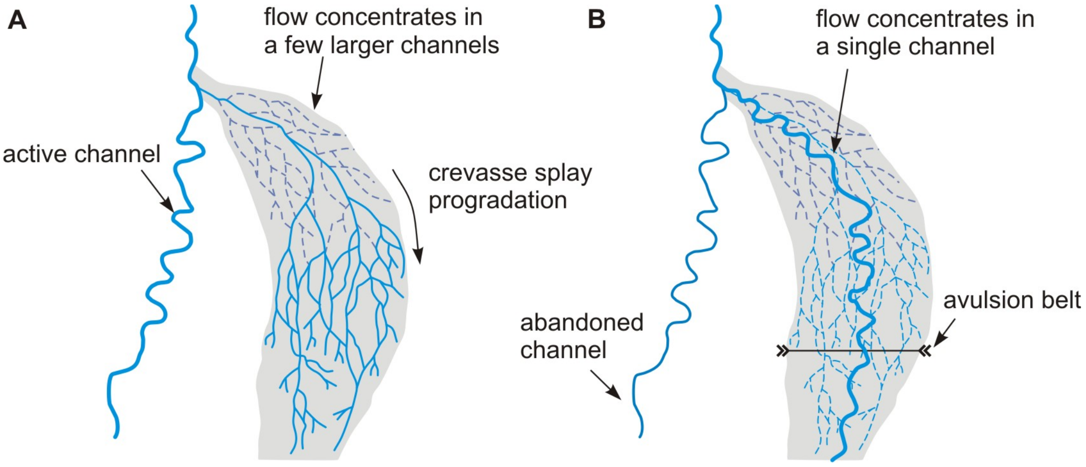

Figure 9.6. Model of avulsion by splay progradation (modified from Smith et al., 1989). A - progradation of the splay drained by network of small channels, B – flow concentrates into single major channel that incises into heterolithic deposits of the splay.

Jones and Hajek (2007) showed that the splay progradation avulsion model could not be applied to every fluvial system; these authors recognised two different types of avulsion successions that they associated with different avulsion styles. The stratigraphically transitional succession is a succession of floodplain deposits equivalent to transition from facies Hm to facies Hsh overlain by a channel sandstone body (Fig. 9.7, A). The stratigraphically abrupt succession can be recognized where a channel sandstone body lies directly on overbank mudstones (facies Hm) (Fig. 9.7, B). The transitional avulsion succession has been related to avulsion by crevasse splay progradation, while abrupt avulsion succession has been thought to represent avulsion by incision/re-occupation (Fig. 9.7).

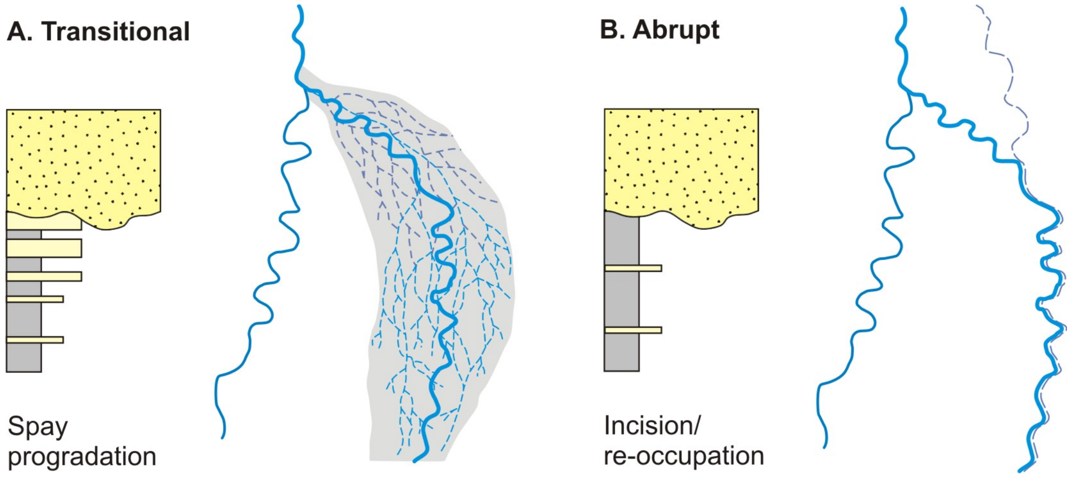

Figure 9.7. Stratigraphically transitional (A) and abrupt (B) types of avulsion successions interpreted to be formed in the result of avulsion by splay progradation and avulsion by incision/re-occupation, respectively (avulsion models are modified from Smith et al., 1989 and Mohrig et al., 2000).

Fluvial systems dominated by one or another avulsion style were considered to correspond to the different splay avulsion successions (Jones and Hajek, 2007). For example, coarsening-upwards transitional avulsion successions in the Willwood Formation were interpreted to have been formed as a result of avulsion by splay progradation, whilst avulsion by incision is proposed to be common during the deposition of the Ferris Formation where the abrupt type of avulsion succession was predominantly observed (Jones and Hajek, 2007). The absence of sheet-like avulsion deposits below the channel sandstone bodies in the Guadalope-Matarranya and Wasatch Formations was explained by occurrence of avulsion by incision/re-occupation on a well-drained floodplain (Mohrig et al., 2000). Coarsening- and thickening-upward overbank successions in the Camargo Formation in Central Andes were interpreted to be a result of avulsion by splay progradation (Horton and DeCelles, 2001). Both avulsion styles were commonly observed for modern distributary channels of the Rhine-Meuse delta (Stouthamer, 2001) and for the Saskatchewan River (Morozova and Smith, 2000). The last two examples demonstrate that both succession types could be common in the deposits of one fluvial system, that is opposite to what has been proposed by Jones and Hajek (2007).

Additionally, stratigraphically transitional avulsion successions were also related to a dominance of local over regional avulsions and to splay-proneness of a fluvial system (Jones and Hajek, 2007). A channel formed as a result of regional avulsion flows within and outside of the avulsion splay and therefore both transitional and abrupt types of avulsion successions can be formed within one fluvial system. During local avulsion channels are likely to stay within the avulsion splay creating only the transitional type of succession. This discussion does not take into account the size of the avulsion splay in the case of regional avulsion. For example, the current avulsion splay on the Taquari DFS stretches downstream to the toe of the fan (Fig. 2 in Buehler et al., 2011) and a new channel would probably flow within the splay through the whole DFS. A stratigraphically transitional avulsion succession would therefore be expected to be formed everywhere along the channel.

Splay-proneness of a fluvial system has been considered to be controlled by the grain size distribution of sediment load, cohesiveness of channel banks, dimensions of channel levees, superelevation of channel water level above the floodplain and variable hydrograph (Jones and Hajek, 2007 and references therein). Gain size distribution and channel bank stability were emphasised by Jones and Hajek (2007) suggesting that abundant silt and mud in the sediment load and easily breached channel banks promote the formation of sandy splays and therefore formation of stratigraphically transitional avulsion successions. In contrast, a fluvial system that lacks coarse-grained suspended load or has cohesive channel banks would be possibly characterised by sparser very fine-grained splays leading to formation of stratigraphically abrupt avulsion successions. However, other factors controlling splay formation have to be also considered. For example, one of the important factors controlling splay formation is frequency and magnitude of flooding events (Knighton and Nanson, 1993).

Consideration of the above discussion reveals a few drawbacks to the avulsion succession classification and their interpretation proposed by other authors. In the next section the proposed classification system is tested for the floodplain deposits of the Huesca DFS succession. On this basis it is possible to interpret the main avulsion styles of the Huesca DFS which in turn gives an insight into some aspects of system behaviour.

9.5 Succession of avulsion deposits in the Huesca DFS succession

9.5.1 Apparent successions of avulsion deposits

The heterolithic overbank deposits of the Huesca DFS succession show both what appear to be transitional and abrupt avulsion successions. Subtype 3/2 sandstone bodies intercalated with fine-grained deposits of facies Hm form a stratigraphically transitional avulsion succession. The proportion and thickness of subtype 3/2 sandstone bodies appear to increase upward and channel sandstone bodies of Type 1 or 2 overlie the succession (Fig. 9.8, A). The coarser, upper part of the succession is considered to represent proximal splay deposits while the lower, finer part represents more distal splay deposits. A stratigraphically abrupt avulsion succession is made up of a channel sandstone body of Type 1 or 2 overlying a package of fine-grained overbank deposits of facies Hm (distal splay / floodbasin) (Fig. 9.8, B).

Apparent transitional avulsion deposit successions are observed more frequently than apparent abrupt avulsion deposit successions. According to the interpretation of Jones and Hajek (2007), predominance of a transitional avulsion deposit succession would indicate dominance of avulsion by splay progradation and prevalence of local avulsions over regional. This interpretation would also imply abundant fine-grained sediment in the suspended load of the Huesca DFS and non-cohesive, easily eroded channel banks.

9.5.2 Successions of avulsion deposits; are they real?

Due to the extensive, good quality outcrops of the Huesca DFS succession it is possible to trace observed avulsion successions laterally. This revealed that avulsion deposits are truncated by overlying channel sandstone body to a different depth in different places along the outcrops (Fig. 9.9). In places, packages of amalgamated sandstone bodies of subtype 3/2 (proximal splay) were observed immediately below the channel sandstone body forming a stratigraphically transitional avulsion succession. A few meters laterally, the same channel sandstone body is found incising into fine-grained deposits of facies Hm (distal splay) forming a stratigraphically abrupt avulsion succession (Fig. 9.9, E-G). Thus, one or the other type of avulsion succession could be produced as the result of variable depth of channel incision. Mohrig et al. (2000) also mentioned that subsequent erosion could remove avulsion deposits. Reworking by subsequent channel flow has been proposed to be one of the causes of absence of splay deposits below deposits of distributary channels of Rhine-Meuse delta (Stouthamer, 2001), hence erosion results in the formation of a stratigraphically abrupt succession. These observations demonstrate that in the case of limited

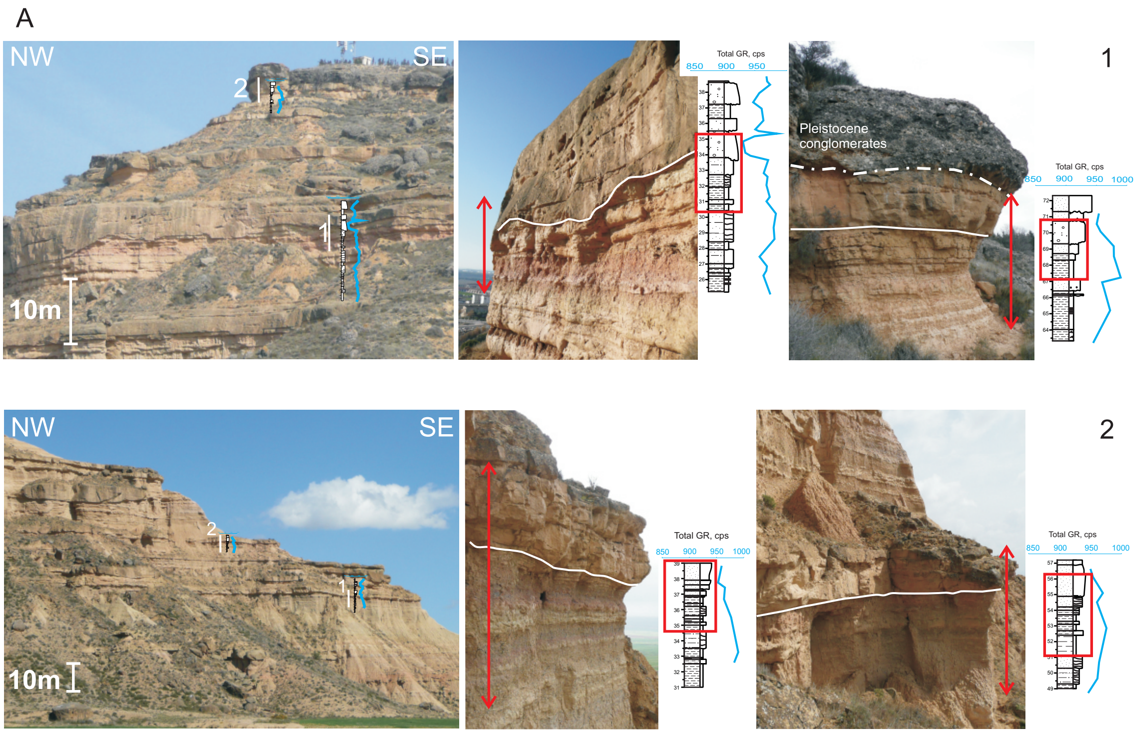

* red bars on the photographs correspond to sedimentary log intervals in red boxes

* arrows indicate fine-grained deposits of facies Hm immediately below major channel sandstone body

Figure 9.8. Examples of apparent stratigraphically transitional (A) and abrupt (B) avulsion deposit successions in the Huesca DFS succession; 1 - Monźon and 2 - Castelflorite outcrops.

exposure it would be difficult to determine whether a stratigraphically transitional avulsion succession that is preserved immediately below a channel sandstone body is related to either the avulsion that formed this particular channel or any of previous avulsion events.

Moreover, there is a chance of failed avulsion (Stouthamer, 2001; Jones and Hajek, 2007) where avulsion splays do form, but flow is not transferred completely and a new permanent channel is not established. For example, failed avulsions forming splay deposits occurred on the floodplain of the Mississippi River down-valley of the Old River (Aslan et al., 2005) and on Rhine-Meuse delta forming the shortly active Schoonrewoerd system originating from the Werkhoven distributary (Makaske et al., 2007). In addition, Stouthamer (2001) observed crevasse splays that did not lead to full, partial or failed avulsion, but formed deposits with the same architecture as deposits of the splays related to avulsion. The author emphasised that it is impossible to differentiate these three cases in 2D outcrops. Therefore, preserved splay deposits might be overlain by a channel sandstone body which is not related to the splay and was formed by a channel diverted to this place by a separate, later avulsion.

In addition, if an avulsion splay had a limited extent (in contrast to Taquari DFS example, Buehler et al., 2011), a channel sandstone body could incise into splay deposits only in the area close to the avulsion site. Further downstream channels could incise into previously formed floodplain deposits that could be either fine-grained deposits of facies Hm or previously formed splay deposits. In this scenario, both stratigraphically abrupt and transitional successions might be formed. The relative age of splay deposits preserved below the channel sandstone body would be difficult to differentiate in ancient fluvial deposits, although dating could be used to understand relationships between modern splay and channel deposits (e.g. Rhine-Meuse delta avulsions, Stouthamer, 2001; Stouthamer and Berendsen, 2001).

Furthermore, Buehler at al. (2011) observed that the Taquari DFS splay has a positive topography and is elevated above the surrounding floodplain. The authors suggested that if the channel eventually avulses it would most likely flow between the avulsion splay and the current alluvial ridge. This is in contrast to the avulsion successions proposed by Jones and Hajek (2007) in which a channel sandstone body overlies the coarsening-upward deposits of an avulsion splay.

Finally, it is unlikely at all for avulsion splay deposits to be preserved directly underneath a channel scour formed in the result of the same avulsion event as it was proposed by Jones and Hajek (2007). The base of the channel scour producing the splay will be deeper than any point on the adjacent floodplain where splay occurs. If

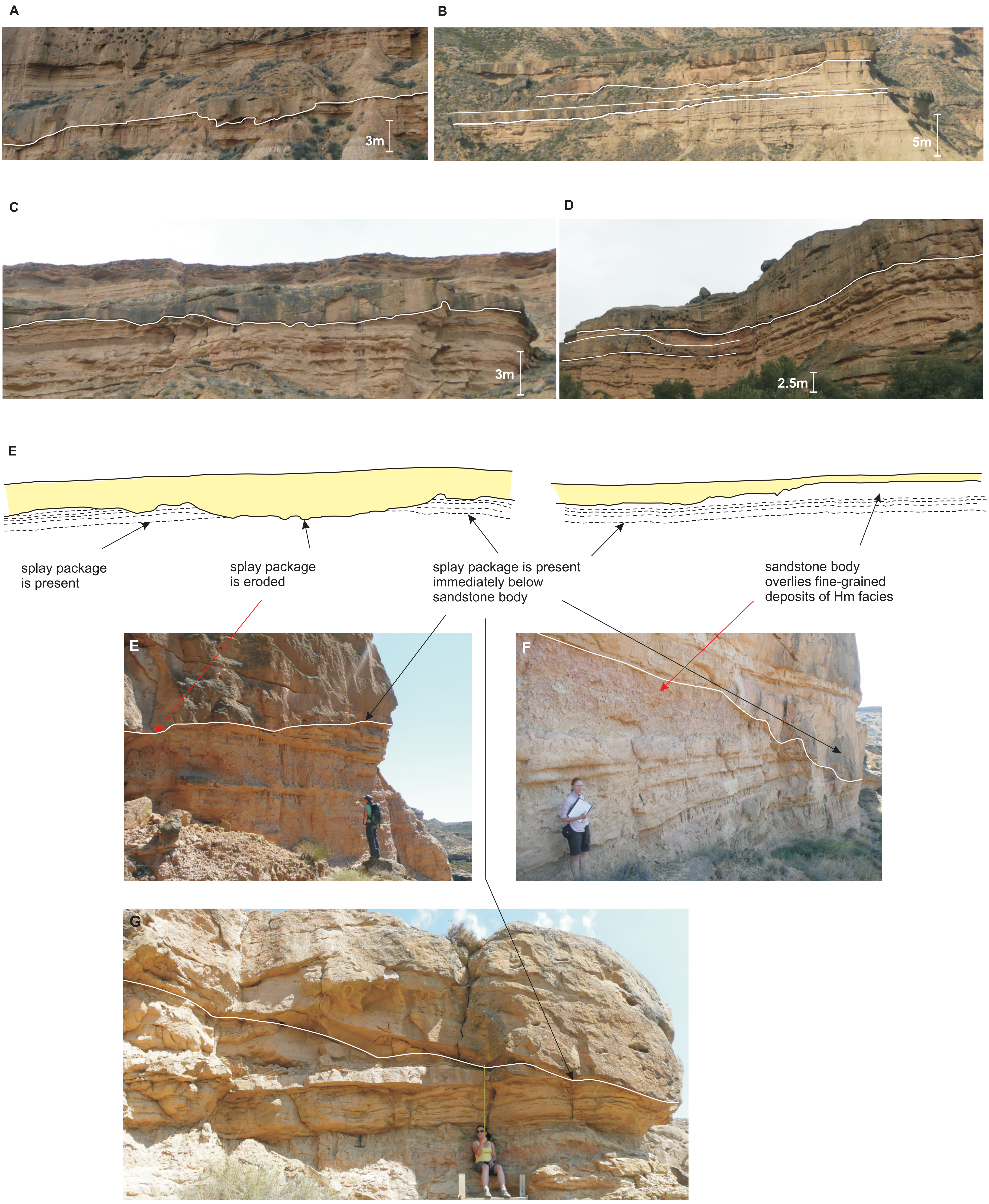

Figure 9.9. Examples of splay deposits truncated by subsequent channel sandstone bodies forming both stratigraphically transitional and stratigraphically abrupt avulsion deposit successions. A, D – Monźon outcrop; B, C – Castelflorite outcrop; E, F, G - close up examples form Piracés, Monźon and Monte Aragón outcrops, respectively. Black and red arrows indicate places where apparent transitional and abrupt avulsion successions are observed.

the new channel will scour as deep as the old channel, it would remove related avulsion deposits below it (Fig. 9.10, A), unless the splay deposits are thicker than the erosion depth of a new channel. Even in the latter case they will be only partially preserved (Fig. 9.10, B).

A. Floodplain succession (including avulsion deposits) is eroded by subsequent channel

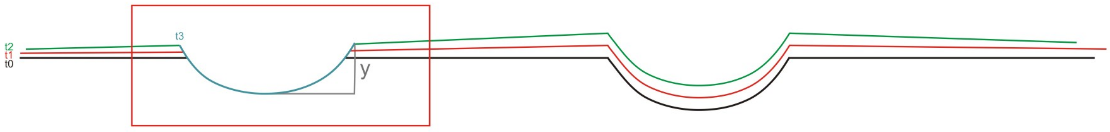

Channel and floodplain complex aggrade less than the incision depth (y) of the subsequent channel.
This possibly occurred in the Huesca DFS (see photographs below).

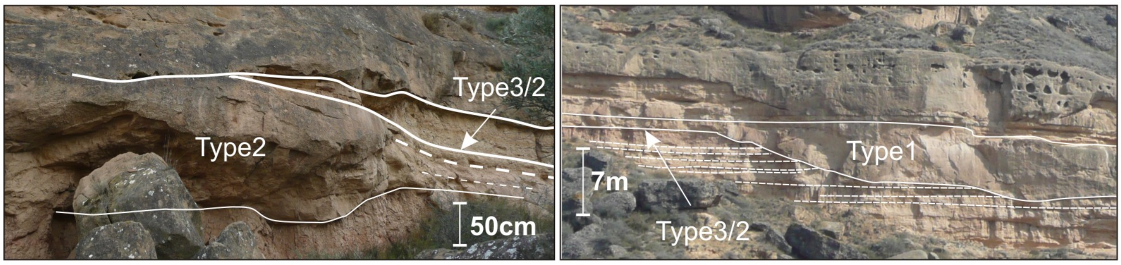

* Monźon outcrop examples (case A)

B. Floodplain succession (including avulsion deposits) could be partially preserved below channel

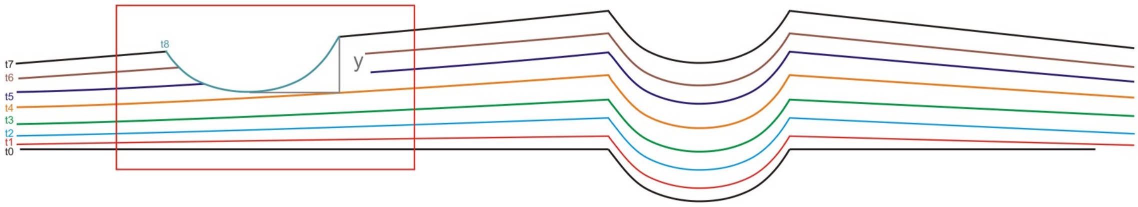

Channel and floodplain complex aggrade significantly more than the incision depth (y) of the subsequent channel.

Figure 9.10. Preservation of avulsion deposits. A - the floodplain succession formed by a channel during flooding and avulsion events would probably be removed by the new channel after avulsion (t3). B - the floodplain succession could be partly preserved in the case when channel-floodplain complex aggrades significantly and accumulates floodplain deposits with thickness greater than the incision depth (y) of the new channel (t8). The case A is considered to be the most probable for the Huesca DFS.

In summary, although there is a probability that a succession related to channel avulsion can be preserved immediately below a related channel sandstone body, the two types of avulsion successions distinguished by Jones and Hajek (2007) appear to be artificial and could be formed in the result of reworking by a subsequent channel flow. It is therefore thought that in most cases, resulting avulsion successions do not provide information about avulsion of the channel that formed the sandstone body at the top of the avulsion succession. In outcrops with limited lateral extent, that are commonly available for sedimentological studies, observation of avulsion successions could lead to incorrect conclusions about avulsion styles and overall fluvial system behaviour. Sandy fluvial successions where only a small portion of floodplain deposits are preserved in lenses between amalgamated sandstone bodies (e.g. Salt Wash DFS succession, Appendix 5.4) are also not suitable for such studies.

Original avulsion deposits could be possibly observed next to the edge of the sandstone body (channel bank) rather than below erosional surface of a new channel. To observe this relationship the outcrop has to be close to the avulsion site. Splay deposits in the Huesca DFS succession were found attached to the top edge of the channel sandstone bodies of Type 1 and 2 (Fig. 5.8, Chapter 5) and could possibly represent avulsion deposits related directly to the avulsion-generating channel. It could be suggested that all splay deposits that can be traced laterally into an adjacent channel sandstone body, originated from that channel.

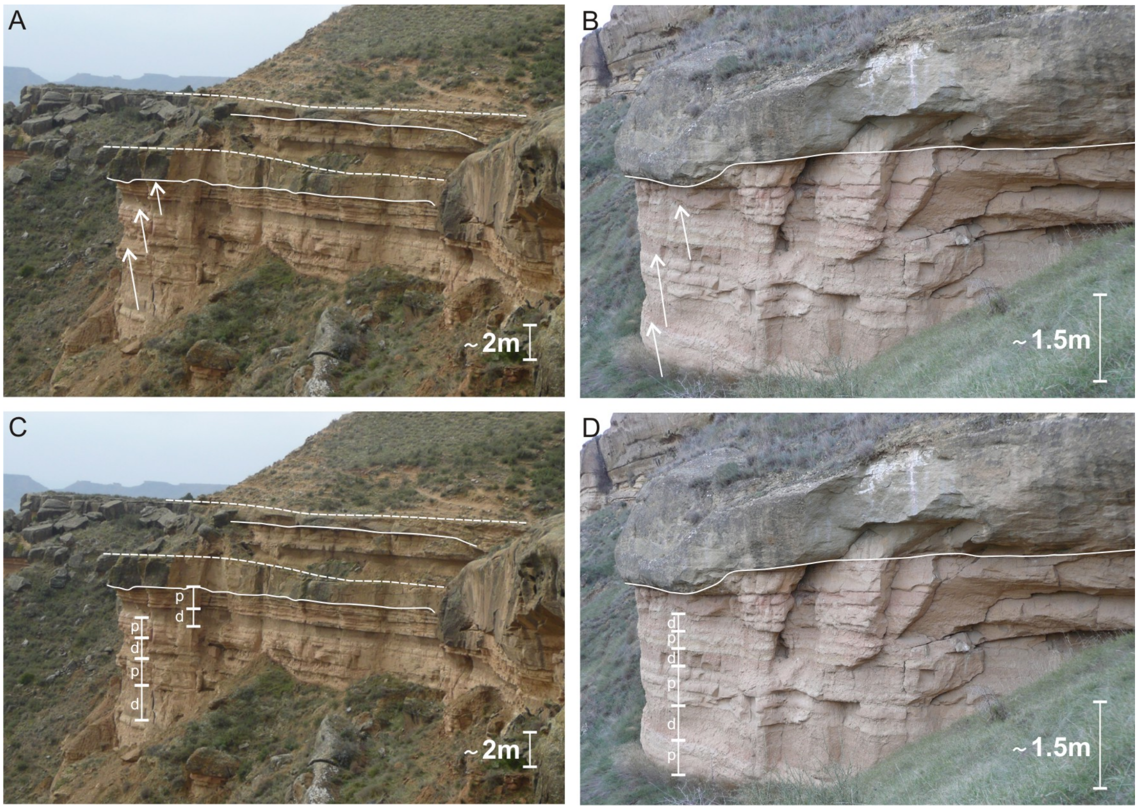

Figure 9.11. Two interpretation of packages of splay deposits in the Huesca DFS succession. A, B – stacked apparently coarsening- and thickening-upward packages. C, D – stacked relatively proximal and distal splay packages. A, C – Castelflorite and B, D – Monźon outcrops. Distal splay deposits (d) - fine-grained, more weathered intervals. Proximal splay deposits (p) – packages of Type 3 sheet-like sandstone bodies interbedded with thin mudstone layers.

Nevertheless, the architecture of floodplain intervals of the Huesca DFS succession quite clearly shows that splays were formed often on the Huesca DFS. Independently of channel sandstone body position, floodplain succession intervals usually consist of vertically stacked packages of distal and proximal splay deposits which appear to coarsen and thicken upwards (from distal to proximal splay deposits) (Fig. 9.11, A-B). Each package could represent either the deposits of a splay that was associated with avulsion or not.

9.5.3 Vertical trends in avulsion deposits; are they real?

Apparent coarsening- and thickening-upward trends in the heterolithic overbank deposits of the Huesca succession were recognised qualitatively by outcrop observations (Fig. 9.11, A-B). The same visual method was used in previous work where similar trends were described for other fluvial successions (Kraus, 1996; Kraus and Wells, 1999; Horton and DeCelles, 2001; Morozova and Smith, 2000; Stouthamer, 2001; Jones and Hajek, 2007).

To test the hypothesis of the presence of coarsening- and thickening-upward trends within the overbank successions, 32 detailed stratigraphic logs have been recorded between vertically subsequent channel sandstone bodies in different locations in the study area (Fig. 3.1). Detailed sedimentological analysis of the recorded overbank successions revealed more complex architecture of the floodplain successions and vertical trends have not been confirmed (Section 9.1; appendices 2.13-18). Order metric statistics (Chapter 10) has been used for 19 logs to quantify visual observations and interpretations. As a result of this analysis vertical trends in thickness or grain size were not found in any of the analysed overbank successions. The methodology and results of the analysis are discussed in the following Chapter 10.

Therefore, the avulsion deposits do not show coarsening- or thickening-upward transitions and are not ordered as it was thought previously. Alternatively they can represent intercalation of relatively proximal and distal splay deposits related to a separate splay events that could be or could not be related to avulsion events (Fig. 9.11, C-D).

9.6 Interpretation and discussion of the results

9.6.1 Splays of the Huesca DFS

Channel avulsion was an important process on the Huesca DFS that controlled sediment distribution and the resulting succession architecture (Section 9.3; chapters 4 and 5). Root traces in the floodplain deposits of the Huesca DFS succession (Chapter 4) indicate a vegetated floodplain (Hamer et al., 2007a) that could have promoted deposition during the avulsion process (Mohrig et al., 2000) and influenced the development of avulsion splays. The high variability of grain sizes in floodplain deposits and the high percentage of fine-grained deposits (Fig. 9.5), together with coarse-grained channel-fill sandstones in the Huesca DFS succession, indicate a wide grain size distribution in the sediment load of the Huesca DFS (Chapter 6). This also suggests that there was enough suspended sediment in the top portion of a channel flow to form splay sandstones and siltstones (Jones and Hajek, 2007).

Abundant Type 3 sandstone bodies (Chapter 6) indicate that splays were often generated from DFS channels. The heterolithic overbank succession is dominated by very fine- to medium-grained sandstones and siltstones with small amounts of mudstones and claystones (appendices 2.13-18). Therefore, the splays of the Huesca DFS were much sandier than, for example, splays of the Rhine-Meuse delta where sand was observed only in splay channels (Stouthamer, 2001; Makaske et al., 2007), but similar to sandy splays of the Saskatchewan (Smith et al., 1989) and Mississippi (Aslan et al., 2005) rivers.

Splay channel sandstone bodies (sandstone bodies of subtype 1/3, facies Sils) have rarely been observed within splay deposits of the Huesca DFS succession, while abundant anastomosing channels have been previously reported to form on avulsion splays of modern fluvial systems (Assine, 2005; Buehler et al., 2011; Smith et al., 1989; Makaske et al., 2007). Three possible explanations could be proposed: 1) the sediment transport in splays of the Huesca DFS was dominated by unconfined flow rather then channelised flow (Fisher et al., 2007(a)); 2) exposed overbank deposit successions represent splay deposits downstream of the avulsion site where channels and scours became smaller (Stouthamer, 2001) and finally transformed into unconfined flow (Buehler et al., 2011); or 3) the sandstone bodies are rarely exposed due to small dimensions of their cross section and because they are widely scattered across the splay. The combination of these interpretations could be the reason for sparse occurrence of splay channel sandstone bodies in the succession. Unfortunately, this question could not be confidently resolved in 2D outcrops. It also could not be determined whether the splay channels were anastomosing or not for the same reason.

9.6.2 Bank cohesiveness of the Huesca DFS

Sandy and silty splay deposits on the Huesca DFS floodplain would form non-cohesive floodplain substrate in relatively proximal and medial areas of the Huesca DFS that could have favoured subsequent crevassing and splay formation (Jones and Hajek, 2007). However, abundant vegetation on the surfaces of the Huesca DFS (Hamer et al., 2007a) could have made banks more cohesive.

In addition, lack of evidence of differential compaction in the Huesca DFS succession suggests that the channel and floodplain deposits may have been dried and cemented to relatively the same degree prior to burial. Abundant limestone grains in the Huesca deposits (Appendix 3 Table 6) may have produced early-stage cement forming cohesive banks. If the conclusion about relatively cohesive banks of the Huesca DFS is correct, it indicates that cohesiveness of channel banks is not important control on splay formation and splay-proneness of a fluvial system as it was proposed by Jones and Hajek (2007).

9.6.3 Avulsion styles of the Huesca DFS

Avulsion by splay progradation

Frequent overbank splays could have been a part of channel avulsion process similar to avulsion by splay progradation. This avulsion style has been often observed on modern fluvial systems (Smith et al., 1989; Perez-Arlucea and Smith, 1999; Morozova and Smith, 2000; Stouthamer, 2001; Assine, 2005; Makaske et al., 2007; Burhler et al., 2011) and therefore is a reasonable interpretation. Some of the splay deposits, however, could be also not related to avulsion (Stouthamer, 2001).

The absence of coarsening- and thickening-upward trends in the overbank successions suggests that avulsion by splay progradation, and floodplain deposition in general, is a complex process that does not create perfect quantitatively recognisable coarsening- and thickening-up successions that have frequently been interpreted in the avulsion deposits. For example, single Mississippi River avulsion involved several avulsion mechanisms, including splay formation, incision into floodbasin deposits and floodplain channel re-occupation (Aslan et al., 2005). The processes were described substituting each other in time during the Mississippi avulsion and laterally downstream along the avulsion site (Aslan et al., 2005). Such combination of processes would have prevented formation of any regular trends and created deposits with complex organisation.

Avulsion by re-occupation

Vertically connected two- and multi-storey subtype 1/1 and Type 2 sandstone bodies with stepped edges were occasionally observed in the Huesca DFS succession (Fig. 9.12). These sandstone body amalgamations were previously stated to indicate avulsion by incision/re-occupation (Mohrig et al., 2000; Martínez et al., 2010 “avulsion by annexation” of Slingerland and Smith, 2004; Aslan et al., 2005). This avulsion style was thought to occur under low aggradation rate conditions (Slingerland and Smith, 2004) on a well-drained, not vegetated floodplain (Mohrig et al., 2000). In contrast as has been shown above, the floodplain of the Huesca DFS was vegetated (Hamer et al., 2007(a)) and subjected to frequent sediment deposition by overbank slays. Abundant channel scours filled with heterolithic overbank deposits in the Huesca DFS succession also indicate that topographically low channel scours on the floodplain were filled with sediment from splays rather than re-occupied by a new channel flow.

Annexation of re-occupied channels could remove any evidence of previous channel and, therefore, evidence of re-occupation (Slingerland and Smith, 2004; Jones and Hajek, 2007). Thus, avulsion by re-occupation / annexation could have occurred on the Huesca DFS, but is not related to any specific avulsion deposits such as the stratigraphically abrupt avulsion deposit succession proposed previously by Jones and Hajek (2007).

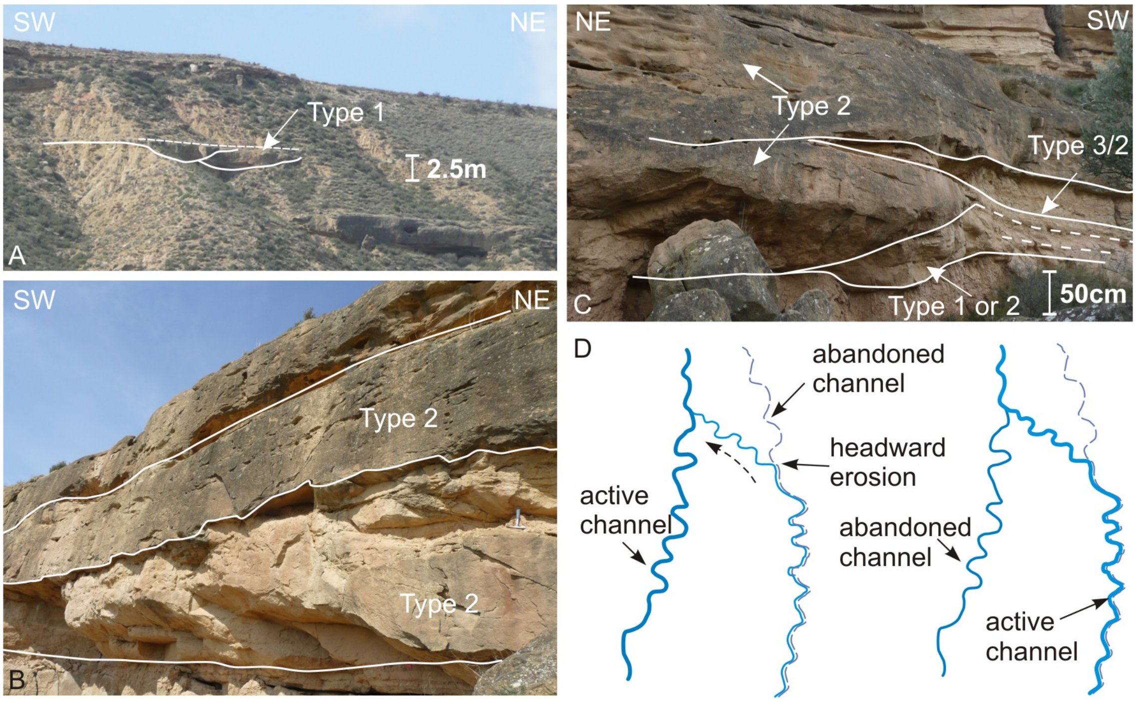

Figure 9.12. Vertically connected two- and multi-storey subtype 1/1 and Type 2 sandstone bodies with stepped edges which could indicate avulsion by re-occupation/annexation. A, B – Castelflorite outcrop; C – Monźon outcrop. D – schematic representation of the mechanism of avulsion by incision/re-occupation (modified from Mohrig et al., 2000).

9.6.4 Deposits of individual avulsion event or multiple avulsion events

Vertically stacked intervals of relatively distal and proximal splay deposits (Fig. 9.11, C-D) could have been probably formed by several episodes of full or failed avulsions that originated from channels located closer to or further from the place of observation. The presence of paleosols within the successions of avulsion deposits indicates that there was sufficient time between splay episodes and therefore supports the interpretation of multiple splay events and rejects the interpretation of deposition by a single splay progradation event. In other words every interval of relatively distal or proximal splay deposits could indicate an individual avulsion episode. Each of these avulsion events in turn could represent a complex combination of different avulsion processes including splay progradation, incision and re-occupation (Section 9.6.3).

This interpretation, however, poses the question as to whether the thickness of the deposits interpreted to correspond to a single avulsion episode is comparable with what may be deposited during one avulsion event. Reported thicknesses of avulsion deposits observed in modern fluvial settings vary between 0.5 to 6 m. For example, the thickness of the avulsion deposits for the Saskatchewan River is 2 to 3 m (Morozova and Smith, 2000), for the Mississippi River is 6 m (Aslan et al., 2005), and for the distributive channels of the Rhine-Meuse delta varies from 0.5 to 4 m (Stouthamer, 2001). The thicknesses of relatively proximal and distal splay deposit intervals in the Huesca DFS succession vary between about 0.5 and 2 m (facies Hsh and Hm, Chapter 4) and therefore are close to the lower boundary of the range of thicknesses for the modern avulsion deposits. This smaller thickness could be explained by smaller size of the Huesca fluvial system in comparison with modern fluvial system examples, but could also be related to other factors. The thickness of the preserved avulsion deposits could be controlled by a combination of factors including fluvial system scale, magnitude and type of the avulsion (nodal, regional, local), amount of sediment influx, aggradation rate of the fluvial system, depth of subsequent erosion and post-depositional compaction. Most of these factors cannot be determined from the available outcrop data.

As far as we know there are no studied modern examples similar to the Huesca DFS. Without data from the modern DFS avulsions and considering how many different factors could control the deposition during the avulsion, conclusions about the thickness of deposits of individual avulsion event on the Huesca DFS cannot be made. Therefore available outcrop data do not allow differentiation of splay deposits formed as a result of individual or multiple avulsion events or individual splays which did not lead to avulsion.

9.6.5 Possible factors promoting avulsion on the Huesca DFS

The association of sandstone bodies of Type 1 and subtype 3/1 observed in the Huesca succession represent a bankfull filled channel scour overlain with sandstone sheet formed by unconfined flow (Chapter 5, Fig. 5.6). As a result of these events a channel would have been blocked leading to a diversion of the flow to a new location on the floodplain, hence avulsion (Sheets et al., 2007). Channel blocking with sediment reduces channel transport capacity and has often been recognised as one of the causes of channel avulsion (Kelly and Olsen, 1992; McCarthy et al., 1992; Slingerland and Smith, 2004; Jones and Schumm, 1999; Field, 2001; Bridge, 2003; Smith et al., 1989; Morozova and Smith, 2000; Makaske, 2001; Stouthamer and Berendsen, 2001, Aslan et al., 2005). Channel blocking requires high sediment supply to water discharge ratio in the system. Filling of a channel with sediment causes decrease in channel depth (Field, 2001) and promotes flooding events (Slingerland and Smith, 2004), especially during relatively high flow regime. While during change to relatively low flow regime, more sediment is deposited causing additional aggradation of the channel floor (Cain and Mountney, 2009). Therefore, the variable water discharge interpreted for the Huesca DFS (Chapter 4) could perhaps provide frequent flooding events and facilitate channel blocking promoting avulsion (Knighton and Nanson, 1993; Field, 2001, Slingerland and Smith, 2004). In addition, a downstream decrease in flow strength (Chapter 8) increases deposition in the channels that could also lead to channel blockage.

Cross-valley and down-valley slope ratio was proposed to be a threshold condition for the avulsion occurrence (Aslan et al., 2005 and references therein). The gradient advantage, however, was recognised to be not a necessary factor for occurrence of an avulsion on the Mississippi River (Aslan et al., 2005). The substrate cohesiveness and presence of active and abandoned channels on the floodplain were found to be more important (Aslan et al., 2005). Evidence of high channel levees or elevation of a channel above floodplain were not observed in the Huesca DFS succession and therefore gradient advantage was perhaps not the main avulsion trigger. Bank cohesiveness perhaps did not play a major role in this process as well because despite of the fact that overbank deposits of the Huesca system are relatively cohesive (vegetated and probably cemented) avulsion splay deposits are very abundant. The presence of active and abandoned channels and their role in the avulsion process cannot be determined from available outcrop data.

In summary, the most probable factors promoting avulsion of the Huesca DFS include reduction in channel capacity through increase in deposition rate caused by high sediment supply to water discharge ratio, variable flow discharge and decrease in the discharge downstream. The role of the presence of active and abandoned channels on the floodplain could have been important in avulsion process, but no evidence is preserved. In general, the Huesca DFS seems to have been splay-prone system and favoured aggradation and preservation of floodplain deposits.

9.7 Conclusions

In this chapter the architecture of the heterolithic deposits of the Huesca DFS succession have been described and their origin have been discussed. Channel scours on the Huesca DFS were filled with both sandy (sandstone bodies) and heterolithic deposits that was controlled by variable water discharge in the Huesca DFS channels. Abundant and extensive heterolithic overbank deposits of the relatively proximal and medial Huesca DFS successions are interpreted to represent avulsion and non-avulsion splay deposits.

Both avulsion successions distinguished by Jones and Hajek (2007) were recognised in the Huesca DFS succession, but were found to be not related to a specific avulsion style, as proposed by those authors. Instead observed successions are formed as a result of erosion by subsequent channel flow. Moreover, the channel flow that eroded the avulsion deposits did not necessarily originate from the same avulsion event. Therefore, sandstone bodies in the Huesca DFS successions are not usually related to underlying avulsion deposits. It is emphasised that the proposed two types of avulsion successions could not be used to interpret avulsion styles and infer characteristics of fluvial system behaviour, especially in outcrops of limited lateral extend or with high degree of sandstone body amalgamation.

The study of architecture of the heterolithic overbank deposits made it possible to interpret depositional style on the floodplain of the Huesca DFS. The Huesca DFS was characterised by a wide grain size distribution in its sediment load. Overbank splays were formed often and contributed the most sediment to the floodplain deposits. The splays might have led to channel avulsion or ceased without completing diversion of the main flow. Avulsion on the Huesca DFS occurred through a combination of splay development, incision and re-occupation of pre-existing channels on the floodplain. Among them, splay formation played the main role.

The complex architecture of the heterolithic overbank deposits reflects this complex avulsion process and simplified coarsening- and thickening-upward vertical trends, usually associated with avulsion deposits formed by splay progradation, were not observed. Avulsion deposits formed as a result of individual avulsion events or individual splays which did not lead to avulsion could not be differentiated using available outcrop data. Avulsion by re-occupation could have occurred on the Huesca DFS but is not related to any specific avulsion deposits.

Reduction of channel capacity due to in-channel aggradation governed by high sediment to water discharge ratio was the main trigger of the avulsion on the Huesca

DFS. Overall the Huesca DFS behaviour favoured floodplain aggradation and preservation of overbank deposits. The behaviour of both the Huesca and Salt Wash DFSs is further discussed in chapters 10, 11 and 12.

10. Evidence for ordered facies and thickness successions in the DFS deposits

10.1. Introduction

Identification of cyclicity in stratigraphic successions forms the basis of many sedimentological interpretations. Middleton (2003) defines “cycle” as “a series of connected events which return to a starting point”. “Cycle” in a sedimentary succession is explained as a distinctive series of lithologies arranged in a predictable vertical pattern in which at least one lithology is repeated and is a starting point of the “cycle” (Schwarzacher, 1975).

Identification of cyclicity is important because cyclic strata are formed by an ordered progression of depositional processes that may be indicative of external forcing by a periodic signal such as glacioeustasy (e.g. Burgess 2006). For example, a succession of asymmetric coarsening-upward cycles within marine siliciclastic deposits can be interpreted to be shallowing-upward cycles related to repeated relative sea level rise followed by its gradual fall. Unfortunately, many such interpretations are too subjective to be useful, because interpretation is often only qualitative and also many apparent patterns could probably occur by chance. Willkinson et al. (1997) noted that shallowing-up cyclicity in peritidal carbonates is typically identified only by subjective, qualitative methods, yet is often confidently interpreted to indicate external forcing by eustatic sea level.

Robust identification of cyclicity in fluvial strata is also an issue. Apparent fining-upward cycles in fluvial deposits are often described in outcrops and are typically assumed to be associated with fluvial deposits of sinuous/meandering streams (Allen, 1970; Leeder, 1973; Cant and Walker, 1976; Donselaar and Overeem, 2008). Apparent coarsening-upward trends in avulsion deposits in fluvial successions have been also interpreted to represent splay progradation process (Kraus, 1996; Perez-Arlucea and Smith, 1999; Horton and DeCelles, 2001; Stouthamer, 2001; Morozova and Smith, 2000, Chapter 9). Subjectively defined fluvial cycles are also described and interpreted from well log data (e.g. in Rider, 2001; Emery and Myers, 1996).

The few quantitative studies of cyclicity in fluvial successions that have been carried out suggest that quantitative methods are useful. One method that has been applied in a few cases is Markov Chain analysis (e.g. Miall, 1973; Tewari and Casshyap, 1983; Johnson, 1984). The authors of these studies pointed out that quantitative analysis helps to reveal unexpected relationships between facies within the succession or between different successions, which could not be seen from outcrop observations.

In this chapter a new quantitative method (Burgess, in prep.) is explored to analyse the degree of order present in strata that helps to understand the strata organisation in more detail. This work is part of a preliminary study conducted to test the method, to understand links between the data and the results and to assess its applicability to fluvial successions.

10.2. Method

10.2.1. Order metric calculations

Three metrics are calculated to quantify order of the recorded successions using facies and facies unit thickness. The Markov order metric and the coarsening trend metric are based on facies transitions, and the runs order metric is calculated from thickness data.

The Markov order metric (MOM)

Davis (1986) defines a Markov chain as “a sequence in which the state at one point is partially dependent, in a probabilistic sense, on the preceding state”. The Markov order metric evaluates the degree of this dependence, i.e. probability of one facies to be followed by another facies, by computing a transition frequency (TF) matrix (e.g. Davis, 1986). The TF matrix represents the number of transitions observed from one facies (in rows) to another facies (in columns). The probability of such transitions is shown in transition probability (TP) matrix (Fig.10.1) by calculating the fraction of TFs in every matrix cell relative to the total sum of TFs in each row. The diagonal of the TP matrix is zero because same to same facies transitions are not present in the recorded successions. The difference between minimum (min_j) and maximum (max_j) probabilities is calculated in each row of the TP matrix and the mean of these differences is found to obtain the Markov order metric.

$m = \frac{\sum_1^J (max_j - min_j)}{J}$, where J is number of rows, hence number of facies.

The Markov order metric (MOM) for a perfectly ordered facies succession is 1 (Fig. 10.1, A, B, D). In contrast the MOM value for an example of a randomly generated facies succession is 0.43 (Fig. 10.1, C, D). The MOM has been found to be sensitive to the length of succession (number of facies units) when the total length is less than 20 (Fig. 10.2, A). The metric value is also sensitive to the number of different facies, and is difficult to interpret in cases with fewer than five facies (Fig. 10.2, B).

Diagram explanation, part 1 (for Figures 10.1 and 10.8-19, A, D, E)

Synthetic (Fig. 10.1) and recorded (Fig 10.8 – 10.19, A, D, E) strata were analysed using three main diagrams. The facies and unit thickness successions are represented

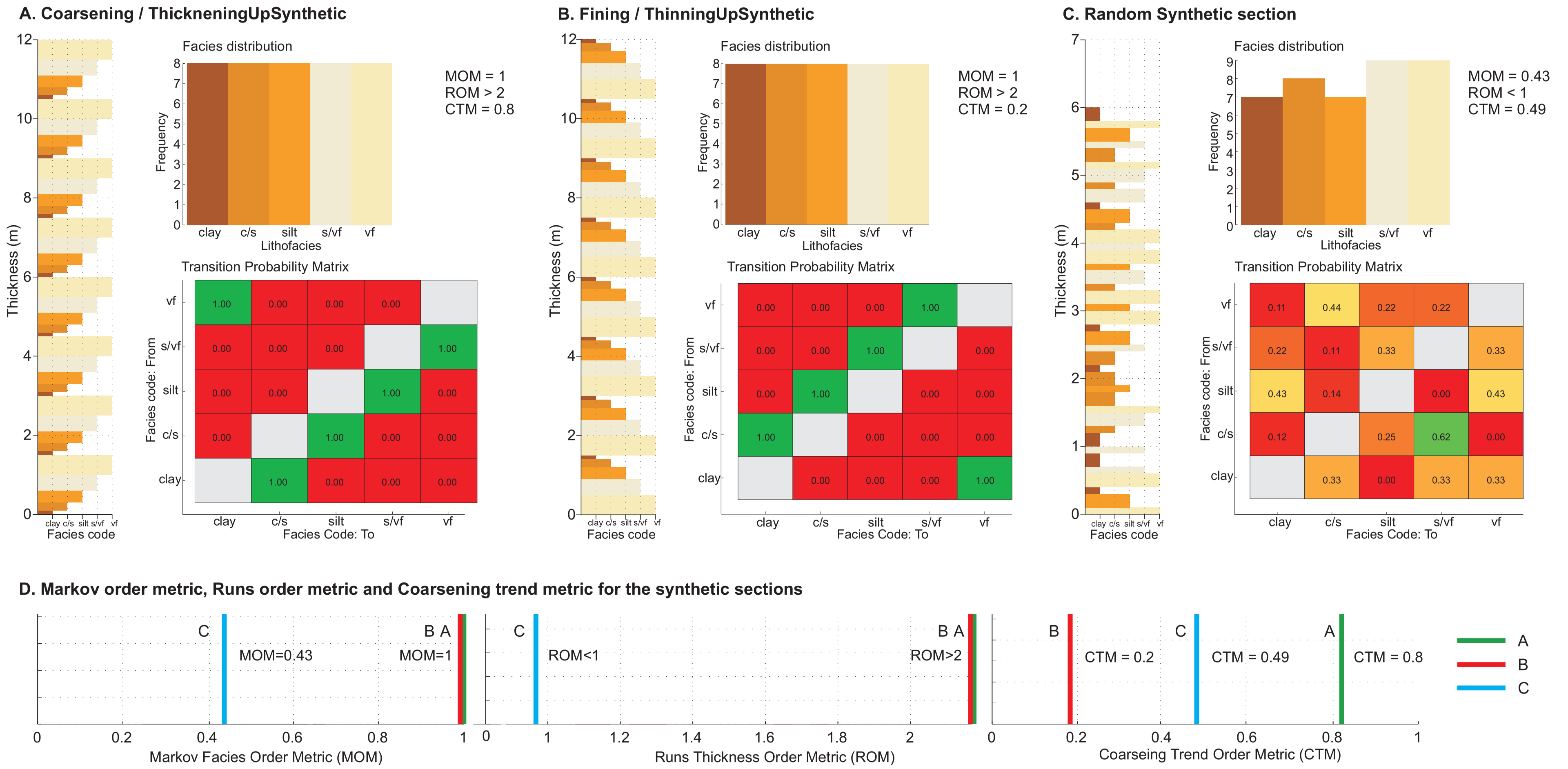

Figure 10.1. Coarsening- and thickening-upward (A), finning- and thinning-upward (B) and random (C) synthetic successions. Facies frequency distribution show uniform distribution for ordered successions. Note that transition probability matrices (TP matrices) have different look for ordered and random successions. D - Range of metric values for two perfectly ordered and random synthetic successions.

with standard sedimentary logs. Facies colour codes and occurrence frequency are presented on the facies frequency distribution plots. The transition probability matrix demonstrates the relationships of facies in the succession. The green to red colour scale for the TP matrix cells indicates a range of transition probabilities from 1 to 0, respectively.

The runs order metric (ROM)

A run is a succession of states which represent a change in j-th facies unit thickness relative to the previous unit. Thickness may either increase (run up) or decrease (run down). Two successions are produced to record the length of runs for increasing thickness (I) and decreasing thickness (D). ROM, the runs order metric (r), is eventually calculated by summing mean values of increasing and decreasing successions:

$r = \left(\frac{\sum_1^n I_j}{n}\right) + \left(\frac{\sum_1^n D_j}{n}\right)$, where n is number of facies units in analysed succession.

Runs in a random thickness succession are shorter than in an ordered one and therefore ROM will be lower. Typical values for random thickness successions are less than 2 (Fig. 10.1, C, D), whereas ROM is between 2 and 3 for ordered thickness successions (Fig. 10.1, A, B, D). Runs order metrics have also been found to be sensitive to the length of the succession when the total length of the succession is 20 facies units or lower (Fig. 10.2, A). The value of the runs metric, however, is independent of the total number of facies units (Fig. 10.2, B).

The coarsening (shallowing) trend metric (CTM)

The shallowing trend metric (s) was defined by Wilkinson et al. (1997) where it was applied to carbonate strata, and is simply

$s = \frac{n_s}{n-1}$, where n_s is the number of transitions between facies that represent a decrease in depositional water depth and n is the total number of facies units in the succession.

For this work on fluvial strata, the shallowing metric has been redefined as a more directly observable coarsening trend metric (CTM). It has been calculated only for the floodplain sections of the Huesca DFS succession where facies are directly related to grain size.

Coarsening metric values equal to 0.8 for perfectly coarsening trend examples and to 0.2 for perfect fining trends (Fig. 10.1 A, B, D). On average, for randomly generated sections the CTM is ~ 0.5 (Fig. 10.1, C-D) (cf. Wilkinson et al., 1997). In contrast to the MOM and ROM, variations in CTM values at small section lengths (Fig. 10.2, A) record coarsening successions present at this scale and are not artificial (Wilkinson et al.,

A. Section length, total number of facies units

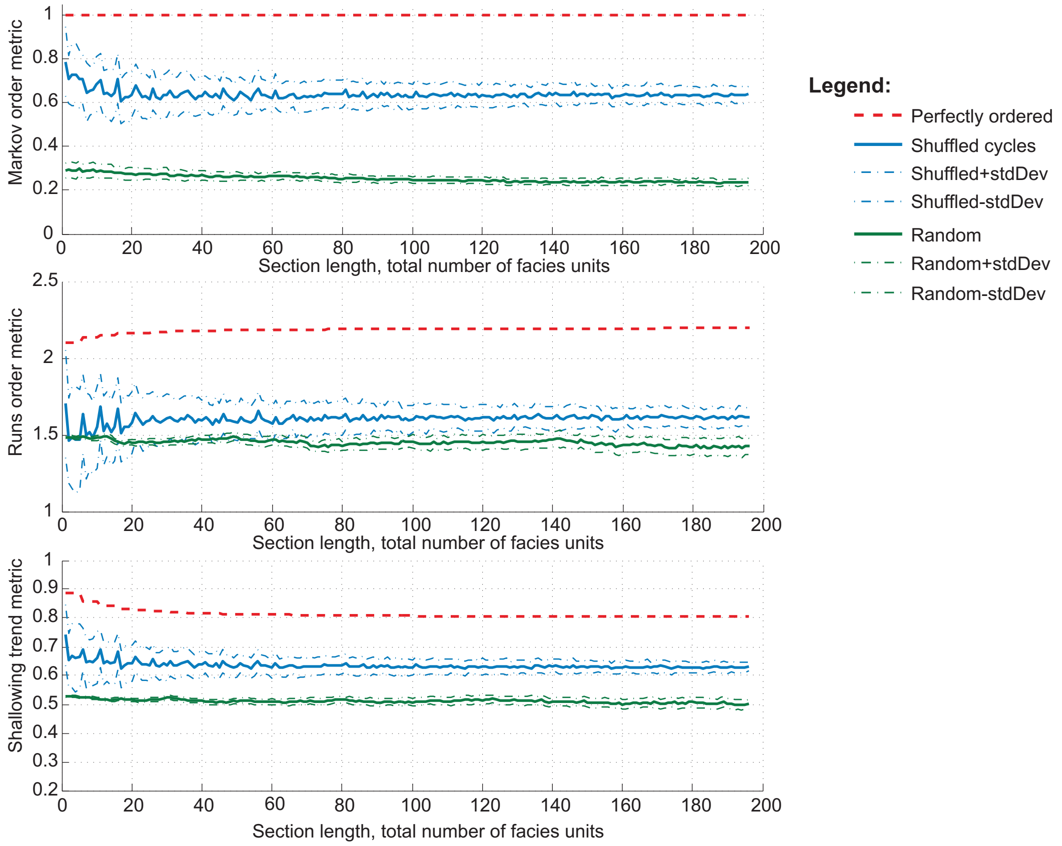

B. Number of different facies

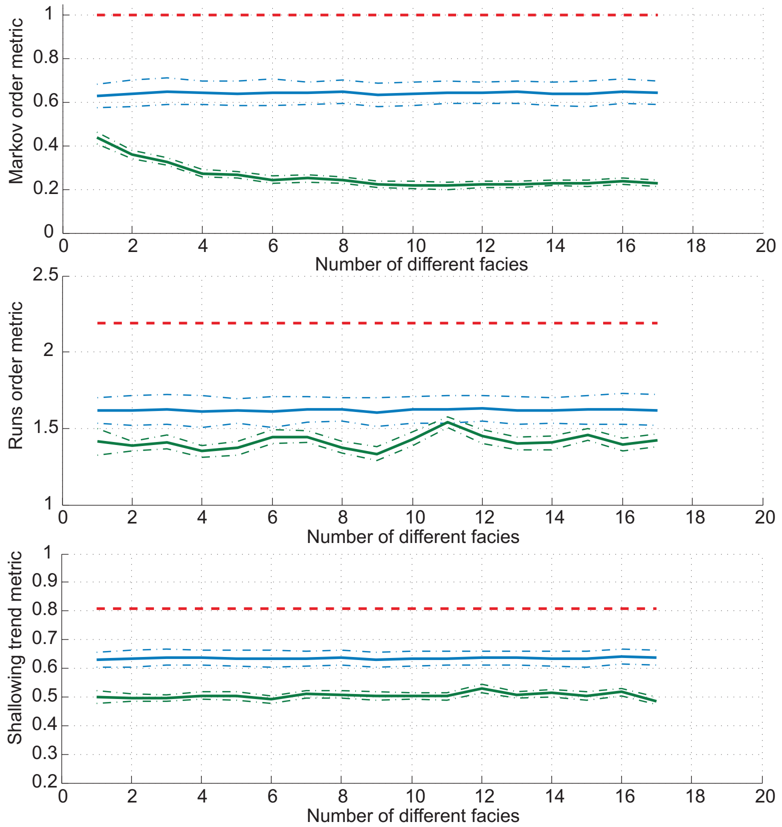

Figure 10. 2. Effect of section length (number of facies units) (A) and number of different facies in the section (B) on the order metrics for synthetic perfectly ordered cyclical, shuffled cycles and random successions (modified from Burgess, in prep.).

1997). The metric is also independent of the number of facies units in the succession (Fig. 10.2, B).

10.2.2. Comparison with synthetic models

The analysis of facies and thickness successions in recorded sections considers a hypothesis that the order is present and an alternative hypothesis that order is not present. If the alternative hypothesis can not be rejected, a succession can be interpreted as a succession of ordered depositional processes, indicating the possibility of forcing by an ordered external signal such as periodic climate cycles, otherwise a different interpretation needs to be found. The hypothesis is tested here using comparison between order metrics for observed successions and disordered synthetic successions. Conclusions about order can then be made based on similarity or difference between the metrics. Three disordered synthetic models are used for the comparison test and include a randomly shuffled same-data model, a randomly shuffled cycles model, and a random model. These three models are explained below.

The randomly shuffled same-data model

The randomly shuffled same-data model represents randomly shuffled facies units of the observed succession, where number of shuffles is equal to the number of facies units in the succession (*n*). Shuffling involves swapping two facies units in the succession, and repeating this process *n* times for randomly selected pairs of facies. Positioning of a unit on top of a unit of the same facies is not permitted; if this occurs another swap is made instead. This swapping process results in a succession with the same frequency distribution and number of facies units as the original successions, but on average with a lack of any order. Generally, the higher the number of shuffles, the more disordered synthetic succession becomes. Importantly, even after *n* shuffles in an *n* unit long succession, some order may remain due to chance of juxtaposition of particular facies or additional order could even be created relative to the original succession. To address this issue, the process of shuffling (n times) is repeated 1000 times and the frequency distribution of all obtained values can then be used to compare with the value calculated for the original succession (Fig. 10.8-19, C).

The randomly shuffled cycles model

The base succession for the randomly shuffled cycles model consists of facies units arranged as perfectly ordered thickening-upward asymmetrical cycles (e.g. Fig. 10.1, A). The ordered succession is characterised by the same number of facies units as the observed succession and has the same number of different facies. These are then randomly shuffled using the same algorithm as the randomly shuffled same-data model. Note that the facies frequency distribution for this model is uniform, meaning that on average all facies occur with the same frequency.

The random model

The random model is created by assigning a random thickness value within a specified range, and a random facies number to each unit in the succession. Thickness and facies values are sampled from a uniform distribution of facies and thicknesses values. The only constraints on facies choice are the range of possible facies that occur (the same as in the observed succession), and that same-facies to same-facies transitions are not permitted. Thickness values are picked from the interval of all possible floating-point numbers between zero and the number of facies in the recorded succession. For example, a succession with 10 facies would have a possible range of thicknesses such that $0 < t \leq 10$. Since the thickness and facies of successive units are selected at random, on average there should be no significant patterns present, so thickness runs should be short and the TP matrix should be uniform, with generally similar probabilities for a transition from one facies to any other facies (Fig. 10.1, C). However, as in the randomly shuffled models, more ordered intervals can occur in a random model just by chance, so as with the shuffled models 1000 random successions are generated and the frequency distribution of the values for each of these sections can then be compared with observed succession data.

The meaning of the comparison between models and observed data

The synthetic models explained above are characterised by pre-defined, known degrees of order or disorder, so comparison of metrics obtained for the models with equivalent metrics calculated for the observed section allow interpretation of the degree of order present in the observed succession.

MOM for randomly shuffled cycles model

Even a small number of shuffles reduces the MOM value for the perfectly ordered cyclical succession and n-times shuffled model would give much lower MOM values than unshuffled perfectly ordered succession. This could be demonstrated on the Figure 10.3, A. Each vertical column on the plot corresponds to a section with different number of facies (x-axis). The colour of column cells represents number of shuffles as a proportion of the total section length) and so ranges from 0 (green), indicating an unshuffled succession, to 1 (red) where the section has been shuffled n times, where n is the section length. The MOM and ROM values for the progressively shuffled ordered cyclical succession are plotted along the y-axis. The green area on the plot represents either unshuffled cases, or cases with only a small number of shuffles. The green area extends from, for example, MOM values of close to 1 to around 0.5, showing that even a small number of shuffles will reduce MOM value significantly. The orange and red area is relatively smaller in size, showing that the MOM value is less sensitive to increasing number of shuffles in the upper range of shuffle values. The same is true for ROM data (Fig. 10.3, B). Thus, randomly shuffled cycles model on average would give low MOM values indicating low degree of order.

MOM for random model

The random model on average lacks any order and is therefore also characterised by low MOM values (e.g. Fig. 10.1, C). Facies for the random model are picked randomly from a uniform facies distribution but note that this could still result in non-uniform facies distribution with one dominant facies in the succession. In such cases the Markov order metric would be higher than for shuffled cycles model, because transitions from any facies to the dominant facies would be more frequent than other transitions. Frequent transitions give higher TP values and consequently higher MOM. Note also that ordered strata can occur by chance in both the random model and the shuffled perfect cycles model. Individual realizations of the random model succession could give higher MOM metrics than for the shuffled cycles model, and vice versa.

Despite these complications, on average, both random and shuffled cycles models have a similar low degree of order with low MOM. Therefore, MOM values calculated from the observed succession that are similar to the mean of MOM values from the random and shuffled models indicate a similar, low degree or no order in the observed data. For such low values the alternative hypothesis of randomness could not be rejected. The MOM value in the ordered succession should be much higher than the MOM values for random and shuffled cycles models.

MOM for shuffled same-data model

The shuffled same-data model is simply shuffled facies units of the recorded succession. Comparison of the MOM values obtained for the observed succession with the MOM distribution of the shuffled same-data model shows the effect of shuffling on the value of the MOM. If the succession is ordered and its facies distribution is close to uniform, the MOM distribution for shuffled same-data model should be located very close to the shuffled cycles model or random model distributions. In this case MOM for the observed succession and shuffle same-data model will be different. Alternatively, if the observed succession is originally not ordered, the MOM values for the observed succession and its shuffled version should be similar. The MOM value for such data succession would be located closer to the random and shuffled cycles model as well.

There is, however, the possibility of some order to be created by chance during shuffling. Apparent order might also arise if the recorded succession is strongly dominated in term of frequency of occurrence by just one or more facies. The resulting MOM values for the recorded succession would be high because the probability of transition to a dominant facies in the distribution would be much higher than for other facies. The metric for the shuffled same-data model would be high as well, because there are fewer variants of facies combinations during the shuffling process when it is restricted by prohibiting same-to-same facies transitions. The MOM value for the recorded succession with one or more dominant facies is expected to be close to the MOM distribution for the shuffled same-data model and higher than MOM distribution for other two models.

Thus, If MOM value for observed succession is similar to the mean MOM for the same-data shuffled model the succession is either disordered, or its facies distribution is strongly dominated by just one or two facies. Additional comparison with random and shuffled cycles models and examination of the transition probability matrix is required to select between these two interpretations.

Diagram explanation, part 2 (for figures 10.8-19, C)

For each studied section, frequency distributions of metric values (MOM, ROM and CTM) are constructed from 1000 iterations of each synthetic model (Fig. 10.8-19, C). The green spike represents MOM, ROM or CTM value for the recorded succession for comparison with model distributions.

10.3. Metric analysis results, their interpretation and discussion

The method described above was applied to analyse facies and thickness successions for 12 system-scale sections in the Huesca and Salt Wash DFS successions (Table 10.1) and 19 floodplain sections in the Huesca DFS succession (Table 10.2). System-scale sedimentary successions represent almost complete succession of facies and unit thickness of DFS deposits exposed in the studied outcrops (appendices 2.1-2.12). The system-scale succession up to 100 m thick could be considered to record succession of events for long period of DFS activity. Floodplain successions represent intervals of overbank deposits between two subsequent channel sandstone bodies in the Huesca DFS succession (appendices 2.13-2.18) that record overbank deposition events for a period before channel re-occurrence at the same location on the floodplain.

10.3.1. Preparation of stratigraphic sections

The word “facies” is used in two slightly different sense in this chapter: For the system-scale sections of the Huesca and Salt Wash DFS succession (Table 10.1) “facies” represents sedimentological facies defined in the Chapter 4. For floodplain sections of the Huesca DFS succession (Table 10.2) “facies” is limited to the grain size of the lithology. Facies codes of system-scale successions are presented in the same order as they were described in the Chapter 4, while facies for floodplain successions are ordered in terms of grain size, from fine to coarse.

Facies of each recorded succession were re-numbered, so that the facies values are continuous (1-2-3-4-…) even if some facies have not been observed in the location. Occurrences of the same facies adjacent to one another were combined into one unit so that the same facies code never occurs twice in succession. Any intervals of no exposure were also removed from the successions for simplicity (note there are only 2 examples in all the strata studied). Intervals of non-exposure probably represent fine-grained overbank facies Hm, Ssh and Hsh but could also contain some rare facies such as Sil, Sils. The number of removed intervals is small and will not noticeably affect these results.

The recorded stratigraphic successions contain from 4 to 9 facies but most of the sections have 6 to 7 facies. Miall (1973) stated that a simplified scheme of 5 to 6 facies is suitable for the Markov chain analysis because higher number of facies makes patterns of facies transitions more difficult to interpret and tend to distort the results. Combining or splitting facies units would give different results. The facies classification for Huesca and Salt Wash DFS successions described in the Chapter 4 includes rare facies such as, for instance, facies Sil and Sils (isolated lenses of sandstones). Although these facies reduce transition probabilities for other facies and could be excluded from the analysis for large-scale studies, they reflect real heterogeneity in the strata, so it is important to include them.

Based on the results of the earlier sensitivity analysis (Fig. 10.2, Section 10.2.1), sections containing minimum 4 facies and not less than 20 facies units were selected for the analysis (Tables 10.1-2).

10.3.2. Metric values for the observed successions

System-scale Huesca and Salt Wash successions

Markov and runs order metrics and parameters of the recorded system-scale successions (appendices 2.1-2.12) are presented in Table 10.1. The MOM shows values between 0.62 and 0.94. The MOM values for the medial and distal sections of the Huesca DFS succession (Castelflorite and Alcolea) are much higher (MOM > 0.9) than the MOM for relatively proximal Monźon sections of the Huesca DFS (MOM = 0.62 – 0.72) and higher than values for all sections of the Salt Wash DFS succession (MOM = 0.64 - 0.8). The runs order metric for all successions varies between 1.1 and 1.4.

N	Logs	Parameters of recorded successions			Metrics for recorded successions	
		Number of beds	Number of facies	Average bed thickness	MOM	ROM
Salt Wash DFS successions						
1	Bullfrog 2 Log 125	70	7	1.299	0.695	1.2429
2	Bullfrog 3 Log 34	40	7	1.370	0.782	1.175
3	Slick Rock Log 1	40	6	1.632	0.675	1.325
4	Little Park 2 Log 12	44	9	1.034	0.795	1.1364
5	Little Park 1 Log 456	27	5	1.281	0.702	1.3333
6	Little Park 3 Log 7	35	8	1.053	0.645	1.3429
	Average for Salt Wash	43	7	1.278	0.716	1.2593
	MAX	70	9	1.632	0.795	1.3429
	MIN	27	5	1.034	0.645	1.1364
Huesca DFS successions						
7	Monźon 4 Log 1	60	6	1.188	0.619	1.1167
8	Monźon 1 Log 12	66	7	0.902	0.723	1.1515
9	Castelflorite 4 Log 1	74	6	1.240	0.934	1.2027
10	Castelflorite 2&3 Log2	57	6	1.279	0.907	1.1404
11	Castelflorite 2 Log 3	36	4	0.994	0.92	1.4167
12	Alcolea 1&2 Log 1	83	8	0.906	0.943	1.1084
	Average for Huesca	63	6	1.085	0.841	1.1894
	MAX	83	8	1.279	0.943	1.4167
	MIN	36	4	0.902	0.619	1.1084

Table 10.1. Metric values and parameters of the recorded system-scale sections of the Huesca and Salt Wash DFS successions.

Floodplain successions of the Huesca DFS

The order metrics and parameters of the recorded floodplain sections of the Huesca DFS succession (appendices 2.13-18) are presented in Table 10.2. The calculated MOM values vary between 0.47 and 0.74, and so are in general lower than metric values for the system-scale successions (MOM = 0.62 – 0.94). The values of the runs order metric for the floodplain succession are low and vary between 0.96 and 1.29. Additionally the coarsening trend metric was computed for the floodplain successions. The values range from 0.45 to 0.58 (~ 0.5). The highest obtained CTM value is still very close to 0.5 (CTM = 0.58 for Monte Aragón 2).

N	Logs	Parameters of recorded successions			Metrics for recorded successions		
		Number of beds	Number of facies	Average bed thickness	MOM	ROM	CTM
Floodplain succession of the Huesca DFS							
1	Bolea 1	35	8	0.192	**0.563**	**1.1321**	**0.52**
2	Bolea 2	61	8	0.180	**0.581**	**1.0164**	**0.48**
3	Piracés 3	23	9	0.396	**0.685**	**1.1739**	**0.45**
4	Piracés 4	21	9	0.407	**0.630**	**1.0476**	**0.55**
5	Piracés 5	21	7	0.326	**0.700**	**1.1429**	**0.50**
6	Piracés 6	20	7	0.407	**0.476**	**1.2500**	**0.47**
7	Pertusa 1	31	4	0.231	**0.739**	**1.0645**	**0.47**
8	Pertusa 3	21	7	0.381	**0.476**	**1.0476**	**0.50**
9	Pertusa 5	21	7	0.271	**0.619**	**1.0952**	**0.50**
10	Monźon 1	44	8	0.323	**0.577**	**1.0909**	**0.56**
11	Monźon 3	35	9	0.370	**0.468**	**1.2571**	**0.47**
12	Monźon 4	33	7	0.214	**0.695**	**1.0000**	**0.56**
13	Lierta 1	22	6	0.307	**0.648**	**1.2727**	**0.48**
14	Monte Aragón 2	34	8	0.293	**0.483**	**1.0882**	**0.58**
15	Monte Aragón 3	24	8	0.162	**0.571**	**0.9583**	**0.48**
16	Monte Aragón 4	44	9	0.300	**0.639**	**1.1136**	**0.53**
17	Castelflorite 1	51	9	0.321	**0.556**	**1.2941**	**0.48**
18	Castelflorite 2	34	7	0.399	**0.565**	**1.1765**	**0.52**
19	Castelflorite 3	35	8	0.419	**0.543**	**1.2000**	**0.53**
	Average for Huesca	32	7	0.310	**0.590**	**1.1275**	**0.51**
	Max	61	9	0.419	**0.739**	**1.2941**	**0.58**
	Min	20	4	0.162	**0.468**	**0.9583**	**0.45**

Table 10.2. Metric values and parameters of the recorded floodplain sections of the Huesca DFS succession.

10.3.3. Comparison between MOM values of the observed successions and synthetic models

Comparison with randomly shuffled cycles and random models

System-scale Huesca and Salt Wash successions

The shuffled cycles and random models based on the system-scale successions give low mean MOM values between 0.32 and 0.5 and between 0.3 and 0.46, respectively (Table 10.3). The distributions of MOM values computed for shuffled cycles and random models are usually located close together on graphs (Fig. 10.8-13, C) and are characterised by similar mean values for system-scale successions with the maximum difference of 0.064 (Little Park 3 Log 7) (Table 10.3). In general the random model shows higher MOM values than the shuffled cycles model. This is probably due to non-uniform distribution of facies in the random succession compared to a uniform distribution in the shuffled cycles succession (Section 10.2.2). The MOM values of the system-scale successions are higher than the mean and maximum MOM for shuffled cycles and random models (Table 10.3) that indicate that observed system-scale successions contain significant element of order.

Floodplain successions of the Huesca DFS

The values for the shuffled cycles and random models based on the floodplain successions are similar and vary from 0.36 to 0.57 and from 0.32 to 0.53, respectively (Table 10.3). The difference between mean values of MOM distributions computed for shuffled cycles and random models (Fig. 10.8-13, 10.14-19) is also low and equals to 0.13 (Piracés 4) (Table 10.3). The MOM values for the floodplain succession are higher than the mean MOM for both disordered synthetic models that demonstrate presence of order in the floodplain successions. The degree of order is slightly lower than that for the system-scale successions and will be discussed in further sections.

The MOM values for the system-scale and floodplain successions are plotted on the graph from Figure 10.3 and fall in the green area (Fig. 10.5, A-B) suggesting they represent a degree of order equivalent to a perfectly cyclical succession in which only a few facies were shuffled. It is, however, a question whether the order style is truly cyclical or the successions have dominant facies that would give high MOM values as well (Section 10.2.2). To investigate these two possibilities the shuffled same-data model need to be compared with MOM values for the recorded successions. This is discussed in the next section.

Comparison with randomly shuffled same-data model

System-scale Huesca and Salt Wash successions

The Markov order metric values for the system-scale strata are close or higher to the mean MOM of the shuffled same-data model. The absolute difference between these values is low and varies between 0.01 and 0.14 (Table 10.3) indicating that random shuffling does not affect the degree of order of the observed successions. The similarity suggests that the observed strata are either not ordered or are strongly dominated by a few facies (e.g. the Alcolea 1&2 Log 1, Fig. 10.8).

Floodplain successions of the Huesca DFS

The same is observed for the floodplain successions. The mean MOM value of the shuffled same-data model and MOM value for the floodplain data differ by the small value between 0 and 0.13 (Table 10.3) indicating very small influence of shuffling on the order of the original successions. This could again be caused by an absence of order or a dominance of one or more facies (e.g. Monźon 3, Fig. 10.19).

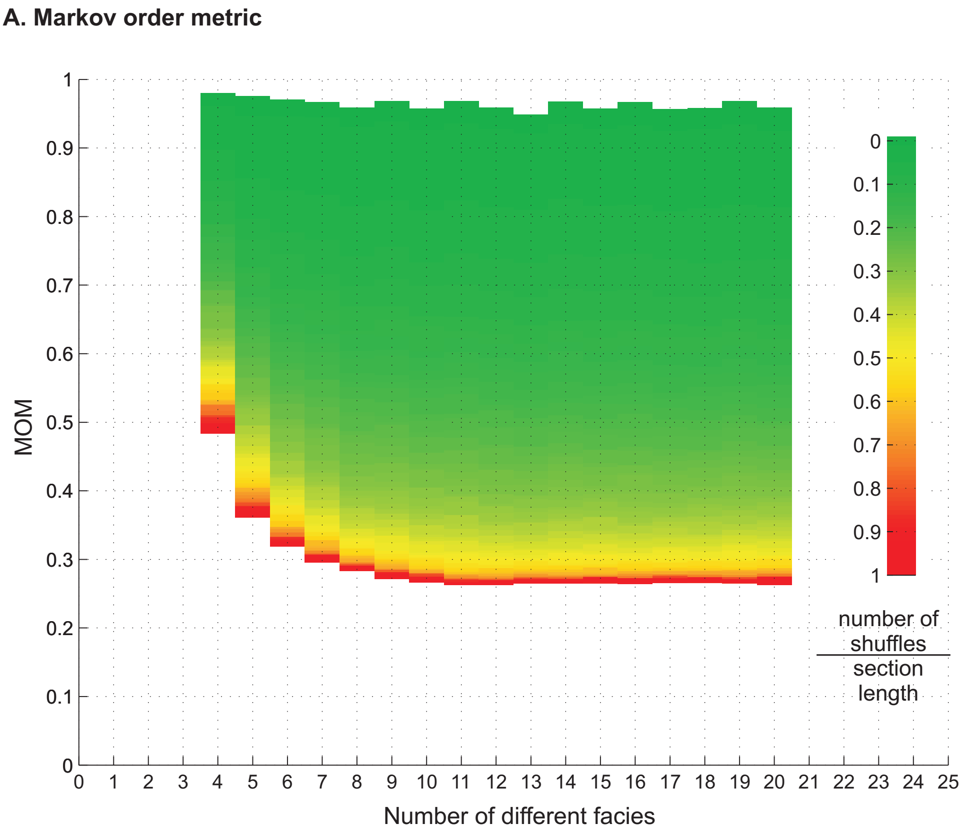

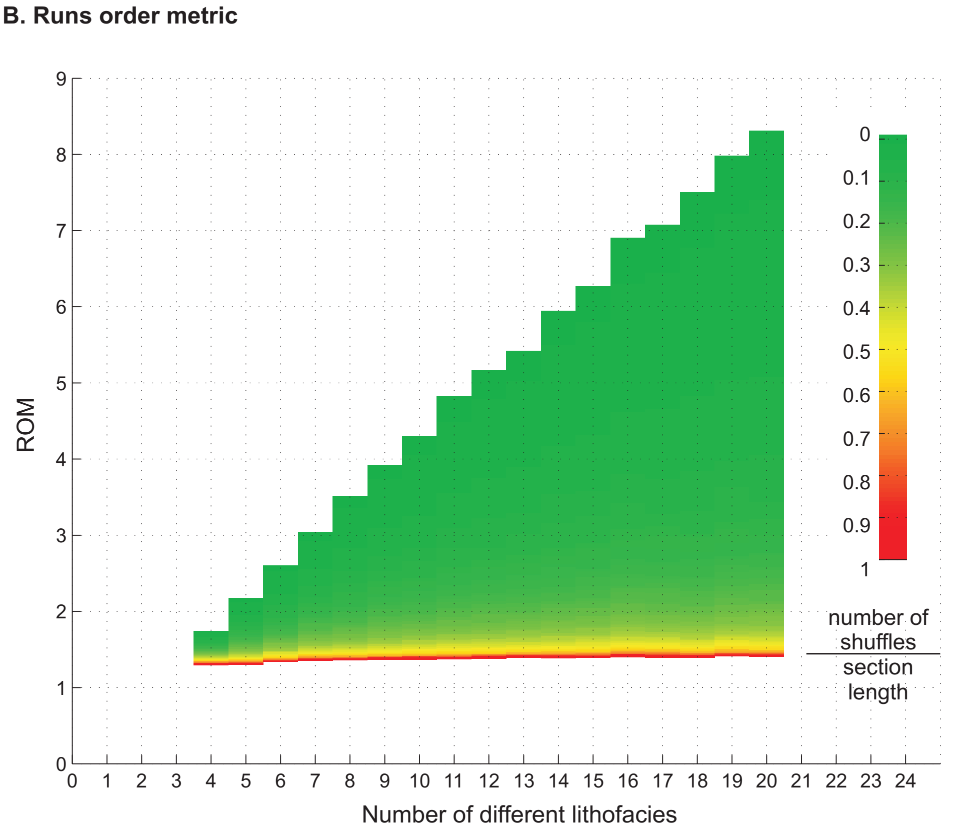

Figure 10.3. Variation in Markov order metric (A) and runs order metric (B) value of the perfectly ordered cyclical succession with number of shuffles for different number of facies.

The same trends are observed for the system-scale and floodplain successions, such that in general shuffling does not change the observed succession MOM values by very much. The interpretation of the absence of order can be rejected for both system-scale and floodplain successions because it has been shown above that there is a difference between MOM values of the observed successions and the mean MOM for random and shuffled cycles model. This suggests that successions are ordered. The similarity between MOM values of the observed successions and the mean MOM for shuffled same-data model discussed in this section indicates, however, that the succession are ordered but not in the same way as the perfectly ordered cyclical succession is ordered. The most likely interpretation is that the observed successions contain one or more dominant facies and it is these dominant facies that lead to the high MOM values. This interpretation is consistent with the facies frequency distributions of the system-scale successions that clearly show the dominance of one facies (Fig. 10.8-12), but the dominance of one facies is not as pronounced in the floodplain successions (Fig. 10.13-19).

Comparison between system-scale and floodplain successions

Examination of the transition probability matrices and facies frequency distributions help to understand MOM values calculated from strata. The facies distributions of the observed system-scale strata are often dominated by one or two facies. For example, Hm/Hsh facies dominate the Alcolea 1&2 Log 1 and St facies dominate Bullfrog 3 Log 34 system-scale successions (Fig. 10.8 and 10.11). The transition probability matrix reflects this facies distribution. The probability of transition to the dominant facies approaches 1, while probabilities for transitions into other facies are much lower, approaching zero. This is because in these successions each non-dominant facies has a high probability of being overlain by the dominant facies. In addition, facies successions include rare facies (e.g. Sil, Sils, Sr, Scr, Sb) which occur once or twice, and also give high TP values in the matrix (e.g. Fig. 10.10). The resulting high probabilities in the TP matrix values produce high MOM values.

These observations from the facies frequency distribution and TP matrices are consistent with the metric analyses results presented above. The difference between MOM for shuffled cycles model and the Alcolea 1&2 Log1 system-scale succession is quite high and equals to 0.64 (Table 10.3, Fig. 10.4 and 8) that is indicative of ordered succession. The difference between MOM values for unshuffled Alcolea 1&2 Log 1 system-scale succession and its shuffled same-data model is only 0.014 (Table 10.3, Fig. 10.8) that supports the presence of a dominant facies in the succession. In this case, since same-to-same facies transitions are prevented during shuffling, there are not many variants of facies sequence combinations that could be obtained by shuffling.

The MOM values are therefore high and almost independent of the number of shuffles. This indicates order style defined by the dominance of one facies.

Some system-scale strata are composed of a more diverse set of facies and therefore have a more uniform frequency distribution and give slightly lower MOM values as well as a much lower difference between shuffled cycles model and unshuffled data. For example, the Bullfrog 2 Log 125 system-scale succession is characterised by smaller MOM (0.695) and lower difference between MOM values for shuffled cycles model and unshuffled data (0.37) (Table 10.3, Fig. 10.10) than the Alcolea 1&2 Log 1 system-scale succession (0.64) (Table 10.3, Fig. 10.8). Strata with more diverse facies have more possible facies combinations that can arise from shuffling and therefore the shuffled succession differs more from the original succession (difference equals to 0.08 in the Bullfrog 2 Log 125, Table 10.3), assuming there is any order present in the original strata.

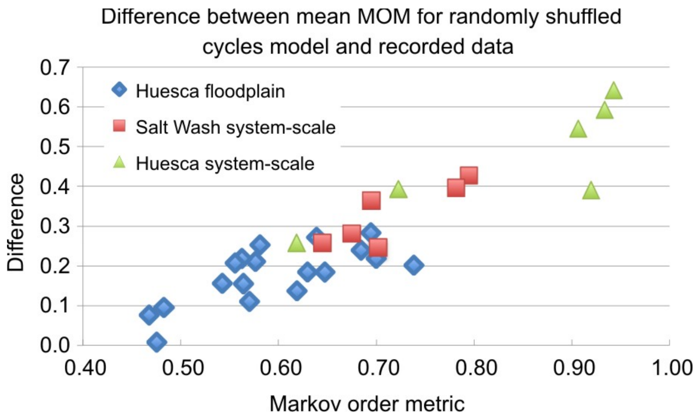

Figure 10.4. Variation in difference of MOM values for shuffled cycles model and recorded successions (y-axis). The difference is plotted against MOM for the recorded successions (x-axis). The difference and MOM values are higher for the system-scale successions than for the floodplain successions.

In comparison to the system-scale successions, facies in the floodplain successions are generally more diverse and are usually not dominated by one facies (Fig. 10.14-19). However, some facies seem more abundant then others. Consequently, MOM values are slightly lower (0.46 - 0.74 – floodplain succession; 0.62 - 0.94 – system-scale successions, Fig. 10.5; Tables 10.1-2) and the difference between the MOM values for the unshuffled data and mean MOM values for the shuffled cycles model is smaller (0.005 - 0.285) (Fig. 10.4; Table 10.3). The difference between system-scale and floodplain facies successions is also demonstrated in the Figure 10.4. The floodplain successions, therefore, are less ordered than system-scale successions, but still show higher degree of order than disordered models and also are not affected by facies unit shuffling much. This result demonstrates that the nature of the order in

A. System-scale successions

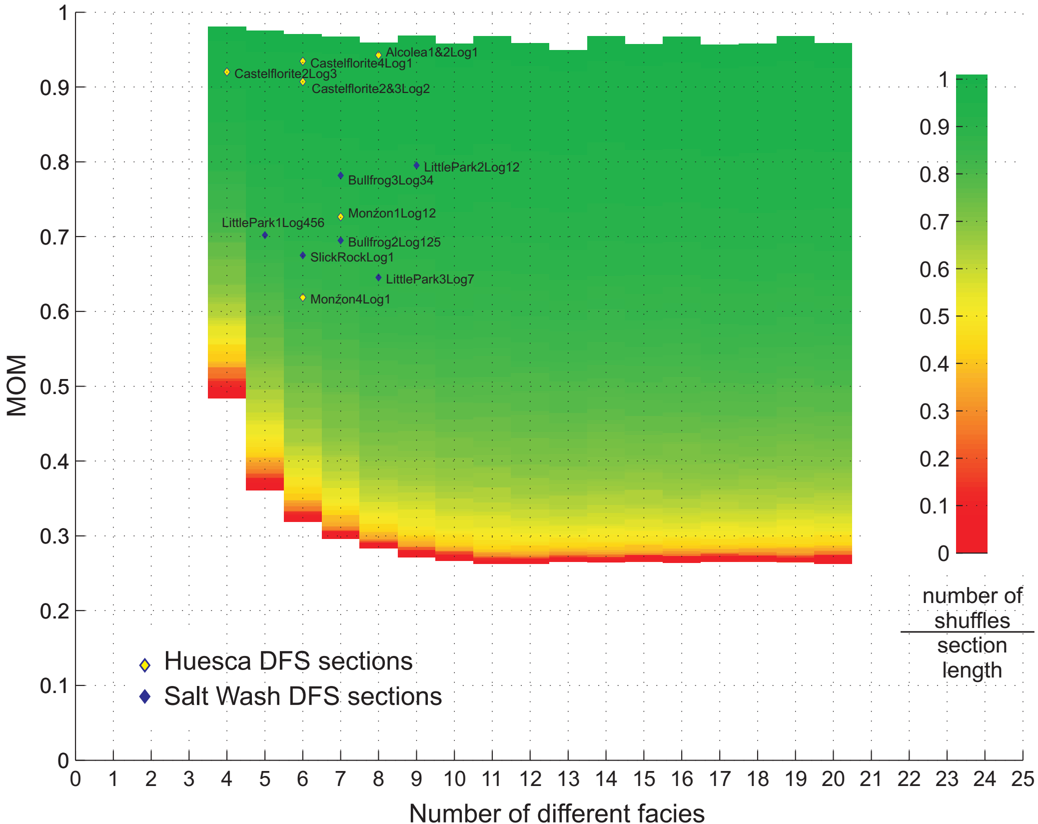

B. Floodplain successions

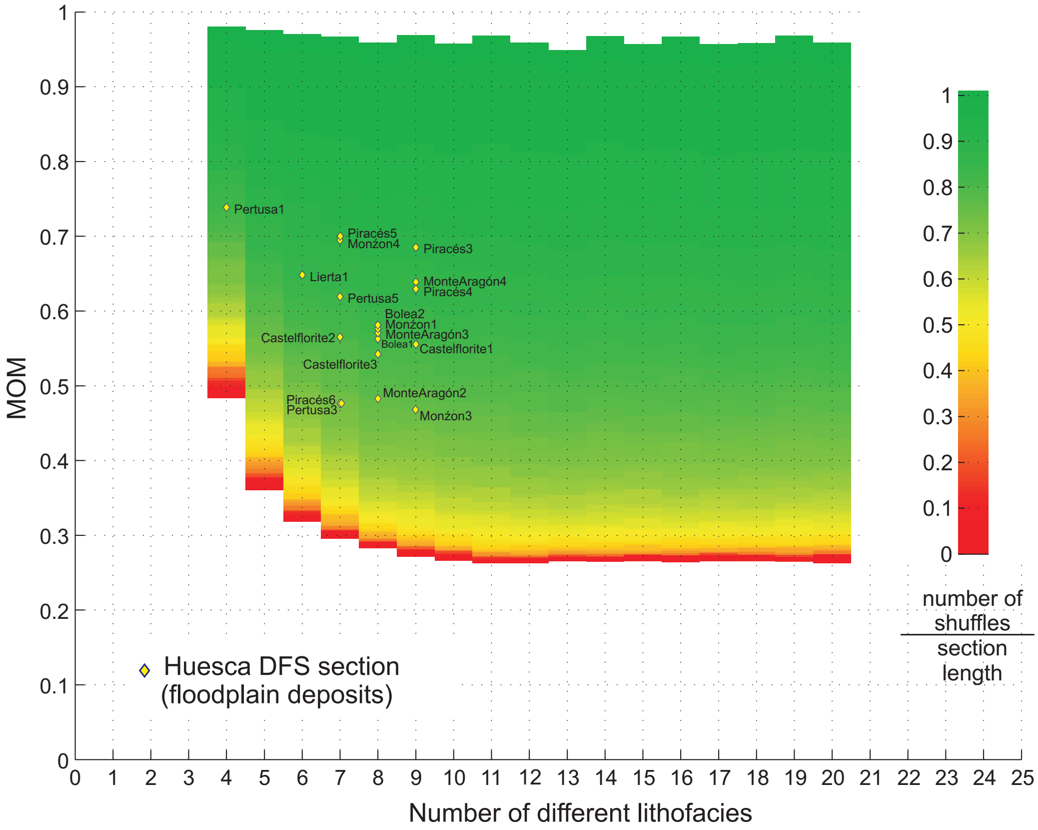

Figure 10.5. Markov order metric values for the system-scale succession of the Huesca and Salt Wash DFS successions (A) and floodplain succession of the Huesca DFS succession (B). The coloured background represent variation in MOM values for perfectly ordered cyclical succession with number of shuffles for different number of facies (see Fig 10.3, A).

floodplain facies successions is different from perfectly cyclical succession and from succession with dominant facies.

Logs	**Random**		**Randomly shuffled cycles**		**Randomly shuffled same data**		**Difference**		**Field section**	**Differ-ence**
	mean	**STD**	**mean**	**STD**	**mean**	**STD**	**Random & recorded data**	**shuffled cycles & recorded data**	**sorted**	**shuffled same data & record data**
Salt Wash DFS successions										
Little Park 2, Log12	0.414	0.053	0.367	0.040	0.805	0.040	**-0.381**	**0.428**	0.795	**-0.010**
Bullfrog 3, Log34	0.426	0.053	0.385	0.038	0.748	0.031	**-0.357**	**0.397**	0.782	**0.034**
Little Park, 1 Log456	0.501	0.066	0.456	0.056	0.692	0.055	**-0.201**	**0.247**	0.702	**0.010**
Bullfrog 2, Log125	0.350	0.034	0.330	0.029	0.613	0.037	**-0.345**	**0.365**	0.695	**0.082**
Slick Rock, Log1	0.419	0.050	0.393	0.044	0.615	0.052	**-0.256**	**0.282**	0.675	**0.060**
Little Park 3, Log7	0.452	0.062	0.387	0.044	0.621	0.074	**-0.194**	**0.258**	0.645	**0.024**
Huesca DFS successions										
Alcolea 1&2	0.324	0.029	0.300	0.025	0.930	0.030	**-0.619**	**0.643**	0.943	**0.014**
Castelflorite 4 Log1	0.361	0.032	0.341	0.029	0.910	0.032	**-0.573**	**0.593**	0.934	**0.024**
Castelflorite 2 Log3	0.506	0.053	0.528	0.071	0.846	0.064	**-0.415**	**0.392**	0.920	**0.074**
Castelflorite 2&3 Log2	0.386	0.039	0.361	0.034	0.863	0.038	**-0.521**	**0.546**	0.907	**0.044**
Monźon 1 Log12	0.357	0.036	0.330	0.029	0.752	0.047	**-0.366**	**0.393**	0.723	**-0.029**
Monźon 3 Log 1	0.381	0.038	0.361	0.033	0.760	0.079	**-0.238**	**0.258**	0.619	**-0.141**
Floodplain successions of the Huesca DFS										
Pertusa1	0.523	0.058	0.536	0.073	0.747	0.028	**-0.216**	**0.203**	**0.739**	**0.008**
Piracés5	0.553	0.087	0.480	0.067	0.650	0.062	**-0.147**	**0.221**	**0.700**	**-0.050**
Monźon4	0.457	0.063	0.410	0.046	0.585	0.055	**-0.239**	**0.285**	**0.695**	**-0.110**
Piracés3	0.556	0.087	0.445	0.052	0.686	0.052	**-0.129**	**0.240**	**0.685**	**0.001**
Lierta1	0.536	0.081	0.463	0.065	0.750	0.095	**-0.112**	**0.185**	**0.648**	**0.102**
Monte Aragón 4	0.415	0.055	0.367	0.041	0.595	0.388	**-0.224**	**0.272**	**0.639**	**-0.044**
Piracés4	0.575	0.092	0.445	0.053	0.603	0.056	**-0.055**	**0.185**	**0.630**	**-0.027**
Pertusa5	0.554	0.087	0.480	0.067	0.747	0.074	**-0.065**	**0.139**	**0.619**	**0.128**
Bolea2	0.360	0.029	0.328	0.030	0.495	0.037	**-0.221**	**0.253**	**0.581**	**-0.087**
Monźon1	0.409	0.051	0.365	0.035	0.520	0.040	**-0.168**	**0.212**	**0.577**	**-0.057**
Monte Aragón 3	0.538	0.083	0.460	0.059	0.500	0.054	**-0.033**	**0.111**	**0.571**	**-0.071**
Castelflorite2	0.453	0.062	0.409	0.047	0.587	0.053	**-0.112**	**0.156**	**0.565**	**0.022**
Bolea1	0.380	0.043	0.344	0.033	0.518	0.033	**-0.184**	**0.219**	**0.563**	**-0.045**
Castelflorite1	0.387	0.046	0.349	0.033	0.535	0.038	**-0.169**	**0.207**	**0.556**	**-0.021**
Castelflorite3	0.452	0.062	0.386	0.043	0.543	0.522	**-0.091**	**0.157**	**0.543**	**0.000**
Monte Aragón 2	0.458	0.064	0.387	0.044	0.493	0.048	**-0.025**	**0.096**	**0.483**	**0.010**
Piracés6	0.565	0.090	0.481	0.067	0.520	0.064	**0.089**	**-0.005**	**0.476**	**0.044**
Pertusa3	0.553	0.086	0.481	0.067	0.550	0.064	**0.077**	**-0.005**	**0.476**	**0.074**
Monźon3	0.461	0.064	0.391	0.049	0.408	0.049	**-0.007**	**0.077**	**0.468**	**-0.060**

Table 10.3. Comparison of MOM values for synthetic models and recorded system-scale successions of the Huesca and Salt Wash DFS deposits and floodplain successions of the Huesca DFS deposits. Table is sorted by MOM values of the recorded successions.

Summary and interpretation

In summary, the successions with very high MOM values are found to have facies distributions dominated by one or more facies. Their MOM values do not change much after shuffling and are markedly higher than MOM values for the shuffled cycles and random models. These results indicate that the degree of order measured by MOM in observed strata is high, but the nature of this order is different from the order in perfectly ordered cyclical successions. The studied successions show systematic variations but they are not cyclical. Such apparent order arises from an alternation of several different facies with one or more dominant facies, leading to a high probability of transition to the dominant facies. The more diverse facies distribution the less ordered the facies successions. The system-scale successions of the Huesca and Salt Wash DFS have been found to be strongly dominated by one or two facies, while floodplain successions of the Huesca DFS is characterised by more diverse facies set and therefore a lower degree of order.

The order at system-scale could have been mainly controlled by long-term factors. For examples, the dominance of the fine-grained facies in the Huesca DFS succession could have been determined by the high degree of aggradation and preservation of overbank deposits in endorheic Ebro Basin (Fisher and Nichols, 2013). In contrast, the dominance of sandstone facies in the proximal and medial Salt Wash DFS could have been a consequence of a high degree of reworking of floodplain deposits by channels in a lower accommodation setting for the DFS (Weissmann et al., 2013 in press). However, the most proximal areas of the Huesca DFS has not been studied in this project and may have an architecture similar to the relatively proximal Salt Wash DFS.

The diverse facies set in the floodplain strata and lower degree of order might result from local depositional processes on the floodplain and reflect variability and complexity of the combination of these processes. The variability of depositional elements distinguished in the heterolithic floodplain deposits of the Huesca DFS (Chapter 9) support this conclusion. Burgess (2006) showed that autogenic factors could also create order in carbonate deposits while degree of disorder probably results from complex combination and complex variability of the control factors. This could be true for the fluvial deposits as well.

In conclusion, the Markov order metric includes information about order but on its own does not allow distinction between systematic transitions to dominant facies and truly cyclical strata. Comparison of MOM values for observed successions with metric distributions for synthetic models makes it possible to recognise these two order styles in facies successions with high MOM. The method, however, did not provide information about the order style for the floodplain successions with intermediate high MOM values and more work is required to investigate this further.

10.3.4. Comparison between ROM values of the observed successions and synthetic models

All system-scale and floodplain successions show very low ROM values (< 1.5) (Tables 10.1-2). The shuffled same-data model and unshuffled data have similar ROM values (Fig. 10.8-13, 10.14-19) meaning that shuffling does not reduce or increase originally low degree of order of thickness successions. Almost all ROM values for the recorded successions are slightly lower than mean ROM values for synthetic models (Fig. 10.8-13, 14-19). The difference, however, is very small (e.g. Table 10.4) and probably reflects the fact that ROM for the observed succession is just one example being compared with a distribution of ROM values for 1000 synthetic models.

Logs	Random		Randomly shuffled cycles		Randomly shuffled same data		Difference		Field section	Diff
	mean	STD	mean	STD	mean	STD	Random & recorded data	shuffled cycles & recorded data	sorted	shuffled same data & recorded data
Salt Wash DFS successions										
Little Park 3 Log 7	1.442	0.035	1.338	0.109	1.288	0.126	**0.099**	**0.005**	**1.3429**	**0.055**
Little Park 1 Log 456	1.437	0.042	1.285	0.107	1.244	0.121	**0.104**	**0.048**	**1.3333**	**0.089**
Slick Rock Log 1	1.435	0.038	1.313	0.969	1.298	0.116	**0.110**	**0.012**	**1.325**	**0.027**
Bullfrog 2 Log 125	1.419	0.041	1.330	0.077	1.244	0.081	**0.176**	**-0.087**	**1.2429**	**-0.001**
Bullfrog 3 Log 34	1.442	0.039	1.326	0.100	1.195	0.094	**0.267**	**-0.151**	**1.175**	**-0.019**
Little Park 2 Log 12	1.418	0.050	1.346	0.103	1.307	0.111	**0.281**	**-0.210**	**1.1364**	**-0.171**
Huesca DFS successions										
Castelflorite 2 Log 3	1.418	0.353	1.283	0.093	1.296	0.126	**0.001**	**0.134**	**1.4167**	**0.120**
Castelflorite 4 Log 1	1.413	0.040	1.320	0.068	1.265	0.084	**0.210**	**-0.117**	**1.2027**	**-0.062**
Monźon 1 Log 12	1.434	0.031	1.333	0.077	1.252	0.088	**0.283**	**-0.182**	**1.1515**	**-0.101**
Castelflorite 2&3, Log 2	1.460	0.046	1.318	0.078	1.301	0.098	**0.320**	**-0.177**	**1.1404**	**-0.160**
Monźon 4 Log 1	1.433	0.039	1.313	0.079	1.307	0.095	**0.316**	**-0.196**	**1.1167**	**-0.190**
Alcolea 1&2 Log 1	1.431	0.030	1.346	0.072	1.127	0.061	**0.323**	**-0.238**	**1.1084**	**-0.018**

Table 10.4. Comparison of ROM values for synthetic models and recorded system-scale successions of the Huesca and Salt Wash DFS deposits. Table is sorted by ROM of the recorded successions.

Similar ROM values between observed strata and the shuffled models suggest that successions of facies unit thicknesses in all studied sections contain no distinguishable order or pattern. For example, Figure 10.6 (A-B) shows that ROM values for system-scale and floodplain succession are below the red area on the plot indicating that the degree of order in the observed succession is lower than the order of n-times shuffled

A. System-scale successions

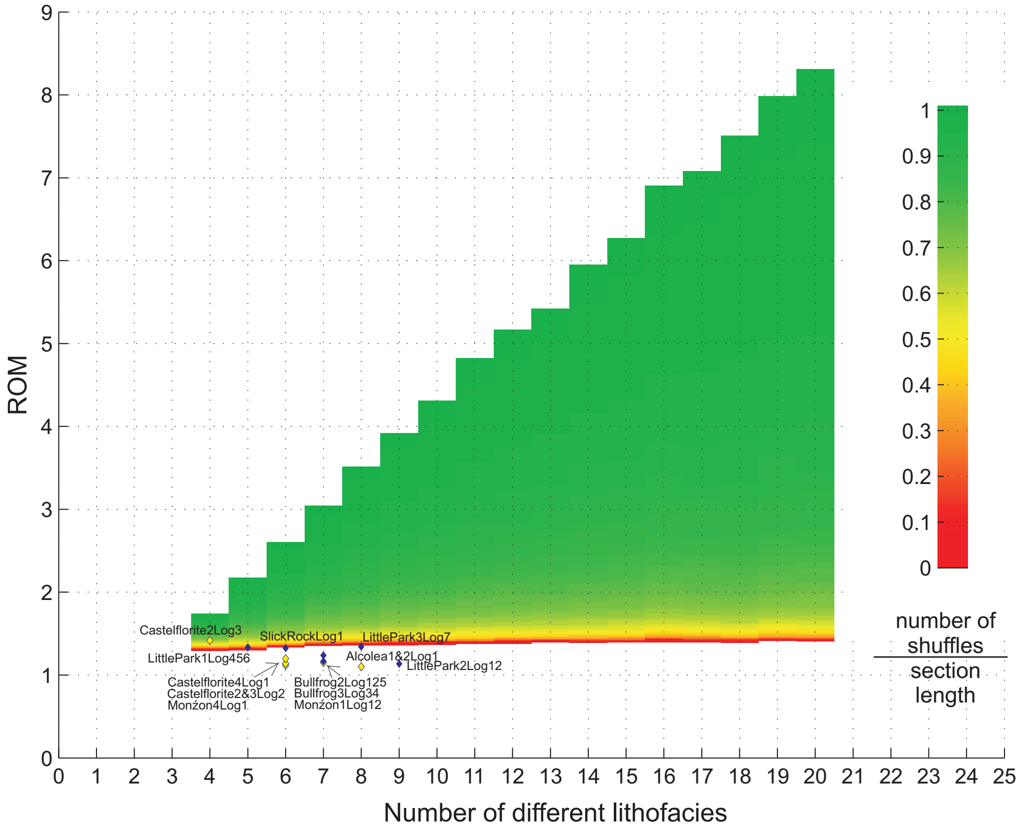

B. Floodplain successions

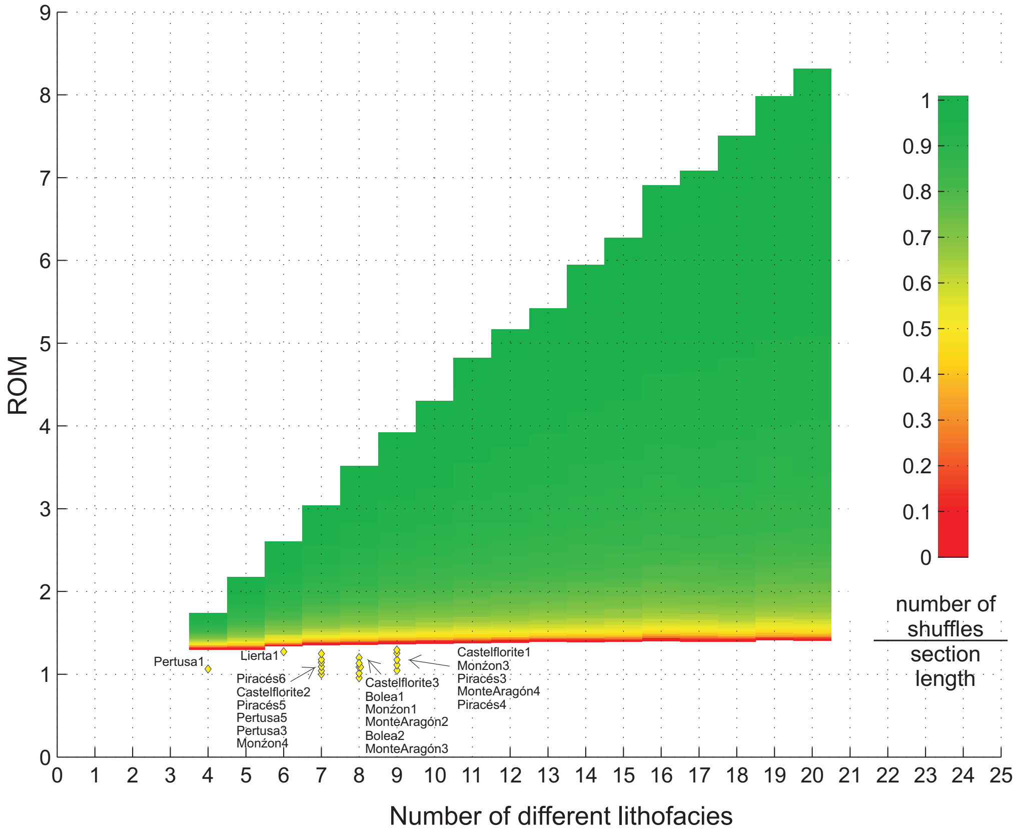

Figure 10.6. Runs order metric values for the ystem-scale succession of the Huesca and Salt Wash DFS successions (A) and floodplain succession of the Huesca DFS succession (B). The coloured background represent variation in ROM values for perfectly ordered cyclical succession with number of shuffles for different number of facies (see Fig 10.3, B).

cyclical succession. The unit thickness successions are therefore indistinguishable from random and can occur by chance. The causes of this pattern are complex succession of events that could not be yet interpreted using current knowledge of depositional processes or the pattern could not be recognised using this method.

10.3.5. Comparison between CTM values of the Huesca floodplain successions and synthetic models

The coarsening trend metric (CTM) was analysed only for the floodplain successions of the Huesca DFS deposits. Calculated values of the CTM range from 0.45 to 0.58 (Table 10.2). Note that to calculate the coarsening metric trend facies numerical codes should be in coarsening order: from 1, the coarsest to *n*, the finest. The CTM values for all floodplain successions are very close to the mean CTM values for all synthetic models (Fig. 10.14-19). The successions, therefore, are not characterised by any coarsening or fining up order because they are close to the mean value for randomly generated and shuffled cyclical successions which are, by definition, not ordered. Moreover, random shuffling does not affect the CTM value for the observed successions as indicated by similar CTM values for the recorded successions and shuffled same-data model. This demonstrates that there is no dominance of either coarsening or finning-upward facies transitions in the floodplain successions.

In the previous Chapter 9 this statistical analysis was referred to to demonstrate that there are no coarsening or thickening-upward trends present in the observed floodplain strata of the Huesca DFS, even though these are commonly qualitatively recognised in avulsion deposits in outcrops and modern examples (Krause and Wells, 1999; Jones and Hajek, 2007; Morozova and Smith, 2000). The CTM and ROM values and their comparison with the synthetic model confirmed that facies and thickness unit successions in the overbank deposits of the Huesca DFS are indistinguishable from random and could occur by chance or in a way that is too complex for resulting patterns to be recognised using method applied here or interpreted using current knowledge of depositional processes and their controls. Thus, interpretation of splay progradation based on the apparent coarsening- and thickening-upward successions in floodplain deposits (Chapter 9) is subjective and should not be made without quantitative analysis.

10.3.6. Comparison of a combination of CTM and MOM values of the observed successions with synthetic models

The coarsening trend metric can be used in combination with the Markov order metric to differentiate cyclical strata from strata that are not cyclical but do show some patterns in facies transitions related to one or more dominant facies. Based on the discussion presented in the previous sections, application of combination of CTM and MOM metrics can be demonstrated for three facies successions with different degree of order.

The CTM and MOM values for a **perfectly ordered coarsening-upward cyclical succession** are close to 0.8 and 1, respectively (Fig. 10.7, A). The mean CTM and MOM values for the shuffled same-data model will be close to the mean values of the CTM and MOM distributions for the shuffled cyclical model and random modes because shuffling would reduce order of the succession considerably. The CTM and MOM values for the observed succession will be much higher than mean CTM and MOM for the three random synthetic models.

The CTM and MOM values for a **randomly generated synthetic succession** are CTM = 0.43 and MOM = 0.49 (Fig. 10.7, B). The distributions of the metric values (CTM and MOM) for all synthetic random models will be close to each other as well as in the previous case. The metric values for the disordered recorded section will be also similar to the mean metric for all synthetic models. Similar results are observed for the Monźon 3 floodplain successions of the Huesca DFS (Fig. 10.7, D).

If the **succession is non-cyclical but has transition patterns related to a dominant facies**, the CTM would be expected to be around 0.5 while MOM values would be relatively higher than ~ 0.6 (Fig. 10.7, C). All CTM distributions for the synthetic models would give similar results. The CTM of the observed data will be the same as mean CTM for all synthetic models. The MOM distribution for shuffled same-data model will be characterised by higher values than the other two models. The MOM value for the observed strata will be similar to the mean MOM for the shuffled same-data model (Fig. 10.7, C).

It is also useful to calculate the coarsening trend metric at different scales within succession to recognise the scale of cycles. That is done by calculating the CTM metric for different thickness intervals (analysis windows) along the succession. The results of this analysis are described in the following section.

10.3.7. Variation in metric values with sample scale (section length)

The importance of stationarity in the observed section was highlighted by Miall (1973) and Willkinson et al. (1997). The statistical properties of facies and thicknesses in a succession could vary with vertical position in the section. Metrics for such non-stationary successions will only give an averaged value when applied across the whole succession, but intervals within the succession may show evidence for greater order. To investigate the presence of order at smaller scales a metric analysis was also conducted with a range of sizes of window that can be moved through the succession

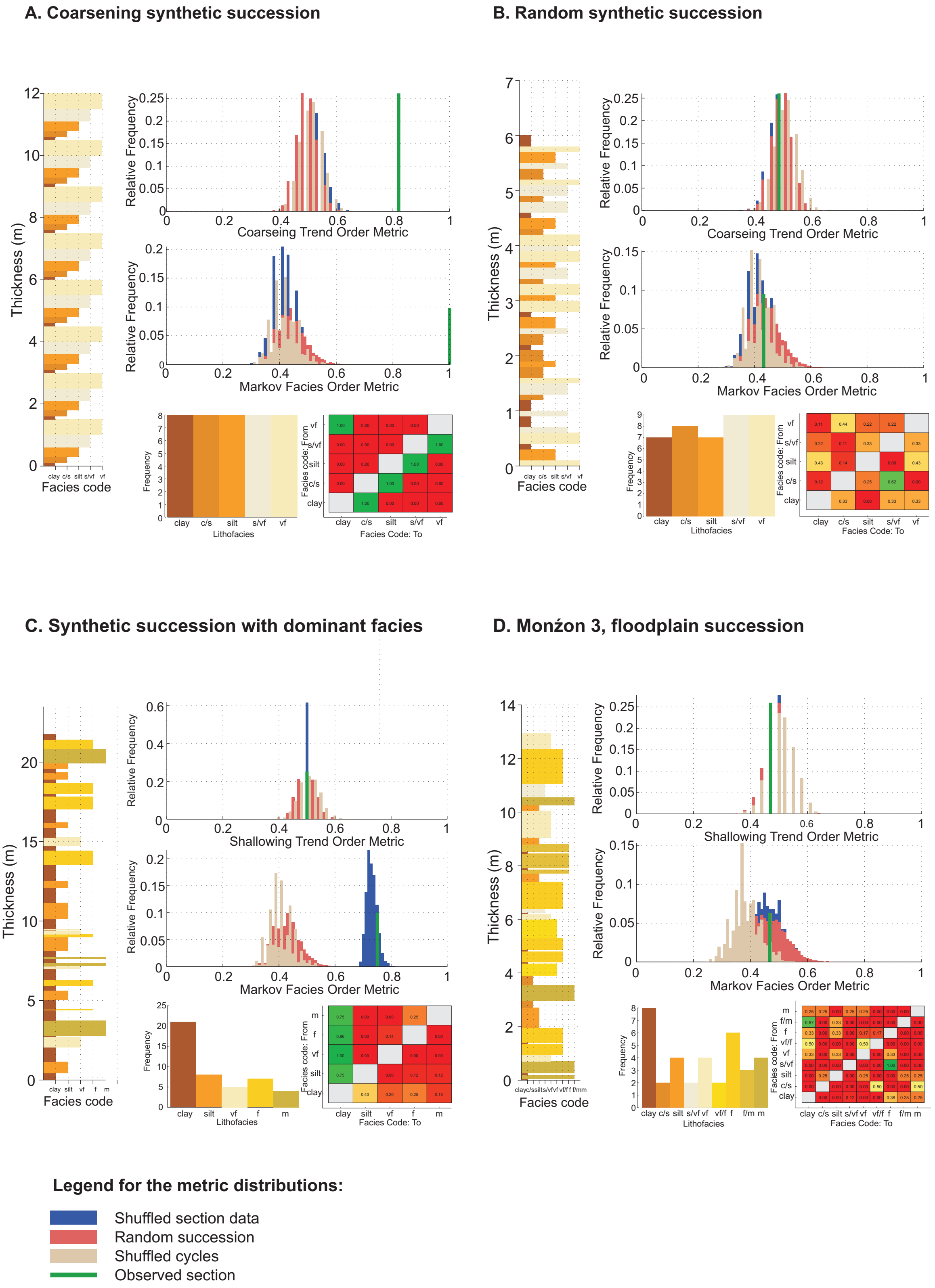

Figure 10.7. Markov order metric and Coarsening upward metric analysis for synthetic coarsening-upward (A), random (B) and dominant facies (C) successions and comparison with floodplain Monźon 3 succession (D). See explanation in the text.

to calculate statistical properties over a limited vertical range at different points in the succession (Wilkinson et al., 1997).

Minimum window size is chosen equal to 10 facies units. The window was then moved up the section and a metric value (MOM, ROM and CTM) calculated for each point. The window size was then increased by 1 and the process repeated (Burgess, in prep). Resulting metric maps are presented in the Figures 10.8-13, B for the system-scale successions and Figures 10.14-19, B for the floodplain successions.

Diagram explanation, part 3 (for Figures 10.8-19, B)

The metric value for the whole succession is shown in the right corner of the triangle map in the Fig. 10.8-19 (B). On the left side of the triangle a metric value for each 10-unit window is plotted. The window size progressively increases from left to right across the triangle. The green to red colour scale shows high to low metric values, respectively, green indicating order and red disorder. Markov and coarsening trend order metrics have the same colour scale from 0 to 1, while runs order metric varies from 1 to 2.5.

Variations in MOM with scale

The variations in MOM values are related to change in the number and types of facies with the section length (window size). System-scale successions, for example, show lower MOM values at small scales indicating less order, because for shorter sections dominance of Hsh or St facies is less pronounced, making the facies distribution more diverse, and reducing apparent order and MOM values (e.g. Alcolea 1&2 Log 1 and Bullfrog 2 Log 125; Fig. 10.8 and 10.10, B).

Markov order metric maps for floodplain successions sometimes show different values for different parts of the succession. For example, the Monźon 4 succession is more ordered in its upper part (between 5 and 7 m) where dominant *clay* facies are repeatedly interbedded with other facies (Fig. 10.14). Conversely, the strata between 7 and 9 m marks are characterised by more variable facies indicated by lower MOM values.

Markov order metric variability appears to be greatest at the smallest scale (10 units) (Fig. 10.8-13) but this may be an artefact because MOM values at window size below 20 units are affected by the section length (Section 10.2.1, Fig. 10.2). For example, in short successions that consist of fewer beds and contain smaller number of facies, some facies could occur only once, leading to anomalously high or low TP matrix values and non-representative MOM values. Thus, variations in MOM values at scales smaller than 20 beds should be interpreted with caution or minimum window size should be chosen equal or higher than 20 units. Perhaps, the length of the section, which degree of order is investigated, should also correspond to the scale and purpose of the study.

Variations in ROM with scale

Runs order metric values do not vary with window size in all studied successions (Fig. 10.8-13 and 10.14-19, B). The ROM triangular maps together with comparative analysis of ROM values for synthetic models indicate that thickness successions truly do not show any evidence for order on the scale of measurement (at all different window sizes).

Variations in CTM with scale

In contrast to the MOM, the CTM is not affected by section length and can record coarsening trends in successions of any length (Wilkinson et al., 1997, Section 10.2.1). Therefore, variations in CTM values with window size for the floodplain succession do reflect real small-scale trends in the strata. Divergence of the CTM value from 0.5 is determined by the number and length of coarsening-upward intervals in a succession.

For example, the CTM map for the Monte Aragón 2 floodplain succession is characterised by the highest CTM = 0.58 (Table 10.3), and dominated by coarsening-up transitions in the upper part of the succession (from 4 to 10 m mark) and highly variable CTM values in its lower part (Fig. 10.18, B). Qualitative interpretation of the upper part of the succession log also suggests the presence of two coarsening-up 4-5 unit long sections that lead to higher CTM values in this part of the succession.

Although sporadic coarsening- and fining-up sections 3-5 beds long are visually observed in a few other successions, floodplain strata in general show more or less similar values of CTM at all scales, suggesting that the strata are stationary, while the small trends could have occurred by chance. Stratigraphic order in the form of “repeated patterns of lithologic variation” (Willkinson et al., 1997) is not present. This result again provides quantitative evidence to support interpreted absence of coarsening-upward trends and “cyclicity” in floodplain avulsion deposits of the Huesca DFS discussed in the Chapter 9.

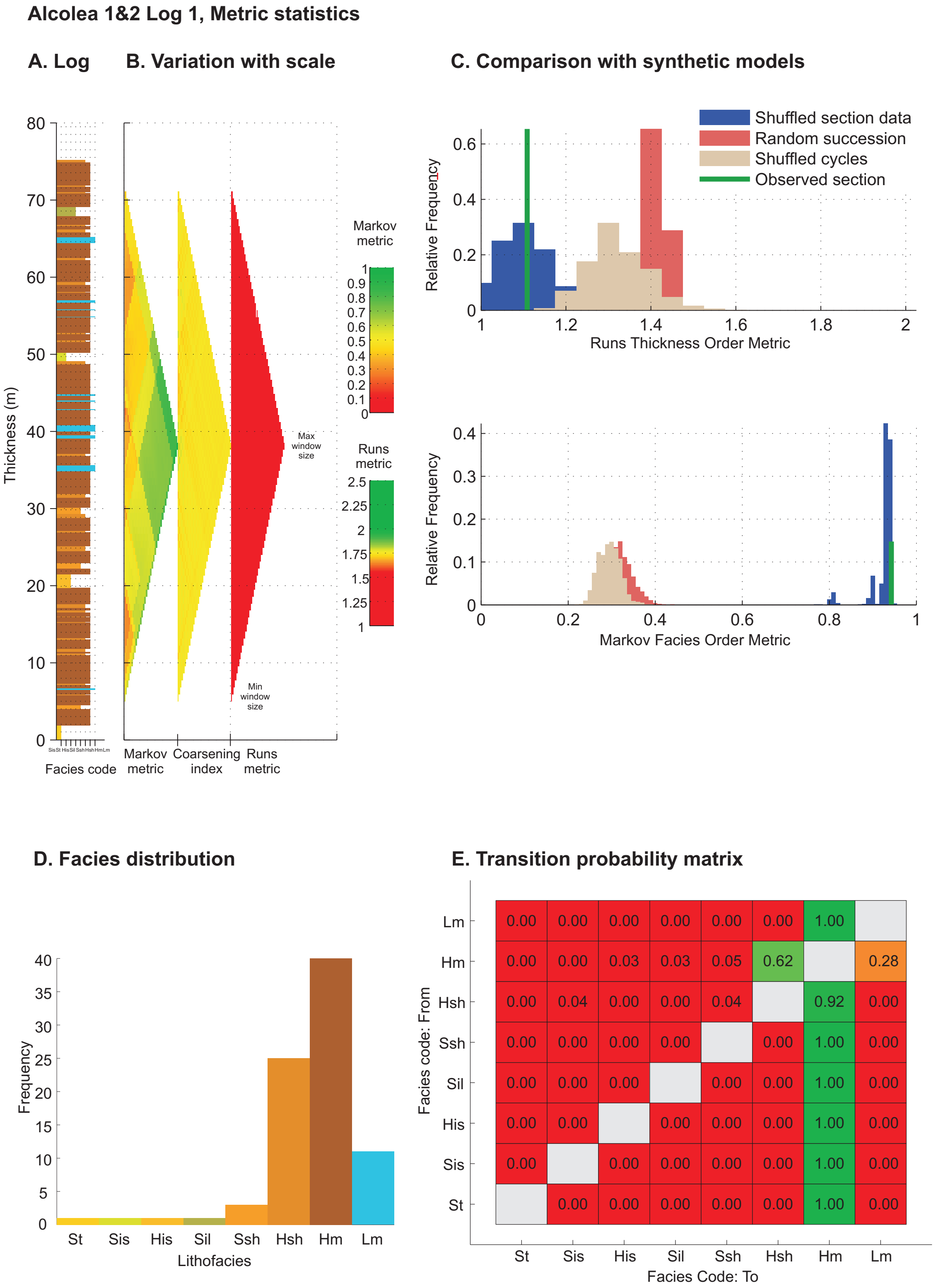

Alcolea 1&2 Log 1, Metric statistics

A. Log

B. Variation with scale

C. Comparison with synthetic models

D. Facies distribution

E. Transition probability matrix

Facies code: From	St	Sis	His	Sil	Ssh	Hsh	Hm	Lm
Lm	0.00	0.00	0.00	0.00	0.00	0.00	1.00	
Hm	0.00	0.00	0.03	0.03	0.05	0.62		0.28
Hsh	0.00	0.04	0.00	0.00	0.04		0.92	0.00
Ssh	0.00	0.00	0.00	0.00		0.00	1.00	0.00
Sil	0.00	0.00	0.00		0.00	0.00	1.00	0.00
His	0.00	0.00		0.00	0.00	0.00	1.00	0.00
Sis	0.00		0.00	0.00	0.00	0.00	1.00	0.00
St		0.00	0.00	0.00	0.00	0.00	1.00	0.00

Figure 10.8. The results of metric analysis for the Alcolea 1&2 Log 1 system-scale succession, Huesca DFS.

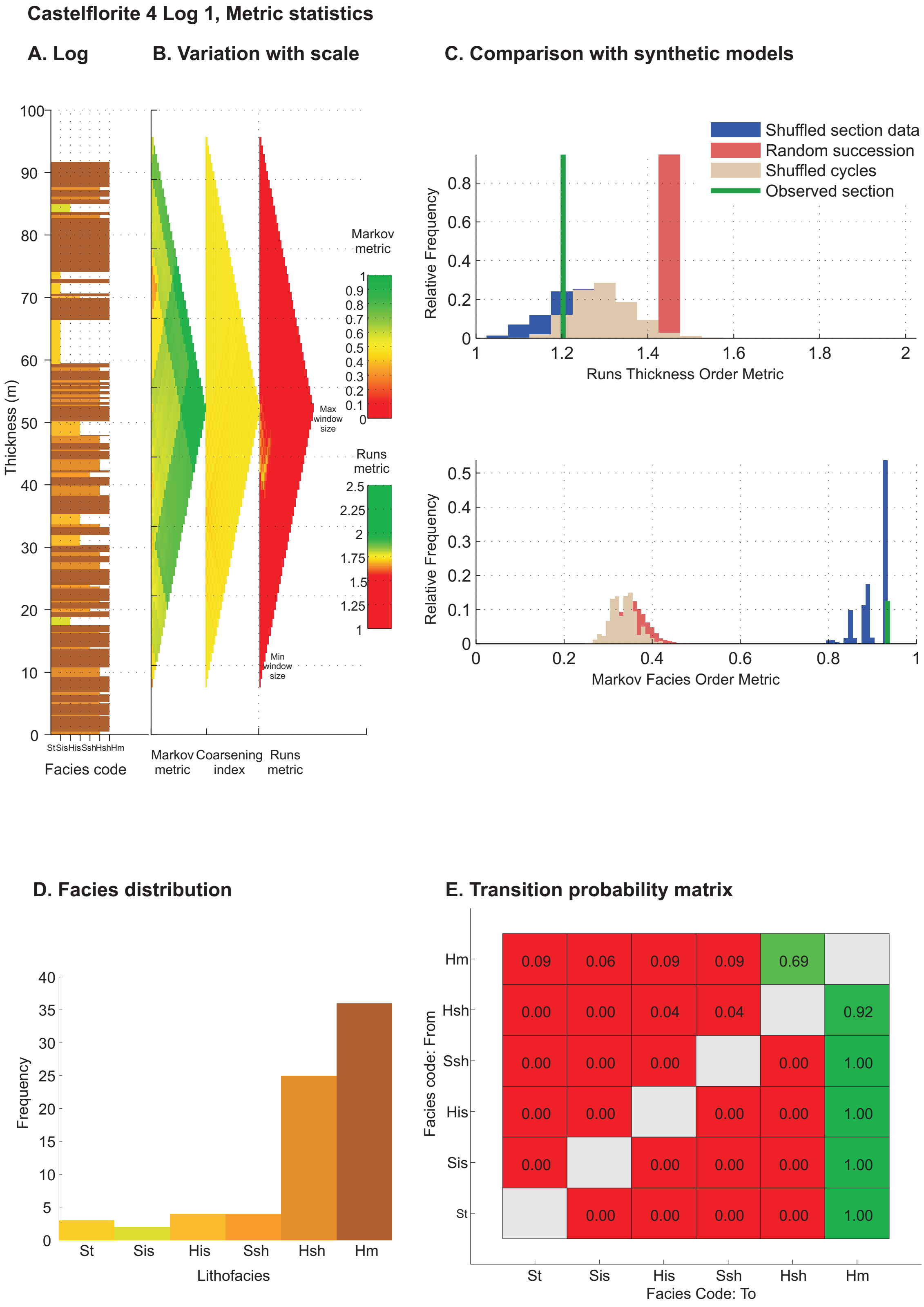

Facies code: From	St	Sis	His	Ssh	Hsh	Hm
Hm	0.09	0.06	0.09	0.09	0.69	
Hsh	0.00	0.00	0.04	0.04		0.92
Ssh	0.00	0.00	0.00		0.00	1.00
His	0.00	0.00		0.00	0.00	1.00
Sis	0.00		0.00	0.00	0.00	1.00
St		0.00	0.00	0.00	0.00	1.00

Figure 10.9. The results of metric analysis for the Castellforite 4 Log1 system-scale succession, Huesca DFS.

Bullfrog 2 Log 125, Metric statistics

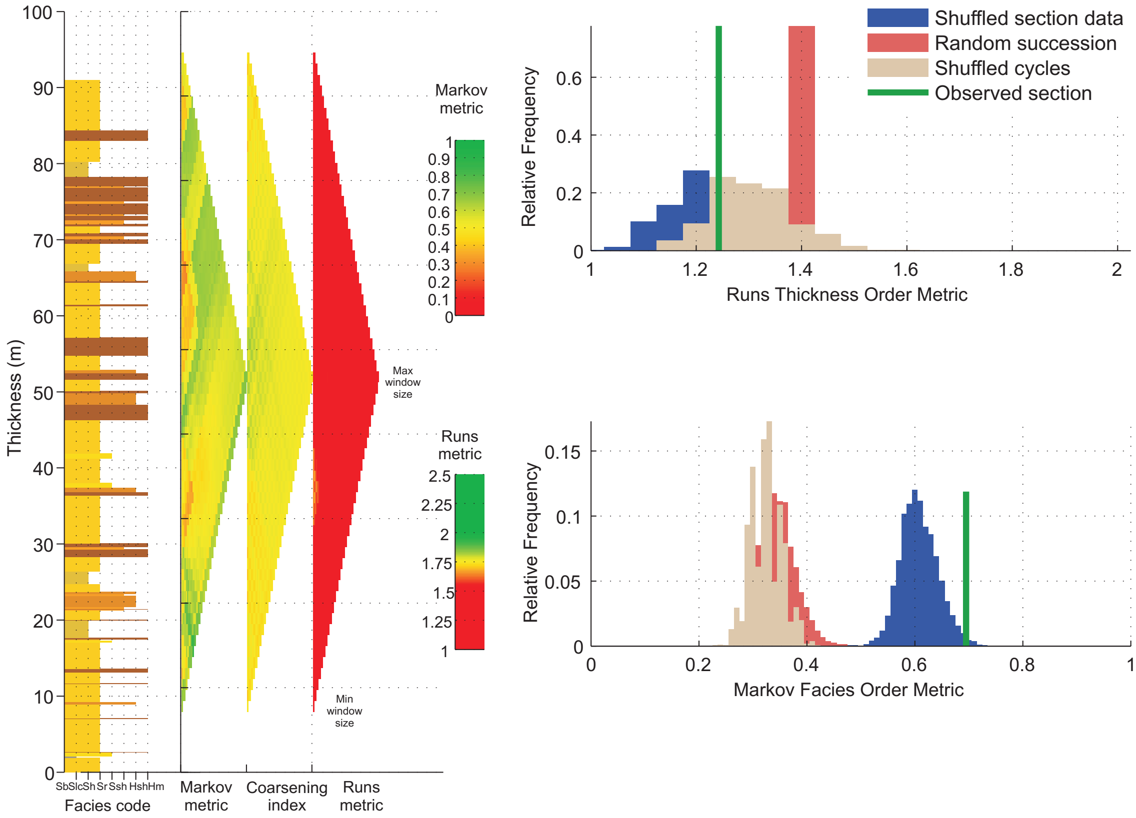

A. Log **B. Variation with scale** **C. Comparison with synthetic models**

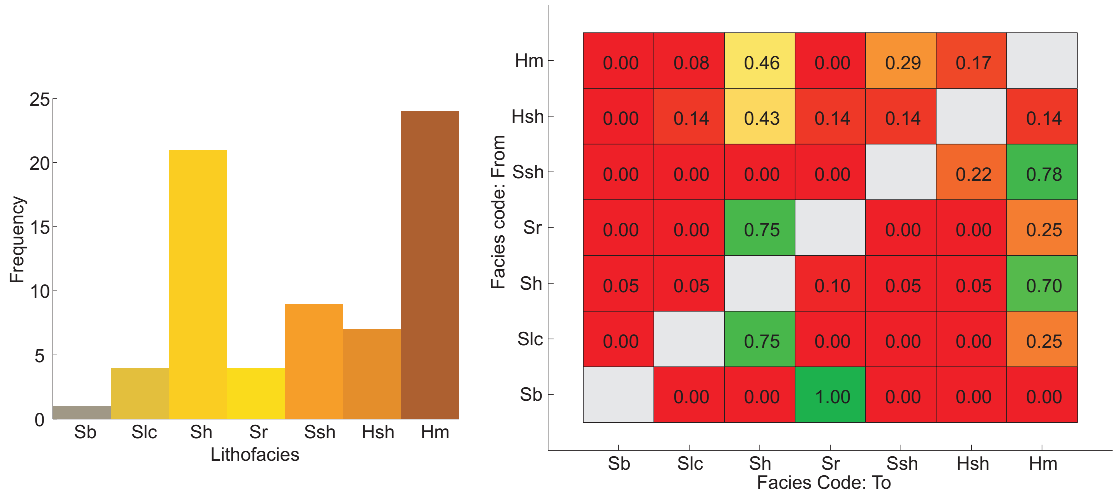

D. Facies distribution **E. Transition probability matrix**

Facies code: From \ To	Sb	Slc	Sh	Sr	Ssh	Hsh	Hm
Hm	0.00	0.08	0.46	0.00	0.29	0.17	
Hsh	0.00	0.14	0.43	0.14	0.14		0.14
Ssh	0.00	0.00	0.00	0.00		0.22	0.78
Sr	0.00	0.00	0.75		0.00	0.00	0.25
Sh	0.05	0.05		0.10	0.05	0.05	0.70
Slc	0.00		0.75	0.00	0.00	0.00	0.25
Sb		0.00	0.00	1.00	0.00	0.00	0.00

Figure 10.10. The results of metric analysis for the Bullfrog 2 Log 125 system-scale succession, Salt Wash DFS.

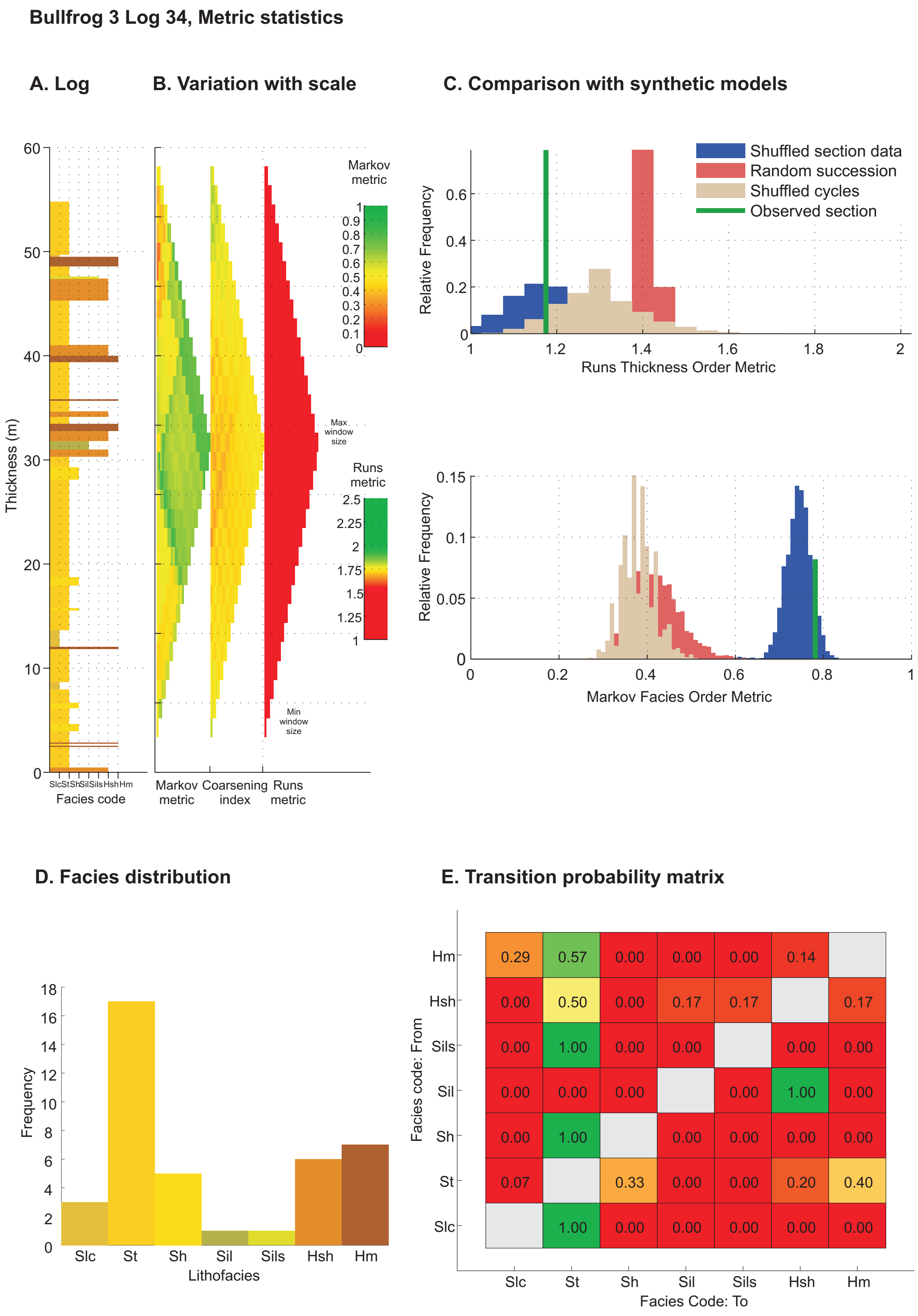

Facies code: From	Slc	St	Sh	Sil	Sils	Hsh	Hm
Hm	0.29	0.57	0.00	0.00	0.00	0.14	
Hsh	0.00	0.50	0.00	0.17	0.17		0.17
Sils	0.00	1.00	0.00	0.00		0.00	0.00
Sil	0.00	0.00	0.00		0.00	1.00	0.00
Sh	0.00	1.00		0.00	0.00	0.00	0.00
St	0.07		0.33	0.00	0.00	0.20	0.40
Slc		1.00	0.00	0.00	0.00	0.00	0.00

Figure 10.11. The results of metric analysis for the Bullfrog 2 Log 34 system-scale succession, Salt Wash DFS.

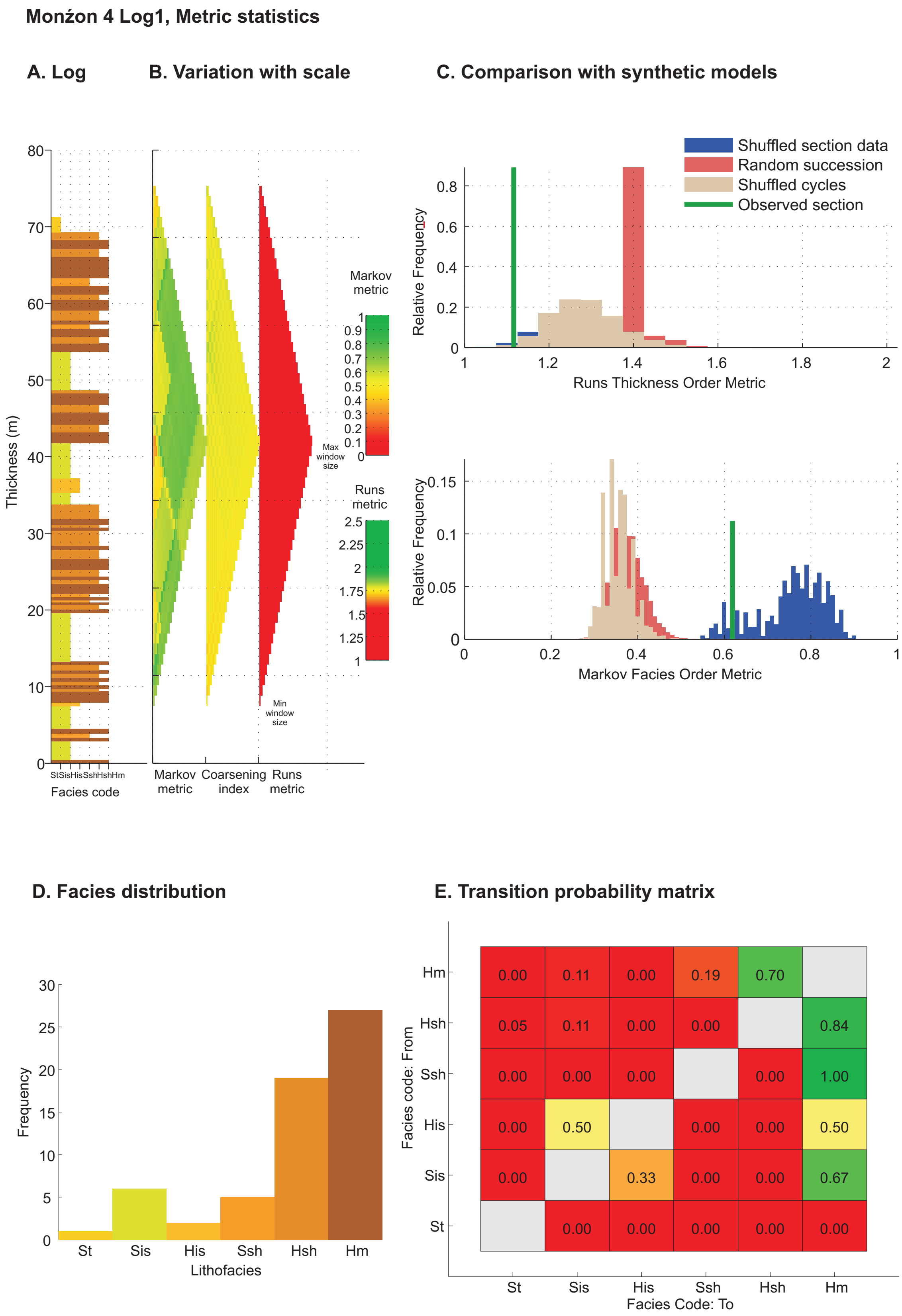

Facies code: From \ To	St	Sis	His	Ssh	Hsh	Hm
Hm	0.00	0.11	0.00	0.19	0.70	
Hsh	0.05	0.11	0.00	0.00		0.84
Ssh	0.00	0.00	0.00		0.00	1.00
His	0.00	0.50		0.00	0.00	0.50
Sis	0.00		0.33	0.00	0.00	0.67
St		0.00	0.00	0.00	0.00	0.00

Figure 10.12. The results of metric analysis for the Monźon 4 Log 1 system-scale succession, Huesca DFS.

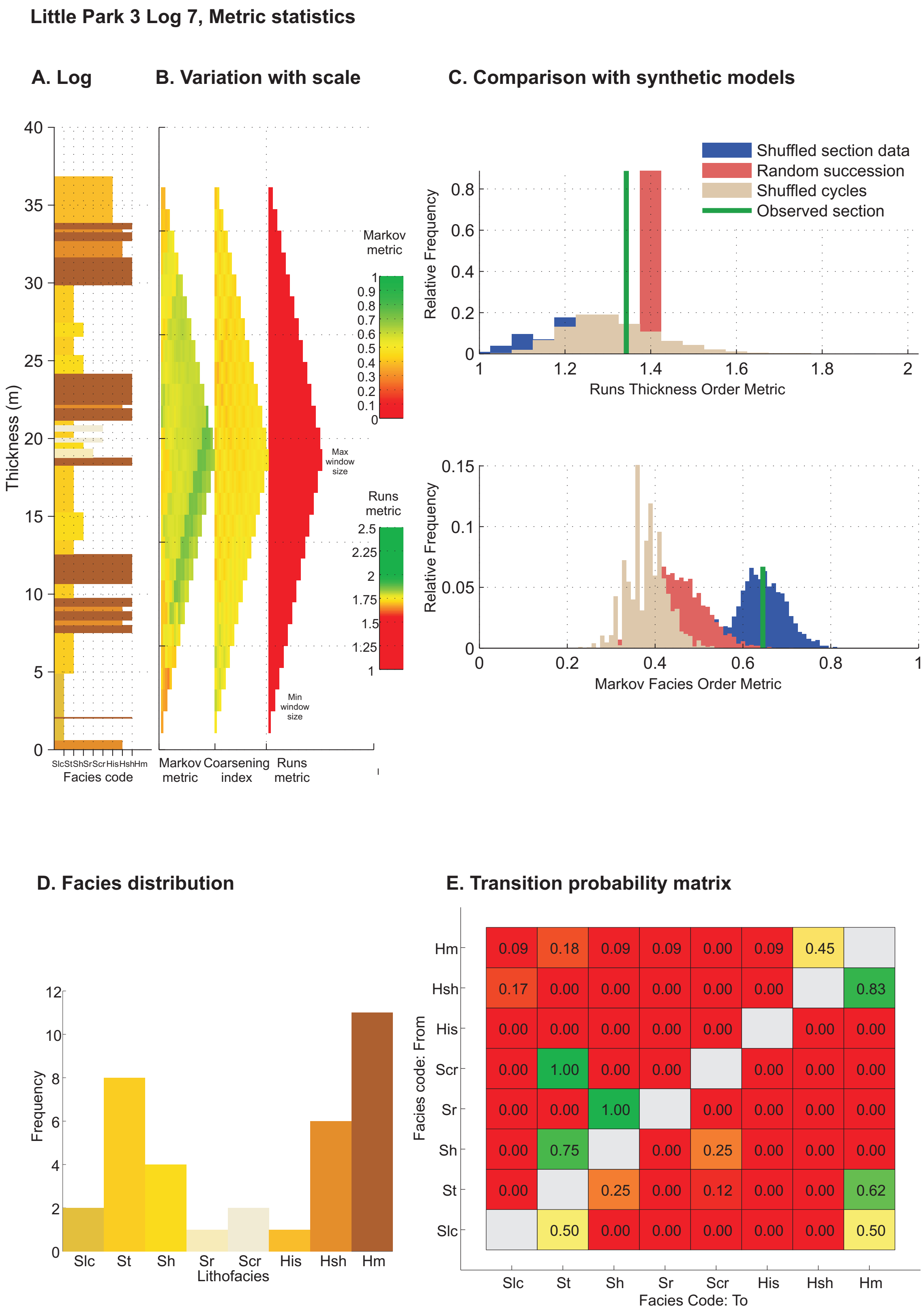

	Slc	St	Sh	Sr	Scr	His	Hsh	Hm
Hm	0.09	0.18	0.09	0.09	0.00	0.09	0.45	
Hsh	0.17	0.00	0.00	0.00	0.00	0.00		0.83
His	0.00	0.00	0.00	0.00	0.00		0.00	0.00
Scr	0.00	1.00	0.00	0.00		0.00	0.00	0.00
Sr	0.00	0.00	1.00		0.00	0.00	0.00	0.00
Sh	0.00	0.75		0.00	0.25	0.00	0.00	0.00
St	0.00		0.25	0.00	0.12	0.00	0.00	0.62
Slc		0.50	0.00	0.00	0.00	0.00	0.00	0.50

Figure 10.13. The results of metric analysis for the Little Park 3 Log7 system-scale succession, Salt Wash DFS. For the results from the other system-scale successions see Appendix 6.

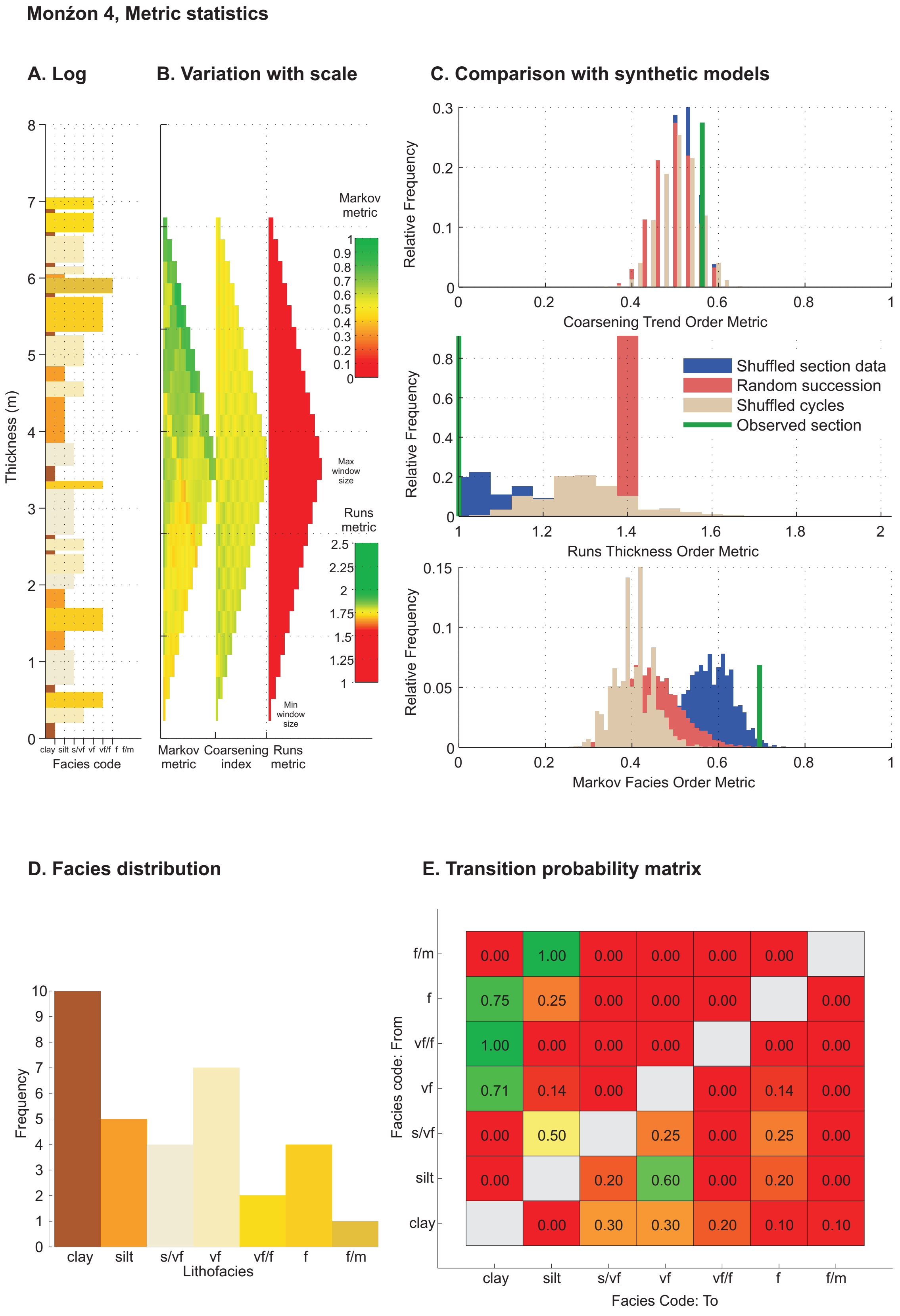

Facies code: From	clay	silt	s/vf	vf	vf/f	f	f/m
f/m	0.00	1.00	0.00	0.00	0.00	0.00	
f	0.75	0.25	0.00	0.00	0.00		0.00
vf/f	1.00	0.00	0.00	0.00		0.00	0.00
vf	0.71	0.14	0.00		0.00	0.14	0.00
s/vf	0.00	0.50		0.25	0.00	0.25	0.00
silt	0.00		0.20	0.60	0.00	0.20	0.00
clay		0.00	0.30	0.30	0.20	0.10	0.10

Figure 10.14. The results of metric analysis for the Monźon 4 floodplain succession, Huesca DFS.

Monte Aragón 4, Metric statistics

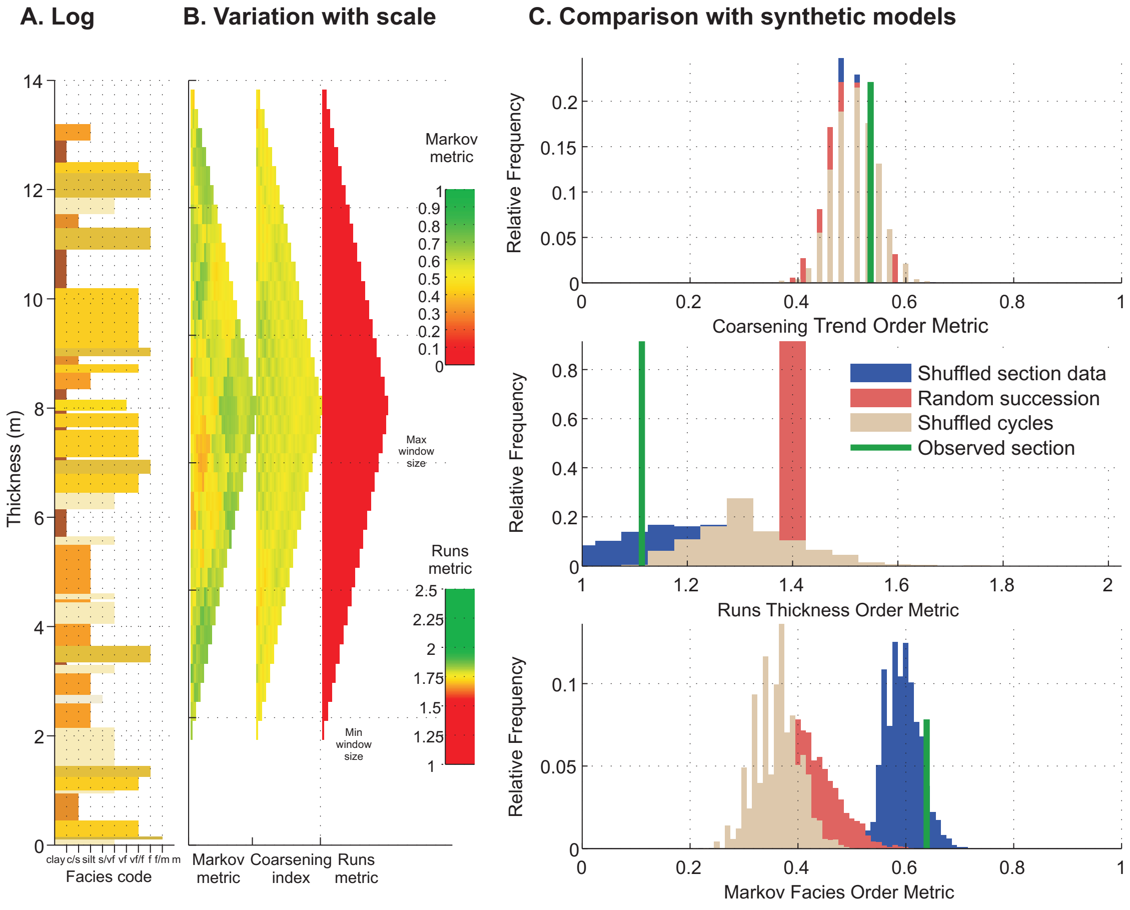
A. Log

B. Variation with scale

C. Comparison with synthetic models

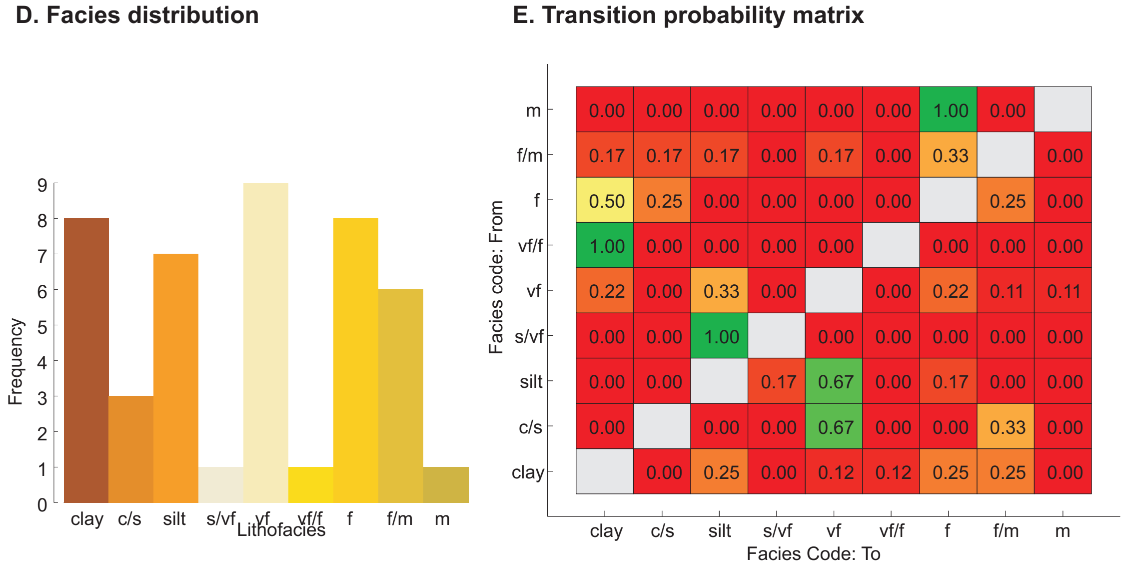
D. Facies distribution

E. Transition probability matrix

Facies code: From \ Facies Code: To	clay	c/s	silt	s/vf	vf	vf/f	f	f/m	m
m	0.00	0.00	0.00	0.00	0.00	0.00	1.00	0.00	
f/m	0.17	0.17	0.17	0.00	0.17	0.00	0.33		0.00
f	0.50	0.25	0.00	0.00	0.00	0.00		0.25	0.00
vf/f	1.00	0.00	0.00	0.00	0.00		0.00	0.00	0.00
vf	0.22	0.00	0.33	0.00		0.00	0.22	0.11	0.11
s/vf	0.00	0.00	1.00		0.00	0.00	0.00	0.00	0.00
silt	0.00	0.00		0.17	0.67	0.00	0.17	0.00	0.00
c/s	0.00		0.00	0.00	0.67	0.00	0.00	0.33	0.00
clay		0.00	0.25	0.00	0.12	0.12	0.25	0.25	0.00

Figure 10.15. The results of metric analysis for the Monte Aragón 4 floodplain succession, Huesca DFS.

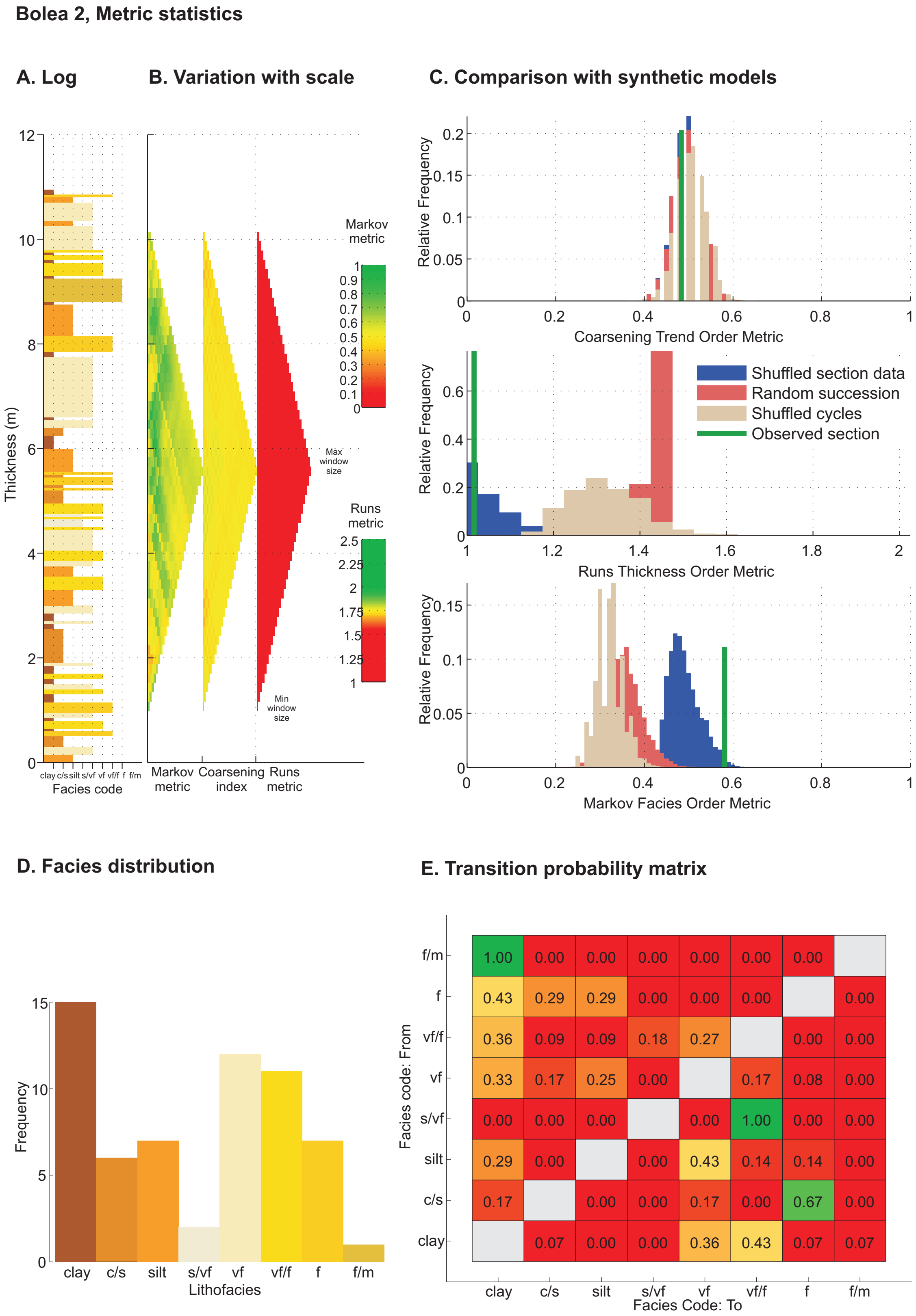

	clay	c/s	silt	s/vf	vf	vf/f	f	f/m
f/m	1.00	0.00	0.00	0.00	0.00	0.00	0.00	
f	0.43	0.29	0.29	0.00	0.00	0.00		0.00
vf/f	0.36	0.09	0.09	0.18	0.27		0.00	0.00
vf	0.33	0.17	0.25	0.00		0.17	0.08	0.00
s/vf	0.00	0.00	0.00		0.00	1.00	0.00	0.00
silt	0.29	0.00		0.00	0.43	0.14	0.14	0.00
c/s	0.17		0.00	0.00	0.17	0.00	0.67	0.00
clay		0.07	0.00	0.00	0.36	0.43	0.07	0.07

Figure 10.16. The results of metric analysis for the Bolea 2 floodplain succession, Huesca DFS.

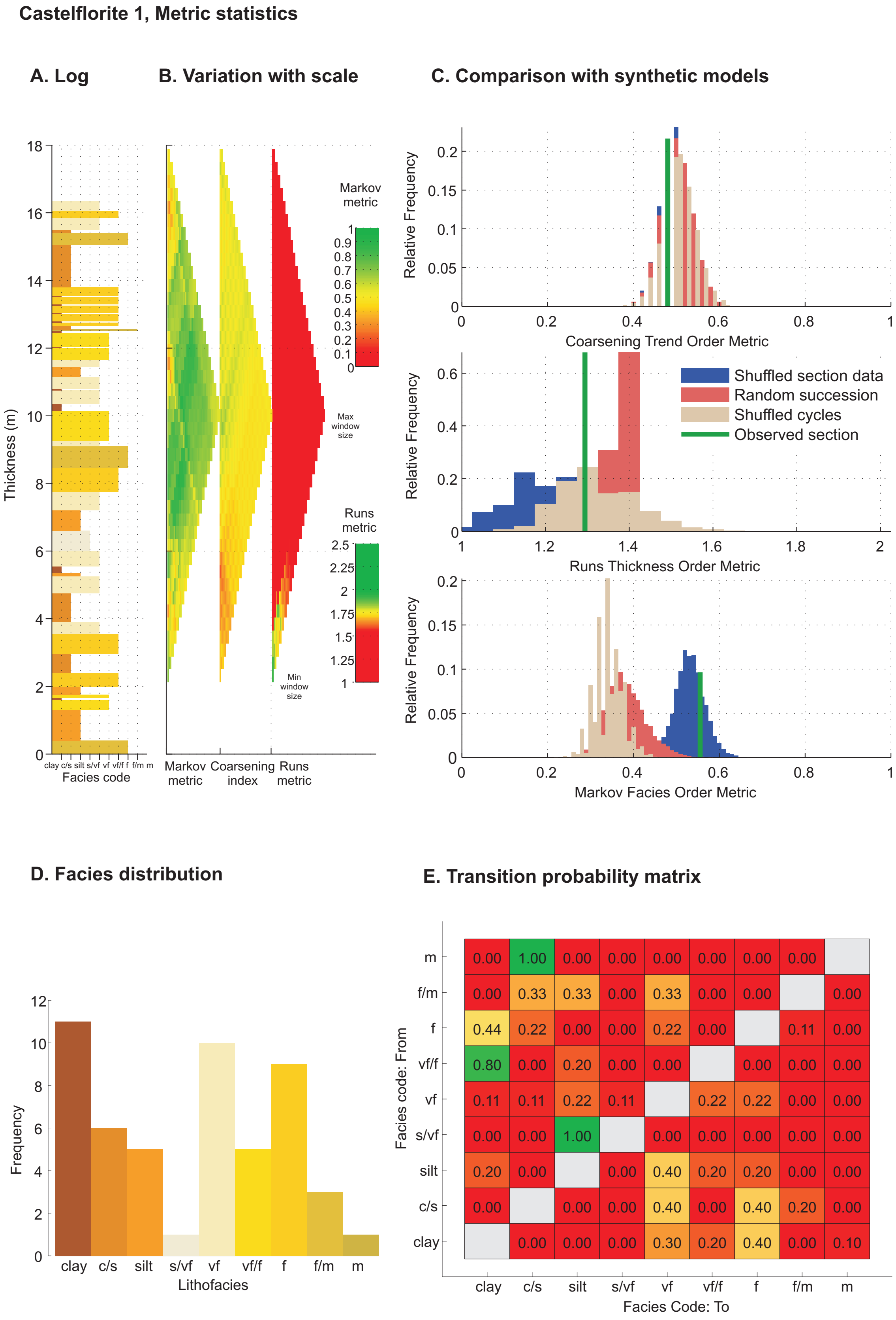

	clay	c/s	silt	s/vf	vf	vf/f	f	f/m	m
m	0.00	1.00	0.00	0.00	0.00	0.00	0.00	0.00	
f/m	0.00	0.33	0.33	0.00	0.33	0.00	0.00		0.00
f	0.44	0.22	0.00	0.00	0.22	0.00		0.11	0.00
vf/f	0.80	0.00	0.20	0.00	0.00		0.00	0.00	0.00
vf	0.11	0.11	0.22	0.11		0.22	0.22	0.00	0.00
s/vf	0.00	0.00	1.00		0.00	0.00	0.00	0.00	0.00
silt	0.20	0.00		0.00	0.40	0.20	0.20	0.00	0.00
c/s	0.00		0.00	0.00	0.40	0.00	0.40	0.20	0.00
clay		0.00	0.00	0.00	0.30	0.20	0.40	0.00	0.10

Figure 10.17. The results of metric analysis for the Castelflorite 1 floodplain succession, Huesca DFS.

Monte Aragón 2, Metric statistics

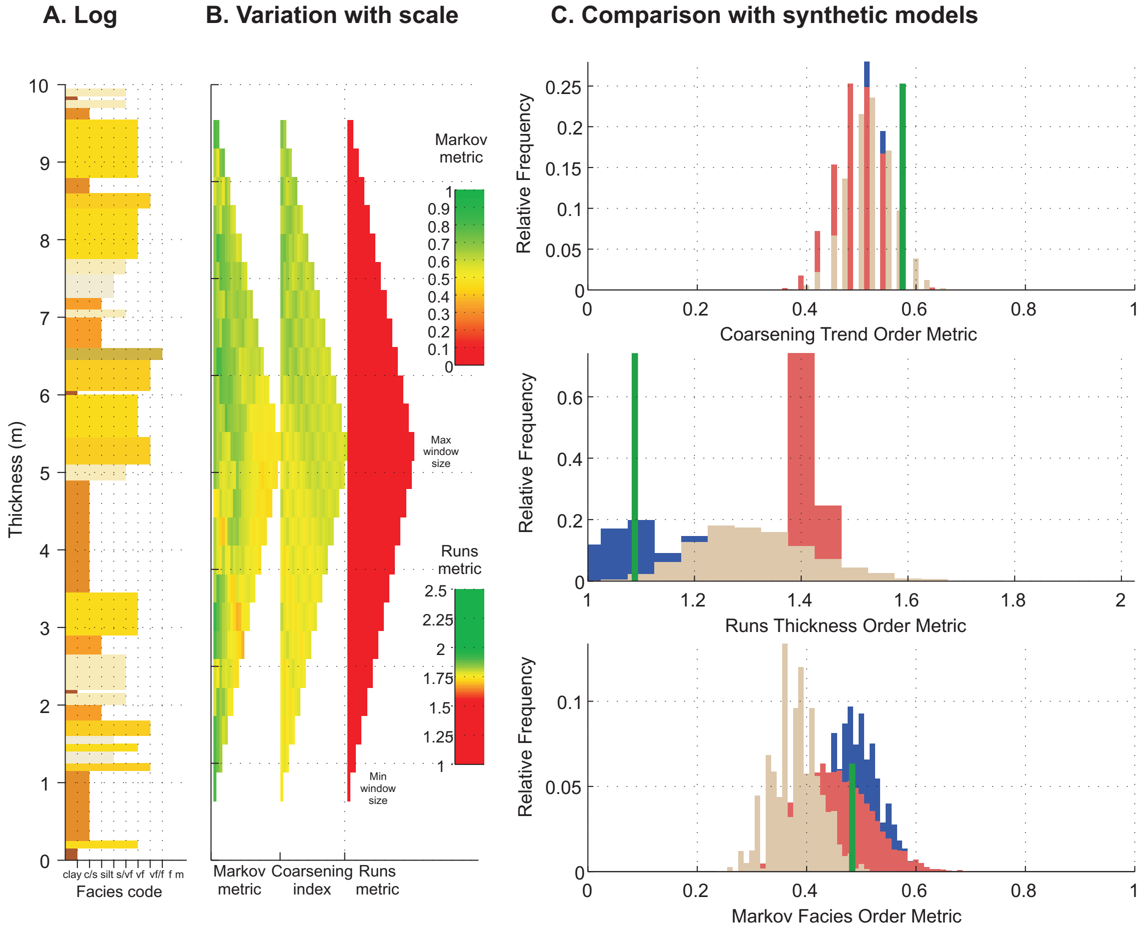
A. Log

B. Variation with scale

C. Comparison with synthetic models

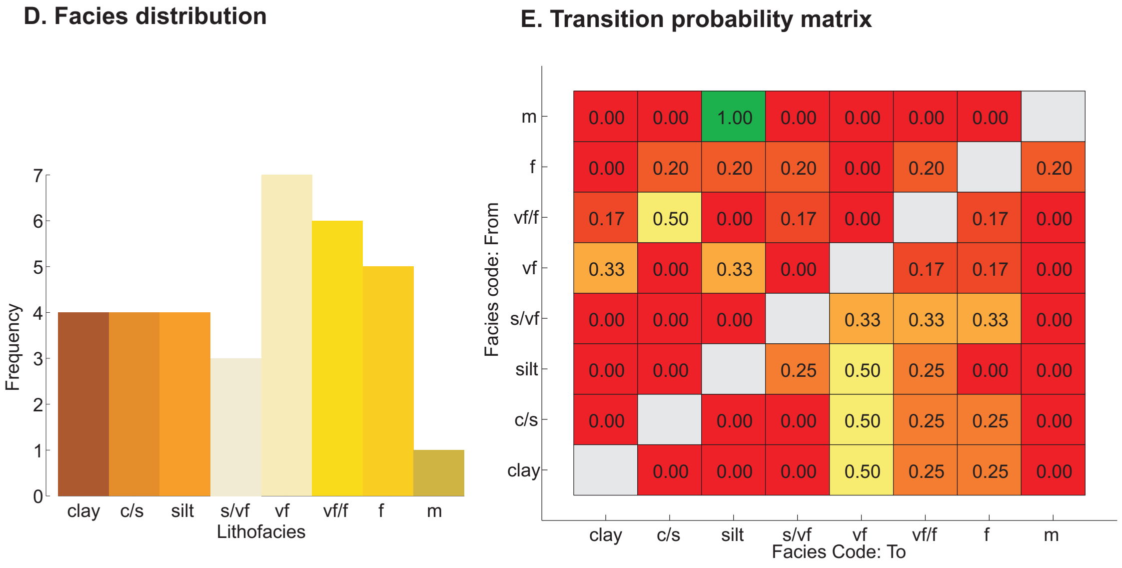
D. Facies distribution

E. Transition probability matrix

	clay	c/s	silt	s/vf	vf	vf/f	f	m
m	0.00	0.00	1.00	0.00	0.00	0.00	0.00	
f	0.00	0.20	0.20	0.20	0.00	0.20		0.20
vf/f	0.17	0.50	0.00	0.17	0.00		0.17	0.00
vf	0.33	0.00	0.33	0.00		0.17	0.17	0.00
s/vf	0.00	0.00	0.00		0.33	0.33	0.33	0.00
silt	0.00	0.00		0.25	0.50	0.25	0.00	0.00
c/s	0.00		0.00	0.00	0.50	0.25	0.25	0.00
clay		0.00	0.00	0.00	0.50	0.25	0.25	0.00

Figure 10.18. The results of metric analysis for the Monte Aragón 2 floodplain succession, Huesca DFS.

Monźon 3, Metric statistics

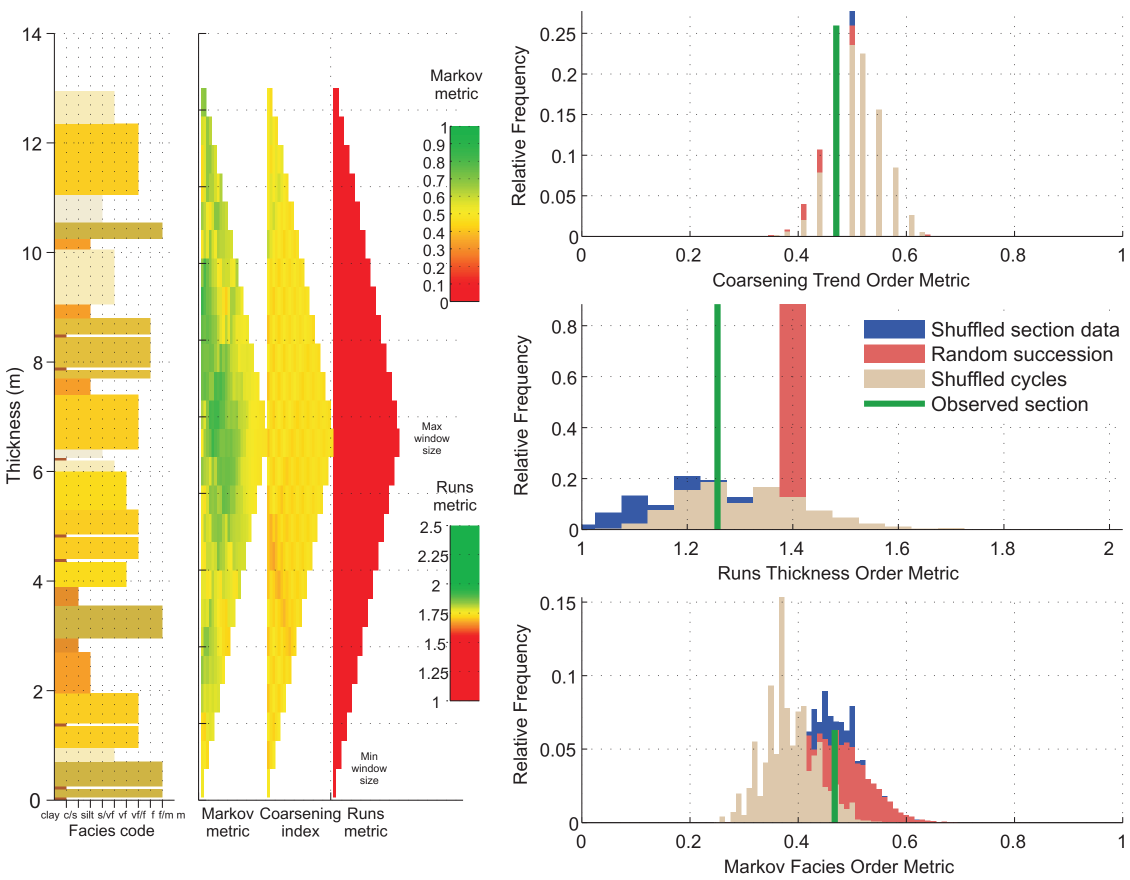

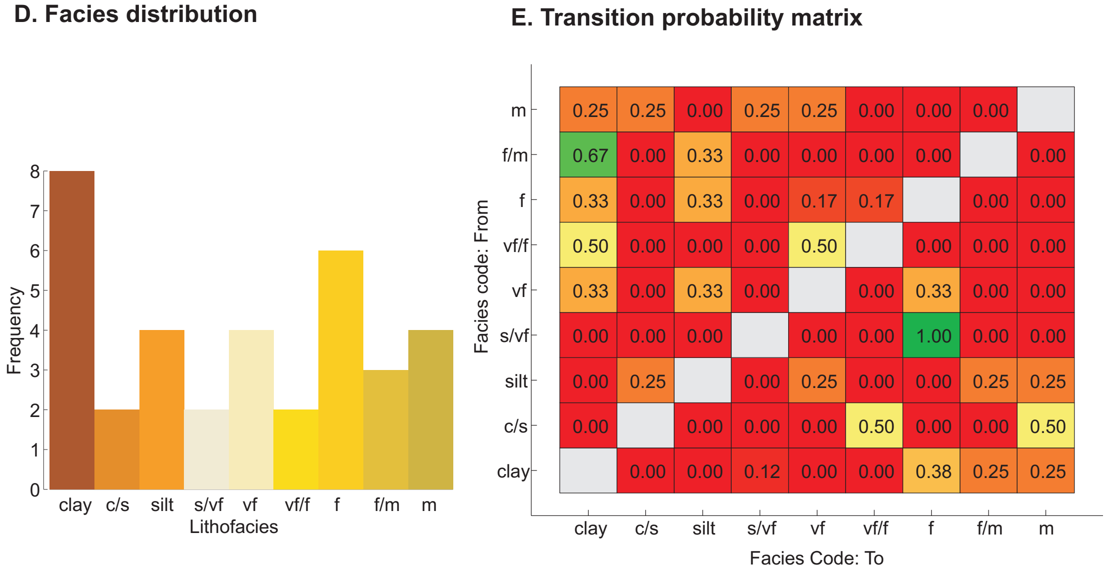

	clay	c/s	silt	s/vf	vf	vf/f	f	f/m	m
m	0.25	0.25	0.00	0.25	0.25	0.00	0.00	0.00	
f/m	0.67	0.00	0.33	0.00	0.00	0.00	0.00		0.00
f	0.33	0.00	0.33	0.00	0.17	0.17		0.00	0.00
vf/f	0.50	0.00	0.00	0.00	0.50		0.00	0.00	0.00
vf	0.33	0.00	0.33	0.00		0.00	0.33	0.00	0.00
s/vf	0.00	0.00	0.00		0.00	0.00	1.00	0.00	0.00
silt	0.00	0.25		0.00	0.25	0.00	0.00	0.25	0.25
c/s	0.00		0.00	0.00	0.00	0.50	0.00	0.00	0.50
clay		0.00	0.00	0.12	0.00	0.00	0.38	0.25	0.25

Figure 10.19. The results of metric analysis for the Monźon 3 floodplain succession, Huesca DFS. For the results from the other floodplain successions see Appendix 6.

10.3.8. Comparison of test of significance with the method used in this research

Another commonly used method for testing for order using Markov statistics compares transition frequencies for an observed succession with a theoretical transition probability matrix that represents a perfectly random succession. The significance of the match between the two is calculated using a χ^2 test (Davis, 1968). In this research similar principles are used to calculate the Markov order metric. The MOM is then compared with the distribution of MOM values calculated for many realizations of random and shuffled synthetic models (Fig. 10.1). The statistical method used here is different from previous methods because it uses many thousands of realizations of three different disordered "random" models for comparison against a single summary statistic (the MOM) from the observed data. The method is both numeric and graphical, and allows more complex distinctions of order styles to be made than simply rejecting or proving a hypothesis about the degree of order using one simple random model.

10.4. Facies transitions and relationships within the DFS successions

The metric analysis for system-scale successions of the Huesca and Salt Wash DFSs reveals a strong relationship between the Markov order metric and the character of the facies distribution in the successions. A TP matrix combined with a facies frequency distribution can be used to create diagrams of facies transitions (Fig. 10.20-21, see also Mail, 1973). The transition diagrams, when used in addition to facies and metric analysis, in turn can help to understand facies relationships and successions of depositional events during development of the Huesca and Salt Wash DFSs in more detail.

10.4.1. The Huesca DFS succession

The facies successions of the Huesca DFS deposits are found to be dominated by floodplain facies Hm and Hsh. The probability of facies transition into one of these facies is high. Transitions from Hm to Hsh and from Hsh to Hm are also characterised by high probability (e.g. 0.62 - 0.92 in the Alcolea 1&2 Log 1 and Castelflorite 4 Log1 successions, Fig. 10.8-9). The facies transition diagrams for these successions have a characteristic shape where Hm and Hsh dominant facies are in the middle and other rare facies all tend to pass into them (Fig. 10.20).

The Hsh facies was formed relatively close to the channel where high-energy unconfined flows transported coarser sediment out of the channel on the floodplain (Chapter 4). Further from the channel the flow had less energy and transported mainly finer-grained suspended load which formed facies Hm. The frequent alternation /

transition between these two facies in the succession (Fig. 10.20) corresponds to repeated flooding events and migration of the channel on the floodplain.

Other floodplain facies such as Sils (channel scours on a splay) and channel fill facies Sil (sandstone lenses formed in confined channels) have very high probability of transition to facies Hm (Fig. 10.20) due to their rare occurrence in the Huesca DFS successions. The facies Sil and Sils are commonly enclosed by finer-grained floodplain Hm facies.

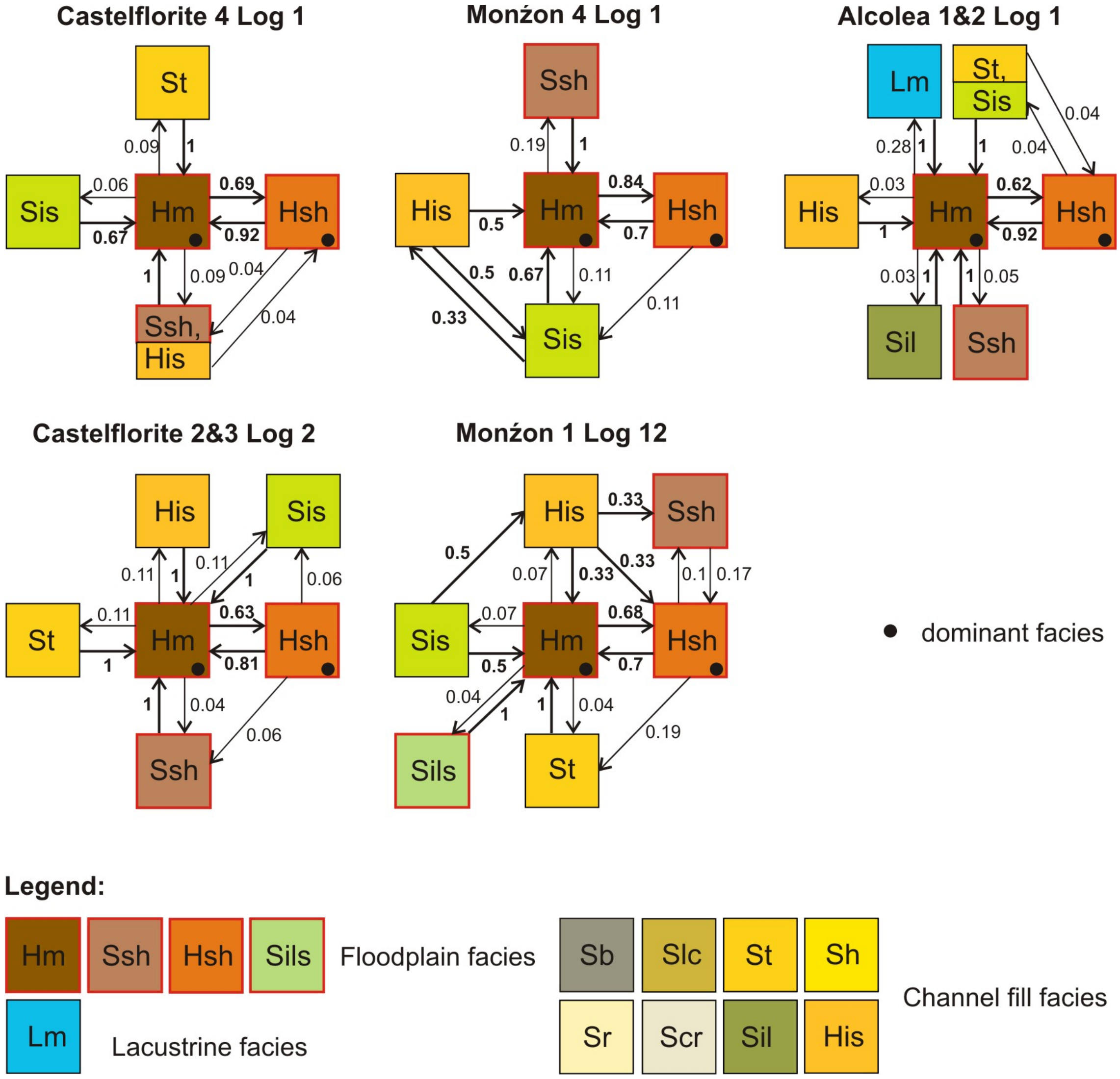

Figure 10.20. Facies transition diagrams for the Castelflorite 4 Log 1; Castelflorite 2&3 Log 2; Monźon 4 Log 1; Monźon 1 Log 12 and Alcolea 1&2 Log 1 successions of the Huesca DFS deposits. The successions are characterised by one or more dominant facies. Thick arrows indicate transitions with high probability. Boxes with two facies indicate facies with the same transition to the other facies. Note that all facies in the succession predominantly pass into one of the dominant facies. Facies colours are approximately the same as on the facies frequency distributions in the Fig 10.8 -13.

Channel fill facies (St, Sis, His) show very high probability of transition to Hm facies (Fig 10.20) that indicates avulsion of a channel to a new place on the floodplain. The place previously occupied by the channel becomes a site of accumulation of floodplain strata. Transition of channel facies Sis into facies His (Monźon 4 Log 1, Monźon 1 Log 12, Fig. 10.20) represents association of the sandy part of a lateral accretion complex and its “upper heterolithic part” (Chapter 4). However, some facies Sis and facies His are observed pass into facies Hm independently from each other (Castelfllorite 4 Log 1, Castelflorite 2&3 Log 2, Fig. 10.20). According to outcrop observations this could indicate independent channel fill deposits, heterolithic LA complex (His2) and sandy LA complex (Sis), formed in different channels (Chapter 4).

It is important to mention that sandstones of channel fill facies very rarely overly facies Hsh (TP = 0.04 for Castelflorite 4 Log 1 and TP = 0.1 for Monźon 4 Log 1, Fig. 10.20). This is another quantitative evidence that does not support previously proposed (Jones and Hajek, 2007) transition of facies from Hm to Hsh and finally to channel fill facies (St, Sis, His) in the stratigraphically transitional avulsion succession (Chapter 9).

In general, the Huesca DFS succession shows intercalation of the floodplain heterolithic facies association (Hm/Hsh/Ssh/Sils) with the minor channel fill facies association (St, Sis/His, Sil). The systematic facies change in the Huesca DFS successions is possibly defined by the high degree of aggradation and preservation of overbank deposits in endorheic Ebro Basin (Fisher and Nichols, 2013), high proportion of fine-grained material in the sediment load of the Huesca DFS and by a set of channel avulsions that resulted in channel reoccurrence at the same lateral position after a period of floodplain deposition.

10.4.2. The Salt Wash DFS succession

Although the Salt Wash DFS successions have been determined to be dominated by one or more facies as well as the Huesca DFS successions, they show more complex facies transitions diagrams (Fig. 10.21) due to slightly more variable set of facies (e.g. Bullfrog 2 Log 125 and Little Park 3 Log 7 successions, Fig. 10.10 and 10.13). This was also seen in slightly lower MOM values for some of the Salt Wash DFS successions in comparison with some of the Huesca DFS successions (Fig. 10.5, A)

Prevailing facies St (trough cross-bedded sandstones) is usually overlain by facies Sh (horizontally / low-angle bedded sandstones) (e.g. TP = 0.75 for Bullfrog 2 Log 125 and for Little Park 3 Log 7, Fig. 10.21), whereas facies St shows less frequent transitions back into facies Sh (e.g. TP = 0.1 for Bullfrog 2 Log 125 and TP = 0.25 for Little Park 3 Log 7, Fig. 10.21). According to the interpretation of facies Sh, a high deposition rate in a channel prevented formation of the dune bedforms necessary for formation of cross-bedding (Chapter 4). In contrast, facies St indicates conditions favourable for dune bedform formation. Additionally facies St is occasionally seen overlain by facies Scr (sandstones with climbing ripple lamination) in the distal successions of the Little Park outcrop (Fig. 10.21). The facies Scr has been interpreted to be a product of migration of ripple bedforms formed at high deposition rates (Chapter 4) that is consistent with the conditions of formation of facies Sh. Another channel fill facies Slc (sandstones with large-scale cross-bedding), representing lager-scale bedforms and higher flow energy, was found predominantly overlain with facies St (e.g. TP = 0.75 for Bullfrog 2 Log 125, Fig. 10.21). Thus, channel facies transitions (Slc - St – Sh or Scr?) observed in the Salt Wash successions are caused by variation in flow regime in the Salt Wash channels. Facies Sr and Scr are observed very rarely leading to a high probability of their transition to other channel fill facies (Fig. 10.21).

Relationships between floodplain facies (Hm, Hsh, Ssh, Sils) and channel fill facies (Slc, St, Sh, Sr) in the Salt Wash successions are different from the Huesca DFS succession and vary between relatively proximal and distal outcrops (Fig. 10.21). The relatively proximal Bullfrog 2 Log 125 succession predominantly shows transitions from channel fill facies (Slc, St, Sh) directly into facies Hm or Hsh and back to channel fill facies (TP = 0.2 - 0.5, Fig. 10.21). Intercalation of Hm and Hsh facies is rare (TP = 0.04 - 0.17, Fig. 10.21). On the logs and outcrop panels facies Hm and Hsh are observed as thin interlayers and lenses within sandstone bodies (appendices 2.7-12 and 5.4). These lenses are remnants of floodplain deposits which were reworked by subsequent avulsing channels; they define these specific facies transitions in the proximal successions. In the distal part of the Salt Wash succession more floodplain deposits are preserved and comprise larger portion of the succession (Chapter 7, Appendix 5.6). For example, the Little Park 3 Log 7 succession shows intervals of interbedded Hm and Hsh facies with TP = 0.4 - 0.8 (Fig. 10.21) that is similar to the Huesca DFS successions where little reworking of floodplain deposits occurred.

Likewise the Huesca DFS succession, the Salt Wash DFS succession shows order in the facies successions, but no distinct cycles can be distinguished. The order of the Salt Wash successions is also partly defined by dominant channel fill facies in proximal and medial areas and by floodplain facies in the distal area. The specific facies transitions observed in the successions were defined by a high degree of reworking of floodplain deposits by channels in a lower accommodation setting for the DFS (Weissmann et al., 2013 in press) (forming remnant fine-grained interlayers). This also resulted in higher proportion of fine-grained material in the distal area because the material reworked in the proximal area was transported downstream.

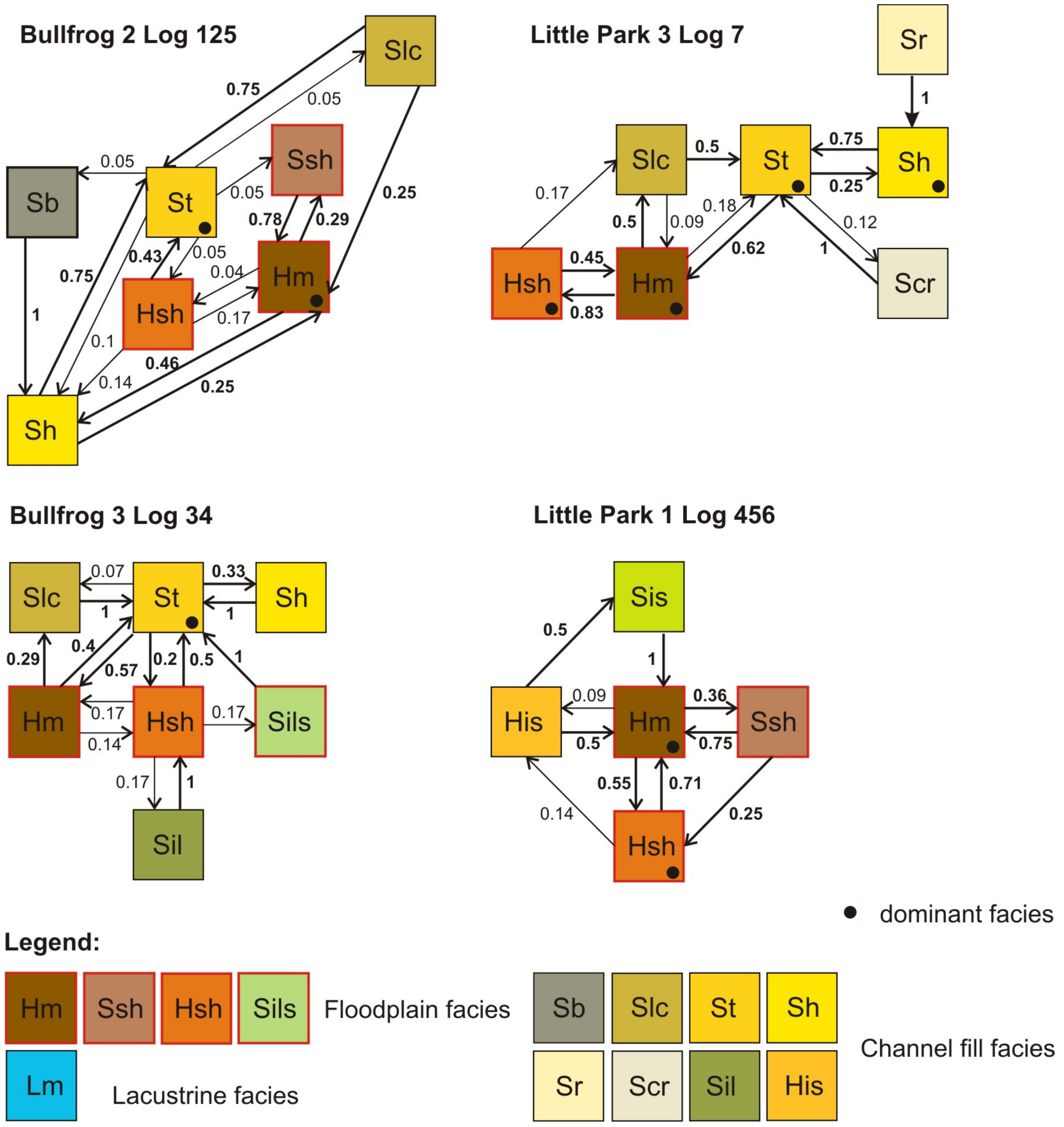

Figure 10.21. Facies transition diagrams for the Bullfrog 2 Log 125, Bullfrog 3 Log 34, Little Park 3 Log 7 and Little Park 1 Log 456 successions of the Salt Wash DFS deposits. The successions are characterised by more diverse facies sets. Thick arrows indicate transitions with high probability. Note difference between successions from the same outcrop and difference between relatively proximal (Bullfrog) and distal (Little Park) successions.

10.4.3. Lateral variability in facies transitions and relationships

Lateral variability in architecture and facies distribution in the Salt Wash DFS succession can be demonstrated by comparison of diagrams for stratigraphic logs from the same outcrop and from proximal and distal parts of the DFSs. The Little Park 1 Log 456 succession is dominated by facies Hm, Hsh and Ssh, while Little Park 3 Log 7 succession is characterised by a more variable facies set including facies St, Sh, Hsh and Hm (Fig. 10.21). Similarly, difference between sections recorded in the relatively proximal Bullfrog outcrop is observed (Fig. 10.21). The facies transition diagrams for the relatively proximal and distal Salt Wash successions are also different (Fig. 10.21).

In comparison successions from all studied parts of the Huesca DFS are dominated by Hm and Hsh facies and facies distributions are not as clearly variable (Fig. 10.20). This difference could be related to relatively even, high preservation of fine-grained floodplain deposits in all studied areas of the Huesca DFS, while in the studied areas of the Salt Wash DFS it varies dramatically due to different degree of reworking across and downstream the system. Note that the most proximal areas of the Huesca DFS has not been studied in this research (chapters 2 and 3, Fig. 3.1 and 3.4) and may have an architecture similar to the relatively proximal Salt Wash DFS. In addition, the analysis is one-dimensional and could not fully reflect lateral heterogeneity of the DFS architecture.

In conclusion, combined analyses of facies, TP matrices, facies transition diagrams and order metrics allowed to investigate the strata and depositional events quantitatively and in more detail that it is possible using only qualitative observations.

10.5. Conclusions

New statistical methods (Burgess, in prep) have been used to analyse the degree of order present in the system-scale successions of the Huesca and Salt Wash DFS deposits and in the floodplain successions of the Huesca DFS deposits.

At the system-scale, the MOM values for the observed successions (0.62 - 0.94) are higher than mean MOM values for the random and shuffled cycles synthetic models that indicates that facies successions are ordered. The MOM of the observed successions is similar to the mean MOM values for the shuffled same-data model indicating that the style of order is defined by strong dominance by one or more facies. The order is therefore apparent and limited to alternation of one or more dominant facies with less abundant facies (see also Miall, 1973). The difference between ordered strata with alternations to a dominant facies and a truly cyclical succession could not be determined using the MOM alone. However, comparison with synthetic models and use of the MOM in combination with the CTM successfully resolved the different types of order present.

The dominance of one or more facies in the system-scale succession perhaps indicate influence of long-term factors such as the high degree of aggradation and preservation of overbank deposits in endorheic Ebro Basin or high degree of reworking of floodplain deposits by channels in a lower accommodation setting in the relatively proximal and medial areas of the Salt Wash DFS.

At the floodplain scale, observed successions have lower MOM values (0.47 - 0.74) than the succession at the system-scale. The MOM values of the floodplain sections are close to mean MOM values of shuffled same-data model and are slightly higher or close to values for two other synthetic models. These relationships indicate lower degree of order in the floodplain succession then in system-scale successions. The CTM values of the observed succession are close to 0.5 and are similar to mean CTM values for all synthetic models indicating no dominance of coarsening or fining upward trends. The lower degree of order is found to be related to more variable facies distribution in the majority of floodplain successions which lack any strongly dominant or very rare facies to increase MOM values. This perhaps indicates that the deposition was influenced by more variable and complex combination and variability of local depositional processes. The succession of such depositional events did not produce patterns that could be clearly recognised using proposed quantitative method. Some degree of order in the floodplain successions of the Huesca DFS is still recognised but evidences of what have caused it could not have been determined.

The Markov order metric varies with the sample size due to non-stationarity of the facies successions. A calculation window applied at different positions through a succession gives different metrics. These variations should be interpreted with respect to the sensitivity of the metric to short section length (e.g. fewer than 20 units). Floodplain successions are in contrast stationary and a coarsening or fining-upward order is not present in them at any scale.

No order can be detected in unit thickness successions in any of the strata at any scale using the runs order metric method. The thickness unit successions are indistinguishable from random and could occur by chance. They could have also been formed in a way that is too complex for resulting patterns to be recognised using the suggested method and too complex to be interpreted using existing knowledge of complex autogenic behaviour of DFSs. This means that may be the process responsible for the formation of the thickness successions exists but could not be interpreted or predicted due to lack of existing information (Burgess, 2006).

One of the important conclusions from the results of the metric analysis is that coarsening and thickening-upwards cyclicity, which is commonly associated with splay progradation during avulsion process, is not characteristic for the floodplain deposits of the Huesca DFS succession (for discussion reader is referred to Chapter 9).

Facies transition diagrams are useful in combination with facies, TP matrices, MOM and CTM analyses. Diagrams for ordered systematic successions with dominant facies and less ordered succession can be differentiated by examination of diagram complexity and can be linked to facies frequency distributions and order metric values.

More detailed examination of the strata and succession of depositional events could be carried out using the combination of those. The comparison of facies transition diagrams between sections recorded in one outcrop and between sections from different outcrops showed difference in facies relationships in the Salt Wash succession across and downstream the DFS. In contrast, all facies successions of the Huesca DFS deposits have been found to be dominated by one or more floodplain facies that results in similar facies transition diagrams for all outcrops. This should be interpreted taking into account that studied outcrops of the Huesca deposits are more distal to the apex of the DFS than the relatively proximal Bullfrog outcrop of the Salt Wash DFS succession.

Although both DFS strata are characterised by the high degree of order related to one or more dominant facies, the Huesca and Salt Wash DFS strata clearly showed variability in facies and sandstone body architecture across and downstream the DFS (chapters 6, 7 and 8). The discussion of heterogeneity in the deposits of both DFSs, presented in the following Chapter 11, could help to investigate this variability further.

The quantitative method of analysis of facies and thickness proposed here needs further development but even at this stage it gives an opportunity to look at the strata quantitatively and understand facies relationships in more detail than is typically possible using more traditional qualitative methods alone.

11. Heterogeneity of DFS deposits

11.1 Introduction

Reservoir heterogeneity is one of main concerns of petroleum geologists and engineers because it influences fluid pathways through the reservoir and therefore defines reservoir production performance (Miall, 1988; Alexander, 1993). As has been observed during this study, the Huesca and Salt Wash fluvial successions are characterised by complex architecture controlled by frequent vertical and lateral changes in facies type and their geometries (chapters 4-10) and these would be difficult to predict in the subsurface. Previously porosity and permeability distribution in fluvial sandstones has been also characterised to be extremely variable (Pryor, 1972, 1973).

Petrographic and detailed outcrop studies of fluvial successions could help to constrain heterogeneity distribution within fluvial reservoirs at microscopic (pore-scale) and mesoscopic (facies, sandstone body connectivity) scales (Jones and Hartley, 1993). The Huesca and Salt Wash DFS successions provide suitable analogues for heterogeneous fluvial reservoirs, and their heterogeneity at different scales is discussed in this chapter.

11.2 Heterogeneity of the Huesca and Salt Wash DFS deposits

Fluvial architecture of the DFS deposits shows heterogeneity at four different scales which are related to particular characteristics of the deposits, including:

- Pore-scale heterogeneity related to the degree of maturity and cementation of the sandstones (Fig. 11.1, A);
- Internal heterogeneity of the sandstone bodies created by sedimentary structures and variations in grain size (Fig. 11.1, B);
- Heterogeneity determined by sandstone body relationships between each other and with fine-grained floodplain deposits (Fig. 11.5, A);
- Fluvial system-scale heterogeneity related to large-scale sandstone body clustering that defines the connectivity of the reservoir (Fig. 11.5, B).

11.2.1 Heterogeneity at pore scale

Porosity of the sandstones and siltstones is estimated from impregnated thin sections using a graphical approach (Chapter 3). Laboratory analyses of porosity and permeability have not been conducted in this research. Although the available data set is limited, some conclusions about reservoir properties could be made based on the porosity estimations and petrographical analysis of the thin sections.

Porosity estimated from the thin sections of the Huesca and Salt Wash sandstones is variable. The difference in porosity values between some samples is up to 15 %. The Huesca sandstones are characterised by porosity ranges between 0.4 % and 15 % (Fig. 11.2) while the Salt Wash sandstones show porosity range between 2 % to 39 % (Fig. 11.3). The estimates could be affected by not accurate estimation procedure (Chapter 3) plus they are made in 2D thin sections while porosity is a volumetric property. According to these limitations, the estimates will be used only for qualitative comparisons.

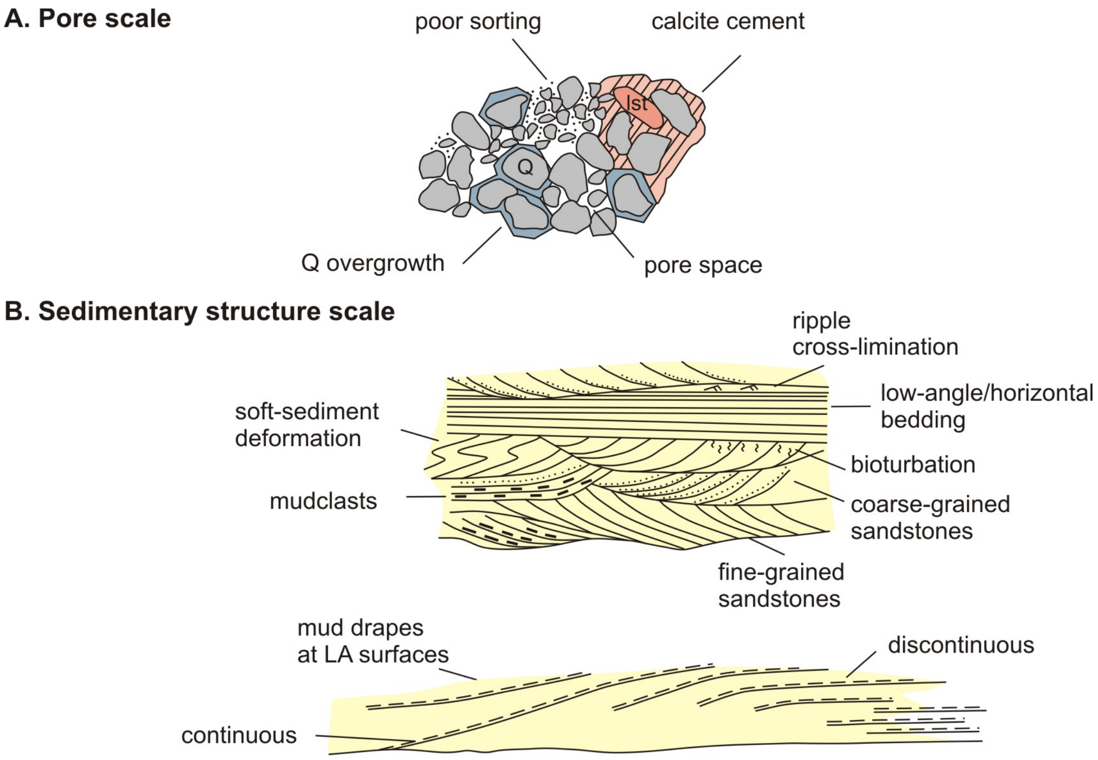

Figure 11.1. Schematic representation of heterogeneity at pore scale (A) and sedimentary structure scale (B) in the Huesca and Salt Wash DFS successions. The diagram is not to scale.

Previously porosity and permeability have been found to increase with increasing grain size (Pryor, 1972; Jiao et al., 2005). Davis et al. (1993) and Jones and Hartley (1993) have also determined that reservoir properties are strongly controlled by depositional facies: porosity and permeability is higher in channel facies and lower in overbank facies. Conversely, the estimated porosity for the Huesca and Salt Wash samples does not show a strong correlation with grain size or facies (Fig. 11.4). Samples from the finer-grained overbank facies show overall lower porosity values (Huesca - 0.4 % – 5 %; Salt Wash – 3 % - 24 %) than samples from coarser-grained channel fill sandstones (Huesca – 2 % – 15 %, Salt Wash – 2 % - 39 %), but some coarse- and medium-grained channel fill sandstones are characterised by porosity values of less than 5 %. Similarly, Pryor (1973) did not find a relationship between the texture of Holocene fluvial sandstones (grain size, sorting) and their porosity. Different porosity and permeability have also been determined for sandstone samples from the same distributary channel facies in the Karamay Formation in China (Jiao et al., 2005).

This heterogeneity in porosity of the Huesca and Salt Wash sandstones could be related to the variable content of cement and matrix in the pore space of the sandstones (Fig. 11.1, A). Davis et al. (1993) also observed a decrease in porosity with an increase in matrix and cement content in Cretaceous fluvial reservoir in Texas.

Abundant limestone fragments in the Huesca sandstones (Section 6.2, Appendix 3 Table 6) led to the formation of calcite cement when they were dissolved and reprecipitated (Appendix 4 Panel 4, B-E; Fig. 11.2, samples 2-3, 2-21, 1-17). The calcite cement is observed mostly in the areas close to the limestone grains (Section 6.2) and is therefore distributed unevenly. The Salt Wash sandstones predominantly consist of quartz grains which in some places are overgrown by quartz cement (Appendix 4 Panel 7, A) and in other places are held together by poikilotopic calcite cement which was formed by dissolution of sparse limestone grains (Appendix 4 Panel 7, D). These cements are also distributed unevenly.

The Huesca sandstones are immature and contain large amounts of lithic fragments which can be aligned between other grains forming a non-uniformly distributed pseudomatrix (Appendix 4 Panel 2, B) (“plastic detritus” in Jiao et al., 2005). Matrix made up of clay material has been observed in only some of the sandstone samples from both DFS successions (sections 6.2 and 7.2). In general, matrix is rarely observed in the sandstones of both successions (Appendix 4 Panel 4, G, Panel 7, F, sample 4-7, Panel 6, C, sample 5-12) and comprises a maximum 10 % – 15 % of the samples (sections 6.2 and 7.2). Thus, cement and matrix in the pore space of the studied DFS sandstones are distributed non-uniformly within individual beds that adds to the degree of heterogeneity created by their variable content in different beds / sandstone bodies (different samples).

Sorting, as determined by grain size analysis, of the sandstones in the Huesca and Salt Wash deposits is generally poor (Appendix 3 Table 3) and this could have reduced porosity within the sandstones (Gaither, 1953). The non-uniform distribution of grains of different sizes is clearly seen in the thin sections of the Huesca sandstones (Fig. 11.2, samples 1-20, 1-21, 2-21, 3-2) and Salt Wash sandstones (Fig. 11.3, samples 5-6, 5-9, 5-14, 7-4). This adds to the variation in porosity defined by the presence of matrix and cements.

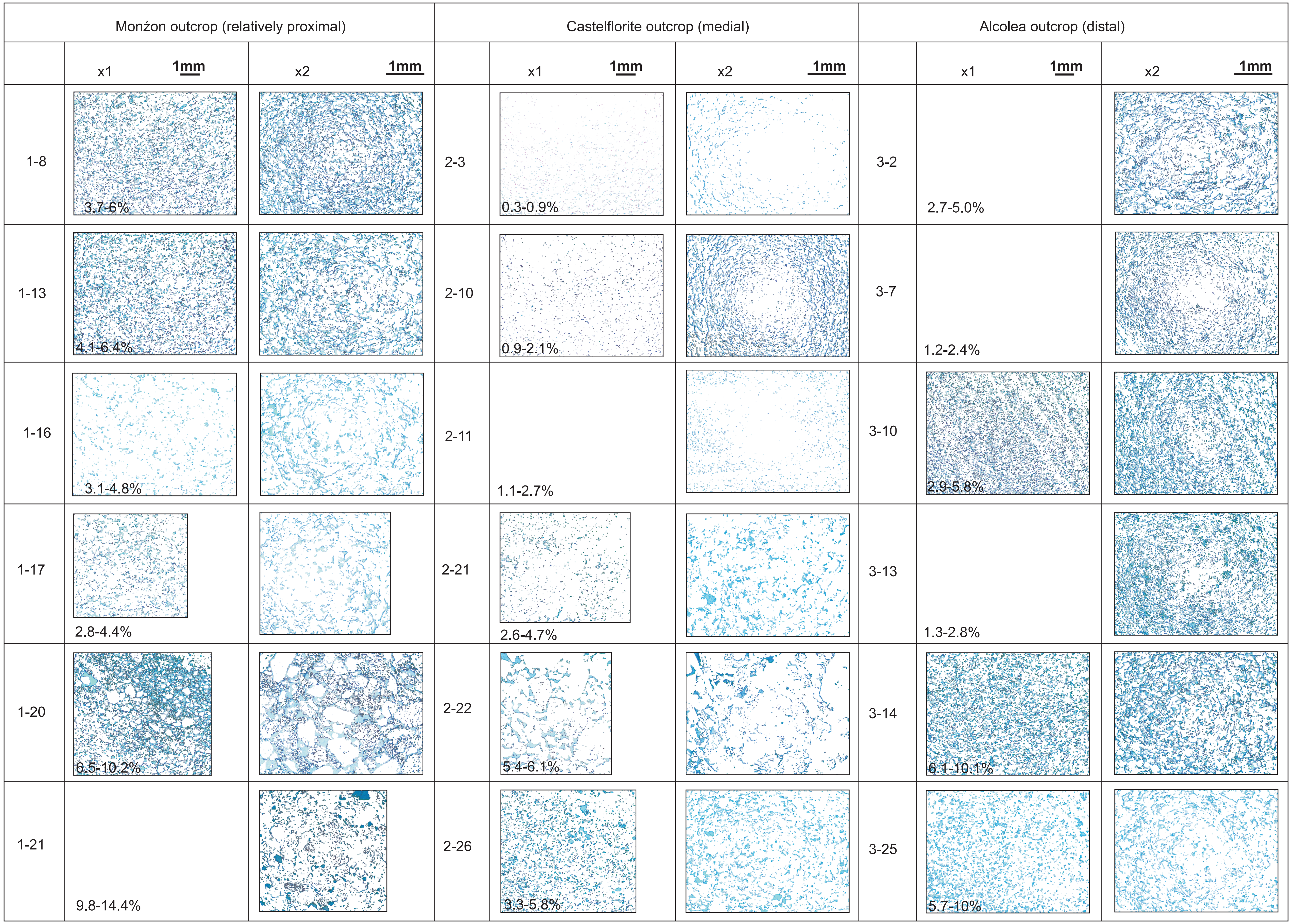

Figure 11.2. Pore space in thin sections of the Huesca sandstones and siltstones used for porosity estimation. The thin sections are shown in x1 and x2 magnifications. Ranges of porosity represent minimum and maximum values obtained using different colour masks during pixel count estimations.

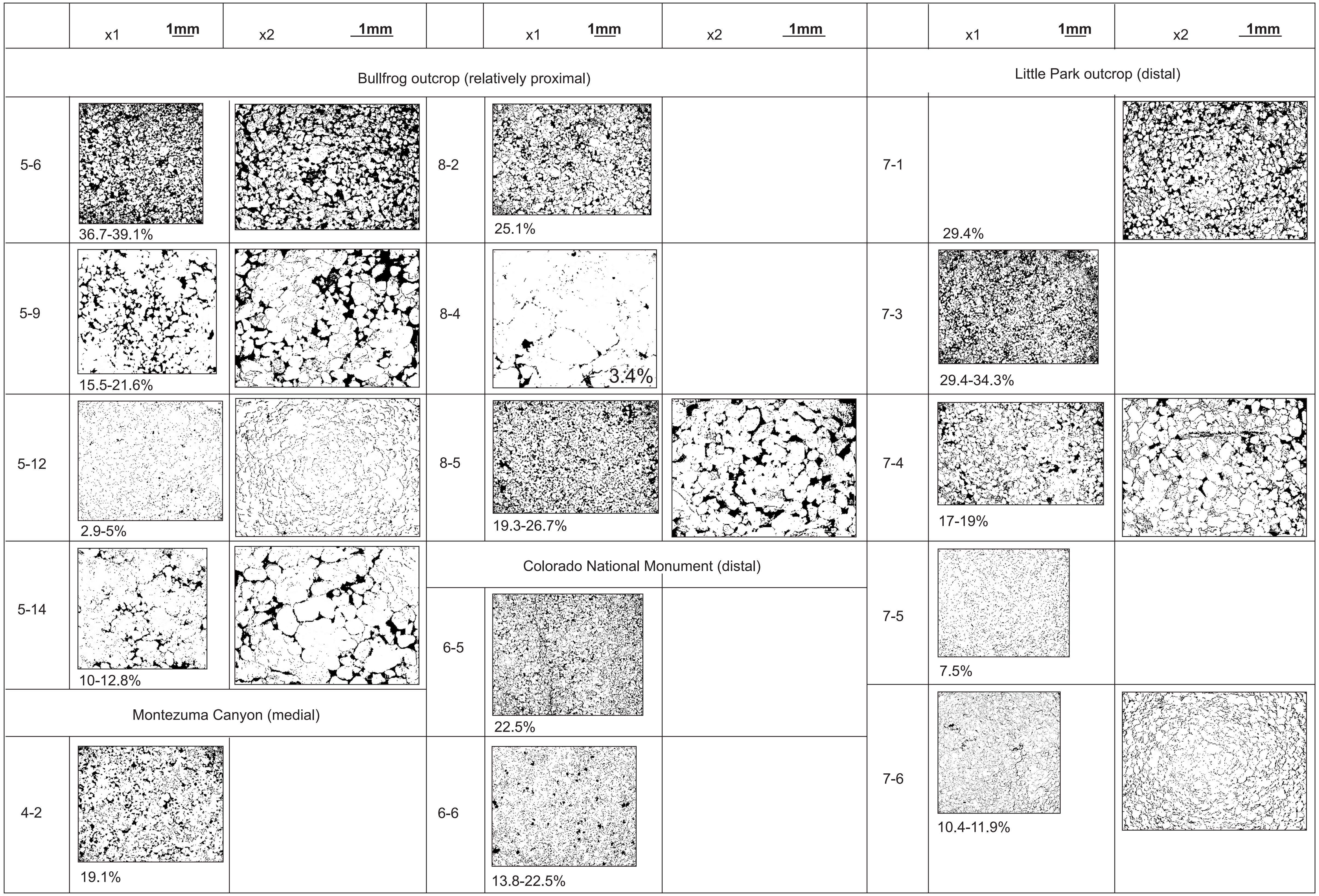

Figure 11.3. Pore space in thin sections of the Salt Wash sandstones and siltstones used for porosity estimation. The thin sections are shown in x1 and x2 magnifications. Ranges of porosity represent minimum and maximum values obtained using different colour masks during pixel count estimation. Where there is only one value, only one colour mask has been used.

A. The Huesca DFS succession

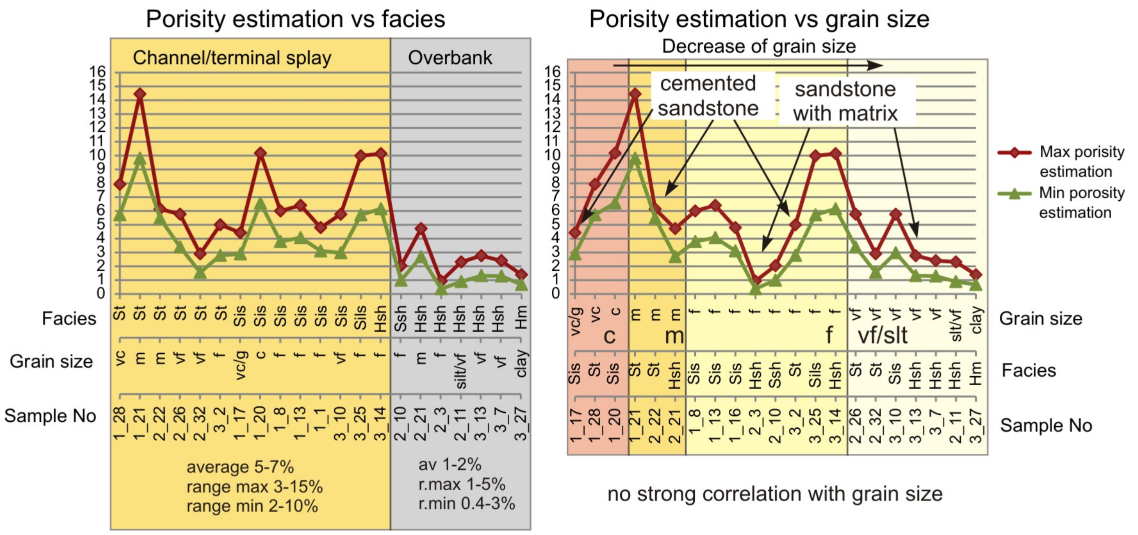

B. The Salt Wash DFS succession

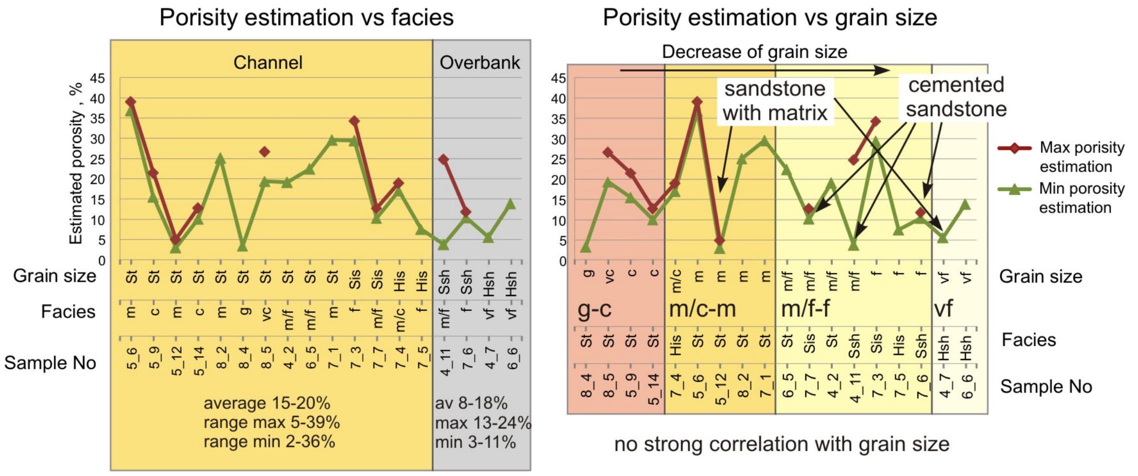

Figure 11.4. Porosity estimated from thin sections of selected samples from the Huesca (A) and Salt Wash (B) DFS successions and its variation between different facies (left, sorted by facies) and with grain size (right, sorted by grain size).

Jiao et al. (2005) have found that the matrix in pores of fluvial sandstones of the Karamay Formation in China reduces permeability rather than porosity of the deposits. It is known that high porosity does not always correlate to high permeability. For example, no clear relationship between permeability and porosity was found in fluvial sandstones by Pryor (1973). Anomalously low permeabilities have been observed due to the presence of fibrous illite in pores between sand grains that reduced permeability dramatically but did not affect porosity values as much (Mikkelsen et al., 1991; Cable and Burke, 2011; Potter et al., 2004). Illite was found to be the main clay mineral in both successions (XRD results in sections 6.2 and 7.2). Permeability or SEM studies have not been done in this work but if the amount of the illite is high in the sandstone pores, relatively low permeability could be expected in the Huesca and Salt Wash sandstones.

The non-uniform distribution of cements, matrix and different sized grains in the studied DFS sandstones defines variation in porosity within one sandstone bed. Illite could possibly reduce permeability of the sandstones locally. The pore-scale heterogeneity in the studied DFS sandstones is caused partly by sandstone origin (source and transport history of sediment) and partly by diagenetic processes. Diagenetic effects on the heterogeneity of porosity is, however, local and are not general characteristic of DFS deposits. Therefore, the main control on the DFS sandstone heterogeneity at the pore-scale is uneven distribution of matrix and poor sorting in general. Distribution of pore-scale heterogeneity is difficult to predict (Pryor, 1972) but needs to be considered during reservoir modelling, for example, using “pore-to-field” modelling approach (Keogh et al., 2007) discussed in Chapter 13.

11.2.2 Heterogeneity at sedimentary structure scale

The medium-scale heterogeneity in the Huesca and Salt Wash succession is associated with mudstone drapes and mudclast horizons along sedimentary bedding surfaces and variations in grain size and sedimentary structures within individual sandstone bodies (Fig. 11.1, B). These heterogeneities are caused by a change in flow regime in the DFS channels (variations between facies Slc, St, Sis and His, Chapter 4). Mudstone drapes and mudclast horizons create discontinuous baffles within the reservoir, while the variations in grain size and structures creates heterogeneity in reservoir properties within individual reservoir bodies.

Mud drapes on lateral accretion surfaces

Some sandstone bodies of Type 2 in the Huesca and Salt Wash DFS successions are characterised by lateral accretion surfaces draped by mudstone in their upper part (Fig. 4.6, B, C, F, H). Other lateral accretion complexes are heterolithic and mudstone drapes cross-cut the sandstone body from the upper boundary to its base (Fig. 4.6, A, J, I). According to 2D modelling experiments conducted by Pranter et al. (2007), the mud drapes in the top part of the point bar sandstone body create permeability baffles and will reduce breakthrough time and sweep efficiency, forcing fluid flow along the lower part of the sandstone body. Ma et al. (1999) also showed that point bar deposits trap the oil in the upper, less permeable part. Heterogeneity of the fluvial reservoir in the Karamay oil field in China has been also associated with changes in properties in the top part of point bars (Jiao et al., 2005). However, 3D modelling showed that only mud drapes that are continuous in three dimensions and have steep slopes affect the sweep efficiency during waterflooding, while 2D models overestimate this effect (Jackson and Muggeridge, 2000). Therefore, only heterolithic lateral accretion facies (His) with continuous mudstone baffles would truly affect behaviour of the DFS reservoirs analogues to the studied successions, while discontinuous mud drapes and mudclast horizons in facies Sis (sandy lateral accretion complexes) would not have the same effect.

Importantly, the effect of the mud drapes on reservoir behaviour would also depend on the type of fluid. For example, in heavy oil reservoirs, which are developed using Steam Assisted Gravity Drainage (SAGD), the discontinuous mud drapes would slow down development of a steam chamber and, consequently oil production rate (Le Revalec et al., 2009). Whereas the mud drapes or mud clasts could not be effective barrier for the gas reservoirs.

Variations in grain size

The effect of discontinuous baffles in point bars in some cases could be reduced if wells are drilled parallel to the paleoflow, while a decrease in grain size would affect the reservoir performance the most (Pranter et al., 2007) independently on the well orientation. Variation in grain size is usually observed between bed sets in both Type 1 and Type 2 sandstone bodies within facies St and between interbedded facies St and Sh (Fig. 4.3 and 4.4).

Varley (1984) showed that filtration properties of a reservoir are controlled by texture and composition of the sandstones. A contrast in reservoir properties that could be partly related to grain size variations in sandstone bodies causes major oil bypass in fluvial reservoirs (Barthel, 1991). This could result in faster flow paths through parts of sandstone body with better filtration properties (coarse-grained bed sets) and bypass areas with poorer filtration properties (finer-grained bed sets), trapping the oil or slowing its displacement.

For example, the coarse-grained central part of channel sandstone bodies was found to create fluid-flow units due to its better filtration properties (Jiao et al., 2005). The sandstones of facies St and Sh within Type 1 and 2 sandstone bodies in the Huesca and Salt Wash successions do not show grain size trends from the base to the upper part of a sandstone body, instead grain size varies between bed-sets, and therefore might be expected to be swept better than those described by Jiao et al. (2005). Nevertheless, frequent change in grain size, hence filtration properties, between bed sets in the observed sandstone bodies would decrease the percentage of oil extraction due to tortuous fluid paths (Weber, 1982 and references therein).

The facies St and Sis are the dominant facies of channel fill deposits in both DFS successions and therefore most of the sandstone bodies would be characterised by heterogeneity in porosity and permeability due to variable grain size and mud drapes.

Type of sedimentary structures

Miall (1988) and Davis et al. (1993) pointed out that sandstones with different sedimentary structures will also have different reservoir properties. Sedimentary structures in sandstone bodies of the Huesca and Salt Wash DFS successions are predominantly represented by through cross-bedding (facies St) and horizontal bedding (facies Sh), while ripple cross-laminated sandstones (facies Sr and Scr) occur rarely. Alternating trough cross-bedded sandstones and sandstones with horizontal / low-angle cross-bedding are common for the sandstone bodies of the Salt Wash DFS succession (Fig. 4.3 and 4.4). According to Miall (1988) and Davis et al. (1993), structureless and horizontally bedded sandstones would have the best filtration properties, planar and trough cross-bedded sandstones - intermediate filtration properties and ripple cross-laminated sandstones - the worst filtration properties. Sandstones of facies St in both the Huesca and Salt Wash DFS successions indeed show variation in grain size along and between individual beds within cross bed set (Fig. 4.3, B, H) that would affect vertical and horizontal permeability ratio (Pryor, 1972, 1973; Weber, 1982). Thus, horizontally bedded sandstones in the Salt Wash DFS succession would be swept more easily than the trough cross-bedded and ripple cross-laminated ones. This would make flow path through the sandstone bodies more tortuous and some parts of sandstone body with poorer properties could be bypassed.

Abundant mudclast accumulations are also associated with bounding surfaces between cross bed sets or between every bed in a cross set in sandstones of facies St (Fig. 4.2, A, E-F, and 4.3, E-F). Mudclasts horizons could act as discontinuous baffles/barriers similar to mud drapes (Jiao et al., 2005; Jones and Hartley, 1993; Larue and Hovadik, 2006). For example, mudclast horizons in channel lag deposits of Lower Cretaceous Cutbank Sandstone of Southern Alberta were found to be the major control on reservoir quality (Farshori, 1989). The presence of mudclasts in the facies St makes it even more heterogeneous in comparison to facies Sh.

Other internal heterogeneities within sandstone bodies such as diagenetic concretions (Jiao et al., 2005), bioturbation (Verdier et al., 1980) and soft sediment deformations (Weber, 1982) could also affect variation in reservoir properties within sandstone bodies. No large diagenetic concretions have been observed in the studied outcrops. Bioturbation is common only in thin Type 3 overbank sandstone bodies in the Salt Wash and Huesca DFS successions and very rarely occurs in major channel sandstone bodies (Fig. 4.3, J). Soft sediment deformation was also only occasionally observed in major sandstone bodies of Type 1 and 2 in the Salt Wash succession (Fig. 4.3, I). Therefore, these heterogeneities would have only a minor effect on reservoir properties.

In summary, internal heterogeneity of sandstone bodies in the Huesca and Salt Wash DFS successions is caused by change in flow regime in DFS channels (change in sedimentary structures and grain size) and to a lesser extent by syn-depositional or diagenetic changes of their deposits. Discontinuous and continuous mud drapes on the bedding surfaces within lateral accretion complexes and mudclast horizons at the boundary surfaces of bed sets create baffles which reduce the breakthrough time and sweep efficiency of the reservoir. Maximum effect would be observed from continuous mud drapes in light hydrocarbon reservoir and from all types of baffles in heavy oil reservoirs. Variation in grain size and sedimentary structures within sandstone bodies results in variation in reservoir properties that in turn forces flow to follow tortuous paths and reduces oil production rate and recovery.

11.2.3 Heterogeneity at sandstone body scale

Individual, internally heterogeneous sandstone bodies are organised into large amalgamated complexes (Chapter 5). Abandoned scours filled with heterolithic deposits and heterolithic lateral accretion complexes (facies His2), associated with Type 2 and more rarely with Type 1 sandstone bodies, and heterolithic overbank deposits are preserved in lenses within these amalgamated complexes (Fig. 11.5, A1). Sandstone bodies in the complexes can be vertically connected in some places but may be split laterally by a wedge of fine-grained floodplain deposits (Fig. 11.6, A-C). The remnants of finer-grained deposits within amalgamated sandstone body complexes form discontinuous baffles for fluid flow creating large-scale vertical and lateral heterogeneity. These heterogeneities are the result of frequent variation in depositional processes on the DFS including variation in flow regime within a channel (occurrence of facies Sis and His2) and channel avulsion (intercalation of floodplain intervals and channel sandstone bodies and presence of abandoned channel scours) that creates a mosaic of deposits of different facies and with different reservoir properties.

The Huesca DFS succession is dominated by fine-grained deposits and therefore fine-grained baffles are a common element within amalgamated sandstone bodies in its relatively proximal part that forms tortuous reservoir body (Fig. 11.6, A-B). In contrast, relatively proximal and medial Salt Wash successions are dominated by sandstone bodies and floodplain packages occur much rarer, and they are mostly discontinuous, that results in a more connected reservoir volume (Fig. 11.6, C). Note that the deposits

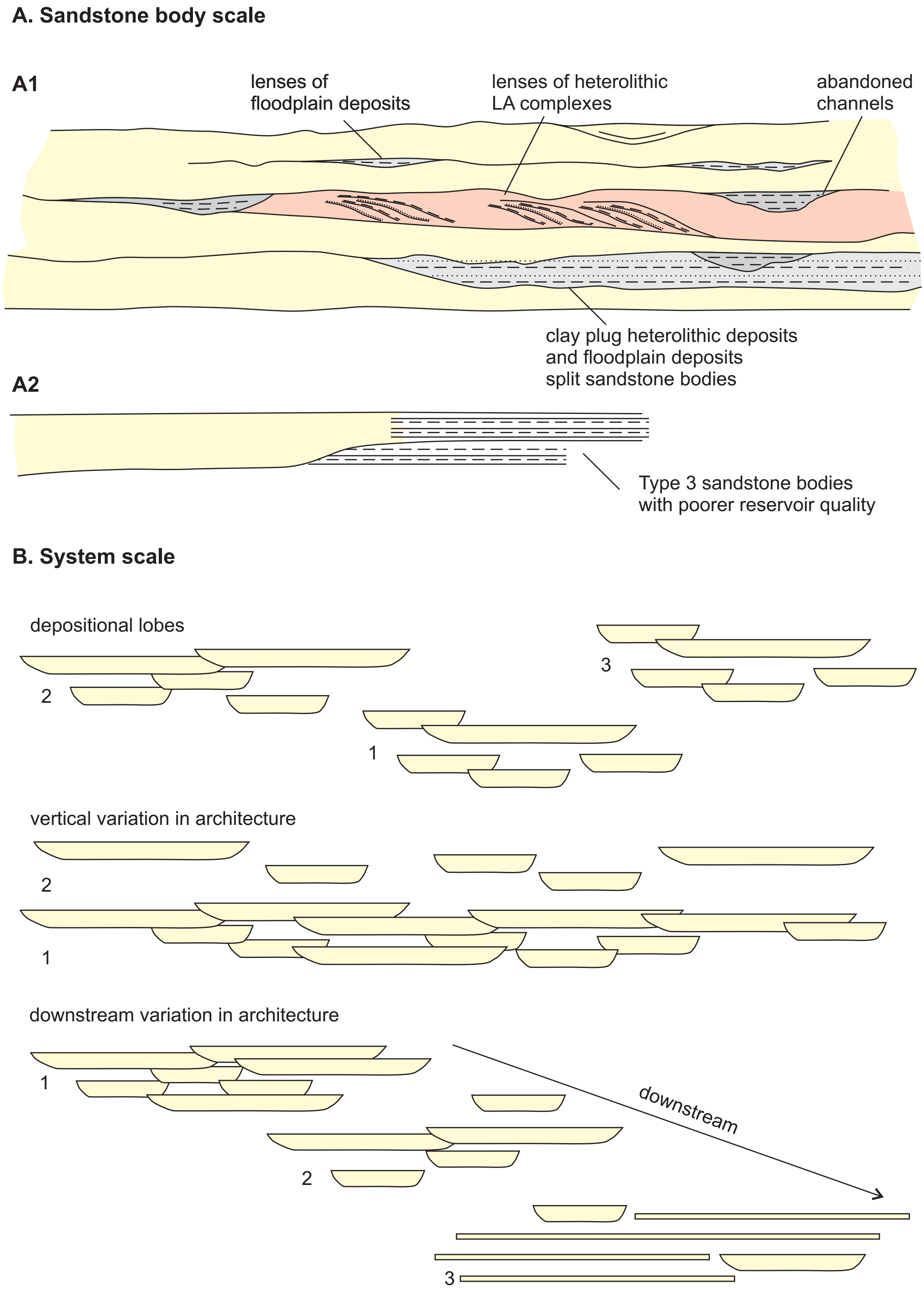

Figure 11.5. Schematic representation of heterogeneity in the Huesca and Sat Wash DFS successions at the sandstone body scale (A) and system scale (B). Diagram is not to scale.

in the most proximal part of the Huesca DFS succession, which have not been studied in this project (chapters 2 and 3), could have formed connected sandstone bodies similar to those observed in the relatively more proximal Bullfrog outcrop of the Salt Wash DFS succession.

Although all sandstone bodies in the relatively proximal and medial Salt Wash DFS successions are connected, lateral heterogeneity in facies relationships even in one outcrop of the Salt Wash DFS succession has been recognised using statistical order metric and facies transition diagram analyses (Fig. 10.21, Chapter 10). This could have been caused by the presence of discontinuous heterolithic floodplain intervals within the amalgamated sandstone bodies. The distribution of heterolithic intervals have been also recognised as the main heterogeneity within the potential Salt Wash sandstone reservoir that controls its sweep efficiency, total production and water cut by Robinson and McCabe (1997). Therefore, the flow path could be still affected by the presence of the heterolithic baffles within the large amalgamated sandstone bodies in the relatively proximal and medial DFS deposits, but perhaps much less than within “jig-saw”-like amalgamated sandstone body in the relatively proximal Huesca deposits (Fig. 11.6, A-C).

Jones and Hartley (1993) discussed that sandstone body scale heterogeneities related to fine-grained facies have unpredictable dimensions and could significantly affect vertical and horizontal permeability and net-to-gross (NTG) ratio. Miall (1988) also pointed out that heterogeneities of this scale in fluvial successions are impossible to map due to internal erosion, amalgamation and absence of markers within fluvial successions and therefore difficult to predict.

The dimensions of the relict flood-plain intervals within amalgamated sandstone bodies in the Salt Wash succession are provided by Robinson and McCabe (1997). The heterolithic deposits of the relatively proximal successions of the Salt Wash DFS deposits include abandoned channel fills with W / T = 33 and overbank deposits with W / T = 70 (Robinson and McCabe, 1997). The heterolithic deposits within amalgamated sandstone bodies in the relatively proximal succession of the Huesca DFS deposits could reach thicknesses from 5 cm to 3 m and continue laterally from 10 m to more than 300 m (W / T is up to 200). The dimensions of the baffles within the Huesca and Salt Wash DFS successions vary considerably (Appendix 5) and it is not vey useful to provide dimensions for them because they would not be representative for any other fluvial succession. However, it could be that ranges of baffle dimensions are similar for fluvial systems of similar styles and therefore may be useful if database of many outcrop analogues for fluvial systems of different styles is created and such link is established.

Thin, sheet-like overbank sandstone bodies of subtypes 3/1 and 3/2 and amalgamated packages of them are commonly connected with larger channel sandstone bodies either when truncated by them or when they gradually pass into them laterally (Fig. 11.5, A2, Fig. 5.5-6). The sandstone bodies of Type 3 differ in their origin and therefore by their lithology (they are finer) and sedimentary structures (they tend to be structureless or ripple cross-lamination) consequently, as it was discussed in previous sections, this would create differences in filtration properties. The Type 3 sandstone bodies would possibly have poorer porosity and permeability than coarser channel sandstone bodies. The difference in properties could result in bypass of Type 3 sandstone bodies with poorer quality (Weber, 1982; Barthel, 1991, Dromgoole and Speers, 1997) and concentration of flow within channel sandstone bodies (thief zones). Farshori (1989) showed that during waterflooding fluid flow can be concentrated between sandstone bodies with the best filtration properties. The effect, however, will be different for different fluid types in the reservoir. The contrast in reservoir properties will not be as significant for gas reservoirs as for heavy oil reservoirs. Therefore, Type 3 sandstone bodies could increase volume and connectivity of a gas reservoir and should be taken into account.

The heterogeneities at sandstone body scale add tortuosity to the path of fluid flow that is already affected by the smaller-scale heterogeneities within individual sandstone bodies discussed in previous sections. Sandstone bodies in both DFS successions are interconnected into complex reservoir body where NTG ratio differs within single sandstone body complex (Fig. 11.6) and some zones with poorer reservoir qualities (Dromgoole and Speers, 1997) or zones sheltered by lenses of fine-grained heterolithic deposits (Jackson and Muggeridge, 2000) could be unswept. The complexity of the reservoir body seems to be higher in the Huesca DFS succession and therefore production properties of such reservoir could be worse. However, more proximal deposits of the Huesca DFS, which have not been studied here (chapters 2 and 3), could have similar architecture and reservoir properties to the relatively proximal Salt Wash succession. The order metric and facies transition diagram analyses (Chapter 10) did not recognise the high degree of heterogeneity in the Huesca DFS succession and it appeared less heterogeneous than the Salt Wash DFS succession. This could be because the analysis has been done for 1D vertical facies successions that provides information only about vertical facies relationships and does not consider lateral facies variability.

11.2.4 Heterogeneity at succession scale

Large-scale heterogeneity in fluvial reservoirs (Fig. 11.5, B) has been shown to be a cause of oil bypass and trapping due to the effect on the degree of sandstone body

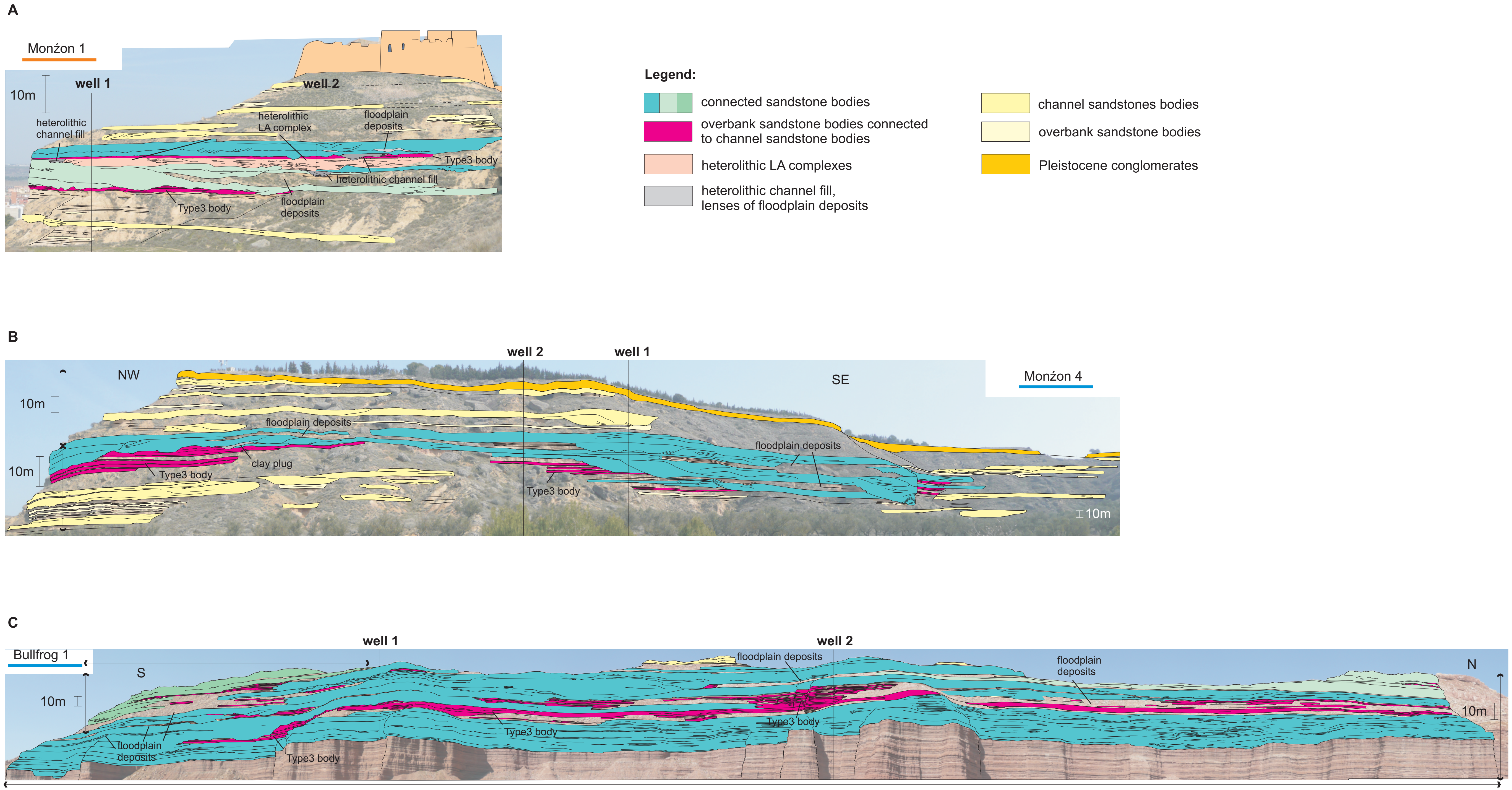

Figure 11.6. Potentially connected sandstone bodies in Monźon outcrop of the Huesca DFS succession (A-B) and in the Bullfrog outcrop in the Salt Wash DFS succession (C). Blue / green - connected sandstone bodies, pink – thin, sheet-like overbank sandstone bodies of Type 3 connected to channel sandstone bodies. Annotations indicate sandstone body scale heterogeneities described in Chapter 11. Note difference in NTG ratio in imaginary wells 1 and 2 in all outcrops.

connectivity (Barthel, 1991). For example, vertical variations in sandstone body proportion and their thickness within the Carboniferous Pennant Measures succession was also stated to affect NTG ratio and connectivity of the reservoir (Jones and Hartley, 1993).

Downstream variations in sandstone body proportion relative to heterolithic floodplain deposits, their dimensions and the degree of their amalgamation (chapters 6, 7 and 8) result in variations in degree of heterogeneity and sandstone body connectivity within the Huesca and Salt Wash DFS successions (Fig. 11.5, B). For instance, the distal succession of the Salt Wash DFS deposits in the Little Park outcrop contains only two large channel sandstone bodies which are connected only in their middle part and split laterally by impermeable floodplain deposits (Appendix 5.6). Other sandstone bodies in the outcrop are thinner and are vertically isolated. In the relatively proximal and medial succession of the Salt Wash DFS deposits all sandstone bodies are connected (Appendix 5.4). The distal succession of the Huesca DFS deposits in the Alcolea outcrop is also characterised by a small proportion of vertically isolated sandstone bodies (Appendix 5.3) while relatively proximal part has at least 30 % of major sandstone bodies that are mostly connected (Appendix 5.1). The degree of heterogeneity in the distal part differs considerably from the degree of heterogeneity in relatively proximal outcrops resulting in strongly contrasting NTG ratio and degree of sandstone body connectivity in different parts of a DFS (Fig. 11.5, B). This variation has to be considered during DFS reservoir characterisation and modelling. Variations in sandstone body architecture vertically have not been observed within the studied DFS outcrops.

Large-scale clustering of sandstone bodies has been recorded in the Ferris DFS succession exposed in Wyoming, USA and interpreted to be a result of autogenic processes including regional avulsions causing depositional lobe migration by Hajek et al. (2010). Nichols (1987) has also suggested higher concentration and connectivity of sandstone bodies in the core part of the depositional lobes than in areas between them (Fig. 11.5, B) based on the data collected in the Luna DFS succession exposed in Ebro Basin next to the Huesca DFS succession. The clustering therefore could also define lateral and vertical system-scale heterogeneity in NTG ratio and sandstone body connectivity.

Lobes on a DFS have been interpreted to migrate as a consequence of a compensation mechanism (Straub et al., 2009; Hajek et al., 2010). Larue and Hovadik (2006) emphasised that compensational stacking could reduce connectivity of the reservoir because sandstone bodies or their amalgamations “avoid” previously deposited ones. Larue and Hovadik (2006) questioned that it is important to know at what scales the compensational stacking occurs, depositional lobes or/and individual channels that would affect the heterogeneity of the DFS succession at different scales. If each channel avulses in a compensational manner it will be placed away from the previous elevated channel ridge and separated by floodplain deposits that could lead to lower sandstone body connectivity. The effect of avulsion mechanism at a channel scale (sandstone body stacking patterns) on the NTG ratio and sandstone body connectivity will be addressed in Chapter 12 using 2D geometric model (Fig. 12.30).

The studied outcrops of the Huesca and Salt Wash DFS succession, however, are not extensive enough to demonstrate lateral variation related to lobe migration. Clustering have not been observed, but could occur at a larger scale. Larger scale outcrop studies are required to confirm lateral sandstone body clustering.

In summary, large-scale heterogeneity in DFS deposits can be created by variation in proportion, dimensions and relationships between sandstone bodies and heterolithic floodplain intervals that occurs vertically and laterally downstream and across a DFS. Such variations could be defined by combination of long-time scale external and internal controls. The main large-scale heterogeneity that was observed in the DFS successions is downstream variations in NTG ratio and sandstone body connectivity. The heterogeneity related to lateral sandstone body clustering and channel avulsion mechanism could also occur.

11.3 Net-to-gross ratio and reservoir connectivity in the Huesca and Salt Wash DFS deposits

Net-to-gross (NTG) ratio is one of the main parameters that are used for estimation of reservoir connectivity, numerical modelling and STOIIP/reserves estimation. It is commonly thought that the higher NTG ratio the higher reservoir body proportion and connectivity (Allen, 1979; King, 1990; Larue and Hovadik, 2006; Robinson and McCabe, 1997). Connectivity of sandstone bodies in 3D space could be higher than visible connectivity in 2D outcrop due to connections between sandstone bodies in the third dimension. Several models of channelized reservoir were created by Larue and Hovadik (2006) to show the relationship between NTG ratio and reservoir-to-well connectivity for 2D and 3D reservoirs. The reservoir-to-well connectivity has been defined as connectivity of the reservoir between producing and injecting wells. The connectivity was found to have positive, but non-linear correlation with NTG ratio. The connectivity does not significantly increase before the NTG ratio is higher than 60 % for 2D case and 30 % for 3D case (Fig. 11.7).

Due to the heterogeneous architecture of the DFS deposits, NTG ratio in a single 1D section could not be correlated with 2D or 3D sandstone body connectivity directly. For example, imaginary well 1 in the Monźon 4 outcrop of the Huesca DFS succession penetrates three large amalgamated sandstone bodies of Type 1 (Fig. 11. 6, B), while well 2, several metres to the north-west from the well 1, finds only vertically isolated sheet-like sandstone bodies of Type 2. The difference in the NTG ratio could be seen for wells 1 and 2 in the Monźon 1 outcrop (Fig. 11. 6, A). A smaller difference is observed for the wells 1 and 2 in the Bullfrog 1 outcrop of the Salt Wash DFS succession (Fig. 11.6, C) but it is still apparent. Therefore, despite the high NTG ratio in one well, neighbouring wells (already at 50 to 150 m away) could have much lower NTG ratios and overall reservoir volume and connectivity would not correlate directly to 1D NTG ratio.

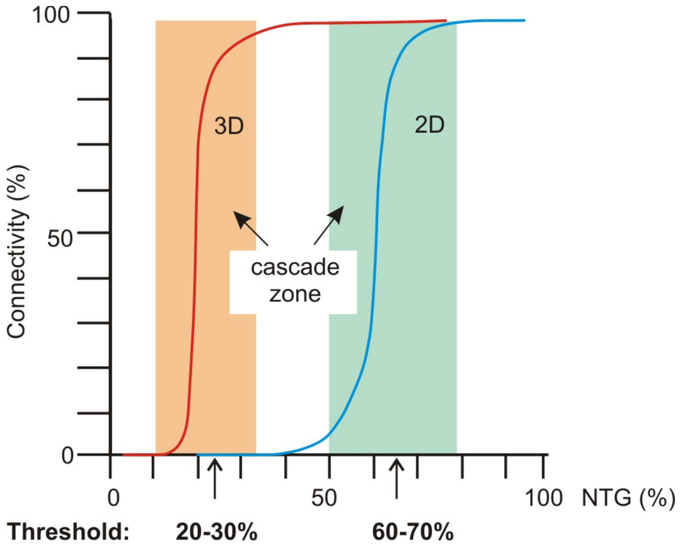

Figure 11.7. Correlation between NTG ratio and 2D / 3D reservoir-to-well connectivity. The cascade zones show zone of rapid increase of reservoir connectivity with small increase in NTG ratio (modified from Larue and Hovadik, 2006).

The NTG ratio in this research is estimated in 1D stratigraphic logs and in 2D photo panels in every outcrop including all sandstone bodies (NTGall) or including channel sandstone bodies of Type 1 and 2 but excluding Type 3 and subtype 1/3 overbank sandstone bodies (NTGmain). The latter scenario is considered because of the possibility of bypass of finer-grained Type 3 and subtype 1/3 sandstone bodies by fluids due to their poorer reservoir quality (Section 11.2.3). The results of NTG ratio estimations are presented in the Table 11.1.

If we assume, for simplification, that sandstone bodies in the studied successions have reservoir properties higher than imaginary cut-offs, reservoir-to-well connectivity of the reservoir can be demonstrated using estimated NTG ratios and Fig. 11.7. The relatively proximal Monźon outcrop shows 1D NTG ratio between 39 % and 66 % and 2D NTG ratio between 30 % and 36 % (Table 11.1), and this corresponds to a high 3D reservoir-to-well connectivity in both cases (> 50 %, ~ 100 %) (Fig. 11.7). The relatively medial Castelflorite outcrop gives already lower 1D and 2D NTG ratios, from 25 % to 43 % and from 13 % to 24 %, respectively. The net-to-gross ratio below 0.20 indicates that less than a half of the reservoir is connected to well in 3D volume (≤ 50 %) (Fig. 11.7). The NTG ratios for the distal succession at Alcolea outcrop are the lowest and vary between 8 % and 20 % in 1D logs and between 1 % and 12 % in 2D panels. Less than 10 % of the reservoir volume or none is connected in this part of the succession (< 10 %) (Fig. 11.7).

The average 1D NTG for the Huesca DFS succession was estimated to be from 26 % to 45 %. Previously the Huesca DFS succession has been also characterised as low-net-to-gross fluvial succession with 2D NTG ratio of 40 % in its relatively proximal DFS deposits outcrop (Piracés / La Serreta outcrop, Fig. 3.1) by Donselaar and Schmidt (2005) and Donselaar and Overeem (2008).

	1D		**2D**		**2D**
Outcrop	**NTGmain,%**	**NTGall,%**	**NTGmain,%**	**NTGall,%**	**?**
Huesca (mean)	**25.8**	**44.5**			
Monźon	39.27	65.95	30.07	35.63	40 % (Donselaar and Overeem, 2008)
Castelflorite	25.38	42.50	13.30	23.93	
Alcolea	7.98	19.95	1.26	11.69	
Salt Wash (mean)	**63.78**	**72.25**			
Bullfrog	77.44	87.14	83.21	86.05	80 % (Robinson and McCabe, 1997)
Slick Rock	56.10	58.00	58.09	58.09	
Little Park	51.20	61.80	35.80	41.61	

Table 11.1. Estimated NTG ratios in 1D stratigraphic logs and 2D photo panels in the Huesca and Salt Wash DFS successions. Note the difference between NTGmain and NTGall ratios that reflects influence of thin sheet-like sandstone bodies on the NTG ratio of the potential reservoirs.

The NTG ratio in the Salt Wash DFS succession is not as variable as in the Huesca succession. The relatively proximal Bullfrog outcrop (more proximal than the Monźon outcrop of the Huesca DFS succession) is characterised by 1D NTG ratio between 77 % and 87 % and 2D NTG ratio between 83 % and 86 %. The Slick Rock medial outcrop shows values around 56 % to 58 % for both 1D and 2D NTG ratios. The Slick Rock NTG ratios are affected by large non-exposure intervals and therefore should be interpreted with caution. The Salt Wash succession in its distal part at Little Park outcrop shows the lowest 1D and 2D NTG ratios, from 51 % to 62 % and from 36 % to 42 %, respectively. The values of NTG ratio in the Salt Wash DFS succession indicate very high 3D reservoir-to-well connectivity in all parts of the Salt Wash DFS succession (> 50 %) (Fig. 11.7). The average 1D NTG ratio in the Salt Wash succession varies between 63 % and 72 %. Robinson and McCabe (1997) reported 2D NTG ratio > 80 % for the relatively proximal outcrops of the proximal Salt Wash succession in the Henry Mountains region. Robinson and McCabe (1997) showed that geological model created based on the data from the Salt Wash succession acts as a homogeneous reservoir during the flow simulation.

As expected, the NTG ratio values in the studied DFS successions decrease downstream with decrease in sandstone body proportion (chapters 6 and 7). The NTG ratios obtained from 1D stratigraphic logs are higher than the ones estimated from 2D panels because they capture small-scale sandstone bodies within the successions which cannot be resolved in the 2D outcrop panels. Both estimates together give an approximate range of the NTG ratios within the successions.

As discussed in Section 11.2.3, thin overbank sheet-like sandstone bodies of subtypes 3/1 and 3/2 are commonly connected with larger channel sandstone bodies (Fig. 5.10, Fig. 11.5, A2). Calculated NTG ratios demonstrate that Type 3 sandstone bodies could increase NTG ratio of the reservoir (compare NTGall and NTGmain in Table 11.1) and therefore increase connected reservoir volume (Fig. 11.6) (see also Nichols, 1987; Donselaar and Overeem, 2008). Larue and Novadik (2006) have also found that floodplain sandy facies improve reservoir-to-well connectivity.

Sandstone bodies of Type 3 contribute considerably to the NTGall ratio in the Huesca DFS succession. The NTGall ratio is higher than the NTGmain ratio by 15 % to 25 % in 1D logs and by 5 % to 10 % in 2D panels (Table 11.1). The NTGall and NTGmain ratios of the Salt Wash succession differ much less by 2 % to 10 % in 1D logs and by 0 % to 5 % in 2D panels. The large difference between NTGmain and NTGall ratios in the Huesca DFS succession is related to the high proportion of Type 3 sandstone bodies in the succession which is in general dominated by heterolithic floodplain deposits in all studied parts of the DFS. In contrast the Salt Wash succession is dominated by sandstone bodies and therefore the effect is smaller. The maximum difference between NTGall and NTGmain ratios is observed in the distal part of the Salt Wash DFS succession due to an increase in the proportion of Type 3 sandstone bodies in this outcrop and decrease in the proportion of Type 2 sandstone bodies which dominate the two other outcrops. Note that the most proximal deposits of the Huesca DFS, which have not been studied in this project, could have also had NTG ratios similar to the relatively proximal and medial Salt Wash deposits.

A fluid preserved in sandstone bodies with poorer reservoir quality (Type 3 sandstone bodies), however, may be bypassed due to high contrast in reservoir properties (Barthel, 1991) between channel and overbank sandstone bodies. Thus, finer-grained sheet-like sandstone bodies most likely improve reservoir behaviour only for light fluids, such as gas, where the contrast in reservoir properties does not create baffles for fluid flow. The presence of thin sheet-like overbank sandstone bodies in the succession therefore has important implications for reservoir behaviour and should be considered.

In summary, the Huesca DFS can form a less connected, low-NTG, tortuous reservoir due to the presence of abundant heterolithic barriers which were probably determined by the high degree of aggradation and preservation of overbank deposits in endorheic Ebro Basin (Fisher and Nichols, 2013). The unstudied most proximal area of the Huesca DFS could, however, form homogeneous reservoir body due to higher degree of reworking caused by lower accommodation space relative to sediment supply in this area in comparison with more distal areas (Weissmann et al., 2013 in press). Thin overbank sandstone bodies in the floodplain intervals in the Huesca DFS succession may provide additional reservoir volume and connectedness for light hydrocarbon reservoirs. On the other hand, the Salt Wash DFS can form well connected, high-NTG, less heterogeneous reservoir as a consequence of a high degree of reworking of heterolithic floodplain deposits (barriers) by channels in a lower accommodation relative to sediment supply setting in both relatively proximal and medial areas of the DFS (Weissmann et al., 2013 in press). The deposits of both DFSs show a downstream trend in reservoir properties. In addition, similar smaller-scale heterogeneities within individual sandstone bodies in both DFS successions will reduce quality of analogous reservoirs and affect their performance.

The above discussion is based on the 1D and 2D estimations of NTG ratio and outcrop observations and contains only hypothetical interpretations. Larue and Novadik (2006) listed a number of factors that could affect NTG ratio and sandstone body connectivity of channelized reservoirs. They include such characteristics as sandstone body W / T ratio, the presence of continuous and discontinuous barriers and baffles, aggradation rate during deposition, scale and type of sandstone body stacking (e.g. compensational stacking). A numerical modelling approach is used in the next Chapter 12 to investigate the sensitivity of the large-scale reservoir properties (NTG ratio and sandstone body connectivity) to a range of variable controls on the DFS architecture including degree of floodplain aggradation relative to degree of channel incision and lateral erosion, and channel avulsion mechanism (sandstone body stacking patterns).

11.4 Conclusions

The deposits of the Huesca and Salt Wash DFSs are very heterogeneous. The heterogeneity is caused by variability of depositional processes and localised diagenetic alterations. Four scales of heterogeneity could be distinguished within the studied successions.

The estimated 2D porosity of the DFS sandstones varies independently from the variation in grain size or facies. The pore-scale heterogeneities are defined by poor sorting of the sandstones and non-uniform distribution of matrix and cement within their pore space (Fig. 11.1, A) and could affect distribution of filtration properties in the DFS sandstones.

The heterogeneities at sedimentary structure scale include continuous and discontinuous mud drapes and mudclast horizons at the bed set boundaries and variations in the grain size and sedimentary structure type within sandstone bodies (Fig. 11.1, B). These heterogeneities are related to changes in flow regime in DFS channels. The variation in grain size could create a contrast in reservoir properties while mud drapes and mudclast horizons could create baffles for fluid flow. The structure-scale heterogeneities may form a tortuous path for the fluid flow within a reservoir body and affect breakthrough time and sweep efficiency of the reservoir, especially for the heavy oil reservoirs. A small effect on reservoir performance could be also caused by syn-depositional and post-depositional processes such as bioturbation and soft sediment deformation.

Amalgamated sandstone bodies within the DFS successions include discontinuous lenses of heterolithic deposits formed in abandoned channel scours, in lateral accretion complexes within channels, and on the floodplain (Fig. 11.5, A). The sandstone body scale heterogeneity is related to variation in facies within channel deposits and on the DFS as a whole that could be controlled by flow regime in a channel and degree of reworking of floodplain deposits in different DFS areas. A mosaic of deposits with different reservoir qualities is formed as a result. These heterogeneities could reduce NTG ratio of the reservoir and add tortuosity to the fluid path that is already affected by smaller-scale heterogeneities within sandstone bodies. Consequently, reservoir sweep efficiency could be affected and some zones of the reservoir could be bypassed.

System-scale heterogeneities in DFS deposits could be related to vertical, lateral and downstream variations in sandstone body distribution relative to the fine-grained floodplain intervals (Fig. 11.5, B) that could be controlled by external factors and internal organisation of the DFSs. These variations control large-scale variations in NTG ratio and sandstone body connectivity in the DFS reservoirs. In the Huesca and

Salt Wash DFS successions NTG ratio varies from relatively proximal to distal outcrops and laterally within each of them. The NTG ratio measured in 1D section is found not representative of the extremely variable NTG ratio of the entire succession. Large-scale outcrop studies are required to recognise heterogeneity at the system-scale.

The floodplain-dominated Huesca succession is characterised by a lower NTG ratio than the sandstone-body-dominated Salt Wash DFS. Sandstone bodies are well connected only in the relatively proximal part of the Huesca DFS succession and they are vertically isolated in other parts of the succession. Thin sheet-like sandstone bodies of Type 3 contribute considerably to the NTG ratio and sandstone body connectivity of the Huesca potential reservoir; however, fluid type will control their effectiveness as a reservoir. All channel sandstone bodies are connected within relatively proximal and medial parts of the Salt Wash DFS succession. Type 3 sandstone bodies contribute to NTG ratio only in the distal part where they dominate. The Huesca reservoir could be very tortuous while the Salt Wash reservoir could behave as a well-connected high net-to-gross reservoir (Fig. 11.6). The difference in reservoir quality and reservoir connectivity between two DFS successions is related to the difference in the degree of floodplain preservation.

The next Chapter 12 presents a study of sensitivity of the NTG ratio and sandstone body connectivity to a range of variable controls on a stratal architecture. This is undertaken using 2D geometrical model that was created based on the data and observations collected in outcrops of the Huesca and Salt Wash DFS successions. This modelling exercise could also help to investigate the causes of the difference in large-scale reservoir architecture and reservoir properties between the Huesca and Salt Wash DFS successions.

As was shown above, heterogeneities in the DFS deposits at all scales could affect reservoir properties and reservoir production performance and therefore all of them should be considered during reservoir modelling. Chapter 13 discusses how detailed sedimentological studies of DFS deposit and analysis of their heterogeneity could be implemented in reservoir modelling.

12. Two-dimensional geometric modelling of fluvial architecture

12.1. Introduction

Numerical modelling is widely applied with the aim of better understanding the controls on the architecture of fluvial strata (Bridge and Leeder, 1979; Bridge and Mackey, 1995; Straub et al., 2009, Deutsch and Tran, 2002), specifically channel behaviour (Jerolmack and Paola, 2007; Bridge and Mackey, 1995), overbank depositional processes (Fisher et al., 2007(b)) and also the more general behaviour of fluvial system (Clevis et al., 2006; Reitz et al., 2007; Dalman and Weltje, 2008; Krassenberg and Bridge, 2008). Recent geometric rule-based models published by Straub et al. (2009) and Wang et al. (2011) provided an initial tool to determine the scale of internal organization of fluvial systems controlled by autogenic factors. The results from all of these previous numerical models have inspired the modelling exercise presented in this chapter.

The main objective of this study is to document the formulation and application of a simple geometrical model to help understand the relationship between the main characteristics of the DFS deposits and the factors which control deposition. The model has also been applied to try to understand the reasons for the differences in architecture observed between the Huesca and Salt Wash DFS successions documented in chapters 4-7, 10 and 11. The input parameters of this numerical model are proxies of the factors that are usually thought to control architecture of fluvial deposits: sediment supply, water discharge, degree of lateral migration of a channel and grain size of sediment load. The effects of variable input parameters and different avulsion and floodplain aggradation algorithms on the main large-scale reservoir qualities of the succession, such as NTG ratio and sandstone body connectivity, which have been discussed based on outcrop data in Chapter 11, will be also investigated.

A geometric modelling approach was chosen not only because of its simplicity, but also because it does not require knowledge of complex hydraulic processes, sediment transport and deposition processes and uses only geometric input data that could be measured from the outcrops or outcrop analogues. The model is two-dimensional (2D) although there are drawbacks to this approach. The limitations of the 2D modelling and importance of 3D modelling, especially for DFS deposits, are discussed later in this chapter.

Although a prototype 3D model was constructed it could not be completed within given the time frame of this PhD project which had a strong focuse on the field-based outcrop studies: there was therefore insufficient time to develop the necessary 3D algorithms. The 2D model is original to this thesis and was coded in Matlab by the author. Previously developed programming codes were not used but the model algorithms developed here were influenced by and incorporate work by Bridge and Leeder (1978), Bridge and Mackey (1993), Mackey and Bridge (1995), Karssenberg et al. (2001), Karssenberg and Bridge (2008), Jerolmack and Paola (2007), Fisher et al. (2007(b)), Clevis et al. (2007), Straub et al. (2009) and Wang et al. (2011).

12.2. Elements and input parameters of the 2D model

Fluvial strata in the model are created by populating the model domain with geometric objects representing channel and floodplain deposits (Fig. 12.1, A-C). Model dimensions, object geometry, input parameters and how objects are distributed will be described in this section. Variables corresponding to model input parameters are highlighted in *italics* throughout this chapter and are summarised in Table 12.1.

12.2.1. Model dimensions, boundaries and grid

The model uses a simple Cartesian grid with vertical scale representing stratigraphic thickness of DFS deposits or elevation (m) and horizontal scale representing lateral extent of the DFS deposits perpendicular to the average palaeocurrent direction (number of cells). Each model run is 2500 cells wide (*modelWidth*) with a cell horizontal dimension of 20 m (*cellSize*), so the total horizontal extent of the model is 50 km. This grid dimension represents a substantial part of a small DFS. For example, the Huesca DFS extends laterally for approximately 100 km (Fig. 2.2).

Wrapping boundary conditions are applied to the algorithm for finding the position of the channel element after avulsion, while truncating boundary conditions are used when the channel-floodplain element is placed ("deposited"), meaning that the channel-floodplain elements can be truncated by the model boundary (e.g. Fig. 12.2).

12.2.2. Initial floodplain topography

The initial floodplain topography is flat and horizontal. Prior to the first time step small uniformly distributed random perturbations between 0 and 0.01 m are applied to this surface (see also Jerolmak and Paola, 2001).

12.2.3. Subsidence

Subsidence is not explicitly modelled in the model but is assumed to be in balance with average aggradation across the basin at every time step (Fig. 12.7, Straub et al., 2009). No differential subsidence occurs in the model.

12.2.4. Channel element

Channel deposits are modelled as a number of rectangular elements each with a certain thickness (*maxThickness*) and width (*channelWidth*) (cf. rectangles in Bridge and Leeder, 1978; triangles in Straub et al., 2009; Wang et al., 2011) (Fig. 12.1, A). The channel sandstone body thickness (*maxThickness*) is a sum of channel erosion depth (*erosionDepth)* and channel aggradation thickness *(chAggradThick)*. The channel aggradation thickness *(chAggradThick)* represents the elevation of the channel ridge above the floodplain or thickness of channel “wings”, while erosion depth determines the thickness of channel element below the floodplain level (Fig. 12.1, A).

Each rectangle represents all the channel fill deposits formed by the channel including sand bars and abandoned channel scours filled with heterolithic overbank deposits (Fig.12.1, D). The channel width therefore corresponds to the width of a preserved channel sandstone body that could be formed as by a laterally stable or a laterally unstable channel. A high *channelWidth* parameter value implicitly simulates sandstone body formed by a laterally unstable channel.

12.2.5. Floodplain element

Jerolmack and Paola (2001) showed that floodplain topography affects channel paths on the floodplain and, consequently, distribution of channel facies. In the 2D model floodplain aggradation can be calculated using one of four different algorithms including “uniform” and “depth-dependent” floodplain aggradation based on work by Jerolmack and Paola (2001), floodplain aggradation that decreases exponentially away from a channel (Bridge and Mackey, 1995; Tornqvist and Bridge, 2002; Karssenberg and Bridge, 2008) and floodplain aggradation calculated as a combination of exponential and depth-dependent cases.

Floodplain aggradation is calculated at every time step after a channel element is positioned (Fig.12.1, C). Overbank flooding events are assumed to flood the whole model area to the elevation of the top of the channel element (see also Jerolmack and Paola, 2001). The supply of overbank fine-grained sediment is assumed to be unlimited (see also Jerolmack and Paola, 2001). Floodplain deposition is allowed only where the floodplain elevation is lower that the channel elevation and in cells which do not belong to the channel.

To simplify the model, sediment compaction (Bridge and Leeder, 1979; Mackey and Bridge, 1995) is not included (see also Lyons, 2004). It is assumed that differential burial compaction does not greatly affect the geometries generated by the model. There is no clear evidence of compaction in the outcrops of the Huesca or Salt Wash DFS deposits.

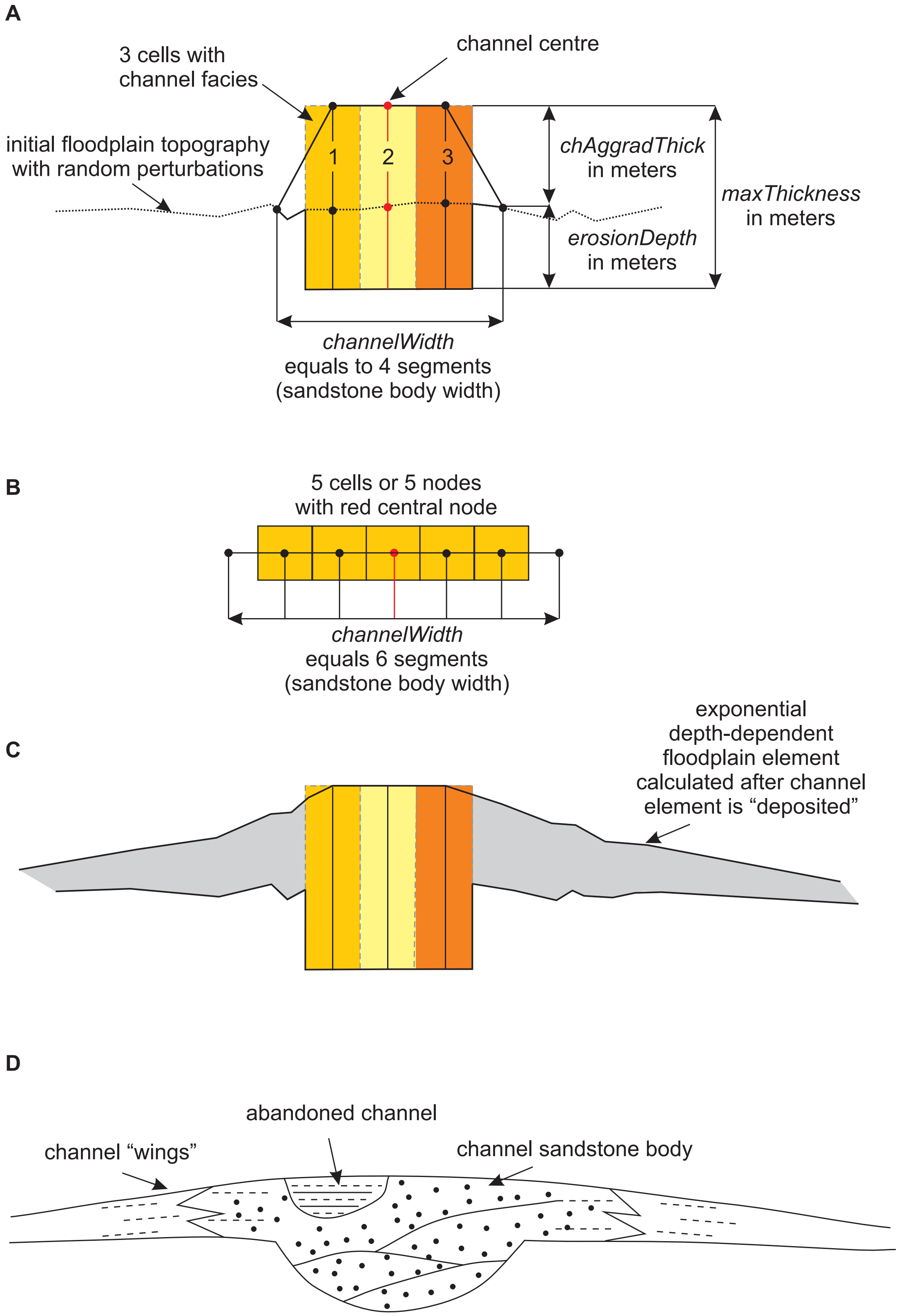

Figure 12.1. Schematic diagram explaining characteristics of channel element (A), relationship between channel width and number of cells/nodes assigned to channel facies (B), calculation of floodplain element after channel element (C). Diagram D is a schematic representation of deposit architecture that is represented by object element in the model.

Uniform floodplain aggradation

For the uniform floodplain algorithm (*floodMethod = 4*) aggradation rate is the same in every point on the floodplain, except the channel element location, independent of floodplain topography: *UniformFloodplainAggradation* (t, x) = constant.

In the case of uniform floodplain aggradation floodplain topography is preserved through time. The uniform floodplain aggradation represents a fraction of the model subsidence.

Depth-dependent floodplain aggradation

The depth-dependent floodplain aggradation algorithm (*floodMethod = 3*) takes into account concentration of the suspended sediment in the body of water during flooding. Uniform floodplain aggradation rate is corrected according to the depth of floodwater column (Jerolmack and Paola, 2001). The higher the flood water thickness or the deeper the depression on the floodplain, the more floodplain sediments will be deposited. This has the effect of smoothing floodplain topography and reducing relief over time by preferential filling of topographic lows:

DepthDependFloodplainAggradation (t, x) = *UniformFloodplainAggradation* (t, x) + *UniformFloodplainAggradation* (t, x) * *floodDepth* (t, x) / *chAggradThick,*

where *floodDepth* (t, x) is flood depth equal to the elevation difference between the top of the channel element edge and elevation at x on the floodplain at the previous time step, *chAggradThick* equals *maxThickness* minus *erosionDepth* and is the elevation of channel element edge above the floodplain.

Exponentially decreasing floodplain aggradation

An exponential decrease in floodplain aggradation with horizontal distance away from a channel (*floodMethod = 2*) is modelled using the formulae from Tornqvist and Bridge (2002) and Karssenberg and Bridge (2008):

ExponentialFloodplainAggradation (t, x) = *chAggradThick* * c + *chAggradThick* * (1 - c) * exp (- d (t, x) / *aggradExp)*,

where *c* is a theoretical aggradation rate at infinite distance from the channel that equals zero for all models in this study, *d (t, x)* is a distance of the point x on the floodplain from channel edge at time step t, and *aggradExp* is an aggradation exponent that represents the rate with which the thickness of floodplain deposits decreases away from the channel element edge (Section 12.2.7).

Exponentially decreasing depth-dependent floodplain aggradation

The most complex method of flood plain aggradation used here combines depth-dependent floodplain aggradation with exponential decay of aggradation rate away from the current channel (*floodMethod = 1*) so that:

DepthDependFloodplainAggradation (t, x) = *ExponentialFloodplainAggradation* (t, x) * *floodDepth* (t, x) / *chAggradThick*

Exponential depth-dependent floodplain aggradation algorithm is used for all model experiments except those experiments where the effects of various floodplain algorithms are investigated.

12.2.6. Channel migration and avulsion

Two algorithms are used to model channel avulsion. 1) The channel is relocated into the lowest elevation point on current floodplain horizon (*chMigrMethod* = 1) assuming that avulsion occurred upstream and flow went to the lowest point and constructed a channel at that point. 2) The channel avulses randomly to any point on the floodplain irrespective of elevation (*chMigrMethod* = 2). For every channel avulsion algorithm an additional channel avulsion rule can be applied where the channel avulses every *n*-th time step after it has randomly locally avulsed for (*n - 1*) steps within certain migration distance (*migration*) (Straub et al., 2009; Wang et al., 2011) (Fig. 12.2). Variable *n* in this case could represent the frequency of major avulsions.

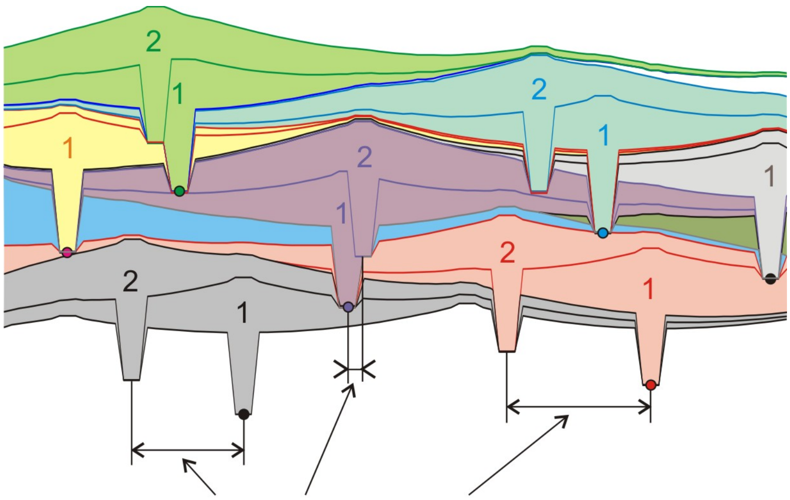

Position of channel(2) = Position of channel(1) + **migration**;
migration = *1* + *(migrationDistance-1)* * ***rand()*** - *0.5* * *migrationDistance*

Figure 12.2. Example of channel element avulsion with frequency of major avulsions (*n*) equal to two that includes one local channel avulsion between major channel avulsions. At the first step channel element avulses randomly within certain distance (*migration*) and at the second step it avulses to the minimum on the current floodplain horizon.

A channel element is positioned at every time step. The horizons of older strata are clipped to account for erosion by the channel base. To do this, elevation at every point of the channel base is compared with elevation of horizons deposited before this. Any points where elevation of those horizons is higher than the base of the channel, it is replaced by the current base-channel elevation (see also Martin, 2007; Straub et al., 2009).

12.2.7. Input parameters

The input parameters and ranges of their values are discussed in this section. The ranges are selected based on values determined from outcrops of the Huesca and Salt Wash DFS successions and on values provided in published studies of other modern and ancient fluvial systems. The increment of variation in input parameters within the set ranges are chosen so that the number of sensitivity model runs equals 20, except where it is specified otherwise.

Time steps

Each model is run for 500 time steps (*TimeSteps*). If the avulsion frequency is *n,* the number of avulsions (*N*) in the model run equals to rounded *TimeSteps / n.*

Channel aggradation thickness

Thickness of channel "wings" observed in the Huesca and Salt Wash DFS strata vary from 0.3 to 4 m (chapters 4-5). The *chAggradThick* variable (Fig. 12.1, A), was set to range from 0.5 to 4.3 m with 0.2 m increments to reflect this range observed in outcrops.

Channel erosion depth

Incision depth observed for the channel sandstone bodies in the Huesca and Salt Wash DFS succession ranges from 1 to 10 m (chapters 5-7). Erosion depths less than 1 m are characteristic for the sandstone sheets formed by poorly-confined flows that do not form confined channels and therefore are not taken into account. Correspondingly, the variable *erosionDepth* (Fig. 12.1, A) in the model is set to vary from 1 to 10.5 m with a 0.5 m increment. Taking into account ranges of values for channel aggradation thickness and channel erosion depth, channel thickness changes from a minimum of 1.5 m to a maximum of 15 m, that is similar to the range observed in the outcrops.

Channel sandstone body width

The values of the channel sandstone body width were chosen in the range from 50 to approximately 1000 m based on the observed widths of major sandstone bodies in the

Huesca and Salt Wash DFS successions (chapters 5-7). However, the maximum value of sandstone body width is difficult to determine with confidence due to amalgamation of the sandstone bodies and the limited lateral extent of exposures. The channel sandstone body width in the model is represented by a number of segments between channel element nodes and could vary from a minimum of 4 segments with the step of 2 or another even number so that the central node of the channel can be found (Fig. 12.1, A-B). The channel facies are assigned to the cells which correspond to nodes of the channel element. A channel width of 4 segments equals to 3 cells and, consequently, to 60 m. The variable *channelWidth* in the model is varied from 4 to 42 segments or from 60 to 820 m, respectively, with increment of 2 cells (40 m).

Floodplain aggradation exponent

The value for the floodplain aggradation exponent is taken to be equal 900 m (cf. Karssenberg and Bridge, 2008) based on observations and numerical modelling from Fisher et al. (2007(b)). The authors found that thickness of splay deposits with grain size up to 3.3 ϕ decreases from 0.2 m to 0.02 m within 2000 m.

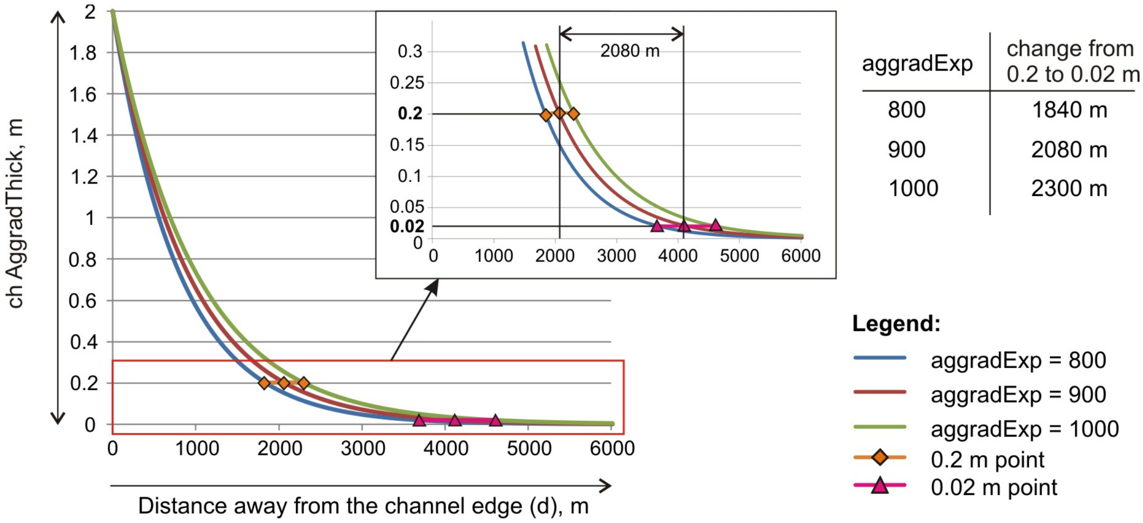

aggradExp	change from 0.2 to 0.02 m
800	1840 m
900	2080 m
1000	2300 m

Figure 12.3. Curve calculated using exponential floodplain aggradation formulae for the channel element with aggradation thickness (*chAggradThick*) equal to 2 m. The figure demonstrates that decrease in floodplain thickness from 0.2 m to 0.02 m occurs within 2000 m (Fisher et al., 2007(b)) for the aggradation exponent (*aggradExp*) equal to 900 m.

Analysis of the exponential floodplain aggradation formulae (Section 12.2.5) for different channel aggradation thicknesses (*chAggradThick*) showed that the thickness of floodplain deposits in the model decreases from 0.2 to 0.02 m within 2000 m for an aggradation exponent (*aggradExp*) equal to 900 m (Fig. 12.3). The variable *aggradExp* is, therefore, assigned to be varied around 900 m from 550 to 1500 m with an increment of 50 m per model run.

Avulsion frequency

Avulsion frequency (*n*) is the least constrained parameter in the model because the time interval between avulsions is unknown. For the experiments in this chapter an avulsion frequency (*n*) equal to 1 and 3 are used. If, for instance, every time step (time needed for deposition of one channel element and floodplain associated with it) represents 500 years, the inter-avulsion period would be equal to 500 and 1500 years respectively.

Inter-avulsion periods have been reviewed for different fluvial systems by Stouthamer and Berendsen (2001, Table 2 therein) and have been found to vary from minimum 3 to maximum 4480 years with an average ranging between 13 and 1400 years for different fluvial systems. Kraus and Aslan (1993) have shown that longer periods between major channel avulsions (e.g. 20,000 years) could also exist. The shortest inter-avulsion periods are not taken into account in this model because the time is not sufficient to deposit channel sandstone body and associated floodplain deposits represented in the model with one channel/floodplain element. The high values could be used for the experimental purposes in the future work and could represent inter-avulsion periods of major nodal avulsions or avulsion of DFS lobes (Fig. 12.4).

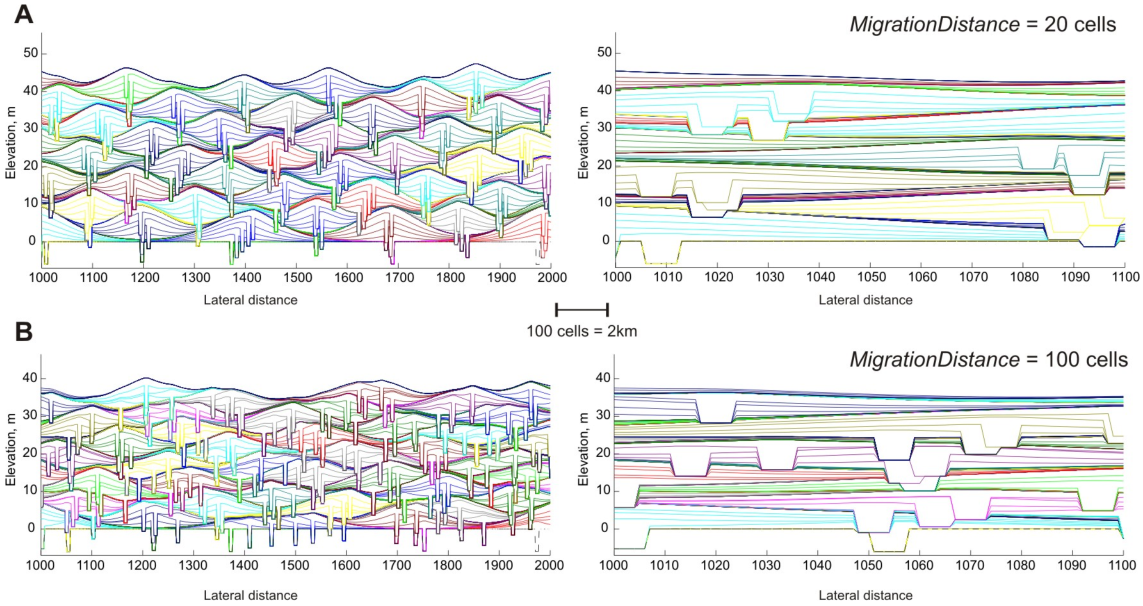

Figure 12.4. Examples of modelled strata with *channelWidth* equal to 8 segments, avulsion frequency n = 5 and *migrationDistance* equal 20 and 100 cells. The diagrams demonstrate contrasting cases with low *migrationDistance* (A) and high *migrationDistance* (B). See explanations in the text.

Migration interval of channel element during local avulsion

The distance of local channel avulsions (*migrationDistance*) between major avulsions is another poorly constrained parameter in the model. During local avulsions the channel element avulses laterally to the left or right from the centre of the previous channel element to a distance which is randomly chosen from the interval between 0 and *migrationDistance* (Fig. 12.2). The following migration distances have been used: 1) from 0 to (*channelWidth* + 20) cells; 2) from 0 to (*channelWidth* + 40) cells and 3) from 0 to (*channelWidth* + 100) cells.

If *migrationDistance* is small, this rule accounts for a low probability of avulsion at short time scales when the channel migrates within the channel belt (local avulsions) (Straub et al., 2009, Wang et al., 2011) and creates closely-spaced or amalgamated channel sandstone bodies (Fig. 12.4, A). If *migrationDistance* is large this algorithm creates depositional lobes within which channels avulse randomly and sandstone bodies may or may not be connected (Fig. 12.4, B). Nodal avulsion relocates the depositional lobe to a new place every *n*-th step.

12.3. Output parameters of the 2D model

The results of every 2D model run are analysed to calculate several output parameters which are explained in this section.

12.3.1. Net-to-gross (NTG) ratio

To calculate NTG ratio (*NTG2D*) the cross-section of layered modelled strata, where the thickness between each chronostratigraphic horizon is variable, is converted to a regular grid of cells with horizontal number of cells equal to the *modelWidth* (2500 cells) and vertical number of cells is approximately equal to the thickness of modelled strata divided by *cellHeight* (0.1 m). Thickness of cells is recorded in the following way: 1) if the thickness of the layer can be divided by the *cellHeight* without a remainder, then the cell thicknesses are set to be equal to the thickness of the layer divided by *cellHeight*; 2) if the thickness of the layer cannot be divided by *cellHeight* without a remainder, one cell is added to the cell number with a thickness equal to the remaining thickness of the layer after division by *cellHeight*, 3) if the thickness of the layer is less than the *cellHeight* one cell is added with a thickness equal to the thickness of this layer.

Once the model has been “gridded” the area of all cells containing the channel facies is calculated and its percentage as a proportion of the gross cross-sectional area of the model is output as NTG ratio. The NTG ratios in outcrops (Chapter 3) and in the model are calculated using a similar approach and therefore can be compared. However, the NTG ratio calculated from the modelled strata does not include sandstone bodies preserved as part of the floodplain deposits, Type 3 sandstone bodies formed by splays (chapters 5-7). The NTG ratio calculated from the model corresponds most closely to the percentage of Type 1 and Type 2 sandstone bodies calculated form 2D outcrop photo panels (Tables 6.1 and 7.1, or see *NTGmain* in Table 11.1).

12.3.2. Sandstone body connectivity

To calculate the sandstone body connectivity in the modelled strata, the succession is represented as a grid of uniform area cells with channel and floodplain facies. To convert modelled strata into grid, the thickness of each layer is divided by the *cellHeight* (0.1 m) and rounded. The horizontal dimension of the cells is the same as described in the previous section.

Channel cells are checked to see if they connect to other channel cells with their sides, and if they do they are counted. This is repeated for every individual connected sandstone body found in the modelled strata. The result of the calculation is a vector that contains the number of connected cells within every individual connected sandstone body in the model (*Connect*). The number of cells counted in this way is representative of the area of connected sandstone bodies. The number of individual connected bodies is also counted (*NumOfIslands*). In the following discussion the number of connected sandstone bodies in the model strata (*NumOfIslands*) is used as a metric of connectivity (Fig. 12.5, A-B). The smaller the number of individual connected sandstone bodies, the higher the connectivity.

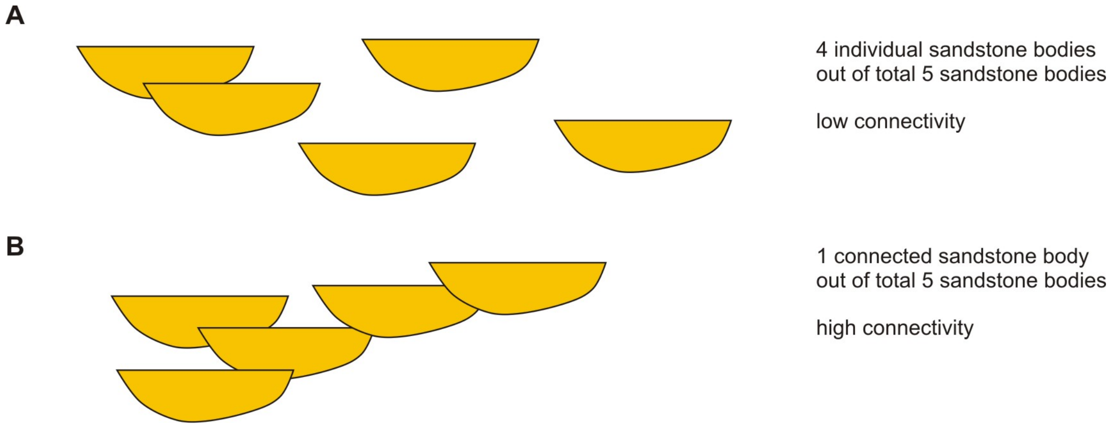

Figure 12.5. Definition of the connectivity metric. The higher the number of individual sandstone bodies (out of the total number of deposited sandstone bodies in the model), the lower the connectivity. The total number of deposited sandstone bodies in every model experiment is 499 which equals *TimeSteps* - 1.

Note that the gridding algorithm used to construct the facies map for connectivity calculation creates the grid that is only an approximation of the modelled strata. This approximation has consequences for the connectivity calculation because layers thinner than half of the cell height in the model are omitted in the grid. This results in overestimation of connectivity, especially vertical connectivity.

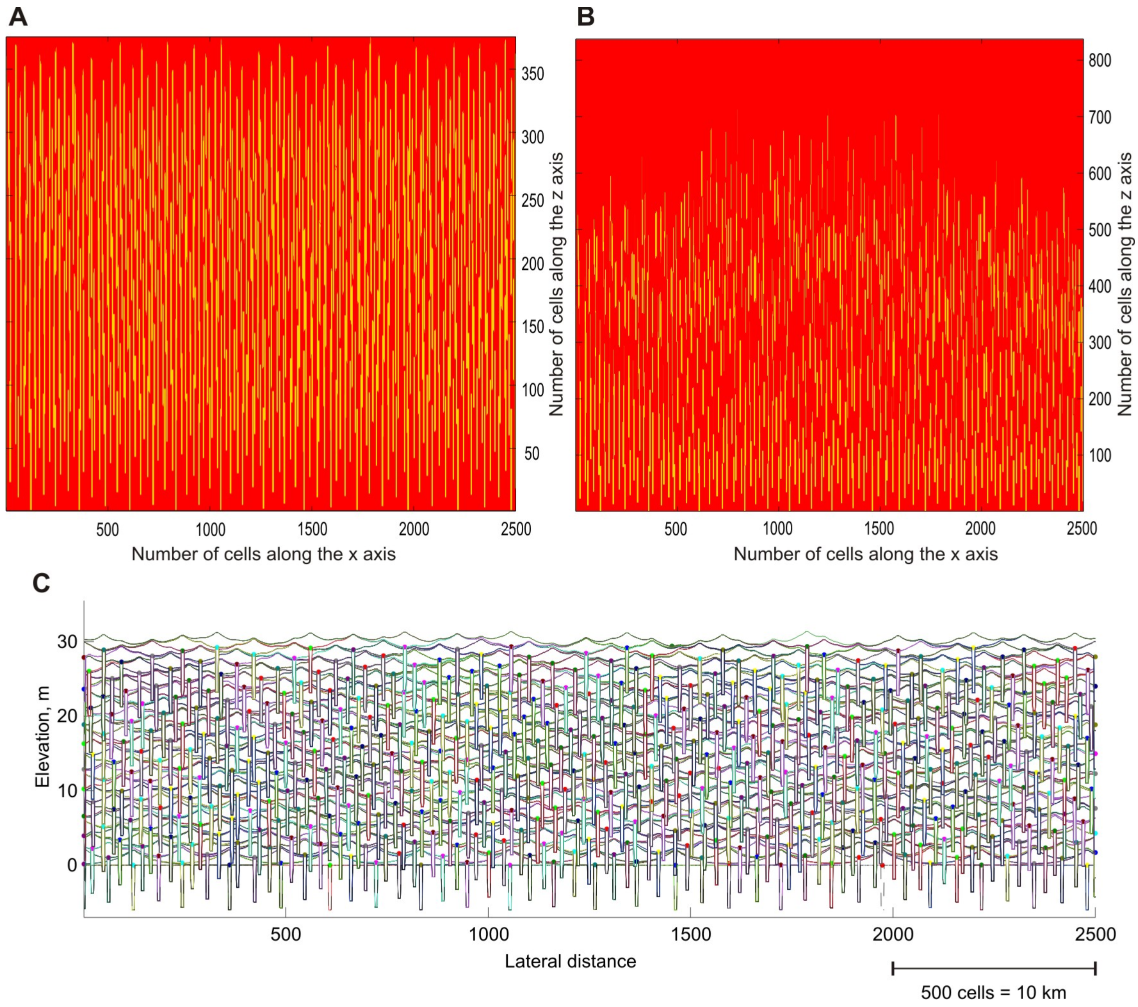

Figure 12.6. Two gridding algorithms for connectivity calculation. Light yellow parallelograms represent cells of channel facies while red background surrounding them represents cells of floodplain facies. A – grid where cells are of the same height (0.1 m) and their number is rounded when calculated from the layer thickness (Section 12.3.2). B – grid where cells are of the same height but the number of cells is calculated including the thinnest of them (Section 12.3.1). C - the modelled strata that has been converted to the facies grid A and B. Compare A and C to see that the current gridding algorithm represents channel distribution reasonably in contrast to the algorithm B.

The gridding algorithm used for NTG ratio calculations (Section 12.3.1) accounts for vertical compartmentalisation more accurately than this method because it includes even the thinnest layers that act as barriers between sandstone bodies. However, in the current algorithm of connectivity calculation the number of cells calculated using improved gridding algorithm could not be used. This is because the cells are assigned the same cell height and this leads to a vertical shift of sandstone bodies or their parts within the grid producing unrealistic strata due to exaggerated thickness of floodplain interlayers (Fig. 12.6, compare B and C).

The simplified algorithm (Section 12.3.2) reproduces channel positions relative to each other more realistically than the gridding method used for NTG ratio calculations (Section 12.3.1) (Fig. 12.6, compare grids A and B with modelled strata C). The simplified algorithm gives a reasonable approximation of the connectivity for the various distributions of channel bodies encountered in the experiments run in this work. For example, it can distinguish between cases with low connectivity (315 bodies) due to high floodplain aggradation and cases with high connectivity (1 body) due to high degree of reworking (Section 12.7, Fig. 12.11 and 12.18). Alternatively, a new algorithm of connectivity calculation that does not include gridding could be developed in the future.

12.3.3. Distance between avulsion positions

In each model run the coordinates of channel element centres after their avulsion are recorded. From these data the horizontal distances (m) between avulsion positions through time are calculated and the mean distance between avulsion positions (*MeanAvulDist)* in the model is found. The distance between avulsion positions can be plotted for every time step and displayed in a cross section to demonstrate its variation with time and spatial distribution (e.g. Fig. 12.11, D).

12.3.4. Distance between channel centres

The coordinates of channel element centres at every time step are also preserved and the distance to the centre of the closest channel (*minDist*) and mean distance to the centres of other channels in the model (*meanDist*) are calculated for the channel at each time step. Mean, standard deviation, maximum and minimum of the calculated distances are output. The mean distances could be plotted for the every time step and their frequency distributions can be output for comparison (e.g. Fig. 12.11, C).

12.3.5. Calculation of spatial variability of sedimentation to subsidence ratio

The spatial variability of sedimentation to subsidence ratio has been discussed by Sheets et al. (2002), Lyons (2004), Straub et al. (2009) and Wang et al. (2011). Sheets et al. (2002) stated that at the long time-scales sedimentation and subsidence are nearly in balance because the depositional locus has time to visit every point on the floodplain many times to balance the subsidence. The ratio of sedimentation to subsidence in this case is close to unity (Fig. 12.7, A-B, Time 3). While at the short time-scales local flow processes affect the deposition rather than the subsidence and aggradation to subsidence ratio is higher or lower than unity meaning that sedimentation is localised (Sheets et al., 2002) (Fig. 12.7, A-B, Time 1). Finally, the authors suggested that variance in sedimentation to subsidence ratio measures the degree of effect of subsidence on sedimentation and it decreases with time interval (Sheets et al., 2002) or thickness interval (Lyons, 2004; Straub et al., 2009; Wang et al., 2011). Furthermore Straub et al. (2009) and Wang et al. (2011) explore the time/thickness window that shows when deposition controlled by local autogenic processes changes to deposition that is in balance with subsidence. This has been done in various strata recorded in experiments, outcrops and seismic data. The time/thickness window is called the **stratigraphic integral scale** or **compensation time/thickness scale**.

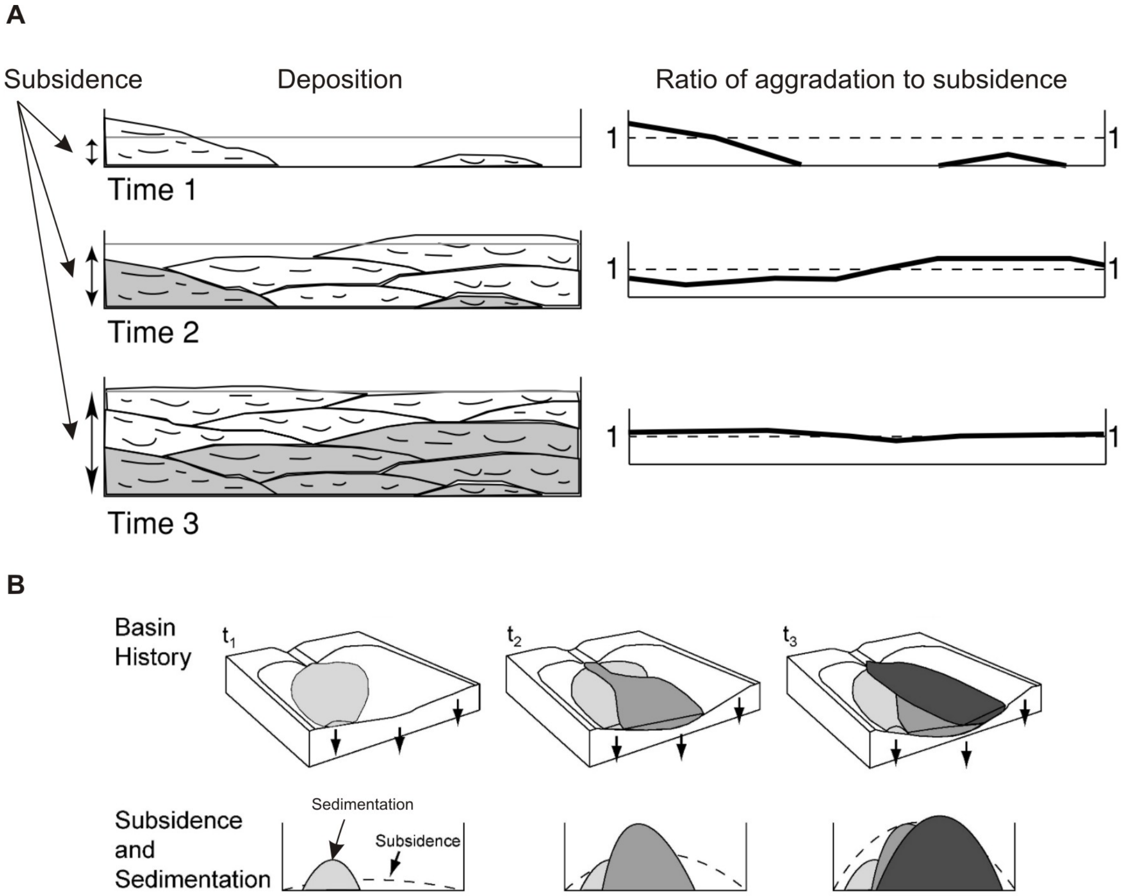

Figure 12.7. Schematic diagrams illustrating deposition by a fluvial system in a basin and corresponding change in value and variability of aggradation to subsidence ratio across the basin with time. The sedimentation is not controlled by subsidence at short time-scales and becomes in balance with subsidence with time. (A - from Sheets et al., 2002 and B - from Lyons, 2004 and Straub et al., 2009).

For every model run the spatial variability of sedimentation to subsidence ratio is calculated between all possible pairs of stratigraphic horizons (Fig. 12.8, A) to determine the stratigraphic integral scale using the method described in Lyons, 2004 and Straub et al., 2009. This method uses thickness to approximate subsidence assuming that there is a balance between subsidence and mean aggradation (Lyons, 2004). The same assumption is accepted for the 2D model in this chapter (Section 12.2.3).

Firstly, normalised subsidence for the modelled stratigraphy is found at each *x* location of the model (*SubsidNorm*) by dividing the thickness between first and the last horizons by the maximum thickness between these two horizons (Fig. 12.8, A).

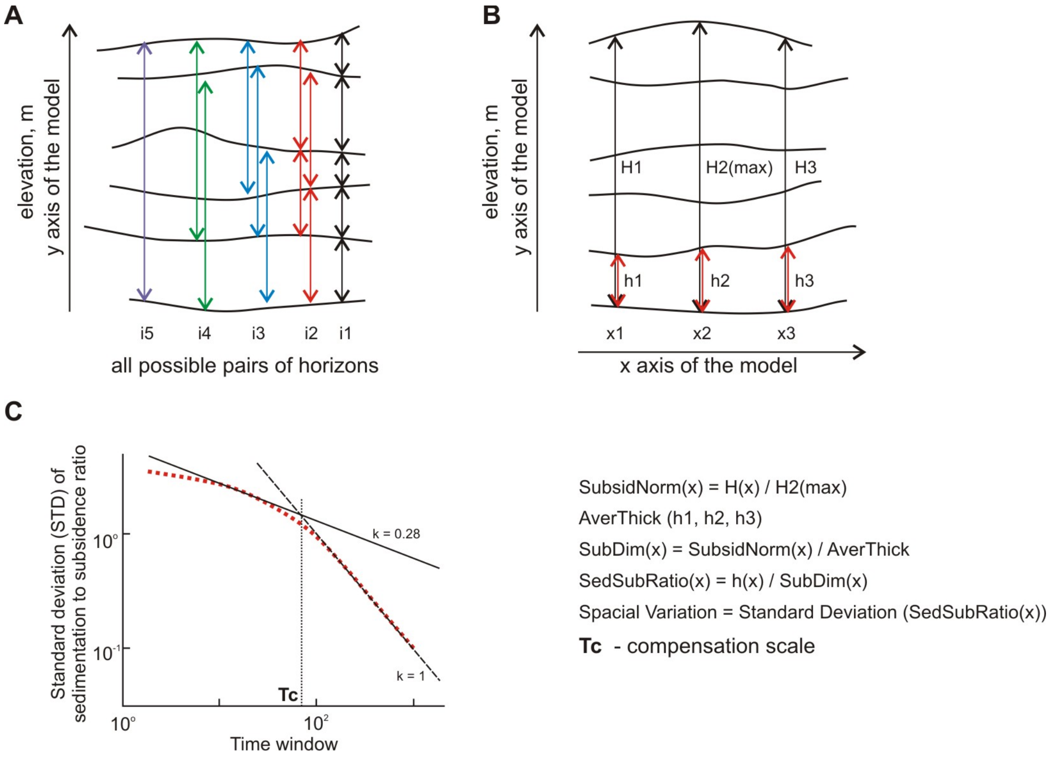

Figure 12.8. Explanation of calculations of compensation thickness scale. A – the variation in sedimentation to subsidence ratio is calculated for all possible combinations of stratigraphic horizons within modelled succession with different window intervals (here, from 1 to 5). B – parameters calculated for every possible pairs of stratigraphic horizons. C – determination of compensation time/thickness scale from Wang et al. (2011).

To calculate the spatial variability metric the following steps are performed for every possible pair of layers (Fig.12.8, B):

- Average thickness (*AverThick*) is calculated for a pair of horizons.
- Normalised subsidence (*SubsidNorm*) at every x location of the model is then multiplied by the average thickness (*AverThick*) which gives dimensional subsidence (*SubDim*).
- The thickness (*Thickness*) between two horizons at each x location is divided by the dimensional subsidence (*SubDim*) at the same location to obtain sedimentation to subsidence ratio (*SedSubRatio*) in every x position of the model.
- Standard deviation of the ratio is computed.

The results are grouped by the thickness window size where mean standard deviation of sedimentation to subsidence ratio and average thickness in the group are found. Mean standard deviation of the ratio is plotted versus average thickness interval (Fig. 12.8, C).

Straub et al. (2009) and Wang et al. (2011) have demonstrated that sedimentation to subsidence ratio decays with increase of time/thickness window as a power-law. They also showed that compensation thickness scale can be found where trend lines (linear regression to log-log data), fit to two segments of the obtained curve, intersect (where one of the lines represents pure compensation with k=1; Fig. 12.8, C;). For some of the modelled successions compensation thickness scale has been found approximately, following this method (Fig. 12.11, E).

12.4. Summary of model assumptions

Following the description of the model set up and input and output parameters, the list of assumptions accepted in the model can be summarised:

- The channel is at the avulsion threshold at each time step;
- Channels avulse in a compensational manner (except in models where the avulsion algorithm effect is investigated);
- When the channel avulses it avulses upstream of the modelled 2D cross section so that it has time to find the easiest flow path into the minimum elevated position on the floodplain (applied to the compensational channel avulsion algorithm, Section 12.2.6);
- All channel sandstone bodies in the strata have the same averaged dimensions;
- During flood events all the model domain is flooded to the level of the channel banks;
- There is unlimited fine-grained sediment supply from the channel during floods;
- Compaction does not greatly affect the geometries generated by the model;
- Subsidence in the model is in balance with the average sedimentation at every time step (Section 12.2.3 and 12.3.5);

12.5. Input parameters of the 2D model and physical processes

The variations in input parameters need to be understood with respect to physical processes represented in the model. The two main processes investigated in the model experiments are floodplain and in-channel aggradation and sediment reworking through channel incision and lateral migration.

12.5.1. Channel/floodplain aggradation thickness

The channel aggradation thickness defines how much a channel aggrades above the initial floodplain elevation (Fig. 12.1, A). At the same time it defines the aggradation of the floodplain that in this model fills the wedge-shape space on both sides of the elevated channel element (Fig. 12.1, C). Therefore, if the aggradation thickness parameter increases, channel and floodplain thickness increase together.

Aggradation in the channel and on the surrounding floodplain is thought to occur when the sediment supply to water discharge (transport capacity) ratio is high (Holbrook et al., 2006; Fisher and Nichols, 2013). The increase in channel aggradation thickness creates a model scenario where an increase in sediment supply relatively to the water discharge causes aggradation of channel floor reducing its transport capacity that in turn causes more frequent flooding events leading to aggradation of floodplain areas (Bryant et al., 1995; Field, 2001; Singerland and Smith, 2004) (see also Chapter 9, Section 9.6.5). A high sediment supply to water discharge ratio, therefore, results in aggradation and preservation of channel and floodplain deposits. Aggradation could be also caused by high subsidence but it is not modelled explicitly in this study.

12.5.2. Erosion depth

Incision of the channel (erosion depth) has been stated to indicate an increase in the water discharge relative to the sediment supply (Holbrook et al., 2006; Fisher and Nichols, 2013) or decrease in base level (Shanley and McCabe, 1994). Incision could be also caused by low subsidence but it is not modelled explicitly in this study. It has been shown that change in base level does not affect upstream reaches of a fluvial system with a low gradient at their termination (Schumm, 1993; Holbrook et al., 2006). The discussion presented previously in Chapter 8, Section 8.3.7 showed that base level probably did not affect the architecture of the Huesca and Salt Wash DFS deposits much.

Therefore, variations in the erosion depth parameter in the model imitates variation in water discharge relative to sediment supply. High erosion depth, representing relatively high water discharge, would result in reworking of channel and floodplain deposits.

12.5.3. Floodplain aggradation exponent

The aggradation exponent parameter defines the distance over which thickness of the floodplain deposits decreases away from the channel edge. This parameter, therefore, controls how much sediment is transported out of the channel within a period between channel avulsions. The amount of sediment transported during a flood can be controlled by a combination of factors such as the length of the channel life/activity between avulsions, availability and supply of fine-grained sediment in a channel (grain size distribution in the sediment load) and magnitude of flooding events.

Abbreviation of the variable	Definition	Values and Explanations
General		
cellSize	Horizontal dimension of a cell	20 m
cellHeight	Height of the cell in the facies grid	0.1 m
modelWidth	Width of the model domain	2500 cells = 50 km
TimeSteps	Number of time steps in the model run	*N* * *n* = 500
Channel Element		
channelWidth	Width of channel element (number of segments) or channel sandstone body	4 segments = 3 cells = 60 m
erosionDepth	Incision depth of channel element below the floodplain level	
chAggradThick	Elevation of the channel ridge above the floodplain level	
maxThickness	Thickness of channel element	*erosionDepth* + *chAggradThick*
chMigrMethod	Algorithm of channel avulsion	1 – channel is relocated to a global minimum 2 – channel avulses randomly
n	Major avulsion frequency	
N	Number of major avulsions	*TimeSteps / n*
migrationDistance	Channel element avulses locally laterally to the left or right from the centre of the previous channel element to a distance which is randomly chosen from the interval between 0 and *migrationDistance.*	*channelWidth* + 20 *channelWidth* + 40 *channelWidth* + 100
Floodplain element		
floodMethod	Floodplain aggradation algorithm	1 – exponential depth-dependant 2 – exponential 3 - depth dependent 4 - uniform
aggradExp	Aggradation exponent - rate with which thickness of floodplain deposits decreases away from the channel element edge	
Output parameters		
NTG2D	Percentage of sandstone bodies relative to the gross cross-section area of the model strata (NTG ratio)	
Connect	Vector that contains number of connected cells within every individual connected sandstone body in the model	
NumOfIlands	Number of individual connected bodies in the model	
MeanAvulDist	Mean distance between avulsion positions within the model	
meanMinDist	Mean of distances to the centre of the closest channel in the model calculated for every channel	
meanMeanDist	Mean of mean distances to the centre of the other channels in the model calculated for every channel	
SubsidNorm	Normalised subsidence - thickness between first and the last horizons divided by maximum thickness between these two horizons at each x location	
AverThick	Average thickness between current pair of horizons	
SubDim	Dimensional subsidence - normalised subsidence divided by average thickness of the horizon	*SubsidNorm* * *AverThick*
SedSubRatio	Sedimentation to subsidence ratio	*Thickness / SubDim*
Tc	Compensation thickness scale	

Table 12.1. Abbreviations used in the chapter and in the programming code for input and output model parameters.

It is known that whether sediment is transported in bedload or suspended load depends on the flow power and the immersed weight of the grains (Reid and Frostick, 1994). The latter is proportional to the grain size assuming the grains have a similar by composition excluding a small percentage of heavy minerals. Therefore, the lack of fine-grained material in the sediment load means that during relatively low magnitude flood only that small amount of suspended sediment would be transported on to the floodplain. In contrast, during relatively high magnitude flood more sediment including some bedload material, which would become suspended, can be carried out of the channel. This amount would probably still be less than in the case when channel flow is rich in suspended fine-grained sediment. In addition, if a channel operates without avulsion for long time, more sediment would be transported by floods out of the channel assuming there is enough sediment to support the process. All these processes are not simulated explicitly in the model and only discussed here as possible controls.

In this model the floodplain aggradation exponent together with the channel aggradation thickness define overall aggradation of the modelled strata. Consequently, the relationships between these two parameters, erosion depth and channel sandstone body width determine the degree of preservation of floodplain strata in the model.

12.5.4. Channel sandstone body width

Channel elements in the model represent sandstone bodies formed by channel deposition, for example by migrating bedforms in the channel, during periods between avulsions (Section 12.2.4). Relatively narrow channel sandstone bodies represent the deposits of laterally stable channels. Wider channel sandstone bodies are formed by lateral migration of a channel and lateral and downstream accretion of bedforms in the channel. Channel sandstone body width in the model, therefore, corresponds to a degree of lateral migration of a channel between avulsions. The lateral migration of a channel results in reworking of previously deposited sediments.

Laterally stable channels observed in the Huesca and Salt Wash DFS successions do not exceed 100 m in width (Chapter 5) which corresponds to 4 to 6 grid segments in the model. The sandstone bodies with widths higher than that are considered to occur in laterally unstable channels.

Schuum (1985) stated that channel patterns change when sediment supply and water discharge change. It is unclear, however, what combination of sediment supply and water discharge actually leads to lateral migration or alternatively to vertical aggradation and avulsion of a channel. It could be speculated that perhaps a high discharge would result in a higher probability of avulsion since avulsion probably requires higher energy flows to create a new path across the floodplain, versus the lower energy needed to erode and trigger lateral channel migration. In addition, if the channelised sediment load lacks fine-grained sediment, the channel belt would probably not aggrade. Therefore, conditions for an avulsion (superelevation and high floodplain to channel gradient ratio, Slingerland and Smith, 2004 and references therein) would not be reached and instead channel would erode laterally to accommodate water and sediment discharge. However, in this conditions channel could also be bankfull filled and avulse due to transport capacity reduction. Low accommodation in the relatively proximal and medial areas of a DFS (Weissmann et al., 2013 in press) could also force channels to migrate laterally and rework previously deposited sediment, but could also lead to more frequent avulsions, that might result in similar reworking.

Substrate cohesiveness is usually used to explain lateral stability of a channel (Allen et al., 1983; Hirst, 1983; Schuum, 1985; Hirst and Nichols, 1986; Nadon, 1994) which in turn could be partially related to the bedload to suspended load ratio in the supplied sediment (Schuum, 1985). For example, a decrease in stream power downstream in a DFS results in deposition of bedload upstream while suspended fine-grained load is being carried downstream creating a more cohesive substrate in the distal areas (Chapter 8). This leads to formation of more laterally stable channels in the distal areas (chapters 6-8, Appendix 5). Jones and Hajek (2007) have also discussed grain size distribution of the sediment load as a potential control of bank stability and splay-proneness of the system. Cohesiveness of the floodplain is also controlled by vegetation (Nadon, 1994).

In summary, the controls on lateral channel migration versus avulsion are poorly understood, but based on the concepts and ideas discussed above, this model assumes that a channel sandstone body with a high width to thickness ratio represent a situation where the floodplain is not cohesive or where accommodation space is low. The parameters discussed above, however, are not simulated explicitly in the model and are only discussed as possible controls on sandstone body width and lateral reworking to demonstrate how results of the modelling in this chapter could be related to real depositional processes.

12.6. Modelling experiments

Several model experiments have been conducted within this study to investigate how variation in input parameters and different avulsion and floodplain aggradation algorithms affect the characteristics of the modelled fluvial architectures.

12.6.1. Variable input parameters

Experiment 1: Every possible combination of four input parameters, including channel sandstone body width, channel aggradation thickness, channel erosion depth, and floodplain aggradation exponent, have been modelled. Each parameter has been varied for across a range with 20 increments (Section 12.2.7), apart from channel sandstone body width which has been varied for 7 increments to reduce the required computer run-time. The model results have been used to investigate how stratal properties such as NTG ratio and sandstone body connectivity depend on the input parameter values, and to find out which input parameters create specific values of those properties in best-fit outcrop models. The best-fit models represent model outcomes that replicate features observed in the outcrops of the Huesca and Salt Wash DFS. The results are discussed in Section 12.7.

Experiment 2: The best-fit models for the relatively proximal successions of the Huesca and Salt Wash DFSs (Monźon and Bullfrog outcrops) have been selected to show the sensitivity of modelled strata to the variations in input parameter values. For this purpose values of every possible pair of four input parameters have been varied for 20 increments with the ranges of values presented in Table 12.2, while two other parameters were kept the same as in the best-fit model. The results are discussed in Section 12.8.

Model **Experiments 1 and 2** were conducted for compensational channel migration algorithm assuming that channel avulses to a minimum on the floodplain at every time step. Experiments 1 and 2 create strata which could have formed under many possible combinations of sediment supply, water discharge, availability of fine-grained sediment and degree of lateral migration of channels. These factors are expressed in the model in the degree of reworking (erosion and lateral migration of channels) and aggradation (aggradation thickness and floodplain aggradation exponent) of the fluvial deposits. The results of the sensitivity analyses are discussed using these main factors.

12.6.2. Variable channel avulsion algorithm

Experiment 3: The same model runs as in the **Experiment 1** have been conducted using a random avulsion mechanism.

Experiment 4: In addition the sensitivity analysis for the Monźon best-fit model has been also done for 1) random avulsion mechanism and 2) compensational avulsion mechanisms with avulsion frequency (*n)* equal to 3 and 5.

Experiment 5: The best-fit Monźon model with compensational avulsion mechanisms and variable avulsion frequency (Experiment 4) has been also run for three different migration distances (Table 12.2).

The results of these three experiments are analysed in terms of the effect of avulsion mechanism on the output parameters of the modelled strata and on compensation thickness scale. The results are discussed in Section 12.9.

12.6.3. Variable floodplain algorithm model

Experiment 6: The best-fit model for the Monźon outcrop was run with the compensational channel migration algorithm and four different floodplain aggradation algorithms (Section 12.2.5) to demonstrate the effect on the output parameters of the modelled strata and on the compensation thickness scale. The models with uniform and depth-dependent floodplain aggradation have been run for four different uniform aggradation constants (Table 12.2). The results are discussed in Section 12.10.

12.6.4. Variation in input parameters with time

Due to the lack of vertical variation in the architecture in 100 m-thick outcrops of the Huesca (appendices 5.1-3) and Salt Wash DFS successions (appendices 5.4-6) changes in input parameters with time have not been modelled.

Input parameter	**Best-fit Monźon**	**Best-fit Bullfrog**	**Experiments 1, 2 and 3**	**Experiments 4 and 5**	**Experiment 6**
n	1	1	1	**1, 3, 5**	1
N	500	500	500	500, 166, 100	500
channelWidth	**8**	**42**	**4 : 2 : 42**	8	8
chAggaradThick	**2**	**3**	**0.5 : 0.2 : 4.3**	2	2
erosionDepth	**6**	**8**	**1 : 0.5 : 10.5**	6	6
aggradExp	**900**	**900**	**550 : 50 : 1500**	900	900
unifromFloodplAggrad	0	0	0	0	**0.01, 0.02, 0.05, 0.1**
migrationDistance	0	0	0	**0, 28, 48, 108**	0
floodMethod	1	1	1	1	**1, 2, 3, 4**
chMigrMethod	1	1	**1, 2**	**1, 2**	1

Table 12.2. Model input parameters for the Monźon and Bullfrog best-fit case models and range of input parameters for six model experiments (Section 12.6). Explanations for ranges of values see in the Section 12.2.7. Best-fit models are discussed in Section 12.7.

12.7. Modelling successions of the Huesca and Salt Wash DFSs

The results of the **Experiment 1** provide the basis data for the modelling of the observed successions. The ranges of input parameters that resulted in the strata with NTG ratios equal to the ratios estimated from the Huesca and Salt Wash outcrop panels have been selected from the output file of the **Experiment 1** (Fig. 12.10 and 12.17). Note that the NTG ratio in the models corresponds to the percentage of Type 1 and 2 sandstone bodies estimated in the outcrops (Tables 6.1, 7.1 and 11.1), not including Type 3 sandstone bodies.

Next the model has been tested with the averaged input parameters measured from the outcrop data. The best-fit models for each outcrop are constructed and the applicability of the model for simulating the observed DFS strata is discussed.

12.7.1. The Huesca DFS succession

The NTG ratios estimated in the Huesca DFS succession vary from 30 % to 15 % and to 1 % in the relatively proximal, medial and distal parts of the strata, respectively. Qualitatively the sandstone body connectivity also varies from partially connected sandstone bodies in the Monźon outcrop to vertically compartmentalised sandstone bodies in the Castelflorite outcrop and to vertically and laterally isolated sandstone bodies in the Alcolea outcrop (appendices 5.1-3).

Relatively proximal succession (Monźon outcrop)

The relatively proximal succession of the Huesca DFS deposits (Monźon outcrop, NTG = 30 %) can be reconstructed by the model with a range of input parameters presented in Figure 12.10. Parameter values for best-fit models vary for different channel sandstone body widths. For example, for a channel sandstone body width of 60 m (4 segments) the strata could have been formed under the following conditions: the lowest aggradation thickness (0.5 - 0.9 m), high erosion depth (5 - 10.5 m) and medium floodplain aggradation exponent (550 – 950 m) (Fig. 12.10, A; e.g. Fig. 12.9, A). The NTG ratio of 30 % in the models with channel sandstone body width equal to or higher than 100 m (6 segments) can be achieved by a combination of much wider range of input parameters (Fig. 12.10, B-G; e.g. Fig. 12.9, B). Although the NTG ratio of the modelled succession of these two examples is similar, their stratal geometry and sandstone body connectivity is different. In the first example every two sandstone bodies are connected (Fig. 12.9, A), while in the second example all bodies are isolated (Fig. 12.9, B). Thus, the NTG ratio cannot be used alone to fully describe stratal architecture and additional data about the succession are needed to support conclusions about stratal architecture.

The succession exposed in the Monźon outcrop is characterised by channel sandstone body widths from 35 to 350 m including both Type 1 and 2 sandstone bodies (chapters 5-6). The 2D model uses only one channel sandstone body width and therefore channel sandstone body width is averaged to 140 m (8 segments). Channel aggradation thickness measured as a thickness of the channel “wings” varies from 1 to 2.5 m and averaged to 2 m. The depth of scours of sandstone bodies is recorded from 6 to 9 m with the most common value equal to 6 m. Floodplain aggradation is an unknown parameter and is assigned to 900 m (Section 12.2.7).

Model with input parameters measured from the outcrop (Table 12.3) produce successions with 28.9 % of sandstone bodies relative to the floodplain deposits (Fig. 12.11, A-B) and this is very close to the values estimated from the outcrop. The sandstone body connectivity in the Monźon model is 315 bodies out of 499 sandstone bodies indicating that on average around 1.5 bodies are connected (Fig. 12.5). The sandstone body connectivity in the outcrop is slightly higher than in the resulting modelled strata (Appendix 5.1). This could be because lateral connection in the modelled succession is not reproduced well because only one type of sandstone bodies is used while in reality wider sandstone bodies can connect narrower sandstone bodies.

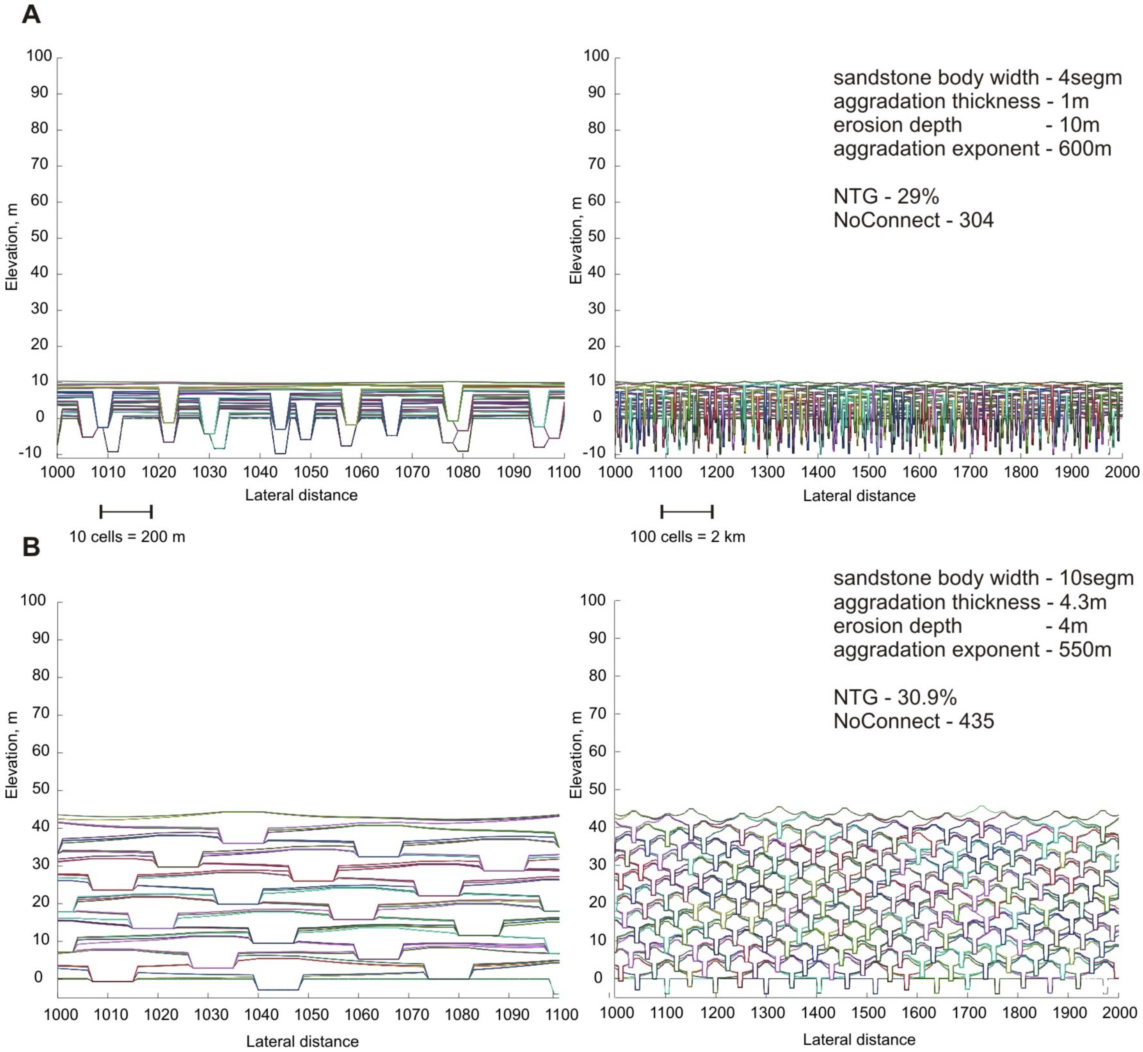

Figure 12.9. Examples of modelled succession with NTG ratio around 30 %. The models are created with contrastingly different input parameters: A – low aggradation thickness and deep erosion (low sediment supply to water discharge ratio), B – high aggradation and relatively shallow erosion (somewhat balanced sediment supply – water discharge ratio). Note different sandstone body connectivity.

The input parameters of the model corresponding to the architecture of the Monźon outcrop could indicate relatively high to moderate reworking (erosion and lateral migration) but also moderate aggradation and preservation of the floodplain deposits.

The apparent similarity of the modelled and real strata could reflect an element of circular reasoning. The 2D model has been created initially based on the observations

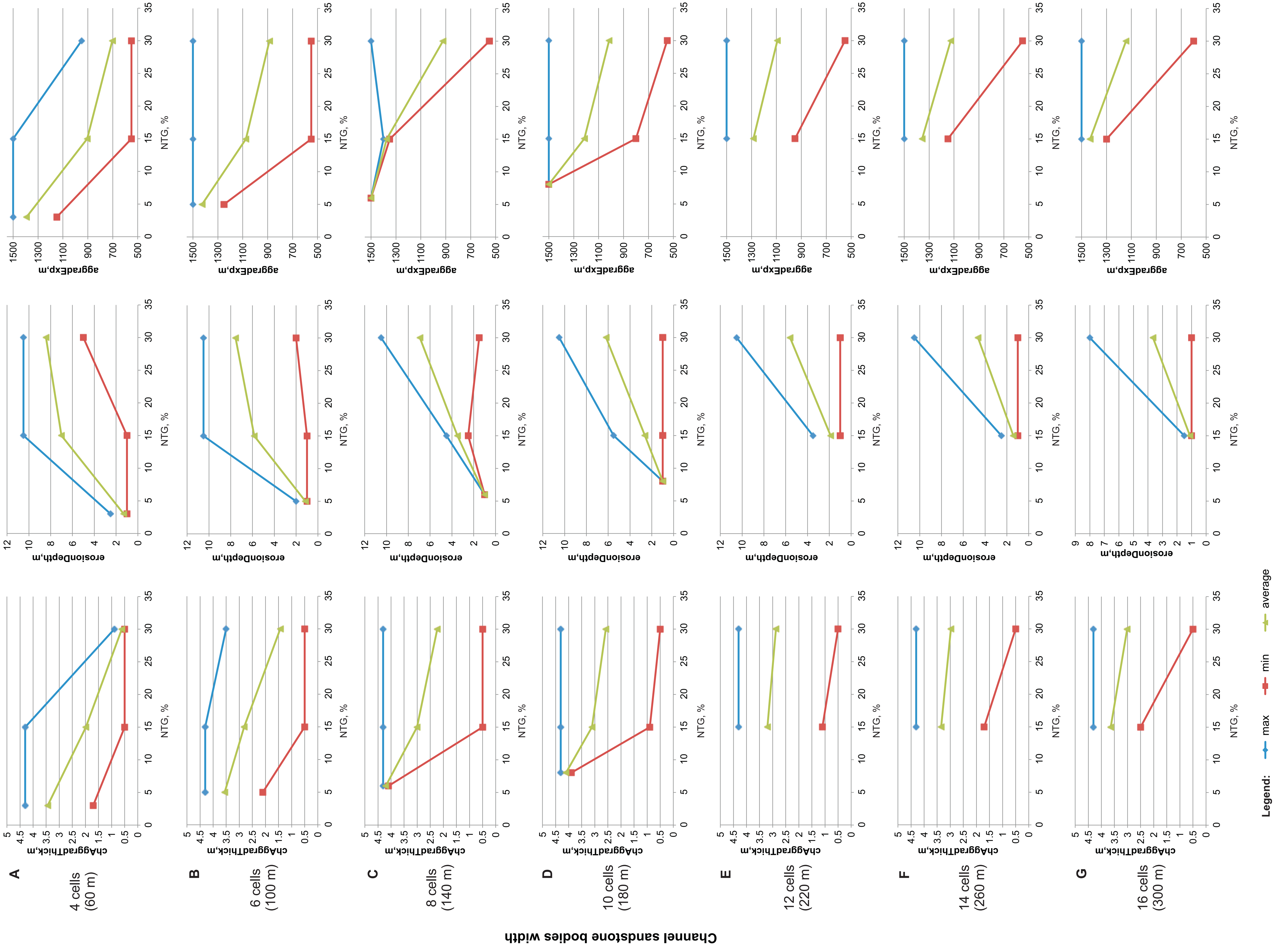

Figure 12.10. Ranges of model input parameters that can produce NTG ratio similar to the relatively proximal (30 %), medial (15 %) and distal (1 - 3 %) outcrops of the Huesca DFS succession. The input parameter ranges are shown for channel sandstone body width of A - 4 (60 m), B - 6 (100 m), C - 8 (140 m), D - 10 (180 m), E - 12 (220 m), F - 14 (260 m), G - 16 (300 m) segments.

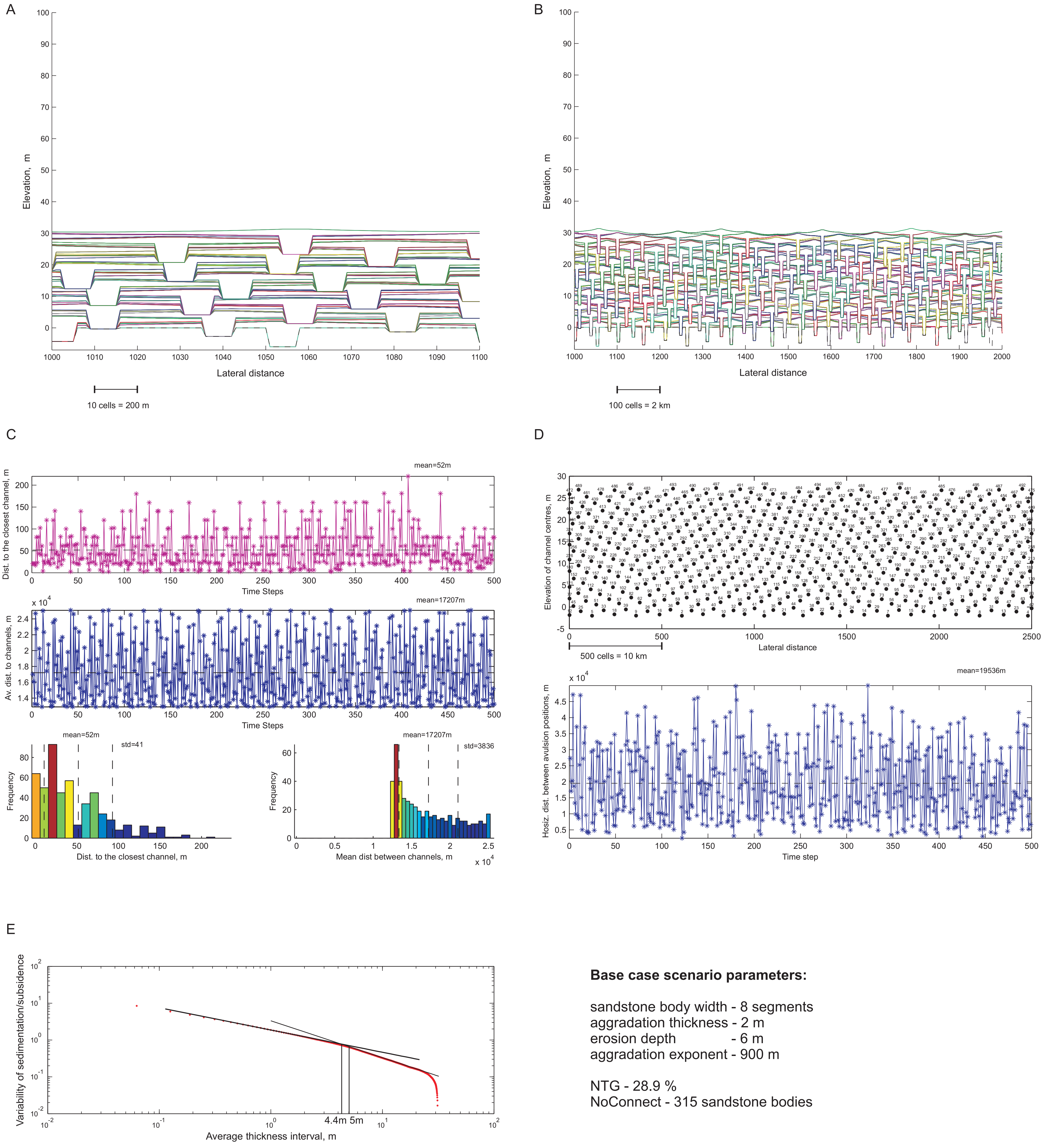

Base case scenario parameters:

sandstone body width - 8 segments
aggradation thickness - 2 m
erosion depth - 6 m
aggradation exponent - 900 m

NTG - 28.9 %
NoConnect - 315 sandstone bodies

Figure 12.11. Best-fit model of the Monźon outcrop. A - 2 km of the modelled strata, B - 20 km of the modelled strata, C - variation of the mean distance between channels and mean distance to the closest channel with time step and frequency distributions of the distances, D - channel position map and variation in mean avulsion distance with time step, E - variability of the sedimentation to subsidence ratio with average thickness windows and approximate estimation of the compensation thickness scale.

and measurements of DFS deposits in the outcrops that are modelled and discussed in this section. Thus, the match between NTG ratio and connectivity for the outcrop and modelled strata here and in the following discussions should not be over interpreted. Nevertheless, the model includes unknown input parameters such as aggradation exponent and type of floodplain aggradation and avulsion mechanisms that have not been determined from the outcrop data indicating that model outcomes are not entirely constrained by outcrop observation, suggesting partial but not complete dependence.

		Monźon	**Castelflorite**	**Alcolea**
Input	*n*	1	1	1
	N	500	500	500
	channelWidth	**8**	**6**	**4**
	chAggradThick	**2**	**1.5**	**0.5**
	erosionDepth	**6**	**3**	**1.5**
	aggradExp	**900**	**1000**	**1500**
	floodMethod	1	1	1
	chMigrMethod	1	1	1
Output	**NTG ratio**	**28.9**	**14.68**	**8.59**
	Number of individual connected bodies	**315 (499)**	**468 (499)**	**442 (499)**
	No of connected elements	1.58	1.07	1.13

Table 12.3. Input and output parameters for the best-fit models for the outcrops of the Huesca DFS succession.

Medial succession (Castelflorite outcrop)

The medial succession of the Huesca DFS deposits (Castelflorite outcrop, NTG = 15 %) can be generated with a very wide range of input parameters (Fig.12.10, A-G). For instance, the medial succession can be created with a combination of following parameters: low channel sandstone body width of 60 m (4 segments), very high aggradation thickness (4.3 m), very deep channel scours (10 m) and very low aggradation exponent (650 m) (Fig. 12.10, A; e.g. Fig. 12.12, B). The medial succession can also be reproduced by model with the same channel sandstone body width, but contrastingly lower aggradation thickness (0.5 m) and erosion depth (2 m) and higher aggradation exponent (900 m) (Fig. 12.10, A; e.g. Fig. 12.12, A). If modelled strata are created with very high channel sandstone body width (300 m), the highest aggradation thickness and floodplain exponent together with the lowest erosion depth are required which will compensate each other to form strata with NTG ratio of 15 % (Fig. 12.10, G).

Sandstone body connectivity of these two examples is only slightly different: in the first case low aggradation and relatively high reworking resulted in connection of few sandstone bodies (Fig. 12.12, A) and in the second case all sandstone bodies are isolated (Fig. 12.12, B). This shows again the limitations of using the NTG ratio parameter without additional data for interpretation of the reservoir connectivity.

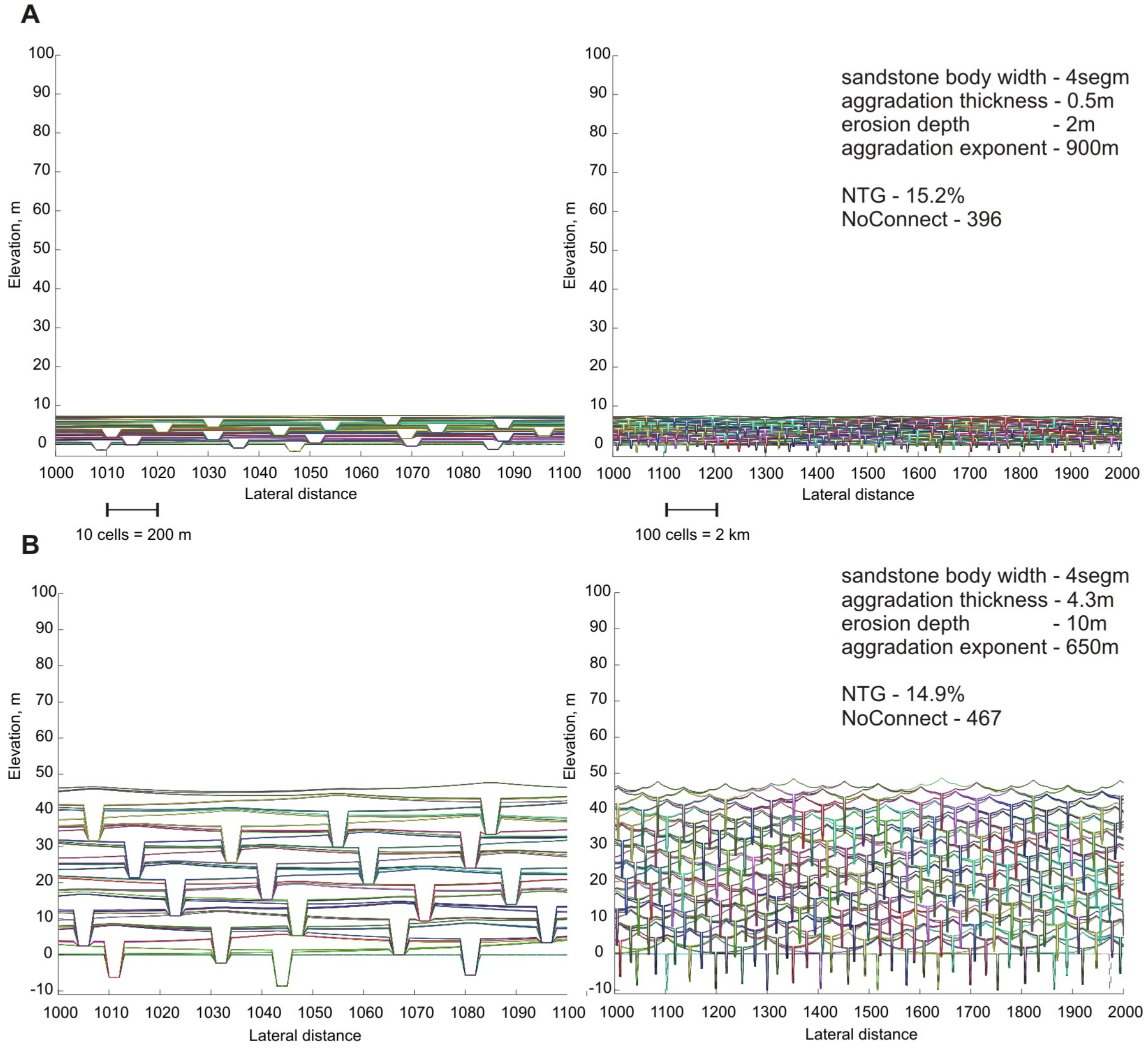

Figure. 12.12. Examples of modelled succession with NTG ratio of 15 % (Castelflorite outcrop). The models are created with contrastingly different input parameters: A – very low aggradation and shallow erosion (low sediment supply and low water discharge), B – high aggradation and deep erosion (high sediment supply and high water discharge). Note slightly different sandstone body connectivity.

The succession in the Castelflorite outcrop is characterised by the sandstone bodies which are from 20 m to 180 m wide. The strata are dominated by Type 1 sandstone bodies, but Type 2 sandstone bodies are also present. To reflect this relationship channel sandstone body width is assigned to 100 m (6 segments). The aggradation thickness measured by the “wings” thickness is equal or below 1.5 m while sandstone body scour depth varies from 3 to 6 m with the most common value equal to 3 m. The floodplain aggradation is unknown and is assigned to 900 - 1000 m (Section 12.2.7).

The model with input parameters measured in outcrop (Table 12.3) produces NTG ratio equal to 14.7 % (Fig 12.13, A-B) that is similar to the estimated from the outcrop. The sandstone body connectivity of the Castelflorite model replicates the outcrop architecture well. The number of individual connected bodies is 468 out of 499

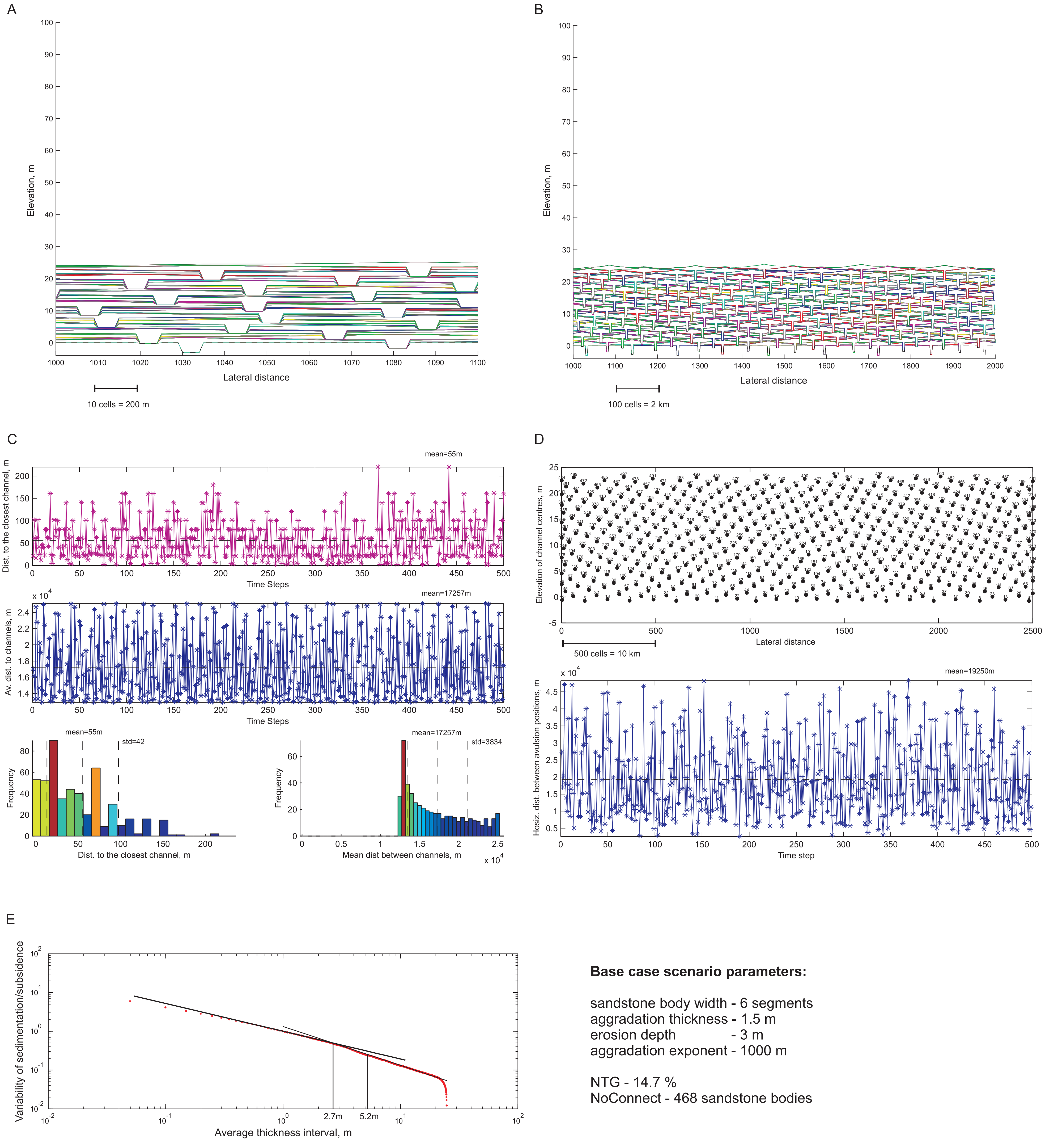

Base case scenario parameters:

sandstone body width - 6 segments
aggradation thickness - 1.5 m
erosion depth - 3 m
aggradation exponent - 1000 m

NTG - 14.7 %
NoConnect - 468 sandstone bodies

Figure 12.13. Best-fit model of the Castelflorite outcrop. A - 2 km of the modelled strata, B - 20 km of the modelled strata, C - variation of the mean distance between channels and mean distance to the closest channel with time step and frequency distributions of the distances, D - channel position map and variation in mean avulsion distance with time step, E - variability of the sedimentation to subsidence ratio with average thickness windows and approximate estimation of the compensation thickness scale.

deposited bodies meaning that only occasionally two bodies are connected (Fig. 12.5) and this is also seen in the medial outcrop (Appendix 5.2). Interestingly, some sandstone bodies are stacked vertically one above another separated by floodplain deposits (Fig.12.13, A) which was also observed in the Castelflorite outcrop (Appendix 5.2, B).

A small proportion of the medial strata are represented by the sheet-like sandstone bodies of terminal splays that are not simulated by the 2D model. In the model this is compensated by lower floodplain aggradation exponent that is less realistic if we take into account how much floodplain deposits is preserved in the succession (Appendix 5.2). The absence of sandstone bodies of variable width in the 2D model may affect the result as well.

The modelling input parameters show that medial succession of the Huesca DFS could have formed under similar conditions as the succession in the relatively proximal area but with slightly higher degree of floodplain preservation, controlled by a smaller degree of reworking due to smaller erosion depth and more laterally stable channels (smaller width). This in turn could have been caused by a decrease in the flow strength and more cohesive finer-grained substrate in the medial area in comparison with the relatively proximal area (Section 12.5, Chapter 8).

Distal succession (Alcolea outcrop)

The NTG ratio estimated in the distal succession of the Huesca DFS deposits (Alcolea outcrop) is 1 %. The minimum NTG ratio that can be produced by the 2D model with input parameters that are within assigned ranges is 3 % to 5 % (Fig. 12.10, A-C). For instance, such strata can be created with minimum channel sandstone body width of 60 m (4 segments), minimum erosion depth equal to 1 m, high aggradation thickness ranging from 1.7 to 4.3 m and maximum aggradation exponent of 1500 m (Fig. 12.14, A-B). However, the high aggradation thickness used in the examples (Fig. 12.14) is not a characteristic for the distal succession of the Huesca DFS deposits. The observed channel “wings” thickness that is measured in the outcrop and represent aggradation thickness is around 0.2 - 0.5 m (Chapter 4).

The model with input parameters measured in the distal Alcolea outcrop results in much higher NTG ratios than is estimated from the photo panels (Table 12.3). For instance, the model with minimum channel sandstone body width, aggradation thickness equal to 0.5 m, erosion depth equal to 1.5 m and aggradation exponent equal to 900 m, gives NTG ratio equal 12 %. An increase in aggradation exponent to 1500 m will reduce NTG ratio to 8.6 % that is the minimum NTG ratio that can be created with realistic outcrop parameters (Fig. 12.10). The increase in aggradation exponent is realistic because the distal succession of the Huesca DFS is dominated by fine-grained deposits. Although a decrease in erosion depth to 0.5 m will additionally reduce NTG ratio to 4.7 %, erosion depth of 0.5 m is unrealistic because erosion depths up to 2 m have been observed in the Alcolea outcrop (Appendix 5.3). None of the sandstone bodies are connected in all the modelled examples of the distal succession and this is seen in the Alcolea outcrop (Appendix 5.3).

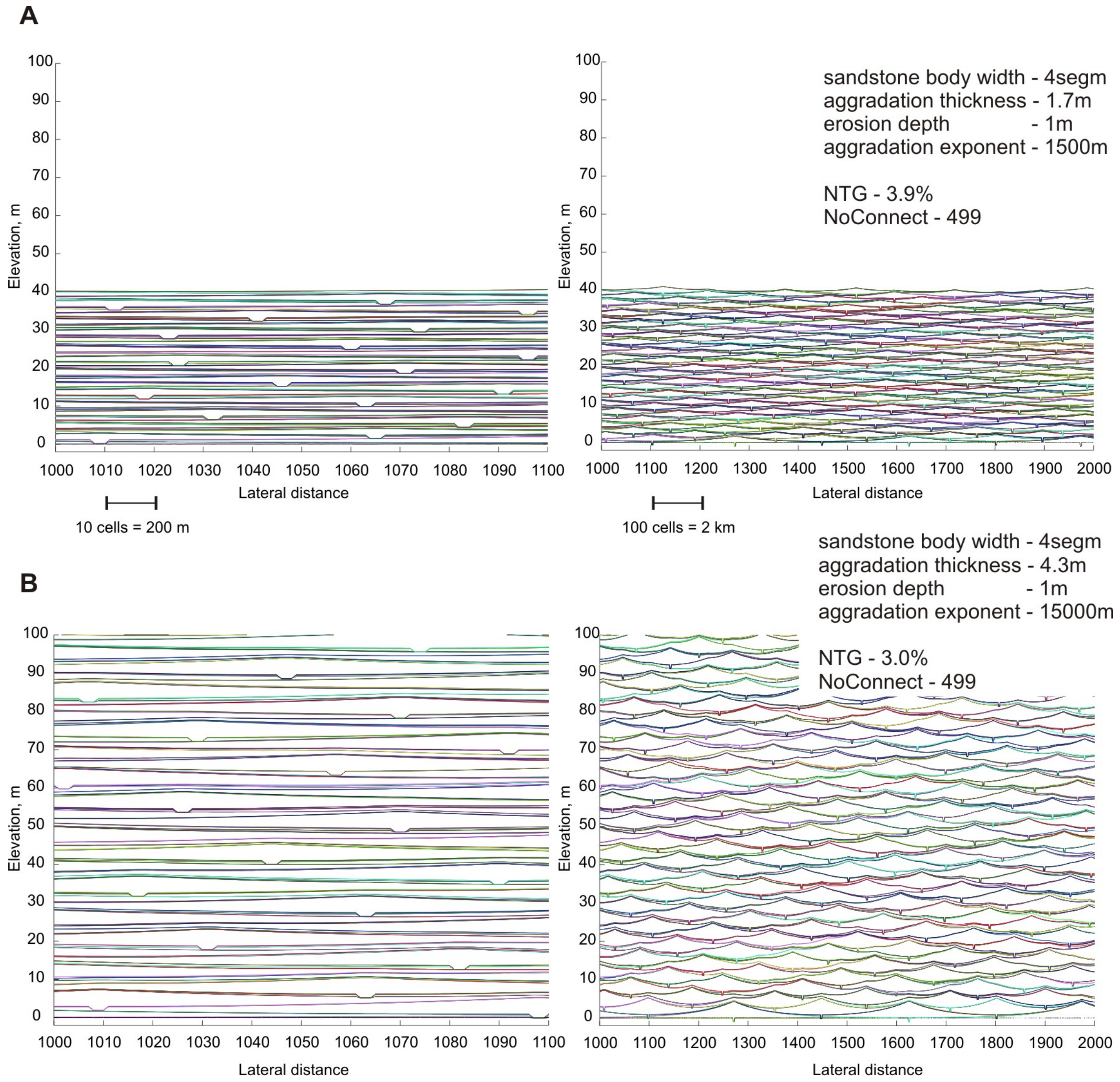

Figure. 12.14. Examples of modelled succession with NTG ratio of 3 %. The models are created with input parameters reflecting high aggradation, abundant fine-grained sediment and minimum of reworking (high sediment supply to water discharge ratio): A – moderate aggradation thickness, B – high aggradation thickness. Sandstone bodies are not connected.

Thus, the distal Alcolea succession of the Huesca DFS deposits cannot be recreated by the 2D model. There are several reasons for this. Firstly, the channel sandstone body width of 60 m is the minimum possible width in the model, while the Type 1 sandstone bodies in the Alcolea outcrop are all less than 11 m wide. Only one sandstone body of Type 2 with width of 100 m has been observed (Appendix 5.3).

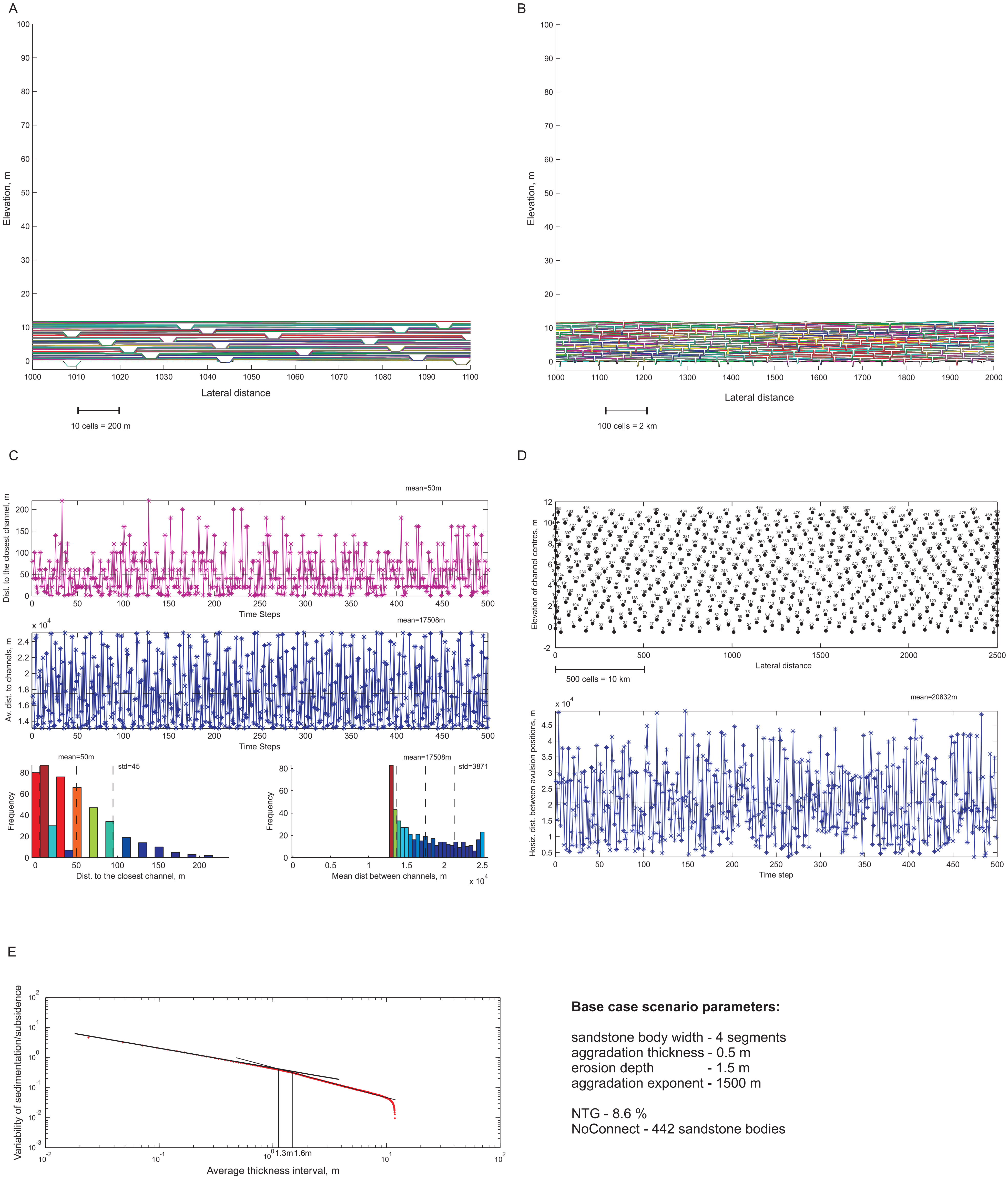

Figure 12.15. Best-fit model of the Alcolea outcrop. A - 2 km of the modelled strata, B - 20 km of the modelled strata, C - variation of the mean distance between channels and mean distance to the closest channel with time step and frequency distributions of the distances, D - channel position map and variation in mean avulsion distance with time step, E - variability of the sedimentation to subsidence ratio with average thickness windows and approximate estimation of the compensation thickness scale.

Base case scenario parameters:

sandstone body width - 4 segments
aggradation thickness - 0.5 m
erosion depth - 1.5 m
aggradation exponent - 1500 m

NTG - 8.6 %
NoConnect - 442 sandstone bodies

Thus the model is a poor representation of distal architecture due to limitations of the grid cell size used in these model runs.

Secondly, the 2D model does not simulate sheet-like sandstone bodies formed by terminal splays that comprise a large portion of the distal Huesca DFS deposits (chapters 4-6). In the current best-fit model configuration, thick floodplain intervals in the distal succession are modelled through high floodplain aggradation thickness that compensates for the lack of floodplain deposits formed by terminal splays.

Finally, the distal area of the Huesca DFS is wider than its proximal area. This basic fan shape means that distal channels should be more widely separated and so rare, relative to their frequency in the proximal DFS (Chapter 8, see also Nichols, 1987). The model, in contrast, has a fixed grid width that was used to model both proximal and distal strata and therefore does not account for proximal to distal variation in sand body spacing.

The current 2D model is less realistic when applied to the distal outcrops of the Huesca DFS. Nevertheless, it could be seen from the modelling attempts and best-fit model input parameters that high floodplain aggradation and abundance of fine-grained sediment played one of the main roles in the formation of the low-NTG distal strata, while degree of reworking was minimal.

12.7.2. The Salt Wash DFS succession

The Salt Wash DFS succession is characterised by much higher NTG ratios than the Huesca DFS succession, ranging from 35 % in the distal part to 85 % in the relatively proximal part and with intermediate NTG ratios in its medial outcrops (50 – 60 %). Qualitatively the sandstone body connectivity varies from occasionally connected sandstone bodies in the distal Little Park outcrop to completely amalgamated sandstone bodies in the relatively proximal Bullfrog outcrop (appendices 5.4-6).

Relatively proximal succession (Bullfrog outcrop)

The relatively proximal succession (Bullfrog outcrop, NTG >= 85 %) can be constructed with the current model set up if the channel sandstone body width is higher than 260 m (14 segments) (Fig. 12.17, G). For example the model with channel sandstone body width of 300 m (16 segments), high erosion depth from 5.5 to 10.5 m, low aggradation thickness from 0.5 to 0.9 m and low aggradation exponent from 550 to 900 m results in a succession with NTG ratio from 80 % to 86 % (Fig. 12.17, G; Fig. 12.16, A). In the models with a higher channel sandstone body width of 580 m (30 segments) the NTG ratio of 85 % can be achieved with a much wider range of input parameters (e.g. Fig. 12.16, B). All sandstone bodies are connected within both modelled examples.

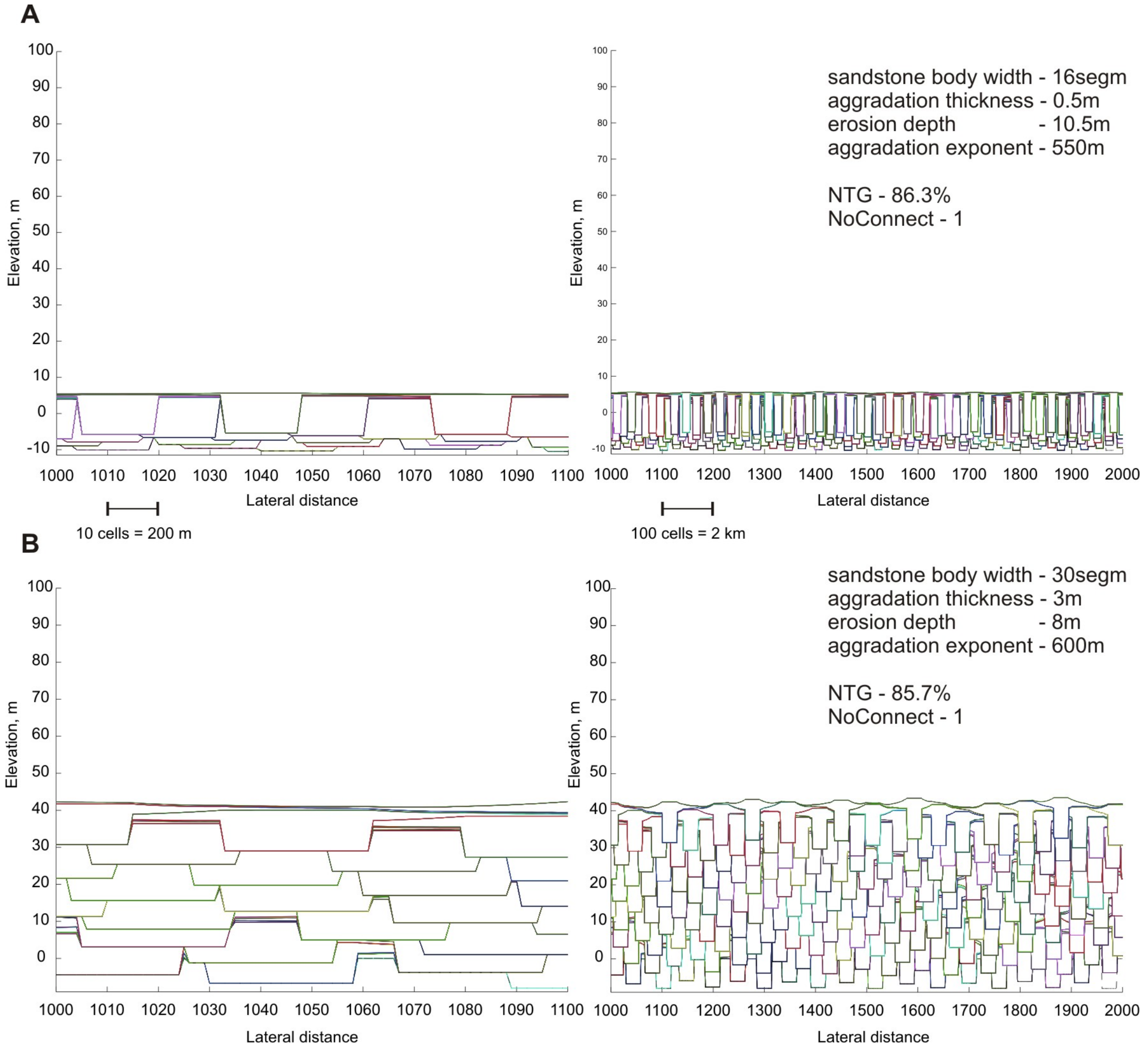

Figure. 12.16. Examples of modelled succession with NTG ratio of 85 % (Bullfrog outcrop). The models are created with contrastingly different input parameters: A – low aggradation and deep erosion (low sediment supply to water discharge ratio), B – relatively high aggradation, deep erosion and high degree of lateral migration (high sediment supply and high water discharge). All sandstone bodies are connected.

The succession exposed in the Bullfrog outcrop is characterised by the sandstone bodies with scour depths from 5 to 10 m, sandstone body widths from 22 m (Type 1) to more than one kilometre (Type 2) (chapters 5 and 7). The Bullfrog strata are dominated by very wide Type 2 sandstone bodies and therefore channel sandstone body width is assigned to the maximum value in the model equal 820 m (42 segments). Channel “wings” are from 1.5 to 4 m thick with an average of 3 m.

The model with input parameters measured from the outcrop (Table 12.4) and an aggradation exponent of 900 m gives NTG ratio of 84.5 % (Fig. 12.18, A-B) that is close to the value estimated from the Bullfrog outcrop. Every sandstone body is connected within the modelled strata as well as in the Bullfrog outcrop, where only few intervals of floodplain deposits are occasionally preserved (Appendix 5.4).

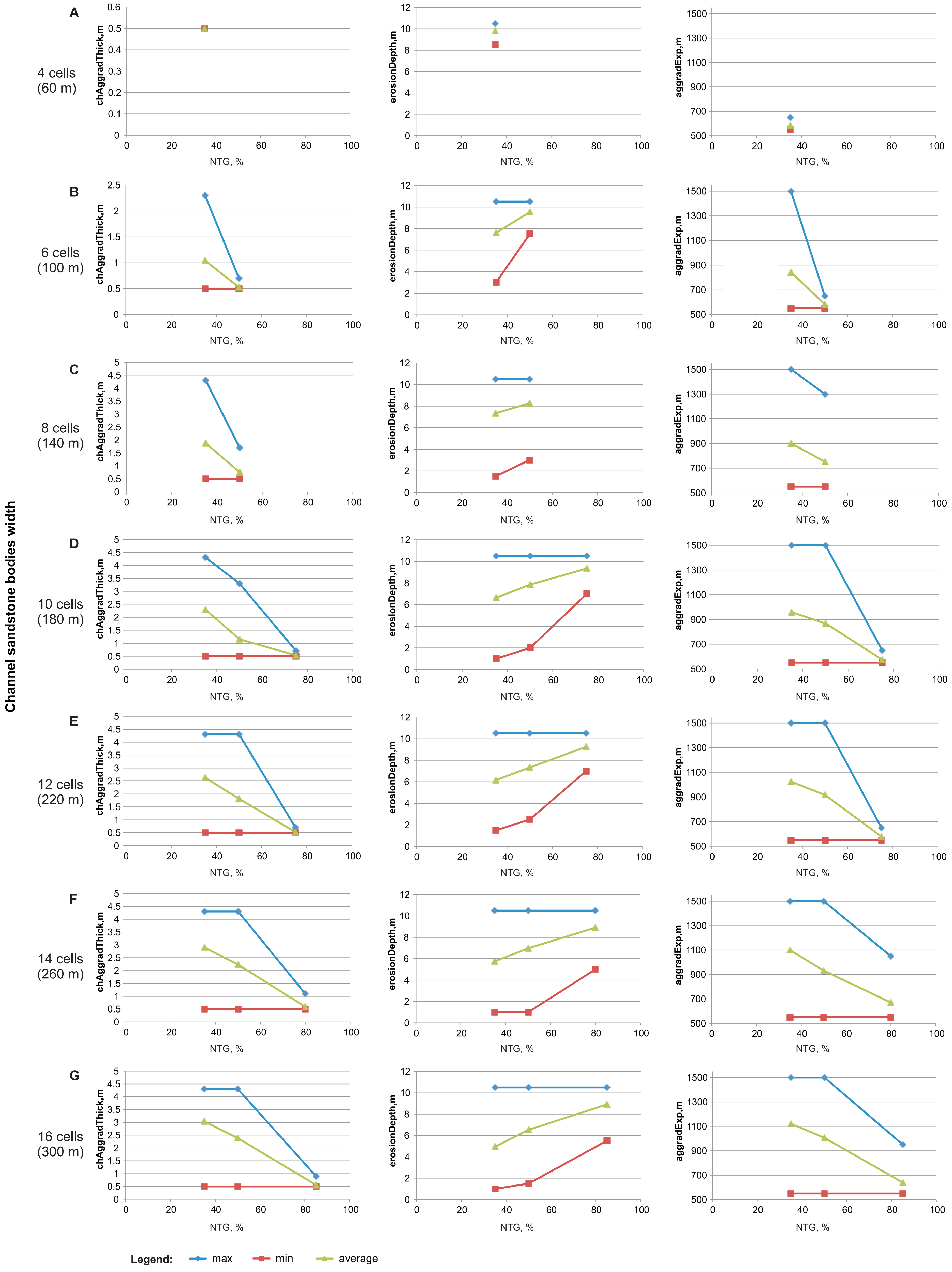

Figure 12.17. Ranges of model input parameters that can produce NTG ratio similar to the relatively proximal (> 85 %), medial (50 - 60 %) and distal (35 %) outcrops of the Salt Wash DFS succession. The input parameter ranges are shown for channel sandstone body width of A - 4 (60 m), B - 6 (100 m), C - 8 (140 m), D - 10 (180 m), E - 12 (220 m), F - 14 (260 m), G - 16 (300 m) segments.

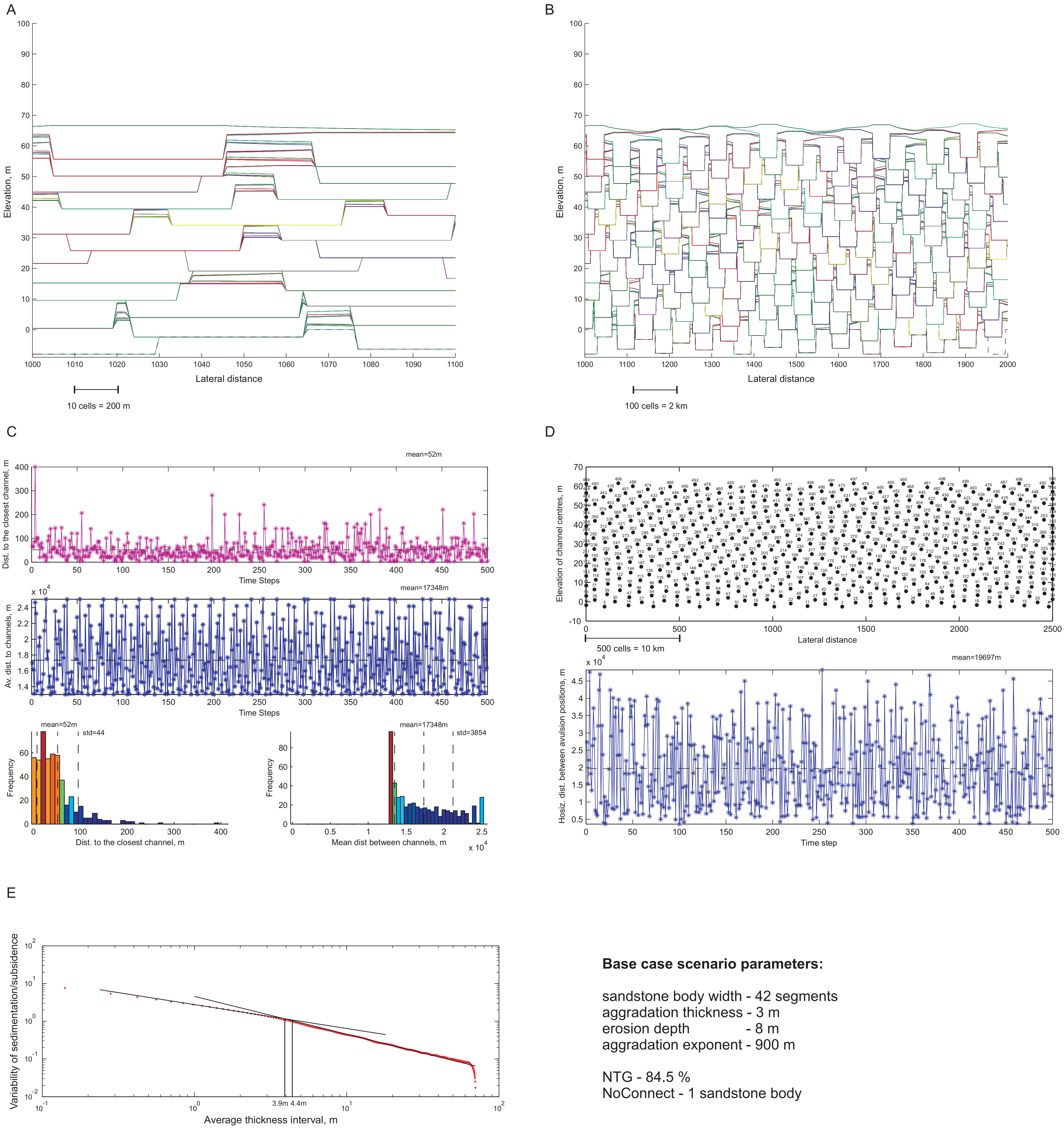

Base case scenario parameters:

sandstone body width - 42 segments
aggradation thickness - 3 m
erosion depth - 8 m
aggradation exponent - 900 m

NTG - 84.5 %
NoConnect - 1 sandstone body

Figure 12.18. Best-fit model of the Bullfrog outcrop. A - 2 km of the modelled strata, B - 20 km of the modelled strata, C - variation of the mean distance between channels and mean distance to the closest channel with time step and frequency distributions of the distances, D - channel position map and variation in mean avulsion distance with time step, E - variability of the sedimentation to subsidence ratio with average thickness windows and approximate estimation of the compensation thickness scale.

The modelling parameters of the Bullfrog strata showed that a smaller channel sandstone body width would reduce NTG ratio significantly. For example, the model with the same input parameters and channel width of 300 m (16 segments) creates successions with NTG ratio of only 48.2 %. To increase the NTG ratio of this modelled strata to ~ 85 %, the aggradation thickness and exponent have to be reduced to 0.5 m and 550 m, while the erosion depth increased to its maximum (10 m), implying that the floodplain deposition on the Salt Wash DFS was limited. However, the very thick intervals of floodplain deposits (up to 10 m) have been observed (Appendix 5.4) and therefore low floodplain aggradation is unrealistic. It is more likely that a high degree of reworking was the main control on sandstone body proportion and connectivity. In the model a high degree of reworking is represented by wide and deeply scoured sandstone bodies.

		Bullfrog	**Slick Rock**	**Little Park**
Input	n	1	1	1
	N	500	500	500
	channelWidth	**42**	**24**	**16**
	chAggradThick	**3**	**3**	**1.5**
	erosionDepth	**8**	**6**	**3**
	aggradExp	**900**	**1000**	**1300**
	floodMethod	1	1	1
	chMigrMethod	1	1	1
Output	**NTG ratio**	**84.53**	**58.2**	**34.81**
	Connected Bodies	**1 (499)**	**106 (499)**	**313 (499)**
	No of connected elements	**499**	**4.71**	**1.59**

Table 12.4. Input and output parameters for the best-fit models of the outcrops of the Salt Wash DFS successions.

Medial succession (Slick Rock outcrop)

The medial succession of the Salt Wash DFS deposits (Slick Rock outcrop, NTG = 50 – 60 %) can be modelled with very wide range of input parameter values (Fig. 12.17, B-G). The NTG ratio of the medial succession could not be reached in the model with a set range of input parameters and the sandstone body width less than 100 m (6 segments) (Fig. 12.17, A). If the sandstone body width equals to 100 m, such a high NTG ratio could be only produced if the erosion depth is very high and aggradation thickness is very low (Fig. 12.19, A). Contrastingly different parameters can be also used to create a model with the same NTG ratio but with a different architecture (Fig. 12.19, B). The nature of the sandstone body connectivity in these two examples is different although the number of connected bodies is close. In the first example sandstone bodies are connected due to deep channel incision and very low floodplain aggradation, while in the second example sandstone bodies are connected due to both great depth and width of sandstone body.

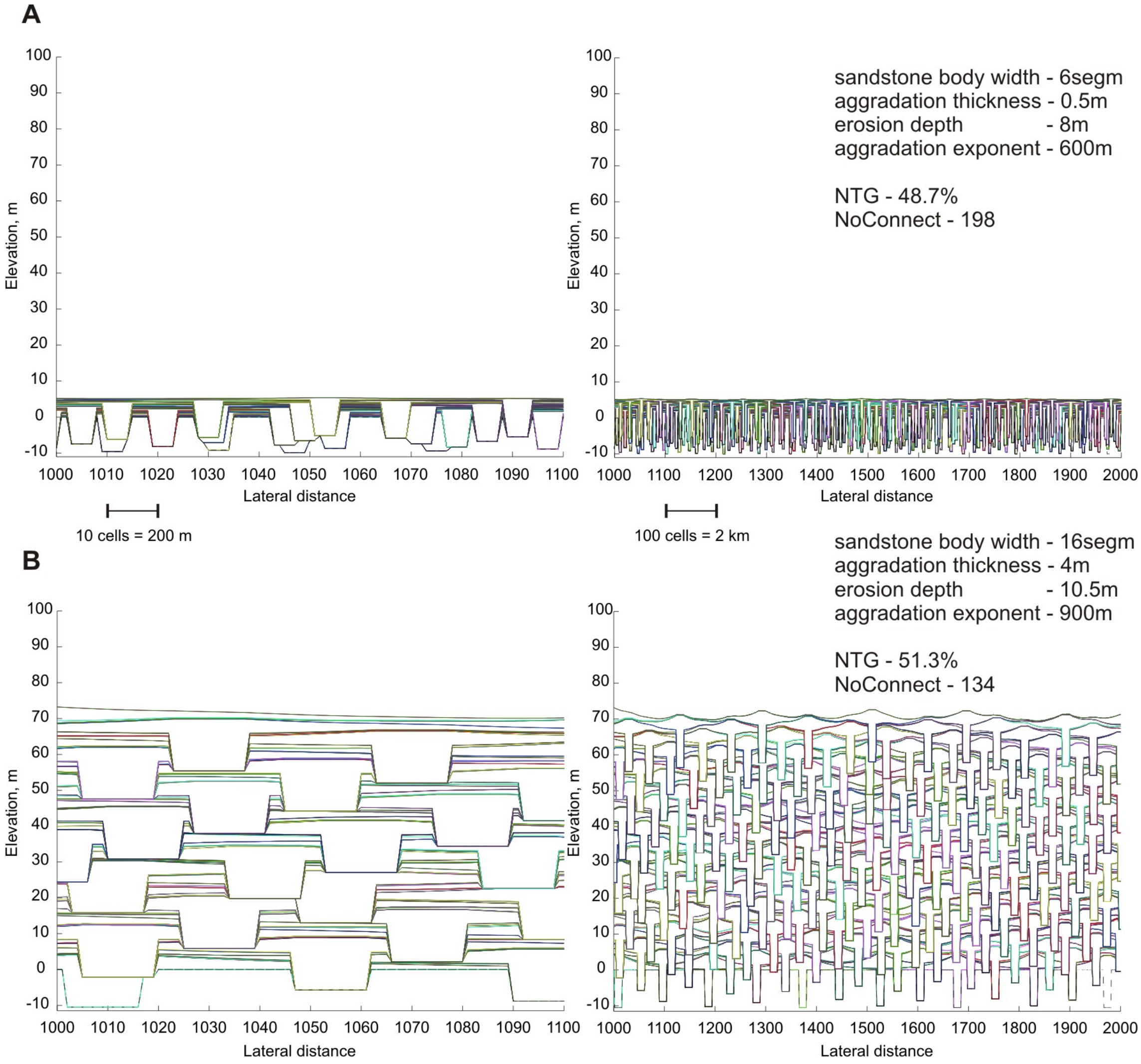

Figure. 12.19. Examples of modelled succession with NTG ratio of 50 % (Slick Rock outcrop). The models are created with contrastingly different input parameters: A – low aggradation and deep erosion (low sediment supply - water discharge ratio), B – high aggradation, deep erosion and high degree of lateral migration (high sediment supply, high water discharge, high degree of lateral migration). Note the different style of the sandstone body connectivity.

The succession exposed in the Slick Rock outcrop is characterised by wide sandstone bodies (200 – 800 m), similar to the Bullfrog succession aggradation thickness (around 2 to 3 m) and a smaller erosion depth (4 – 6 m) (Chapter 7, Appendix 5.5). The model with the input parameters measured in the outcrop, using average sandstone body width (260 m = 24 segments) and maximum aggradation thickness (3 m), produces succession with a NTG ratio of 58.2 % if erosion depth equals 6 m (Fig. 12.20) and a NTG ratio of 49.7 % if erosion depth equals 4 m. On average every 4 sandstone bodies are connected in the strata. Modelled NTG ratio and sandstone body connectivity are similar to those observed in the outcrop.

The modelling of the medial Slick Rock strata suggests that the strata were formed in similar high reworking conditions as the relatively proximal Bullfrog strata but with

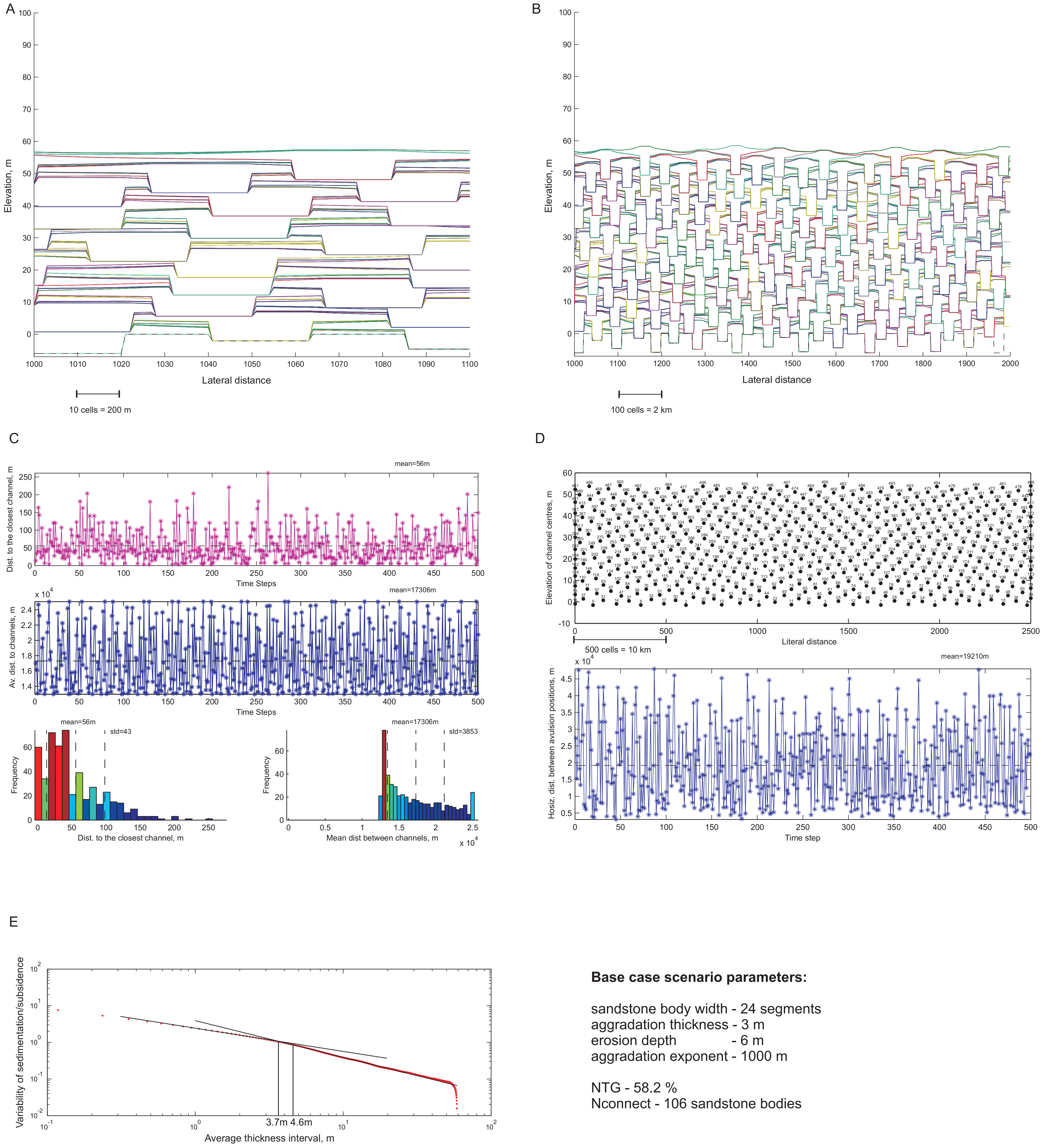

Base case scenario parameters:

sandstone body width - 24 segments
aggradation thickness - 3 m
erosion depth - 6 m
aggradation exponent - 1000 m

NTG - 58.2 %
Nconnect - 106 sandstone bodies

Figure 12.20. Best-fit model of the Slick Rock outcrop. A - 2 km of the modelled strata, B - 20 km of the modelled strata, C - variation of the mean distance between channels and mean distance to the closest channel with time step and frequency distributions of the distances, D - channel position map and variation in mean avulsion distance with time step, E - variability of the sedimentation to subsidence ratio with average thickness windows and approximate estimation of the compensation thickness scale.

slightly smaller incision and degree of lateral migration of the channels. However, parameters measured from the outcrop are highly uncertain due to limited exposure in the Slick Rock outcrop.

Distal succession (Little Park outcrop)

The distal succession of the Salt Wash DFS exposed in the Little Park outcrop (NTG = 35 %) can be also created with a very wide range of input parameters values (Fig. 12.17, A-G). Two examples of modelled strata characterised by the same NTG ratio simulated with contrasting values of input parameters are illustrated in Figure 12.21. Sandstone body connectivity in both modelled examples is slightly different.

The strata exposed in the Little Park outcrop include both Type 1 and Type 2 sandstone bodies as well as abundant Type 3 sandstone bodies. The width of major channel sandstone bodies varies from 60 to 600 m, while the aggradation thickness (channel "wings") and scour depth ranges from 0.2 to 1.5 m and from 1 to 5 m, respectively (Chapter 7, Appendix 5.6). A model with the input parameters measured in the outcrop such as average channel sandstone body width equal to 300 m (16 segments), aggradation rate equal to 1.5 m, average erosion depth equal to 3 m and aggradation exponent equal to 1300 m, produces strata with the NTG ratio of 34.8 % (Fig. 12.22, A-B). The aggradation exponent higher than 900 m is reasonable assumption because a high proportion of fine-grained overbank deposits is observed in the distal Little Park succession (Chapter 7, Appendix 5.6) similarly to the distal Alcolea outcrop in the Huesca DFS succession (Section 12.7.1). The sandstone bodies in the modelled strata are mainly not connected but vertically connected sandstone bodies can occur occasionally and this is also seen in the Little Park outcrop (Appendix 5.6).

Similarly to the distal succession of the Huesca DFS, the modelled distal strata created with outcrop parameters measured from the Little Park outcrop (Fig. 12.22) do not reproduce the architecture of the distal Salt Wash succession realistically. The deposits exposed in the Little Park outcrop show a much smaller number of large sandstone bodies of Type 2 than in the modelled strata, and Type 3 sandstone bodies enclosed by floodplain fine-grained deposits dominate the distal Little Park strata (Chapter 7, Appendix 5.6). The Type 3 sandstone bodies are not simulated by the 2D model and only channel sandstone bodies are considered.

Nevertheless, the modelling experiments suggest that the distal deposits of the Salt Wash DFS succession as well as in the Huesca succession are characterised by higher floodplain aggradation and preservation than medial and relatively proximal successions of the same DFS.

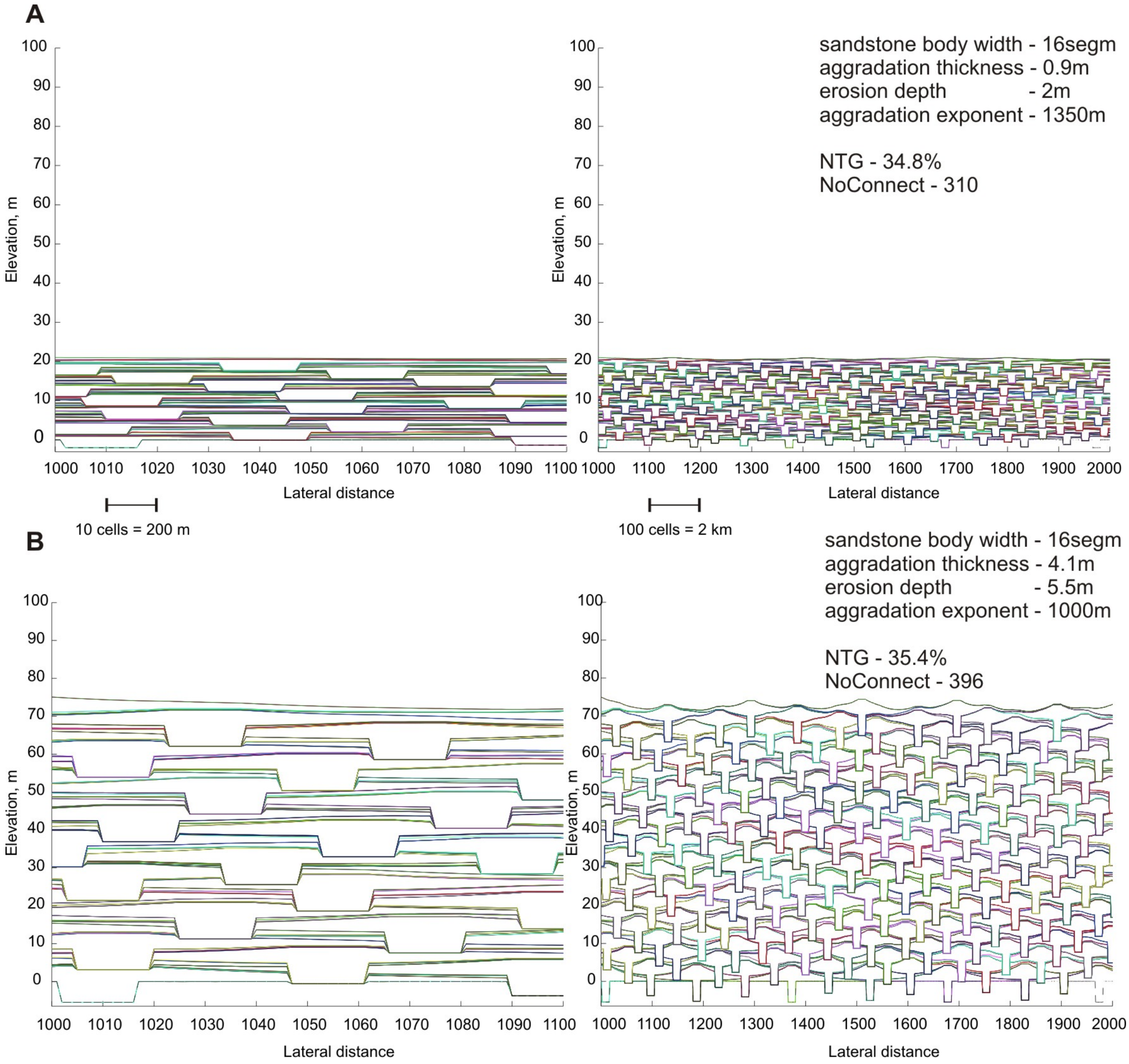

Figure. 12.21. Examples of modelled succession with NTG ratio of 35 % (Little Park outcrop). The models are created with contrastingly different input parameters: A – low aggradation and moderate erosion (relatively low sediment supply - water discharge ratio), B – high aggradation, deep erosion and high degree of lateral migration (high sediment supply, high water discharge, high degree of lateral migration). The sandstone body connectivity between examples is only slightly different.

12.7.3. Summary of main results from the modelling of observed DFS strata

The geometric 2D model has been tested using data measured from the outcrops of the studied DFS successions as input for the model. The model can reproduce strata that match the NTG ratio and sandstone body connectivity estimated from the relatively proximal and medial outcrops. However, the current model set up is purely geometric and almost all input parameters are based on the observations from the same outcrops and therefore there is a risk of circular reasoning that must be taken into account with all interpretations. Nevertheless, the presence of input parameters that cannot be measured from outcrops (aggradation exponent and floodplain aggradation and

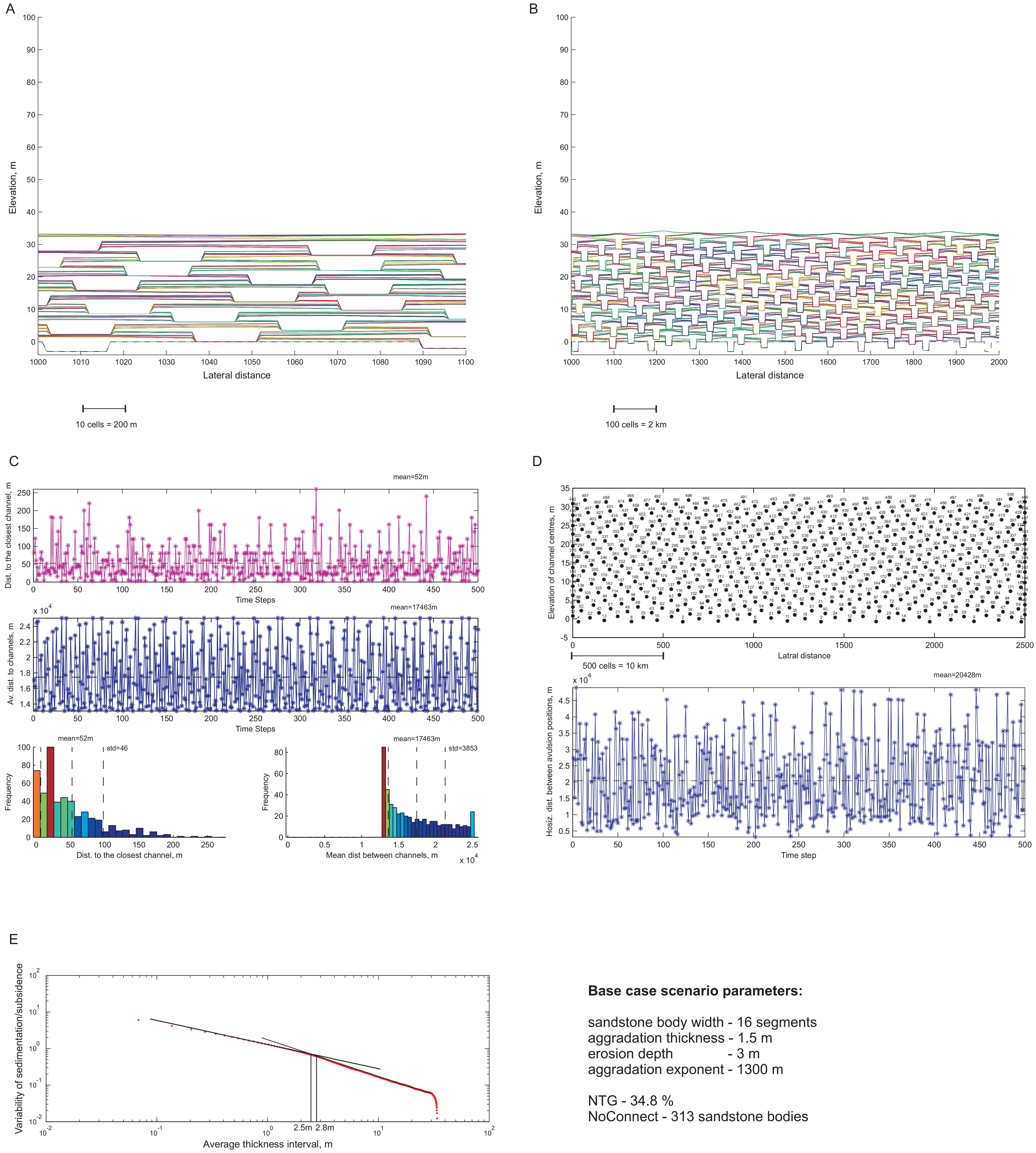

Base case scenario parameters:

sandstone body width - 16 segments
aggradation thickness - 1.5 m
erosion depth - 3 m
aggradation exponent - 1300 m

NTG - 34.8 %
NoConnect - 313 sandstone bodies

Figure 12.22. Best-fit model of the Little Park outcrop. A - 2 km of the modelled strata, B - 20 km of the modelled strata, C - variation of the mean distance between channels and mean distance to the closest channel with time step and frequency distributions of the distances, D - channel position map and variation in mean avulsion distance with time step, E - variability of the sedimentation to subsidence ratio with average thickness windows and approximate estimation of the compensation thickness scale.

avulsion mechanisms) reduce this risk and show that unknown input parameters could be similar to real processes that occurred during formation of the real strata.

It has been shown that relatively proximal, medial and distal DFS strata have to be modelled using different input parameters. Replicated relatively proximal strata require a relatively higher degree of vertical and lateral reworking than more distal strata. Replicated distal strata, in contrast, require a relatively higher degree of floodplain preservation. The 2D model, however, has been found to be limited by lack of flexibility in sandstone body type and dimensions that were observed to be variable in outcrops (Appendix 5). Variable sandstone body dimensions are needed to accurately reproduce the architecture observed in the DFS strata. Distal strata suffer in particular because the 2D model does not simulate terminal splay deposits.

The degree of lateral migration of channels (lateral reworking) has been determined to be the main control on the contrasting architecture characteristics of the Huesca and Salt Wash DFS strata. If sandstone body width is less than 300 m (16 segments), the high-NTG proximal Salt Wash successions could not be modelled using current ranges of input parameters. The higher degree of reworking of floodplain deposits in the Salt Wash DFS could have been a consequence of a lower accommodation setting for the DFS (Weissmann et al., 2013 in press) (see also chapters 8, 10-11).

It has been found that strata with the same NTG ratio can be produced by models with different combinations of contrasting input parameters (Fig. 12.10 and 12.17). The same is true for the strata with the same sandstone body connectivity (see Section 12.8). One single scenario cannot fully explain strata with a particular characteristics unless other parameter values (e.g. outcrop or well data) are available to restrict the number of combinations. For example, strata with the same NTG ratio might have different sandstone body connectivity and geometry of the strata (Fig. 12.23; Fig. 12.9-22).

This finding emphasises that many combinations of external factors could result in the same characteristics of the deposits, suggesting that many DFS stratal architectures may be non-unique, so that it is unlikely many outcrops can be claimed with confidence to be due to any one specific combination of controls. The next section investigates this issue further via a sensitivity analysis.

12.8. Sensitivity analysis: variable input parameters

Model **Experiments 2** (Section 12.6) based on the best-fit models for the relatively proximal strata of the Huesca and Salt Wash DFSs (Monźon and Bullfrog outcrops, Tables 12.3-4; Fig. 12.11 and 12.18) provided the data for sensitivity analysis of the sandstone body architecture to variable input parameters. The analysis is focused on the important reservoir parameters such as NTG ratio and sandstone body connectivity.

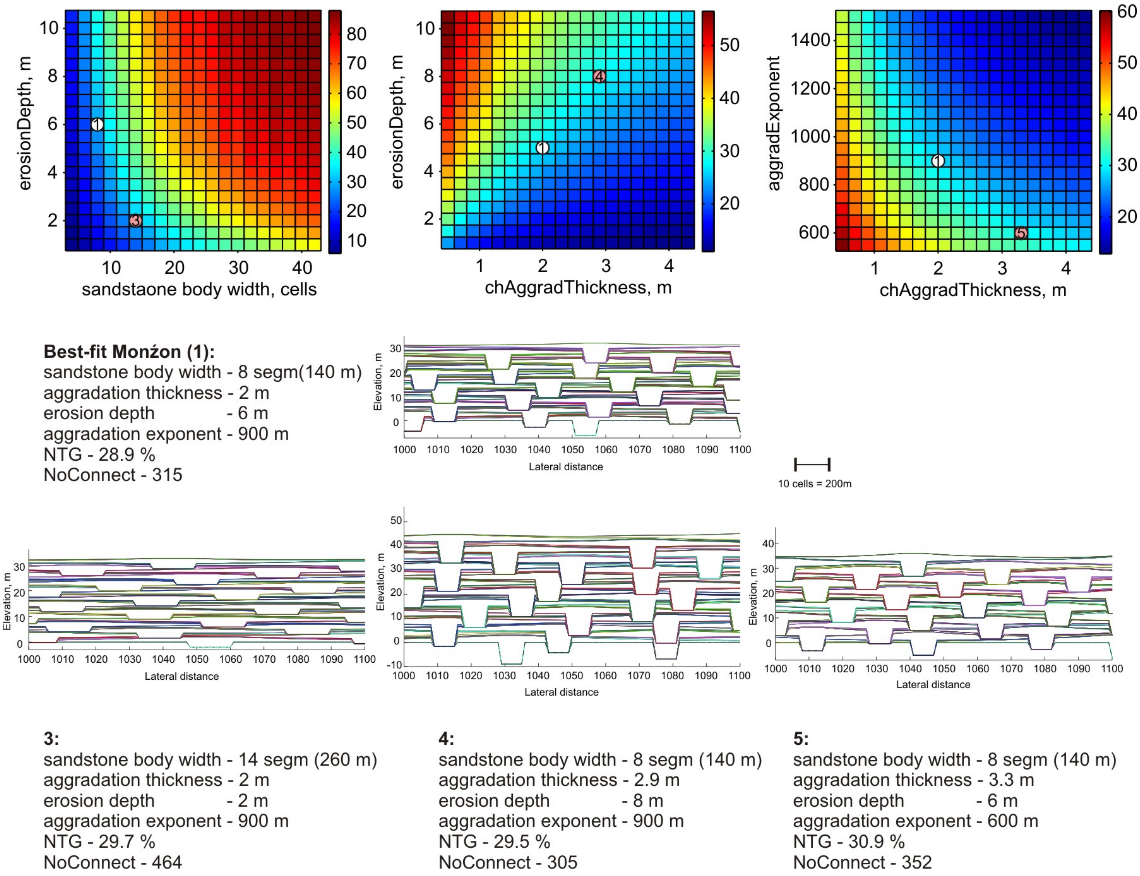

Best-fit Monźon (1):
sandstone body width - 8 segm(140 m)
aggradation thickness - 2 m
erosion depth - 6 m
aggradation exponent - 900 m
NTG - 28.9 %
NoConnect - 315

3:
sandstone body width - 14 segm (260 m)
aggradation thickness - 2 m
erosion depth - 2 m
aggradation exponent - 900 m
NTG - 29.7 %
NoConnect - 464

4:
sandstone body width - 8 segm (140 m)
aggradation thickness - 2.9 m
erosion depth - 8 m
aggradation exponent - 900 m
NTG - 29.5 %
NoConnect - 305

5:
sandstone body width - 8 segm (140 m)
aggradation thickness - 3.3 m
erosion depth - 6 m
aggradation exponent - 600 m
NTG - 30.9 %
NoConnect - 352

Figure 12.23. Non-uniqueness of input parameters, hence factors, that control NTG ratio of the modelled strata. All four models created with different input parameters but produce successions with NTG ratio around 30 % (Monźon outcrop). Note that although the NTG ratio is similar, the number of connected bodies (*Nconnect*) and stratal geometry varies between the models. Explanation of the parameter space maps see in Section 12.8.

Relationships between input and output parameters are shown using parameter space maps (Fig 12.24, 26–27) created following the method of Williams et al. (2012). The output parameters have been plotted in relation to each possible pair of four variable input parameters (Table 12.2). The colour on the maps represents values of the output parameter.

The effects of input parameters on the NTG ratio and sandstone body connectivity of the modelled strata gave results that can be explained using the common understanding of the intercalation between processes of sediment aggradation and reworking. The effect of input parameters on the distance between channels is less obvious but leads to changes in the NTG ratio and sandstone body connectivity of the modelled strata and therefore is worth discussing.

A. Mean avulsion distance (m)

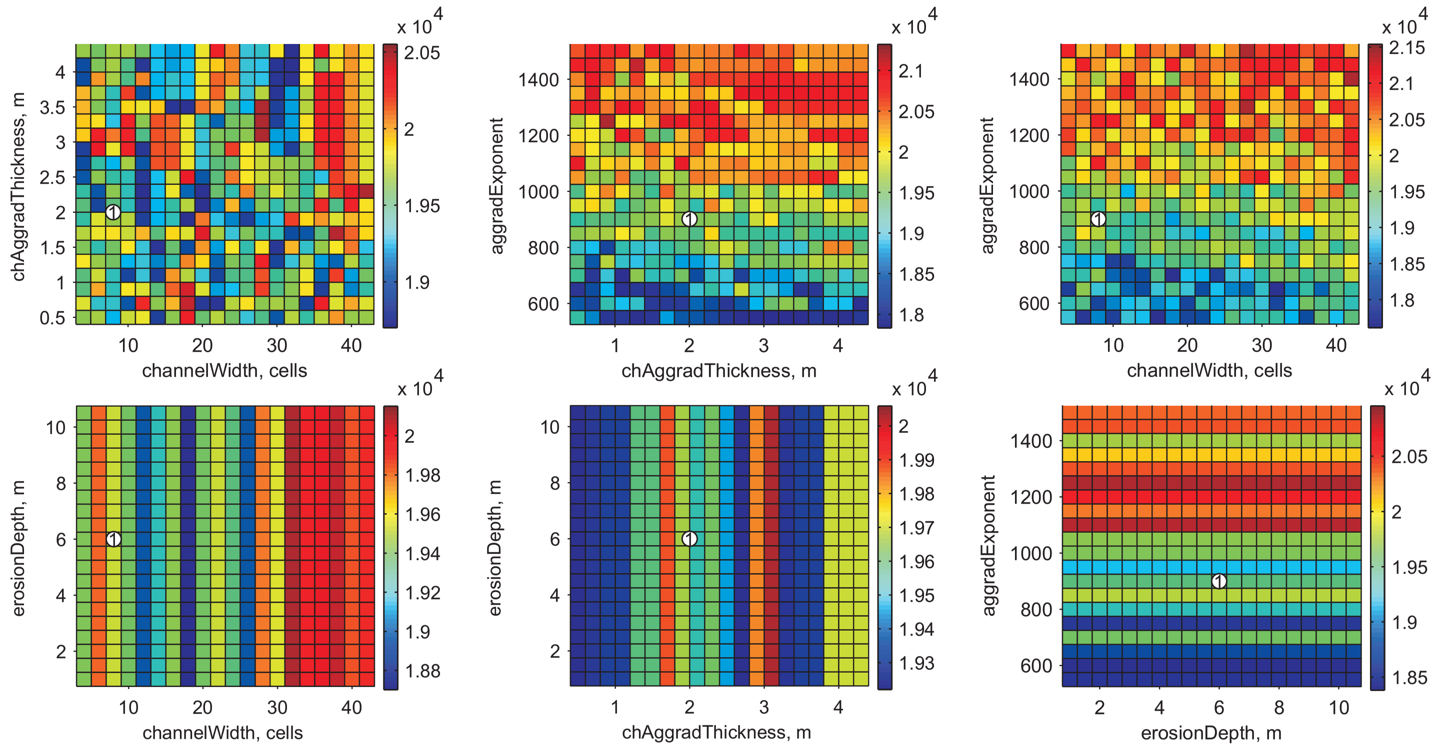

B. Mean distance between channels (m)

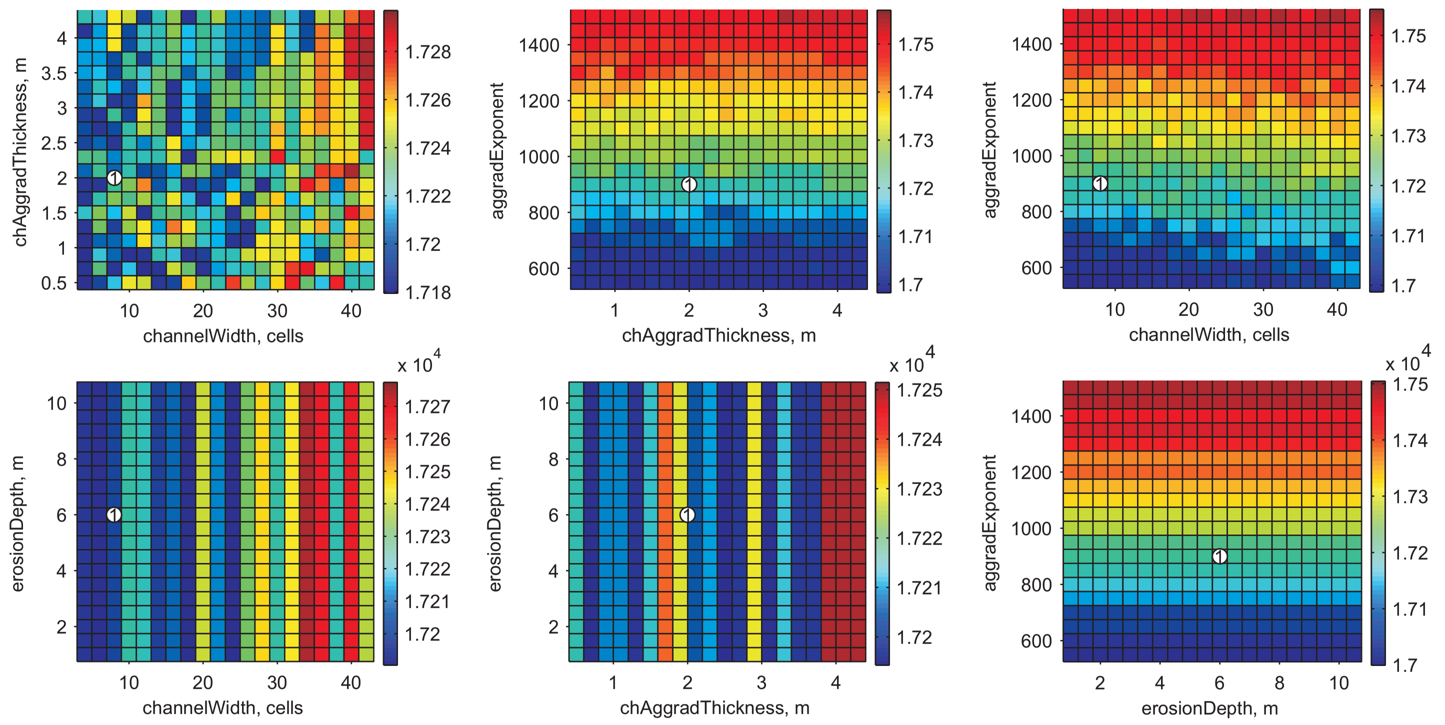

C. Mean distance to the closest channel (m)

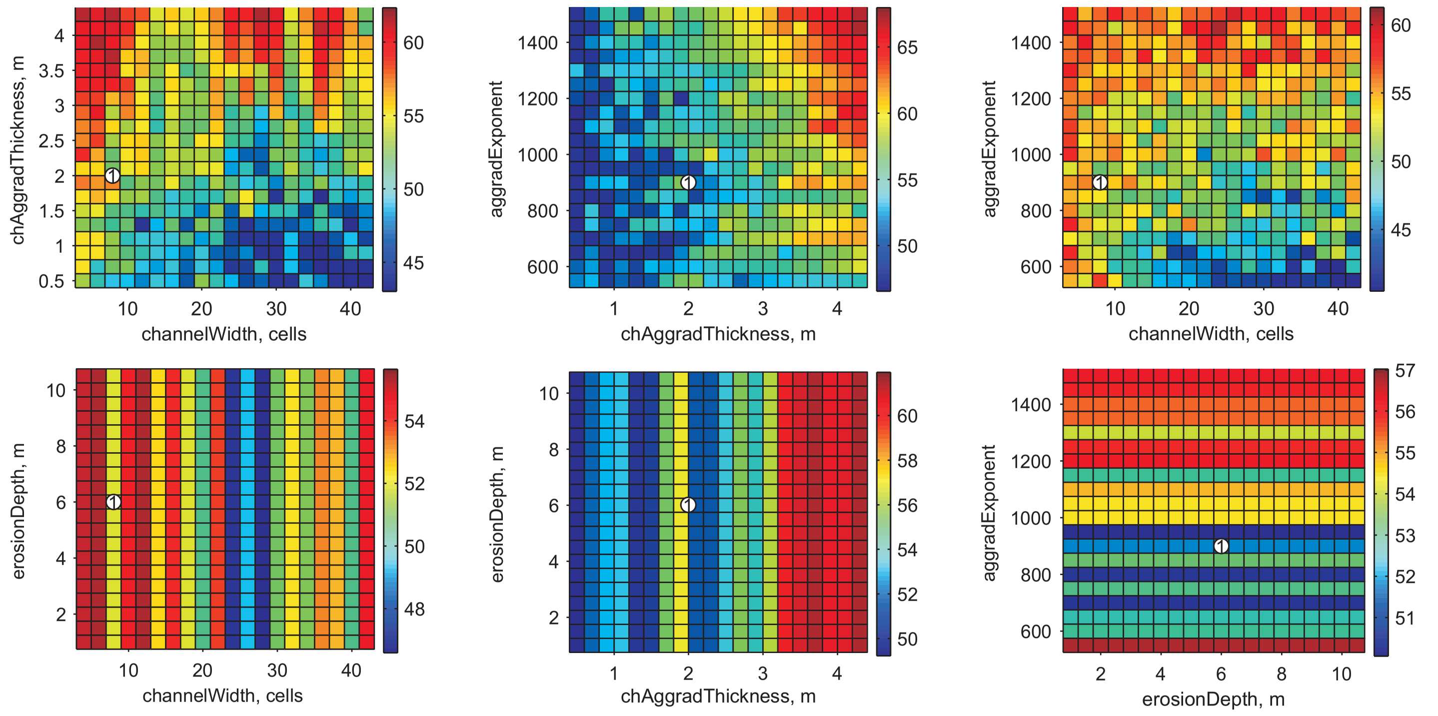

Figure 12.24. Variation in mean avulsion distance (A), mean distance between channels (B) and mean distance to the closest channel (C) with input parameters including channel sandstone body width (*channelWidth*), erosion depth (*erosionDepth*), aggradation thickness (*chAggradThickness*) and aggradation exponent (*aggradExponent*). The sensitivity analysis is based on the best-fit model parameters for the Mońzon outcrop (Table.12.3).

12.8.1. Sensitivity of distance between channel sandstone bodies in the modelled strata to variation in input parameters

The mean distance between avulsion locations (*MeanAvulDist*) in the model is mainly influenced by the floodplain aggradation exponent (Fig. 12.24, A). The higher the floodplain aggradation exponent, the more extensive is the elevated area of floodplain deposits on both sides of the channel element. Consequently, the topographic minimum where next channel is diverted by the next avulsion tends to be further away from the elevated area (see also Sheets et al., 2002). The highest distance between avulsion locations has been obtained for the model with highest floodplain aggradation exponent (1500 m) independently of other parameters (Fig. 12.24).

Variations in the distance between avulsion locations usually define variations in mean distance between channels (*MeanMeanDist*) (Fig. 12.24, B). Each channel element is free to avulse to a topographic minimum anywhere within the entire model domain and therefore the lateral distance between channels is always higher than vertical distance. This is also true for the real strata due to their aspect ratio. Thus, changes in lateral distance caused by changes in the aggradation exponent contribute more to the variation in the mean distance between channels than changes in vertical distance. According to these results, both *MeanAvulDist* and *MeanMeanDist* are theoretically controlled by the amount of fine-grained suspended load transported out of the channel by floods (Section 12.5).

The mean distance to the closest channel (*MeanMinDist*), in contrast, reflects variations in vertical distance between sandstone bodies (Fig. 12.24, C). The main control parameter on the vertical distance in the model is the aggradation thickness (related to sediment supply), but minor effects can also be seen from the floodplain aggradation exponent that contributes to the total succession aggradation (Section 12.5). The smallest distance to the closest channel has been found for the model with the smallest aggradation thickness (0.5 m) and an aggradation exponent (550 m). Thus, *MeanMinDist* reflects the degree of vertical aggradation and preservation of floodplain deposits.

The distance between channel centres is not affected by erosion depth and only slightly affected by channel sandstone body width (Fig. 12.24, A-C). The proximity of the channel sandstone bodies in turn controls changes in NTG ratio and sandstone body connectivity discussed in the following two sections.

12.8.2. Effect of the floodplain aggradation parameters on the NTG ratio and sandstone body connectivity of the modelled strata

The high aggradation of the floodplain deposits (high aggradation thickness and exponent), probably caused by high sediment supply to water discharge ratio, and implicitly by high availability of fine-grained sediment in the stream load (Section 12.5), makes the distance between channels increase (Fig.12.24, A-C) and, consequently, reduces the sandstone body connectivity in the strata (Fig. 12.26, B). Additionally, high subsidence rate can be another factor controlling aggradation but it is not considered in this study. The result is a high degree of floodplain preservation that reduces the proportion of sandstone bodies relative to floodplain deposits and hence reduces the NTG ratio of the strata.

The aggradation thickness (sediment supply) affects NTG ratio and connectivity more than the floodplain aggradation exponent (abundance of fine-grained sediment) (Fig. 12.26, A-B) due to the greater effect on vertical distance between channels, hence vertical sandstone body connectivity, and greater contribution to the floodplain interval aggradation, hence floodplain deposit proportion. The floodplain aggradation exponent still contributes to overall floodplain aggradation and preservation.

12.8.3. Effect of reworking parameters on the NTG ratio and sandstone body connectivity of the modelled strata

The high degree of reworking of previously accumulated channel fill and floodplain deposits (deep incision and high degree of lateral migration of channels), probably caused by a low sediment supply to water discharge ratio and implicitly by low cohesiveness of channel banks or low accommodation (Section 12.5), leads to an increase in both NTG ratio and sandstone body connectivity of a succession (Fig. 12.26, A, B). The effect on the sandstone body connectivity is not entirely related to the distance between channels. If width and thickness of channel sandstone bodies are high the connectivity would be controlled by sandstone body cross-sectional area rather than distance between channel centres. The erosion depth does not affect the distance between channel centres (Section 12.8.1) but it affects the NTG ratio and connectivity due to the increased area of reworked floodplain strata.

Reworking due to erosion depth (water discharge) affects the output parameters of the modelled strata less than the degree of lateral channel migration (Fig. 12.26, A-B) for simply geometrical reasons such as the relative cross sectional area of channel sandstone bodies.

12.8.4. Sensitivity of the NTG ratio and sandstone body connectivity in the modelled strata to the width of sandstone bodies

The data from the model **Experiment 1** have been grouped by width of channel sandstone bodies in the experiment and maximum, minimum and average values have been calculated within each group (Table 12.5). The obtained data showed an expected increase in maximum, minimum and average values of the NTG ratio with channel sandstone body width (Fig. 12.25, A), hence with the degrees of reworking due to lateral migration of channels. The increase in maximum NTG ratio slows down when it reaches 75 % and subsequent increase is not as great (Fig. 12.25, A). This change is possibly related to reworking of previously deposited sandstone bodies by subsequent channel elements and overlap of sandstone bodies and does not have great effect on already high NTG ratio. The same trends are seen for the number of individual sandstone bodies in the model which decreases with increase in channel sandstone body width as connectivity increases (Fig. 12.25, B; Fig. 12.5).

Channel sandstone body width, segments	**4**	**6**	**8**	**10**	**12**	**14**	**16**
Maximum NTG ratio, %	37.4	54.7	67.7	75.1	79.9	83.5	86.3
Minimum NTG ratio, %	3	5	6.9	8.8	10.6	12.4	14.1

Table 12.5. Minimum and maximum NTG ratios for different channel sandstone body width.

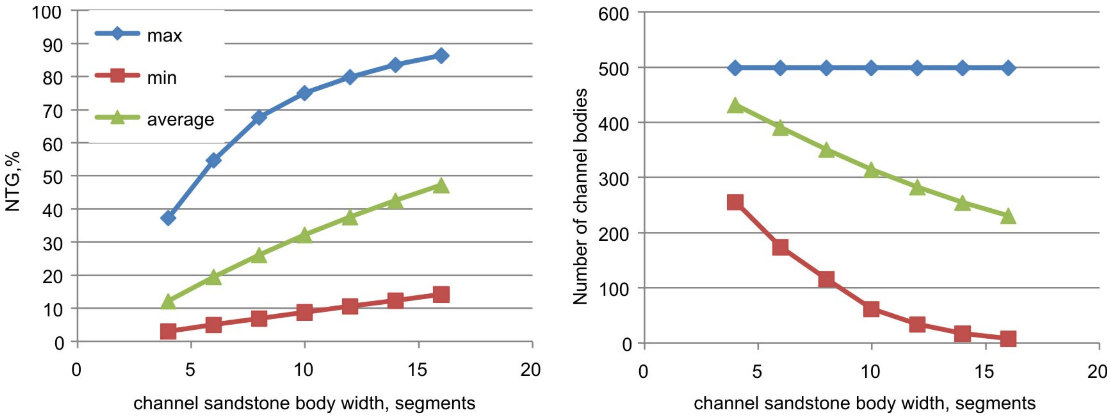

Figure 12.25. Increase in the maximum, average and minimum NTG ratio (A) and number of individual sandstone bodies (B) in the model with the increase in channel sandstone body width.

Independently of the channel sandstone body width, maximum NTG ratio values (data from **Experiment 1**) correspond to the models with the lowest floodplain/channel aggradation, highest erosion depth and lowest floodplain aggradation exponent, hence a high degree of reworking and a low degree of aggradation. In contrast, the lowest values of the NTG ratio correspond to a high degree of aggradation and low degree of

A. Net-to-Gross (%)

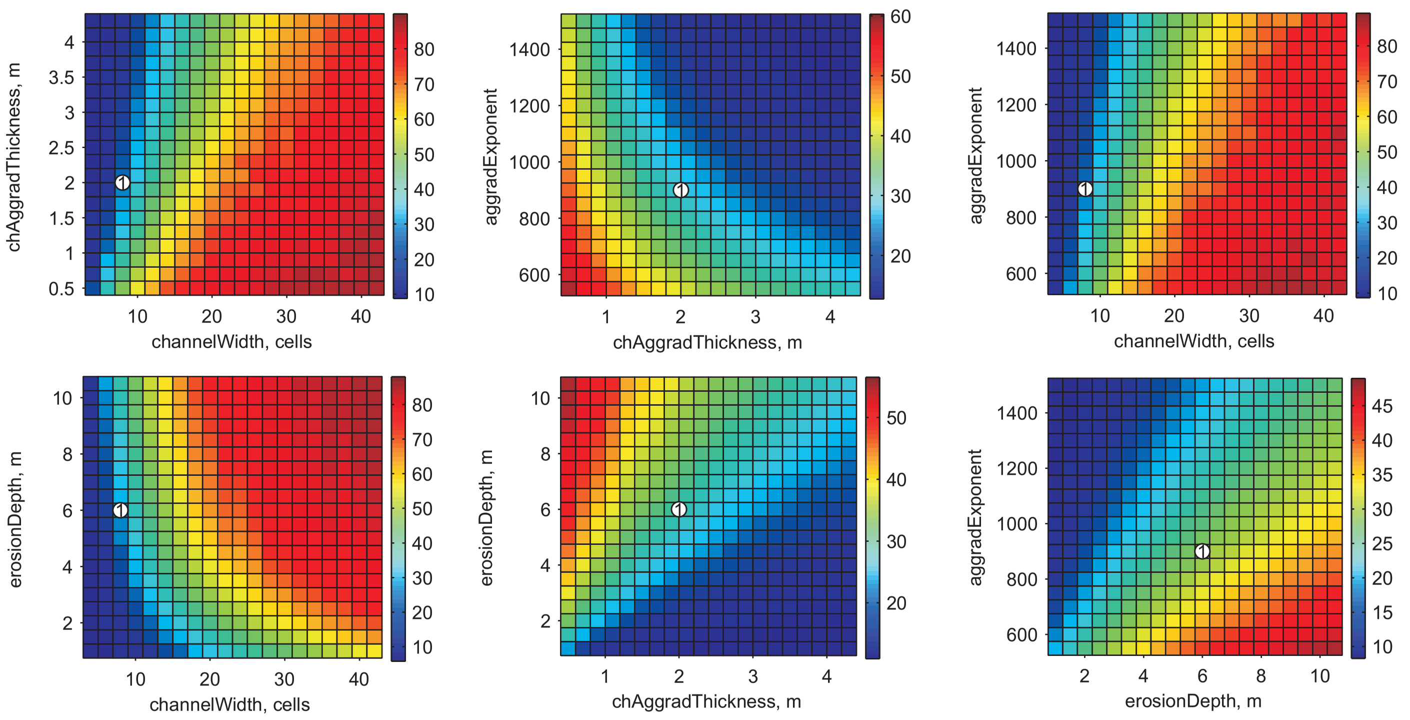

B. Number of sandstone bodies (m)

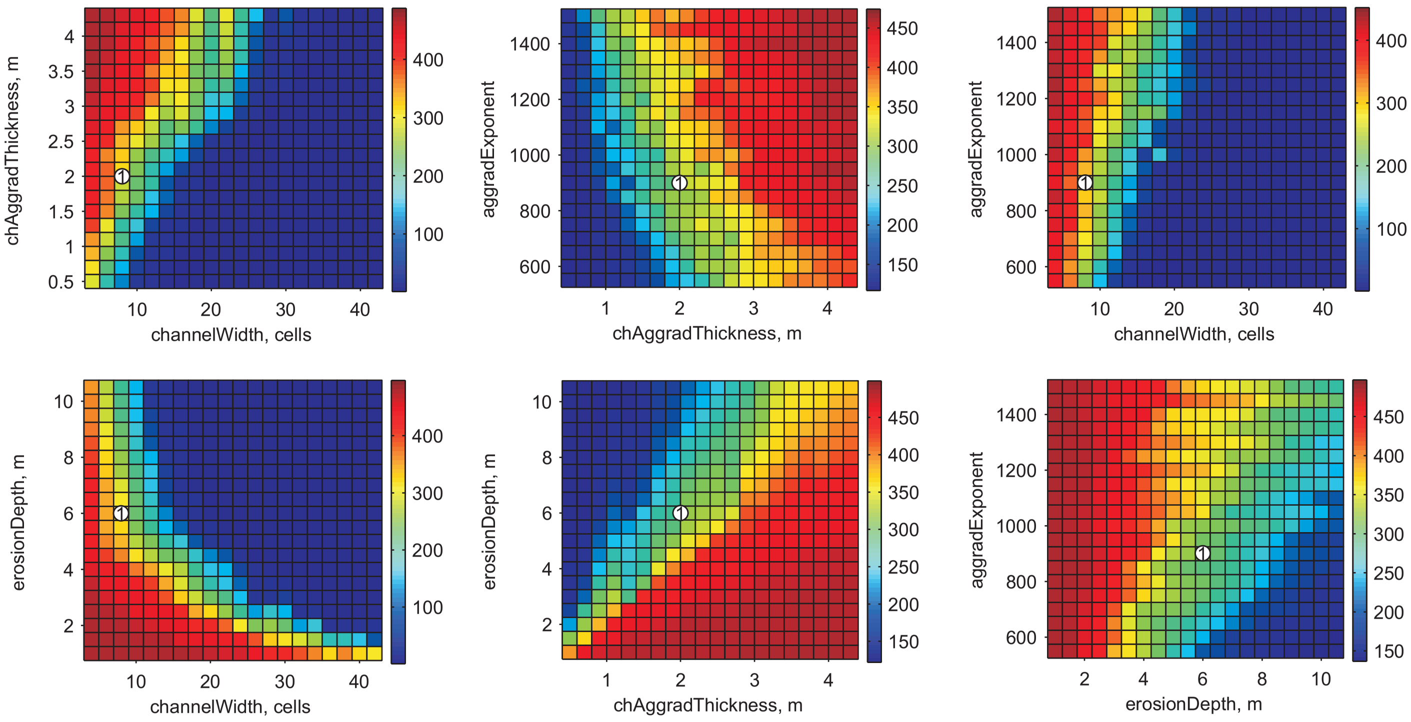

C. Average thickness of the modelled strata (m)

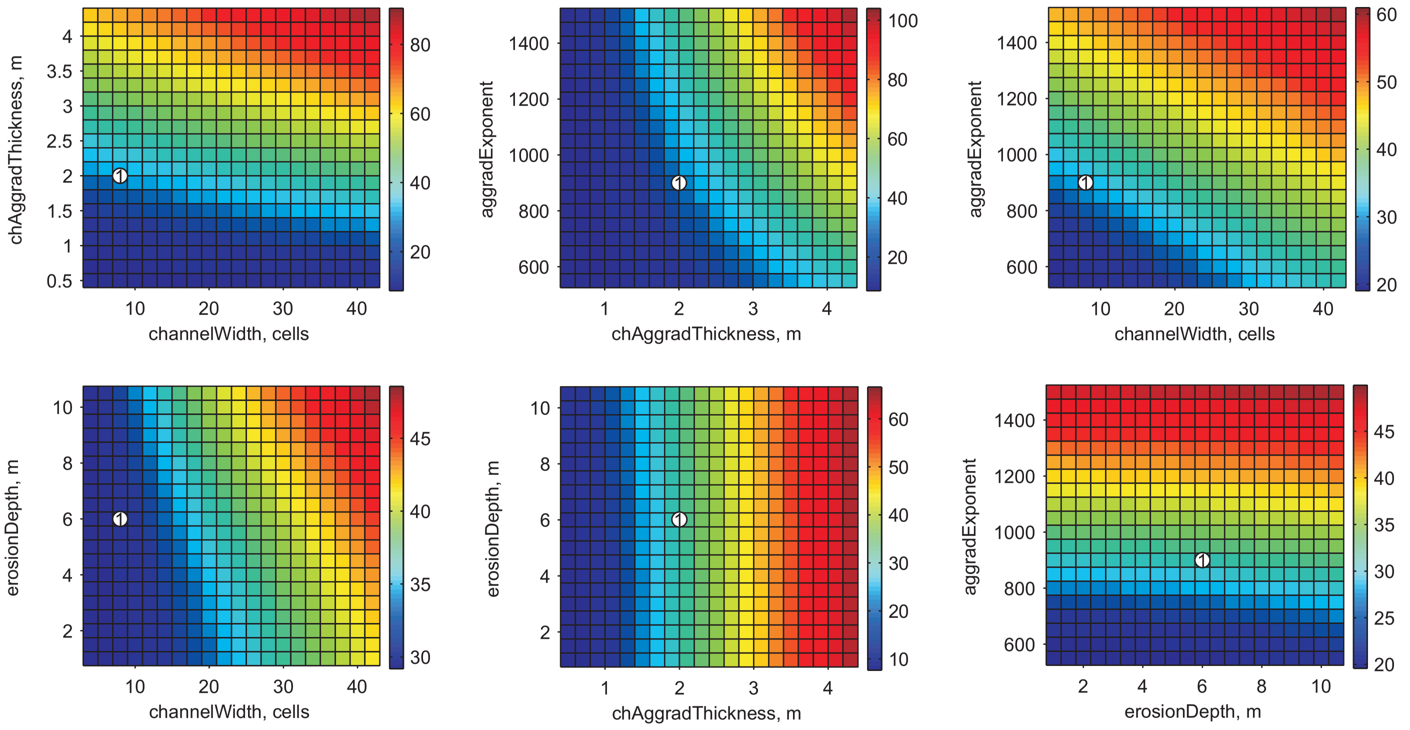

Figure 12.26. Variation in net-to-gross (A), number of sandstone bodies (B) and average thickness of the modelled strata (C) with input parameters including channel sandstone body width (*channelWidth*), erosion depth (*erosionDepth*), aggradation thickness (*chAggradThickness*) and aggradation exponent (*aggradExponent*). The sensitivity analysis is based on the best-fit model parameters for the Monżon outcrop (Table.12.3).

reworking. Intermediate results could be produced with many different combinations of input parameters (Fig.12.10 and 12.17) suggesting again that many fluvial architectures are rather non-unique.

12.8.5. Sensitivity of characteristics of strata with high and low channel sandstone body width to variations in input parameters

The difference between Monźon and Bullfrog best-fit models is mainly related to channel sandstone body width which is significantly different (8 and 42 segments). Other parameters such as erosion depth, aggradation thickness and aggradation exponent differ less (Tables 12.3-4). Consequently, trends on the sensitivity maps for a pair of input parameters where one of the parameters is channel sandstone body width are similar for both cases because the channel width is varied within the same range in both analyses (Fig. 12.26 and 12.28, A–B; Table 12.6). Insignificant differences between the results of two sensitivity analyses is also observed when channel sandstone body width is kept constant while other input parameters are varied (Table 12.6, grey shaded cells).

The magnitude of changes in NTG ratio and the number of individual sandstone bodies (connectivity) differs for the Monźon and Bullfrog best-fit models when a pair of investigated input parameters does not include sandstone body width (Table 12.6, white cells). For example, variation in the erosion depth from 1 m to 10.5 m at a channel aggradation thickness equal to 2.1 m changes the NTG ratio of the Monźon best-fit model from 13.2 % to 36.8 %. The same variation in the erosion depth and aggradation thickness changes the NTG ratio of the Bullfrog best-fit model more, from 56.2 % to 87.8 %. The change in aggradation thickness from 0.5 m to 4.3 m and constant erosion depth equal to 6 m results in a change of the NTG ratio of the Monźon best-fit model from 49.8 % to 19.8 % while the NTG ratio of the Bullfrog best-fit model changes only from 90.3 % to 74.3 % (Table 12.6).

It could be inferred from this analysis that aggradation thickness affects the NTG ratio of the strata with high channel widths less than the NTG ratio of the strata with smaller channel width (Table 12.6). The variations in aggradation exponent also have a greater effect on the NTG ratio and sandstone body connectivity of the strata with smaller channel sandstone body widths. In contrast, the erosion depth affects the NTG ratio of the strata with small channel body widths less.

The results discussed in sections 12.8.4 and 12.8.5 support that the sandstone body width (degree of lateral migration) is one of the main controls on the reservoir characteristics of the DFS strata that has been also shown in sections 12.7 and 12.8.3.

		Monźon best-fit						Bullfrog best-fit					
		NTG ratio			Number of sandstone bodies (connectivity)			NTG ratio			Number of sandstone bodies (connectivity)		
Constant parameter	**Variable parameter**	**from**	**to**	**difference**	**from**	**to**	**difference**	**from**	**to**	**difference**	**from**	**to**	**difference**
erosionDepth = 6m	Aggradation thickness	49.8	19.8	30	130	463	-333	90.3	78.4	11.9	1	5	-4
Aggradation thickness = 2.1m	erosionDepth	13.2	36.8	-23.6	494	213	281	56.2	87.8	-31.6	318	1	317
aggradation Exponent = 900 m	Aggradation Thickness	49.8	19.8	30	130	463	-333	91.3	78.4	12.9	1	5	-4
Aggradation Thickness = 2.1m	aggradation Exponent	40	19.2	20.8	232	405	-173	86.9	79.9	7	9	1	8
aggradation Exponent = 900 m	erosion depth	13.3	37.5	-24.2	494	207	287	51.2	86.7	-35.5	371	1	370
erosionDepth = 6m	aggradation Exponent	40.7	19.8	20.9	21	371	-350	86.3	70.4	15.9	8	111	-103
chanel SB width = 8m	Aggradation thickness	49.8	19.8	30	130	463	-333	53.7	22.9	30.8	130	421	-291
Aggradation Thickness = 2.1m	chanel SB width	13	83.7	-70.7	405	1	404	15.2	86	-70.8	394	1	393
chanel SB width = 8m	erosionDepth	13.3	37.5	-24.2	494	207	287	11.9	31.4	-19.5	494	285	209
erosionDepth = 6m	chanel SB width	13.4	84	-70.6	412	1	411	10.7	81.3	-70.6	469	1	468
chanel SB width = 8m	aggradation Exponent	40.7	19.8	20.9	221	371	-150	38.9	18.5	20.4	258	413	-155
aggradation Exponent = 900 m	chanel SB width	13.4	84	-70.6	412	1	411	12.5	84.6	-72.1	444	1	443

Table 12.6. Results of the sensitivity analysis for the Monźon and Bullfrog best-fit models.The table shows relative magnitude of the effect of input parameters on the NTG ratio and nuber of sandstone bodies (metric of connectivity) of the modelled strata. The column "difference" shows variation in the output parameters if the variable input parameters changed within the set range (Table 12.2, Section 12.2.7) while the other input parameter is kept the same. Note small difference for the analyses where channel sandstone body width (channel SB width) is taking part (tow left columns marked by grey).

A. Mean avulsion distance (m)

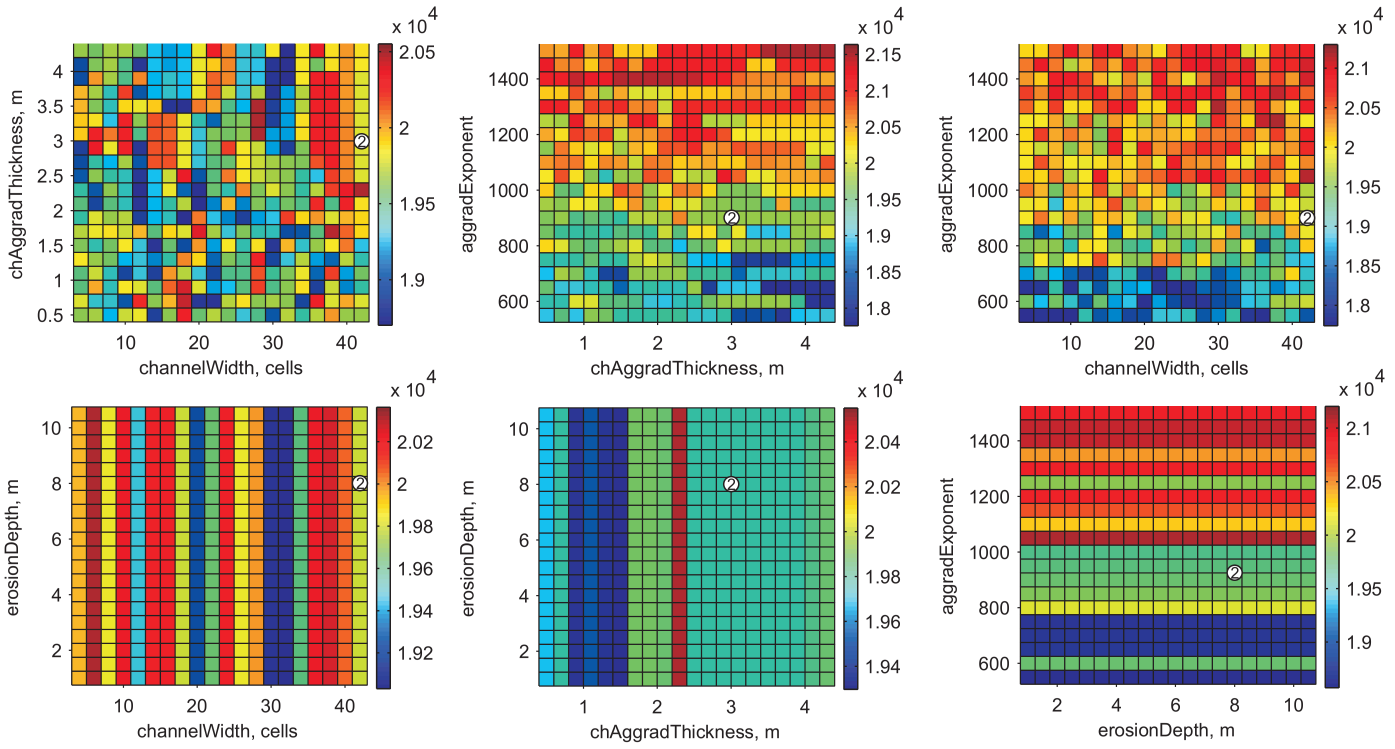

B. Mean distance between channels (m)

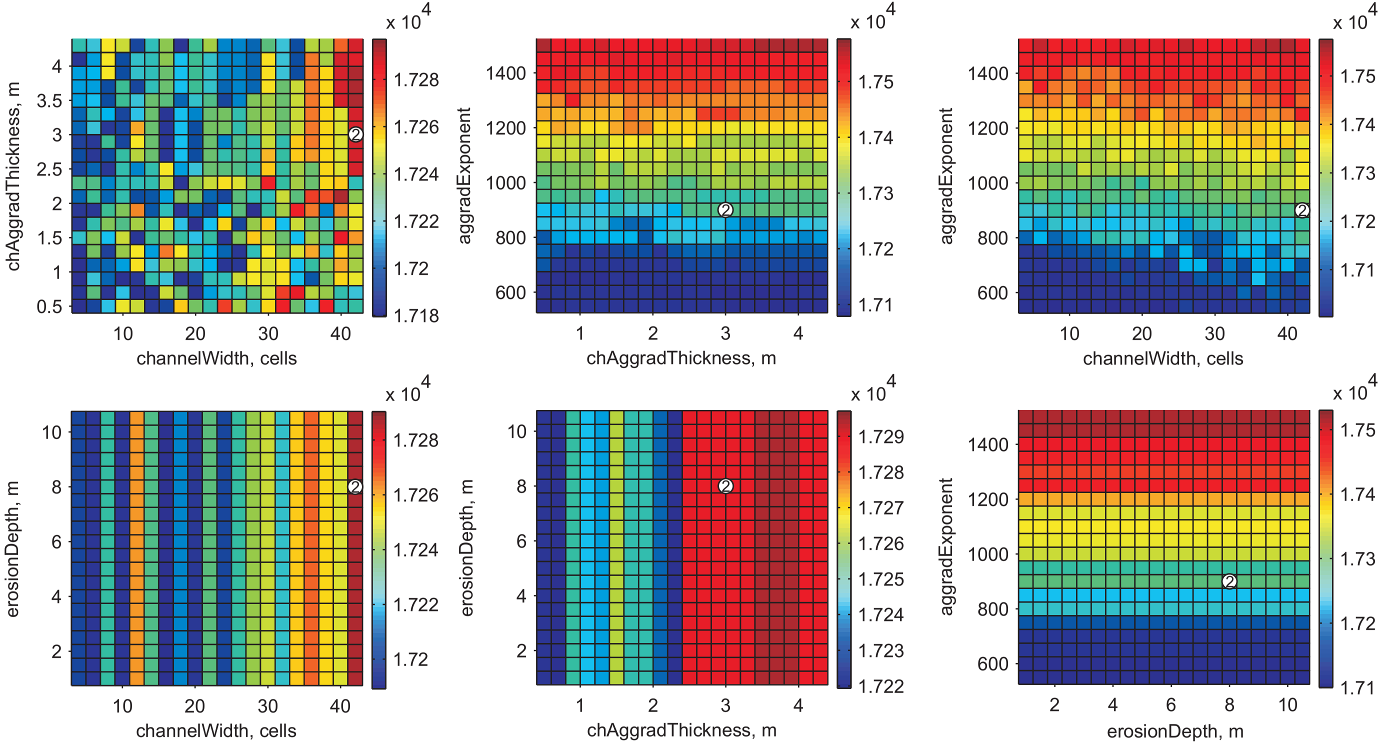

C. Mean distance to the closest channel (m)

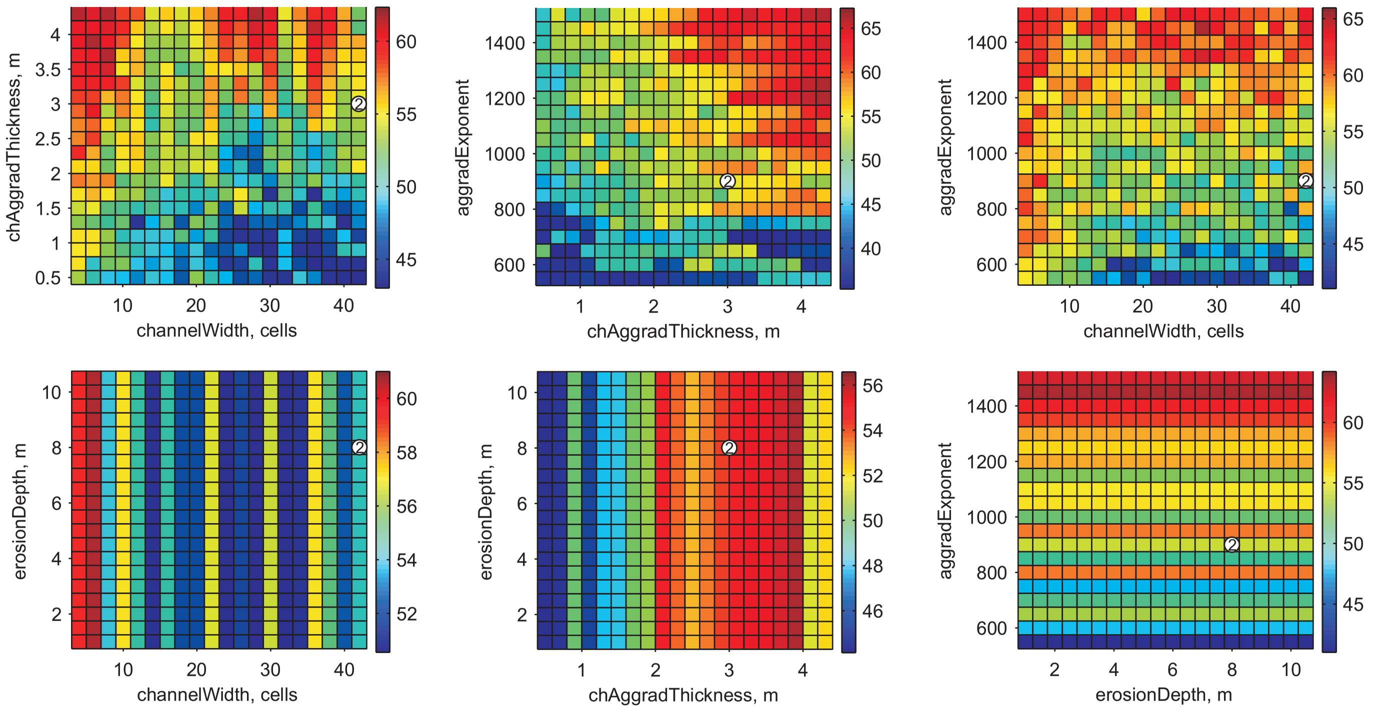

Figure 12.27. Variation in mean avulsion distance (A), mean distance between channels (B) and mean distance to the closest channel (C) with input parameters including channel sandstone body width (*channelWidth*), erosion depth (*erosionDepth*), aggradation thickness (*chAggradThickness*) and aggradation exponent (*aggradExponent*). The sensitivity analysis is based on the best-fit model parameters for the Bullfrog outcrop (Table.12.4).

A. Net-to-Gross (%)

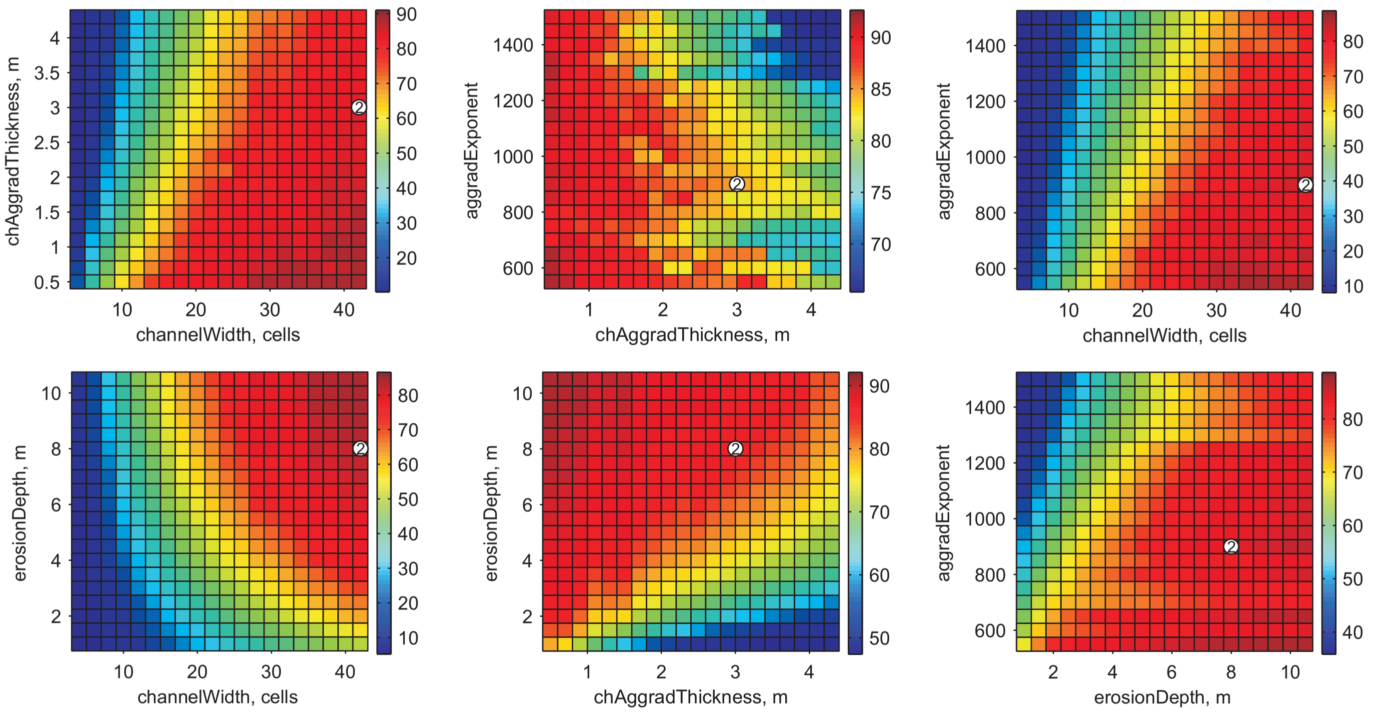

B. Number of sandstone bodies (m)

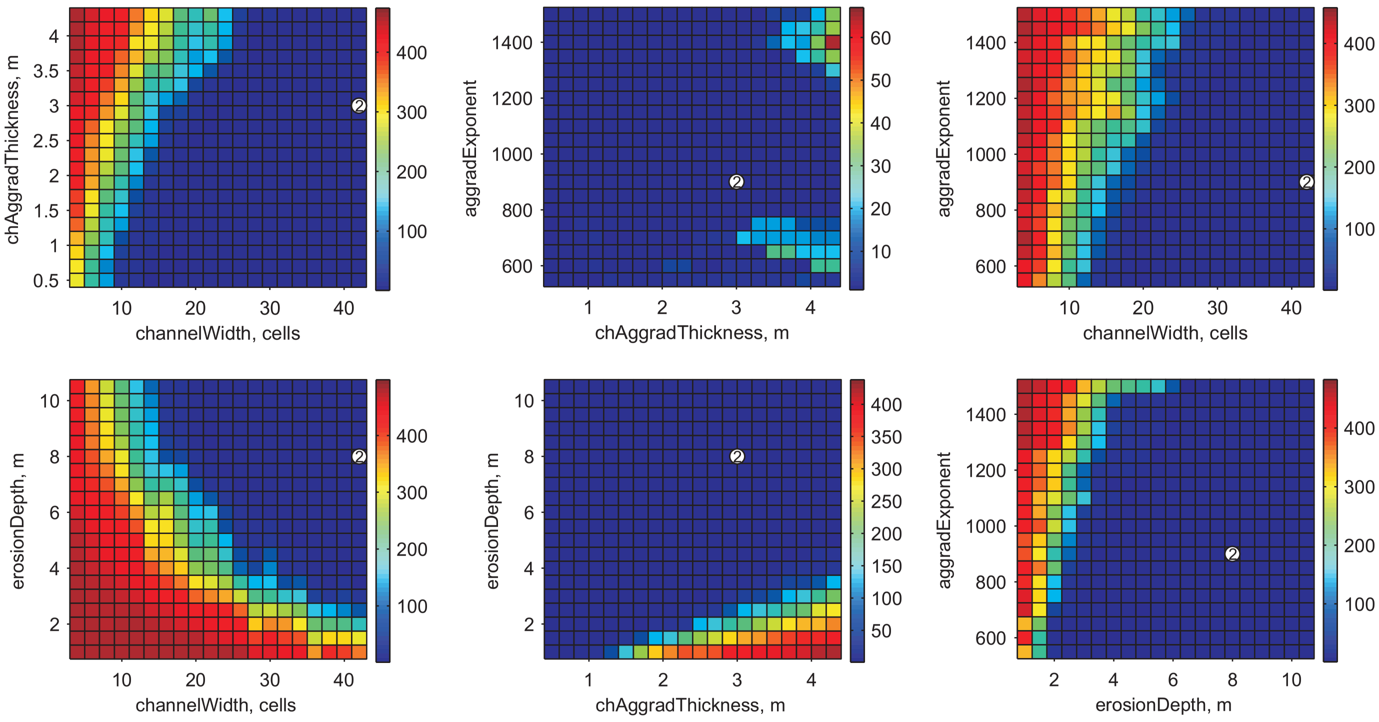

C. Average thickness of the modelled strata (m)

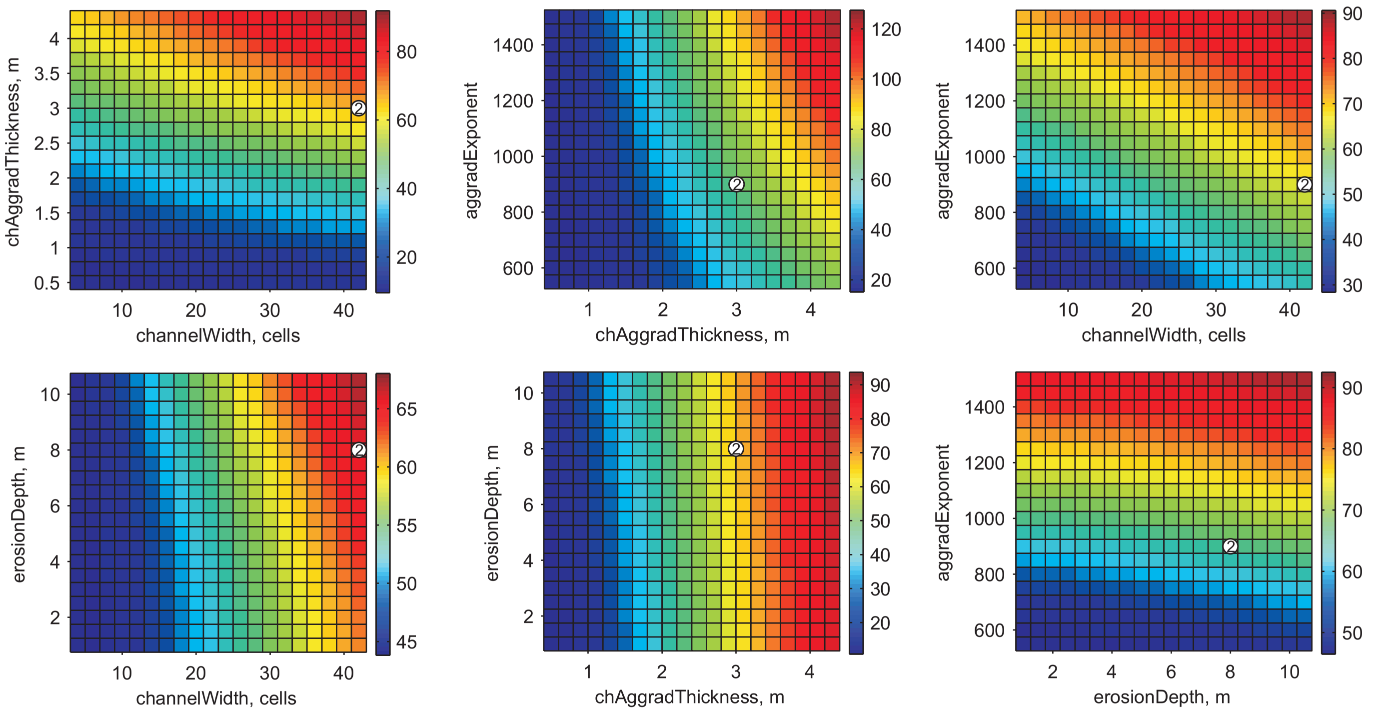

Figure 12.28. Variation in net-to-gross (A), number of sandstone bodies (B) and average thickness of the modelled strata (C) with input parameters including channel sandstone body width (*channelWidth*), erosion depth (*erosionDepth*), aggradation thickness (*chAggradThickness*) and aggradation exponent (*aggradExponent*). The sensitivity analysis is based on the best-fit model parameters for the Bullfrog outcrop (Table.12.4).

12.8.6. Artefacts within the models with compensational channel migration algorithm

The striping and irregularities on the sensitivity maps for Monźon and Bullfrog best-fit models are possibly caused by gridding algorithm artefacts and model boundary effects. The number of connected sandstone bodies is clearly affected by the algorithm that is used to create the facies grid to count connected cells. The limitations of the algorithm are described in Section 12.3.2. The truncating boundary condition in the model (Section 12.2.1) could introduce some discrepancies to the mean distance between channels and therefore to the NTG ratio that are seen on the sensitivity maps. This effect seems to affect models with higher sandstone body width (Bullfrog best-fit model) more than the models with low sandstone body width (Monźon best-fit model) (Fig.12.24, 26-28). More work is required to understand some of these artefacts completely. However, the trends obtained on the sensitivity maps and average values are still recognised and the model is considered suitable for qualitative analysis, with careful consideration that some results may be affected by gridding algorithm and the model boundary effect.

12.9. Sensitivity analysis: variable avulsion mechanism

The sensitivity analysis of the reservoir parameters and compensation thickness scale of the modelled strata to the channel avulsion mechanism is based on the data obtained in the **Experiments 3, 4 and 5** (Section 12.6; Table 12.2).

12.9.1. Sensitivity of NTG ratio and sandstone body connectivity in the modelled strata to channel avulsion mechanism

In general the results of the **Experiment 3** showed that NTG ratio for the modelled strata where channels avulse randomly is lower than in the strata modelled with the compensational avulsion algorithm (Fig. 12.29, A). This is because channel sandstone bodies in the model with random avulsions have a chance to be placed close to or on top of each other and therefore partially rework each other, leading to smaller cross sectional area occupied by an amalgamated sandstone body (Fig. 12.30, C). The number of individual sandstone bodies shows lower values (higher connectivity (Fig. 12.5)) for the models with random channel migration for the same reason (Fig. 12.29, B).

The trend in the output parameters with increase in sandstone body width is the same for the modelled strata with compensational and random channel avulsions (Fig. 12.29). In the strata modelled with random channel avulsion a few sandstone bodies are always connected while there are models created with compensational channel migration algorithm where all sandstone bodies are isolated (Fig. 12.29, B). This and results of the Experiment 3 confirm the suggestion made by Larue and Hovadik (2006) that strata formed with compensational avulsion mechanism would have lower sandstone body connectivity because channels would be avulsing away from their previous position into a topographic minimum and therefore would be separated by floodplain deposits laterally and vertically with a low probability of being connected (see also Chapter 11).

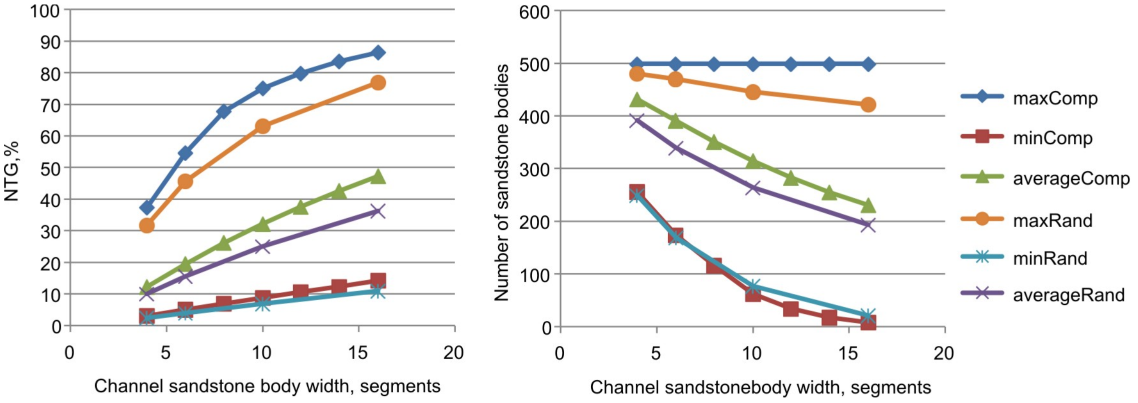

Figure 12.29. Increase in the maximum, average and minimum NTG ratio and number of individual sandstone bodies with increase in sandstone body width. Compare values between models with random and compensational channel migration algorithms.

The results of **Experiment 4,** where best-fit Monźon strata have been modelled with random and combined random and compensational channel avulsion algorithms, show that reworking of sandstone bodies by subsequent bodies explains the lower NTG ratios for these models as well being due to the random component present in both avulsion algorithms (Fig. 12.30, A, C-D).

The Monźon best-fit modelled strata simulated with the random channel avulsion algorithm shows exactly the same sensitivity trends in output parameters as seen for the same model simulated with compensational channel avulsions (compare Fig. 12. 24 and 26 with Fig. 12.31 and 32). Due to the same seed number used during the sensitivity analysis, the distance between avulsion locations in all models with random channel migration algorithm is independent of the input parameters and therefore are not presented.

An increase in the migration distance parameter (*migrationDistance*) in the model with combined random and compensational channel avulsion algorithms during **Experiment 5** causes the increase in the NTG ratio due to a decrease in the degree of channel-channel reworking (Fig.12.30, A, D).

The models with a random channel avulsion mechanism seem to be less affected by the model artefacts described in Section 12.8.6. For example, boundary effects might

A. NTG ratio and number of sandstone bodies in the modelled strata simulated with different channel avulsion algorithms

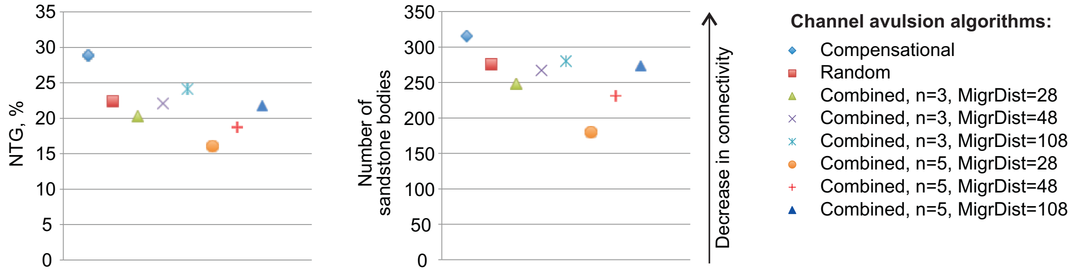

B. Compensational avulsion mechanism

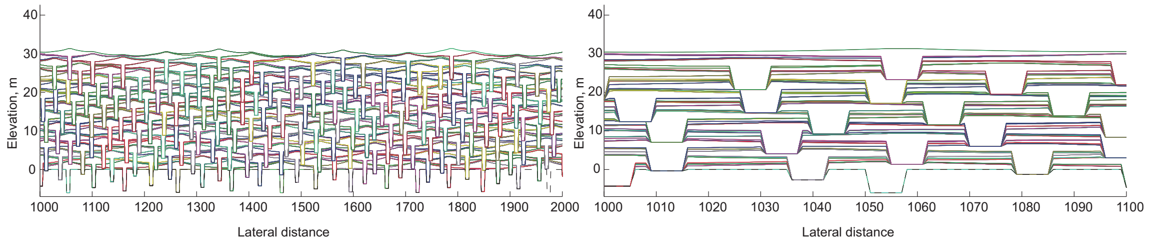

C. Random avulsion mechanism

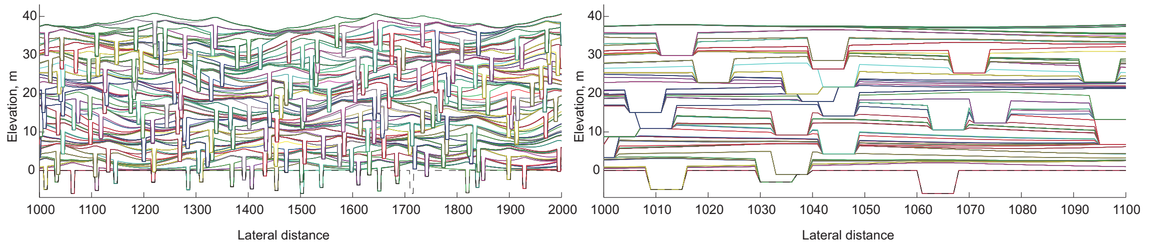

D. Combined compensational and random avulsion mechanism with avulsion frequency n = 3 and *migrationDistance* = 28 cells (upper) and 108 cells (lower)

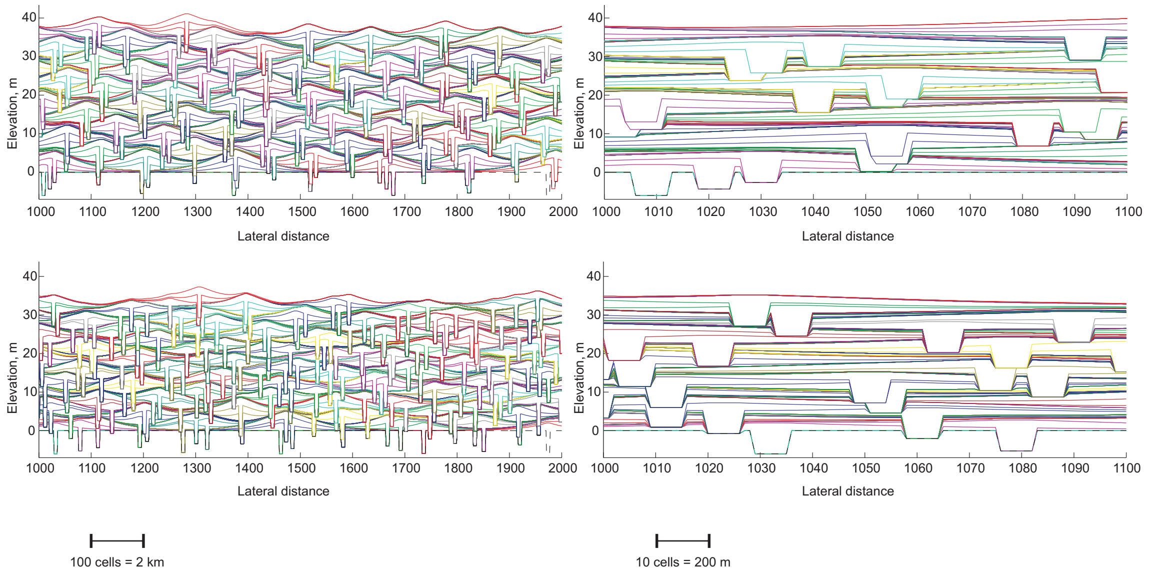

Figure 12.30. Variation in NTG ratio and number of sandstone bodies in the Monźon best-fit model with different channel avulsion algorithms.

A. Net-to-Gross (%)

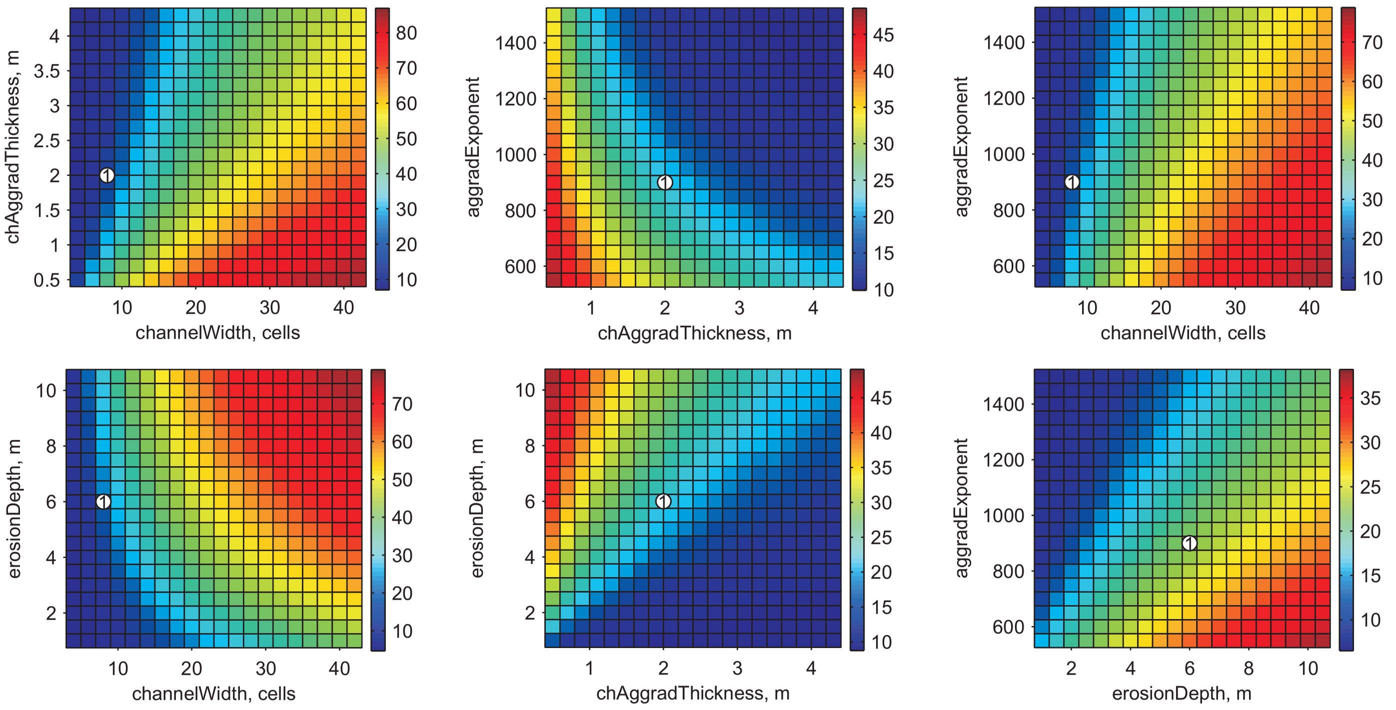

B. Number of sandstone bodies (m)

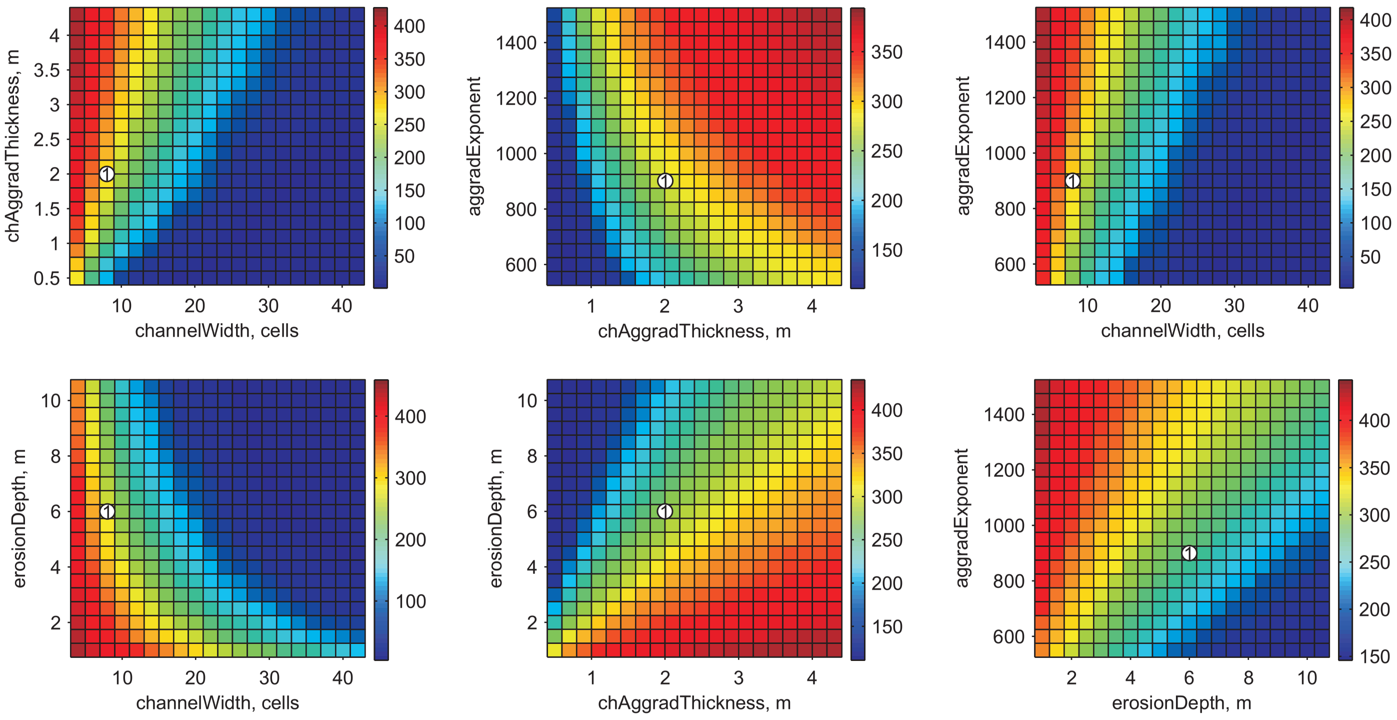

C. Average thickness of the modelled strata (m)

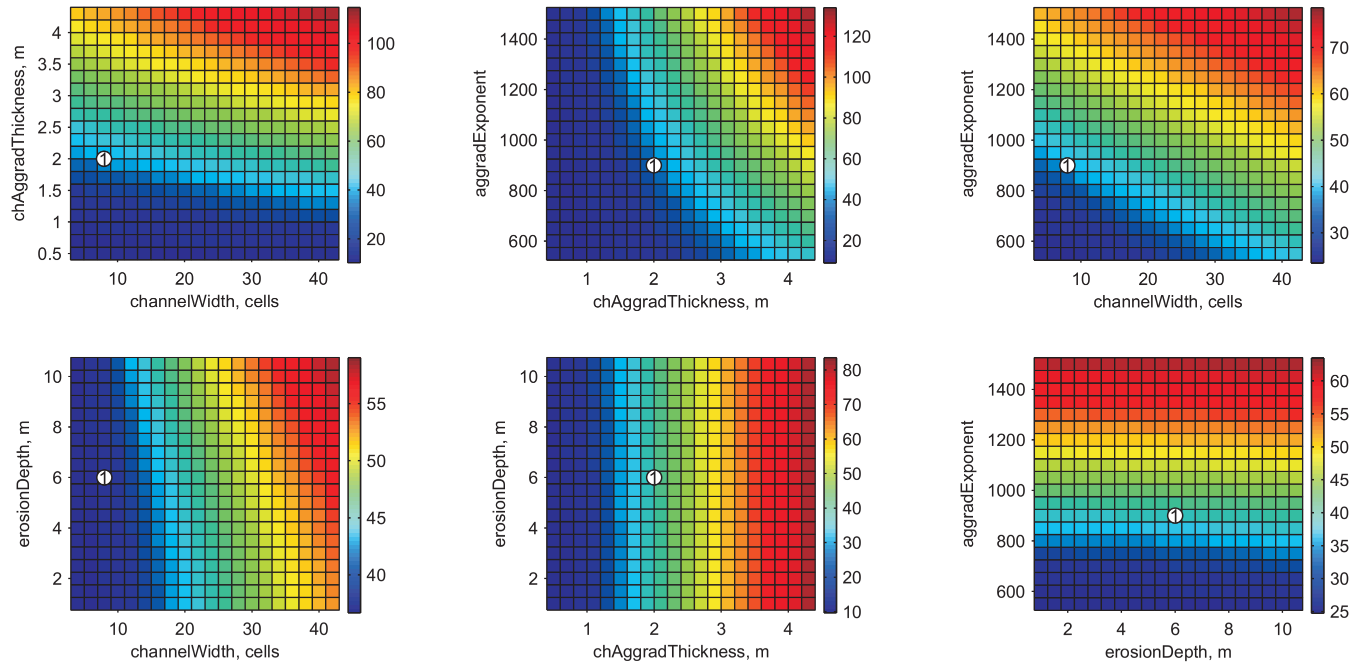

Figure 12.31. Variation in net-to-gross (A), number of sandstone bodies (B) and average thickness of the modelled strata (C) with input parameters including channel sandstone body width (*channelWidth*), erosion depth (*erosionDepth*), aggradation thickness (*chAggradThickness*) and aggradation exponent (*aggradExponent*). The sensitivity analysis is based on the best-fit model parameters for the Monźon outcrop (Table.12.3) with random channel avulsion algorithm.

A. Mean distance between channels (m)

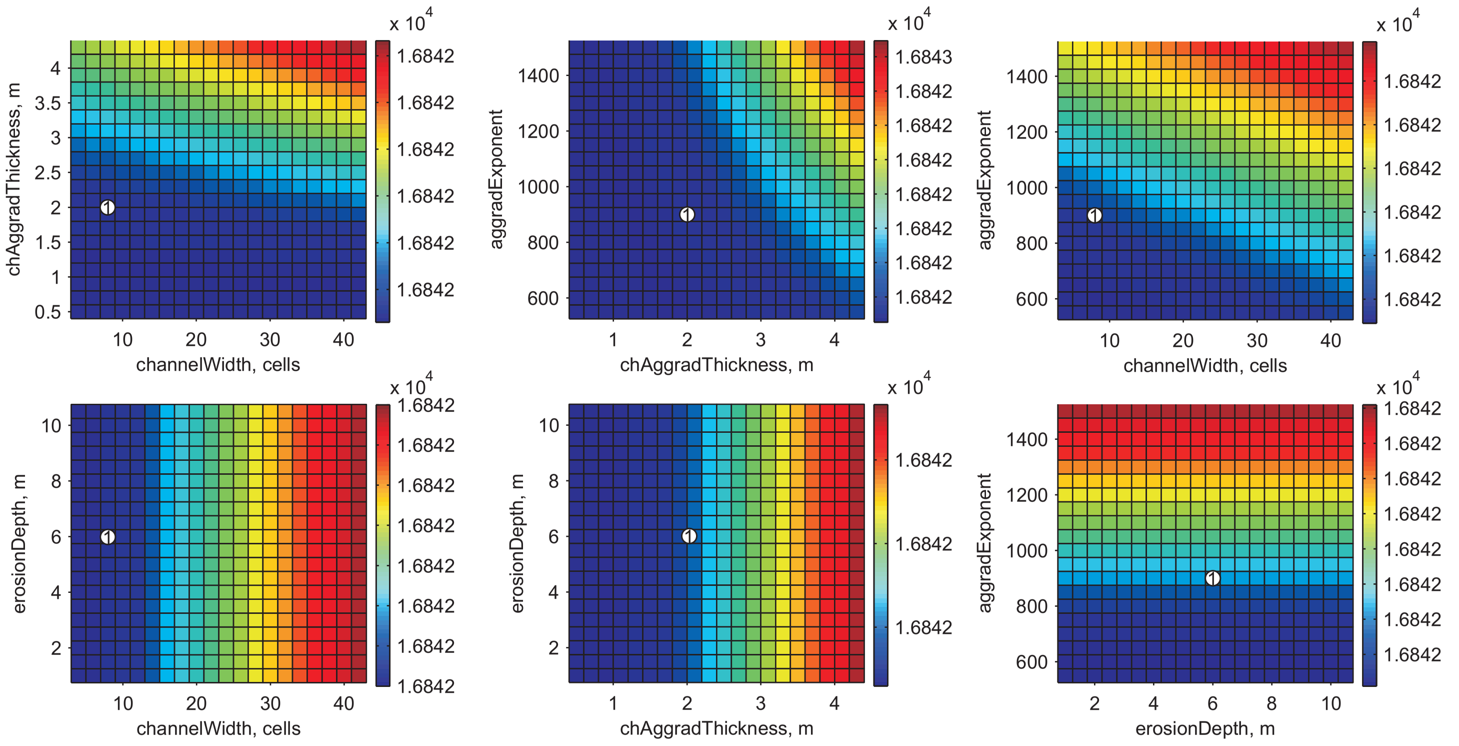

B. Mean distance to the closest channel (m)

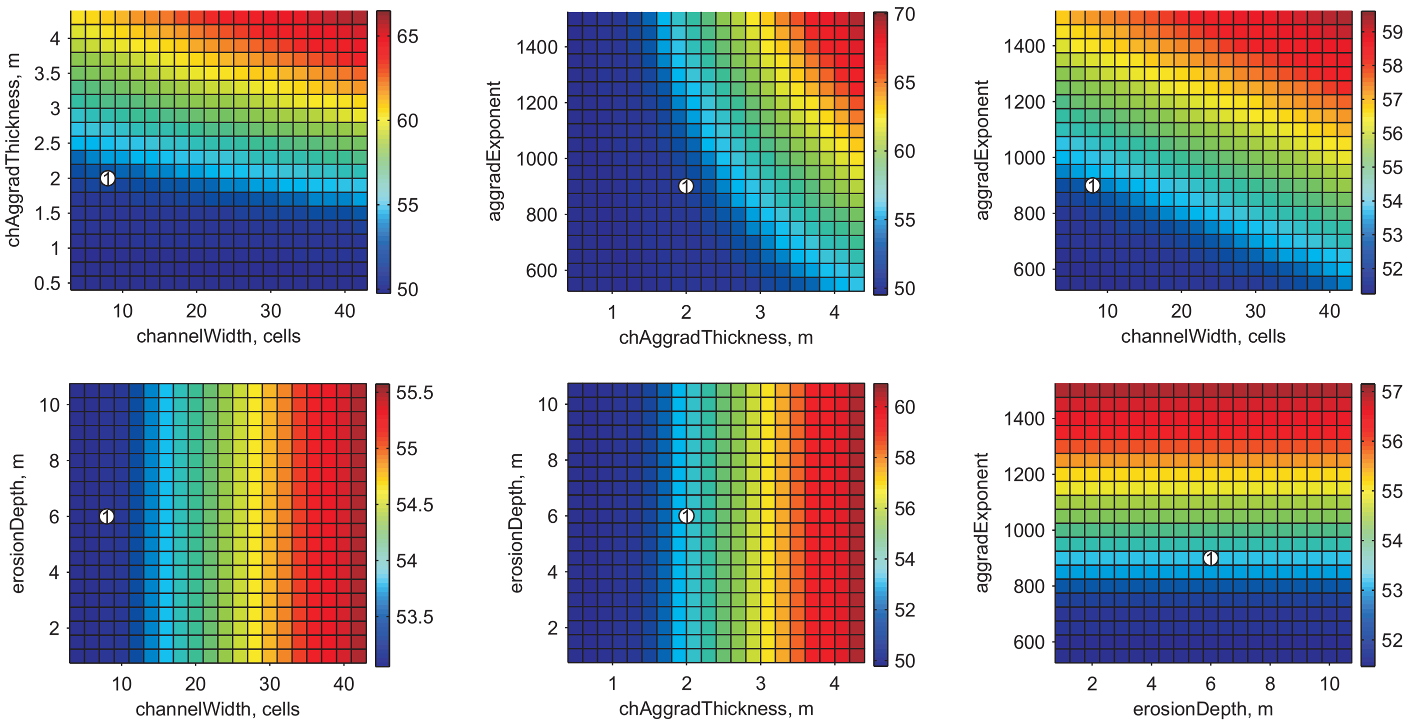

Figure 12.32. Variation in mean avulsion distance (A), mean distance between channels (B) and mean distance to the closest channel (C) with input parameters including channel sandstone body width (*channelWidth*), erosion depth (*erosionDepth*), aggradation thickness (*chAggradThickness*) and aggradation exponent (*aggradExponent*). The sensitivity analysis is based on the best-fit model parameters for the Monźon outcrop (Table.12.3) with random channel avulsion algorithm. Distance between avulsion positions does not change in these models because the seed number in the model is kept the same for all sensitivity runs.

influence the strata characteristics less because the channel elements are distributed randomly and fewer are restricted by model boundaries (Fig. 12.30, B and C).

12.9.2. Sensitivity of the compensation thickness scale in the modelled strata to channel avulsion mechanism

The variation of sedimentation to subsidence ratio and compensation thickness scale was compared for the Monźon best-fit models (Table 12.3) created with different avulsion algorithms (Fig. 12.33) during the **Experiment 4** and with different migration distances during **Experiment 5**.

Compensational avulsion mechanism

The compensational avulsion type is by definition expected to compensate the floodplain topography efficiently. In the best-fit Monźon model the strata is compensated when its average thickness reaches approximately 4.4 - 5 m (Fig. 12.34, A). Note that compensation thickness is determined approximately and could include some error and therefore a range is given.

Random avulsion mechanism

Compensation in the strata is reached at a much higher average thickness if random channel avulsion algorithm is used. The compensational thickness scale for this model ranges from 6.3 m to 14 m (Fig. 12.34, B). This is due to the channel element sometimes occurring at random on top of an older channel element creating "anticompensational stacking" (Straub et al., 2009), increasing the channel to floodplain relief and consequently increasing time needed to compensate this relief.

Combined random and compensational avulsion mechanism

In **Experiments 4 and 5** the Monźon best-fit model has been run with the compensational avulsion algorithm but with different avulsion frequencies (*n* = 3 and n = 5) and migration distances (*migrationDistanc*e = 28, 48 and 108 cells). The compensational thickness scale for all these models is low (~ 3 - 4.8 m) and similar to the compensation thickness scale of the models with the compensational avulsion algorithm (Fig. 34, A and C).

The increase in avulsion frequency (*n*) changes the compensation scale by ~ 1 m (Fig. 12.35, A and C, B and D). This difference might be affected by the uncertainty in the compensational thickness determination due to the uncertainty in the fit of the approximation lines. It also could be that there is not much difference between models with different avulsion frequencies because the channel element in these models still avulses in to topographic minima and then locally avulses and deposits within these

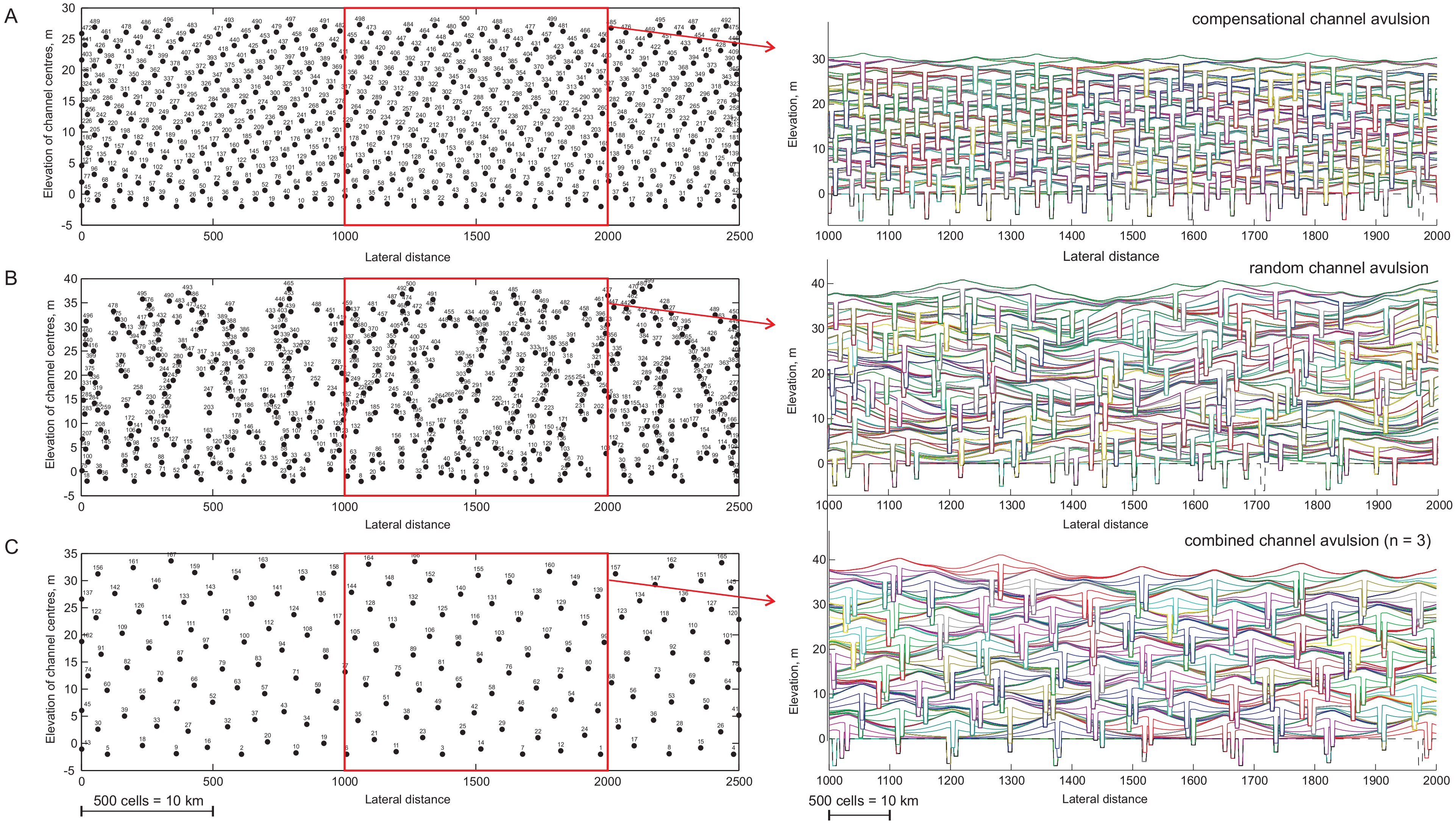

Figure 12.33. Modelled strata with Monźon best-fit model parameters (Table 12.3) with three different avulsion algorithms and corresponding stacking patterns.

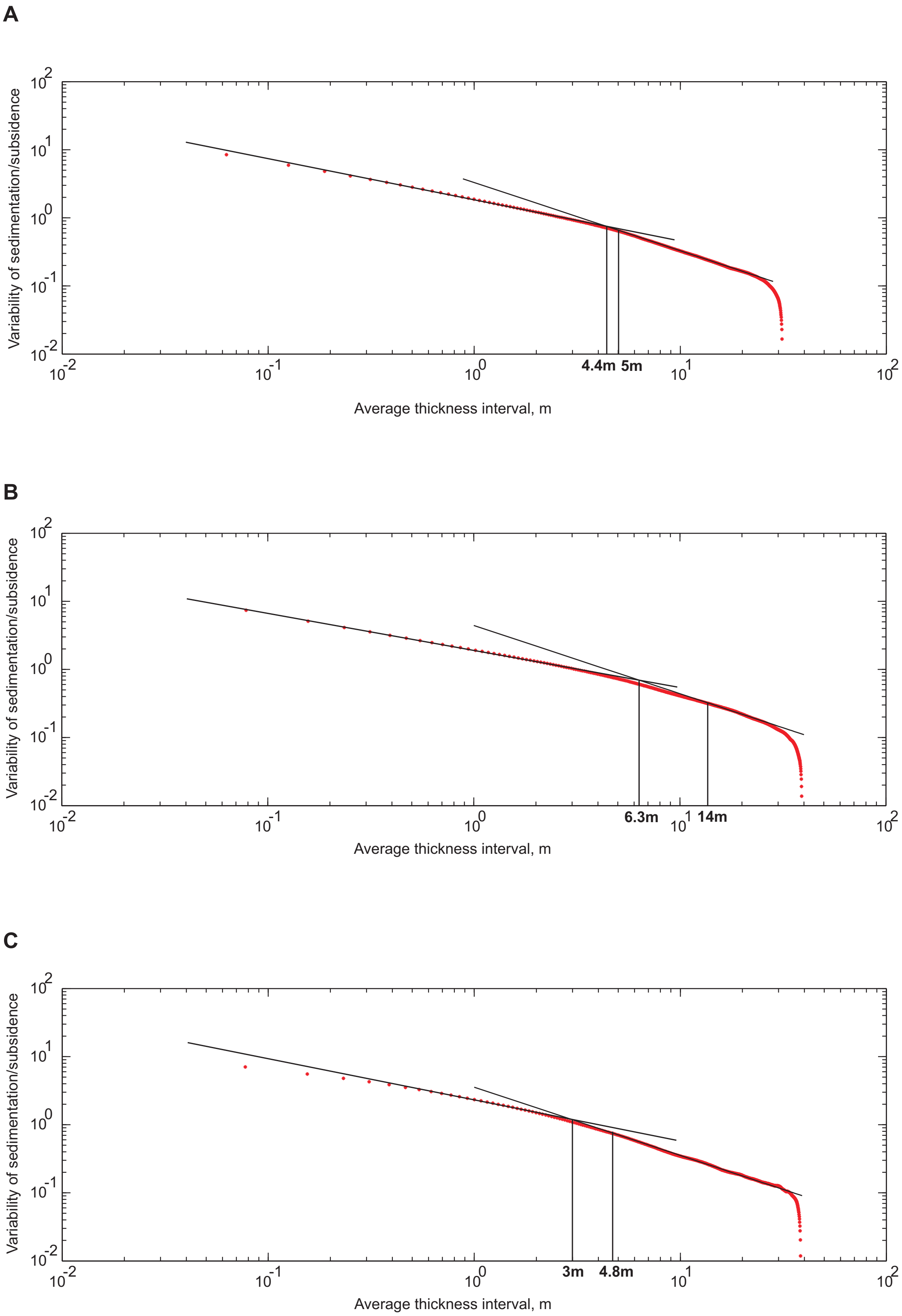

Figure 12.34. Variation in sedimentation to subsidence ratio (standard deviation) for Monźon best-fit model strata with A - compensational channel avulsion algorithm, B - random channel avulsion algorithm and C - combined compensational and random algorithms with avulsion frequency equal 3 and migration distance equal 28 cells.

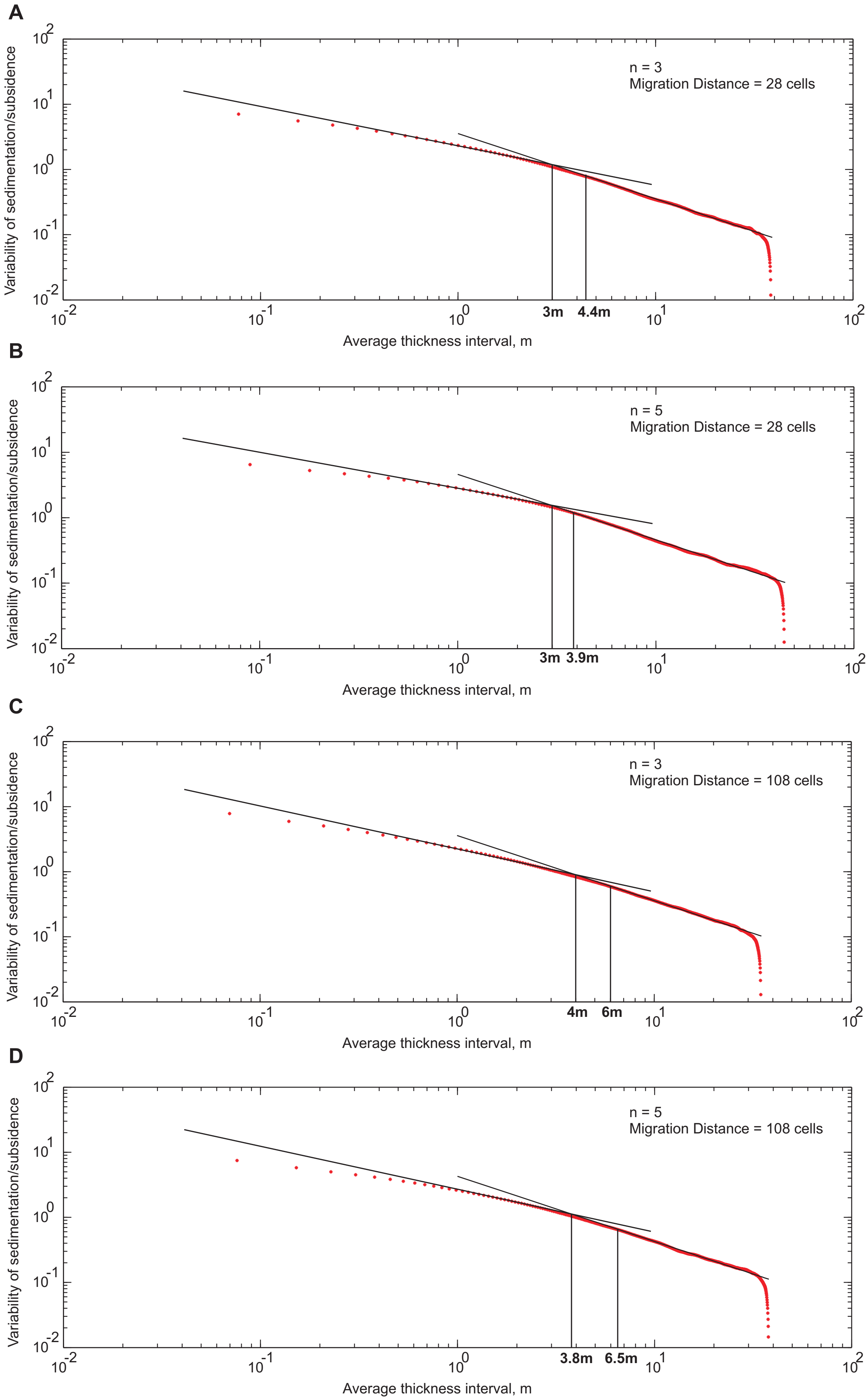

Figure 12.35. Variation in sedimentation to subsidence ratio (standard deviation) for Monźon best-fit model strata with combined compensational and random channel avulsion algorithm with different avulsion frequencies and migration distances.

minima, filling the topography. Therefore the relief could be compensated at a similar rate in both models.

The increase in migration distance (*migrationDistanc*e) raises the compensation thickness scale from approximately 3 – 4.4 m up to 4.8 - 6.5 m (compare A and C, B and D in the Fig.12.35) which might be caused by more variable topography created by the greater distance between channels after local avulsions and due to a chance of anti-compensational stacking (Fig. 12.35, C). This scenario could be compared with lobe formation within a DFS where depositional lobes move into lower topography on the DFS surface by nodal major avulsions but within lobes channel avulses within relatively limited distance.

12.10. Sensitivity analysis: variable floodplain algorithm

Previously created fluvial models use different floodplain aggradation algorithms, such as 1) exponentially decreasing floodplain aggradation away from the channel (Leeder and Bridge, 1979; Clevis et al., 2006; Dalman and Webrje, 2008; Krassenberg and Bridge, 2008), depth-dependent aggradation (Jerolmack and Paola, 2007; Turker et al., 2009), uniform and with random noise floodplain aggradation (Jerolmack and Paola, 2007). It is interesting therefore to see how different algorithms affect the modelled strata. Jerolmack and Paola (2007) have already discussed how the floodplain topography affects channel avulsion and distribution of sandstone bodies. In this section the data from **Experiment 6** are used to investigate the sensitivity of the output parameters to floodplain aggradation algorithms.

12.10.1. Sensitivity of NTG ratio and sandstone body connectivity in the modelled strata to floodplain aggradation algorithm

Exponential depth-dependant and exponential floodplain aggradation

The exponential depth-dependant floodplain aggradation is used for the Monźon best-fit model (Fig. 12.11) and all models discussed in the previous sections. The Monźon strata simulated with other floodplain aggradation algorithms are compared here with the best-fit model (Fig. 12.36, A-D).

The modelled strata created with exponential floodplain aggradation show a similar but slightly lower NTG ratio and lower sandstone body connectivity (Fig.12.36, A-C). The exponential depth-dependent floodplain aggradation accounts for floodplain topography and deposits a greater thickness in depressions than on elevated areas. This behaviour results in annealing of the channel ridge topography over time (see also Jerolmack and Paola, 2007) so that channel elements are able to migrate on top of the previous element creating amalgamated sandstone bodies and produces strata with

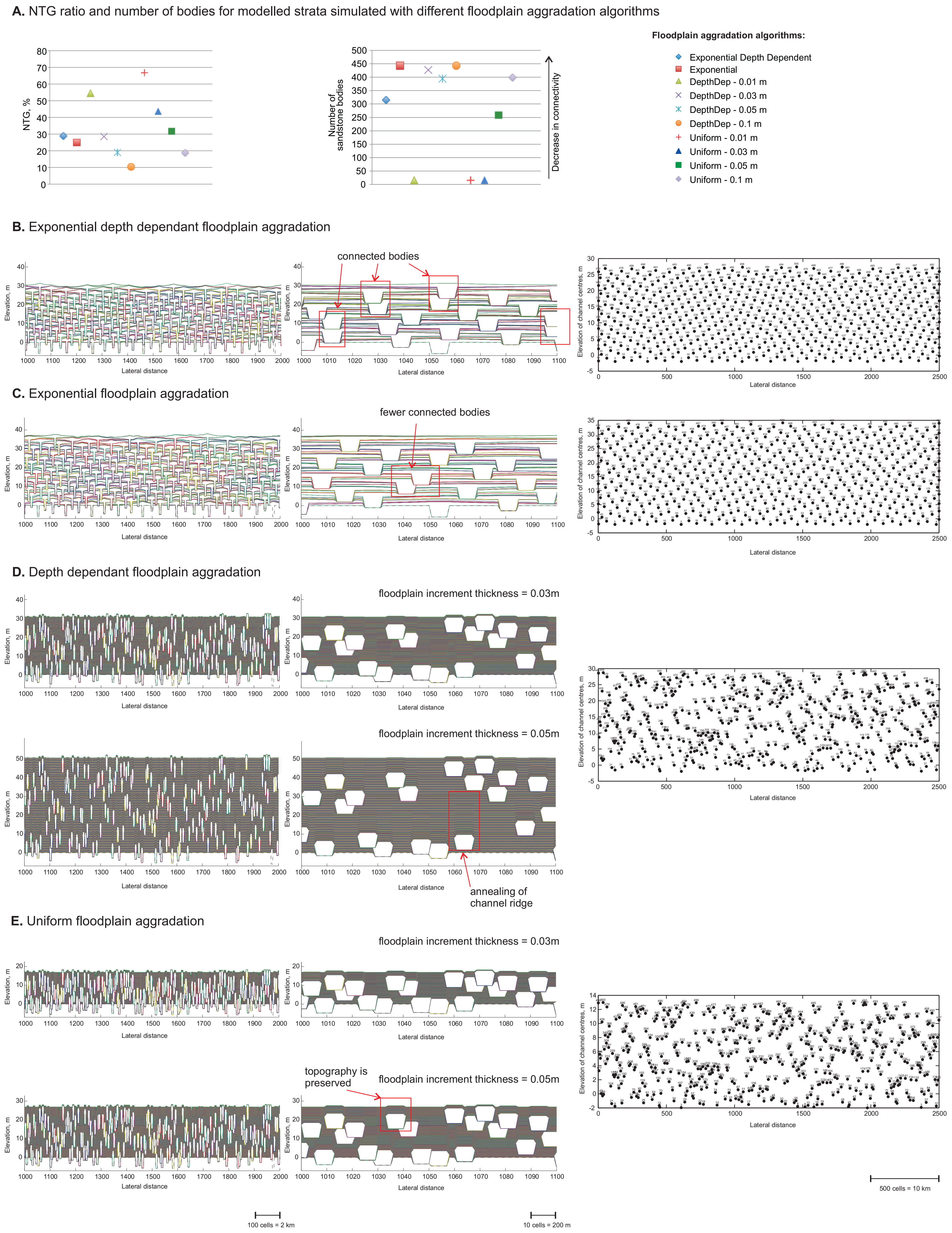

Figure 12.36. Variation in NTG ratio, number of sandstone bodies and sandstone body distribution patterns in modelled strata simulated with Monźon best-fit input parameters and different floodplain aggradation algorithms.

relatively higher connectivity (Fig. 12.36, B and C). In contrast, the exponential floodplain aggradation preserves floodplain topography and the elevation of the channel ridges. The ridges define the next channel position that will be away from the previous elevated channel ridge (see also Sheets et al., 2007; Jerolmack and Paola, 2007) reducing the possibility of channel connection. The difference can be also seen in the distribution of channel centres on the maps (Fig. 12.36, B and C).

Depth-dependant and uniform floodplain aggradation

The modelled strata created with depth-dependant floodplain aggradation also have a lower NTG ratio and sandstone body connectivity in comparison to the model with simple uniform floodplain aggradation (Fig. 36, A, D, E). The resulting proportion of floodplain strata in the model with depth-dependent aggradation is greater than in the model with uniform aggradation (Fig. 36. D and E), while other parameters are the same. A higher floodplain strata proportion relative to the channel strata explains the lower NTG ratio and sandstone body connectivity. The relationships are simply due to the formula used to calculate depth-dependent floodplain aggradation (Section 12.2.5). The NTG ratio and sandstone body connectivity for both models obviously increases as floodplain aggradation decreases (Fig. 36, A).

Channel element distribution is not affected by these two floodplain aggradation algorithms. This is perhaps because the initial topography and compensational avulsion mechanism controls the position of the channels more than change in these two floodplain algorithms.

12.10.2. Sensitivity of the compensation thickness scale in the modelled strata to floodplain aggradation algorithm

The compensation thickness scale increases slightly with the change in the floodplain algorithm from exponential depth-dependant to exponential (Fig. 12.37, A and B) or from depth-dependent to uniform (Fig. 12.37, C and D). Floodplain aggradation algorithms with depth-dependant correction fill of depressions on the floodplain and smooth topography perhaps facilitating compensation of the model topography and resulting in smaller compensational thickness scale. In the current configuration of the 2D model it is unclear at what value of uniform floodplain aggradation the modelled strata could be compared to the strata modelled with exponential floodplain aggradation and therefore these analyses have not been done. More future work is needed to investigate this issue further.

In summary, analyses presented in sections 12.9-10 demonstrate that channel avulsion and floodplain aggradation algorithms affect the resulting stratal

A. Exponential depth-dependant floodplain aggradation

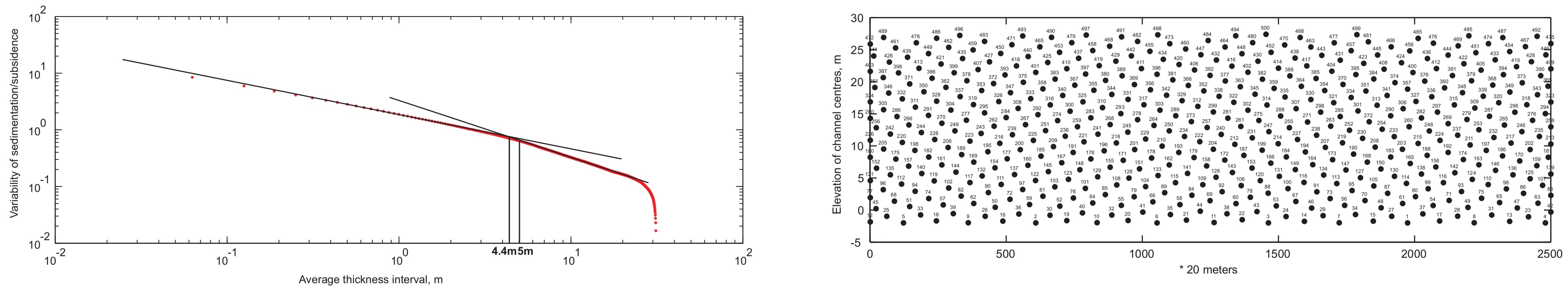

B. Exponential floodplain aggradation

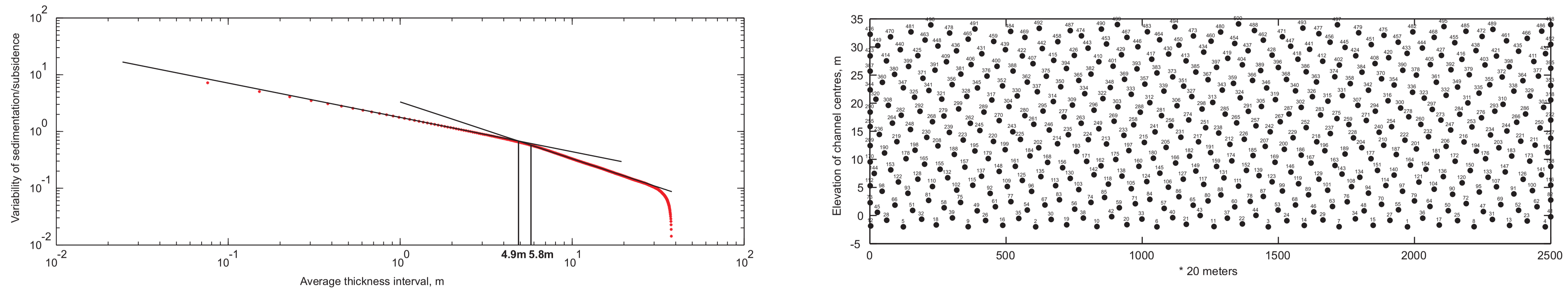

C. Depth-dependant floodplain aggradation

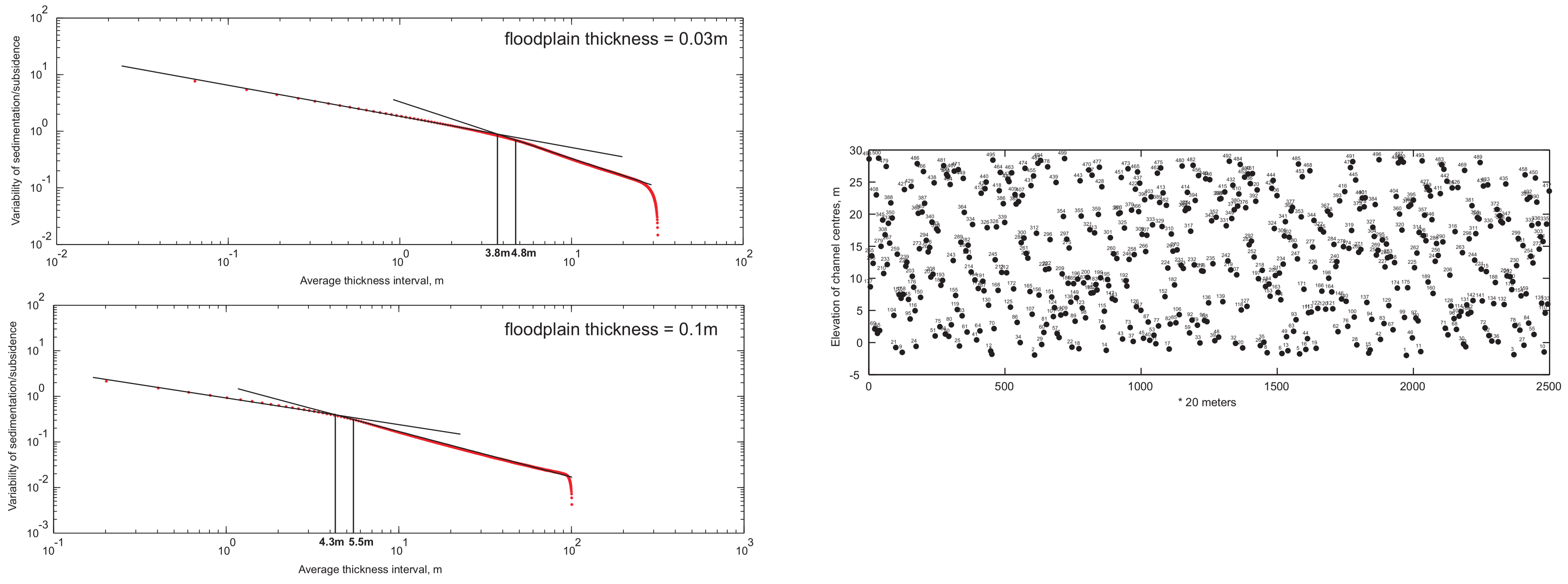

C. Uniform floodplain aggradation

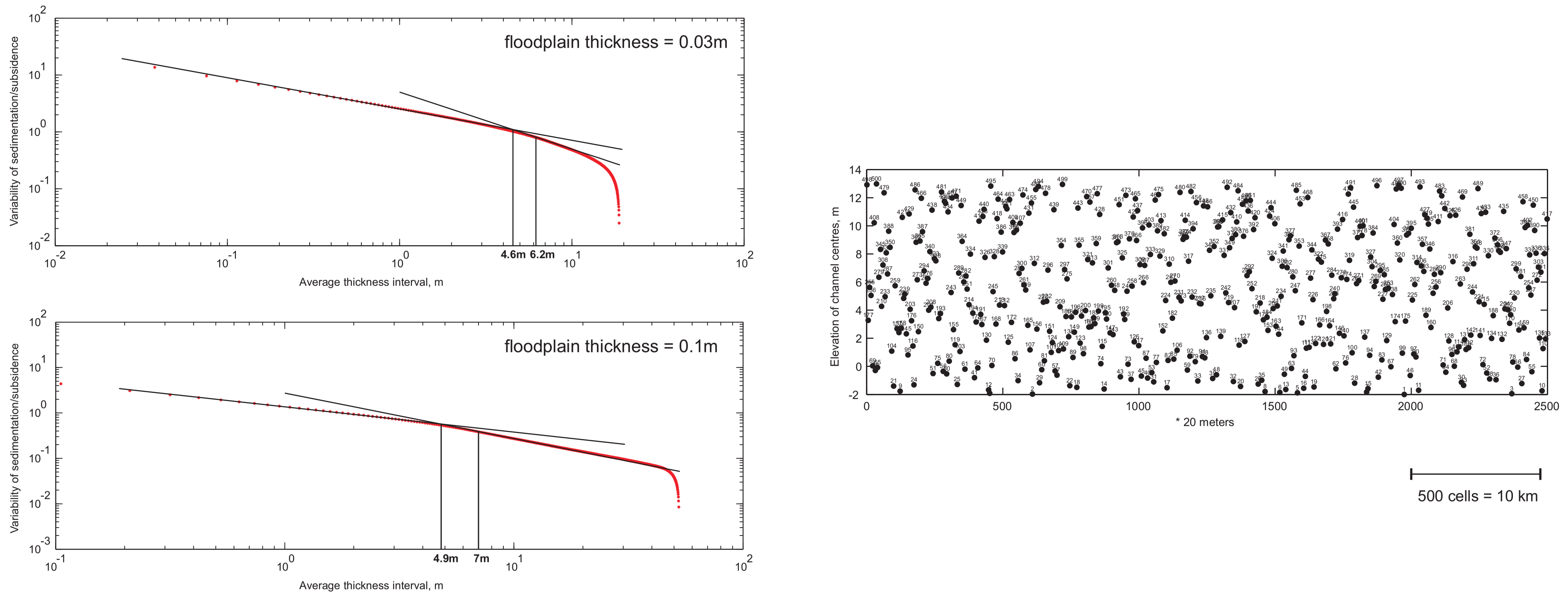

Figure 12.37. Variation in sedimentation to subsidence ratio (standard deviation) and sandstone body distribution patterns for modelled strata with Monźon best-fit input parameters and different floodplain aggradation algorithms.

characteristics and therefore, need to be chosen carefully when numerical models are created.

12.11. Discussion of the results, limitations of the 2D model and recommendations for future work

12.11.1. Modelling of the Huesca and Salt Wash DFS strata

The 2D model has been used to create strata similar to those observed in the outcrops of the Huesca and Salt Wash DFS successions to better understand the factors controlling contrasting architecture between the study areas and from proximal to distal parts of each area. It was found that to model the high-NTG strata observed in the Salt Wash outcrops, the model input requires greater widths of channel sandstone bodies than for the Huesca strata, while other input parameters are relatively similar. This indicates that the degree of lateral migration of channels (hence lateral reworking) is the main control on the difference between stratal architecture of the studied DFS successions. Modelling of DFS strata in proximal, medial and distal areas showed that a higher degree of vertical and lateral reworking is needed to model proximal successions while greater floodplain preservation is needed to model more distal successions.

These results support the interpretations of outcrop data presented in chapters 8-11: the degree of reworking of floodplain deposits in the Salt Wash DFS is higher than in the Huesca DFS where floodplain deposits are predominantly preserved. The difference could have been caused by a lower accommodation setting for the Salt Wash DFS (Weissmann et al., 2013 in press). The downstream differences in DFS architecture are also related partly to a change in amount of accommodation space relative to sediment supply and consequently in a degree of reworking downstream (Weissmann et al., 2013 in press; Chapter 8) and partly to a decrease in flow discharge downstream in each DFS (Chapter 8).

Several limitations of the model have been discovered. Firstly, the 2D model uses constant dimensions of all sandstone bodies while in reality three different types of sandstone bodies have been distinguished in both DFS successions (Chapter 5). Use of the averaged sandstone body dimensions is a reasonable approximation but is not entirely correct. All three sandstone body types need to be included in the future, especially Type 3 terminal splay sandstone bodies which comprise a significant part of the distal low-NTG DFS strata (chapters 6, 7 and 11). The distal strata cannot be modelled accurately without introducing terminal splay depositional processes to the model. This also restricts the application of the model to the reservoirs where Type 3 sandstone bodies could increase reservoir volume and NTG ratio (Chapter 11).

Secondly, in real outcrops some sandstone bodies are often oriented in a plane oblique to the palaeocurrent direction and this could be modelled correctly if a third dimension is added to the model (Fig. 12.38). Such cross sections would more realistically represent the sandstone body geometries observed in outcrops.

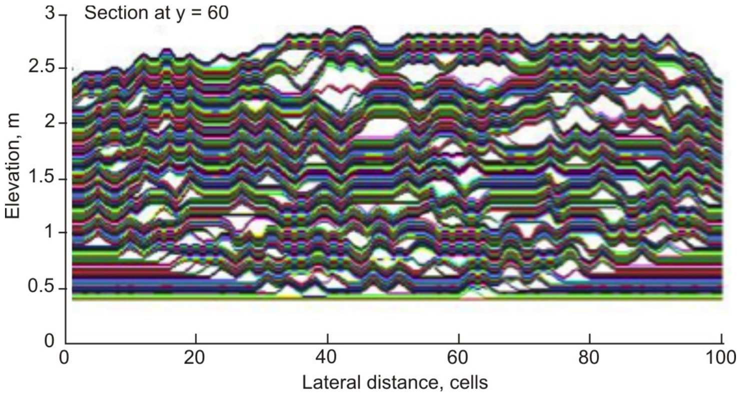

Figure 12.38. Examples of cross-section from the prototype of the 3D model of the DFS. Every coloured line represents time step. White triangles represent channel elements. Erosion is not simulated. Note narrow and wide channel sandstone bodies that are formed by the same channel element geometry but cut by the cross section at different angles to the paleocurrent direction.

In addition, the exponential depth-dependent floodplain aggradation algorithm used in the best-fit outcrop models and in most sensitivity experiments is only a partial representation of overbank deposition processes. In reality floodplain deposition occurs not only by channel ridge aggradation but also by filling floodplain depressions by lateral splay deposits as has been described for the Mississippi River by Aslan and Autin (1999). The deposition in splays has been also determined to be a common process in the Huesca DFS (Chapter 9). The future models, therefore, should include deposition by splays.

Finally, the gridding algorithm used for the calculations of the sandstone body connectivity in the current 2D model is only an approximate method (sections 12.3.2 and 12.8.6). In this thesis this algorithm is used to simplify the calculation in order to reduce computation time and the time spent on code writing. In the future this algorithm could be improved or an alternative algorithm that does not involve “gridding” could be developed. Furthermore, the 2D model cannot reproduce complex 3D architecture that exists in reality and therefore it does not reflect 3D sandstone body connectivity that is usually higher than what is observed in 2D outcrops (cf. Larue and Hovadik, 2006). In contrast, the 2D model might be sufficient to simulate deposits of an axial tributary river because its strata would not show significant lateral variations.

Although there are several limitations to the current 2D model, it can be used to create a close representation of the architecture of relatively proximal and medial DFS successions which was tested on the data collected from the studied outcrops. However, these results might represent some element of circular reasoning because the model was originally created based on the observations made from the same outcrops. Despite this, the match between modelled strata and observations was not entirely predictable because the model includes input parameters and algorithms that cannot be determined from the outcrops (floodplain aggradation exponent, floodplain aggradation and avulsion mechanisms). These unconstrained parameters and algorithms used for creation of the best-fit models can be considered to be close to the processes that occurred in reality because the model produces strata similar to those observed in the outcrops. However, it does not mean that combinations of other values for aggradation exponent and different floodplain and avulsion algorithms could not produce the same matching results. This requires further investigation.

12.11.2. Non-unique controls on strata characteristics

An important conclusion from the modelling experiments of this study is that a wide range of combinations of input parameters produces modelled fluvial architecture with the same characteristics (NTG ratio or sandstone body connectivity). The strata with intermediate NTG ratio can be produced with a wider range of input parameters while extreme input parameters are required to reproduce extreme architecture characteristics such as in relatively proximal Salt Wash succession (NTG = 85 %) or in distal Huesca succession (NTG = 1 – 3 %). Note that although the NTG ratio of the strata is the same, the geometry of the strata and sandstone body connectivity can be different (Fig. 12.23).

These results emphasise non-uniqueness of combinations of factors that could have controlled strata with particular characteristics (see also Burgess and Allen, 1996; Burgess, 2006; Waltham et al., 2006; Prince and Burgess, 2013 in review). One scenario should not be chosen without trying to limit the number of combinations of input parameters for the model using additional parameters measured from the outcrop or subsurface data.

This result is important when interpretation of the controls on stratal architecture or static reservoir modelling is concerned. For example, if the observed strata are characterised by high NTG (e.g. Bullfrog strata, Section 12.7.2) at least two interpretations could be suggested. The strata could be formed by a system with low fine-grained material content in the sediment load or by a system characterised by a high degree of reworking due to low subsidence or a low sediment supply to water discharge ratio. If extensive outcrop data are available and thick intervals of fine-grained overbank deposits are observed within amalgamated sandstone body complexes (e.g. Bullfrog outcrop, Appendix 5.4), the second interpretation is more probable. It could be difficult to choose one interpretation if only limited 1D well data are available. For instance, if all wells show high NTG ratio both interpretations are still valid.

In reservoir modelling usually one interpretation of strata architecture and well correlation is chosen as input for the static geological model and this, as demonstrated here, is not correct. In the absence of additional information a better way of looking at this is to consider all combinations of controls and types of architecture corresponding to observed stratal characteristics as possible. In this case the combinations of input parameters and stratal geometries with particular reservoir characteristics obtained from the 2D model experiments in this study are useful.

12.11.3. Sensitivity of NTG ratio and sandstone body connectivity in the modelled strata to variable input parameters of the model

The sensitivity analysis showed that NTG ratio and sandstone body connectivity are related to input parameters such as water discharge, sediment supply, availability of fine-grained sediment in ways predicted by existing models. For example, increasing the degree of reworking of floodplain deposits through incision and lateral migration of channels increases the NTG ratio and connectivity of the modelled strata. In contrast, the higher floodplain aggradation, the lower the NTG ratio and sandstone body connectivity. These results do not mean that DFSs behave in an entirely predictable way, but rather show that a simple geometric 2D model is not able to demonstrate the more complex behaviour of a DFS. Complex behaviour of DFS and many other depositional systems probably arises from processes that occur in 3D. A 3D model is needed to further investigate this complexity. For example, the 3D model of Karssenberg and Bridge (2008) can simulate some downstream variations observed in the architecture of DFS strata. Nevertheless, results from the sensitivity analysis conducted using 2D model in this research do tend to confirm relationships between controls and fluvial architecture characteristics that are commonly used to interpret the variations observed in outcrop and subsurface data (Weissmann et al., 2002; Holbrook et al, 2007; Kjemperud et al., 2008; Nichols, 2005; Fisher and Nichols, 2013).

In the result of more detailed sensitivity it has been also found that variations in the erosion depth (water discharge) affect reservoir characteristics and stratal geometry less than variations in the degree of lateral channel migration (lateral reworking). The variations in the aggradation thickness (sediment supply) also have a greater effect than variations in the floodplain aggradation exponent (availability of fine material). The analysis of model realisations with different sandstone body widths (degrees of lateral reworking) demonstrated that if sandstone body width is high it becomes the main control on the stratal architecture (Section 12.8.4). In addition the sandstone body width affects the sensitivity of the reservoir characteristics of the modelled strata to the other input parameters (Section 12.8.5).

12.11.4. Sensitivity of NTG ratio and sandstone body connectivity in the modelled strata to variable avulsion and floodplain aggradation mechanisms

The studies presented here also show that different channel avulsion and floodplain aggradation algorithms affect absolute values of the characteristics of modelled fluvial architecture and therefore need to be chosen carefully during modelling. However, general trends in strata characteristics with variable input parameters are not affected by avulsion algorithms (e.g. compare Fig 12.32 and 12.26).

The importance of the floodplain topography and processes has been emphasised by Jerolmack and Paola (2007), and the effects of floodplain topography on reservoir properties of the resulting deposits have been noted in the experiments presented here. For example, the connectivity of strata modelled with the exponential floodplain algorithm is lower than the connectivity of strata modelled with the exponential depth-dependent algorithm. In the latter model floodplain topography is annealing faster, allowing channels to come back to the same location and form amalgamated sandstone bodies. The NTG ratio in this case is lower due to channel-channel reworking (Section 12.10). Channel re-occupation was not considered in this study.

The channel-to-channel reworking resulting in overlap of sandstone bodies, was found to be a key control on variations in NTG ratio in the strata. The overlap reduces the area occupied by sandstone bodies and therefore their proportion relative to the floodplain strata. Thus, amalgamated sandstone bodies do not always mean that the succession has a high NTG ratio because the relative position of individual bodies within amalgamated bodies and distribution of amalgamated bodies are also important controls of the NTG ratio.

Lower sandstone body connectivity in strata formed by a fluvial system avulsing in a compensational manner has been suggested by Laru and Hovadik (2006) and is also demonstrated by the experiments in this work. The strata modelled with compensational avulsion algorithm showed a higher NTG ratio and lower sandstone body connectivity than the strata created with the random avulsion algorithm. This relates to the positioning of channel elements in a compensational way, further away from the previous elements that in turn reduces the probability of sandstone bodies being amalgamated (Section 12.9).

12.11.5. Compensation thickness scale and its sensitivity to avulsion and floodplain aggradation algorithms

The 2D model has also been used to determine the compensation thickness scale that is related to the time required for the depositional element to revisit every spot on the model floodplain many times and fill the topography so that the sedimentation to subsidence ratio is close to unity (Sheets et al., 2002; Straub et al., 2009). Wang et al. (2011) stated that during the time before the compensation is reached the architecture is mainly controlled by local autogenic forces. The scale's sensitivity to different channel migration and floodplain aggradation algorithms has also been investigated.

The compensation thickness scale for the strata modelled with the random avulsion algorithm is high (~ 14 m) while the topography in the model with compensational or combined avulsion algorithms is compensated faster (~ 5 m) (Section 12.9.2). These relationships are the same as in the modelling experiments of Straub et al. (2009) and Wang et al. (2011). This is related to a possibility of channels which avulse randomly to be stacked on top of each other and form greater relief that would increase compensation time.

Different floodplain algorithms affect the compensation thickness scale in the modelled strata less than the different channel migration algorithms (only by 1 - 2 m). A higher compensation thickness scale is found for non-exponential floodplain aggradation algorithms (uniform and depth-dependent) that do not produce lobe-like geometries causing channels to avulse in a different way (Fig. 12.36-37). The depth-dependent floodplain aggradation algorithms anneal the topography and result in smaller compensation time than algorithms without this correction (Section 12.10.2). However, the compensation thickness scale determination in this study is approximate and therefore some error is expected. Small variations in compensation scale might be a result of this error that needs to be taken into account when interpreting the results.

Using analogue experiments, Sheets et al. (2002) found that compensation thickness scale (stratigraphic integral scale) is equal to 5 - 10 channel depths independently of the subsidence rate. Subsequently Wang et al. (2011) suggested that the compensation scale equals to one channel depth for systems where avulsion is the lowest frequency autogenic process, but for systems with strong external control and high sediment cohesiveness the compensation scale can be much higher. In this work the compensation scale determined for the modelled strata simulated with the Monźon best-fit input parameters (Table 12.3) and purely compensational channel behaviour (~4 ~ 5.5 m) is also close to the one channel erosion depth (6 m). The strata simulated with the same input parameters but with the random channel avulsion mechanism give a higher compensation scale (~ 14 m). According to the discussion in Wang et al.

(2011), the latter case could represent a scenario where the architecture is controlled by some external / internal forces that make some channels stack in an anti-compensational manner, increasing the time before compensation.

Straub et al. (2009) demonstrated that real depositional successions have somewhat intermediate channel behaviour between purely compensational and random (k = 0.75), e.g. deposition in lobes. This could be true for the observed DFSs as well. The application of the method suggested by Wang et al. (2011) will make it possible to find the compensation thickness scale for the outcrop data in the same way as for the modelled successions. The compensation scale of the DFS strata could then be compared with the compensation scale of modelled strata and channel migration method could be adjusted in the model to match outcrop data. Unfortunately, although this work had been planned in collaboration with the authors of the method, it could not be carried out in the time frame of this project. This study is recommended for the future research (Chapter 14).

12.11.6. Regularity in channel distribution within the modelled strata: proposal for future research

The sandstone bodies in some modelled strata created in this study appear to be more regularly distributed (e.g. Fig. 12.9, B and 12.14, B) than in others (e.g. Fig. 12.9, A and 12.12, A). Controls on the apparent regularity are not immediately obvious or easy to explain, even in this simple model.

The channel elements in almost all model experiments are by definition distributed in a compensational way that might result in regularly spaced depositional elements. However, the avulsion mechanism is not the only parameter that controls the regularity because other modelled strata created with the same avulsion mechanism do not show similar apparent regularity (Fig. 12.39).

Input parameters that control distance between sandstone bodies would probably affect apparent regularity. The distance to the closest channel sandstone body (*MinDist*) and shape of frequency distribution of the distances can be probably used as a metric of regularity. The higher the minimum distance and the less skewed the frequency distribution the more regular the modelled strata (Fig. 12.39, A-B).

To investigate this metric two apparently regular modelled strata have been subjected to sensitivity analysis with variable input parameters (Fig. 12.40-41). The aggradation thickness seems to be the main control on the metric of the regularity perhaps because it controls the vertical distance between channel elements (Fig. 12.40-41, A). This relationship could also occur because thick floodplain elements quickly smooth irregularities in initial floodplain topography and diminish its control on the channel avulsion location. The depth-dependent nature of the floodplain aggradation in the model also could contribute to this by smoothing previous topographic relief. The strata modelled with exponential floodplain aggradation algorithm show a noticeably less regular channel patterns and lower metric (Fig. 12.40, D).

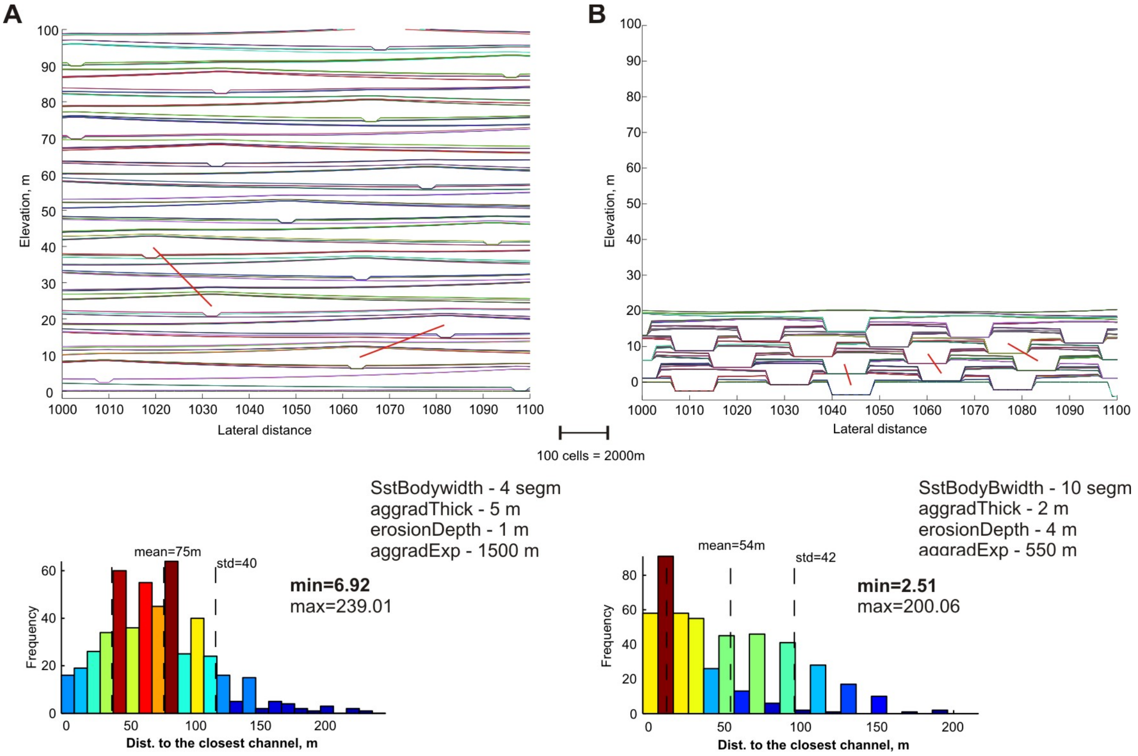

Figure 12.39. Apparently regular (A) and not regular (B) modelled strata. Note difference in the minimum values of the distance to the closest channel (marked by red lines on the strata) and in shape of frequency distribution of the values of the distance to the closest channel.

A high aggradation exponent and wide sandstone bodies make the depositional element wider and it would cover a significant part of the initial floodplain and smoothing its topography over a wider area so that there would be fewer possible avulsion locations for the next element (Fig. 12.40-41, B-C). After the initial floodplain has been covered and smoothed by a few depositional elements, the location of previous channel elements controls subsequent avulsions that happen in a regular compensational manner.

The distance to the closest channel seems to be a suitable metric for assessing regularity of the channel distribution within the strata. However more studies are required to investigate this further. The regular channel distribution in the modelled strata could also be a result of more indirect and as yet unknown relationships between input and output model parameters that are not obvious. As shown in Chapter 10, interpretation of stratal order has to be supported by quantitative evidences and qualitative, subjective interpretation of regularity should not be used. In the future research, facies and thickness order analysis carried out for the successions recorded

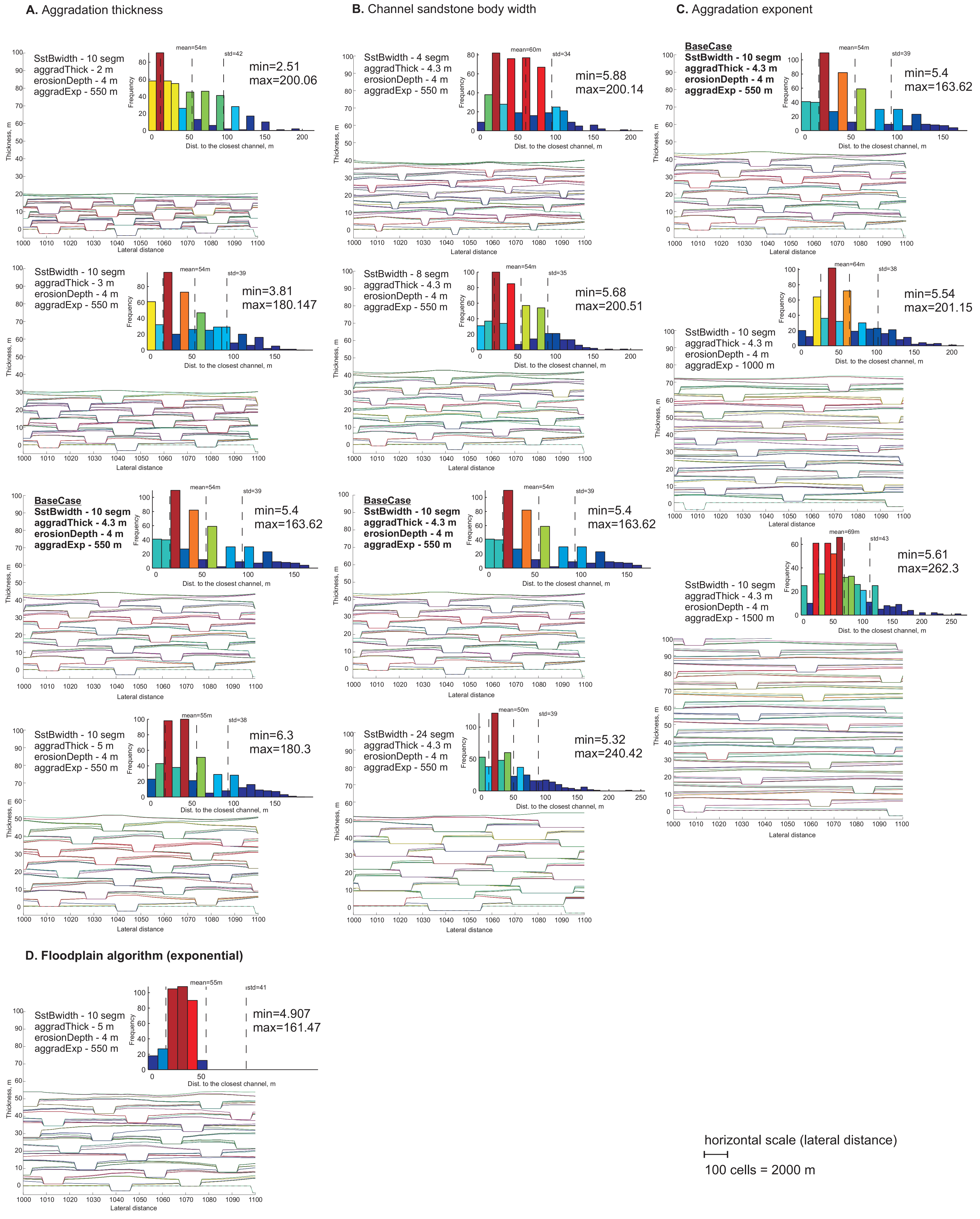

Figure 12.40. Sensitivity of the distance to the closest channel to variable input parameters (Base case 1) to: A - input aggradation thickness, B - channel sandstone body width, C -aggradation exponent and D - exponential floodplain algorithm in contrast to all other examples modelled with exponential depth dependent floodplain algorithm. It is suggested that increase in minimum distance to the closest channel element and change in shape of frequency distribution indicate regularity/order architecture of modelled strata: the lower the minimum distance and the less distribution is screwed towards small values the more regularly sandstone bodies distribution.

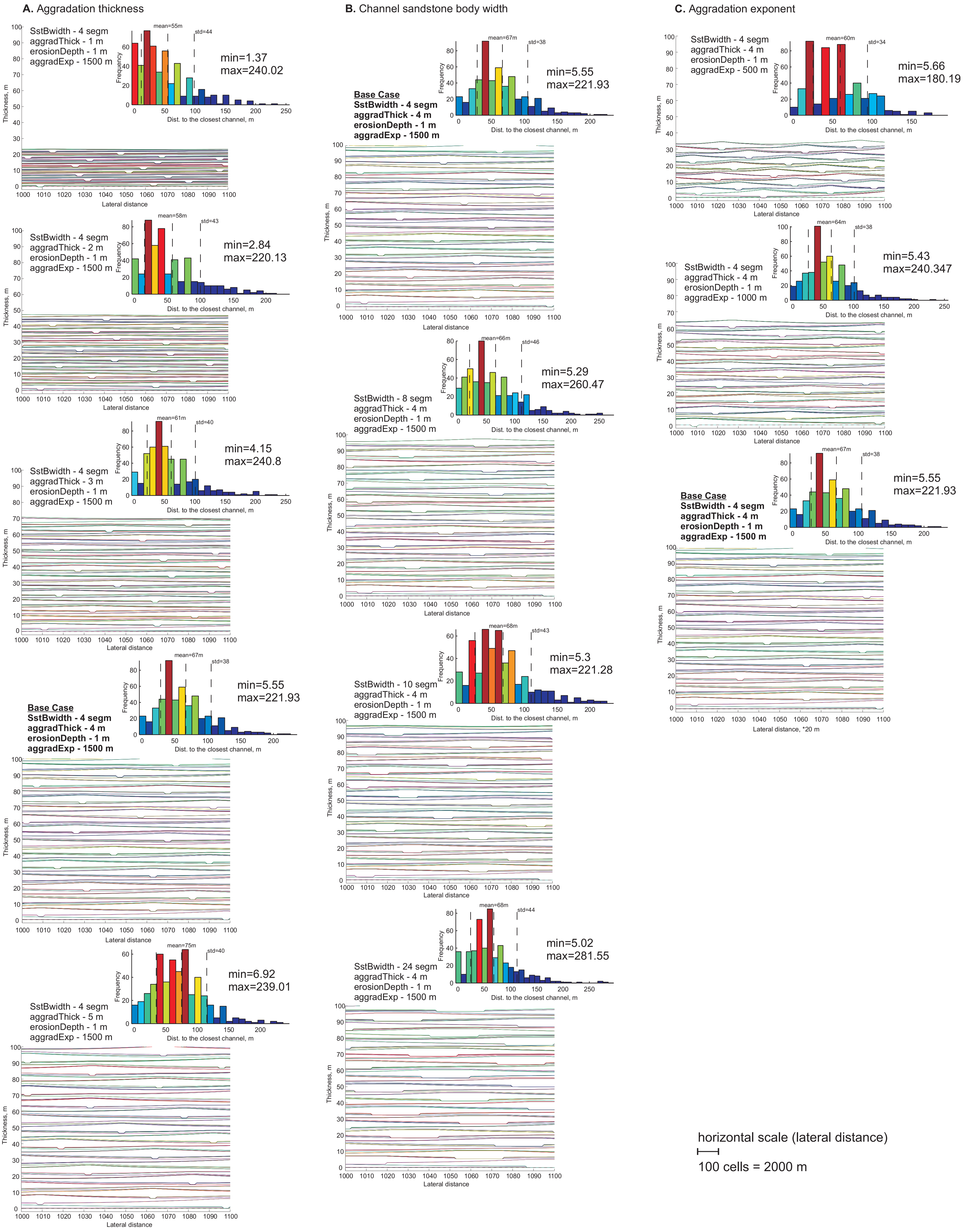

Figure 12.41. Sensitivity of the distance to the closest channel to variable input parameters (Base case 2) to: A - input aggradation thickness, B - channel sandstone body width, C -aggradation exponent and D - exponential floodplain algorithm in contrast to all other examples modelled with exponential depth dependent floodplain algorithm. It is suggested that increase in minimum distance to the closest channel element and change in shape of frequency distribution indicate regularity/order architecture of modelled strata: the lower the minimum distance and the less distribution is screwed towards small values the more regularly sandstone bodies distribution.

in the Huesca and Salt Wash outcrops (Chapter 10) could be conducted for the modelled strata with increase number of facies for comparison. Furthermore, the channel-belt clustering analysis developed by Hajek et al. (2010) could be also applied to assess the degree of regularity in spatial distribution of channel elements in the modelled strata.

12.12. Conclusions

In this chapter the formulation, applications and limitations of the 2D geometric model are documented. Despite of the limitations of the 2D model, applying it in comparison with outcrop observations is useful for investigating relationships between the characteristics of the DFS strata and their controlling factors.

Models with input parameters measured in outcrops produce strata with NTG ratio and sandstone body connectivity similar to outcrop observations recorded in the relatively proximal and medial Huesca and Salt Wash DFS deposits. The difference between the architecture of the Huesca and Salt Wash successions has been found to be controlled mainly by degree of lateral reworking of floodplain deposits by channel flow. Proximal, medial and distal DFS strata have to be modelled with different input parameters corresponding to the architecture characteristics described in chapters 5, 6 and 7. These results support interpretation of the outcrop observations and statistical analyses presented in chapters 8-11.

The 2D modelling demonstrated that strata with particular reservoir characteristics can be reconstructed using a wide range of input parameters and therefore controls on their architecture are non-unique. In the absence of additional observations from the outcrop or subsurface data or additional metric characterising architecture all realisations should be considered as possible. Multiple strata geometries produced by the 2D model in this research could be used as examples of those variants or used to eliminate some variants of architecture geometry. This result influences interpretation of possible controls on the deposit architecture and outcome of static reservoir modelling.

The sensitivity analyses conducted using the 2D model showed that reservoir characteristics of modelled strata change with the variation in sediment supply and water discharge in a predictable way and confirm the relationships between controls and fluvial architecture characteristics that are commonly used for interpretations of the variations observed in outcrop and subsurface data. The degree of lateral reworking and aggradation thickness was found to be the main controls on the stratal characteristics. The degree of lateral reworking (sandstone body width) also affects sensitivity of the strata characteristics to the other external controls.

The sensitivity analysis has also shown that different channel avulsion and floodplain aggradation algorithms affect the important reservoir qualities of modelled strata and therefore have to be chosen carefully during numerical modelling that is used for reservoir studies. Occurrence of channel-to-channel reworking was found to be a key control on these variations. The depth-dependent element in floodplain aggradation and random avulsions result in higher connectivity of the sandstone bodies that is related to annealing of the floodplain topography and possibility of channel positioning on top of each other. Models without depth-dependent component in floodplain aggradation and compensational channel avulsions displayed much lower connectivity because floodplain topography is preserved and channel elements are avulsing farther from each other and are separated by floodplain strata.

The preliminary results of the compensation scale studies for the modelled DFS strata have been presented in this chapter. The model demonstrated the same relationships between compensation scale and avulsion mechanisms as described previously (Straub et al., 2009; Wang et al., 2011): high compensation scale for model with random channel avulsion and low compensation scale for model with compensational avulsion style. Lower compensational scale was also found for models where floodplain deposition occurs preferably in depressions smoothing the topography of the floodplain surface (depth-dependent) and therefore facilitates compensation of the relief. The compensation thickness scale needs to be determined for each particular succession from the outcrop data so that it can be matched with the channel avulsion algorithm in its model. Further investigations of the effects of combined compensational and random channel avulsion algorithms on stratal characteristics and sensitivity of compensation scale to external controls would be useful (see also Wang et al., 2011).

The simplicity of the 2D model needs to be considered when interpreting these results because the model does not capture all the details of the complex behaviour of DFSs. Three types of sandstone bodies need to be introduced into the model, especially splay deposits (Type 3) that are an important part of the architecture of the DFS strata, especially in their distal areas. Downstream variations in architecture and reservoir properties of the DFS strata might be emergent properties of the model if third dimension is added. Development and application of a 3D model is required to investigate DFSs characteristics further.

Despite of the limitations and simplicity of the 2D geometric model, it has potential to be useful for 1) studies of relationships between DFS deposit architectures and their controlling factors when used in combination with outcrop and/or subsurface data, 2) modelling of many possible variants of stratal architectures corresponding to particular reservoir characteristics and 3) studies of order within the DFS strata. Implications of the geometric process-imitating modelling and the results presented in this chapter to reservoir modelling will be further discussed in Chapter 13.

13. Implications of the studies to reservoir modelling

13.1 Introduction

The main part of this thesis comprises the detailed documentation of two distributive fluvial system successions to provide an insight into the architecture of the deposits and the main factors and processes that control styles of sediment deposition during the development of a DFS. As suggested by Weissmann et al., 2010 and Hartley et al., 2010(a), the deposits of DFS are likely to be preserved in the geological record and therefore potentially form hydrocarbon reservoirs, aquifers or host economic minerals and coal, e.g. uranium-rich sandstones of the Salt Wash DFS (Craig et al., 1955; Mullens and Freeman, 1955; Tyler and Ethridge, 1983) and coal-bearing DFS deposits of Tongue River Member of Fort Union Formation (Ayers et al., 1986; Jonson and Pierce, 1990).

This final discussion chapter is mainly concerned with the implications of the studies presented in earlier chapters to reservoir characterisation. This chapter discusses how outcrop data and results from 2D geometric modelling can be used in reservoir modelling but also provides information about the limitations of these applications.

The data collected in this research and their interpretation provide analogues for reservoir and aquifer characterisation and input for reservoir modelling. The comparison of two DFS successions with contrasting architectures provides an opportunity to better understand the controls on their deposition. This information could then help to determine suitable analogues for reservoirs and aquifers.

Outcrop studies of reservoir analogues are generally used to reduce uncertainties in reservoir modelling by collecting dimensional data for sandstone bodies, studying small- and large-scale heterogeneity of both the whole succession and its individual elements, and statistical analyses of quantitative data sets. Despite this, there is almost always a difference between the modelled architecture and properties of the reservoir and its performance when history matching is attempted (Miall, 2006). Reducing uncertainties in reservoir models leads to better estimations of the amount of recoverable hydrocarbons and this is the main aim of the reservoir modelling (Alexander, 1993). The reservoir modelling in turn serves to predict the behaviour of the reservoir during field development.

Fluvial reservoirs, in particular, are reservoirs with low recovery because they are characterised by complex architecture that results in trapped oil even in mature fields (Holden et al., 1998). Therefore, studies of fluvial deposits are extremely useful.

13.2 Use of modern and outcrop analogues in reservoir modelling

Keogh et al. (2007) emphasised that modern and outcrop analogues have to be the main focus in order to improve knowledge of fluvial reservoirs of different types. Alexander (1993), Geehan (1993), North (1996), Kolterman and Gorelik (1996), Bridge and Tye (2000) and Miall (2006) discussed the advantages and disadvantages of using modern and outcrop analogues for reservoir modelling. They all agreed that studies of ancient and modern fluvial deposits should be continued and are valuable for the characterisation of hydrocarbon reservoirs.

13.2.1 Outcrop analogues

Outcrop analogues are generally the main source of information about how reservoirs could be described in the subsurface. Alexander (1993) emphasised that although outcrop data could be described in detail, using outcrops for prediction of facies and reservoir property distributions requires an understanding of reservoir architecture beyond what is often possible with only limited outcrop. For example, the architecture of the fluvial deposits could change laterally and vertically within one succession as a result of intercalation of several upstream and downstream controls acting at different time scales (Miall, 2006). All outcrop analogues are also limited due to the difference in temporal and spatial scales (Alexander, 1993). Suitable reservoir analogues have to be also chosen in relation to the climatic and tectonic setting and temporal and spatial scales. Many of these parameters are unknown or difficult to infer from the outcrop data.

Nevertheless, the outcrops are still the main source of information about what is preserved in the geological record and provide much more information than spatially limited subsurface data. A limited number of documented outcrop analogues makes the choice of outcrop analogue for the reservoir even more difficult (Alexander, 1993). Therefore any detailed outcrop studies that are undertaken with the aim of describing the reservoir properties of fluvial deposits formed in different settings and understanding the links to their controls are useful. The more of these studies are done the higher the possibility that the links between reservoir characteristics and control factors on their variations would be better understood.

More specifically, only few examples of documented ancient DFS successions exist and could be used as outcrop analogues for DFS reservoirs. These are DFS successions formed in different geological settings including the Luna DFS successions (Ebro Basin, Spain, Hirst and Nichols, 1986; Nichols, 1987), Fort Union Formation, Tonger River Member (Wyoming, USA, Ayers et al., 1986; Johnson and Pierce, 1990), Camargo Formation (Eastern Cardillera, Horton and DeCelles, 2001) and the Organ Rock Formation in Paradox Basin, USA (Cain and Mountney, 2009) (Chapter 5). Moreover, not all of these outcrop examples are well documented.

The Huesca and Salt Wash DFS successions studied in this thesis provide suitable outcrop analogues due to their excellent exposure where both the large-scale architecture and small-scale facies studies could be carried out. The studied deposits are examples of DFS reservoirs formed at different scales, in different depositional setting (climate, basin configuration) (Chapter 2) and are characterised by contrasting architecture and net-to-gross (NTG) ratios (Chapter 11). The Huesca DFS deposits provide an analogue of DFS reservoirs formed in endorheic basins. Moreover it is an example of low-NTG succession (Chapter 11) where the distribution of sandstone bodies and their connectivity is the most difficult to predict. In contrast, the relatively proximal and medial deposits of the Salt Wash DFS could form high-NTG reservoir due to lower accommodation in these areas of the DFS (Weissmann et al., 2013 in press). Both DFS successions showed downstream variations in sandstone body geometries and connectivity caused by downstream variation in depositional processes typical for the DFSs (Chapter 8). This study demonstrated that high-NTG DFS reservoir could become low-NTG DFS reservoir over distances from 40 km (Huesca) to 200 km (Slat Wash) (chapters 8 and 11).

As there are only few documented examples of DFS successions and their deposits can be characterised by specific trends in reservoir characteristics related to specific behaviour of the DFS, more studies are required to expand the database of DFS outcrop analogues and research presented in this thesis contributes to this database.

13.2.2 Modern analogues

Modern analogues are often used to demonstrate the types of fluvial channel pattern that are thought to be analogous to the reservoir or support the observations from seismic and well-log data (e.g. Carter, 2003). Bridge and Tye (2000) reviewed strengths and drawbacks of outcrop analogues for reservoir characterisation and also suggested using modern (Holocene) analogues instead of ancient outcrops because it is possible to establish direct links between the deposits and the depositional processes.

However, in contrast to outcrop analogues, modern day analogues of fluvial depositional elements and architecture of recent deposits of modern fluvial systems (e.g. seen by Ground Penetrating Radar) do not necessarily reflect the characteristics of the preserved strata that would form hydrocarbon reservoirs (Miall, 2006). For example, the dimensions and architecture of large-scale amalgamated sandstone bodies, formed as a result of avulsions and lateral migration of channels, and vertical variations in architecture and sandstone body dimensions in fluvial successions cannot be predicted from modern analogues (see also Miall, 2006; Alexander, 1993). Therefore, only outcrop analogues provide realistic information on the architecture of fluvial deposits that are preserved as a result of long-term depositional processes (Miall, 2006).

In addition, modern fluvial analogues do not reflect depositional processes in the past when, for example, vegetation was not widespread or climate was different. Holocene climate, for instance, was highly variable and the frequency of abrupt climate changes has been shown to increase from the middle Holocene to the present day (Mayewski et al., 2004). Past climate variations and therefore the scale of depositional events might have been very different, making Holocene analogues unsuitable for the interpretation of ancient deposits.

Observations of modern fluvial systems together with experimental modelling have been playing a greater role in understanding of fluvial processes that have been used for the construction of process-based models of fluvial systems by engineers, geomorphologists and geologists (see also reviews by Paola, 2002; Sheets et al., 2002, 2007; Straub et al., 2009; Hajek and Wolynski, 2012) and therefore are still useful but not for direct application as reservoir analogues. Thus outcrop analogues remain to be the main source of realistic information for subsurface studies.

13.3 Geometry of facies bodies as input for reservoir modelling

The shape and dimensions of facies bodies determine the reservoir volume and are the main input parameter for stochastic reservoir modelling (Bridge and Tye, 2000; Bridge, 2008). Problems during field production caused by unrealistic predictions of reservoir body dimensions and connectivity would result in increased production costs due to the need for additional actions to enhance recovery (Bridge and Tye, 2000). The need to develop wider data sets of sandstone and shale body dimensions was emphasised by Robinson and McCabe (1997), who demonstrated that there is high sensitivity of modelled reservoir heterogeneity and sweep efficiency to the correct correlation and dimensions of lithofacies within a succession. Since sandstone body dimensions are an important component used in the reservoir modelling, a significant part of the research presented in this thesis has been focused on this subject (chapters 3-7).

13.3.1 Sandstone body geometry

Fluvial sandstone body geometry and dimensions have been studied and classified previously by several authors including Friend et al. (1979), Friend (1983), Fielding and

Crane (1987), Hirst (1991) and Reynolds, (1999). An extensive review of the literature on the external geometry of channel bodies and valley fills is provided by Gibling (2006). The sandstone bodies in these studies are usually related to the styles of fluvial systems, e.g. meandering or braided, distributive fans and deltas (Gibling, 2006).

The classification presented in this thesis is based on the data collected from the Huesca and Salt Wash DFS successions (Chapter 5). Three sandstone body types have been recognised firstly through observations of their shapes and dimensions and then have been interpreted in terms of the depositional processes. The emphasis was given to studies of the geometric characteristics of the sandstone bodies and the nature of their amalgamation styles (Chapter 5) because the channel styles/patterns (meandering, straight or braided) are difficult to define in the subsurface and sometimes even in the outcrops (see discussion in Section 13.3.3.).

In contrast to the previous studies of sandstone body geometries in the Huesca (Hirst, 1991) and Salt Wash (Robinson and McCabe, 1997; Kjemperud et al., 2008) DFS successions, the classification in this thesis has combined data from two ancient DFS successions that have been collected from three transect outcrops representing proximal, medial and distal areas of the DFSs and therefore accounts for downstream changes in sandstone body geometries in both DFS successions. In addition, the descriptions include a quantitative analysis of sandstone body types and their specific subtypes that have different origins and distribution across DFS (chapters 4-7).

The studies of individual sandstone body types are useful, but sandstone bodies usually amalgamate in various ways that can make them wider, thicker, more connected and of different shape than individual sandstone bodies. Characteristic amalgamation styles for the two DFS successions have been also studied in this research (Chapter 5) and this provides information about possible connections between different sandstone body types. One of the important outcomes of this part of the research is that major channel sandstone bodies in low-NTG successions could be connected with thin sheet-like sandstone bodies (Type 3) that are attached to the sides of large sandstone bodies or truncated by them and could improve the quality of the potential reservoir (chapters 5 and 11).

13.3.2 Measurements of sandstone body dimensions in outcrop and on photo panels

Measurements of the sandstone body dimensions are the basis of quantitative analysis of outcrop analogues. During this research it has been found that measurements of sandstone body width and thickness in outcrops are not always representative of the true dimensions of the sandstone bodies. The measurements are inaccurate in cases of poor exposure, small outcrop length, oblique orientation of the outcrop to the palaeocurrent direction and low accuracy of palaeocurrent direction estimations (chapters 3-5). Furthermore, sandstone body dimensions vary within the same outcrop and only ranges of thicknesses and widths could be determined (Chapter 5).

There is also some error when the sandstone body dimensions are measured from photo panels, such as the ones used in this thesis (Appendices 5.1-6). These errors are related to the distortion of the images (Section 3.3.1). If more precise measurements are needed LIDAR techniques can be used (Pringle et al., 2006). However, even LIDAR techniques cannot reduce errors related to outcrop exposure quality and the other limitations mentioned above. Moreover this technique is much more expensive and time consuming.

A high degree of sandstone body amalgamation introduces another challenge when measuring sandstone body dimensions. For instance, individual sandstone bodies within amalgamated complexes in the relatively proximal deposits of the Huesca and Salt Wash DFSs are difficult to distinguish (Fig. 13.1, A-B). If remnants of finer-grained deposits are present between sandstone bodies, the boundaries could be traced in the outcrop and on photo panels, otherwise the task becomes very difficult. Even if individual sandstone bodies can be recognised, their thickness is incomplete because they are truncated by subsequent erosion events (Fig.13.1, A-B). Bridge and Tye (2000) have highlighted the difficulty of separating individual sandstone bodies from amalgamated complexes and estimating thicknesses and widths of individual sandstone bodies within them in the subsurface (Fig.13.1, C). Outcrop analogues are usually used to overcome this difficulty. However, the discussion above shows that outcrop data also have limitations that should be taken into account when applying them to reservoir characterisation, especially when sandstone body geometries are used for well correlation.

13.3.3 Sandstone body correlation between wells

Bridge (2008) and North (1996) emphasised that it is difficult to define input parameters for stochastic reservoir modelling, especially the shapes and lateral dimensions of sandstone and shale bodies, and their location between wells which is limited by well spacing. Analogue outcrop data of sandstone body widths and thicknesses are usually used as a basis for correlation of sandstone bodies between wells. This is based on the common assumption that sandstone body width to thickness ratio is related to the vertical succession of deposits and a channel pattern, i.e. meandering or braided (Bridge and Tye, 2000). For example, high connectivity is related to the deposits of braided streams and even different modelling approaches are used, based on the

A. Monźon 1 outcrop

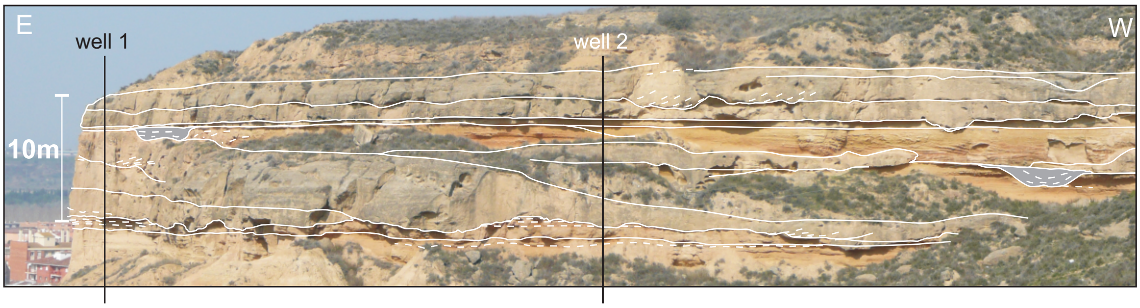

B. Bullfrog 1 outcrop

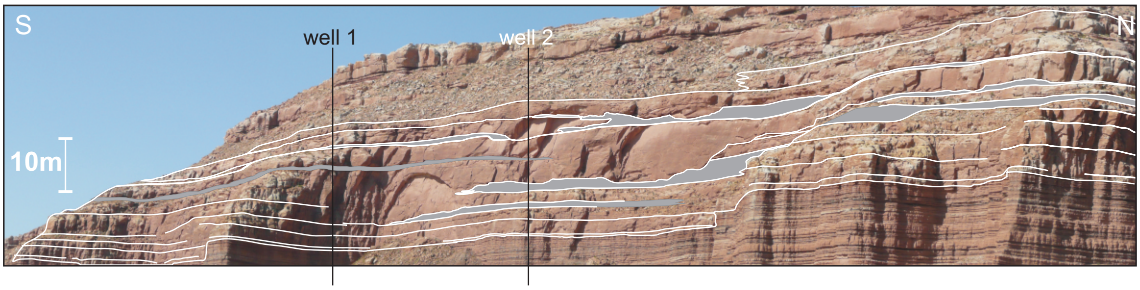

C

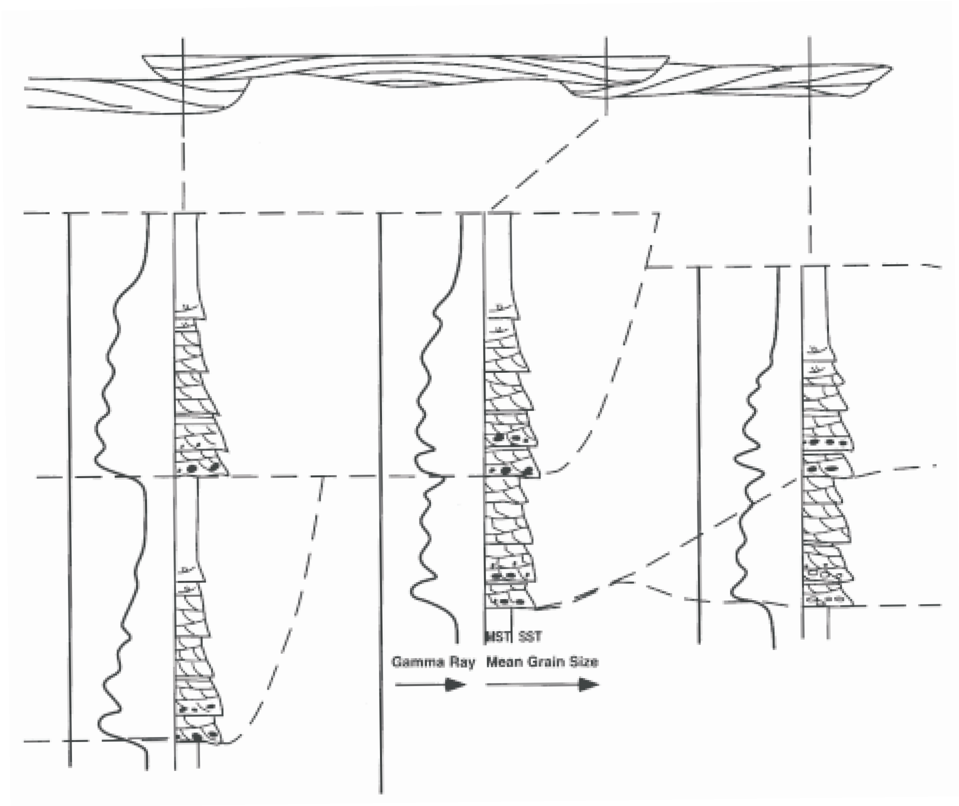

Figure 13.1. Amalgamated sandstone body complexes in the relatively proximal successions of A - the Huesca DFS (Monźon 1, Appendix 5.1) and B - the Salt Wash DFS (Bullfrog 1, Appendix 5.4). Boundaries between individual sandstone bodies not always could be seen within amalgamated sandstone bodies. C - Schematic diagram demonstrating difficulty of distinguishing individual sandstone bodies from well-log and core data (from Bridge and Tye, 2000). Also compare wells 1 and 2 on the photo panels.

interpretation of channel pattern (Martin, 1993; Martin et al., 1988; Robinson and McCabe, 1998).

Bridge and Tye (2000) further emphasised that channel pattern is difficult to recognise in wells/core and therefore outcrop analogues and empirical equations that are chosen for specific channel patterns cannot be used with confidence for the determination of sandstone body dimensions. Outcrop studies in this research have showed that recognition of channel pattern even in outcrops is not easy. For example, the amalgamated sandstone bodies in the relatively proximal deposits of the Salt Wash DFS represent what is usually interpreted as deposits of braided streams (Fig. 13.1, B) (Peterson, 1984; Tyler and Ethridge, 1958). However, another relatively proximal outcrop near Caineville (Fig. 3.4) revealed sandstone bodies with large-scale inclined stratification perpendicular to the palaeocurrent direction (Fig. 13.2, A-B) indicating sediment accretion on a point bar in sinuous channels (Thomas et al., 1987). The Google Earth satellite image of the Caineville outcrop area also shows preserved meander loop traces (Fig. 13.2, D). The large-scale inclined stratification in the sandstone bodies in the Bullfrog outcrop may be obscured by other sedimentary structures (Miall, 1985) such as abundant trough cross-bedding observed in the channel fill sandstones (Fig. 13.2, C; Fig. 4.3, Chapter 4). In addition, in the relatively proximal part of the Salt Wash DFS inclined heterolithic stratification at the top part of a point bar sandstone body, which is usually seen due to mud drapes along the inclined surfaces, could have been removed due to erosion by subsequent channels. The high degree of reworking in the relatively proximal area of the Salt Was DFS has been also confirmed by the modelling results presented in Chapter 12 and supports this interpretation.

Fining-upward vertical successions of the facies observed in outcrops and log data are often being associated with the deposits formed in sinuous (meandering) channels (Allen, 1970; Leeder, 1973; Cant and Walker, 1976; Donselaar and Overeem, 2008; Rider, 2001; Emery and Myers, 1996). The facies analysis of the Huesca and Salt Wash DFS deposits showed that the grain size varies between cross-sets within sandstone bodies without any trend or sometimes with coarsening-upward trend (Chapter 4, Fig. 4.3). The order analysis of the vertical facies and thickness successions in the DFS deposits also showed that there are no facies or thickness trends within the deposits (Chapter 10), although deposits formed in sinuous channels are present in both DFSs (Fig. 4.6; Fig. 13.3, C-E).

Thus, evidence of channel style could be unclear in 2D outcrops and therefore vertical signature from well logs is considered even less reliable source of information about

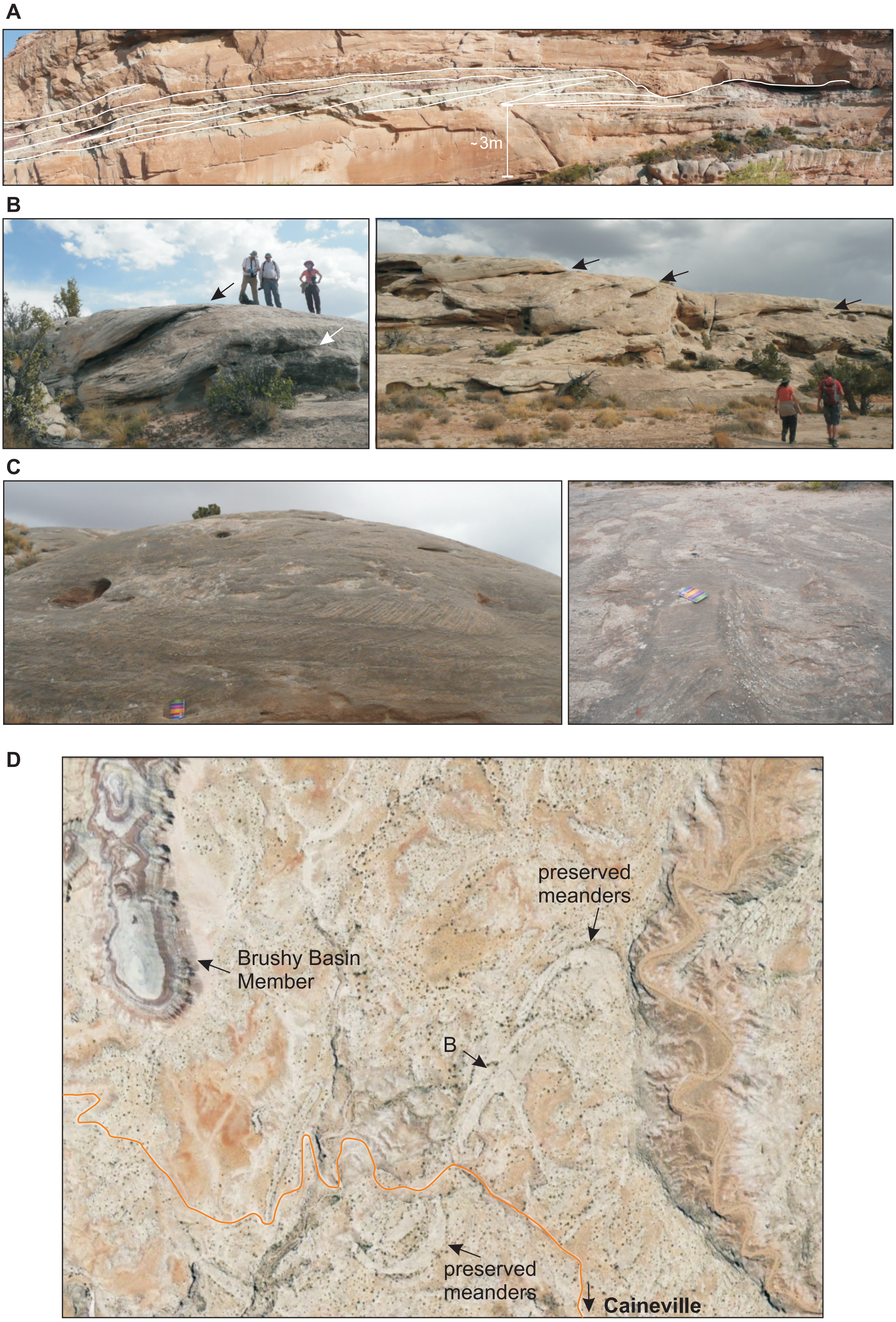

Figure 13.2. Lateral accretion complexes in relatively proximal deposits of the Salt Wash DFSnear Caineville (for location see Fig. 3.4): A - heterolithic LA complexes and B - large-scale LA surfaces within large sandstone body characterised by abundant trough cross-bedding (C), long side of the notebook for scale is 20 cm). D - Preserved traces of meander loops on the Google Earth satellite image of the Caineville outcrop area.

depositional processes or channel pattern and could cause subsequent erroneous sandstone body dimension estimations.

Geometric conclusions drawn from the studied Huesca and Salt Wash DFS successions could be used when correlating sandstone bodies. Bridge and Tye (2000) stated that correlation between wells has to be based on the principle that sandstone body bases and tops are not horizontal. In this research it has been found that most of the sheet-like sandstone body bases are flat and horizontal, while their tops can behorizontal, inclined or gradational (Fig.13.3, A-E, Appendix 5) and therefore the sandstone bodies should be correlated accordingly. Miall (2006) has also argued that sheet-like sandstone bodies have horizontal bases (Fig. 13.3, G).

Three-dimensional seismic data could be used to realistically interpret channel patterns and map actual sandstone bodies in the subsurface (Bridge and Tye, 2000; Miall, 2002). Extensive studies of different fluvial styles from subsurface seismic data (Miall, 2006) in combination with outcrop analogues where channel styles can be confidently determined could provide the link between preserved sandstone body geometries and channel patterns. In addition, well logging and Ground Penetrating Radar surveys behind the well-documented outcrop surfaces could be also conducted with this aim (Miall, 2006). These suggestions will indeed help to provide the link between 1D well data, 2D outcrop data and 3D seismic data.

Unfortunately, seismic data resolution is limited and only sandstone bodies with thickness higher than 10 m (Bridge and Tye, 2000) can be recognised. For example, majority of sandstone bodies in the studied DFS deposits are thinner than 10 m and would not be seen on seismic data even in large Salt Wash DFS. However, if large amalgamated sandstone body complexes could be seen on and mapped from seismic data, it would give information about how continuous are these sandstone bodies between wells.

Apart from the channel pattern, bank stability and avulsion frequency were also mentioned as possible controls on sandstone body dimensions and the degree of their amalgamation (Bridge and Tye, 2000) and therefore affect the style of sandstone body correlation between wells. The modelling exercise in this thesis (Chapter 12) has also shown that degree of lateral migration of channels, which could partially relate to amount of accommodation space and partially to bank stability in the system, controls the proportion and connectivity of the sandstone bodies in the succession. In addition, downstream decrease in sandstone body dimensions and the degree of their amalgamation and connectivity was probably related to more cohesive substrate and higher avulsion frequency in the distal areas of the DFS caused by downstream decrease in water discharge (Chapter 8). These factors, however, are still poorly

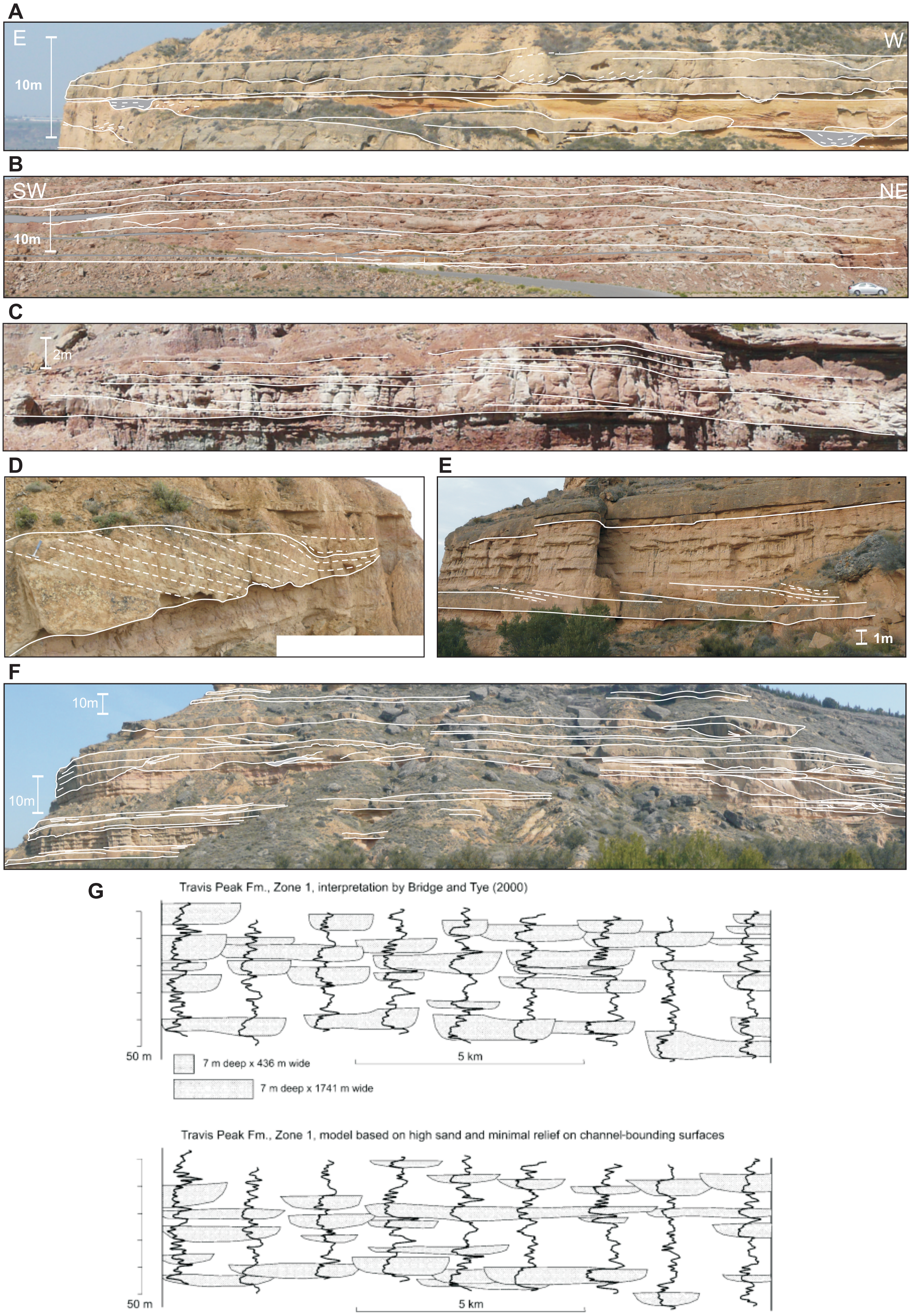

Figure 13.3. Flat bases of the main channel sandstone bodies in the Huesca DFS succession (A, D, E) and Salt Wash DFS succession (B, C). The sandstone bodies in the relatively proximal Huesca succession (Monźon 4 outcrop, Appendix 5.1) are characterised by scoured bases with flat middle area (F). Example of well correlation at the diagram G shows two different variants of correlation based on the assumptions of non-flat and flat bases (from Miall, 2006) (not for comparison with studied successions).

understood (Bridge and Tye, 2000). Process-based modelling could give an insight into the relationships between channel patterns, discussed above controlling factors and the resulting sandstone body dimensions (Bridge, 2008). The implications and limitations of the process-based modelling are discussed in Section 13.6.

The pressure-test data and 4D seismic surveys are the other techniques used in the industry to determine which sandstone bodies are connected and therefore to determine correlation distance of sandstone bodies between wells (see examples in Miall, 2006).

13.3.4 Net-to-gross and sandstone body correlation between wells

Bridge and Mackey (1993(b)) showed that all sandstone bodies can be connected and therefore correlated between wells if sandstone body percentage relative to fine-grained floodplain deposits is higher than 75 % in 2D cross section. Cross sections with a sandstone body percentage of less than 40 % were found to contain isolated sandstone bodies (Bridge and Mackey, 1993(b)). The 2D model presented in Chapter 12 demonstrated that a high sandstone body proportion in the modelled strata can be reached if sandstone bodies have sheet-like continuous geometries. For instance, relatively proximal, sandy succession of the Salt Wash DFS where almost all sandstone bodies are connected and NTG ratio reaches 85 % (Appendix 5.4) can only be modelled with a channel width not less than 800 m (Fig. 12.17-18) given other input parameters values measured from the outcrop (Chapter 12). This result supports the finding for high-NTG reservoirs of Bridge and Mackey (1993(b)) and means that almost all sandstone bodies in the succession could be correlated. In contrast to the results of Bridge and Mackey (1993(b)), in this study the modelled strata with low NTG ratio (30 %) could include a few connected sandstone bodies (Fig. 12.11 and 12.23). However in general, 2D model is unable to predict sandstone body connectivity in 3D space that could be higher than the connectivity in 2D cross section.

The 2D geometric model has also shown that modelled strata with the same NTG ratio (lower than 75 %, Fig. 12.25) could show different geometry and sandstone body connectivity (Fig. 12.23) (Chapter 12). Therefore NTG ratio can not be directly used to predict continuity of sandstone bodies between wells.

In addition, the NTG ratio or sandstone body proportion determined from well data are limited by one-dimensional character of the data and by their specific locations. Just a few metres away from the well the NTG ratio might change dramatically (see discussion in Chapter 11, Section 11.3). Moreover, if only a few wells are available close to each other, the downstream variation in architecture of DFS deposits (chapters

6-8) could be missed and prediction of the NTG ratio in the reservoir and its architecture would be incorrect.

Therefore, the NTG ratio determined from wells or based on the results of 2D modelling does not reduce the uncertainty in sandstone body continuity and correlation and is uncertain parameter to base the interpretation on. Above-mentioned 3D seismic attribute analysis and production data, with some limitations, could help to map sandstone bodies between wells and perhaps help to determine the two- or three-dimensional sandstone body proportion and connectivity.

13.4 Detailed sedimentological and petrographical studies

Detailed sedimentological and petrographic studies provide information about the set of possible facies that could occur in a DFS and also the small-scale characteristics of the facies. The detailed facies description in Chapter 4 was carried out using data collected from both the Huesca and Salt Wash DFS successions and therefore includes wider set of facies. The detailed analysis of the internal characteristics of the facies has revealed different scales of heterogeneity within sandstone bodies (reservoir bodies), for example, heterogeneities related to uneven matrix distribution in a pore space or variation in grain size and sedimentary structures (Fig. 11.1). These heterogeneities would result in variations in petrophysical properties within reservoir bodies that in turn affect hydrocarbon and water flow paths and, consequently, sweep efficiency of the reservoir (Chapter 11; Holden et al., 1998). The mosaic of facies in the strata creates heterogeneity at larger scales affecting NTG ratio and sandstone body connectivity in the reservoir and therefore hydrocarbon volume and recovery.

Keogh et al. (2007) reviewed advances in reservoir modelling and highlighted the “pore-to-field” modelling approach (Fig.13.4). The idea includes integration of models that capture reservoir heterogeneity at different scales. For example, models of heterogeneous pore-space or lithological interbedding are built and then flow simulated to analyse the effect of the heterogeneities at this scale on flow behaviour (produce relative permeability curves), for instance using SBED software (Keogh et al., 2007 and references therein). The results are integrated as input parameters into the models at the next higher scale. This approach requires detailed studies of sandstone texture and petrography, lithofacies and facies associations in outcrop analogues similar to studies carried out in this thesis.

Samples from the studied outcrops have been analysed in thin sections and in loose material that revealed poor sorting and uneven matrix and cement distribution in the pore space of the sandstone facies (chapters 6-7 and 11, Appendix 4, Appendix 3 Table 3). Although cementation is a local characteristic of the particular succession,

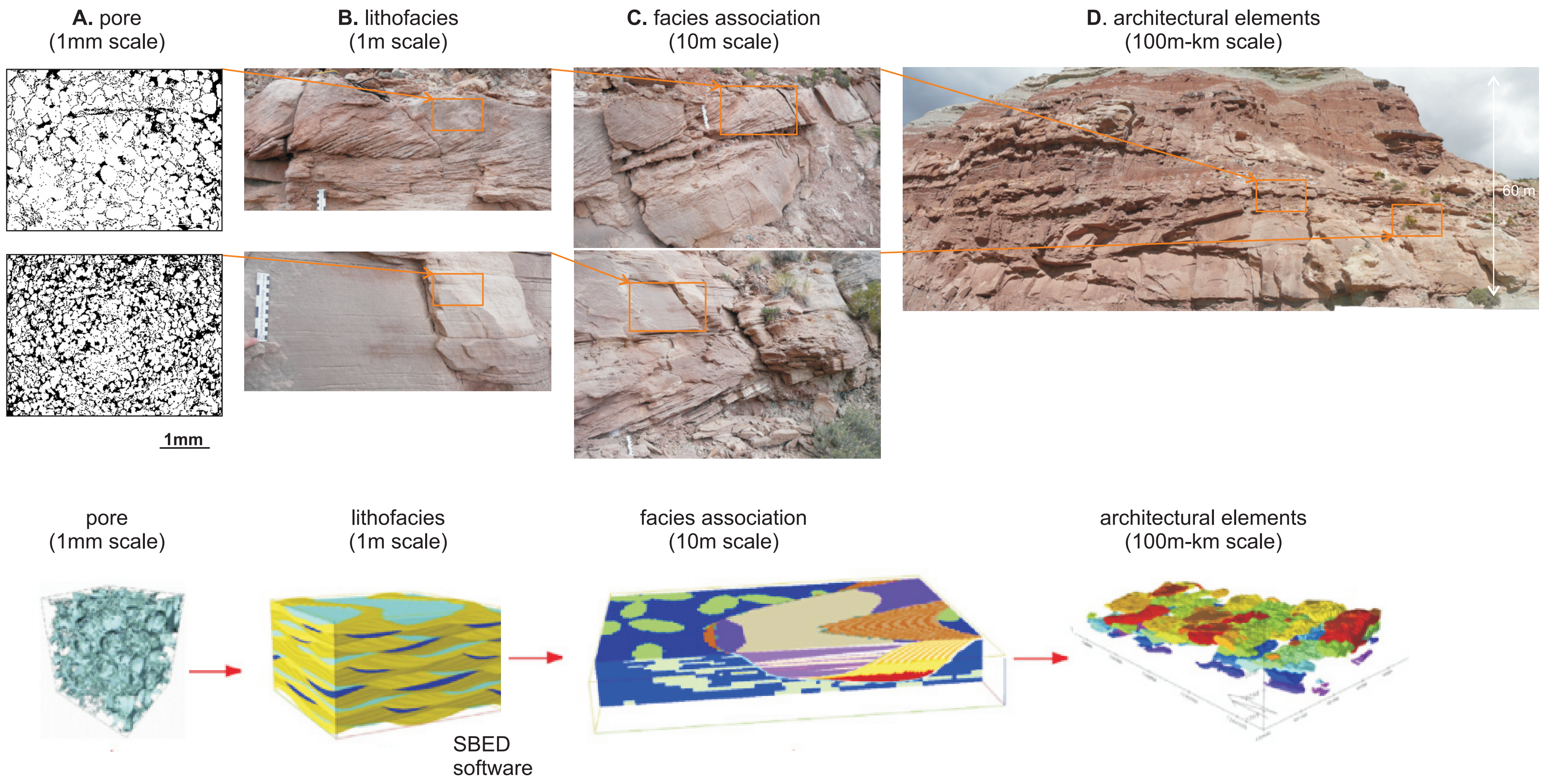

Figure 13.4. Workflow of "pore-to-field" scale modelling modified from Keogh et al. (2007). The thin section and outcrop examples are from the distal succession of the Salt Wash DFS in the Little Park 3 outcrop (Appendices 2.10-12 and 5.6).

this and other sandstone characteristics could be taken into account when creating pore-scale model (Fig. 13.4, A). Porosity estimated from the samples (Fig.12.2-4) cannot be used directly for subsurface predictions due to weathering of the rocks at the surface and because it was estimated in 2D thin sections, but observed heterogeneity in porosity might be useful to consider.

Sedimentary logs together with extended descriptions and photographs of each lithofacies bed recorded in the field (Appendix 2) can be used at the second stage of the “pore-to-field” modelling (Fig. 13.4, B). In comparison with core data, which are limited by the core diameter, the outcrop data provides more information about each lithofacies which can be incorporated into a model of similar lithofacies inferred from the core data (e.g. using SBED software). From the previous experience of the author of the thesis (Kulikova, 2006) core data are not always enough to confidently model the lithofacies in the SBED software because the software requires process-based input parameters that in turn require lithofacies observations more extensive than in 10 cm-wide core (Fig. 13.4, B-C), unless trial and error approach is used to match lithofacies bed geometry in core and in the model.

Although petrographic and lithofacies studies can be conducted using only core data recovered from subsurface wells, the degree of heterogeneity observed within facies associations cannot be predicted using well data alone. Detailed sedimentary logging, extended descriptions and photographs of facies (Appendix 2), and outcrop photo panels (Appendix 5) recorded during this research provide such information for analogous DFS reservoirs. Heterogeneity at sedimentary structure and sandstone body scales which needs to be considered in the facies association-scale models (Fig. 13.4, C) has been discussed in Chapter 11.

However, the heterogeneity at these scales observed in outcrops could not necessarily be applied directly to subsurface DFS successions of similar type. For instance, a point bar sandstone body formed in a sinuous channel might be characterised by inclined stratification with mudstone drapes that continue from the top to the bottom of the sandstone body, or with mudstone drapes that occur only at the top of the body, or there may be no mudstone drapes (Fig. 13.5, A-C). In addition, subsequent erosion could remove the heterolithic top part of a sandstone body creating large, amalgamated, almost homogeneous sandstone bodies such as those observed in the relatively proximal parts of the Salt Wash DFS succession (Fig. 13.1, B). These reservoir bodies with different structures would behave differently during reservoir production (see review in Section 11.2.2) and it is often unclear which variant to choose as an analogue for the reservoir bodies.

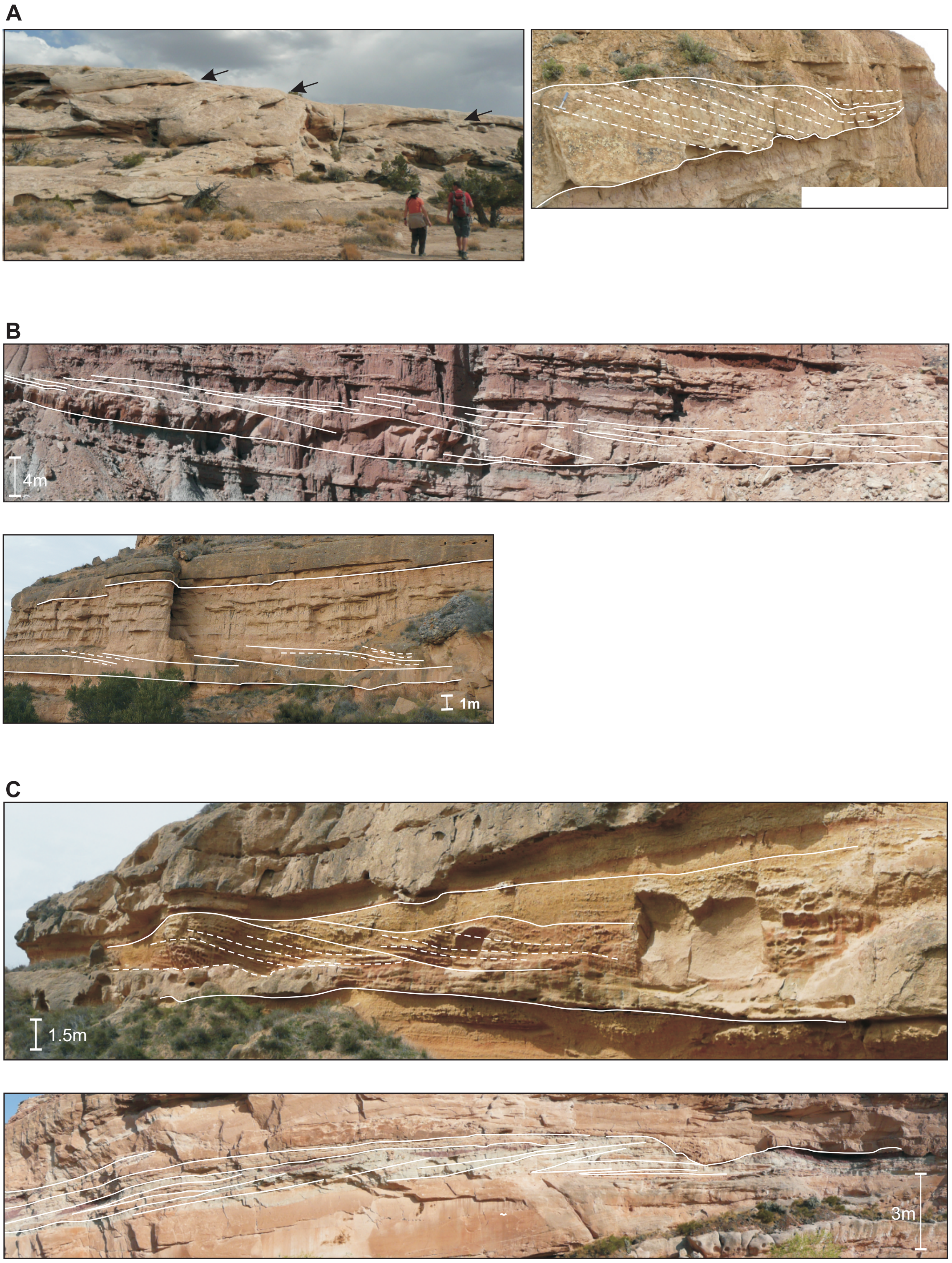

Figure 13.5. Examples of lateral accretion complexes without mud drapes along the inclined surfaces (A), with mud drapes that continue to the middle of the sandstone body (B) and heterolithic lateral accretion complexes with continuous mudstone layers along the inclined surfaces (C). Examples are from both the Huesca and Salt Wash DFS successions.

Knowledge of several possible variants of internal sandstone body characteristics gained from extensive studies of outcrop analogues of fluvial systems of different style makes it possible to be aware of and anticipate all scenarios that could occur in a particular subsurface example and look for the evidence that support one scenario or another. This emphasises again the need for extensive database of outcrop analogues of different styles of fluvial architecture. If one scenario could not be chosen all possible variants have to be considered and modelled. Perhaps the most heterogeneous variant should be used to prevent underestimation of the reservoir heterogeneity.

Implications of the architecture studies carried out in this thesis (chapters 6-12) to the last stage of “pore-to-field” modelling (Fig. 13.4, D) are discussed in the following section.

13.5 Sandstone body architecture and population of reservoir model with facies

The most common reservoir modelling approach includes object-based or pixel-based facies distribution and continuous population of reservoir properties within facies. In this discussion the facies modelling is the main focus. The parameters of the facies bodies or facies indicator and rules of their distribution within the model are commonly based on the data from core, well-logs, seismic survey and outcrop analogues. As discussed above, the first two data sources do not provide much information about facies distribution between wells. The architecture of sandstone bodies determined from outcrop analogues are usually used to investigate this problem. Other possible sources of information about sandstone body architecture are also discussed in this section.

13.5.1 Facies distribution, NTG ratio and outcrop analogues

The facies objects in the model are commonly distributed to preserve the proportion of facies or NTG ratio determined from well data. The main drawback of this method is associated with highly variable facies proportion in fluvial deposits that could change dramatically vertically and laterally, perpendicular and downstream to the palaeocurrent direction. The lateral changes are especially characteristic of the DFS deposits, as has been observed previously and discussed in this thesis. For example, downstream variations in the architecture of the DFS deposits have been described in detail in chapters 6-8 (Fig. 13.6, A and B) and in previous studies of the DFS deposits (e.g. Nichols and Hirst, 1998; Cain and Mountney, 2009). The lateral and vertical variation in channel sandstone body density (clustering) in the DFS deposits in the Ferris Formation has been also recognised by Hajek et al. (2010) (Fig. 13.6, C). The sandstone body clustering has been related to deposition in lobes such as has been

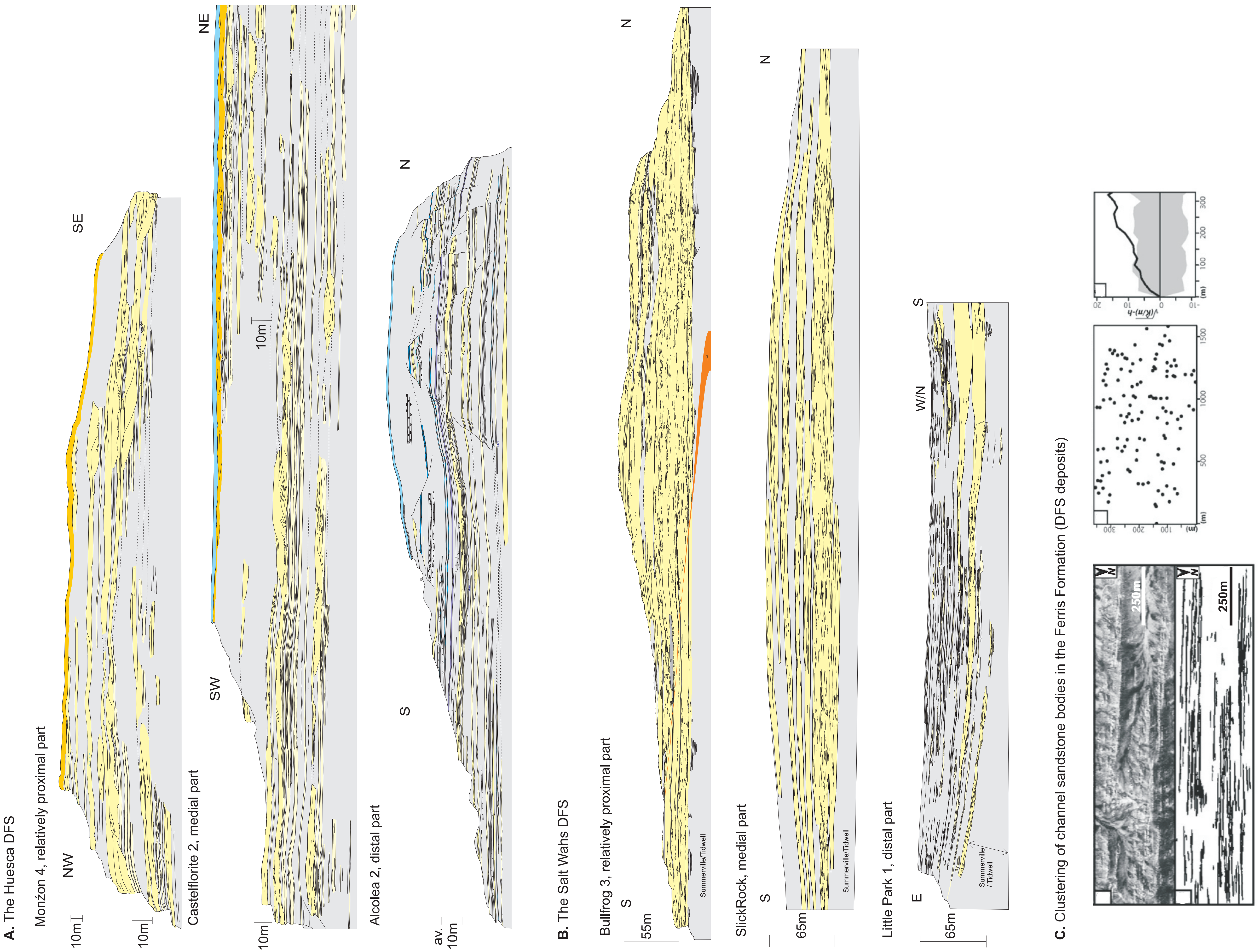

Figure 13.6. Lateral variations in architecture of DFS deposits. Downstream variations in architecture of the Huesca DFS (A) and the Salt Wash DFS (B) deposits, C - sandstone body clustering within the Ferris Formation in Wyoming, USA from Hajek et al. (2010) including: aerial photograph of the outcrop of the Ferris Formation, sandstone body interpretation based on the photograph, point pattern of channel centres in the outcrop and K-function plot showing clustering for distances greater than approximately 120m (for explanations see Hajek et al., 2010).

observed in the modern Kosi DFS by Chakraboty et al. (2010). Therefore, NTG ratio in DFS successions varies vertically and laterally and this heterogeneity should be considered. The heterogeneity and trends in reservoir architecture that could not be determined from well data could be conditioned using 2D and 3D data from outcrop analogues, seismic surveys and numerical process-based and process-imitating modelling (sections 13.5.2-3 and 13.6).

Furthermore, 2D geometrical modelling presented in this thesis (Chapter 12) showed that strata with the same proportion of sandstone bodies (NTG ratio) could have contrastingly different stratal geometry under different input parameters. In reservoir modelling one interpretation of reservoir architecture or well correlation is usually suggested and used as an input for the static model. The results of the 2D modelling show that this approach is not correct. Perhaps many variants of the architecture that could be conditioned to the NTG ratio from available well data should be modelled to account for any possible heterogeneity in the reservoir architecture. In this case the database of fluvial architecture styles from outcrops, seismic data and numerical modelling would be useful. Although single outcrop analogue is difficult to define for a particular reservoir, data collected from multiple outcrop studies could help to describe multiple strata architectures that could possibly occur in the subsurface (e.g. data base in Colombera et al., 2011, 2012). The process-based or process-imitating modelling can be also used to create all possible variants of the reservoir architecture corresponding to specific reservoir characteristics determined from subsurface data (Chapter 12); however the modelled strata would be difficult to condition on the well data (Keogh et al., 2007). The applicability and limitations of the process-based and process-imitating numerical modelling will be discussed in Section 13.6.

13.5.2 3D seismic data for reservoir architecture predictions

Improvement of geophysical technologies has made it possible to use seismic data for high-resolution stratigraphic correlations and interpretation of depositional environment and reservoir architecture in 3D that could not be confidently made using only well data (Carter, 2003). Bridge and Tye (2000) argued that seismic amplitude images can be confidently used to recognise fluvial system channel patterns, help to chose outcrop analogues and conduct sandstone body correlations between wells. Seismic data, for instance, revealed that fluvial architecture styles (channel types, channel spacing) and reservoir body dimensions vary dramatically within a short stratigraphic interval of the Pleistocene gas-prone Pilong Formation in Thailand that was previously modelled using a uniform fluvial architecture (Miall, 2002). Some other examples of successful seismic data integration, which have helped to improve the understanding of the origin of the reservoir and its architecture, have been cited by Miall (2006).

The main problem with the application of seismic data that has been highlighted by many authors is the limited resolution. Channel sandstone bodies have to be at least 10 m thick to be recognised on a seismic section (Bridge and Tye, 2000). The channel sandstone bodies in the Huesca and Salt Wash DFS successions, however, are rarely thicker than 10 m (chapters 5-7), unless they are amalgamated. Therefore individual sandstone bodies would not be distinguished on seismic sections or time slices. Thin sheet-like sandstone bodies of Type 3 and their packages are an important part of the Huesca DFS architecture and make up a large proportion of all the sandstone bodies in the succession, and hence make up a large proportion of reservoir volume (Fig. 13.7, B-C). The Type 3 sandstone bodies have been also observed in floodplain intervals in the Salt Wash DFS succession (Fig. 13.7, A, D). Due to the low resolution of seismic data, Type 3 or similar sandstone bodies would not be resolved (see also Miall, 2002; Jones and Hajek, 2007), but could contribute to reservoir volume and connectivity (Chapter 11, Table 11.1).

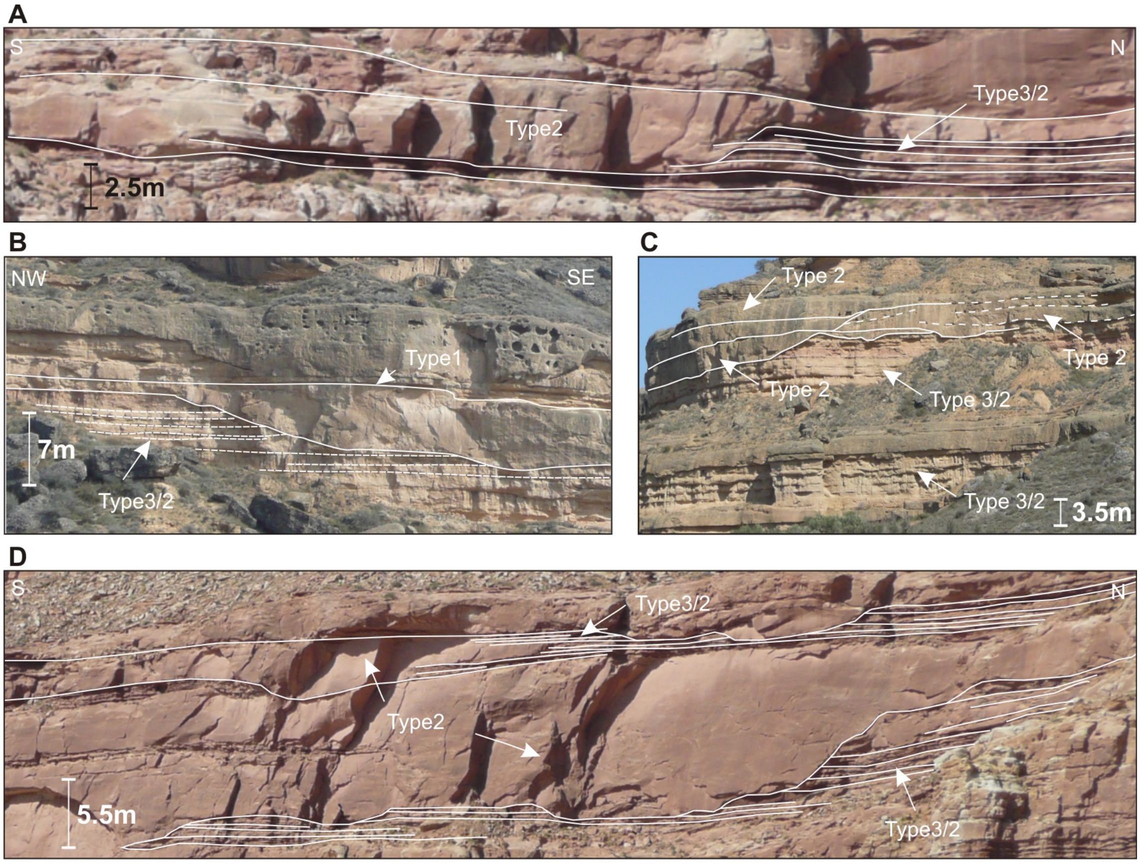

Figure 13.7. Abundant thin sheet-like subtype 3/2 sandstone bodies in the Huesca (B, C) and Salt Wash (A, D) DFS successions that contribute to reservoir volume and could connect major channel sandstone bodies.

Therefore outcrop analogues provide more detailed information about sandstone body architecture, some details of which could not be seen on seismic data, but affect the prediction of reservoir behaviour. Therefore seismic data should be used in combination with outcrop data. Seismic data interpretation could perhaps help to determine fluvial style and large-scale architecture, and to choose the type of outcrop analogue for the reservoir, whereas interpretation of detailed sandstone body architecture can be based on the outcrop data.

13.5.3 “Training images” and outcrop analogues for reservoir architecture predictions

A semi-variogram-based geostatistical method is used to distribute facies indicator between wells in conventional pixel-based reservoir modelling. Caers and Zhang (2004) stated that this approach can not reflect the degree of heterogeneity observed in outcrop analogues: the authors demonstrated examples of three different reservoir heterogeneities that result in similar semi-variograms. Multiple-point geostatistical approach uses “training images” (Fig. 13.8, A) to replace the semi-variogram although it is still a stochastic approach (Caers et al., 2002; Caers and Zhang, 2004). “Training images” are an intuitively-produced “database of geological patterns” that include information about reservoir heterogeneity and statistical information (typical geometry and their spatial relations) that is used to produce multiple realisations of a reservoir pattern which can be conditioned to well, seismic and production data (Caers and Zhang, 2004; Maharaja, 2008).

In the multiple-point geostatistics initial “training images” are not constrained by hard data (Keogh et al., 2007) so their construction is based on theoretical understanding of geological patterns and their variations in 3D space. Outcrop analogues are the primary source of the theoretical ideas used for construction of the “training images”. However, direct application of outcrop data (e.g. photo panels) for the creation of “training images” is limited due to lack of stationarity in the outcrop data (Caers and Zhang, 2004). Non-stationarity is indeed very typical for heterogeneous fluvial deposits, especially DFS deposits. Therefore, only elements of real 3D architecture observed in outcrops, for example geometry of facies bodies and their spatial relations, could be used to construct “training image” (Fig. 13.8, A and C).

Distributive patterns and downstream variations described for the DFS succession could be captured to some extent when using multiple-point geostatisitc method, “training images” and trend maps (e.g. Fig. 13.8). Note, however, that in real DFS deposits facies are not distributed as elongated bodies as it is shown in Figure 13.8, D. Thus, reservoir models produced with multiple-point geostatistcs, and in fact all models, and “training images” themselves have to be critically assessed in terms of their realism. For instance, channel facies representation as “noodle-like” objects of sandstone facies (e.g. Larue and Hovadik, 2006) is in most cases an unrealistic representation of channel fill deposits that in reality consist of individual or amalgamated sandstone bodies of different geometries (Chapter 5). Detailed outcrop studies could help to construct realistic “training images”. Three-dimensional outcrops that are not always available are preferable for this task.

The library of “training images” (Caers and Zhang, 2004) for different fluvial styles that contain many possible variants of reservoir heterogeneity could be used to choose suitable “training image” for the reservoir modelling according to the interpretation of other available subsurface data. The database of well-documented DFS outcrops would assist in creation of such library. For example scaling trends or regions (Fig. 13.8, B-C) could be created based on the downstream trends in sandstone body dimension and proportion observed in the Huesca and Salt Wash DFS outcrops (chapters 6-8).

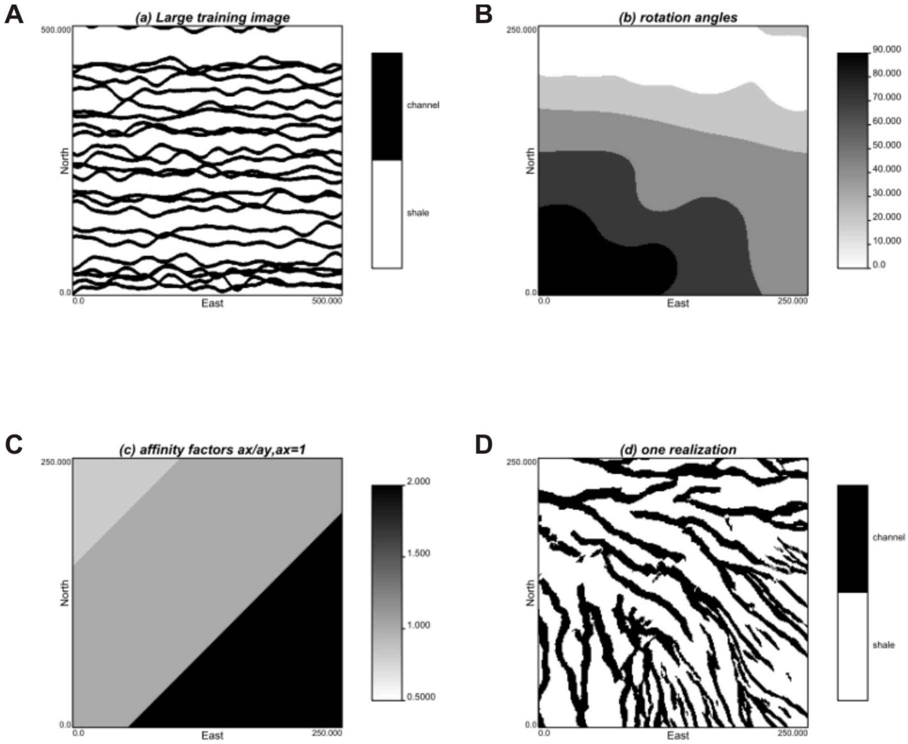

Figure 13.8. Examples of one of the model realisations (D) created using stationary “training image” (A), locally varying rotation angle (B) and locally varying affinity factor or scaling regions (e.g local shrinking or stretching by a certain factor) (C) (from Caers and Zhang, 2000). The model reflects downstream variations and radial pattern of DFS deposits. Note, however, that facies are not distributed as elongated bodies within the real DFS successions.

13.6 Implications of process-based / process-imitating modelling to modelling of reservoir architecture

Process- based and process-imitating numerical modelling have become a widely-used tool for exploring the relationships between architecture of fluvial deposits and controlling factors that determine one or another architecture style. However, although the process-based and process-imitating modelling has advanced significantly it have not yet been incorporated into the reservoir modelling workflow (see reviews by Kolterman and Gorelik, 1996; Paola, 2000; Keogh et al., 2007; Bridge, 2008, Wolinsky and Hajek, 2011). Probabilistic approaches such as semi-variogram and multiple-point geostatistical methods are usually used.

Numerical models based on the understanding of depositional system behaviour has been argued to be capable of predicting fluvial architecture between wells better than stochastic approach that cannot predict architecture outside data areas (Bridge, 2008). Keogh et al. (2007) and Bridge (2008), however, also argued that our knowledge of physical sedimentary, climatic and tectonic processes affecting fluvial architecture is still too poor. Consequently, the process-based models include many assumptions and simplifications. The 2D model created in this research is an example of such simplified models (Chapter 12). Use of process-based modelling based on an incomplete knowledge of processes is therefore limited for reservoir modelling. Nevertheless, some models are useful and their implications to reservoir modelling can be discussed. For example, modelled strata could be used for conditioning of stochastic reservoir models through “training images”, facies transition probabilities or trend maps.

13.6.1 “Training images” and parameters for multiple-point geostatistics

Large-scale process-based models can help to constrain “training images” that are then applied to condition stochastic pixel-based reservoir modelling. Large-scale, field-size process-based models are difficult to create due to the incomplete understanding of fluvial system behaviour (Bridge, 2008), the large number of details and processes that have to be considered and the unmanageable computation time of such models. Plus most of reservoir models do not need that level of details (Maharaja, 2008). Instead process-imitating, rule-based models can be used for the large-scale, long-term architecture modelling (Bridge, 2008).

The 2D rule-based, geometric model of DFS strata created during this study (Chapter 12) is considered a large-scale model (2500 cells * 20 m = 50 km laterally) that could be used to study effects of large-scale processes and therefore a suitable basis for cross-sectional 2D “training images”. However, reservoir models are three-dimensional and 3D versions of the process-imitating model and “training images” are required. Furthermore, the 3D model that takes into account specific processes of a DFS, including formation of radial channel pattern, deposition in lobes and downstream variation in depositional processes, would be able to capture lateral heterogeneities in the architecture of DFS deposits described in chapters 6-11. The information about depositional patterns and their variations learned from the 3D model could be used as input for the 3D “training images” and for identification of transformation parameters (rotation angle, affinity factor, Fig. 13.8) for multiple-point geostatistical modelling.

For example, an approach that combines process-based models, “training images” and multiple-point geostatistics was used to model 3D subsurface heterogeneity of an aquifer by Michael et al. (2010). Kolterman and Gorelik (1996 and references therein) also exemplified use of “training images”, created using a process-imitating approach, in hybrid reservoir modelling that combines conditioned architecture patterns (“training images”) and stochastic approaches.

Paola (2000) in his review of different types of process-based and process-imitating models stated that 2D model slices, such as ones that have been produced based on the relatively proximal, medial and distal outcrop data in this study (Fig. 13.9; Chapter 12), can be used to understand 3D depositional system with the condition that downstream fluxes control deposition more than lateral fluxes. The latter could be true for the studied DFSs. Thus, 2D slices of DFS strata produced in this study could give some information about depositional patterns and especially their trends that can be used in reservoir modelling with a multiple-point geostatistical approach.

The 2D model presented in this research is a “work in progress” (e.g. the 2D model cannot realistically model distal successions) and therefore needs further development to be ready to be applied to reservoir modelling. A 3D model of DFS strata would clearly have wider implications in this area.

13.6.2 Markov chain models

Markov facies transition probability (TP) can be used to model discrete facies distributions (Bridge, 2008; Kolerman and Gorelik, 1996 and references therein) as an alternative to the semi-variogram or multiple-point geostatistical method. For example, a Markov chain model has been created by Elfeki and Dekking (2001) to predict the facies distribution between imaginary wells through an outcrop. The model applicability was demonstrated by an accurate prediction of fluvial facies distribution in this outcrop. The input parameters for the method are vertical and horizontal facies TPs. Vertical facies TPs can be derived from sedimentary logs, outcrop panels, well-logs and core data, while the horizontal facies TPs can be determined from transects on geological maps (Elfeki and Dekking, 2001). Both are uni-dimensional and limited by their location and could be not entirely representative of the whole succession, and therefore cannot capture complex heterogeneity of the fluvial reservoir. The drawbacks of the coupled Markov chain models that use combined 1D vertical and horizontal chains (e.g. Elfeki and Dekking, 2001) and a need for 2D Markov models (e.g. used in remote sensing, Patil and Taillie, 2001) has been recognised. The latter, however, would be difficult to apply in reservoir modelling due to insufficient density of the well data for creating lateral facies distribution maps (Li and Zhang, 2008), but could be based on data from ancient and modern analogues.

Markov chain method has not yet been commonly incorporated in 3D reservoir modelling software. Only a few published examples of Markov chain modelling exist. Most of them use Markov chain models to simulate facies distributions in 2D cross sections (Elfekki and Dekking, 2001, 2005, 2007; Li, 2007), but an attempt to modify sequential indicator simulation (SIS) algorithm to account for facies TPs by incorporating Markov chain analysis has been carried out by Carle et al. (1998) and Weissmann et al. (1999) to create 3D facies model.

The fluvial architecture created by process-based / process-imitating models could perhaps be used to determine facies TPs for 2D and 1D Markov chain models either from several 2D cross sections similar to ones modelled in Chapter 12 or from 3D modelled strata if a 3D model is available. The outcrop panels and logs documented in this research could be also used for creation of 2D and 1D Markov chain models for the analogous reservoirs. The outcrop data would be a more reliable basis for this task than the numerical model output because the model only uses theoretical understanding of the depositional processes and includes many assumptions and simplifications.

The facies TPs calculated for the sedimentary logs of the Huesca and Salt Wash DFS successions (Chapter 10) do not consider same to same facies transitions and only record succession of different states or events. Vertical or horizontal facies TPs obtained using this method do not reflect lateral and vertical dimensions of the facies bodies, and therefore reservoir heterogeneity cannot be captured using these Markov chains. The faices TPs simply show how different facies units are organised and intercalate.

Markov chains of this type obtained from facies successions in outcrops or modelled strata could be used to predict vertical and lateral succession of facies objects during object-based simulation of facies distribution in a reservoir model. Whereas dimensions of facies objects can be defined by thickness and width probability distributions based on the data from outcrop analogues. The question that arises here again is how representative the modelled strata or outcrop analogues that are used as a basis for the Markov chain analysis of a particular reservoir (see also Section 13.2.1).

13.6.3 NTG ratio, reservoir connectivity and reservoir architecture

Reservoir connectivity and heterogeneity in channelized reservoirs has been found to influence fluid recovery the most (Larue and Freedman, 2005). The studies of heterogeneity of the DFS strata in this research (Chapter 11) have been done by means of documentation of 2D - 2.5D outcrops (chapters 4-7, 9) and 2D geometric modelling (Chapter 12). The results of Larue and Hovadik (2006) indicate that connectivity in 2D and 3D reservoirs are different and therefore 2D modelling and 2D outcrop analogues do not reflect complex sandstone body connectivity of the 3D reservoir. The same conclusion has been made in this study when 2D geometric model has been applied for modelling of the complex DFS strata (Chapter 12). It is therefore clear that a 3D model is required. However, some important conclusions concerning with sandstone body connectivity and NTG ratio can be inferred from the results of these numerical studies and are discussed below.

Sensitivity of NTG ratio to model input parameters

The geometrical 2D modelling exercise in this research concerns the sensitivity of the NTG ratio and sandstone body connectivity to the variation in input parameters of the model that represent proxies of depositional processes and external controlling factors (Chapter 12). The analysis has showed that strata characterised by the same NTG ratio could be formed in the results of wide range of combinations of input parameters and be characterised by contrasting architectures and different sandstone body connectivity (Fig. 12.23). This suggests that strata architecture does affect the sandstone body connectivity. Thus, NTG ratio should be used with caution when applied as an indicator of the reservoir architecture and sandstone body connectivity during well correlations (Section 13.3.4) and facies distribution simulations.

Larue and Hovadik (2006) found that reservoir architecture affects 2D and 3D reservoir connectivity in channelized reservoirs with NTG ratio lower than 60 % and 35 %, respectively, while the connectivity is not affected by reservoir architecture if NTG ratio is above these thresholds. In this study sandstone body connectivity in high-NTG strata (NTG > 75 %) have been found to be not affected by variation in input parameters of the model very much (Fig. 12.25), which confirms similar conclusion for 2D reservoirs of Larue and Hovadik (2006). In contrast, the sandstone body connectivity of low-NTG, highly heterogeneous strata was found to be primary affected by the deposits architecture (see also Larue and Freedman, 2006). To investigate the latter the sensitivity analysis has been carried out for the modelled DFS strata with a sandstone body proportion equal to 30 % (Monźon outcrop, Section 12.8). The main result of this modelling experiment is that the width (degree of lateral migration of channels) and thickness (channel erosion depth plus aggradation thickness) of the sandstone bodies, given constant floodplain aggradation, influences sandstone body connectivity the most. Unfortunately, these two parameters, especially width, are the most difficult to predict in the subsurface. The difficulty with thickness identification arises when individual sandstone bodies cannot be distinguished due to high degree of amalgamation (Fig. 13.1; Section 13.3.2). Thus, very careful estimations of ranges of sandstone body dimensions from subsurface data, outcrop analogues and process-imitating modelling is needed when low-NTG reservoir is concerned, and studies presented in this thesis could be used if applicable. Otherwise range of sandstone body widths could be used to produce many possible variants of reservoir architecture to consider the effect of this uncertainty.

Variations in NTG ratio in DFS deposits

The NTG ratio is one of the most uncertain parameter for the DFS reservoirs in particular because it changes laterally due to downstream variation in depositional processes (chapters 8 and 11) and sandstone body clustering in depositional lobes (Fig. 13.6, C, Chapter 11). The 2D geometric modelling of the relatively proximal, medial and distal successions of the Huesca and Salt Wash DFS deposits confirmed downstream trends in NTG ratio and sandstone body connectivity inferred from outcrop data (chapters 11-12; Fig. 13.9, A..). The 2D model, however, is not able to predict how fast NTG ratio changes from the proximal to distal part of the DFS. A 3D model and detailed apex to basin outcrop studies (e.g. Chapter 8) would be useful in resolving this problem. For example, downstream changes in architecture have been modelled using 3D process-based model by Krassenberg and Bridge (2008) (Fig. 13.9, C) where this information could be extracted and applied as trends for facies distribution during reservoir modelling.

The 2D geometrical modelling also showed that modelled strata characterised by a high degree of sandstone body clustering (imitated with combined compensational and random channel avulsion mechanisms and small migration distance parameter) have smaller NTG ratio and relatively higher connectivity than modelled strata with more regularly distributed sandstone bodies (larger migration distance). The lower NTG ratio and high connectivity in the former case have been determined to occur due to higher degree of channel-channel reworking and thick floodplain strata separating the channel clusters (Fig. 12.30, D). The higher NTG ratio and lower connectivity observed for the modelled strata with higher migration distance because channels are placed further from each other and separated by floodplain deposits. This clearly shows that the avulsion mechanism controlling resulting sandstone body clustering affects the reservoir properties (Section 12.3.2). The sensitivity of reservoir properties to channel clustering needs to be investigated further as avulsion mechanisms used in the process-imitating model could be applied as a definition for placement rules during object-based facies modelling.

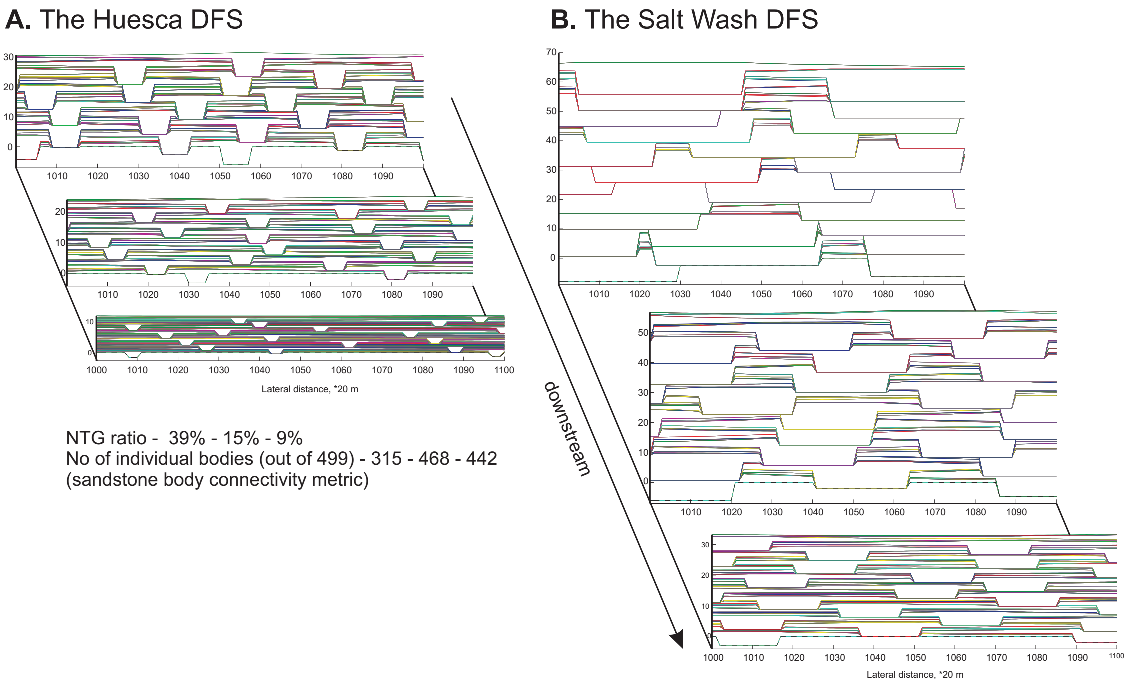

NTG ratio - 39% - 15% - 9%
No of individual bodies (out of 499) - 315 - 468 - 442
(sandstone body connectivity metric)

NTG ratio - 85% - 58% - 34%
No of individual bodies (out of 499) - 1 - 106 - 313
(sandstone body connectivity metric)

C. 3D model by Karssenberg and Bridge, 2008

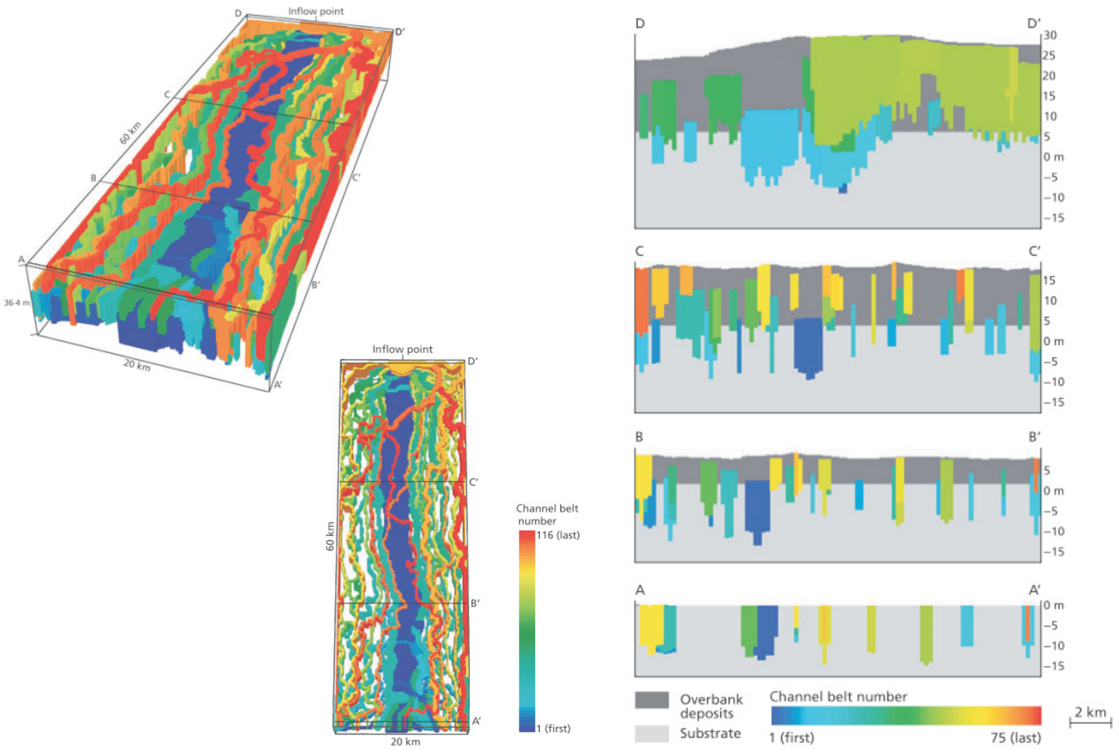

Figure 13.9. Downstream variations in architecture of DFS deposits from the apex to the distal areas modelled using 1) 2D geometric model created in this research based on the data from the Huesca (A) and Salt Wash (B) DFS successions and 2) 3D model created by Karssenberg and Bridge (2008) (C). Note that distal strata of the Huesca and Salt Wash DFSs could not be represented realistically with current configuration of the 2D geometric model (Chapter 12).

As lateral variations in DFS architecture and its characteristics appear to be significant, lateral trends reflecting this heterogeneity should be used to condition stochastic modelling of facies distribution in DFS reservoirs. These trends can be derived from the modelled strata that are characterised with the same reservoir properties as the reservoir it would be applied to. At the same time multiple architecture styles produced by the model with the same NTG ratio have to be considered. A 3D model would again have advantages over 2D models for this.

Sensitivity of sandstone body connectivity to rules of sandstone body distribution

The 2D modelling showed that NTG ratio and sandstone body connectivity are affected by the rules for sandstone body distribution within the model (avulsion mechanism, Section 12.9). Random distribution of sandstone bodies, where sandstone body location is not affected by the location of the previous sandstone body and floodplain topography, results in strata with higher sandstone body connectivity than the strata simulated with compensational channel avulsion, where each subsequent channel is diverted away from the previous channel locations into the minimum depression on the floodplain (Fig. 12.30 B-C and 12.33, A-B). Decrease in connectivity in the strata with compensational stacking of channel sandstone bodies has been also proposed by Larue and Hovadik (2006). Straub et al. (2009) discussed that in reality channels avulsions occur in somewhat intermediate way between pure compensational and random. Although sensitivity analysis has been undertaken for a few models with combined compensational and random avulsion rules (see previous section), it requires further study. In future, when avulsion rules for a particular outcrop or process-imitating model analogue are better understood, they might be applied as distribution rules for facies object when populating a reservoir model.

Compensation thickness scale and rules of sandstone body distribution

The work by Lyons (2004), Sheets et al. (2002), Straub et al. (2009) and Wang et al. (2011) introduced the ideas of “stratigraphic integral scale” or compensation scale that indicates “time needed for channels to visit every spot in the basin, averaging local autogenic effects and bringing the geometry of the long time scale depositional package into balance with the accommodation” (Straub et al., 2009). Wang et al. (2011) proposed that this scale could indicate the transition from fluvial architecture controlled by stochastic autogenic processes such as channel avulsion to fluvial architecture governed by allogenic factors such as sediment supply, water discharge and base level. Wang et al. (2011) emphasised that allogenic controls should not be used to explain variations in fluvial architecture below the compensation scale. If the compensation scale can be identified for an outcrop analogue of a fluvial reservoir, for example by using the method applied to outcrops of Ferris Formation by Wang et al. (2011) (also see discussion in Chapter 11), different rules for the distribution of facies objects could be applied at different architecture scales during reservoir modelling. These ideas are relatively new and future development is expected.

Applications of the 2D model

Although the 2D geometric rule-based model has its limitations (Section 12.11), its results are more easily applied to reservoir modelling than ones generated from process-based models because this model does not require knowledge of complex physical processes of sediment transport and deposition. The 2D model uses object-based geometric approach that is close to the object-based method of the reservoir modelling. Synthetic strata analogous to a reservoir can be created using data measured directly from the outcrop analogue and derived from subsurface data as input into the model. When a desirable match between characteristics of the modelled strata and the reservoir is obtained the architecture style resulting from the model and sandstone body distribution rules used in the model could be adopted for stochastic reservoir modelling using the methods discussed in this section. If conclusions about the best-fit modelled strata cannot be made due to uncertainties in the subsurface data, several variants of modelled strata corresponding to the reservoir characteristics need to be considered as possible representation of the reservoir architecture (Section 12.11.2).

13.6.4 Future of the process-based / process-imitating modelling in reservoir modelling

The process-based and process-imitating models are considered to be more realistic tools for predicting reservoir architecture than models generated using purely stochastic approaches. However, there are several issues to be solved before the process-based and process-imitating models can be used with confidence.

First of all our understanding of sediment transport and depositional processes is incomplete (Bridge, 2008); the process-based / process-imitating models contain many assumptions and simplifications. The models, therefore, do not represent fluvial processes accurately enough to produce realistic architectures. For instance, the 2D model created in this research is indeed very simplified and geological processes are imitated in the model using geometrical rules that do not reflect complexity of real depositional processes occurring on a DFS. For example, compensational avulsion mechanism used in all outcrop models might only partly reflect channel behaviour in real DFSs. In addition, the absence of terminal splay process in the model does not allow reconstructing distal DFS strata. Moreover, the 2D models do not reproduce complexity of DFS deposits in 3D space. For the discussion of model assumptions and limitations see Chapter 12.

Much more work has to be also done in the direction of incorporating more complex processes and more details into process-based models and creating coupled models at different temporal and spatial scales (Keogh et al., 2007; Bridge, 2008). This task requires a multidisciplinary effort from geomorphologists, hydrologists, geologists and computer scientists and ultimately is limited by computer power.

Kolterman and Gorelik (1996), Keogh et al. (2007) and Bridge (2008) also indicated that one of the main issues of process-based models is conditioning of the modelled strata to the hard subsurface data. When process-based model conditioning is possible the modelled strata can be flow-simulated and matched to the reservoir production data. Without this stage modelled strata could be only used in a similar way to outcrop analogues with the advantage of a third dimension, an ability to produce multiple realisations and conduct sensitivity analyses (Section 13.6). Example of the conditioning of process-based models to well data is provided by Karssenberg et al. (2001). However, Keogh et al. (2007) emphasises that at this stage process-based models have to be simplified to be conditioned to the well data and this reduces their ability to create realistic architectures.

Furthermore, the deterministic process-based models can produce complex architecture patterns that are indistinguishable from random (Burgess, 2006) and therefore are not very different from what can be produced using stochastic approaches. Such architecture patterns, therefore, can be predicted using statistical approaches without creating complex process-based models. In this case the advantage of the process-based models is the link they provide to familiar depositional processes and controlling factors which are commonly used and are easier to imagine and understand than complex statistical reasoning in stochastic simulations (e.g. variograms).

Thus, outcrop studies and process-based modelling has to be developed much more to better understand controls on the preserved architecture patterns, including those that are indistinguishable from random, before process-based models could substitute stochastic modelling (see also Keogh et al., 2007).

Lack of publically available programming codes for fluvial models and different formulations and programming languages used for those models, which are available, have necessitated the creation of a new model. This is time-consuming and in some respects a repetition of previous efforts. In addition, in every new model different assumptions and simplifications are introduced.

Construction of process-based models or the interpretation of the results of existing process-based models require advanced understanding of physics of geological processes and their mathematical description, as well as appropriate skills in computer programming. Each of the subjects is difficult on their own.

Before the process-based modelling can be used by any geologist for reservoir modelling, unified formulations of sediment transport and deposition process need to be developed and many more details and processes at different spatial and temporal scales need to be incorporated into the ultimate coupled fluvial process-based model. Some of these geological processes reflected in ancient fluvial deposits might not be known yet, e.g. combination of processes causing the architecture patterns that are indistinguishable from random. In addition, the modelling software that incorporates conditioning on the hard subsurface data would need to be developed.

Despite the limited implications of process-based modelling to reservoir modelling at this stage, it is still a useful tool that if formulated carefully and interpreted taking into account the limitations can provide important results that can be incorporated during reservoir modelling. Among them are: conclusion about non-uniqueness of controls on strata architecture and their reservoir characteristics (Chapter 12; see also Burgess and Allen, 1996; Burgess, 2006; Waltham et al., 2008; Prince and Burgess, 2013 in review), results of sensitivity analyses showing relative importance of different factors controlling fluvial architecture (Chapter 12 sections 12.8-10; see also Burgess and Allen, 1996) and conclusions about different architecture characteristics resulting from different styles of fluvial system behaviour at different time scales (Straub et al., 2009; Wang et al., 2011; Chapter 12). The ways in which these results can be applied in reservoir modelling have been discussed in this chapter.

13.7 Conclusions

The studies conducted within this thesis contribute to a wide range of objectives and stages of reservoir modelling. In this chapter the main implications and possible future implications of detailed facies analysis, architecture studies, quantitative outcrop studies, statistical analysis and process-imitating modelling of DFS deposits and fluvial deposits in general have been discussed. The importance of outcrop studies and process-based modelling specific for the DFS strata are emphasised. This is based on the observations of characteristic vertical and lateral variations in the architecture of highly heterogeneous DFS deposits. The discussion also highlights the main limitations of the collected data, the methods used and the interpretations, to make geologists and geomodellers aware of them when applying the data to reservoir architecture predictions.

The main conclusion that can be made from the discussion above is that to simulate realistic reservoir architecture and properties, integration of all possible data, methods and tools available for the industry geologists is required. Outcrop analogues are still considered the main source of realistic input data for reservoir modelling providing more information about preserved architecture than data obtained from studies of modern fluvial systems and process-based / process-imitating modelling, which implications are currently limited. Thus, more case studies are needed to improve the database of reservoir analogues of different types of fluvial systems especially DFS deposits that are most likely to be preserved as fluvial hydrocarbon reservoirs. The studies in this thesis contribute to this purpose. The process-based modelling is on the way to becoming a reservoir modelling tool. Although it is characterised by many limitations demonstrated in this thesis, it already could contribute to the predication of reservoir architecture.

14. Conclusions and recommendations for future research

This thesis contains various descriptive and quantitative studies of the deposits of the Huesca and Salt Wash distributive fluvial systems (DFS). The main conclusions from these studies are summarized below. Recommendations for future research are also suggested.

14.1. Summary of the main conclusions

- **The sandstone body classification has been created based on outcrop studies of both the Huesca and Salt Wash DFS successions** (chapters 4 and 5). Three sandstone body types have been distinguished: Type 1 - thick sandstone bodies with scoured base (W / T ratio < 15) formed by laterally stable channels, Type 2 - thick sheet-like sandstone bodies (W / T ratio > 15) formed in laterally unstable channels and Type 3 - thin sheet-like sandstone bodies (W / T ratio > 15) formed by poorly-confined and unconfined flows on the floodplain. A detailed description of sandstone body types, subtypes and their dimensions has been provided and the relationships between different sandstone body types and their amalgamation styles have been analysed. Channel avulsion is interpreted to be the main process responsible for the formation of sandstone bodies and their amalgamation complexes, and distribution of these across the DFS floodplain.

  The classification has been tested for documented DFS deposits formed in a number of different climatic settings. Additional outcrop studies of other DFS successions are needed to further test and expand the classifications.

- **Facies analysis and sandstone body classification have been used to quantify the main characteristics of and downstream trends in the deposits of the Huesca and Salt Wash DFSs** (chapters 6, 7 and 8). The downstream changes in the facies associations and sandstone body types and architecture are interpreted to be mainly controlled by decrease in a stream power downstream in a DFS caused by loss of energy of the flow due to entering an open basin from the confined feeder channel, distributive discharge and evaporation and infiltration of water on the way downstream. The following downstream variations in the DFS deposits have been recognised and are common for both studied successions:
  - Increase in the proportion of non-sandstone, fine-grained deposits;
  - Decrease in the degree of sandstone body amalgamation;
  - Decrease in Type 1 and Type 2 sandstone body dimensions;

  - Decrease in the sandstone grain size of Type 1 and Type 2 sandstone bodies;
  - Increase in the proportion of isolated sandstone bodies of subtypes 1/1, 1/2 and/or 2/3 in medial and distal outcrops over Type 2 and amalgamated sandstone bodies in relatively proximal outcrops;
  - Dominance of Type 3 sandstone bodies over other types in the distal outcrop;
  - Change in facies associations from proximal to distal successions: for example, lacustrine mudstones and limestones occur only in the distal outcrop of the Huesca DFS succession.

- **Evidence of avulsion events has been studied within the Huesca DFS succession** where both sandstone bodies and thick floodplain deposits are preserved and well exposed (Chapter 9). The heterolithic floodplain deposits of the Huesca DFS succession form a complex association of heterolithic lateral accretion complexes, channel scours filled with heterolithic deposits, packages of closely-spaced sheet-like sandstone bodies of Type 3, packages of interbedded siltstone and mudstone sheets, small-scale scours filled with sand and the “heterolithic upper part” of lateral accretion complexes. The deposits are interpreted to be mainly formed by lateral splays that may or may not be related to avulsion events.

  The detailed studies show that it is impossible to recognise whether overbank deposits are related to individual or multiple avulsion events, and whether splay deposits were formed in the result of successful or failed avulsion event. The presence of active and abandoned channels on the floodplain could have been also important during avulsion events; however evidence of re-occupation may not be preserved. Thus, channel sandstone bodies are most likely not related to underlying splay deposits, but splay deposits originated from the channel may be found laterally at the edge of the channel sandstone body.

  Both apparent stratigraphically transitional and abrupt avulsion successions (Jones and Hajek, 2007) have been observed in the Huesca DFS succession but are found to be formed by erosion of the deposits by subsequent channels rather than indicating a specific channel avulsion style. An application of avulsion successions proposed by Jones and Hajek (2007) could lead to incorrect conclusions about the avulsion styles and overall fluvial system characteristics, especially in outcrops with limited length and in successions with a high degree of sandstone body amalgamation where only a small portion of the floodplain deposits is preserved (e.g. relatively proximal Salt Wash DFS succession).

The studies of the floodplain deposits allowed interpretation of the Huesca DFS as a splay-prone fluvial system with high proportion of fine-grained material in the sediment load.

- **A new statistical method has been applied to assess the evidence of order in facies and thickness successions in the Huesca and Salt Wash DFS strata** (Chapter 10)**.** The method is based on the comparison between metrics calculated for observed successions and the same metrics calculated for synthetic ordered and disordered models (Burgess, in prep). This study has tested the applicability of this method to the DFS deposits.

  The high degree of order found in system-scale facies successions in the Huesca and Salt Wash DFS strata is not related to coarsening- or fining-upward cyclicity but is defined by the dominance of one or more facies within the DFS successions and therefore apparent. Fining-upward cycles commonly related to lateral accretion complexes have not been recognised by the quantitative methods applied in this study, although the lateral accretion element was observed. The dominance of facies at the system-scale was possibly controlled by long-term large-scale processes and factors such as ones which control preservation of floodplain deposits.

  The lower degree of order found in floodplain facies successions in the Huesca DFS strata is related to the presence of a more diverse facies set. Coarsening-upward cyclicity which is commonly associated with and qualitatively described for deposits formed by splay progradation during avulsion process has not been recognised by the quantitative methods applied in this study. The results possibly indicate that the deposition at this scale was influenced by more variable and complex local processes which do not produce patterns that could be recognised using the statistical methods employed here. The variability of facies distinguished in the heterolithic floodplain deposits of the Huesca DFS (Chapter 9) supports this conclusion.

  The thickness unit successions at both system and floodplain scales show no order and are indistinguishable from random. The thickness successions, therefore, could occur by chance or in a way that is too complex for resulting patterns to be recognised and interpreted using existing methods and knowledge.

The quantitative method of analysis of facies and thickness successions provides an opportunity to look at the strata and facies relationships quantitatively and in more detail. Application of the method to the DFS deposits demonstrate that interpretation of processes based on qualitative interpretations of facies trends and cycles in outcrops or subsurface (e.g. well logs) could lead to incorrect conclusions about depositional processes.

- **Both the Huesca and Salt Wash DFS deposits have been found to be highly heterogeneous.** Heterogeneities at pore, sedimentary structure, sandstone body and succession scales have been distinguished (Chapter 11).

  The pore scale heterogeneities are related to poor grain sorting and uneven matrix distribution in the DFS sandstones. The structure scale heterogeneities are caused by the variations in grain size within and between cross sets, by mudclast horizons and mud drapes along the lateral accretion surfaces; all formed due to changes in flow regime in DFS channels. The amalgamated sandstone bodies in the studied successions include heterogeneities related to intervals of heterolithic deposits preserved within them that could have been controlled by variation in flow regime in channel and by degree of sediment reworking through channel avulsions and lateral migration on a DFS. Succession-scale heterogeneities are determined by variations in sandstone body distribution and clustering vertically, laterally and downstream a DFS that could have been caused by internal organisation of a DFS (deposition in lobes, downstream decrease in water discharge) as well as external factors (accommodation space and sediment supply to water discharge ratio). The heterogeneities at all scales would affect quality and production behaviour of a DFS reservoir and should be considered.

  The relatively proximal and medial Salt Wash DFS deposits could form high-NTG reservoirs where all sandstone bodies are connected. In contrast, studied relatively proximal (almost medial) deposits of the Huesca DFS form low-NTG reservoir where sandstone bodies are connected into very tortuous “jig-saw” reservoir. Importantly for the DFS deposits the NTG ratio and sandstone body connectivity decrease from proximal to distal area. The difference in the degree of heterogeneity is most likely related to difference in the degree of floodplain deposit preservation which is in turn governed by difference in accommodation space available during development of each DFS and between proximal and distal areas within each DFS. The difference in the reservoir qualities of two studied successions exists at the sandstone body and succession scales while pore and structure scale heterogeneities are similar.

An important feature of the studied successions is the abundant Type 3 thin sheet-like sandstone bodies that connect major sandstone bodies and could improve the reservoir quality in cases where the overbank fine-grained sandstone bodies are considered a good reservoir, e.g. for gas reservoirs. The Type 3 sandstone bodies have not been included in the 2D geometric model presented in this thesis and this task could be a focus of the future modelling work.

- **A two-dimensional (2D) geometric model has been created to complement outcrop studies with the aim of providing a better understanding of the controls on the contrasting architecture of the Huesca and Salt Wash DFS deposits and sensitivity of the DFS deposit architecture and large-scale reservoir properties to external forcing factors** (Chapter 12). Despite limitations of the approach and obvious advantages of 3D modelling of DFS strata, the 2D geometric model is useful when used in comparison with outcrop data. Flexible input parameters and different algorithms of channel avulsion and floodplain aggradation have been implemented in the model so that their effects on important reservoir properties such as NTG ratio and sandstone body connectivity can be investigated.

  The model has been tested using input parameters measured in outcrops. The modelled strata showed similar NTG ratio and sandstone body connectivity to relatively proximal and medial Huesca and Salt Wash DFS strata. The main difference between architectures of the DFSs has been found to be mostly related to the difference in the degree of floodplain deposits reworking. Downstream variations in NTG ratio and sandstone body connectivity have been also discovered to be related to the decrease in the degree of reworking downstream the DFSs. These results support the theoretical interpretations of the outcrop observations from two DFSs and could be related to a lower accommodation for the Salt Wash DFS and variation in accommodation within each DFS from proximal to distal areas.

  Strata with particular reservoir characteristics, NTG ratio and sandstone body connectivity, can be modelled with a wide range of input parameters (proxies of external factors) and therefore controls on their architecture are not unique. Multiple combinations of control factors exist for a particular architecture unless observations help to narrow the range. If observations are limited many possible interpretations should be considered. Architecture and sandstone body connectivity of the strata with the same NTG ratio, however, could be different. The NTG ratio, therefore, should not be used solely when interpreting subsurface reservoir architecture. These results influence interpretation of possible controls on the deposit architecture and outcome of static reservoir modelling.

Sensitivity analysis shows that the architecture of modelled strata varies with the input parameters (proxies of external factors) in a predictable way and confirms the results of existing models. The NTG ratio and sandstone body connectivity decreases as floodplain aggradation increases and increases with increasing erosion and lateral reworking by channels. Among all input parameters, the reservoir qualities are mainly influenced by floodplain aggradation rate and lateral migration of the channel (sandstone body width). The latter, if high, could affect sensitivity of stratal architecture to the other controlling factors.

Different channel avulsion and floodplain algorithms also affect the modelled stratal architecture. Channel-channel reworking could be a key control on these variations. The modelled strata simulated with the compensational avulsion style are characterised by higher NTG ratio and lower sandstone body connectivity than the strata simulated with the random channel avulsion mechanism that supports previously suggested ideas (Larue and Hovadik, 2006). Intermediate channel behaviour possibly occurs on real DFSs that is characterised by deposition on lobes and this issue requires further investigation. Depth-dependent component in floodplain aggradation promotes annealing of floodplain topography and results in a higher probability of sandstone bodies being amalgamated and connected. Therefore channel avulsion and floodplain aggradation algorithms should be chosen carefully during numerical modelling.

Preliminary results of sensitivity studies of the compensational thickness scale to channel avulsion and floodplain algorithms have been also presented in the thesis (Chapter 12).

- **The studies conducted within this thesis contribute to a wide range of objectives and stages of reservoir modelling** (Chapter 13). Facies and sandstone body classifications, quantified downstream trends in DFS architecture as well as heterogeneity studies have direct implication to reservoir architecture characterisation where shape, dimensions and distribution of sandstone bodies have to be predicted from limited subsurface data. The outcrops studied in this thesis are reservoir analogues and provide ranges of facies object dimensions and a basis for “training images”, trend maps and Markov chain models used to constrain stochastic reservoir models. Geologists and geomodellers have to be aware of the limitations discussed in the thesis when applying outcrop data to reservoir architecture predictions. The results of the outcrop studies also highlight the need of specific studies of DFS reservoir analogues due to the characteristic lateral variations in the architecture of the DFS deposits.

The outcrop data are the main source of realistic information about reservoir architecture, in comparison with the limited application of studies of modern fluvial systems and process-based / process-imitating modelling. Thus, more case studies are needed to add to the database of reservoir analogues of different types of fluvial systems, especially DFSs, since they are likely to be preserved in the geological record (Weissmann et al., 2010). Studies in this thesis contribute to this database.

The process-based / process-imitating modelling is on the way to becoming a reservoir modelling tool and its limitations are demonstrated in this thesis, but it already could produce results that influence the way reservoir architecture is interpreted and predicted.

14.2. Recommendations for future research

- Outcrop and modern DFS examples formed in different climatic and tectonic settings are required for quantitative documentation and analysis to test and amplify facies and sandstone body classifications presented in this research and to add to the database of DFS reservoir analogues. Large-scale outcrops should be chosen for basin-scale architecture studies. In particular, it would be interesting to see studies where both outcrop and subsurface data (well-log, seismic or GPR data) are available and studied together.
- More specifically, tectonic events that occurred during the formation of the Salt Wash DFS are poorly understood and therefore their influence on the deposition cannot be determined. Correlation of basement structures with variations in thickness and sandstone body architecture across the Salt Wash DFS, synthesis of tectonic and volcanic events in the source area and provenance studies of Salt Wash sandstones could provide some answers to this problem.
- More studies are also required in the most proximal areas of Salt Wash DFS and deformed areas of the Huesca DFS. This would allow correlation of the most proximal successions with the relatively proximal, medial and distal successions studied in this research. More downstream transects could be

studied to investigate rate of downstream changes. The data can be then incorporated into the study presented here to provide complete facies and architectural model for the Huesca and Salt Wash DFSs.

- Detailed studies of the total and spectral gamma ray (GR) data collected from the Huesca and Salt Wash DFS deposits (Chapter 3) could not be conducted during the time frame of this project, but some results are included in the Appendix 7. The collected data demonstrated increase in mean values of total GR and concentrations of Potassium, Thorium and Uranium downstream the DFSs (appendices 7.9-10) with increase in proportion of fine-grained deposits. The difference in these values between different sandstone body types is noticeable but is not distinct enough to be used to differentiate sandstone body types (appendices 7.11-13). A higher resolution GR survey (more than 1 to 3 readings per bed) and focused statistical data analysis might be needed to provide a better link between subsurface GR logs and outcrop data.
- Targeted physical modelling and detailed process-based numerical modelling of lateral splays could help to understand splay deposit architecture and might help to solve questions about the scale of and difference between deposits formed by individual or multiple splay events and between splays that are or are not related to channel avulsion.
- Order analysis of facies and thickness successions conducted for the Huesca and Salt Wash DFS successions can be combined with the results of the 2D numerical modelling to investigate degree of regularity of sandstone body distribution observed in the modelled strata (Chapter 12, Section 12.11.6). The spatial statistics could also be used to determine a metric of the regularity, e.g. the clustering analyses has been used by Hajek et al. (2010) to investigate degree of clustering of sandstone bodies within Ferris Formation in Wyoming, USA.
- The studies of the compensation thickness scale conducted in this thesis on the modelled DFS strata have shown that the 2D geometric model behaves in the same way as was defined by Straub et al. (2009) and Wang et al. (2011). It would be interesting to calculate compensation scale from the outcrop panels of the Huesca and Salt Wash DFS deposits using the method applied by Wang et al. (2011) to outcrop panels of the Ferris Formation (Wyoming, USA). The results could probably be used to condition the interpretation of avulsion mechanisms in the model.

- Since the advantage of the 3D modelling of the DFS strata over 2D modelling is apparent, creation of a geometric 3D numerical model based on the previously created 2D model would be useful. The model would have to take into account specific process that occur on the DFS: single source, radial channel pattern, formation of three types of sandstone bodies, especially Type 3 terminal splay sandstone sheets in the distal area, and changes in substrate cohesiveness downstream. Ultimately modelled 3D strata can be flow simulated to investigate the effects of the 3D stratal architecture on reservoir production properties.
- At the moment the numerical modelling suffers from the lack of publically available computer codes. Although some models are available, they are written using different programming languages and apply different formulations of sedimentary processes. New models are generally created from scratch combining findings from various published studies. Furthermore the process-based modelling requires advanced knowledge of physical processes and their mathematical description as well as appropriate skills in computer programming. Therefore, 3D numerical modelling of DFS deposits would contribute from collaboration across disciplines such as geology, geomorphology, computer science, physics and mathematics.

Bibliography

Alexander, J., 1993, A discussion on the use of analogues for reservoir geology, Geological Society, London, Special Publications, vol. 69, no. 1, p. 175-194.

Allen, J. R. L., 1963, The classification of cross-stratified units with notes on their origin, Sedimentology, vol. 2, no. 2, p. 93-114.

Allen, J. R. L., 1970, A quantitative model of climbing ripples and their cross-laminated deposits, Sedimentology, vol. 14, no. 1-2, p. 5-26.

Allen, J. R. L., 1983(a), Studies in fluviatile sedimentation: Bars, bar-complexes and sandstone sheets (low-sinuosity braided streams) in the brownstones (L. Devonian), welsh borders, Sedimentary Geology, vol. 33, no. 4, p. 237-293.

Allen, J. R. L., December 1965, The sedimentation and palaeogeography of the Old Red Sandstone of Anglesey, North Wales, Proceedings of the Yorkshire Geological and Polytechnic Society, vol. 35, no. 2, p. 139-185.

Allen, J. R. L., 1979, Studies in fluviatile sedimentation: An elementary geometrical model for the connectedness of avulsion-related channel sand bodies, Sedimentary Geology, vol. 24, no. 3, p. 253-267.

Allen, P. A., L. Cabrera, F. Colombo, and A. Matter, 1983, Variations in fluvial style on the Eocene-Oligocene alluvial fan of the Scala Dei Group, SE Ebro Basin, Spain, Journal of the Geological Society, London, vol. 140, no. 1, p. 133-146.

Allen, P., 1982, Cyclicity of Devonian fluvial sedimentation, Cunningsburgh Peninsula, SE Shetland, Journal of the Geological Society, vol. 139, no. 1, p. 49-58.

Alonso-Zarza A. M. and others, 2002, Tertiary, *in* Gibbons, W. and Moreno, M. T. (eds), The Geology of Spain, The Geological Society, London.

Anderton, R., 1985, Clastic facies models and facies analysis, Geological Society, London, Special Publications, vol. 18, no. 1, p. 31-47.

Arenas, A. C., 1993, Sedimentología y paleogeografía del Terciario del margen pirenaico y sector central de la cuenca del Ebro (zona aragonesa occidental, Concepción Arenas Abad.

Arenas, C. and G. Pardo, 1999, Latest Oligocene-Late Miocene lacustrine systems of the north-central part of the Ebro Basin (Spain): sedimentary facies model and palaeogeographic synthesis, Palaeogeography, Palaeoclimatology, Palaeoecology, vol. 151, no. 1–3, p. 127-148.

Arenas, C., H. Millán, G. Pardo, and A. Pocoví, 2001, Ebro Basin continental sedimentation associated with late compressional Pyrenean tectonics (north-eastern Iberia): controls on basin margin fans and fluvial systems, Basin Research, vol. 13, no. 1, p. 65-89.

Arenas, C., J. Casanova, and G. Pardo, 1997, Stable-isotope characterization of the Miocene lacustrine systems of Los Monegros (Ebro Basin, Spain): palaeogeographic and palaeoclimatic implications, Palaeogeography, Palaeoclimatology, Palaeoecology, vol. 128, no. 1, p. 133-155.

Ashley, G. M., J. B. Southard, and J. C. Boothroyd, 1982, Deposition of climbing-ripple beds: a flume simulation, Sedimentology, vol. 29, no. 1, p. 67-79.

Aslan, A. and M. D. Blum, 1999; 2009, Contrasting Styles of Holocene Avulsion, Texas Gulf Coastal Plain, USA, *in* Smith, N. D. and J. Rogers (eds), Fluvial Sedimentology VI, Blackwell Publishing Ltd., p. 193-209.

Aslan, A. and W. J. Autin, 1999, Evolution of the Holocene Mississippi River floodplain, Ferriday, Louisiana; insights on the origin of fine-grained floodplains, Journal of Sedimentary Research, vol. 69, no. 4, p. 800-815.

Aslan, A., W. J. Autin, and M. D. Blum, 2005, Causes of river avulsion: Insights from the Late Holocene avulsion history of the Mississippi River, U.S.A. Journal of Sedimentary Research, vol. 75, no. 4, p. 650-664.

Assine, M. L., 2005, River avulsions on the Taquari megafan, Pantanal wetland, Brazil, Geomorphology, vol. 70, no. 3-4, p. 357-371.

Ayers Jr, W., 1986, Lacustrine and fluvial-deltaic depositional systems, Fort Union Formation (Paleocene), Powder River Basin, Wyoming and Montana, AAPG Bulletin, vol. 70, no. 11, p. 1651-1673.

Barthel, R., 1991, The effect of large-scale heterogeneities on the performance of waterdrive reservoirs, Conference paper, SPE Annual Technical Conference and Exhibition, 6-9 October 1991, Dallas, Texas.

Bertram, G., D. Emery, and K. Myers, 1996, Sequence stratigraphy, Wiley Online Library.

Best, J. L., P. J. Ashworth, C. S. Bristow, and J. Roden, 2003, Three-dimensional sedimentary architecture of a large, mid-channel sand braid bar, Jamuna River, Bangladesh, Journal of Sedimentary Research, vol. 73, no. 4, p. 516-530.

Bilodeau, W. L., 1986, The Mesozoic Mogollon Highlands, Arizona: An Early Cretaceous Rift Shoulder, The Journal of geology, vol. 94, no. 5, p. 724-735.

Blainey, J. B. and J. D. Pelletier, 2008, Infiltration on alluvial fans in arid environments: Influence of fan morphology, Journal of Geophysical Research, vol. 113, no. F3, p. F03008.

Bown, T. M. and M. J. Kraus, 1987, Integration of channel and floodplain suites: I. Developmental sequence and lateral relations of alluvial Paleosols, Journal of Sedimentary Research, vol. 57, no. 4, p. 587-601.

Brady, L. L., 1969, Stratigraphy and petrology of the Morrison Formation (Jurassic) of the Canon City, Colorado area, Journal of Sedimentary Research, vol. 39, no. 2, p. 632-648.

Bridge, J. S. and M. R. Leeder, 1979, A simulation model of alluvial stratigraphy, Sedimentology, vol. 26, no. 5, p. 617-644.

Bridge, J. S. and R. S. Tye, 2000, Interpreting the dimensions of ancient fluvial channel bars, channels, and channel belts from wireline-logs and cores, AAPG Bulletin, vol. 84, no. 8, p. 1205-1228.

Bridge, J. S. and S. D. Mackey, 1993; 2009, A revised alluvial stratigraphy model, *in* Marzo, M. and C. Puigdefabregas (eds), Alluvial sedimentation, IAS Special Publication 17, v. 66, Blackwell Publishing Ltd., p. 317-336.

Bridge, J. S. and S. D. Mackey, 1993(b); 2009, A theoretical study of fluvial sandstone body dimensions, *in* Bryant, I. D and S. S. Flint (eds), The geological modelling of hydrocarbon reservoirs and outcrop analogues, Blackwell Publishing Ltd., p. 213-236.

Bridge, J. S., 1984, Large-scale facies sequences in alluvial overbank environments, Journal of Sedimentary Research, vol. 54, no. 2, p. 583-588.

Bridge, J. S., 2003, Rivers and floodplains: forms, processes, and sedimentary record, Blackwell Pub.

Bridge, J., 2008, Numerical modelling of alluvial deposits: recent developments, *in* de Boer P., G. Postma, K. van der Zwan, P. Burgess, P. Kukla (eds), Analogue and numerical modelling of sedimentary systems: from understanding to prediction, IAS Special Publication, no. 40, p. 97-138.

Bristow C. S., R. L. Skelly and F. G. Ethridge, 1999, Crevasse splays from the rapidly aggrading, sand-bed, braided Niobrara River, Nebraska: effect of base-level rise, Sedimentology, vol. 46, no. 6, p. 1029-1047.

Bryant, M., P. Falk, and C. Paola, 1995, Experimental study of avulsion frequency and rate of deposition, Geology, vol. 23, no. 4, p. 365-368.

Buehler, H. A., G. S. Weissmann, L. A. Scuderi, and A. J. Hartley, 2011, Spatial and Temporal Evolution of an Avulsion on the Taquari River Distributive Fluvial System from Satellite Image Analysis, Journal of Sedimentary Research, vol. 81, no. 8, p. 630-640.

Burgess, P. M. and P. A. Allen, 1996, A forward-modelling analysis of the controls on sequence stratigraphical geometries, Geological Society, London, Special Publications, vol. 103, no. 1, p. 9-24.

Burgess, P. M., 2006, The signal and the noise: forward modelling of allocyclic and autocyclic processes influencing peritidal carbonate stacking patterns, Journal of Sedimentary Research, vol. 76, no. 7, p. 962-977.

Busby-Spera, C. J., 1988, Speculative tectonic model for the early Mesozoic arc of the southwest Cordilleran United States, Geology, vol. 16, no. 12, p. 1121-1125.

Cable, A. and M. Burke, 2011, investigation of permeability anomalies, Abstract, International symposium of the society of core analysis, Austin, Texas, USA.

Cabrera, L., M. Cabrera, R. Gorchs, and F. X. C. de las Heras, 2002, Lacustrine basin dynamics and organosulphur compound origin in a carbonate-rich lacustrine system (Late Oligocene Mequinenza Formation, SE Ebro Basin, NE Spain), Sedimentary Geology, vol. 148, no. 1–2, p. 289-317.

Cadigan, R. A., 1967, Petrology of the Morrison Formation in the Colorado Plateau region, USGS report, US Government Printing Office.

Caers, J. and T. Zhang, 2004, Multiple-point geostatistics: a quantitative vehicle for integrating geologic analogs into multiple reservoir models, *in* Grammer, G. M., P. M. Harris, and G. P. Eberli (eds), Integration of outcrop and modern analogues in reservoir modelling: AAPG Memoir 80, p. 383-394.

Caers, J., S. Srinivasan, and A. Journel, 1999, Geostatistical quantification of geological information for a fluvial-type North Sea reservoir, SPE Annual Technical Conference and Exhibition, 3-6 October 1999, Houston, Texas.

Cain, S. A. and N. P. Mountney, 2009, Spatial and temporal evolution of a terminal fluvial fan system: the Permian Organ Rock Formation, South-east Utah, USA, Sedimentology, vol. 56, no. 6, p. 1774-1800.

Cain, S. and N. Mountney, 2011, Downstream changes and associated fluvial–eolian interactions in an ancient terminal fluvial fan system: the Permian Organ Rock Formation, SE Utah, *in* Davidson S.K., S. Leleu and C. P. North (eds), From river to rock record: The preservation of fluvial sediments and their subsequent interpretation, p. 167-185.

Cant, D. J. and R. G. Walker, 1976, Development of a braided-fluvial facies model for the Devonian Battery Point Sandstone, Quebec, Canadian Journal of Earth Sciences, vol. 13, no. 1, p. 102-119.

Carle, S. F., E. M. Labolle, G. S. Weissmann, D. Van Brocklin, and G. E. Fogg, 1998, Conditional simulation of hydrofacies architecture: a transition probability / Markov approach, hydrogeologic models of sedimentary aquifers, concepts in hydrogeology and environmental geology, vol. 1, p. 147-170.

Carroll, A. R. and K. M. Bohacs, February, 1999, Stratigraphic classification of ancient lakes: Balancing tectonic and climatic controls, Geology, vol. 27, no. 2, p. 99-102.

Carter, D. C., 2003, 3D seismic geomorphology: Insights into fluvial reservoir deposition and performance, Widuri field, Java Sea, AAPG Bulletin, vol. 87, no. 6, p. 909-934.

Castro and others, 2002, Paleozoic Magmatism, *in* Gibbons, W. and Moreno, M.T. (eds), The Geology of Spain, The Geological Society, London.

Chakraborty, T., R. Kar, P. Ghosh, and S. Basu, 2010, Kosi megafan: Historical records, geomorphology and the recent avulsion of the Kosi River, Quaternary International, vol. 227, no. 2, p. 143-160.

Clevis, Q., P. de Boer, and M. Wachter, 2003, Numerical modelling of drainage basin evolution and three-dimensional alluvial fan stratigraphy, Sedimentary Geology, vol. 163, no. 1-2, p. 85-110.

Clevis, Q., P. L. D. Boer, and W. Nijman, 2004, Differentiating the effect of episodic tectonism and eustatic sea-level fluctuations in foreland basins filled by alluvial fans and axial deltaic systems: insights from a three-dimensional stratigraphic forward model, Sedimentology, vol. 51, no. 4, p. 809-835.

Cloyd, K. C., R. V. Demicco, and R. J. Spencer, 1990, Tidal channel, levee, and crevasse-splay deposits from a Cambrian tidal channel system; a new mechanism to produce shallowing-upward sequences, Journal of Sedimentary Research, vol. 60, no. 1, p. 73-83.

Coleman, J. M., 1969, Brahmaputra river: Channel processes and sedimentation, Sedimentary Geology, vol. 3, no. 2-3, p. 129-239.

Collinson, J. D., 1970, Bedforms of the Tana river, Norway, Geografiska Annaler Series A Physical Geography, p. 31-56.

Collinson, J., 1996, Alluvial sediments, Sedimentary environments: processes, facies and stratigraphy, vol. 3, p. 37-82.

Colmenero and others, 2002, Carboniferous, *in* Gibbons, W. and Moreno, M.T. (eds), The Geology of Spain, The Geological Society, London.

Colombera, L., F. Felletti, N. P. Mountney, and W. D. McCaffrey, 2012, A database approach for constraining stochastic simulations of the sedimentary heterogeneity of fluvial reservoirs, AAPG Bulletin, vol. 96, no. 11, p. 2143-2166.

Colombera, L., N. P. Mountney, and W. D. McCaffrey, 2012, A relational database for the digitization of fluvial architecture: concepts and example applications, Petroleum Geoscience, vol. 18, no. 1, p. 129-140.

Coney, P. J., J. A. Muñoz, K. R. McClay, and C. A. Evenchick, 1996, Syntectonic burial and post-tectonic exhumation of the southern Pyrenees foreland fold–thrust belt, Journal of the Geological Society, vol. 153, no. 1, p. 9-16.

Constantine, J. A. and T. Dunne, January, 2008, Meander cut-off and the controls on the production of oxbow lakes, Geology, vol. 36, no. 1, p. 23-26.

Craig, L. C., C. N. Holmes, R. A. Cadigan, V. L. Freeman, T. E. Mullens and G. W. Weir, 1955, Stratigraphy of the Morrison and related formations, Colorado Plateau region, a preliminary report. USGS Bulletin, 1009-E: 125-168.

Crowley, K. D., 1983, Large-scale bed configurations (macroforms), Platte River Basin, Colorado and Nebraska: Primary structures and formative processes, GSA Bulletin, vol. 94, no. 1, p. 117-133.

Currie, B. S., 1997, Sequence stratigraphy of non-marine Jurassic–Cretaceous rocks, central Cordilleran foreland-basin system, GSA Bulletin, vol. 109, no. 9, p. 1206-1222.

Dalman, R. A. F. and G. J. Weltje, 2008, Sub-grid parameterisation of fluvio-deltaic processes and architecture in a basin-scale stratigraphic model, Computers and Geosciences, vol. 34, no. 10, p. 1370-1380.

Davidson, S. K. and C. P. North, 2009, Geomorphological Regional Curves for Prediction of Drainage Area and Screening Modern Analogues for Rivers in the Rock Record, Journal of Sedimentary Research, vol. 79, no. 10, p. 773-792.

Davidson, S. K., A. J. Hartley, G. S. Weissmann, G. J. Nichols, and L. A. Scuderi, 2013, Geomorphic elements on modern distributive fluvial systems, Geomorphology, vol. 180–181, no. 0, p. 82-95.

Davis, J. M., R. C. Lohmann, F. M. Phillips, J. L. Wilson, and D. W. Love, 1993, Architecture of the Sierra Ladrones Formation, central New Mexico: Depositional controls on the permeability correlation structure, GSA Bulletin, vol. 105, no. 8, p. 998-1007.

Davis, J. C., 1986, 2002, Statistics and Data Analysis in Geology: New York, John Wiley and Sons.

Demko, T. M., B. S. Currie, and K. A. Nicoll, 2004, Regional palaeoclimatic and stratigraphic implications of paleosols and fluvial/overbank architecture in the Morrison Formation (Upper Jurassic), Western Interior, USA, Sedimentary Geology, vol. 167, no. 3-4, p. 115-135.

Deutsch, C. V. and T. T. Tran, 2002, FLUVSIM: a program for object-based stochastic modelling of fluvial depositional systems, Computers and Geosciences, vol. 28, no. 4, p. 525-535.

Dickinson, W. R., 2001, Tectonic setting of the Great Basin through geologic time: implications for metallogeny, Regional tectonics and structural control of ore: the major gold trends of northern Nevada: Geological Society of Nevada, Special Publication, vol. 33, p. 27-53.

Dickinson, W. R., 2006, Geotectonic evolution of the Great Basin, Geosphere, vol. 2, no. 7, p. 353-368.

Donselaar, M. E. and I. Overeem, 2008, Connectivity of fluvial point-bar deposits: An example from the Miocene Huesca fluvial fan, Ebro Basin, Spain, AAPG Bulletin, vol. 92, no. 9, p. 1109-1129.

Donselaar, M. E. and J. M. Schmidt, 2005, Integration of outcrop and borehole image logs for high-resolution facies interpretation: example from a fluvial fan in the Ebro Basin, Spain, Sedimentology, vol. 52, no. 5, p. 1021-1042.

Donselaar, M., C. Gozalo, and S. Moyano, 2012, Avulsion processes at the terminus of low-gradient semi-arid fluvial systems: Lessons from the Río Colorado, Altiplano endorheic basin, Bolivia, Sedimentary Geology, vol. 283, no.1, p. 1-14.

Dromgoole, P. and R. Speers, 1997, Geoscore: a method for quantifying uncertainty in field reserve estimates, Petroleum Geoscience, vol. 3, no. 1, p. 1-12.

Dubiel, R. F., 1994, Triassic deposystems, paleogeography, and paleoclimate of the Western Interior, Mesozoic systems of the Rocky Mountain region, USA, p. 133-168.

Dunham, R. J., 1962, Classification of carbonate rocks according to depositional texture, *in* M1: Classification of carbonate rocks – a symposium, p. 108-121.

Ekart, D. D., T. E. Cerling, I. P. Montanez, and N. J. Tabor, 1999, A 400 million year carbon isotope record of pedogenic carbonate: implications for paleoatmospheric carbon dioxide, American Journal of Science, vol. 299, no. 10, p. 805-827.

Elfeki, A. and M. Dekking, 2001, A Markov chain model for subsurface characterization: theory and applications, Mathematical Geology, vol. 33, no. 5, p. 569-589.

Elfeki, A. M. M. and F. M. Dekking, 2005, Modelling subsurface heterogeneity by coupled markov chains: directional dependency, Walther's law and entropy, Geotechnical and Geological Engineering, vol. 23, no. 6, p. 721-756.

Elfeki, A. M. and F. M. Dekking, 2007, Reducing geological uncertainty by conditioning on boreholes: the coupled Markov chain approach, Hydrogeology Journal, vol. 15, no. 8, p. 1439-1455.

Evans, G. and A. Arche, 2002, The flux of siliciclastic sediment from the Iberian Peninsula, with particular reference to the Ebro, Geological Society, London, Special Publications, vol. 191, no. 1, p. 199-208.

Farshori, M., 1989, Fluvial facies and reservoir heterogeneity, Cutbank Sandstone (Lower Cretaceous), Horsefly Lake Pool, Southern Alberta, Core Conference: Geology and Reservoir Heterogeneity.

Field, J., 2001, Channel avulsion on alluvial fans in southern Arizona, Geomorphology, vol. 37, no. 1-2, p. 93-104.

Fielding, C. R. and R. C. Crane, 1987, An application of statistical modelling to the prediction of hydrocarbon recovery factors in fluvial reservoir sequences, *in* Ethridge, F. G., Flores, R. M., and Harvey M. D. (eds) Recent Developments in Fluvial Sedimentology: SEPM, Special Publication 39.

Fielding, C. R., P. J. Ashworth, J. L. Best, E. W. Prokocki, and G. H. S. Smith, 2012, Tributary, distributary and other fluvial patterns: What really represents the norm in the continental rock record? Sedimentary Geology, vol. 261–262, no. 0, p. 15-32.

Fisher J. A. and G. J. Nichols, 2012, Interpreting the stratigraphic architecture of fluvial systems in internally drained basins, Journal of the Geological Society, London, v. 20, p. 1-9.

Fisher, J. A., C. B. E. Krapf, S. C. Lang, G. J. Nichols, and T. H. D. Payenberg, 2008, Sedimentology and architecture of the Douglas Creek terminal splay, Lake Eyre, central Australia, Sedimentology, vol. 55, no. 6, p. 1915-1930.

Fisher, J. A., G. J. Nichols, and D. A. Waltham, 2007(a), Unconfined flow deposits in distal sectors of fluvial distributary systems: Examples from the Miocene Luna and Huesca Systems, northern Spain, Sedimentary Geology, vol. 195, no. 1-2, p. 55-73.

Fisher, J. A., D. Waltham, G. J. Nichols, C. B. E. Krapf and S. C. Lang, 2007(b), A quantitative model for deposition of thin fluvial sand sheets, Journal of the Geological Society, London, vol. 164, no. 1, p. 67-71.

Folk, R. L. and W. C. Ward, 1957, Brazos River bar (Texas): a study in the significance of grain size parameters, Journal of Sedimentary Research, vol. 27, no. 1, p. 3-26.

Folk, R. L., 1980, Petrology of sedimentary rocks, Hemphill Pub. Co.

Friend, P. F., 1983; 2009, Towards the field classification of alluvial architecture or sequence, *in* Collinson J. D. and J. Lewin (eds), Modern and ancient fluvial systems, Blackwell Publishing Ltd., p. 345-354.

Friend, P. F., M. J. Slater, and R. C. Williams, 1979, Vertical and lateral building of river sandstone bodies, Ebro Basin, Spain, Journal of the Geological Society, London, vol. 136, no. 1, p. 39-46.

Friend, P., 1977, Distinctive features of some ancient river systems, Fluvial Sedimentology AAPG Memoir 5, p. 531-542.

Frostick, L., I., J. Jarvis, and H. Eardley, 1988, Triassic sediments of the Inner Moray Firth, Scotland: early rift deposits, Journal of the Geological Society, London, vol. 145, no. 2, p. 235-248.

Gaither, A., 1953, A study of porosity and grain relationships in experimental sands, Journal of Sedimentary Research, vol. 23, no. 3, p. 180-195.

Garcia-Alcalde and others, 2002, Devonian, *in* Gibbons, W. and Moreno, M. T. (eds), The Geology of Spain, The Geological Society, London.

Garcia-Castellanos, D., J. Vergés, J. Gaspar-Escribano, and S. Cloetingh, 2003, Interplay between tectonics, climate, and fluvial transport during the Cenozoic evolution of the Ebro Basin (NE Iberia), J.Geophys.Res., vol. 108, p. 2347.

Geehan, G., T. Lawton, S. Sakurai, H. Klob, T. Clifton, K. Inman, and K. Nitzberg, 1986, Geologic prediction of shale continuity, Prudhoe Bay field; *in* Lake, L. W. and H. B. Jr. Carraoll (eds) Reservoir characterization, Academic Press, London, p. 63-82.

Ghosh, P., S. Sarkar, and P. Maulik, 2006, Sedimentology of a muddy alluvial deposit: Triassic Denwa Formation, India, Sedimentary Geology, vol. 191, no. 1, p. 3-36

Gibbons, W. and M. T. Moreno, 2002, The geology of Spain, Geological Society London.

Gibling, M. R., 2006, Width and Thickness of Fluvial Channel Bodies and Valley Fills in the Geological Record: A Literature Compilation and Classification, Journal of Sedimentary Research, vol. 76, no. 5, p. 731-770.

Gohain, K. and Parkash, B., 1982. Channel pattern changes in the Kosi river, North Bihar (India) and Nepal. II-th International Sedimentological Congress, Abstract volume, p. 32.

Gomez, B., L. A. K. Mertes, J. D. Phillips, F. J. Magilligan, and L. A. James, November, 1995, Sediment characteristics of an extreme flood: 1993 upper Mississippi River valley, Geology, vol. 23, no. 11, p. 963-966.

González-Bonorino, G., F. Colombo, and L. Abascal, 2010, Architecture of an Oligocene fluvial ribbon sandstone in the Ebro Basin, North-eastern Spain, Sedimentology, vol. 57, no. 3, p. 845-856.

Good, S. C., 2004, Paleoenvironmental and paleoclimatic significance of freshwater bivalves in the Upper Jurassic Morrison Formation, Western Interior, USA, Sedimentary Geology; Reconstruction of the Extinct Ecosystem of the Upper Jurassic Morrison Formation, vol. 167, no. 3, p. 163-176.

Gradstein, F. M., J. G. Ogg, and A. G. Smith, 2005, A geologic time scale 2004, Cambridge University Press.

Gutierrez-Marco and others, 2002, Ordovician, *in* Gibbons, W. and Moreno, M. T. (eds), The Geology of Spain, The Geological Society, London.

Hajek, E. A. and M. A. Wolinsky, 2012, Simplified process modelling of river avulsion and alluvial architecture: Connecting models and field data, Sedimentary Geology, vol. 257–260, no. 0, p. 1-30.

Hajek, E. A., P. L. Heller, and B. A. Sheets, 2010, Significance of channel-belt clustering in alluvial basins, Geology, vol. 38, no. 6, p. 535-538.

Hamer, J. M. M., 2007, Interpreting ancient continental environments: a palaeopedological and ichnological approach, Unpublished PhD thesis, Royal Holloway, University of London.

Hamer, J. M. M., N. D. Sheldon, G. J. Nichols, and M. E. Collinson, 2007(a), Late Oligocene-Early Miocene paleosols of distal fluvial systems, Ebro Basin, Spain, Palaeogeography, Palaeoclimatology, Palaeoecology, vol. 247, no. 3-4, p. 220-235.

Hamer, J. M. M., N. D. Sheldon, and G. J. Nichols, 2007(b), Global aridity during the Early Miocene? A terrestrial paleoclimate record from the Ebro Basin, Spain, The Journal of Geology, vol. 115, no. 5, p. 601-608.

Hampson, G. J., W. Davies, S. J. Davies, J. A. Howell, and K. R. Adamson, 2005, Use of spectral gamma-ray data to refine subsurface fluvial stratigraphy: late Cretaceous strata in the Book Cliffs, Utah, USA, Journal of the Geological Society, London, vol. 162, no. 4, p. 603-621.

Harms, J. C., D. B. Mackenzie, and D. G. McCubbin, 1963, Stratification in modern sands of the Red River, Louisiana, The Journal of geology, p. 566-580.

Hartley, A. J., G. S. Weissmann, G. J. Nichols, and G. L. Warwick, 2010(a), Large distributive fluvial systems: characteristics, distribution, and controls on development, Journal of Sedimentary Research, vol. 80, no. 2, p. 167-183.

Hartley, A. J., G. S. Weissmann, G. J. Nichols, and L. A. Scuderi, 2010(b), Fluvial form in modern continental sedimentary basins: Distributive fluvial systems: REPLY, Geology, vol. 38, no. 12, p. e231-e231.

Hasiotis, S., F. Peterson, T. Demko, and C. Turner, 1997, Giant termite (Insecta: Isoptera) nests from the base of the Upper Jurassic Morrison Formation, north-western New Mexico, GSA Abstracts with Program, v. 28, p, A461.

Heller, P. L., C. L. Angevine, N. S. Winslow, and C. Paola, 1988, Two-phase stratigraphic model of foreland-basin sequences, Geology, vol. 16, no. 6, p. 501-504.

Hickey, L., 1980, Paleocene stratigraphy and flora of the Clark's Fork Basin, Early Cenozoic palaeontology and stratigraphy of the Bighorn basin, Wyoming: University of Michigan Papers on Palaeontology, vol. 24, p. 33-49.

Hirst, J. and G. Nichols, 1986, Thrust tectonic controls on Miocene alluvial distribution patterns, southern Pyrenees, *in* Allen P. A. and P. Homewood (eds), Foreland Basins, IAS Special Publications 8, p. 247-258.

Hirst, P. J., 1983, Oligo-Miocene alluvial systems in the Northern Ebro Basin, Huesca Province, Spain, Unpublished PhD thesis, University of Cambridge.

Hirst, P. J., 1991, Variations in alluvial architecture across the Oligo-Miocene Huesca fluvial system, Ebro Basin, Spain; The three-dimensional facies architecture of terrigenous clastic sediments and its implications for hydrocarbon discovery and recovery: SEPM Concepts in Sedimentology and Palaeontology, vol. 3, p. 111-121.

Holbrook, J., R. W. Scott, and F. E. Oboh-Ikuenobe, 2006, Base-level buffers and buttresses: a model for upstream versus downstream control on fluvial geometry and architecture within sequences, Journal of Sedimentary Research, vol. 76, no. 1, p. 162-174.

Holden, L., R. Hauge, Ã. Skare, and A. Skorstad, 1998, Modelling of fluvial reservoirs with object models, Mathematical Geology, vol. 30, no. 5, p. 473-496.

Horton, B. K. and P. G. DeCelles, 2001, Modern and ancient fluvial megafans in the foreland basin system of the central Andes, southern Bolivia: implications for drainage network evolution in fold-thrust belts, Basin Research, vol. 13, no. 1, p. 43-63.

Hunter, R. E., 1977, Terminology of cross-stratified sedimentary layers and climbing-ripple structures, Journal of Sedimentary Research, vol. 47, no. 2, p. 697-706.

Hunter, R. E., 1985, A kinematic model for the structure of lee-side deposits, Sedimentology, vol. 32, no. 3, p. 409-422.

Ingersoll, R. V., T. F. Fullard, R. L. Ford, J. P. Grimm, J. D. Pickle, and S. W. Sares, 1984, The effect of grain size on detrital modes; a test of the Gazzi-Dickinson point-counting method, Journal of Sedimentary Research, vol. 54, no. 1, p. 103-116.

Mapa geológico Peninsular Ibérica, Baleares y Canarias, Insituto Technlógico Geominero de España, 1994.

Jackson, M. and A. Muggeridge, 2000, Effect of discontinuous shales on reservoir performance during horizontal water flooding, SPE Journal, vol. 5, no. 4, p. 446-455.

Jerolmack, D. J. and C. Paola, 2007, Complexity in a cellular model of river avulsion, Geomorphology, vol. 91, no. 3-4, p. 259-270.

Jiao, Y., Jiaxin, L. Sitian, Y. Ruiqi, L. Fengjiang, and Y. Shengke, 2005, Architectural units and heterogeneity of channel reservoirs in the Karamay Formation, outcrop area of Karamay oil field, Junggar basin, northwest China, AAPG Bulletin, vol. 89, no. 4, p. 529-545.

Johnson, E. A. and F. W. Pierce, 1990, Variations in fluvial deposition on an alluvial plain: an example from the Tongue River Member of the Fort Union Formation (Paleocene), south-eastern Powder River Basin, Wyoming, USA, Sedimentary Geology, vol. 69, no. 1, p. 21-36.

Johnson, S. Y., 1984, Cyclic fluvial sedimentation in a rapidly subsiding basin, northwest Washington, Sedimentary Geology, vol. 38, no. 1-4, p. 361-391.

Jones, H. L. and E. A. Hajek, 2007, Characterizing avulsion stratigraphy in ancient alluvial deposits, Sedimentary Geology, vol. 202, no. 1-2, p. 124-137.

Jones, J. A. and A. J. Hartley, 1993, Reservoir characteristics of a braid-plain depositional system: the Upper Carboniferous Pennant Sandstone of South Wales, Geological Society, London, Special Publications, vol. 73, no. 1, p. 143-156.

Jones, L. S. and S. A. Schumm, 1999; 2009, Causes of avulsion: an overview, *in* N. D. Smith and J. Rogers (eds) Fluvial sedimentology VI: IAS Special Publication 28, John Wiley and Sons, p. 169-178.

Jupp, P., B. Spurr, G. Nichols, and J. P. P. Hirst, 1987, Statistical estimation of the apex of a sediment distribution system from paleocurrent data, Mathematical Geology, vol. 19, no. 4, p. 319-333.

Karssenberg, D. and J. S. Bridge, 2008, A three-dimensional numerical model of sediment transport, erosion and deposition within a network of channel belts, floodplain and hill slope: extrinsic and intrinsic controls on floodplain dynamics and alluvial architecture, Sedimentology, vol. 55, no. 6, p. 1717-1745.

Karssenberg, D., J. Bridge, E. Stouthamer, M. Kleinhans, and H. Berendsen, 2003, Modelling cycles of fluvial aggradation and degradation using a process-based alluvial stratigraphy model, Numerical and Physical Modelling of Sedimentary Systems, from Understanding to Prediction, *in* de Boer P., G. Postma, P. Kukla, C. J. Van der Zwan, P. M. Burgess, I. Ritsema and F. Van Den Belt (eds), Numerical and Physical Modelling of Sedimentary Systems, from Understanding to Prediction, Utrecht, the Netherlands.

Karssenberg, D., T. E. Törnqvist, and J. S. Bridge, 2001, Conditioning a process-based model of sedimentary architecture to well data, Journal of Sedimentary Research, vol. 71, no. 6, p. 868-879.

Kasse, C., J. Vandenberghe, J. Van Huissteden, S. Bohncke, and J. Bos, 2003, Sensitivity of Weichselian fluvial systems to climate change (Nochten mine, eastern Germany), Quaternary science reviews, vol. 22, no. 20, p. 2141-2156.

Keller, W. D., 1953, Clay minerals in the type section of the Morrison Formation, Journal of Sedimentary Research, vol. 23, no. 2, p. 93-105.

Kelly, S. B. and H. Olsen, 1993, Terminal fans - a review with reference to Devonian examples, Sedimentary Geology, vol. 85, no. 1-4, p. 339-374.

Keogh, K. J., A. W. Martinius, and R. Osland, 2007, The development of fluvial stochastic modelling in the Norwegian oil industry: A historical review, subsurface implementation and future directions, Sedimentary Geology, vol. 202, no. 1-2, p. 249-268.

King, P., 1990, The connectivity and conductivity of overlapping sand bodies, *in* Buller, A.J. et al. (eds) North Sea Oil and Gas Reservoirs II. Graham and Trotman, London, p. 353-362

Kjemperud, A. V., E. R. Schomacker, and T. A. Cross, 2008, Architecture and stratigraphy of alluvial deposits, Morrison Formation (Upper Jurassic), Utah, AAPG Bulletin, vol. 92, no. 8, p. 1055-1076.

Kleinhans, M., 2004, Sorting in grain flows at the lee side of dunes, Earth-Science Reviews, vol. 65, no. 1, p. 75-102.

Knighton, D. A. and G. C. Nanson, 1993, Anastomosis and the continuum of channel pattern, Earth Surface Processes and Landforms, vol. 18, no. 7, p. 613-625.

Koltermann, C. E. and S. M. Gorelick, 1996, Heterogeneity in sedimentary deposits: A review of structure-imitating, process-imitating, and descriptive approaches, Water Resources Research, vol. 32, no. 9, p. 2617-2658.

Kowallis, B. J., E. H. Christiansen, and A. L. Deino, 1991, Age of the Brushy Basin Member of the Morrison Formation, Colorado Plateau, western USA, Cretaceous Research, vol. 12, no. 5, p. 483-493.

Kowallis, B., E. Christiansen, D. Tingey, A. Deino, F. Peterson, and C. Turner, 1993, Volcanic ash layers in the Tidwell Member of the Upper Jurassic Morrison Formation: Minimum age of the J-5 unconformity on the Colorado Plateau, , vol. 25, no. 6, p. 472-473.

Kraus, M. J. and A. Aslan, 1993, Eocene hydromorphic Paleosols; significance for interpreting ancient floodplain processes, Journal of Sedimentary Research, vol. 63, no. 3, p. 453-463.

Kraus, M. J. and T. M. Wells, 1999; 2009, Recognizing avulsion deposits in the ancient stratigraphical record, *in* Smith N. D. and J. Rogers (eds) Fluvial Sedimentology VI: IAS Special Publication 28, John Wiley and Sons, p. 251-268.

Kraus, M. J., 1996, Avulsion deposits in lower Eocene alluvial rocks, Bighorn Basin, Wyoming, Journal of Sedimentary Research, vol. 66, no. 2, p. 354-363.

Kuenen, P. H., 1959, Experimental abrasion: 3. Fluviatile action on sand, American Journal of Science, vol. 257, no. 3, p. 172-190.

Kulikova A. E., 2006, Effect of mall scale heterogeneities on reservoir properties, Unpublished MSc individual project report, Heriot-Watt University.

Larue, D. K. and F. Friedmann, 2005, The controversy concerning stratigraphic architecture of channelized reservoirs and recovery by water flooding, Petroleum Geoscience, vol. 11, no. 2, p. 131-146.

Larue, D. K. and J. Hovadik, 2006, Connectivity of channelized reservoirs: a modelling approach, Petroleum Geoscience, vol. 12, no. 4, p. 291-308.

Le Ravalec, M., C. Morlot, R. Marmier, and D. Foulon, 2009, Heterogeneity impact on SAGD process performance in mobile heavy oil reservoirs, Oil and Gas Science and Technology-Revue de l'IFP, vol. 64, no. 4, p. 469-476.

Leeder, M. R., 1983; 2009, On the interactions between turbulent flow, sediment transport and bedform mechanics in channelized flows, *in* Collinson J. D. and J. Lewin (eds), Modern and ancient fluvial systems, Blackwell Publishing Ltd., p. 3-18.

Leeder, M., 1973, Fluviatile fining-upwards cycles and the magnitude of palaeochannels, Geological Magazine, vol. 110, no. 03, p. 265-276.

Levinson, A. and G. Coetzee, 1978, Implications of disequilibrium in exploration for uranium ores in the surficial environment using radiometric techniques - a review, Mineral Science and Engineering, vol. 10, no. 1, p. 19-27.

Li, W., 2007, A fixed-path Markov chain algorithm for conditional simulation of discrete spatial variables, Mathematical Geology, vol. 39, no. 2, p. 159-176.

Li, W. and C. Zhang, 2008, A single-chain-based multidimensional Markov chain model for subsurface characterization, Environmental and Ecological Statistics, vol. 15, no. 2, p. 157-174.

Loevborg, L., H. Wollenberg, P. Srensen, and J. Hansen, 1971, Field determination of uranium and thorium by gamma-ray spectrometry, exemplified by measurements in the Ilmaussaq alkaline intrusion, south Greenland, Economic Geology, vol. 66, no. 3, p. 368-384.

Lopez-Gomez and others, 2002, Permian and Triassic, *in* Gibbons, W. and Moreno, M. T. (eds), The Geology of Spain, The Geological Society, London.

Lyons III, W. J., 2004, Quantifying channelized submarine depositional systems from bed to basin scale, Unpublished PhD thesis, Massachusetts Institute of Technology.

Ma, S., J. Zhang, N. Jin, Z. Wang, and Y. Wang, 1999, The 3-D architecture of point bar and the forming and distribution of remaining oil, Conference paper, SPE Asia Pacific Improved Oil Recovery Conference, 25-26 October 1999, Kuala Lumpur, Malaysia.

Mack, G. H., W. C. James, and H. C. Monger, February, 1993, Classification of paleosols, GSA Bulletin, vol. 105, no. 2, p. 129-136.

Mackey, S. D. and J. S. Bridge, 1995, Three-dimensional model of alluvial stratigraphy; theory and applications, Journal of Sedimentary Research, vol. 65, no. 1b, p. 7-31.

Maharaja, A., 2008, TiGenerator: Object-based training image generator, Computers and Geosciences, vol. 34, no. 12, p. 1753-1761.

Makaske, B., H. J. A. Berendsen, and M. H. M. van Ree, 2007, Middle Holocene Avulsion-Belt Deposits in the Central Rhine–Meuse Delta, The Netherlands, Journal of Sedimentary Research, vol. 77, no. 2, p. 110-123.

Mange, M. A. and H. F. W. Maurer, 1992, Heavy minerals in colour, Chapman and Hall London.

Martin-Chivelet and others, 2002, Cretaceous, *in* Gibbons, W. and Moreno, M. T. (eds), The Geology of Spain, The Geological Society, London.

Martin, J. H., 1993, A review of braided fluvial hydrocarbon reservoirs: the petroleum engineer's perspective, Geological Society, London, Special Publications, vol. 75, no. 1, p. 333-367.

Martin, J. M., 2007, Quantitative sequence stratigraphy, Unpublished PhD thesis, University of Minnesota.

Martin, J., A. Evans, and J. Raper, 1988, Reservoir modelling of low-sinuosity channel sands: a network approach, European Petroleum Conference, 16-19 October 1988, London, United Kingdom.

Martínez, J. L. C., L. C. Pérez, A. Marcuello, P. A. Cazo, M. M. Carpio, and F. Bellmunt, 2010, Exhumed channel sandstone networks within fluvial fan deposits from the Oligo-Miocene Caspe Formation, South-east Ebro Basin (North-east Spain), Sedimentology, vol. 57, no. 1, p. 162-189.

Massuel, S., G. Favreau, M. Descloitres, Y. Le Troquer, Y. Albouy, and B. Cappelaere, 2006, Deep infiltration through a sandy alluvial fan in semiarid Niger inferred from electrical conductivity survey, vadose zone chemistry and hydrological modelling, Catena, vol. 67, no. 2, p. 105-118.

Mayewski, P. A., E. E. Rohling, J. Curt Stager, W. Karlén, K. A. Maasch, L. David Meeker, E. A. Meyerson, F. Gasse, S. van Kreveld, K. Holmgren et al, 2004, Holocene climate variability, Quaternary Research, vol. 62, no. 3, p. 243-255.

McCabe, P. J., 1977, Deep distributary channels and giant bedforms in the upper Carboniferous of the Central Pennines, northern England, Sedimentology, vol. 24, no. 2, p. 271-290.

McCaffrey, K. J. W., R. R. Jones, R. E. Holdsworth, R. W. Wilson, P. Clegg, J. Imber, N. Holliman, and I. Trinks, 2005, Unlocking the spatial dimension: digital technologies and the future of geoscience fieldwork, Journal of the Geological Society, vol. 162, no. 6, p. 927-938.

McCarthy, T. S., W. N. Ellery, and I. G. Stanistreet, 1992, Avulsion mechanisms on the Okavango fan, Botswana: the control of a fluvial system by vegetation, Sedimentology, vol. 39, no. 5, p. 779-795.

McKee, E. D., E. J. Crosby, and H. L. Berryhill, 1967, Flood deposits, Bijou Creek, Colorado, June 1965, Journal of Sedimentary Research, vol. 37, no. 3, p. 829-851.

Meunier, J. D., E. Sellier, and M. Pagel, 1990, Radiation-damage rims in quartz from uranium-bearing sandstones, Journal of Sedimentary Research, vol. 60, no. 1, p. 53-58.

Meunier, J., P. Landais, M. Monthioux, and M. Pagel, 1987, Oxidation reduction processes in the genesis of the uranium-vanadium tabular deposits of the Cottonwood Wash mining area (Utah, USA): evidence from petrological study and organic matter analysis, Bulletin de Minéralogie, vol. 110, p. 145-156.

Miall, A. D., 1973, Markov chain analysis applied to an ancient alluvial plain succession, Sedimentology, vol. 20, no. 3, p. 347-364.

Miall, A. D., 1978, Fluvial sedimentology, Stacs Data Service Ltd.

Miall, A. D., 1985, Architectural-element analysis: A new method of facies analysis applied to fluvial deposits, Earth-Science Reviews, vol. 22, no. 4, p. 261-308.

Miall, A. D., 1988, Reservoir heterogeneities in fluvial sandstones: lessons from outcrop studies, AAPG Bulletin, vol. 72, no. 6, p. 682-697.

Miall, A. D., 2002, Architecture and sequence stratigraphy of pleistocene fluvial systems in the Malay Basin, based on seismic time-slice analysis, AAPG Bulletin, vol. 86, no. 7, p. 1201-1216.

Miall, A. D., 2006, Reconstructing the architecture and sequence stratigraphy of the preserved fluvial record as a tool for reservoir development: A reality check, AAPG Bulletin, vol. 90, no. 7, p. 989-1002.

Michael, H. A., H. Li, A. Boucher, T. Sun, J. Caers, and S. M. Gorelick, 2010, Combining geologic-process models and geostatistics for conditional simulation of 3D subsurface heterogeneity, Water Resources Research, vol. 46, no. 5, p. W05527.

Middleton, G. V., M. J. Church, M. Coniglio, L. A. Hardie, and F. J. Longstaffe, 2003, Encyclopedia of sediments and sedimentary rocks, Kluwer Academic Publishers.

Mikkelsen, M., A. Scheie, and O. Rong, 1991, Abnormal permeability behaviour of a north sea sandstone reservoir, Conference paper, SPE Annual Technical Conference and Exhibition, 6-9 October 1991, Dallas, Texas.

Mohrig, D., P. L. Heller, C. Paola, and W. J. Lyons, 2000, Interpreting avulsion process from ancient alluvial sequences: Guadalope-Matarranya system (northern Spain) and Wasatch Formation (western Colorado), GSA Bulletin, vol. 112, no. 12, p. 1787-1803.

Moody-Stuart, M., 1966, High- and low-sinuosity stream deposits, with examples from the Devonian of Spitsbergen, Journal of Sedimentary Research, vol. 36, no. 4, p. 1102-1117.

Mookerjea, D., 1961, The Kosi - a challenge in river control, Journal of the Institution of Engineers (India), vol. 42, no. 3, p. 117-142.

Moore, G. T., D. N. Hayashida, C. A. Ross, and S. R. Jacobson, 1992, Paleoclimate of the Kimmeridgian/Tithonian (Late Jurassic) world: I. Results using a general circulation model, Palaeogeography, Palaeoclimatology, Palaeoecology, vol. 93, no. 1, p. 113-150.

Morozova, G. S. and N. D. Smith, 2000, Holocene avulsion styles and sedimentation patterns of the Saskatchewan River, Cumberland Marshes, Canada, Sedimentary Geology, vol. 130, no. 1-2, p. 81-105.

Mullens, T. E. and V. L. Freeman, 1957, Lithofacies of the Salt Wash Member of the Morrison Formation, Colorado Plateau, GSA Bulletin, vol. 68, no. 4, p. 505-526.

Myers, K. and P. Wignall, 1987, Understanding Jurassic organic-rich mudrocks - new concepts using gamma-ray spectrometry and palaeoecology: examples from the Kimmeridge Clay of Dorset and the Jet Rock of Yorkshire, *in* Legget J. K. and G. G. Zuffa (eds), Marine clastic sedimentology, London, Graham and Trotman, p. 172-189.

Nadon, G. C., 1994, The genesis and recognition of anastomosed fluvial deposits; data from the St. Mary River Formation, south-western Alberta, Canada, Journal of Sedimentary Research, vol. 64, no. 4b, p. 451-463.

Nichols, G. J. and J. A. Fisher, 2007, Processes, facies and architecture of fluvial distributary system deposits, Sedimentary Geology, vol. 195, no. 1-2, p. 75-90.

Nichols, G. J. and J. P. Hirst, 1998, Alluvial fans and fluvial distributary systems, Oligo-Miocene, northern Spain; contrasting processes and products, Journal of Sedimentary Research, vol. 68, no. 5, p. 879-889.

Nichols, G. J., 1987, Structural controls on fluvial distributary systems - the Luna system, northern Spain, Recent Developments in Fluvial Sedimentology, SEPM Special Publication, vol. 39, p. 269-277.

Nichols, G. J., 2005, Sedimentary evolution of the Lower Clair Group, Devonian, West of Shetland: climate and sediment supply controls on fluvial, aeolian and lacustrine deposition, Geological Society, London, Petroleum Geology Conference series, vol. 6, p. 957-967.

Nichols, G., 2011, Endorheic Basins, *in* Bursby C. and A. Azor (eds), Tectonics of Sedimentary Basins, John Wiley and Sons, Ltd, p. 621-632.

North, C. P. and S. K. Davidson, 2012, Unconfined alluvial flow processes: Recognition and interpretation of their deposits, and the significance for palaeogeographic reconstruction, Earth-Science Reviews, vol. 111, no. 1-2, p. 199-223.

North, C. P., 1996, The prediction and modelling of subsurface fluvial stratigraphy, Advanced in fluvial dynamic and stratigraphy: Chichester, John Wiley and Sons Ltd, p. 395-508.

Ogg, J. G., G. Ogg, and F. M. Gradstein, 2008, The concise geologic time scale, Cambridge.

Owen, G., 1996, Experimental soft-sediment deformation: structures formed by the liquefaction of unconsolidated sands and some ancient examples, Sedimentology, vol. 43, no. 2, p. 279-293.

Paola, C., 2000, Quantitative models of sedimentary basin filling, Sedimentology, vol. 47, p. 121-178.

Paola, C., G. Parker, R. Seal, S. K. Sinha, J. B. Southard, and P. R. Wilcock, 1992, Downstream fining by selective deposition in a laboratory flume, Science, vol. 258, no. 5089, p. 1757-1760.

Parrish, J. T. and F. Peterson, 1988, Wind directions predicted from global circulation models and wind directions determined from aeolian sandstones of the western United States: A comparison, Sedimentary Geology, vol. 56, no. 1, p. 261-282.

Parrish, J. T., F. Peterson, and C. E. Turner, 2004, Jurassic “savannah”, plant taphonomy and climate of the Morrison Formation (Upper Jurassic, Western USA), Sedimentary Geology; Reconstruction of the Extinct Ecosystem of the Upper Jurassic Morrison Formation, vol. 167, no. 3, p. 137-162.

Patil, G. P. and C. Taillie, 2001, A multiscale hierarchical Markov transition matrix model for generating and analysing thematic raster maps, Environmental and Ecological Statistics, vol. 8, no. 1, p. 71-84.

Perez-Arlucea, M. and N. D. Smith, 1999, Depositional patterns following the 1870s avulsion of the Saskatchewan River (Cumberland Marshes, Saskatchewan, Canada), Journal of Sedimentary Research, vol. 69, no. 1, p. 62-73.

Pérez-Rivarés, J., M. G. Crespo, M. C. A. Abad, and G. P. Tirapu, 2004, Magnetostratigraphy of the Miocene continental deposits of the Montes de Castejón (central Ebro basin, Spain): geochronological and palaeoenvironmental implications, Geologica Acta, vol. 2, no. 3, p. 221.

Peterson, F., 1984, Fluvial sedimentation on a quivering craton: Influence of slight crustal movements on fluvial processes, upper Jurassic Morrison formation, western Colorado plateau, Sedimentary Geology, vol. 38, no. 1-4, p. 21-49.

Peterson, F., 1986, Jurassic palaeotectonics in the west-central part of the Colorado Plateau, Utah and Arizona, Palaeotectonics and Sedimentation, Rocky Mountain Region, US Mere. Am. Assoc. Pet. Geol, vol. 41, p. 563-596.

Peterson, F., 1988, A synthesis of the Jurassic system in the southern Rocky Mountain region, Geology of North America, vol. 2, p. 65-76.

Peterson, F., 1992, Chronology of the Jurassic system in the western interior basin: Fort Collins, Colorado, SEPM Proceedings, Mesozoic of the Western Interior, p. 53.

Peterson, F., 1994, Sand dunes, sabkhas, streams, and shallow seas: Jurassic paleogeography in the southern part of the Western Interior Basin, Mesozoic systems of the Rocky Mountain region, USA: Denver, Colorado, Rocky Mountain Section SEPM, p. 233-272.

Pettijohn, F. J., P. E. Potter, and R. Siever, 1987, Sand and sandstone, Springer-Verlag.

Pipiringos, G. N. and R. O'Sullivan, 1978, Principal unconformities in Triassic and Jurassic rocks, western interior United States: a preliminary survey, USGS, US Government Printing Office.

Plint, A., 1986, Slump blocks, intraformational conglomerates and associated erosional structures in Pennsylvanian fluvial strata of eastern Canada, Sedimentology, vol. 33, no. 3, p. 387-399.

Posamentier, H. W., G. P. Allen, D. P. James, and M. Tesson, 1992, Forced regressions in a sequence stratigraphic framework: concepts, examples, and exploration significance (1), AAPG Bulletin, vol. 76, no. 11, p. 1687-1709.

Potter, D. K., P. W. M. Corbett, S. A. Barclay, and R. S. Haszeldine, 2004, Quantification of Illite Content in Sedimentary Rocks Using Magnetic Susceptibility - A Rapid Complement or Alternative to X-Ray Diffraction, Journal of Sedimentary Research, vol. 74, no. 5, p. 730-735.

Pranter, M. J., A. I. Ellison, R. D. Cole, and P. E. Patterson, 2007, Analysis and modeling of intermediate-scale reservoir heterogeneity based on a fluvial point-bar outcrop analog, Williams Fork Formation, Piceance Basin, Colorado, AAPG Bulletin, vol. 91, no. 7, p. 1025-1051.

Prince G. D. and P. M. Burgess, 2013 (in review), Numerical modelling of falling-stage topset aggradation, Journal of Sedimentary Research.

Pringle, J., J. Howell, D. Hodgetts, A. Westerman, and D. Hodgson, 2006, Virtual outcrop models of petroleum reservoir analogues: a review of the current state-of-the-art, First Break, p. 33-42.

Pryor, W. A., 1973, Permeability-porosity patterns and variations in some Holocene sand bodies, AAPG Bulletin, vol. 57, no. 1, p. 162-189.

Pryor, W., 1972, Reservoir inhomogeneities of some recent sand bodies, Old SPE Journal, vol. 12, no. 3, p. 229-245.

Puigdefabregas, C., 1973, Miocene point-bar deposits in the Ebro Basin, Northern Spain, Sedimentology, vol. 20, no. 1, p. 133-144.

Reid, I. and L. Frostick, 1994, Fluvial sediment transport and deposition, *in* Pye K. (eds), Sediment transport and depositional processes, p. 89-155.

Reitz, M. D., D. J. Jerolmack, and J. B. Swenson, 2010, Flooding and flow path selection on alluvial fans and deltas, Geophysical Research Letters, vol. 37, no. 6, p. L06401.

Reynolds, A. D., 1999, Dimensions of paralic sandstone bodies, AAPG Bulletin, vol. 83, no. 2, p. 211-229.

Riba, O., S. Reguant, and J. Villena, 1983, Ensayo de síntesis estratigráfica y evolutiva de la cuenca terciaria del Ebro, Libro homenaje a JM Ríos, Geología de España, vol. 2, p. 131-159.

Rider, M. H., 1996; 2001, The geological interpretation of well logs, Gulf Publishing.

Rietveld, H., 1969, A profile refinement method for nuclear and magnetic structures, Journal of Applied Crystallography, vol. 2, no. 2, p. 65-71.

Robinson, J. W. and P. J. McCabe, 1997, Sandstone-body and shale-body dimensions in a braided fluvial system: Salt Wash Sandstone Member (Morrison Formation), Garfield County, Utah, AAPG Bulletin, vol. 81, no. 8, p. 1267-1291.

Sambrook Smith, G. H., J. L. Best, P. J. Ashworth, C. R. Fielding, S. L. Goodbred, and E. W. Prokocki, 2010, Fluvial form in modern continental sedimentary basins: Distributive fluvial systems: COMMENT, Geology, vol. 38, no. 12, p. e230-e230.

Sanford, R. F., 1995, Hydrogeology of Jurassic and Triassic wetlands in the Colorado Plateau and the origin of tabular sandstone uranium deposits, vol. 32, no. 6, p. 257A-257A.

Schumm, S. A., 1985, Patterns of Alluvial Rivers, Annual Review of Earth and Planetary Sciences, vol. 13, no. 1, p. 5-27.

Schumm, S. A., 1993, River response to baselevel change: Implications for sequence stratigraphy, The Journal of Geology, vol. 101, no. 2, p. 279-294.

Schwarzacher, W., 1975, Sedimentation models and quantitative stratigraphy, Elsevier Science Limited.

Shanley, K. W. and P. J. McCabe, 1994, Perspectives on the sequence stratigraphy of continental strata, AAPG Bulletin, vol. 78, no. 4, p. 544-568.

Sheets, B. A., C. Paola, and J. M. Kelberer, 2007; 2009, Creation and preservation of channel-form sand bodies in an experimental alluvial system, *in* Nichols *G. J.*, E. Williams and C. Paopla (eds) Sedimentary Processes, Environments and Basins, Blackwell Publishing Ltd., p. 555-567.

Sheets, B. A., T. A. Hickson, and C. Paola, 2002, Assembling the stratigraphic record: depositional patterns and time-scales in an experimental alluvial basin, Basin Research, vol. 14, no. 3, p. 287-301.

Shelton, J. W. and R. L. Noble, 1974, Depositional features of braided-meandering stream: Geologic notes, AAPG Bulletin, vol. 58, no. 4, p. 742-749.

Shepherd, R. G. and S. A. Schumm, February, 1974, Experimental study of river incision, GSA Bulletin, vol. 85, no. 2, p. 257-268.

Shukla, U., I. Singh, P. Srivastava, and D. Singh, 1999, Paleocurrent patterns in braid-bar and point-bar deposits: examples from the Ganga River, India, Journal of sedimentary research, vol. 69, no. 5.

Singh, H., B. Parkash, and K. Gohain, 1993, Facies analysis of the Kosi megafan deposits, Sedimentary Geology, vol. 85, no. 1-4, p. 87-113.

Singh, I. B. and S. Kumar, 1974, Mega- and giant ripples in the Ganga, Yamuna, and Son Rivers, Uttar Pradesh, India, Sedimentary Geology, vol. 12, no. 1, p. 53-66.

Sinha, R. and P. F. Friend, 1994, River systems and their sediment flux, Indo-Gangetic plains, Northern Bihar, India, Sedimentology, vol. 41, no. 4, p. 825-845.

Slingerland, R. and N. D. Smith, 2004, River avulsions and their deposits, Annual Review of Earth and Planetary Sciences, vol. 32, no. 1, p. 257-285.

Smith, N. D., 1970, The braided stream depositional environment: comparison of the Platte River with some Silurian clastic rocks, North-Central Appalachians, GSA Bulletin, vol. 81, no. 10, p. 2993-3014.

Smith, N. D., 1972, Flume experiments on the durability of mud clasts, Journal of Sedimentary Research, vol. 42, no. 2, p. 378-383.

Smith, N. D., T. A. Cross, J. P. Dufficy, and S. R. Clough, 1989, Anatomy of an avulsion, Sedimentology, vol. 36, no. 1, p. 1-23.

Soil Taxonomy, 1992; 2010, Keys to Soil Taxonomy, 5th edition, Pocahontas press, Blacksburg.

Stanistreet, I. G. and T. S. McCarthy, 1993, The Okavango Fan and the classification of subaerial fan systems, Sedimentary Geology, vol. 85, no. 1-4, p. 115-133.

Steiner, M. B. and C. E. Helsley, 1975, Late Jurassic magnetic polarity sequence, Earth and Planetary Science Letters, vol. 27, no. 1, p. 108-112.

Steiner, M. B. and C. E. Helsley, November, 1975, Reversal pattern and apparent polar wander for the Late Jurassic, GSA Bulletin, vol. 86, no. 11, p. 1537-1543.

Stouthamer, E. and H. J. A. Berendsen, 2001, Avulsion frequency, avulsion duration, and interavulsion period of Holocene channel belts in the Rhine-Meuse Delta, The Netherlands, Journal of Sedimentary Research, vol. 71, no. 4, p. 589-598.

Stouthamer, E., 2001, Sedimentary products of avulsions in the Holocene Rhine–Meuse Delta, The Netherlands, Sedimentary Geology, vol. 145, no. 1-2, p. 73-92.

Straub, K. M., C. Paola, D. Mohrig, M. A. Wolinsky, and T. George, 2009, Compensational stacking of channelized sedimentary deposits, Journal of Sedimentary Research, vol. 79, no. 9, p. 673-688.

Strecker, M., R. Alonso, B. Bookhagen, B. Carrapa, G. Hilley, E. Sobel, and M. Trauth, 2007, Tectonics and climate of the southern central Andes, Annual Review of Earth and Planetary Sciences, vol. 35, p. 747-787.

Teixell, A., 1996, The Ansó transect of the southern Pyrenees: basement and cover thrust geometries, Journal of the Geological Society, vol. 153, no. 2, p. 301-310.

Tewari, R. C. and S. M. Casshyap, 1983, Cyclicity in early Permian fluviatile Gondwana coal measures: An example from Giridih and Saharjuri basins, Bihar, India, Sedimentary Geology, vol. 35, no. 4, p. 297-312.

Thomas, R. G., D. G. Smith, J. M. Wood, J. Visser, E. A. Calverley-Range, and E. H. Koster, 1987, Inclined heterolithic stratification - terminology, description, interpretation and significance, Sedimentary Geology, vol. 53, no. 1-2, p. 123-179.

Thorman, C. H., K. B. Ketner, W. E. Brooks, and F. Peterson, 1992, The Elko orogeny in north-eastern Nevada, Structural Geology and Petroleum Potential of Southwest Elko County, Nevada, Nevada Petroleum Society, Fieldtrip Guidebook, Nevada Petroleum Society Inc., Reno, p. 1-3.

Thorman, C., K. Ketner, and F. Peterson, 2004, The Middle to Late Jurassic Elko orogeny in eastern Nevada and western Utah, GSA Abstracts with Programs, vol. 24, p. 66.

Tooth, S., 2000, Downstream changes in dryland river channels: the Northern Plains of arid central Australia, Geomorphology, vol. 34, no. 1-2, p. 33-54.

Tooth, S., 2005, Splay formation along the lower reaches of ephemeral rivers on the Northern Plains of Arid Central Australia, Journal of Sedimentary Research, vol. 75, no. 4, p. 636-649.

Törnqvist, T. E. and J. S. Bridge, 2002, Spatial variation of overbank aggradation rate and its influence on avulsion frequency, Sedimentology, vol. 49, no. 5, p. 891-905.

Trotter, C., 1963, Palyno-botanical and stratigraphic studies of three lignite drill cores (Paleocene) from Harding County, South Dakota: Unpublished PhD thesis, Pennsylvania State University, University Park, Pennsylvania.

Tucker, G. E., S. T. Lancaster, N. M. Gasparini, and R. L. Bras, 2001, The channel-hillslope integrated landscape development model (CHILD), Landscape erosion and evolution modelling, vol. 349, p. 388.

Tucker, G. E., S. T. Lancaster, N. M. Gasparini, R. L. Bras, and S. M. Rybarczyk, 2001, An object-oriented framework for distributed hydrologic and geomorphic modelling using triangulated irregular networks, Computers and Geosciences, vol. 27, no. 8, p. 959-973.

Tunbridge, I. P., 1981, Sandy high-energy flood sedimentation - some criteria for recognition, with an example from the Devonian of SW England, Sedimentary Geology, vol. 28, no. 2, p. 79-95.

Turner, C. E. and F. Peterson, 2004, Reconstruction of the Upper Jurassic Morrison Formation extinct ecosystem - a synthesis, Sedimentary Geology, vol. 167, no. 3-4, p. 309-355.

Tyler, N. and F. G. Ethridge, 1983, Depositional setting of the Salt Wash Member of the Morrison Formation, Southwest Colorado, Journal of Sedimentary Research, vol. 53, no. 1, p. 67-82.

Valdes, P. J. and B. W. Sellwood, 1992, A palaeoclimate model for the Kimmeridgian, Palaeogeography, Palaeoclimatology, Palaeoecology, vol. 95, no. 1, p. 47-72.

Valladares and others, 2002, Precambrian, *in* Gibbons, W. and Moreno, M. T. (eds), The Geology of Spain, The Geological Society, London.

Van Fossen, M. C. and D. V. Kent, 1992, Palaeomagnetism of the Front Range (Colorado) Morrison Formation and an alternative model of Late Jurassic North American apparent polar wander, Geology, vol. 20, no. 3, p. 223-226.

Van Niekerk, A., K. R. Vogel, R. L. Slingerland, and J. S. Bridge, 1992, Routing of heterogeneous sediments over movable bed: model development, Journal of Hydraulic Engineering, vol. 118, no. 2, p. 246-262.

Verdier, A., T. Oki, and A. Suardy, 1968, Geology of the Handil field (East Kalimantan - Indonesia), Giant oil and gas fields of the decade, vol. 1978, p. 399-421.

Waltham, D. and D. R. Gröcke, 2006, Non-uniqueness and interpretation of the seawater 87Sr / 86Sr curve, Geochimica et Cosmochimica Acta, vol. 70, no. 2, p. 384-394.

Wang, Y., K. M. Straub, and E. A. Hajek, 2011, Scale-dependent compensational stacking: An estimate of autogenic time scales in channelized sedimentary deposits, Geology, vol. 39, no. 9, p. 811-814.

Webber, K. and L. Van Geuns, 1990, Framework for constructing clastic reservoir simulation models, Journal of Petroleum Technology, vol. 42, no. 10, p. 1248-1253.

Weber, K., 1982, Influence of common sedimentary structures on fluid flow in reservoir models, Journal of Petroleum Technology, vol. 34, no. 3, p. 665-672.

Weissmann, G. S., S. F. Carle, and G. E. Fogg, 1999, Three-dimensional hydrofacies modelling based on soil surveys and transition probability geostatistics, Water Resources Research, vol. 35, no. 6, p. 1761-1770.

Weissmann G. S., Hartley, A. J., Scuderi, L. A., Nichols, G. J., Davidson, S. K., Atchley, S. C., Bhattacharyya, P., Chakraborty, T., Ghosh, P., Nordt, L.C., Owen, A., and Sheldon, N., 2013 (in review), Prograding distributive fluvial systems – geomorphic models and ancient examples.

Weissmann, G. S., A. J. Hartley, G. J. Nichols, L. A. Scuderi, M. Olson, H. Buehler, and R. Banteah, 2010, Fluvial form in modern continental sedimentary basins: Distributive fluvial systems, Geology, vol. 38, no. 1, p. 39-42.

Weissmann, G. S., J. F. Mount, and G. E. Fogg, 2002, Glacially driven cycles in accumulation space and sequence stratigraphy of a stream-dominated alluvial fan, San Joaquin Valley, California, USA. Journal of Sedimentary Research, vol. 72, no. 2, p. 240-251.

Wells, N. A. and J. A. Dorr Jr., 1987, Shifting of the Kosi River, Northern India, Geology, vol. 15, no. 3, p. 204-207.

Wilkinson, B. H., C. N. Drummond, E. D. Rothman, and N. W. Diedrich, 1997, Stratal order in peritidal carbonate sequences, Journal of Sedimentary Research, vol. 67, no. 6, p. 1068-1082.

Williams, G. E., 1971, Flood deposits of the sand-bed ephemeral streams of Central Australia, Sedimentology, vol. 17, no. 1-2, p. 1-40.

Williams, H. D., P. M. Burgess, V. P. Wright, G. Della Porta, and D. Granjeon, 2011, Investigating carbonate platform types: multiple controls and a continuum of geometries, Journal of Sedimentary Research, vol. 81, no. 1, p. 18-37.

Wizevich, M. C., 1991, Photo mosaics of outcrops: useful photographic techniques, The three-dimensional facies architecture of terrigenous clastic sediments and its implications for hydrocarbon discovery and recovery: SEPM Concepts in Sedimentology and Paleontology, vol. 3, p. 111-121.

Wohl, E. and H. Achyuthan, 2002, Substrate influences on incised - channel morphology, The Journal of Geology, vol. 110, no. 1, p. 115-120.

Wohl, E. and H. Ikeda, April, 1997, Experimental simulation of channel incision into a cohesive substrate at varying gradients, Geology, vol. 25, no. 4, p. 295-298.

Young, R., 1993, Introduction to the Rietveld method, The Rietveld Method, vol. 5, p. 1-38.

Appendices

Appendix 1:
GPS waypoints

Appendix 1. Table of GPS waypoints recorded during outcrop documentation (UTM WGS-84 coordinate system)

Huesca				
Point	**Zone**	**E**	**N**	**Altitude**
Main outcrops, outcrop maps and logs				
Monzon				
104	31T	266961	4643317	288
105	31T	266998	4643305	290
111	31T	267024	4643299	292
112	31T	267030	4643298	290
113	31T	267049	4643317	293
114	31T	267043	4643330	303
115	31T	267078	4643346	306
116	31T	267082	4643352	310
117	31T	267131	4643350	312
118	31T	267139	4643339	316
119	31T	267157	4643292	314
120	31T	267167	4643271	317
121	31T	267171	4643238	317
122	31T	267188	4643219	319
123	31T	267162	4643196	308
124	31T	267159	4643185	306
125	31T	267137	4643152	300
126	31T	267090	4643131	306
127	31T	267070	4643116	279
128	31T	267111	4643116	305
129	31T	267112	4643092	307
130	31T	267114	4643067	314
131	31T	267133	4643104	329
132	31T	267143	4643103	332
133	31T	267173	4643093	347
134	31T	267196	4643091	350
135	31T	267116	4643082	310
136	31T	267074	4643045	313
137	31T	267071	4643032	318
138	31T	267065	4643012	319
139	31T	267048	4642982	325
140	31T	267051	4642959	327
141	31T	267114	4642923	339
142	31T	267072	4642966	339
143	31T	267079	4642970	340
144	31T	267093	4642972	351
145	31T	267102	4642969	355
146	31T	267155	4642914	338
147	31T	267166	4642897	330
148	31T	267180	4642858	328
149	31T	267194	4642867	332
150	31T	267190	4642851	330
151	31T	267223	4642828	342
152	31T	267247	4642789	333
153	31T	267281	4642748	333
154	31T	267294	4642740	334
155	31T	267308	4642739	333
156	31T	267340	4642720	334
157	31T	267361	4642661	339
158	31T	267370	4642659	340
159	31T	267367	4642623	346
160	31T	267369	4642601	349
Castelflorite				
211	30T	747693	4633057	386
212	30T	747700	4633082	385
213	30T	747669	4633102	385
214	30T	747661	4633146	386

Salt Wash				
Point	**Zone**	**E**	**N**	**Altitude**
Main outcrops, outcrop maps and logs				
Bullforg				
103	12S	518089	4162921	1185
104	12S	518077	4162932	1190
105	12S	518069	4162941	1195
106	12S	518074	4162938	1199
107	12S	518099	4162909	1203
108	12S	518100	4162907	1206
109	12S	518103	4162900	1208
110	12S	518050	4163121	1191
111	12S	518049	4163123	1199
112	12S	518055	4163124	1200
113	12S	518055	4163113	1202
114	12S	518053	4163110	1205
115	12S	518048	4163110	1201
116	12S	518045	4163110	1202
117	12S	518043	4163107	1207
118	12S	518042	4163132	1211
119	12S	518035	4163132	1213
120	12S	518025	4163126	1211
121	12S	518021	4163123	1215
123	12S	518021	4163123	1217
125	12S	518015	4163115	1222
126	12S	518009	4163113	1218
127	12S	518016	4163216	1221
128	12S	518012	4163225	1220
129	12S	518013	4163228	1237
130	12S	518011	4163233	1235
131	12S	517984	4163248	1230
132	12S	517975	4163256	1222
133	12S	517984	4163269	1234
134	12S	517989	4163271	1239
135	12S	517989	4163271	1242
137	12S	517976	4163261	1242
138	12S	517977	4163272	1250
139	12S	517984	4163277	1266
417	12S	518127	4162870	1207
418	12S	518129	4162869	1206
419	12S	518126	4162868	1210
420	12S	518126	4162866	1210
422	12S	518148	4162804	1210
423	12S	518146	4162794	1211
424	12S	518148	4162791	1209
425	12S	518148	4162788	1211
426	12S	518141	4162795	1208
427	12S	518141	4162792	1214
428	12S	518141	4162791	1216
433	12S	518197	4162644	1221
436	12S	518195	4162642	1226
437	12S	518186	4162643	1227
438	12S	518196	4162632	1224
439	12S	518194	4162624	1233
440	12S	518187	4162627	1233
441	12S	518212	4162587	1235
442	12S	518206	4162584	1237
443	12S	518197	4162583	1236
444	12S	518217	4162548	1239
445	12S	518212	4162547	1246
446	12S	518215	4162545	1249

Point	Zone	E	N	Altitude
215	30T	747687	4633171	404
216	30T	747610	4633190	389
217	30T	747584	4633220	389
218	30T	747721	4633059	384
219	30T	747724	4633069	390
220	30T	747723	4633097	388
221	30T	747727	4633115	390
222	30T	747744	4633165	369
223	30T	747769	4633178	386
224	30T	747767	4633211	388
225	30T	747732	4633230	404
226	30T	747832	4633271	371
227	30T	747836	4633286	373
228	30T	747873	4633296	375
229	30T	747867	4633320	364
230	30T	747874	4633340	371
231	30T	747881	4633343	391
232	30T	747887	4633360	405
233	30T	747887	4633360	408
234	30T	747927	4633404	392
235	30T	747974	4633415	396
236	30T	747976	4633392	406
237	30T	747979	4633357	388
238	30T	747937	4633343	386
239	30T	747938	4633345	386
240	30T	747936	4633363	395
241	30T	748007	4633410	398
242	30T	748051	4633369	395
243	30T	748054	4633380	397
244	30T	748055	4633405	396
245	30T	748047	4633417	407
246	30T	748076	4633426	397
247	30T	748104	4633442	395
248	30T	748128	4633445	398
249	30T	748149	4633443	381
250	30T	748186	4633460	376
251	30T	748210	4633512	406
252	30T	748213	4633547	424
253	30T	748238	4633463	390
254	30T	748324	4633377	397
255	30T	748325	4633388	395
256	30T	748319	4633399	396
257	30T	748314	4633435	396
258	30T	748340	4633461	395
259	30T	748338	4633502	396
260	30T	748320	4633510	408
261	30T	748313	4633588	414
262	30T	748299	4633573	410
263	30T	748371	4633528	378
264	30T	748366	4633537	399
265	30T	748350	4633580	412
266	30T	748338	4633591	422
267	30T	748378	4633584	390
268	30T	748418	4633629	389
269	30T	748428	4633632	394
270	30T	748437	4633661	415
271	30T	748440	4633675	421
272	30T	748458	4633606	388
273	30T	748463	4633603	391
274	30T	748459	4633630	392
275	30T	748466	4633653	389
276	30T	748484	4633669	395

Point	Zone	E	N	Altitude
447	12S	518214	4162540	1248
448	12S	518243	4162532	1248
449	12S	518241	4162528	1252
450	12S	518228	4162526	1251
451	12S	518227	4162527	1256
452	12S	518211	4162526	1259
453	12S	518207	4162519	1260
454	12S	518204	4162517	1262
455	12S	518196	4162516	1261
456	12S	518197	4162514	1265
457	12S	518214	4162511	1266
459	12S	518215	4162510	1273
460	12S	518224	4162498	1270
461	12S	518224	4162497	1272
462	12S	518225	4162498	1278
463	12S	518229	4162495	1278
464	12S	518221	4162497	1273
465	12S	518218	4162492	1278
466	12S	518216	4162492	1282
467	12S	518215	4162486	1282
468	12S	518211	4162490	1287
469	12S	518209	4162489	1289
470	12S	518201	4162488	1286
471	12S	518203	4162480	1289
472	12S	518217	4162474	1291
473	12S	518212	4162468	1295
474	12S	518219	4162458	1298
475	12S	518247	4162456	1298
476	12S	518244	4162460	1292
477	12S	518359	4162346	1297
478	12S	518349	4162358	1292
479	12S	518341	4162364	1289
480	12S	518327	4162390	1292
481	12S	518318	4162403	1294
482	12S	518303	4162416	1280
483	12S	518301	4162421	1289
484	12S	518296	4162432	1297
485	12S	518290	4162432	1288
486	12S	518290	4162444	1298
487	12S	518283	4162448	1292
488	12S	518275	4162453	1290
489	12S	518268	4162454	1293
490	12S	518258	4162458	1290
491	12S	518251	4162466	1289
492	12S	518232	4162457	1293
493	12S	518216	4162461	1293
494	12S	518211	4162473	1291
Caineville				
147	12S	497797	4242074	2819
148	12S	497073	4250282	1566
149	12S	496930	4250453	1553
150	12S	496919	4250457	1556
151	12S	496941	4250580	1565
152	12S	496941	4250587	1562
153	12S	497069	4250632	1561
Slick Rock				
79	12S	680562	4208848	2065
80	12S	680554	4208842	2068
81	12S	680551	4208839	2077
82	12S	680550	4208847	2077
84	12S	680550	4208852	2079
86	12S	680542	4208845	2082

Point	Zone	E	N	Altitude
277	30T	748509	4633684	376
278	30T	748510	4633699	395
279	30T	748503	4633714	406
280	30T	748575	4633681	385
281	30T	748602	4633661	387
282	30T	748612	4633646	390
283	30T	748620	4633652	397
284	30T	748658	4633607	394
285	30T	748641	4633617	391
286	30T	748677	4633563	396
287	30T	748683	4633543	398
288	30T	748695	4633505	397
289	30T	748689	4633496	392
290	30T	748727	4633438	378
291	30T	748747	4633405	360
292	30T	748275	4633408	355
Alcolea				
198	31T	261612	4620023	177
200	31T	261597	4620071	226
201	31T	261610	4620079	206
202	31T	261630	4620089	196
302	31T	261244	4620080	269
304	31T	261422	4620053	282
305	31T	261450	4620053	271
306	31T	261497	4620108	272
307	31T	261540	4620138	261
308	31T	261552	4620149	255
309	31T	261560	4620144	254
310	31T	261566	4620138	244
311	31T	261556	4620126	241
312	31T	261532	4620113	241
313	31T	261577	4620152	242
314	31T	261602	4620161	240
315	31T	261612	4620161	241
316	31T	261623	4620153	235
317	31T	261631	4620150	230
318	31T	261633	4620145	225
319	31T	261597	4620203	241
320	31T	261607	4620216	241
321	31T	261585	4620204	250
322	31T	261590	4620219	248
323	31T	261599	4620228	240
324	31T	261607	4620239	238
325	31T	261607	4620286	214
326	31T	261616	4620209	239
327	31T	261622	4620201	238
328	31T	261614	4620174	233
329	31T	261649	4620170	223
330	31T	261641	4620130	207
331	31T	261650	4620119	208
332	31T	261651	4620113	200
333	31T	261628	4620105	224
334	31T	261606	4620101	223
335	31T	261600	4620085	224
336	31T	261592	4620068	222
337	31T	261591	4620059	219
338	31T	261594	4620052	222
339	31T	261592	4620039	225
340	31T	261581	4620044	230
341	31T	261586	4620013	230
342	31T	261623	4619987	212
343	31T	261618	4619970	209
344	31T	261573	4619982	212

Point	Zone	E	N	Altitude
87	12S	680535	4208848	2087
88	12S	680534	4208841	2090
89	12S	680520	4208855	2105
90	12S	680520	4208855	2107
91	12S	680517	4208858	2100
92	12S	680509	4208861	2111
93	12S	680498	4208861	2114
94	12S	680483	4208860	2104
95	12S	680471	4208828	2121
96	12S	680475	4208832	2127
97	12S	680477	4208831	2131
98	12S	680472	4208832	2136
99	12S	680346	4208776	2150
100	12S	680342	4208775	2152
Montezuma Canyon				
1	12S	651642	4182984	1733
2	12S	651638	4182980	1733
3	12S	651625	4182973	1724
4	12S	651614	4182967	1722
5	12S	651606	4182951	1732
6	12S	651601	4182940	1742
7	12S	651554	4182857	1616
8	12S	651573	4182938	1738
9	12S	651566	4182927	1744
10	12S	651548	4182919	1741
11	12S	651531	4182901	1743
12	12S	651501	4182892	1752
13	12S	651488	4182889	1733
14	12S	651473	4182873	1761
15	12S	651456	4182852	1759
16	12S	651457	4182852	1759
17	12S	651436	4182827	1764
18	12S	651418	4182813	1765
19	12S	651079	4182808	1828
20	12S	651085	4182817	1829
21	12S	651096	4182824	1836
22	12S	651124	4182845	1841
23	12S	651142	4182851	1840
24	12S	651166	4182856	1843
25	12S	651185	4182867	1844
26	12S	651198	4182875	1847
27	12S	651165	4182853	1843
28	12S	651154	4182849	1843
29	12S	651145	4182853	1842
30	12S	651140	4182850	1841
31	12S	651109	4182832	1837
32	12S	651095	4182819	1832
33	12S	651079	4182809	1830
34	12S	651075	4182802	1828
35	12S	651053	4182654	1794
36	12S	651414	4182810	1755
37	12S	651420	4182818	1752
38	12S	651426	4182827	1750
39	12S	651432	4182833	1746
40	12S	651444	4182843	1748
41	12S	651451	4182855	1742
42	12S	651459	4182869	1743
43	12S	651469	4182879	1741
44	12S	651469	4182885	1736
45	12S	651476	4182886	1738
46	12S	651496	4182881	1745
47	12S	651507	4182888	1747
48	12S	651510	4182892	1746

Point	Zone	E	N	Altitude
345	31T	261547	4619966	210
346	31T	261549	4619939	208
347	31T	261544	4619917	209
348	31T	261536	4619887	209
349	31T	261532	4619864	210
350	31T	261523	4619894	216
351	31T	261535	4619945	214
352	31T	261554	4619982	218
353	31T	261577	4619998	219
354	31T	261572	4619999	219
355	31T	261562	4620008	228
356	31T	261540	4620003	223
357	31T	261535	4619983	219
358	31T	261516	4620036	240
359	31T	261453	4620029	239
360	31T	261444	4620013	243
361	31T	261428	4620031	255
362	31T	261448	4620055	253
363	31T	261629	4619944	192
364	31T	261633	4619979	191
365	31T	261620	4619994	199
370	31T	261588	4619923	200
371	31T	261601	4619915	191
372	31T	261626	4619897	186
373	31T	261655	4619911	197
374	31T	261643	4619922	200
375	31T	261616	4619883	186
376	31T	261584	4619874	196
377	31T	261585	4619870	198
Logs in floodplain successions				
Rio Alcanadre (Aquero), road bridge N240				
20	30T	738977	4663411	
21	30T	738960	4663400	
Pertusa				
23	30T	737589	4653899	
25	30T	737662	4653948	
26	30T	737683	4654024	
35	30T	737828	4654496	
36	30T	737156	4654325	
Novales				
37	30T	725284	4655964	
38	30T	725372	4655840	
Lierta				
39	30T	706638	4679293	
Piraces				
40	30T	721959	4654350	
41	30T	721795	4654774	
42	30T	722165	4655153	
43	30T	722134	4655171	
44	30T	722094	4654847	
45	30T	722215	4654692	
Monte Aragon				
46	30T	719200	4670150	
47	30T	718927	4670139	
48	30T	718416	4670450	
49	30T	718062	4670819	
50	30T	718096	4670866	
Monzon (floodplain logs)				
51	31T	267188	4642827	
52	31T	267066	4642919	
53	31T	267056	4642974	
54	31T	267035	4643459	

Point	Zone	E	N	Altitude
49	12S	651515	4182896	1735
50	12S	651519	4182902	1730
51	12S	651539	4182916	1728
52	12S	651559	4182927	1737
53	12S	651566	4182937	1734
54	12S	651576	4182942	1733
55	12S	651585	4182945	1731
56	12S	651594	4182950	1729
57	12S	651602	4182955	1726
58	12S	651609	4182966	1708
59	12S	651622	4182977	1705
60	12S	651631	4182985	1709
61	12S	651641	4182991	1719
62	12S	651468	4182855	1758
63	12S	651739	4183001	1726
64	12S	651792	4183015	1719
65	12S	651955	4183129	1731
66	12S	652082	4183186	1731
Little Park				
319	12S	706531	4321616	1582
320	12S	706549	4321618	1601
321	12S	706549	4321622	1613
322	12S	706543	4321623	1609
323	12S	706532	4321623	1600
324	12S	706564	4321651	1598
325	12S	706544	4321661	1602
326	12S	706536	4321662	1608
327	12S	706540	4321660	1609
328	12S	706539	4321664	1605
329	12S	706547	4321666	1612
330	12S	706575	4321655	1610
331	12S	706577	4321651	1612
332	12S	706556	4321666	1613
333	12S	706558	4321672	1619
334	12S	706552	4321671	1619
335	12S	706552	4321672	1623
336	12S	706532	4321677	1611
337	12S	706481	4321646	1615
338	12S	706531	4321698	1610
339	12S	706541	4321668	1611
340	12S	706551	4321662	1611
341	12S	706594	4321674	1610
342	12S	706592	4321676	1613
343	12S	706618	4321687	1611
344	12S	706633	4321679	1608
345	12S	706628	4321647	1614
346	12S	706630	4321615	1615
347	12S	706634	4321616	1609
348	12S	706632	4321614	1611
349	12S	706633	4321614	1615
350	12S	706576	4321424	1605
351	12S	706611	4321427	1599
352	12S	706603	4321436	1593
353	12S	706582	4321451	1591
354	12S	706581	4321493	1594
355	12S	706591	4321506	1593
356	12S	706569	4321509	1600
357	12S	706594	4321543	1589
358	12S	706582	4321545	1592
359	12S	706607	4321581	1611
360	12S	706578	4321599	1586
361	12S	706623	4321624	1601

Point	Zone	E	N	Altitude
Castelflortie (floodplain logs)				
55	30T	747771	4633105	
56	30T	748138	4633417	
57	30T	748680	4633829	
58	30T	748467	4633650	
Bolea				
59	30T	701776	4681209	
60	30T	701756	4681241	
Piraces (Canal del Cinca)				
61	30T	718367	4654324	
Near Piraces village				
62	30T	722475	4653550	
Canal del Cinca between Tardienta and Tarbenas				
63	30T	710623	4657995	
64	30T	710286	4656657	
65	30T	708732	4653709	
66	30T	708838	4653390	
67	30T	705691	4650870	
68	30T	709784	4656902	
69	30T	704480	4652044	
70	30T	705803	4651219	
71	30T	708188	4652802	
72	30T	708406	4653325	
73	30T	708627	4655633	
74	30T	709845	4658122	
75	30T	709885	4658333	
76	30T	710187	4658823	
77	30T	710567	4659345	
78	30T	711048	4659825	
79	30T	711147	4660547	

Point	Zone	E	N	Altitude
362	12S	706618	4321640	1605
363	12S	706606	4321652	1598
364	12S	706604	4321661	1600
365	12S	706586	4321648	1595
366	12S	706593	4321636	1593
367	12S	706587	4321642	1593
368	12S	706568	4321646	1587
369	12S	706556	4321623	1588
370	12S	706570	4321614	1588
371	12S	706523	4321612	1589
372	12S	706522	4321612	1589
373	12S	706508	4321609	1595
374	12S	706501	4321611	1593
375	12S	706518	4321569	1583
376	12S	706454	4321614	1589
377	12S	706437	4321602	1581
378	12S	706359	4321542	1596
379	12S	706429	4321611	1570
380	12S	706460	4321658	1587
381	12S	706466	4321691	1578
382	12S	706358	4321736	1578
383	12S	706357	4321742	1583
384	12S	706383	4321755	1573
385	12S	706428	4321754	1577
386	12S	706430	4321728	1596
387	12S	706423	4321736	1588
388	12S	706446	4321729	1575
389	12S	706452	4321716	1587
390	12S	706452	4321721	1587
391	12S	706431	4321733	1614
392	12S	706439	4321733	1610
393	12S	706443	4321731	1608
394	12S	706453	4321734	1610
395	12S	706467	4321726	1612
396	12S	706462	4321735	1609
397	12S	706485	4321725	1605
398	12S	706491	4321727	1614
399	12S	706498	4321728	1610
400	12S	706498	4321732	1613
401	12S	706506	4321729	1609
402	12S	706515	4321744	1617
403	12S	706586	4321420	1597
404	12S	706614	4321409	1595
405	12S	706617	4321412	1596
406	12S	706624	4321399	1602
407	12S	706627	4321401	1608
408	12S	706623	4321406	1608
409	12S	706627	4321403	1611
410	12S	706633	4321399	1610
411	12S	706639	4321396	1620
412	12S	706637	4321405	1621
413	12S	706638	4321398	1625
414	12S	706640	4321404	1623
Colorado National Monument (CNM)				
180	12S	696352	4326166	1963
181	12S	696258	4326266	1963
182	12S	696270	4326273	1961
183	12S	696564	4326658	1930
184	12S	696635	4326736	1928
185	12S	696642	4326780	1924
186	12S	696635	4326800	1920
187	12S	696624	4326821	1925

Point	Zone	E	N	Altitude

Point	Zone	E	N	Altitude
188	12S	696615	4326904	1913
189	12S	696591	4326862	1926
190	12S	696571	4326875	1922
191	12S	696544	4326887	1916
192	12S	696506	4326903	1910
193	12S	696460	4326918	1913
194	12S	696432	4326930	1913
195	12S	696394	4326982	1903
196	12S	696401	4326986	1900
197	12S	696445	4327003	1898
198	12S	696445	4327002	1899
199	12S	696477	4327008	1900
200	12S	696496	4327019	1898
201	12S	696519	4327044	1897
202	12S	696541	4327070	1901
203	12S	696561	4327099	1893
204	12S	696581	4327117	1891
205	12S	696615	4327127	1892
206	12S	696645	4327145	1887
207	12S	696666	4327173	1887
208	12S	696667	4327206	1884
209	12S	696704	4327256	1883
210	12S	696688	4327265	1879
211	12S	696666	4327200	1892
212	12S	696650	4327177	1882
213	12S	696639	4327163	1881
214	12S	696635	4327149	1883
215	12S	696631	4327141	1887
216	12S	696618	4327135	1889
217	12S	696599	4327132	1892
218	12S	696591	4327133	1919
219	12S	696571	4327113	1904
220	12S	696551	4327094	1901
221	12S	696529	4327071	1902
222	12S	696522	4327058	1905
223	12S	696519	4327063	1903
224	12S	696500	4327038	1905
225	12S	696493	4327027	1906
226	12S	696473	4327016	1907
227	12S	696472	4327015	1905
228	12S	696431	4327006	1906
229	12S	696400	4326998	1913
230	12S	696387	4326985	1914
231	12S	696431	4326920	1913
232	12S	696445	4326913	1907
233	12S	696499	4326892	1911
234	12S	696534	4326879	1914
235	12S	696549	4326877	1921
236	12S	696581	4326862	1917
237	12S	696574	4326855	1931
238	12S	696589	4326849	1919
239	12S	696618	4326811	1924
240	12S	696624	4326797	1925
241	12S	696626	4326772	1930
242	12S	696632	4326762	1936
243	12S	696626	4326743	1933
244	12S	696613	4326728	1931
245	12S	696569	4326682	1936
246	12S	696557	4326669	1936
247	12S	696548	4326660	1928
248	12S	696422	4326497	1969
249	12S	696422	4326497	1971

Point			N	Altitude

Point	Zone	E	N	Altitude
250	12S	696397	4326481	1966
251	12S	696432	4326513	1967
252	12S	696291	4326305	1956
253	12S	696282	4326297	1959
254	12S	696264	4326281	1959
255	12S	696259	4326276	1960
256	12S	696251	4326267	1960
257	12S	696221	4326239	1960
258	12S	696136	4326245	1973
259	12S	696155	4326256	1981
260	12S	696202	4326300	1975
261	12S	696225	4326311	1979
262	12S	696223	4326315	1980
263	12S	696230	4326323	1979
264	12S	696230	4326337	1975
265	12S	696233	4326341	1973
266	12S	696234	4326348	1972
267	12S	696234	4326353	1972
268	12S	696245	4326365	1975
269	12S	696265	4326375	1973
270	12S	696275	4326385	1976
271	12S	696294	4326396	1981
272	12S	696309	4326409	1978
273	12S	696310	4326423	1974
274	12S	696327	4326434	1977
275	12S	696353	4326452	1980
276	12S	696367	4326457	1979
277	12S	696399	4326471	1972
278	12S	696410	4326481	1972
279	12S	696421	4326499	1966
280	12S	696432	4326513	1964
281	12S	696439	4326528	1962
282	12S	696426	4326550	1963
283	12S	696417	4326576	1961
284	12S	696427	4326594	1954
285	12S	696431	4326613	1953
286	12S	696424	4326635	1951
287	12S	696423	4326669	1947
288	12S	696430	4326688	1956
289	12S	696431	4326699	1961
290	12S	696466	4326760	1954
291	12S	696492	4326759	1946
292	12S	696504	4326773	1948
293	12S	696505	4326787	1947
294	12S	696519	4326804	1946
295	12S	696276	4326025	1977
296	12S	696256	4326015	1975
297	12S	696238	4326005	1974
298	12S	696220	4325992	1976
299	12S	696207	4325982	1973
300	12S	696193	4325981	1975
301	12S	696184	4325979	1976
302	12S	696174	4325977	1981
303	12S	696162	4325975	1979
304	12S	696139	4325974	1987
305	12S	696128	4325971	1986
306	12S	696099	4325959	1989
307	12S	696093	4325945	1989

Appendix 2:
Sedimentary logs

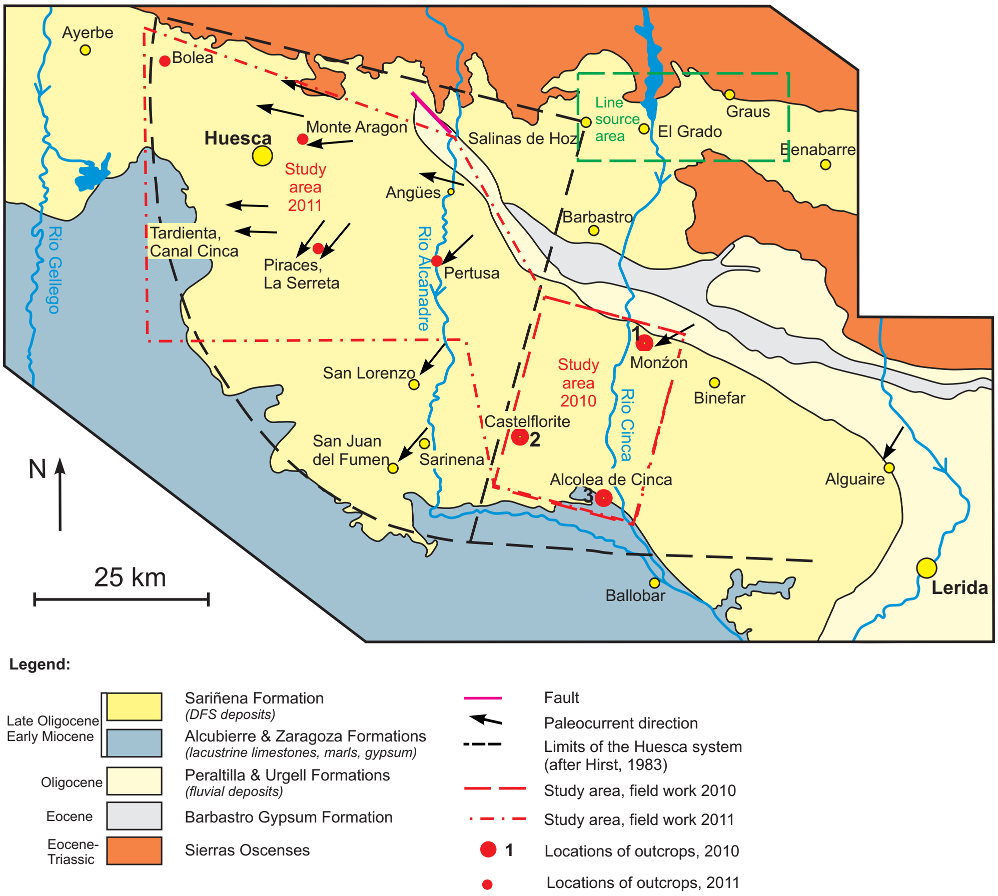

Geological map of the northern part of the Ebro Basin. Red boxes mark study areas.

Red dots indicate locations of sedimentary logs recorded in the Huesca DFS succession (Appendices 2.1 to 2.6) and sedimentary logs recorded in the floodplain deposits of the Huesca DFS succession (Appendices 2.13 to 2.18):

2.1 - Monźon 4 Log 1;
2.2 - Monźon 1 Log12;
2.3 - Castelflorite 4 Log 1;
2.4 - Ccastelflorite 2&3 Log 2;
2.5 - Castelflorite 2 Log 3;
2.6 - Alcolea 1& 2 Log 1.

2.13 - Monźon, Log 3 and 4;
2.14 - Pertusa, Log 3 and 5;
2.15 - Piracés 3 and 5;
2.16 - Castelflorite 1;
2.17 - Monte Aragón 2 and 4;
2.18 - Bolea 2.

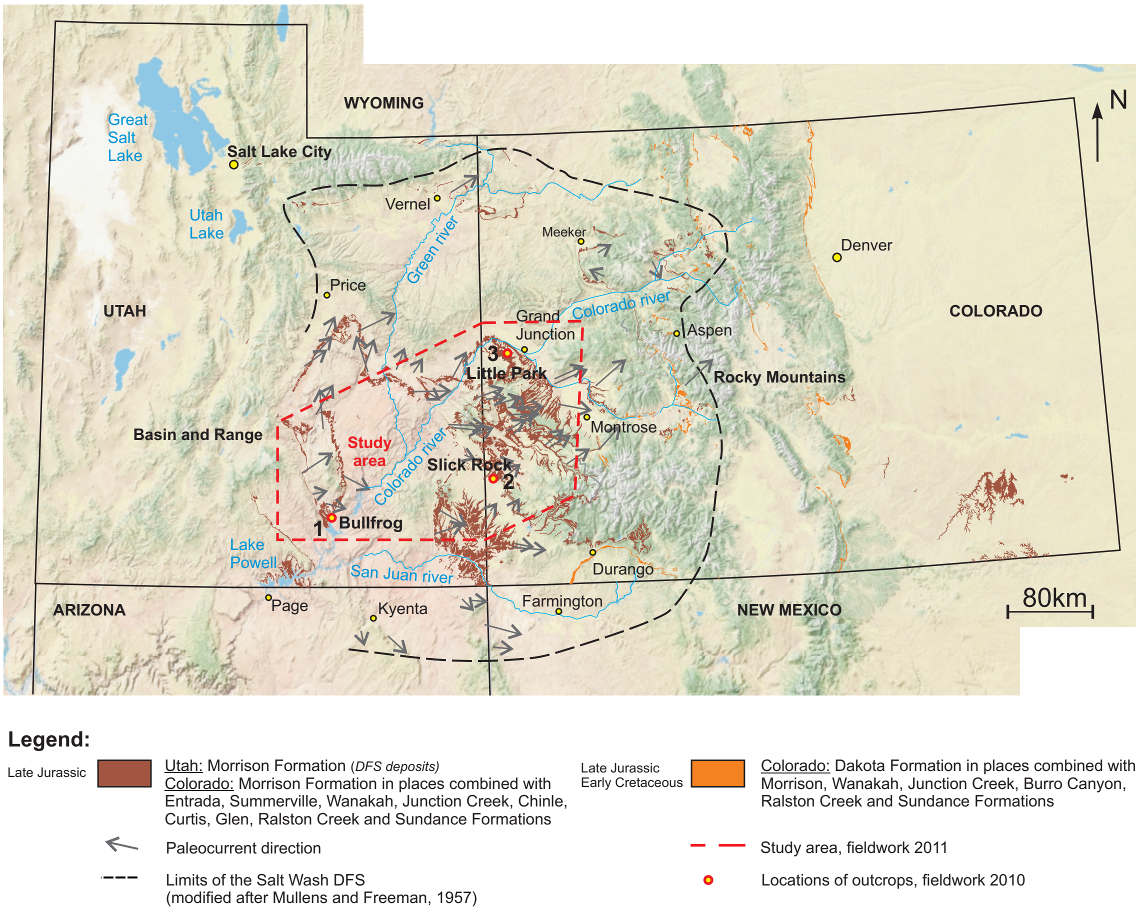

Topographic map of Utah and Colorado states of the USA with outcrops of the Morrison Formation (brown). Black arrows indicate paleocurrent data (Craig et al., 1955) and the dotted line is a limit of the Salt Wash DFS (modified after Mulllens and Freeman, 1957; Tyler and Ethridge, 1983). The red box show the study area.

Dots indicate locations of large outcrop studies and locations of sedimentary logs of the Salt Wash DFS succession presented in Appendices 2.7 - 2.12:

2.7 - Bullforg 3, Log 1, 2, 3 and 4;
2.8 - Bullfrog 2, Log 5;
2.9 - Slick Rock, Log 1;
2.10 - Little Park 2, Log 1 and 2;
2.11 - Little Park 1, Log 4, 5 and 6;
2.12 - Little Park 3, Log 7.

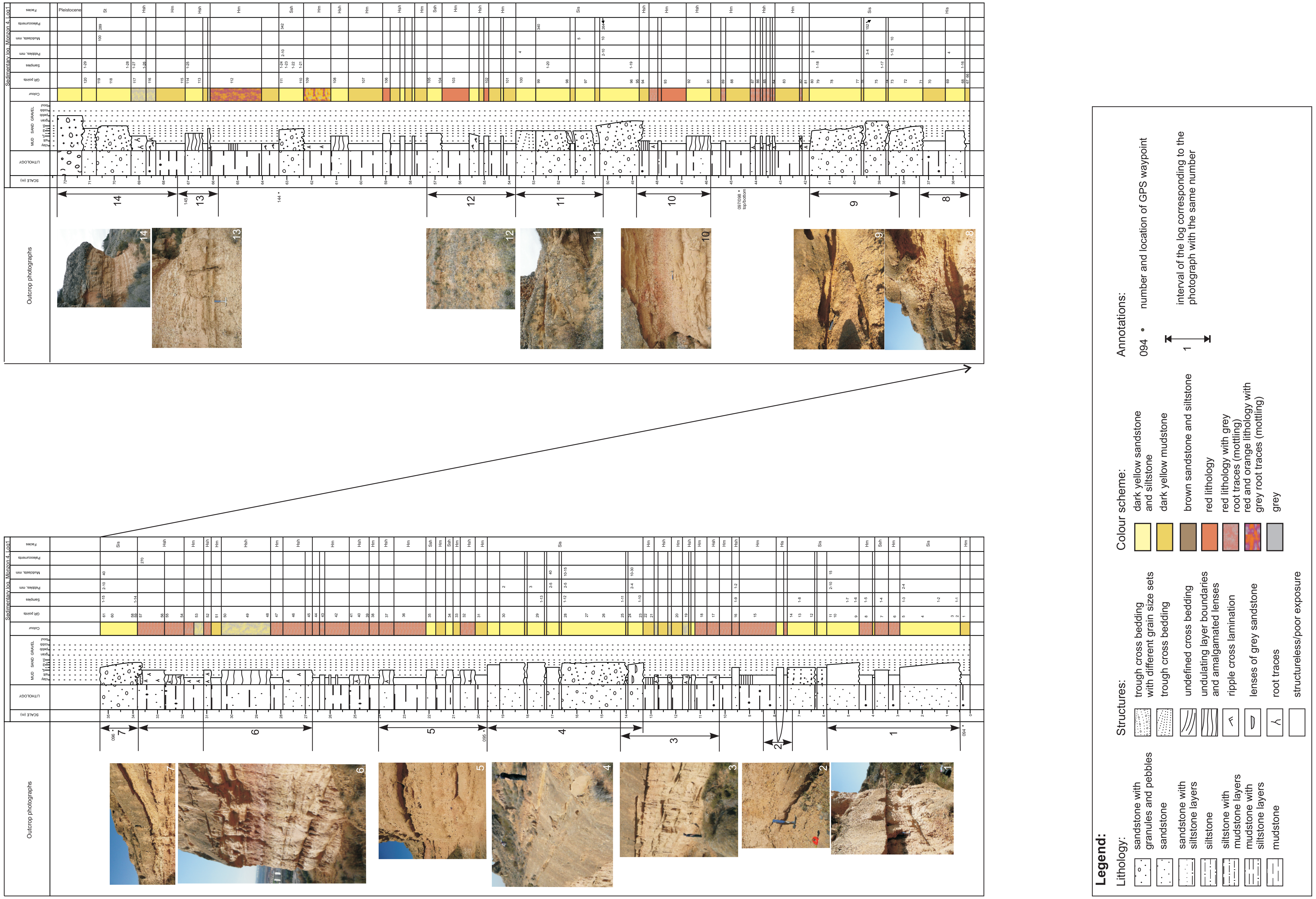

Appendix 2.1. Sedimentary log for the relatively proximal succession of the Huesca DFS deposits (Monzon 4 outcrop panel in the Appendix 5.1).

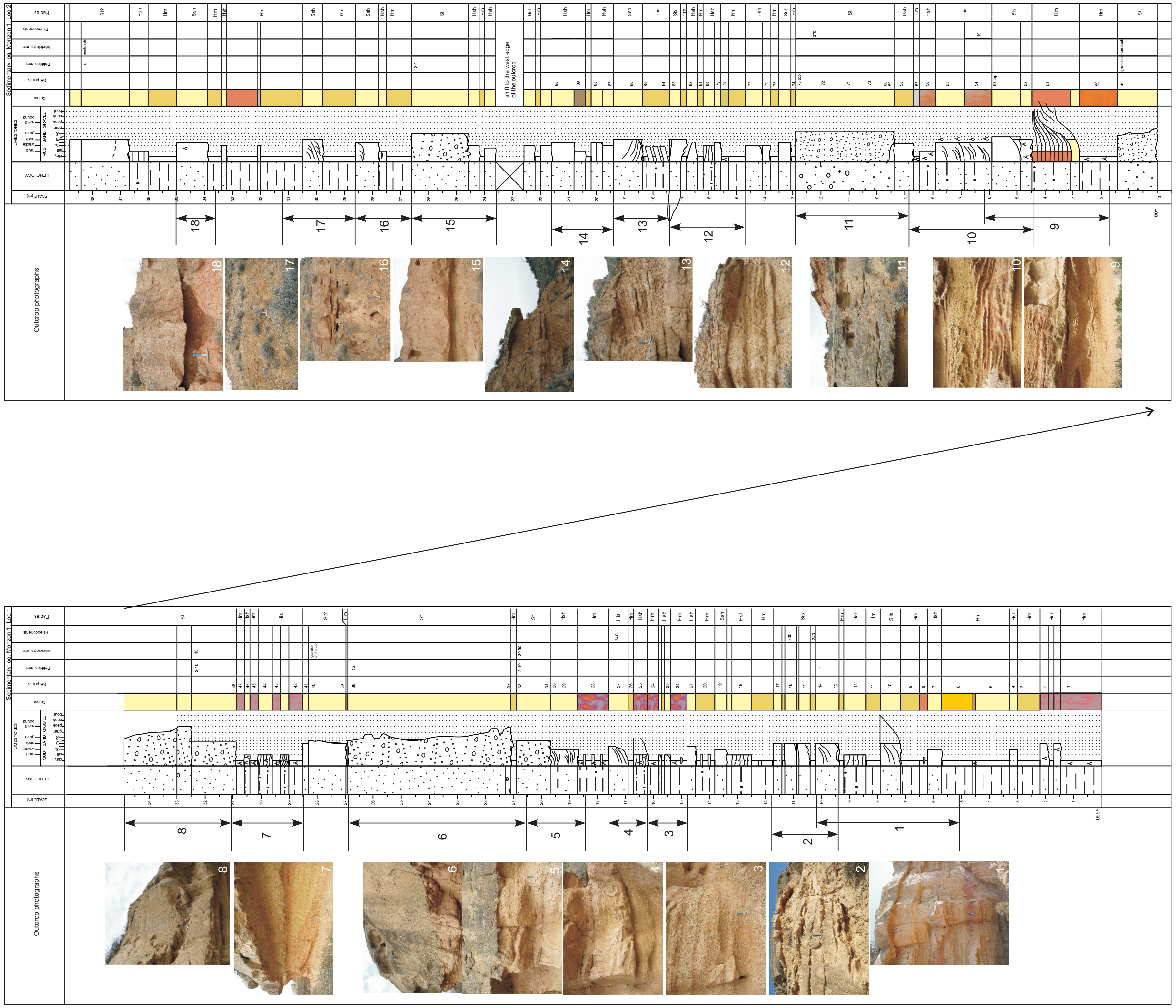

Appendix 2.2. Sedimentary log for the medial succession of the Huesca DFS deposits (Monzon 1 outcrop panel in the Appendix 5.1). For legend see Appendix 2.1.

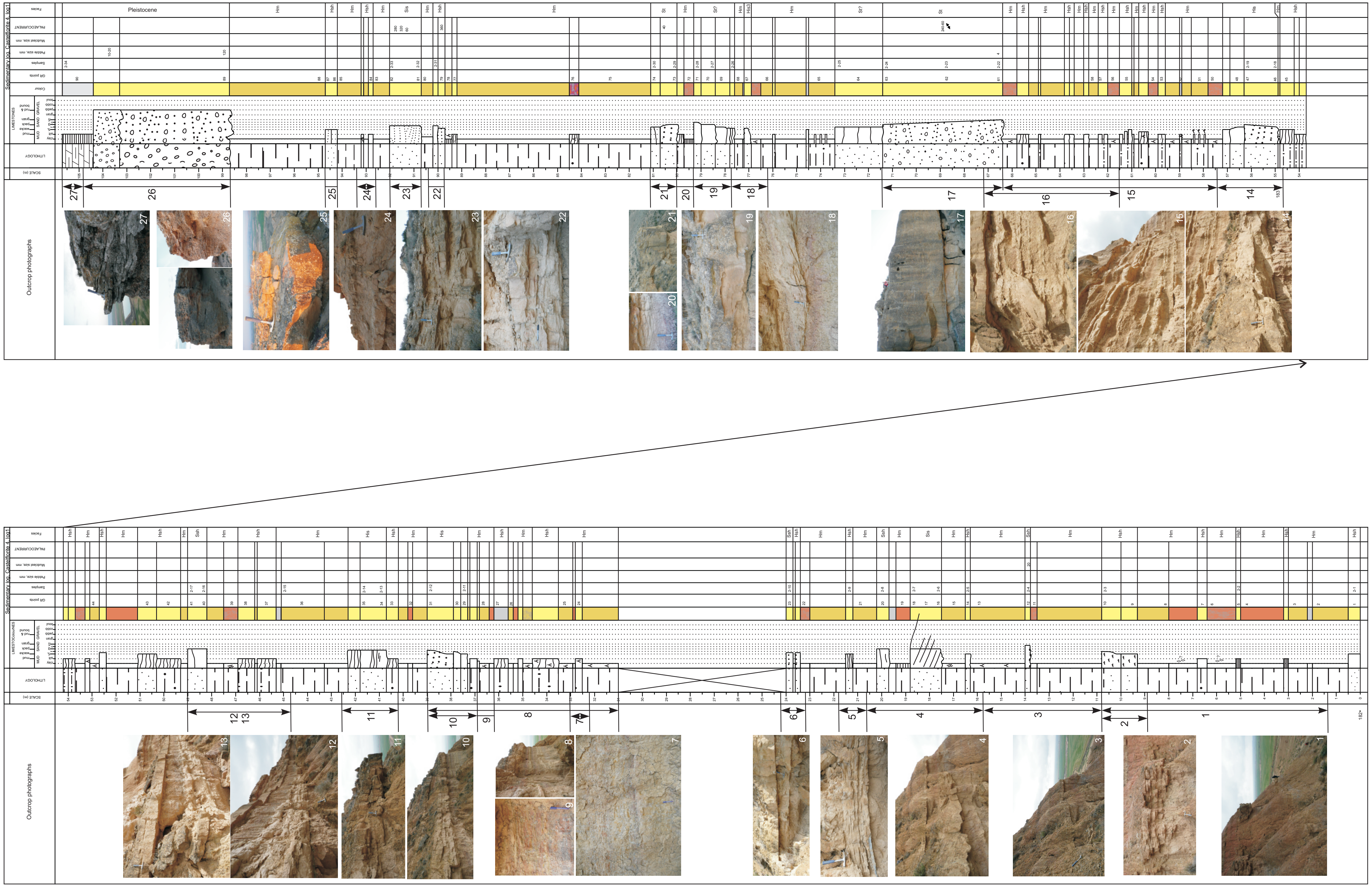

Appendix 2.3. Sedimentary log for the medial succession of the Huesca DFS deposits (Castelflorite 4 outcrop panel in the Appendix 5.2). For legend see Appendix 2.1.

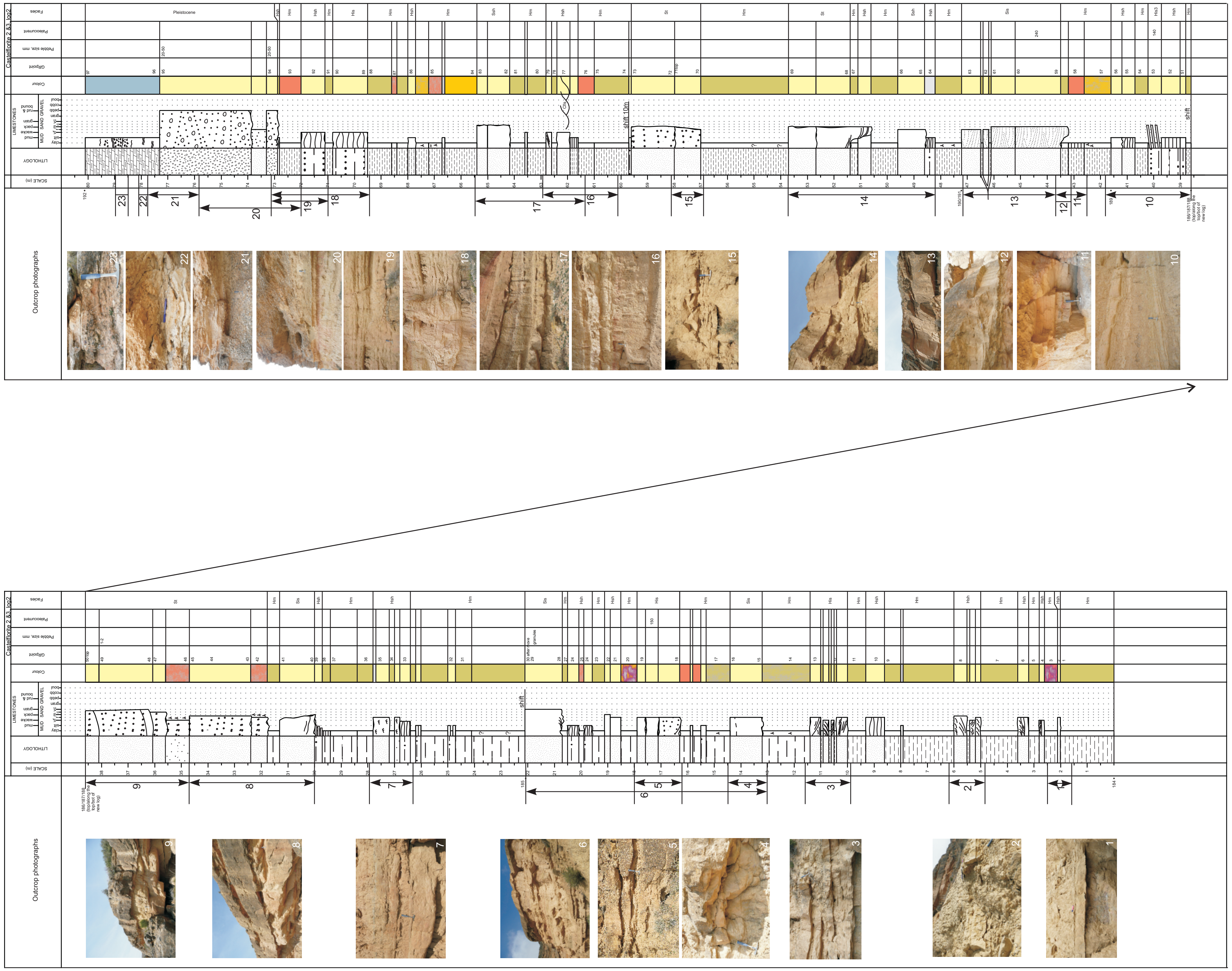

Appendix 2.4. Sedimentary log for the medial succession of the Huesca DFS deposits (Castelflorite 2 and 3 outcrop panel in the Appendix 5.2). For legend see Appendix 2.1.

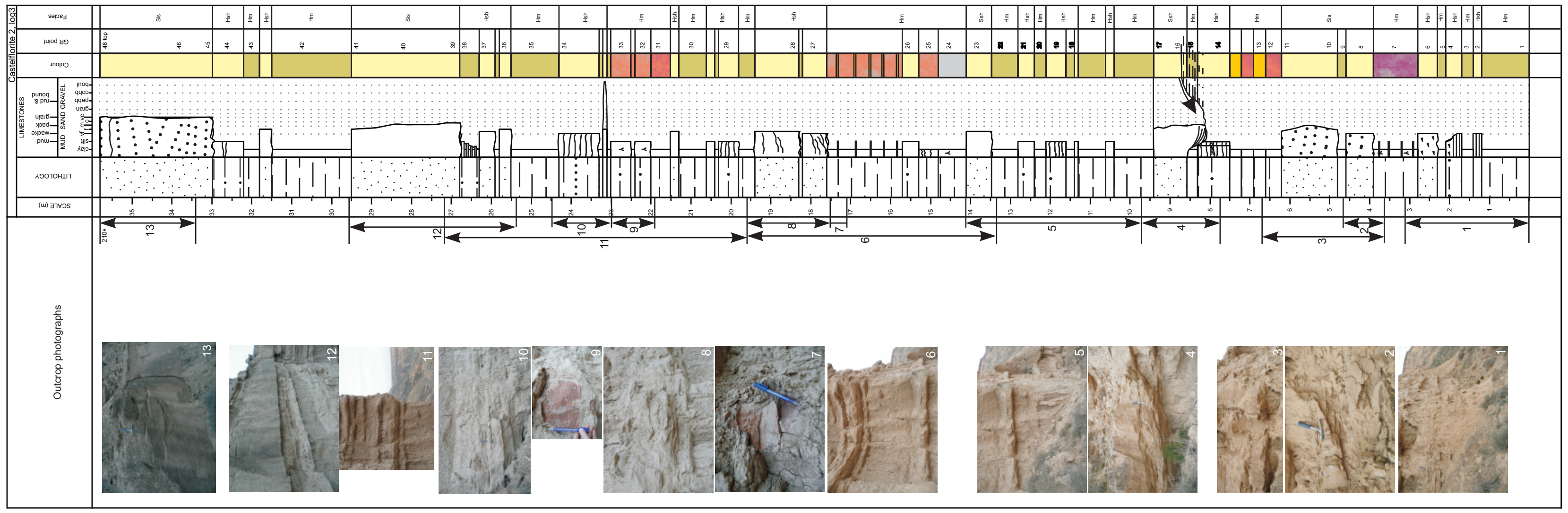

Appendix 2.5. Sedimentary log for the medial succession of the Huesca DFS deposits (Castelflorite 2 outcrop panel in the Appendix 5.2). For legend see Appendix 2.1.

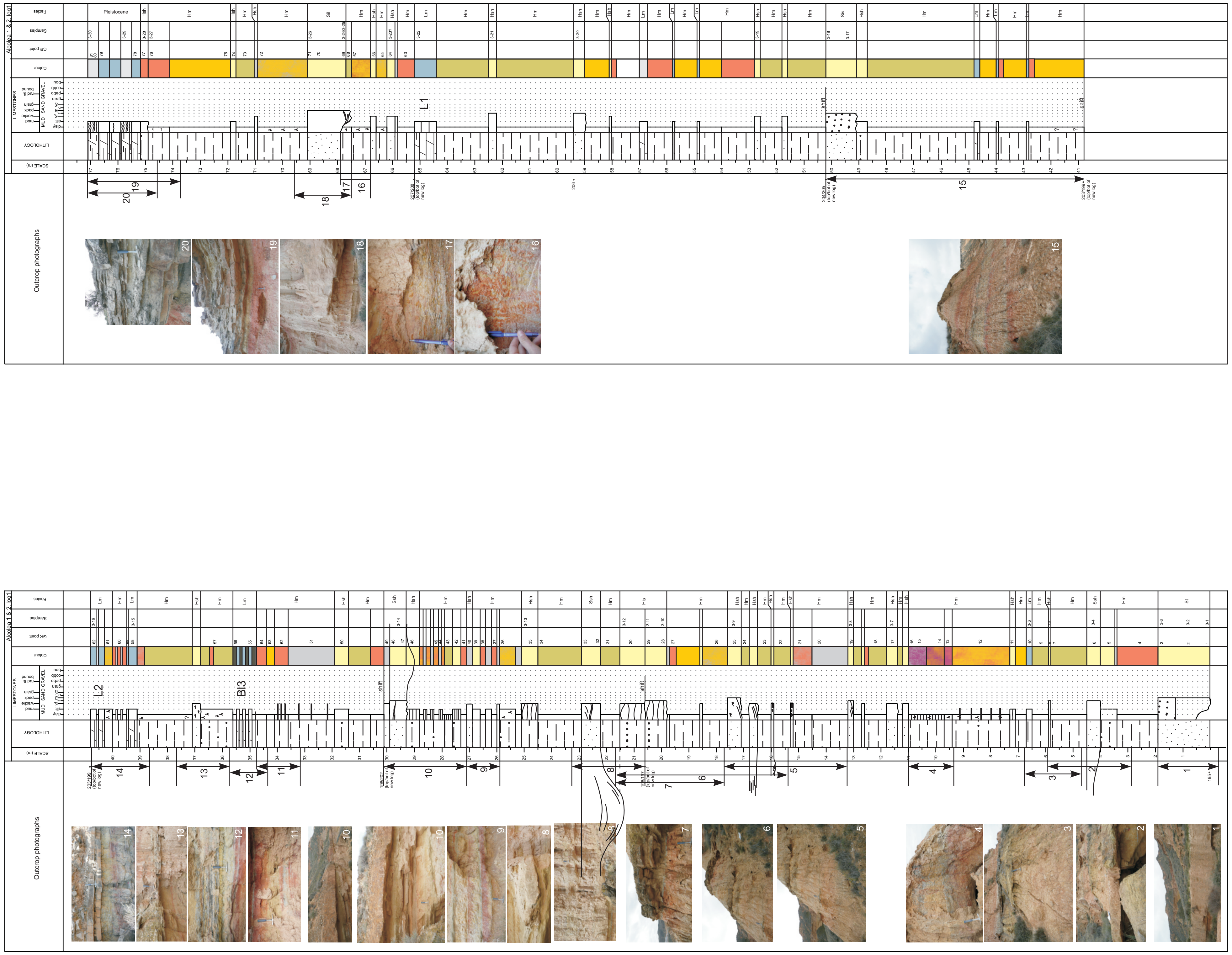

Appendix 2.6. Sedimentary log for the distal succession of the Huesca DFS deposits (Alcolea 1 and 2 outcrop panel in the Appendix 5). For legend see Appendix 2.1.

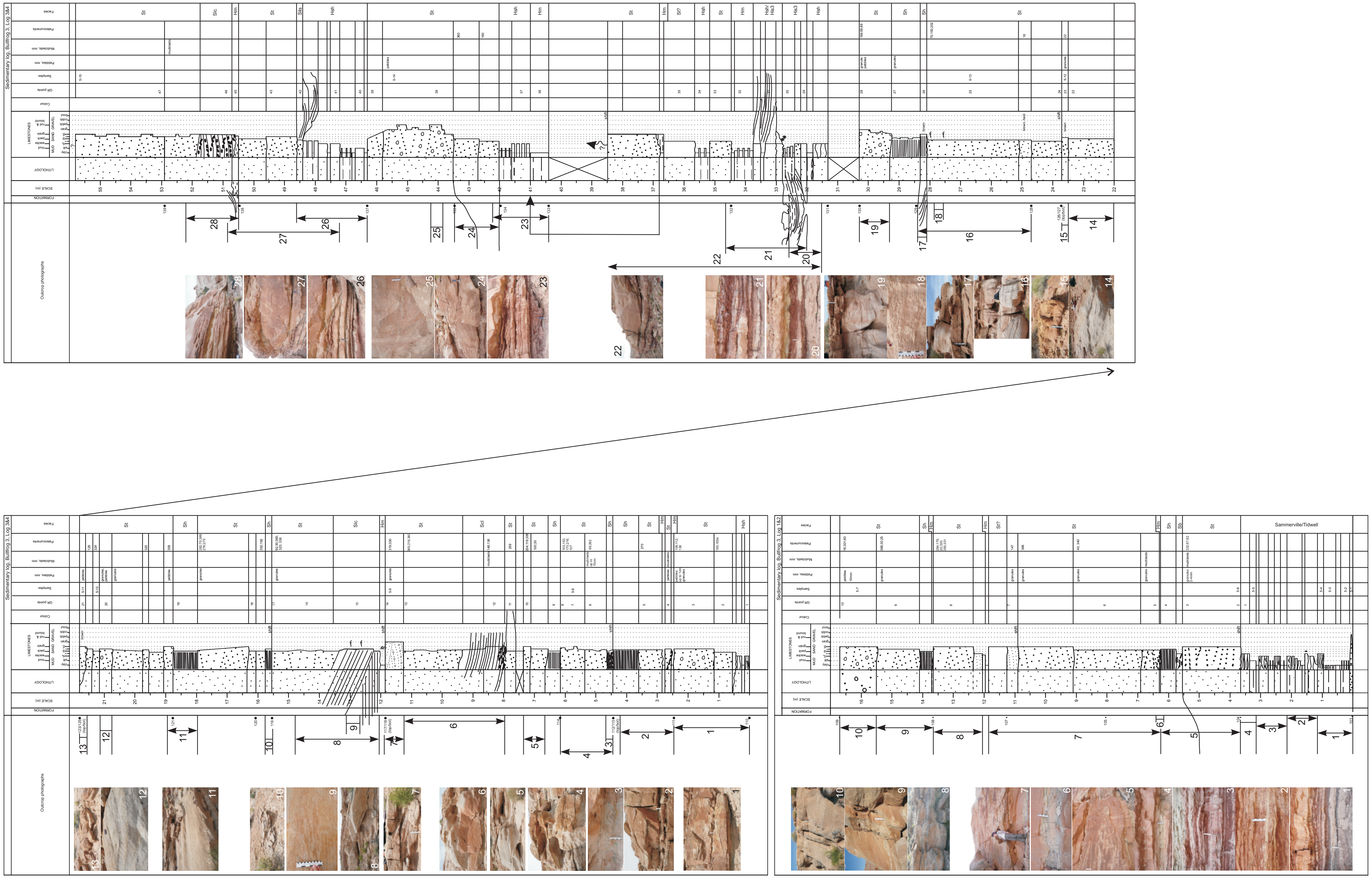

Appendix 2.7. Sedimentary log for the relatively proximal succession of the Salt Wash DFS deposits (Bullfrog 3 outcrop panel in the Appendix 5.4). For legend see Appendix 2.1.

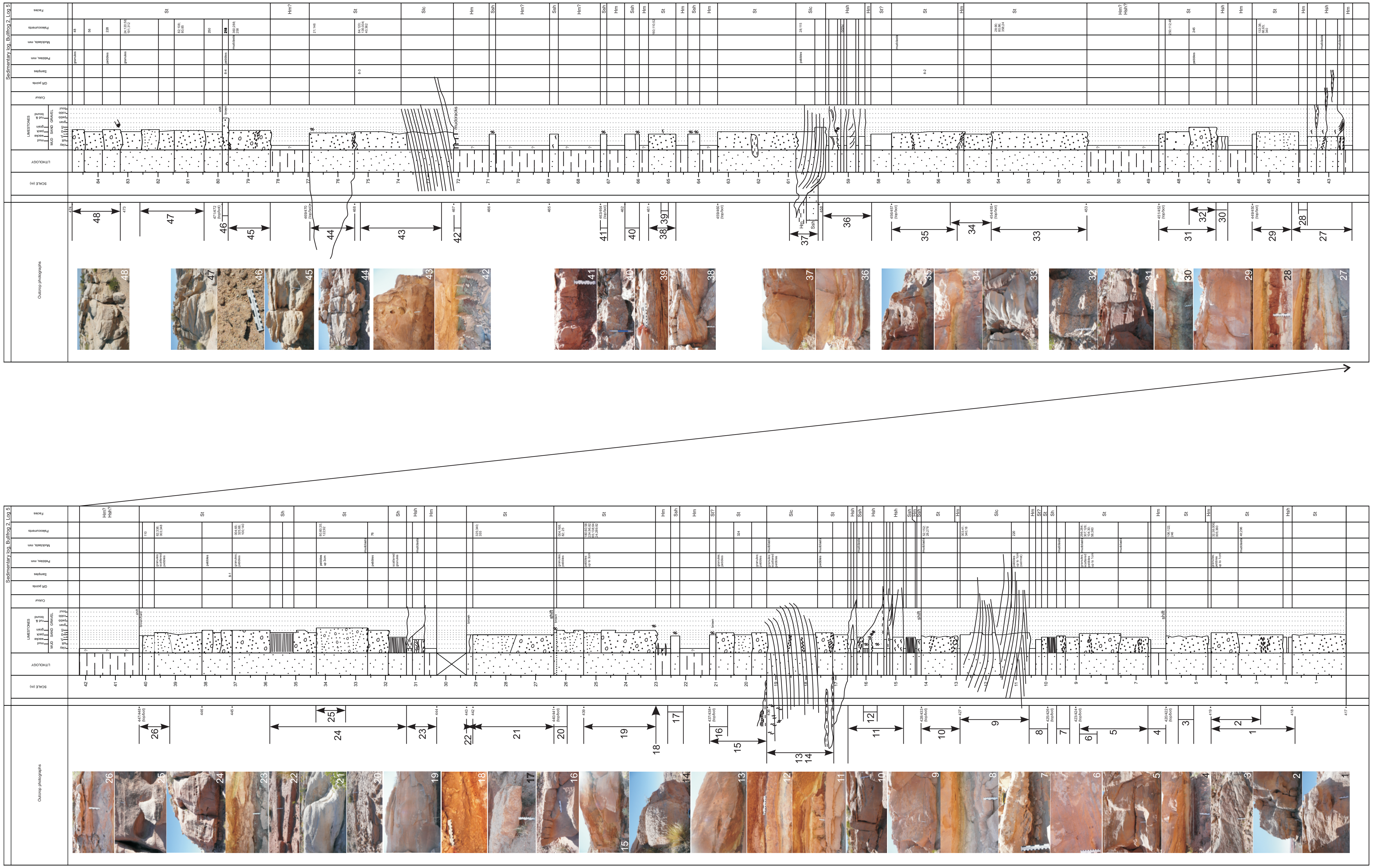

Appendix 2.8. Sedimentary log for the relatively proximal succession of the Salt Wash DFS deposits (Bullfrog 2 outcrop panel in the Appendix 5.4). For legend see Appendix 2.1.

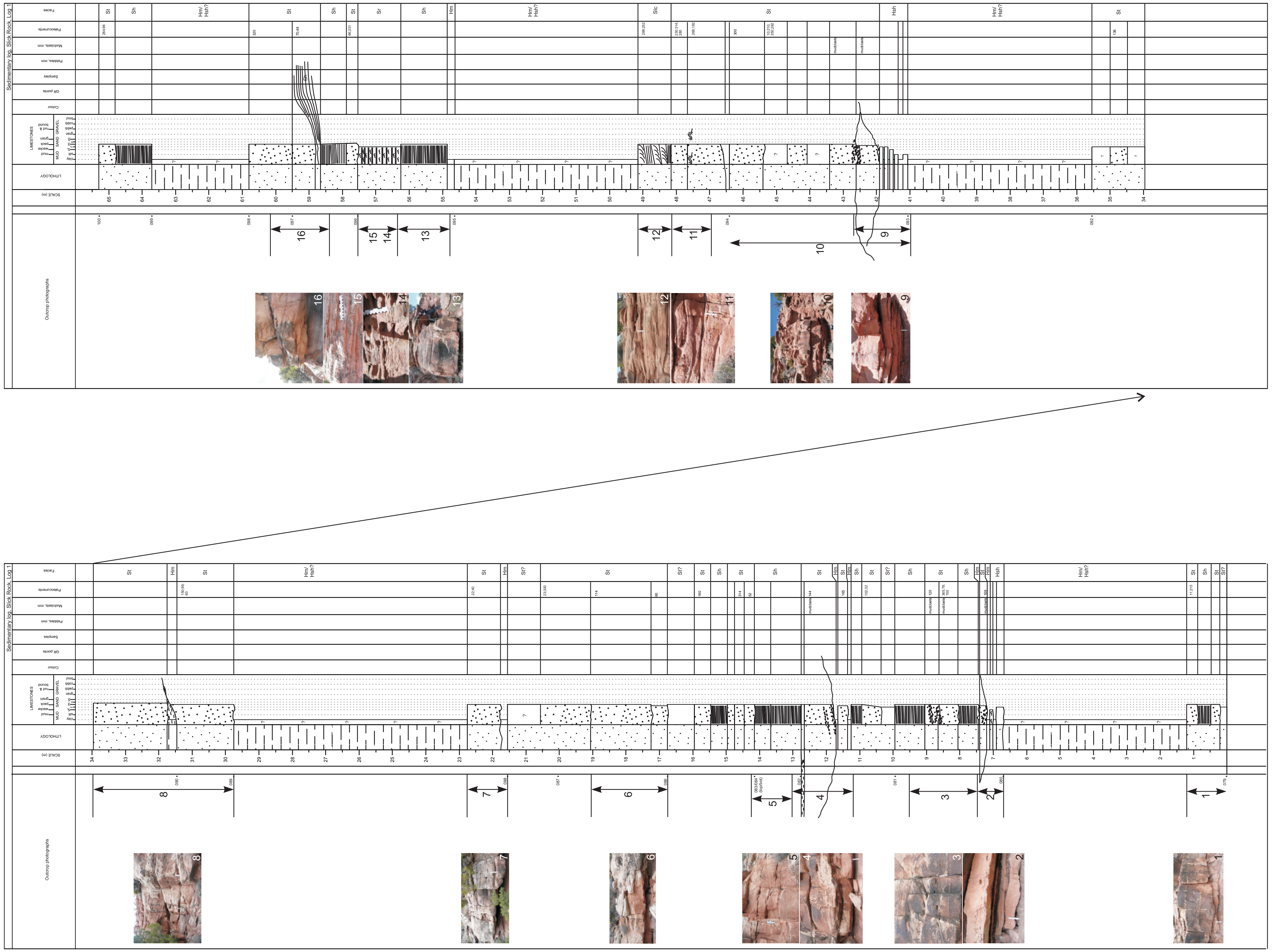

Appendix 2.9. Sedimentary log for the medial succession of the Salt Wash DFS deposits (Slick Rock outcrop panel in the Appendix 5). For legend see the Appendix 2.1. The sedimentary log is recorded in collaboration with A. Owen.

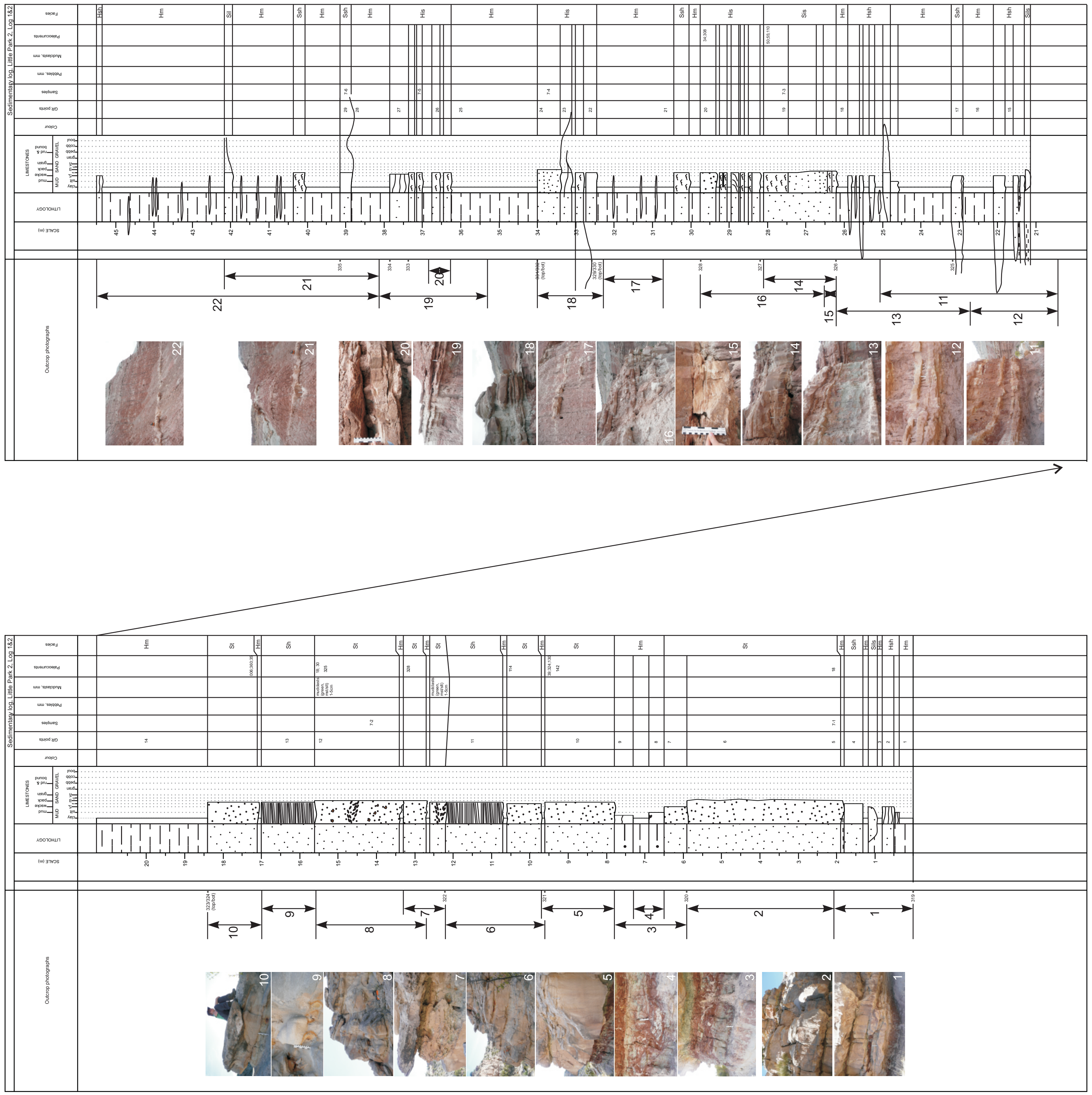

Appendix 2.10. Sedimentary log for the distal succession of the Salt Wash DFS deposits (Little Park 2 outcrop panel in the Appendix 5.6). For legend see Appendix 2.1.

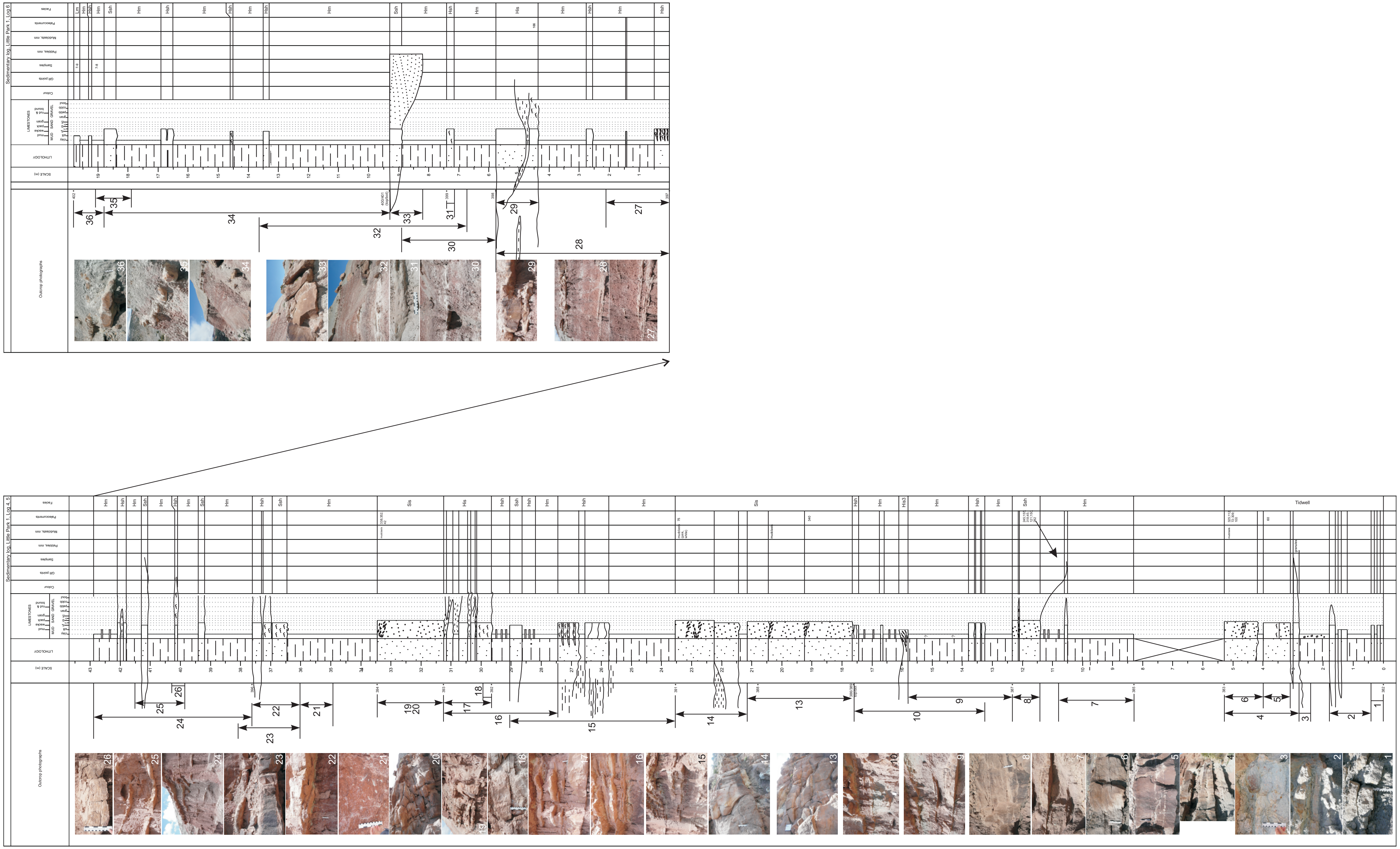

Appendix 2.11. Sedimentary log for the distal succession of the Salt Wash DFS deposits (Little Park 1 outcrop panel in the Appendix 5.6). For legend see Appendix 2.1.

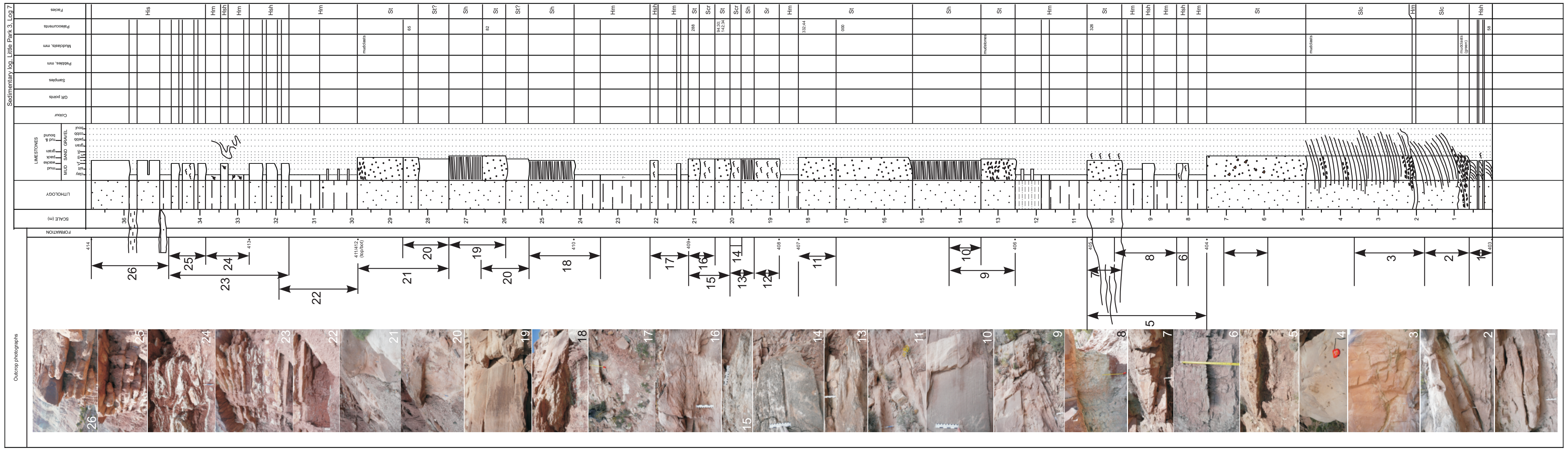

Appendix 2.12. Sedimentary log for the distal succession of the Salt Wash DFS deposits (Little Park 3 outcrop panel in the Appendix 5.6). For legend see Appendix 2.1.

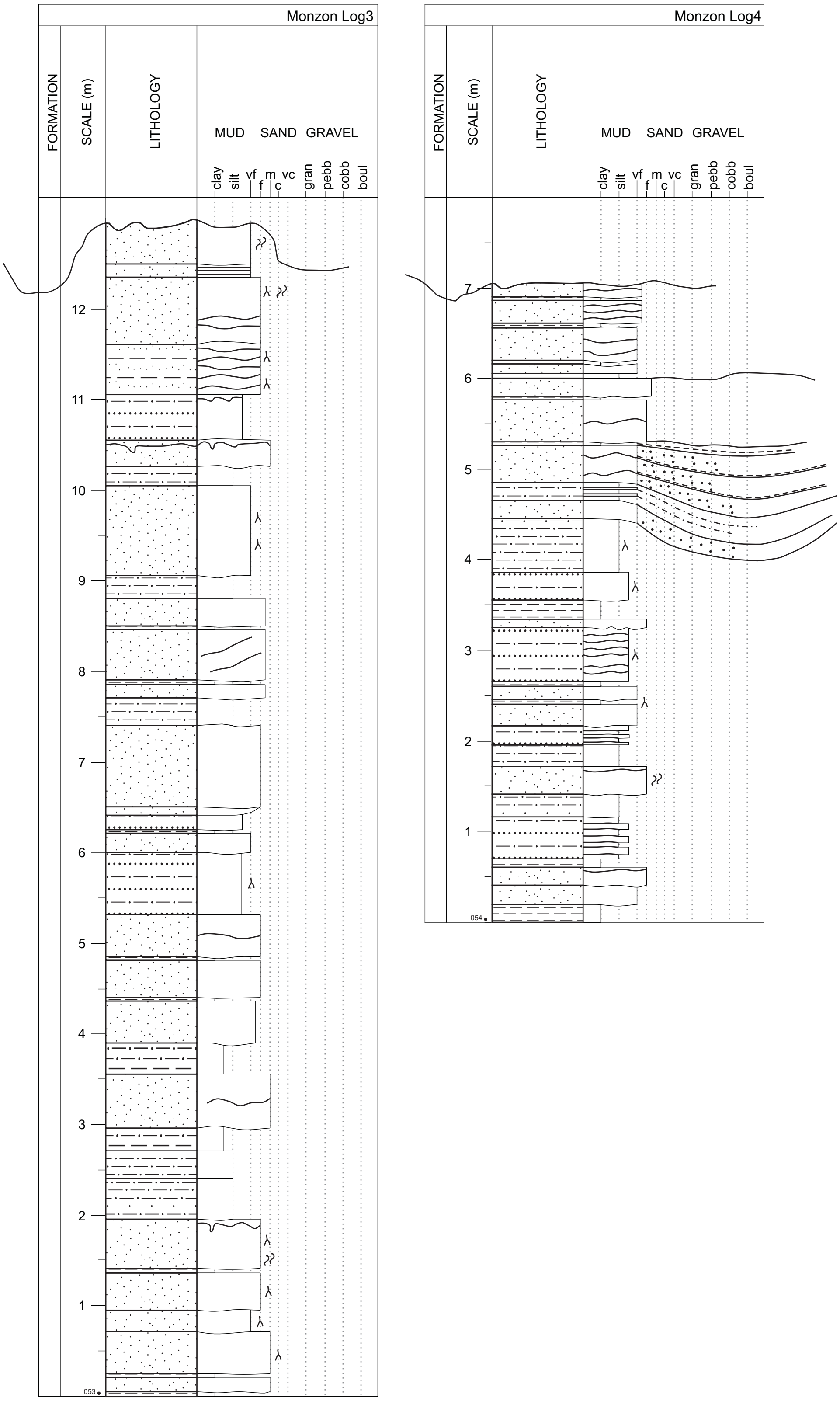

Appendix 2.13. Sedimentary log for the overbank deposits of the Huesca DFS succession (Monzon 3 and 4). For legend see Appendix 2.1.

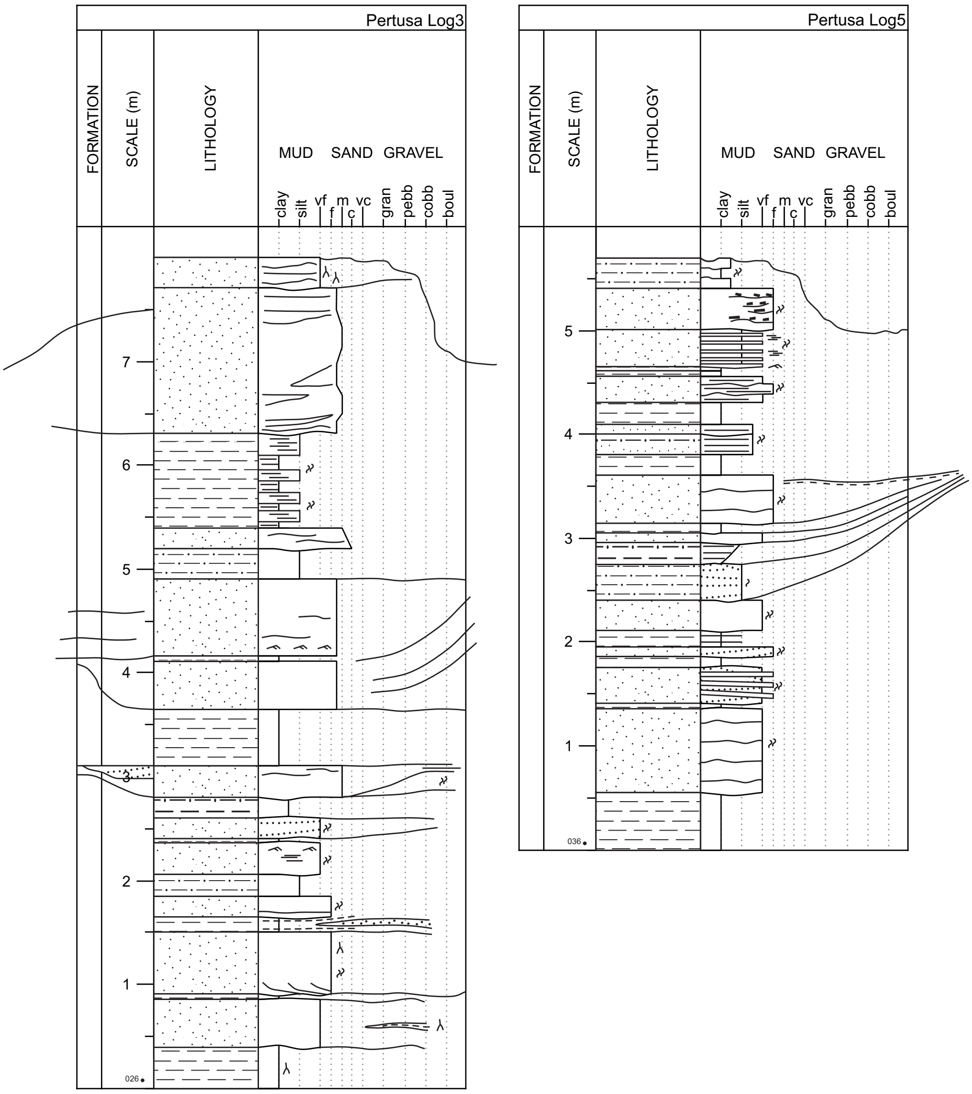

Appendix 2.14. Sedimentary log for the overbank deposits of the Huesca DFS succession (Pertusa 3 and 5). For legend see Appendix 2.1.

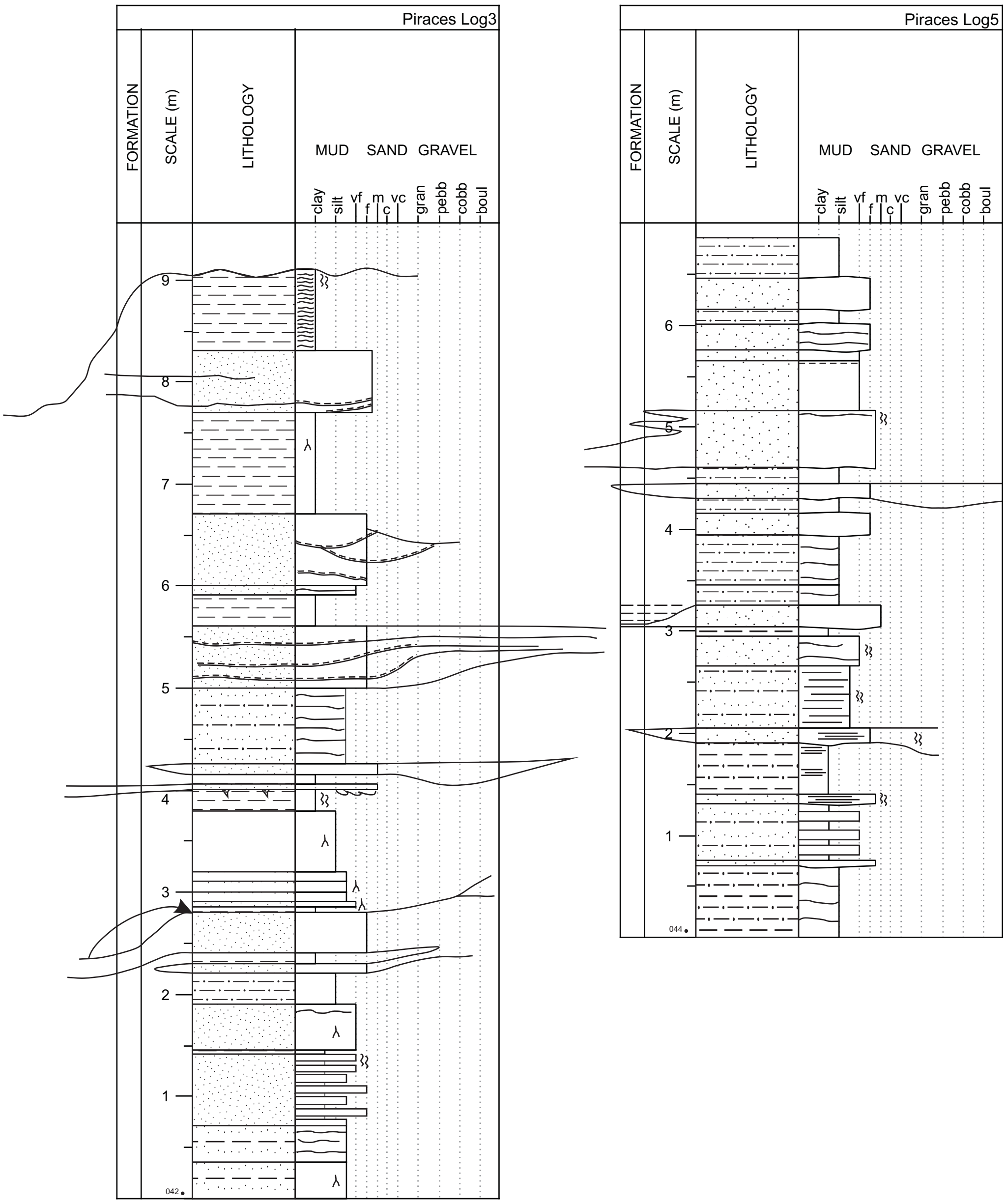

Appendix 2.15. Sedimentary log for the overbank deposits of the Huesca DFS succession (Piraces 3 and 5). For legend see Appendix 2.1.

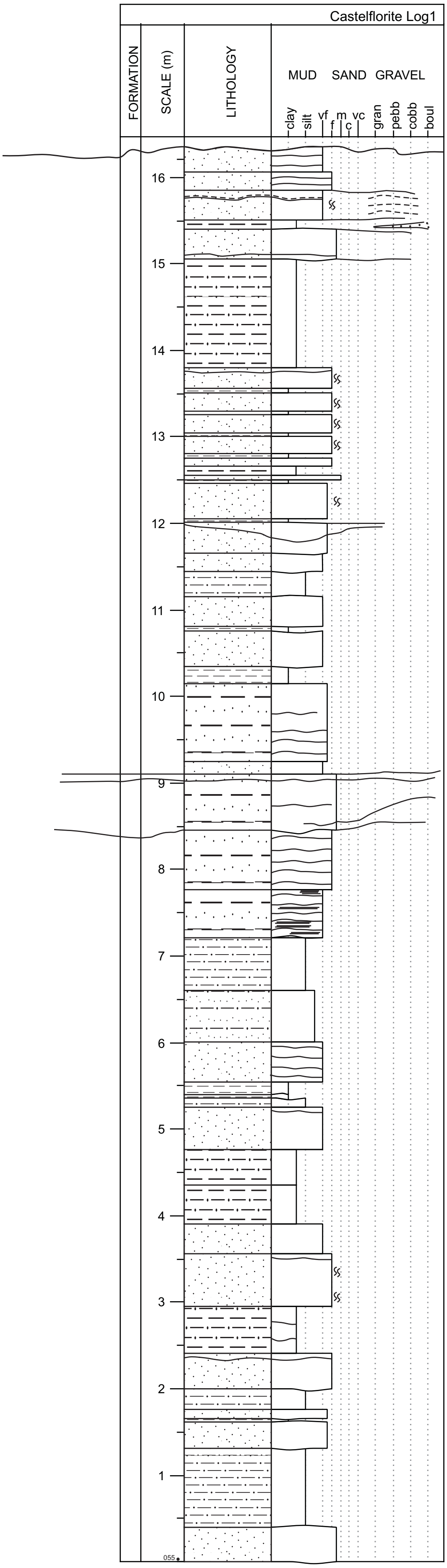

Appendix 2.16. Sedimentary log for the overbank deposits of the Huesca DFS succession (Castelflorite 1). For legend see Appendix 2.1.

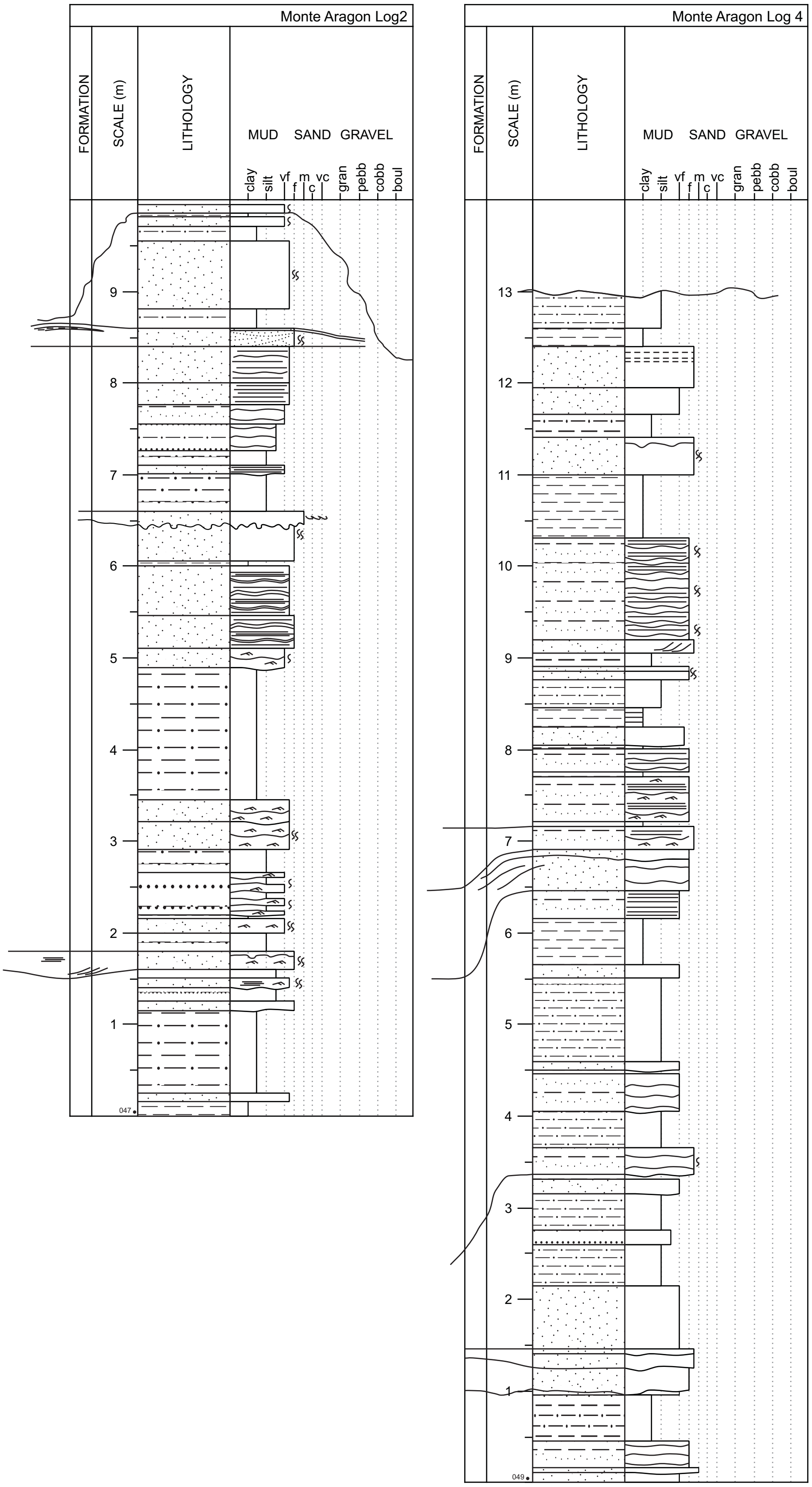

Appendix 2.17. Sedimentary log for the overbank deposits of the Huesca DFS succession (Monte Aragon 2 and 4. For legend see Appendix 2.1.

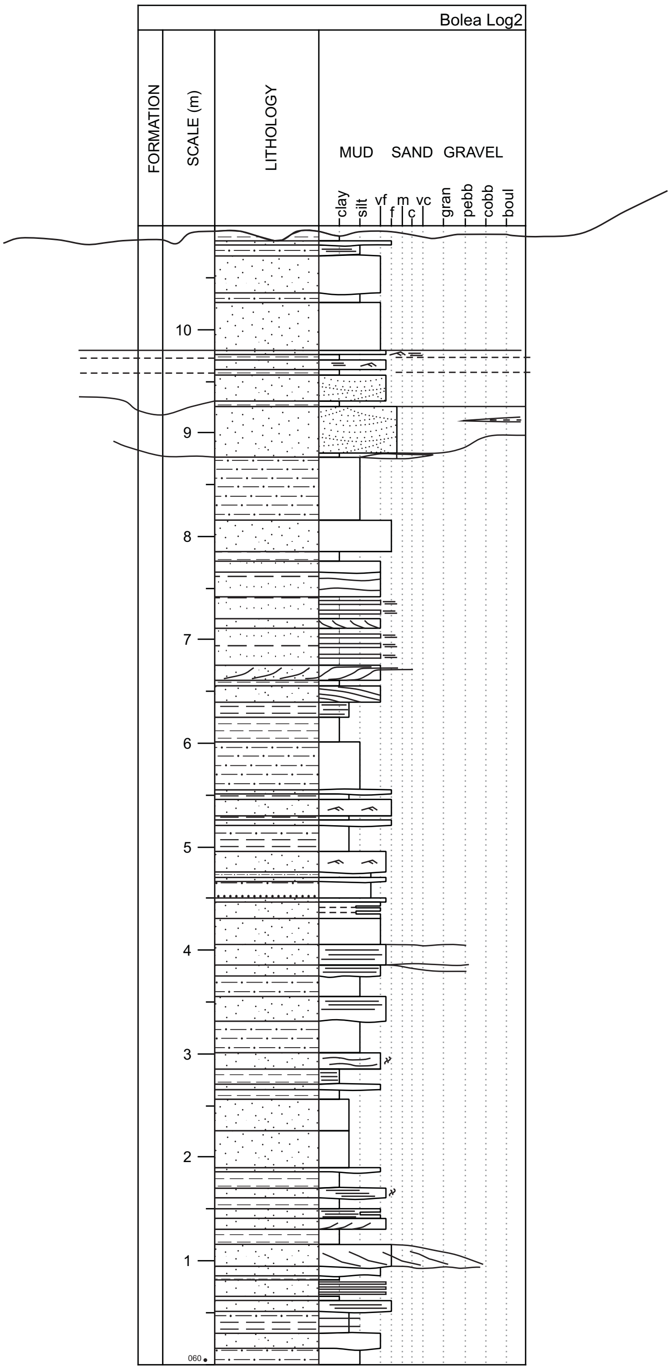

Appendix 2.18. Sedimentary log for the overbank deposits of the Huesca DFS succession (Bolea 2). For legend see Appendix 2.1.

Appendix 3:
Sandstone characteristics

Table 1. Sample analyses

DFS	Outcrop	Sample	Mean grain size	Sorting	Facies	Sandstone body type	Grain size analysis	Thin sections	Acid bath	Heavy mineral separation	XRD
Huesca	Monźon	1_5	very fine *	-	Hm	overbank					-
		1_6	medium	poorly sorted	Sis	Type2	-				
		1_8	fine	poorly sorted	Sis	Type2	-	-	-	-	
		1_13	fine	moderately sorted	Sis	Type2	-	-	-		-
		1_16	fine	poorly sorted	Sis	Type2	-	-	-	-	
		1_17	medium*	-	Sis	Type2		-			
		1_20	coarse	moderately sorted	Sis	Type2	-	-			-
		1_21	medium	poorly sorted	St	Type1	-	-	-	-	-
		1_28	very coarse*	-	St	Type1		-			
	Castelflorite	2_3	fine*	-	Ssh	Type3		-			
		2_10	fine	poorly sorted	Ssh	Type3	-	-			
		2_11	silt*	-	Hsh	Type3		-			-
		2_21	medium	poorly sorted	Hsh	Type3	-	-			-
		2_22	coarse	poorly sorted	St	Type1	-	-			
		2_26	very fine	poorly sorted	St	Type1	-	-	-	-	-
		2_27	medium	poorly sorted	St	Type1	-				
		2_32	very fine	poorly sorted	St	Type1	-	-			-
	Alcolea	3_2	fine	poorly sorted	St	Type1	-	-			-
		3_7	very fine*	-	Hsh	Type3		-			
		3_9	medium	poorly sorted	Hsh	Type3	-				
		3_10	very fine	poorly sorted	Sis	Type2	-	-			-
		3_13	very fine/silt*	-	Hsh	Type3		-			-
		3_14	fine	poorly sorted	Ssh	Type3	-	-	-		
		3_20	fine	poorly sorted	Hsh	Type3	-		-		
		3_25	fine	poorly sorted	Sil	Type1	-	-	-		
		3_27	very fine/silt*	-	Hm	overbank		-			-

DFS	Outcrop	Sample	Mean grain size	Sorting	Facies	Sandstone body type	Grain size analysis	Thin sections	Acid bath	Heavy mineral separation	XRD
Salt Wash	**Montezuma**	4_2	medium	moderately sorted	St	Type2/2	-	-			
		4_4	fine	poorly sorted	Ssh	Type3	-	-			
		4_6	medium	poorly sorted	St	Type2/2	-	-			
		4_7	fine	poorly sorted	Hsh	Type3	-	-			
		4_9	fine	moderately sorted	Ssh	Type4	-	-			
		4_10	medium	moderately sorted	St	Type2/2	-	-			
		4_11	fine*	-	Ssh	Type3		-			
	Bullfrog (Log34)	5_6	medium	moderately well sorted	St	Type2/2	-	-			
		5_9	medium	moderately well sorted	St	Type2/2	-	-			
		5_12	medium	moderately sorted	St (brown)	Type2/2	-	-			
		5_14	coarse	moderately sorted	St	Type2/2	-	-			
	Colorado National Monument (CNM)	6_1	silt*	-	Lm	alluv.plain		-			
		6_5	medium	moderately sorted	St	Type2/2	-	-			
		6_6	fine	poorly sorted	Hsh	Type3	-	-			
		6_8	fine	well sorted	Sh	Type2/2	-	-			
	Little Park (log123)	7_1	medium	poorly sorted	St	Type2/2	-	-			
		7_3	fine*	-	Sis	Type2/3		-			
		7_4	medium	moderately sorted	His	Type2	-	-			
		7_5	fine	poorly sorted	His	Type2	-	-			
		7_6	medium	moderately sorted	Ssh	Type3	-	-			
		7_7	medium	poorly sorted	Sis	Type2	-	-			
	Little Park (log456)	7_9	limestone*	-	Lm	alluv.plain		-			
	Bullfrog (log125)	8_2	medium	moderately sorted	St	Type2/2	-	-			
		8_4	coarse	moderately sorted	St(brown)	Type2/2	-				
		8_5	very coarse	poorly sorted	St	Type2/2	-	-			

* - grains size is determined visually

Table 2. Grain size fractions after seiving

DFS	Samples	Crashed sample weight, gramms	Fraction weight and weight %														SUM	SUM %	loss %
			> 2φ,g	> 2φ,%	2-1φ	2-1φ,%	1-0.5φ	1-0.5φ,%	0.5-0.25φ	0.5-0.25φ,%	0.25-0.125φ	0.25-0.125φ,%	0.125-0.063φ	0.125-0.063φ,%	< 0.063φ	< 0.063φ%			
Huesca	1_6	367.67	8.56	2.33	11.22	3.05	82.85	22.53	152.77	41.55	66.64	18.12	23.70	6.45	20.06	5.46	365.80	99.49	0.51
	1_8	231.86	0.00	0.00	1.71	0.74	4.73	2.04	6.01	2.59	77.04	33.23	85.02	36.67	54.84	23.65	229.35	98.92	1.08
	1_13	195.59	0.00	0.00	0.10	0.05	0.30	0.15	3.56	1.82	123.12	62.95	44.99	23.00	22.24	11.37	194.31	99.35	0.65
	1_16	167.61	0.00	0.00	0.23	0.14	5.63	3.36	35.43	21.14	65.50	39.08	26.50	15.81	27.42	16.36	160.71	95.88	4.12
	1_20	284.88	0.80	0.28	9.37	3.29	120.38	42.26	107.52	37.74	27.92	9.80	11.98	4.21	6.91	2.43	284.88	100.00	0.00
	1_21	234.04	0.00	0.00	0.77	0.33	9.49	4.05	90.75	38.78	85.43	36.50	25.23	10.78	18.12	7.74	229.79	98.18	1.82
	2_1	226.25	0.00	0.00	0.32	0.14	8.96	3.96	16.69	7.38	62.96	27.83	79.43	35.11	53.53	23.66	221.89	98.07	1.93
	2_21	315.91	0.00	0.00	0.00	0.00	3.84	1.22	77.73	24.61	115.51	36.56	74.19	23.48	40.38	12.78	311.65	98.65	1.35
	2_22	269.24	3.74	1.39	43.24	16.06	92.45	34.34	81.29	30.19	25.60	9.51	10.26	3.81	11.20	4.16	267.78	99.46	0.54
	2_26	187.96	0.00	0.00	0.00	0.00	0.38	0.20	2.87	1.53	54.97	29.25	59.80	31.82	64.83	34.49	182.85	97.28	2.72
	2_27	216.93	0.09	0.04	1.90	0.88	46.24	21.32	99.52	45.88	44.59	20.56	11.74	5.41	11.30	5.21	215.38	99.29	0.71
	2_32	249.18	0.00	0.00	0.36	0.14	3.84	1.54	12.36	4.96	66.82	26.82	92.97	37.31	70.70	28.37	247.05	99.15	0.85
	3_2	211.46	0.00	0.00	2.32	1.10	13.51	6.39	23.50	11.11	100.07	47.32	38.17	18.05	30.30	14.33	207.87	98.30	1.70
	3_9	376.19	0.00	0.00	0.00	0.00	19.46	5.17	109.43	29.09	167.15	44.43	51.60	13.72	27.70	7.36	375.34	99.77	0.23
	3_10	204.97	0.00	0.00	0.00	0.00	0.59	0.29	5.25	2.56	47.62	23.23	84.33	41.14	65.83	32.12	203.62	99.34	0.66
	3_14	217.68	0.00	0.00	0.61	0.28	8.67	3.98	27.38	12.58	91.44	42.01	49.96	22.95	36.76	16.89	214.82	98.69	1.31
	3_25	272.28	0.00	0.00	1.93	0.71	8.12	2.98	22.76	8.36	139.52	51.24	76.78	28.20	18.75	6.89	267.86	98.38	1.62
	3_2	249.04	0.00	0.00	0.00	0.00	0.48	0.19	47.53	19.09	107.00	42.96	68.41	27.47	24.49	9.83	247.91	99.55	0.45

DFS	Samples	Crashed sample weight, gramms	Fraction weight and weight %														SUM	SUM %	loss %
			> 2φ,g	> 2φ,%	2-1φ	2-1φ,%	1-0.5φ	1-0.5φ,%	0.5-0.25φ	0.5-0.25φ,%	0.25-0.125φ	0.25-0.125φ,%	0.125-0.063φ	0.125-0.063φ,%	< 0.063φ	< 0.063φ%			
Salt Wash	4_2	264.25	0.00	0.00	0.00	0.00	20.45	7.78	54.94	20.90	142.05	54.04	29.33	11.16	16.08	6.12	262.85	99.47	0.53
	4_4	156.49	0.00	0.00	0.00	0.00	11.36	7.32	15.56	10.02	26.89	17.32	69.08	44.50	32.36	20.84	155.25	99.21	0.79
	4_6	297.68	0.00	0.00	0.00	0.00	29.74	10.04	150.76	50.90	78.63	26.55	18.58	6.27	18.49	6.24	296.20	99.50	0.50
	4_7	226.41	0.00	0.00	0.00	0.00	22.05	9.84	19.54	8.72	78.37	34.96	77.30	34.48	26.91	12.00	224.17	99.01	0.99
	4_9	142.17	0.00	0.00	0.00	0.00	7.55	5.34	10.22	7.23	78.21	55.31	35.24	24.92	10.18	7.20	141.40	99.46	0.54
	4_10	215.26	0.00	0.00	4.95	2.31	11.56	5.39	61.52	28.66	112.82	52.56	14.16	6.60	9.63	4.49	214.64	99.71	0.29
	5_6	232.74	0.00	0.00	0.00	0.00	4.12	1.87	51.54	23.42	137.05	62.27	25.30	11.50	2.08	0.95	220.09	94.56	5.44
	5_9	290.05	0.00	0.00	0.00	0.00	34.02	12.30	174.92	63.26	60.58	21.91	6.52	2.36	0.47	0.17	276.51	95.33	4.67
	5_12	207.08	0.00	0.00	0.21	0.10	8.41	4.08	57.50	27.89	103.95	50.42	25.25	12.25	10.84	5.26	206.16	99.56	0.44
	5_14	279.57	0.00	0.00	6.53	2.35	51.57	18.55	170.83	61.44	33.50	12.05	10.45	3.76	5.16	1.86	278.04	99.45	0.55
	6_5	204.31	0.00	0.00	0.00	0.00	7.90	3.88	26.78	13.15	133.28	65.45	25.23	12.39	10.45	5.13	203.64	99.67	0.33
	6_6	103.80	0.00	0.00	0.00	0.00	16.25	15.78	14.49	14.07	17.41	16.91	31.91	30.99	22.90	22.24	102.96	99.19	0.81
	6_8	188.24	0.00	0.00	0.00	0.00	7.79	4.14	17.77	9.45	124.90	66.44	33.20	17.66	4.34	2.31	188.00	99.87	0.13
	7_1	268.64	0.00	0.00	0.00	0.00	14.26	5.33	119.17	44.55	94.38	35.28	18.87	7.05	20.80	7.78	267.48	99.57	0.43
	7_3	242.95	0.00	0.00	0.00	0.00	8.31	3.44	23.04	9.55	165.55	68.62	37.83	15.68	6.54	2.71	241.27	99.31	0.69
	7_4	289.55	0.00	0.00	0.00	0.00	16.96	5.89	155.09	53.83	89.54	31.08	17.67	6.13	8.84	3.07	288.10	99.50	0.50
	7_5	169.45	0.00	0.00	0.10	0.06	5.19	3.08	16.94	10.06	91.81	54.53	38.23	22.71	16.10	9.56	168.37	99.36	0.64
	7_6	269.91	0.00	0.00	1.96	0.73	14.92	5.58	42.41	15.86	151.81	56.76	43.58	16.30	12.76	4.77	267.44	99.08	0.92
	7_7	273.88	0.00	0.00	0.00	0.00	22.39	8.58	38.76	14.85	135.67	51.99	56.47	21.64	7.68	2.94	260.97	95.29	4.71
	8_2	330.71	0.00	0.00	2.21	0.67	25.51	7.75	135.26	41.09	139.78	42.46	21.76	6.61	4.66	1.42	329.18	99.54	0.46
	8_4	190.07	0.00	0.00	126.90	67.99	28.86	15.46	14.48	7.76	9.60	5.14	3.88	2.08	2.93	1.57	186.65	98.20	1.80
	8_5	209.64	0.00	0.00	7.25	3.46	49.57	23.67	103.85	49.59	40.83	19.50	6.36	3.04	1.55	0.74	209.41	99.89	0.11

Table 3. Results of grain size analysis based on graphic formular (Folk & Ward, 1957)

DFS	Sample	Percentiles					mean, φ	mean	sorting (formula Folk, 1975)	sorting (Harrel, 1984)
Huesca		**5**	**16**	**50**	**84**	**95**				
	1_6	-0.65	-0.05	1.05	2.30	3.80	1.10	medium	1.26	poorly sorted
	1_8	1.35	1.80	2.80	4.23	5.15	2.94	fine	1.18	poorly sorted
	1_13	1.55	1.70	2.27	3.30	4.27	2.42	fine	0.81	moderately sorted
	1_16	0.60	1.10	2.15	4.00	5.40	2.42	fine	1.45	poorly sorted
	1_20	-0.45	-0.20	0.65	1.50	2.85	0.65	coarse	0.93	moderately sorted
	1_21	0.55	0.80	1.70	2.90	4.65	1.80	medium	1.15	poorly sorted
	2_10	0.65	1.70	2.80	4.30	5.20	2.93	fine	1.34	poorly sorted
	2_21	0.70	0.12	2.16	3.40	4.95	1.89	medium	1.46	poorly sorted
	2_22	-1.28	-0.63	0.45	1.70	3.40	0.51	coarse	1.29	poorly sorted
	2_26	1.65	1.97	3.10	4.70	5.45	3.26	very fine	1.26	poorly sorted
	2_27	-0.30	0.20	1.15	2.27	3.85	1.21	medium	1.15	poorly sorted
	2_32	1.15	1.80	2.95	4.40	5.20	3.05	very fine	1.26	poorly sorted
	3_2	0.12	1.25	2.20	3.50	5.00	2.32	fine	1.30	poorly sorted
	3_9	0.50	0.85	1.85	2.85	4.10	1.85	medium	1.05	poorly sorted
	3_10	1.60	2.07	3.10	4.55	5.20	3.24	very fine	1.17	poorly sorted
	3_14	0.60	1.45	2.53	3.75	5.05	2.58	fine	1.25	poorly sorted
	3_20	0.75	1.30	2.23	3.30	4.50	2.28	fine	1.07	poorly sorted
	3_25	0.15	1.07	2.25	3.25	4.50	2.19	fine	1.20	poorly sorted

DFS	Sample	Percentiles					mean, φ	mean	sorting (formula Folk, 1975)	sorting (Harrel, 1984)
Salt Wash	4_2	0.20	0.95	1.80	2.50	3.75	1.75	medium	0.93	moderately sorted
	4_4	0.20	1.35	2.80	4.00	5.05	2.72	fine	1.40	poorly sorted
	4_6	0.00	0.60	1.30	2.40	3.90	1.43	medium	1.04	poorly sorted
	4_7	0.00	1.20	2.45	3.40	4.70	2.35	fine	1.26	poorly sorted
	4_9	0.40	1.55	2.20	3.15	4.15	2.30	fine	0.97	moderately sorted
	4_10	0.00	0.80	1.75	2.45	3.45	1.67	medium	0.94	moderately sorted
	5_6	0.60	1.15	1.85	2.40	3.15	1.80	medium	0.70	moderately well sorted
	5_9	0.15	0.55	1.15	1.85	2.35	1.18	medium	0.66	moderately well sorted
	5_12	0.55	0.95	1.70	2.60	3.50	1.75	medium	0.86	moderately sorted
	5_14	-0.35	0.30	1.00	1.65	2.70	0.98	coarse	0.80	moderately sorted
	6_5	0.6	1	2	2.65	3.5	1.88	medium	0.85	moderately sorted
	6_6	-0.2	0.5	2.6	4.05	5.05	2.38	fine	1.68	poorly sorted
	6_8	0.6	1.55	2.1	2.7	3.5	2.12	fine	0.73	moderately sorted
	7_1	0.25	0.75	1.50	2.45	4.25	1.57	medium	1.03	poorly sorted
	7_4	0.35	0.70	1.30	2.25	3.20	1.42	medium	0.82	moderately sorted
	7_5	0.70	1.55	2.20	3.25	4.50	2.33	fine	1.00	poorly sorted
	7_6	0.25	1.10	2.00	2.80	3.50	1.97	medium	0.92	moderately sorted
	7_7	0.10	1.00	2.00	2.80	3.90	1.93	medium	1.03	poorly sorted
	8_2	0.05	0.70	1.50	2.25	2.95	1.48	medium	0.83	moderately sorted
	8_4	-1.40	-1.25	-0.80	0.60	2.25	-0.48	very coarse	1.02	poorly sorted
	8_5	-0.40	0.05	1.00	1.85	2.40	0.97	coarse	0.87	moderately sorted

Table 4. Concentration (%) of main grain classes for the Huesca DFS sandstones (results from point counting)

DFS	Outcrop	Samples	Qm	Qs	Qp	P	F	Schists	Limestones	Sandstones
Huesca	Monźon	1_13	11.2	2.6	4.6	0.3	3.6	64.7	3.6	0.3
		1_16	15.7	4.9	8.5	1.3	6.9	42	10.8	2.3
		1_17	11.5	5.3	5.6	2	6.3	51	7.2	4.9
		1_20	14.7	8	2	2	1.7	47.5	5.4	14.4
		1_21	18	7.9	6	0.9	4.4	39.2	13.9	0.9
		1_28	21.7	6.3	6.3	1.3	4.3	34.9	10.9	8.6
		Average %	15.5	5.8	5.5	1.3	4.5	46.5	8.6	5.2
		Max %	21.7	8	8.5	2	6.9	64.7	13.9	14.4
		Min %	11.2	2.6	2	0.3	1.7	34.9	3.6	0.3
	Castelflorite	2_3	15.5	2.6	6.3	1.6	3.9	47.7	8.6	3.3
		2_10	18.5	7.3	1.3	0	2.3	44	12.3	2.3
		2_21	17.9	4.7	3.3	1.7	2.7	47.2	11	4.3
		2_22	9.5	8.8	4.2	6.2	5.9	26.1	19.3	14.4
		2_26	18.6	3.3	1.3	0.3	2.9	46.7	13.4	1.3
		Average %	16	5.3	3.3	2.5	3.5	42.4	12.9	5.1
		Max %	18.6	8.8	6.3	6.2	5.9	47.7	19.3	14.4
		Min %	9.5	2.6	1.3	0.3	2.3	26.1	8.6	1.3
	Alcolea	3_2	16.3	2	2	1.7	6	47.7	11	5
		3_10	17.4	2.7	3.7	1.3	2.7	54.8	5	1
		3_14	10.3	4.3	2.7	0	2.3	65.3	10.3	0.7
		3_25	12.3	5	4.7	1.3	3.1	55.7	7.9	2.5
		Average %	14.1	3.5	3.3	1.4	3.5	55.9	8.6	2.3
		Max %	17.4	5	4.7	1.7	6	65.3	11	5
		Min %	10.3	2	2	1.3	2.3	47.7	5	0.7

DFS	Outcrop	Samples	Fe oxides	Igneous	Mica	Heavy minerals	Chert	Quartzite
Huesca	**Monźon**	1_13	2	0.7	5	0	1	0.3
		1_16	2	1	3.9	0.3	0.3	0
		1_17	1	1	2	0.7	0	1.6
		1_20	1	1.3	1.7	0	0.3	0
		1_21	2.2	1.3	1.6	0	1.3	2.2
		1_28	2.3	0.3	2	0.3	1	0
		Average %	1.7	0.9	2.7	0.4	0.8	1.4
		Max %	2.3	1.3	5	0.7	1.3	2.2
		Min %	1	0.3	1.6	0.3	0.3	0.3
	Castelflorite	2_3	2.3	0	3.3	0.3	1.3	3.3
		2_10	2.3	0	6.6	2.3	0.7	0
		2_21	2	0.7	4	0	0.7	0
		2_22	2	1.6	2	0	0	0
		2_26	2	0	6.5	0.7	0	2.9
		Average %	2.1	1.1	4.5	1.1	0.9	3.1
		Max %	2.3	1.6	6.6	2.3	1.3	3.3
		Min %	2	0.7	2	0.3	0.7	2.9
	Alcolea	3_2	2	0.7	4.3	0	1.3	0
		3_10	2.3	0	6	1	0.7	1.3
		3_14	2.3	0	1.3	0	0.3	0
		3_25	4.4	0.6	1.6	0	0.6	0.3
		Average %	2.8	0.6	3.3	1	0.7	0.8
		Max %	4.4	0.7	6	1	1.3	1.3
		Min %	2	0.6	1.3	1	0.3	0.3

Table 5. Concentrations (%) of main minerals determined with X-ray diffraction for the Huesca sandstones

DFS	Sample / Mineral	Concentration,%							
		Kaolinite	Orthoclase	Abite	Muscovite	Chorite	Quartz	Calcite	Gypsum
Huesca	1-5	1.30	2.20	5.80	17.60	2.50	35.80	33.40	1.50
	1-13	0.70	1.80	6.40	22.30	1.00	50.60	16.20	1.00
	1-20	0.60	0.00	8.40	24.80	0.20	54.30	11.30	0.40
	1-21	0.30	1.70	7.20	21.00	0.20	53.10	16.60	0.00
	2-11	0.20	1.10	1.90	12.90	0.10	27.90	55.60	0.20
	2-21	0.20	1.10	5.70	18.20	0.20	41.40	32.80	0.30
	2-26	0.20	0.90	11.20	14.80	0.20	45.10	27.60	0.00
	2-32	0.20	3.30	5.00	17.60	0.20	40.90	32.80	0.10
	3-2	1.20	2.10	6.10	8.30	0.10	38.50	13.70	30.10
	3-10	0.40	0.00	7.10	16.00	0.10	41.90	33.40	1.10
	3-13	1.10	0.00	7.10	37.50	0.50	41.40	11.90	0.50
	3-27	0.10	2.90	6.60	14.90	0.10	31.60	43.80	0.00
	Average	0.54	1.43	6.54	18.83	0.45	41.88	27.43	0.46
	Max	1.30	3.30	11.20	37.50	2.50	54.30	55.60	30.10
	Min	0.10	0.00	1.90	8.30	0.10	27.90	11.30	0.00

Table 6. Carbonate content in the Huesca sandstones

Samples	Weight of fraction 0.25-0.063φ	Weight , g after acid bath	Weight, g of disolved carbonate
1_8	162.06	99.11	38.84
1_13	168.11	124.83	25.75
1_16	92.00	66.45	27.77
1_21	110.66	88.67	19.87
2_26	114.77	70.14	38.89
3_2	138.24	90.04	34.87
3_14	141.40	97.42	31.10
3_25	216.30	135.29	37.45

Table 7. Heavy mineral content in the Huesca sandstones

Samples	Sample weight, g	Light fraction weight, g	Light fraction weight, %	Heavy fraction weight, g	Heavy fraction weight, %
1_8	74.21	72.45	97.63	0.98	1.32
1_16	62.90	61.47	97.73	0.80	1.27
1_21	73.63	71.85	97.58	1.47	2.00
2_26	68.98	67.00	97.13	1.38	2.00

Table 8. Porosity determined from impregnated thin sections

DFS	Outcrop	Sample No.	Porosity range		Grain size	Facies
			Maximum	Minimum		
Huesca	Monźon	1_1	4.8	3.1	f	Sis
		1_8	6.0	3.8	f	Sis
		1_13	6.4	4.1	f	Sis
		1_17	4.4	2.9	vc/g	Sis
		1_20	10.2	6.6	c	Sis
		1_21	14.5	9.8	m	St
		1_28	7.9	5.7	vc	St
	Castelflorite	2_3	0.9	0.4	f	Hsh
		2_10	2.0	1.0	f	Ssh
		2_11	2.3	0.9	silt/vf	Hsh
		2_21	4.7	2.7	m	Hsh
		2_22	6.1	5.5	m	St
		2_26	5.8	3.4	vf	St
		2_32	2.9	1.6	vf	St
	Alcolea	3_2	5.0	2.8	f	St
		3_7	2.4	1.3	vf	Hsh
		3_10	5.8	3.0	vf	Sis
		3_13	2.8	1.3	vf	Hsh
		3_14	10.1	6.2	f	Hsh
		3_25	10.0	5.7	f	Sil
		3_27	1.4	0.7	clay	Hm

DFS	Outcrop	Sample No.	Porosity range		Grain size	Facies
			Maximum	Minimum		
Salt Wash	Bullfrog	5_6	39.1	36.8	m	St
		5_9	21.6	15.5	c	St
		5_12	5.0	3.0	m	St
		5_14	12.8	10.1	c	St
		8_2	-	25.1	m	St
		8_4	-	3.4	granules	St
		8_5	26.7	19.4	vc	St
	Montezuma	4_2	-	19.1	m/f	St
		4_7	-	5.6	vf	Hsh
		4_11	24.9	3.8	m/f	Ssh
	CNM and Little Park	6_5	-	22.5	f/m	St
		6_6	-	13.9	vf	Hsh
		7_1	-	29.6	m	St
		7_3	34.3	29.4	f	Sis
		7_4	19.0	17.0	m/c	His
		7_5	-	7.5	f	His
		7_6	11.9	10.4	f	Ssh
		7_7	12.8	10.3	f/m	Sis

Appendix 5:
Outcrop photo panels (see pocket at the back of the thesis)

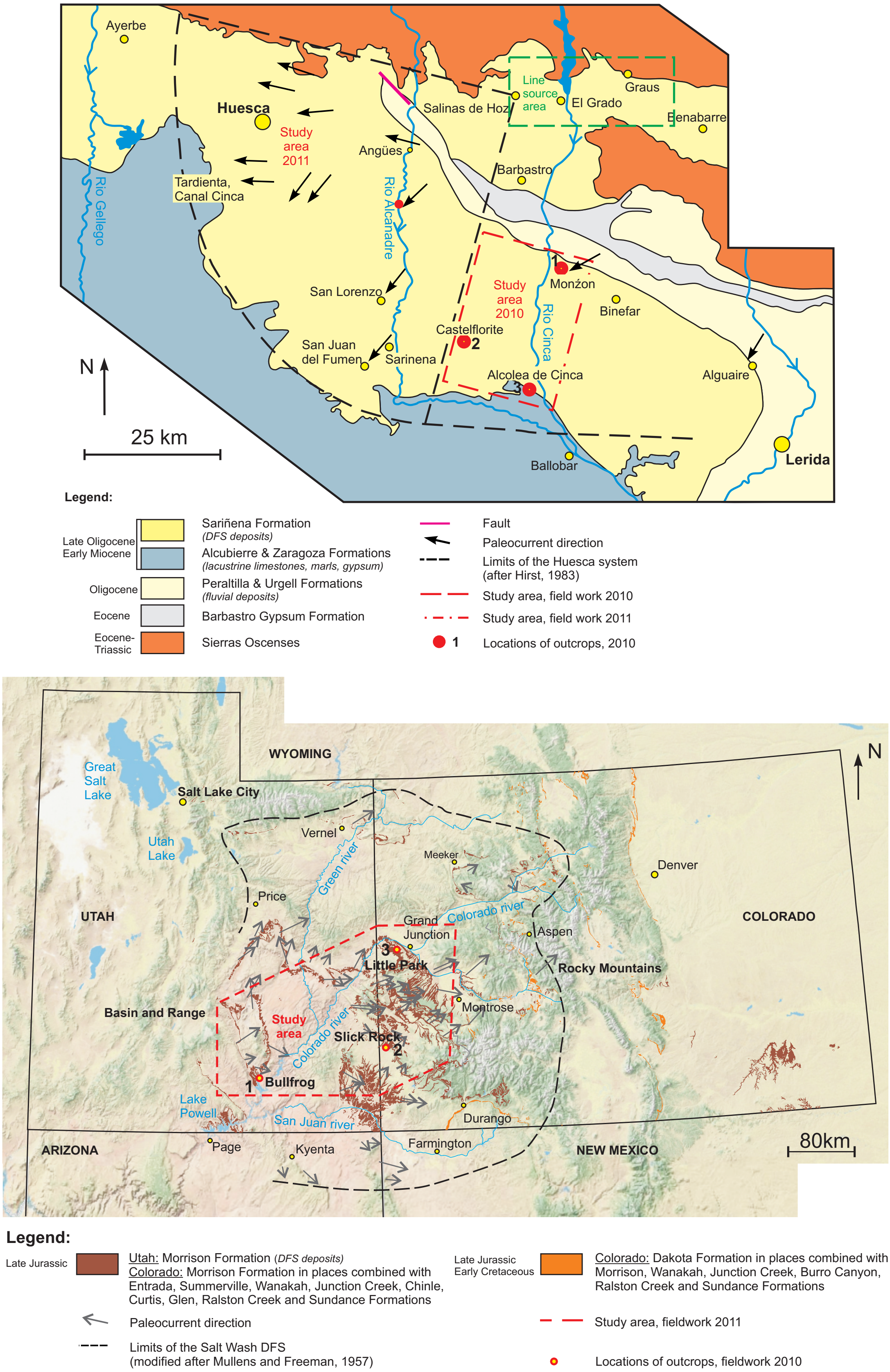

Locations of the outcrop panels documented in Spain (top) and USA (bottom) and presented in Appendices 5.1 - 5.6: Monzon (5.1), Castelflorite (5.2), Alcolea (5.3), Bullfrog (5.4), Slick Rock (5.5) and Little Park (5.6). The panels are folded in the back pocket of the thesis (6 pages).

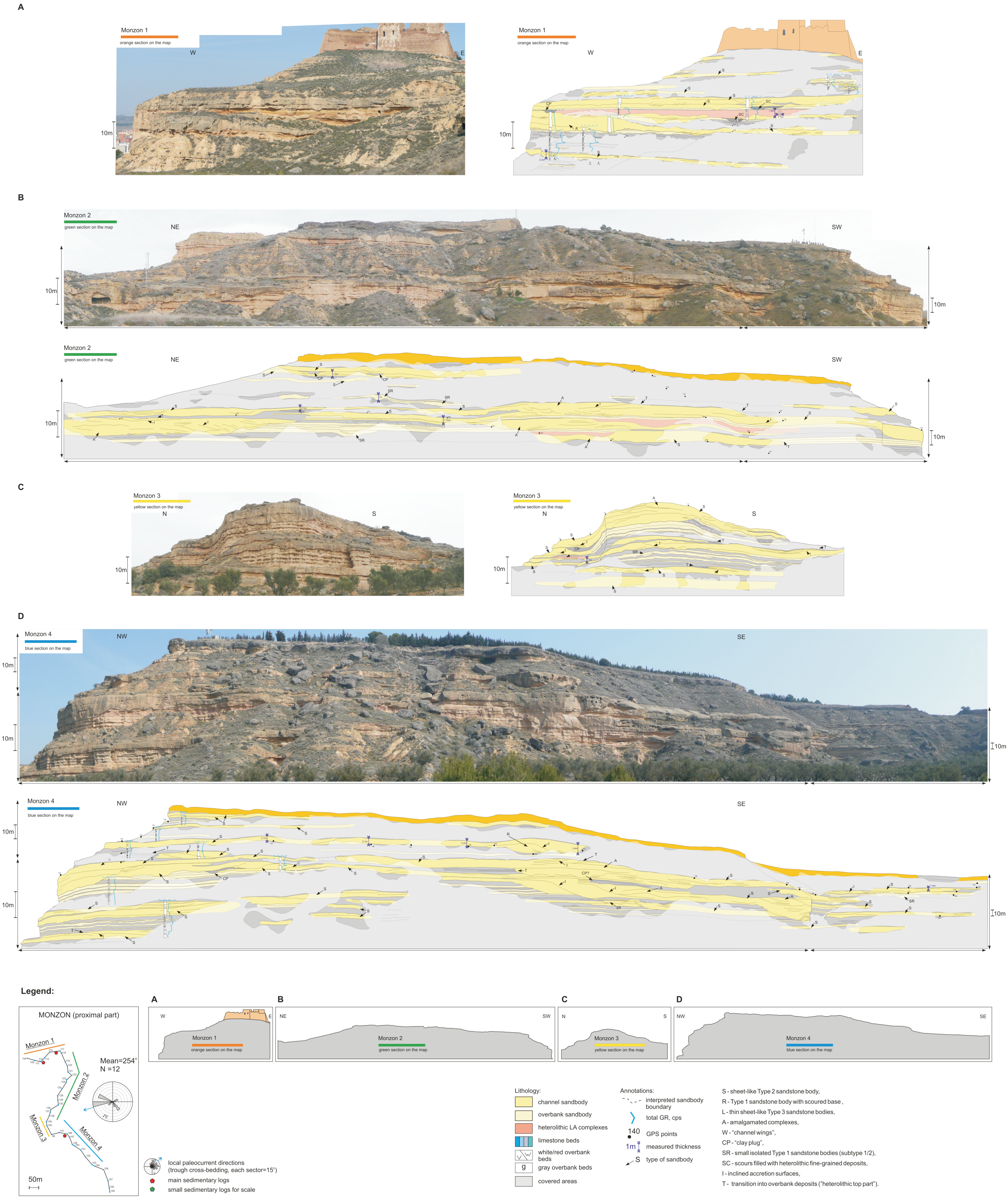

Appendix 5.1. Outcrop photo panels and their interpretation, Monzon outcrop of the relatively proximal Huesca DFS succession.
Map and schematic outcrop diagram show location and orientation of the panels relative to each other and relative to average palaeocurrent direction.

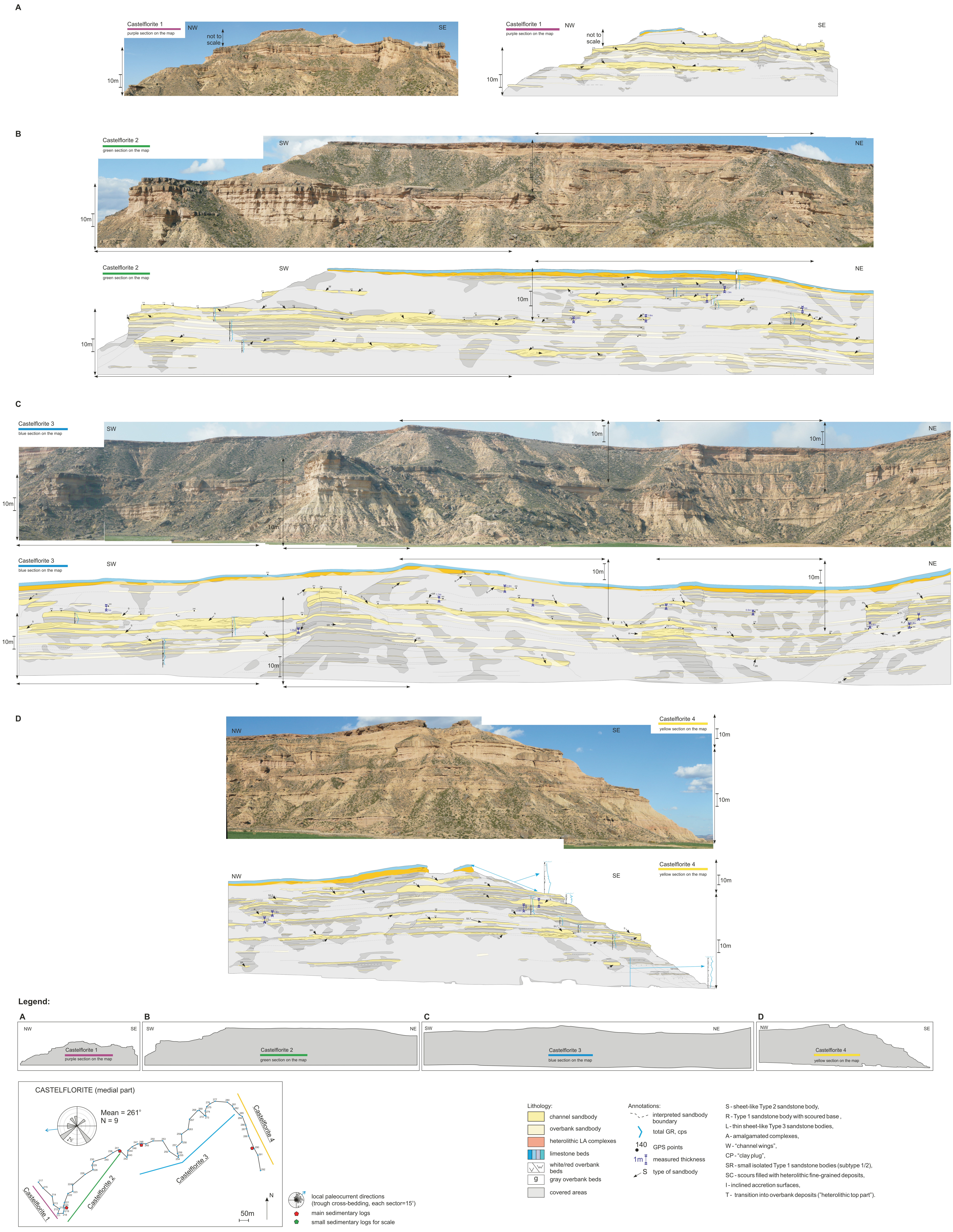

Appendix 5.2. Outcrop photo panels and their interpretation, Castelflorite outcrop of the medial Huesca DFS succession.
Map and schematic outcrop diagram show location and orientation of the panels relative to each other and relative to average palaeocurrent direction.

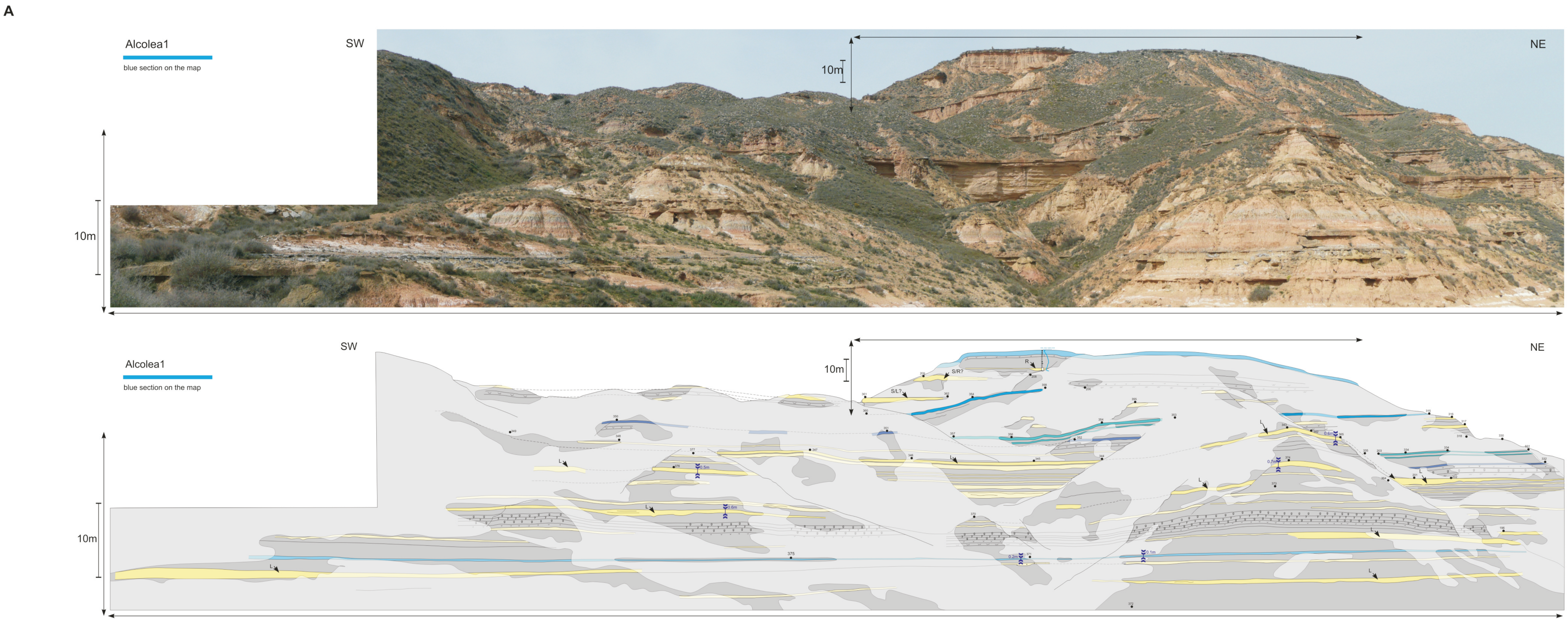

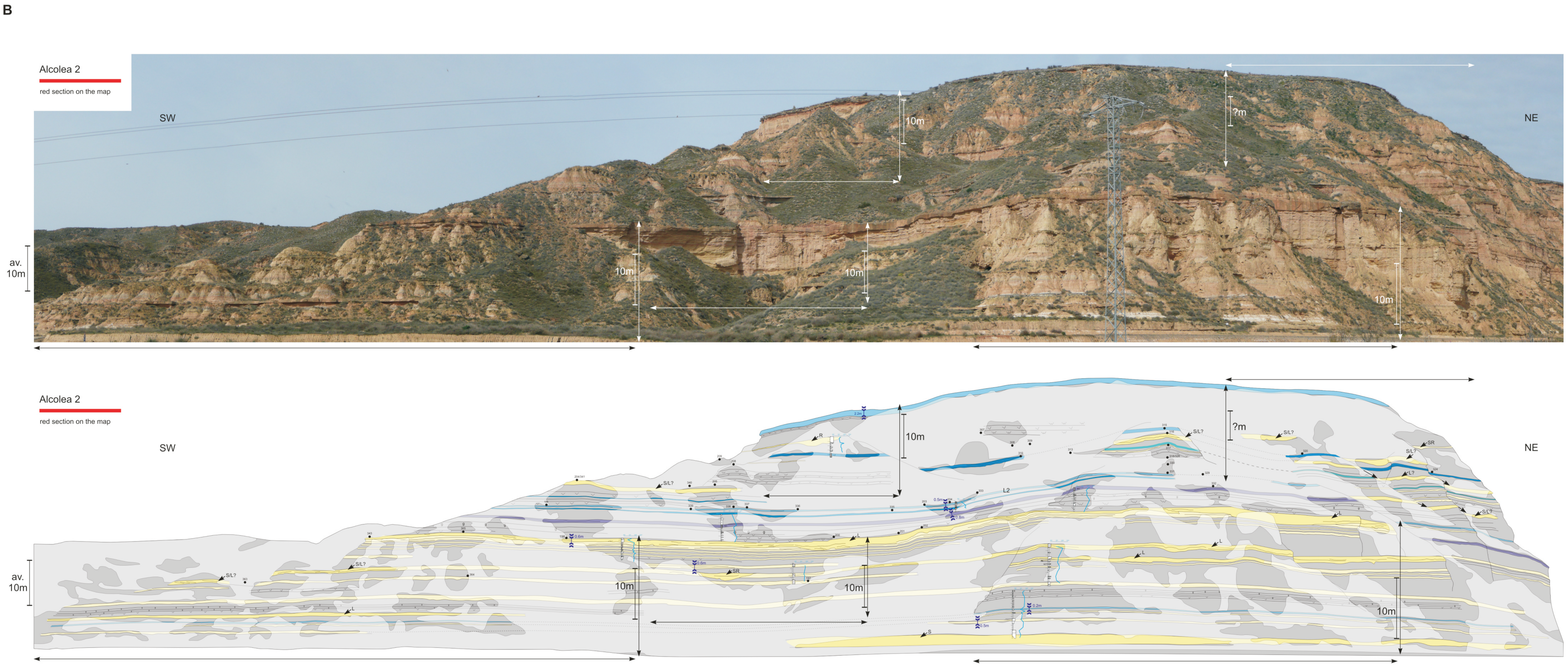

Legend:

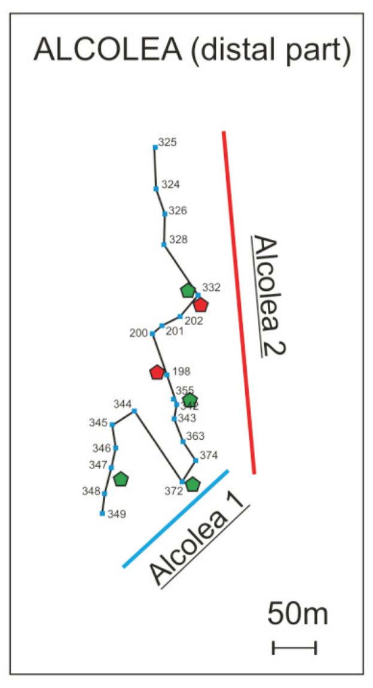

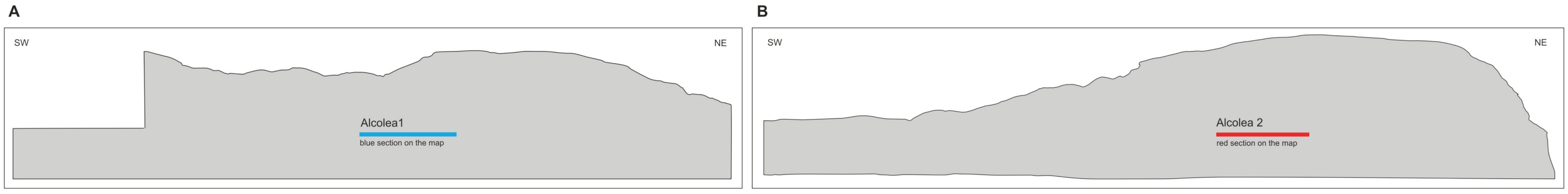

- main sedimentary logs
- small sedimentary logs for scale

Lithology:

🟨	channel sandbody
▭	overbank sandbody
🟧	heterolithic LA complexes
🟦	limestone beds
▨	white/red overbank beds
g	gray overbank beds
▭	covered areas

Annotations:

- - -	interpreted sandbody boundary
〉	total GR, cps
140 ●	GPS points
1m	measured thickness
↙ S	type of sandbody

S - sheet-like Type 2 sandstone body,
R - Type 1 sandstone body with scoured base ,
L - thin sheet-like Type 3 sandstone bodies,
A - amalgamated complexes,
W - “channel wings”,
CP - “clay plug”,
SR - small isolated Type 1 sandstone bodies (subtype 1/2),
SC - scours filled with heterolithic fine-grained deposits,
I - inclined accretion surfaces,
T - transition into overbank deposits (”heterolithic top part”).

Appendix 5.3. Outcrop photo panels and their interpretation, Alcolea outcrop of the distal Huesca DFS succession.
Map and schematic outcrop diagram show location and orientation of the panels relative to each other and relative to average palaeocurrent direction.

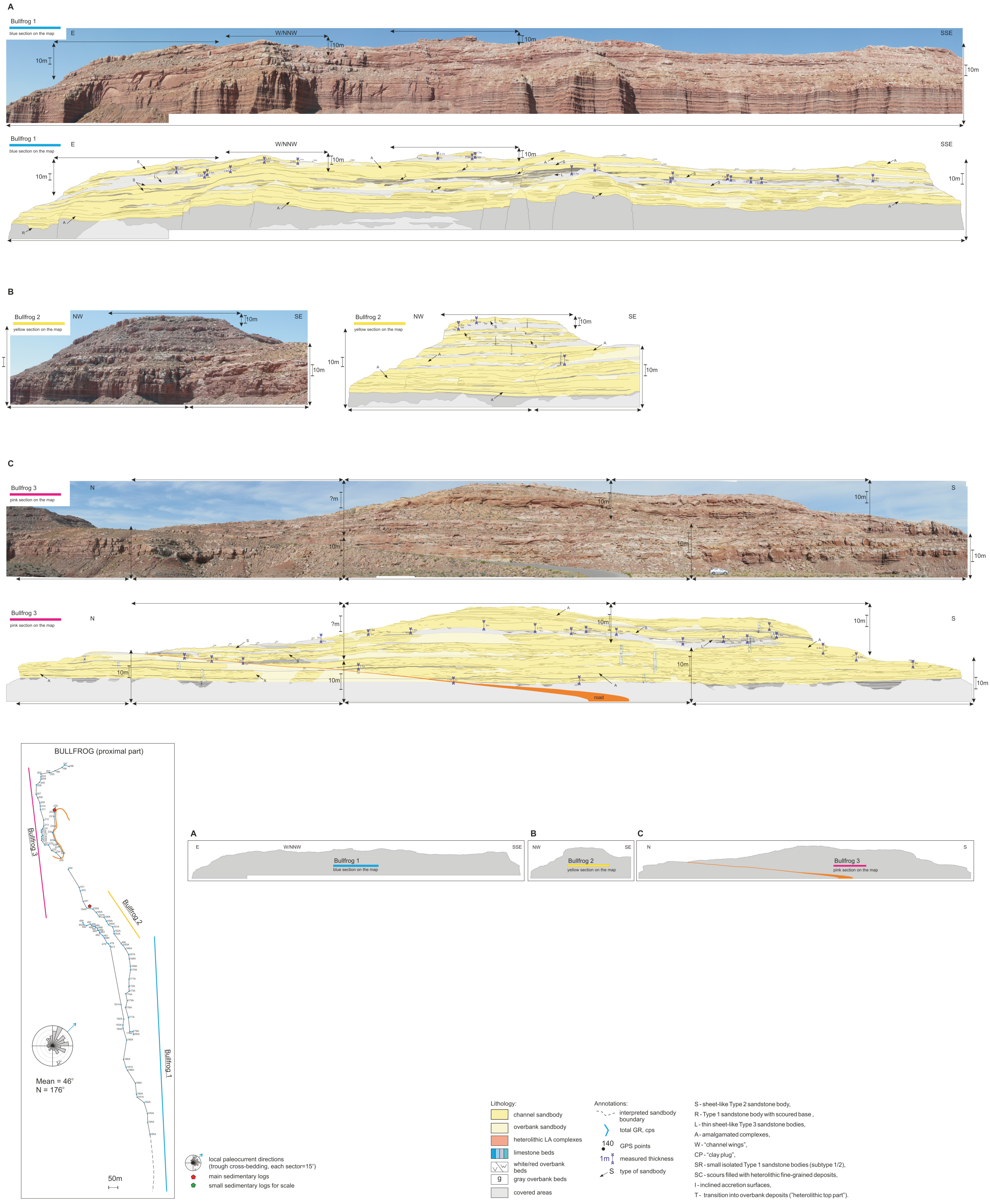

Appendix 5.4. Outcrop photo panels and their interpretation, Bullfrog outcrop of the relative proximal DFS succession.
Map and schematic outcrop diagram show location and orientation of the panels relative to each other and relative to average palaeocurrent direction.

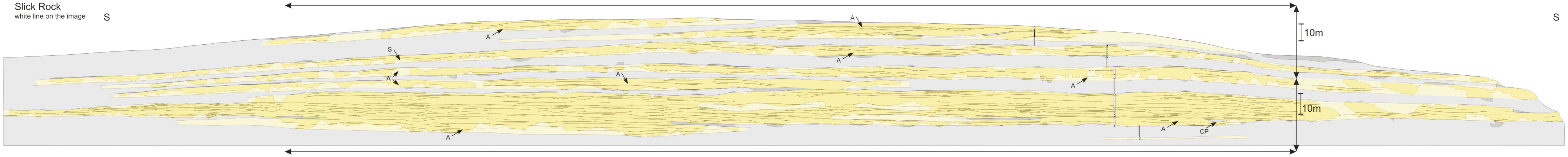

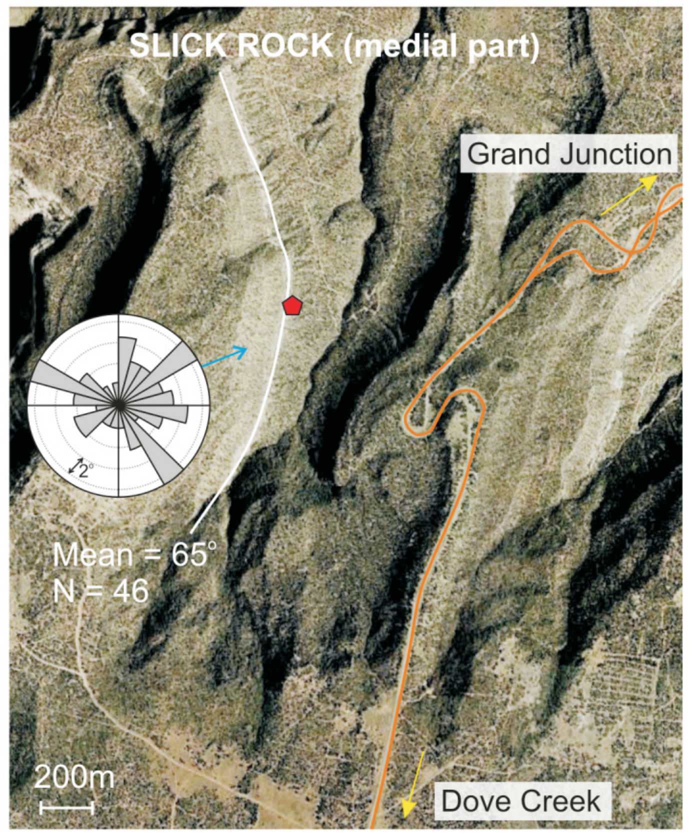

*white line shows orientation of the Slick Rock outcrop

local paleocurrent directions (trough cross-bedding, each sector=15°)

main sedimentary logs

small sedimentary logs for scale

Lithology:

- channel sandbody
- overbank sandbody
- heterolithic LA complexes
- limestone beds
- white/red overbank beds
- g gray overbank beds
- covered areas

Annotations:

- interpreted sandbody boundary
- total GR, cps
- 140 GPS points
- 1m measured thickness
- S type of sandbody

S - sheet-like Type 2 sandstone body,
R - Type 1 sandstone body with scoured base ,
L - thin sheet-like Type 3 sandstone bodies,
A - amalgamated complexes,
W - “channel wings”,
CP - “clay plug”,
SR - small isolated Type 1 sandstone bodies (subtype 1/2),
SC - scours filled with heterolithicfine-grained deposits,
I - inclined accretion surfaces,
T - transition into overbank deposits (”heterolithic top part”).

Appendix 5.5. Outcrop photo panels and their interpretation, Slick Rock outcrop of the relatively proximal Salt Wash DFS succession.
Google Earth image and schematic outcrop diagram show location and orientation of the panels relative to each other and relative to average palaeocurrent direction.

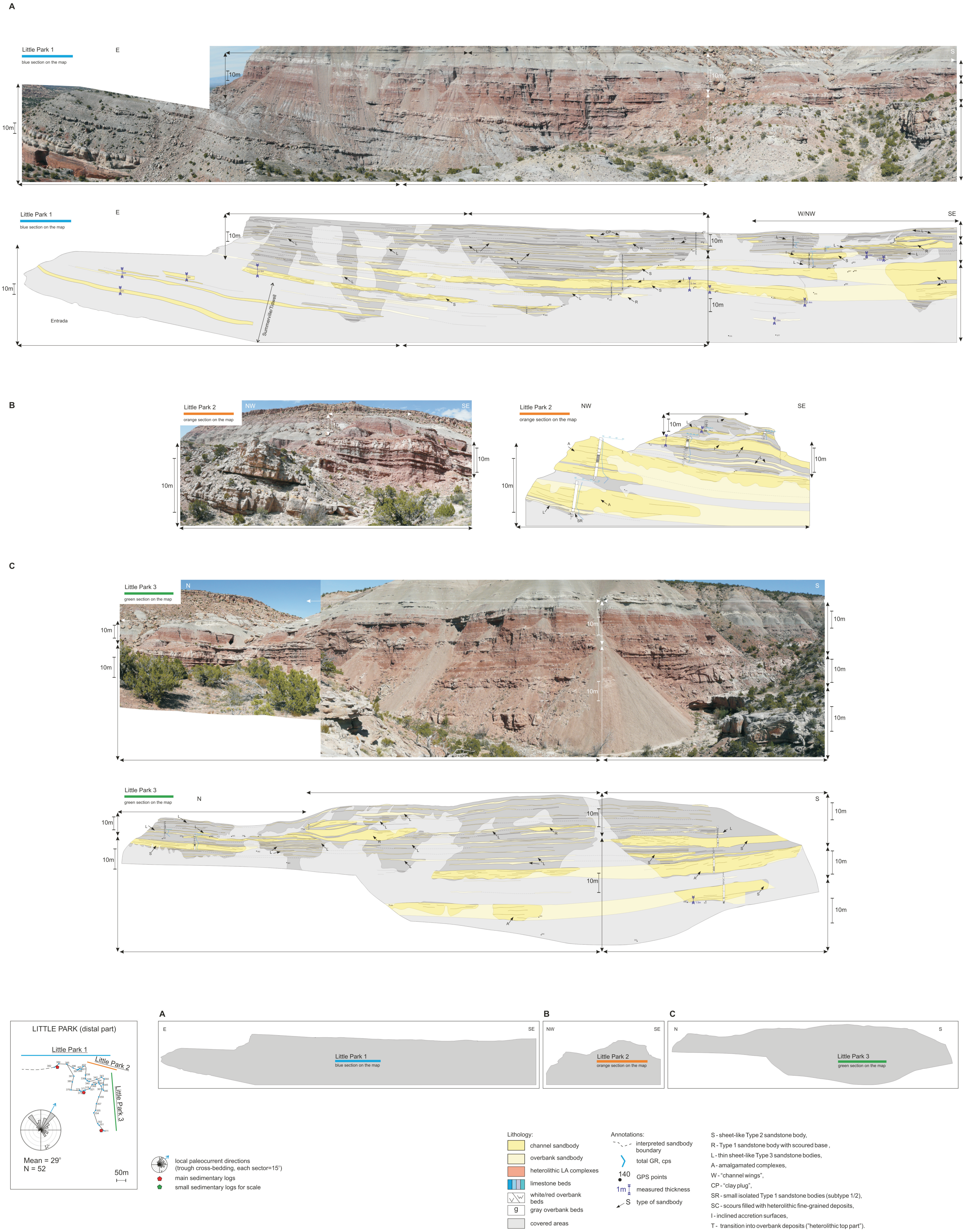

Appendix 5.6. Outcrop photo panels and their interpretation, Little Park outcrop of the relatively proximal Salt Wash DFS succession.
Map and schematic outcrop diagram show location and orientation of the panel relative to each other and relatively to average palaeocurrent direction.

Appendix 6:

Order analysis results:
System-scale successions - 1-10
Floodplain successions - 11-22

Alcolea 1&2 Log 1, Metric statistics

A. Log **B. Variation with scale** **C. Comparison with synthetic models**

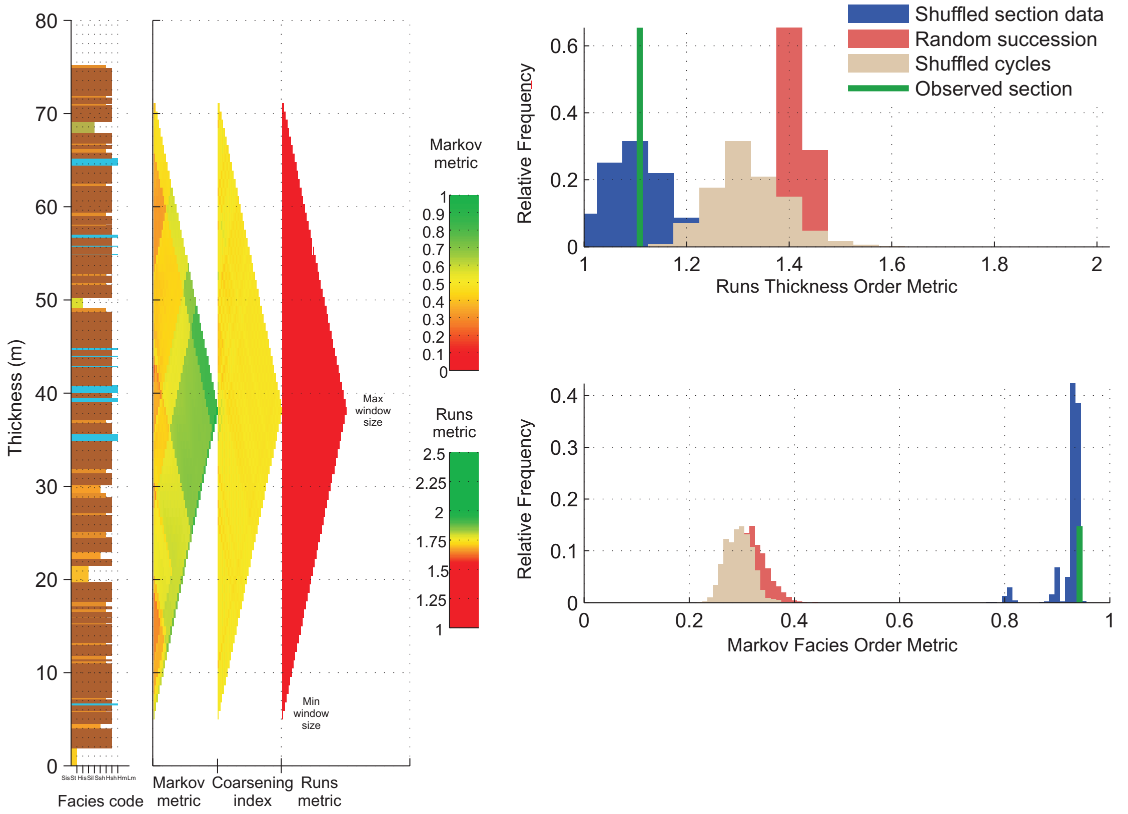

D. Facies distribution

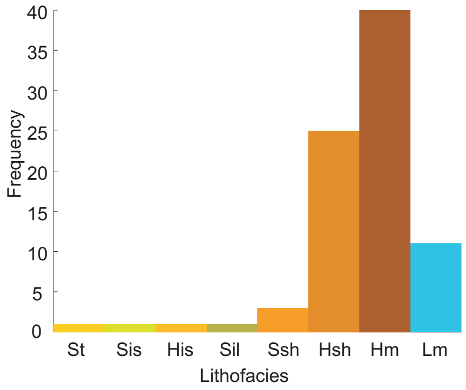

E. Transition probability matrix

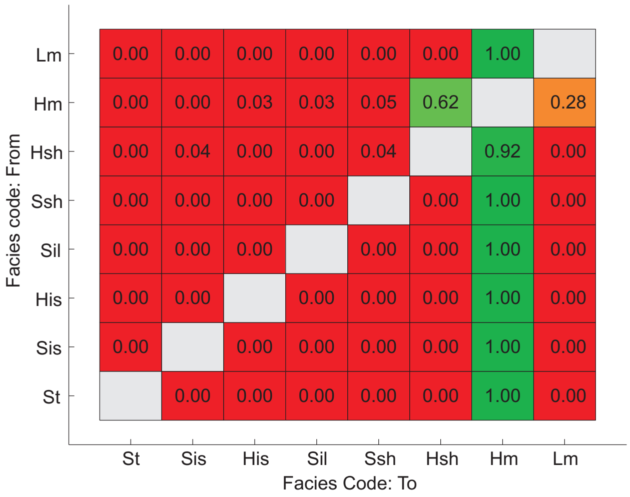

Facies code: From	St	Sis	His	Sil	Ssh	Hsh	Hm	Lm
Lm	0.00	0.00	0.00	0.00	0.00	0.00	1.00	
Hm	0.00	0.00	0.03	0.03	0.05	0.62		0.28
Hsh	0.00	0.04	0.00	0.00	0.04		0.92	0.00
Ssh	0.00	0.00	0.00	0.00		0.00	1.00	0.00
Sil	0.00	0.00	0.00		0.00	0.00	1.00	0.00
His	0.00	0.00		0.00	0.00	0.00	1.00	0.00
Sis	0.00		0.00	0.00	0.00	0.00	1.00	0.00
St		0.00	0.00	0.00	0.00	0.00	1.00	0.00

Appendix 6.1. Results of the order analysis for the Alcolea 1 & 2, Log 1, Huesca DFS.

Castelflorite 4 Log 1, Metric statistics

A. Log **B. Variation with scale** **C. Comparison with synthetic models**

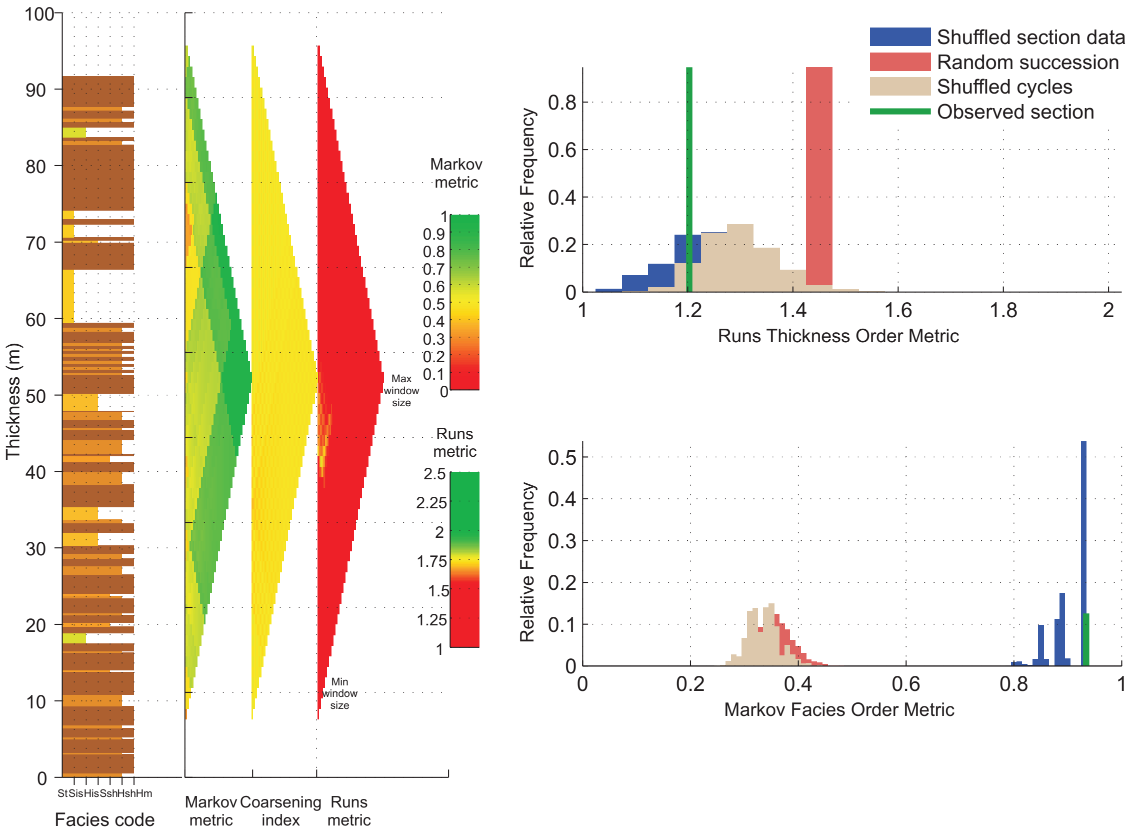

D. Facies distribution **E. Transition probability matrix**

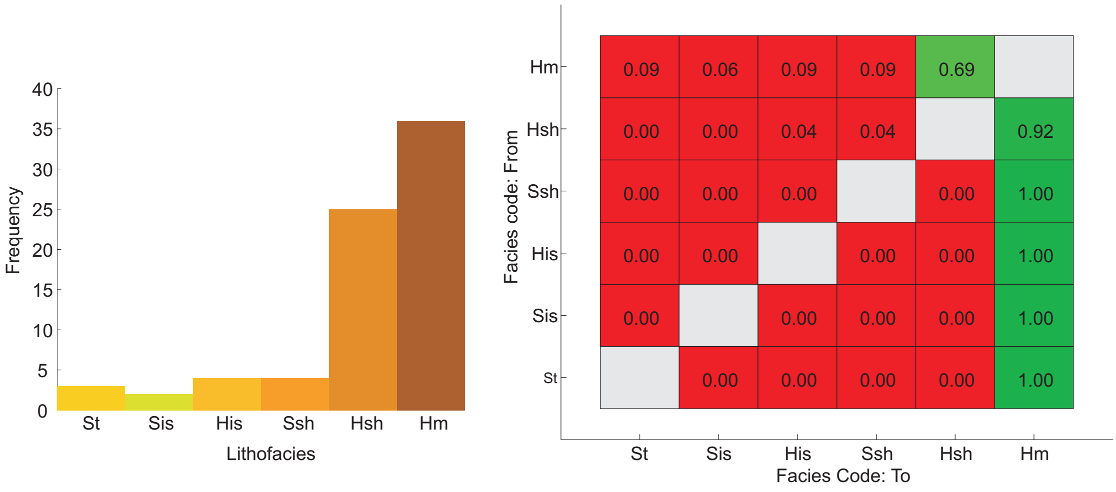

Facies code: From \ Facies Code: To	St	Sis	His	Ssh	Hsh	Hm
Hm	0.09	0.06	0.09	0.09	0.69	
Hsh	0.00	0.00	0.04	0.04		0.92
Ssh	0.00	0.00	0.00		0.00	1.00
His	0.00	0.00		0.00	0.00	1.00
Sis	0.00		0.00	0.00	0.00	1.00
St		0.00	0.00	0.00	0.00	1.00

Appendix 6.2. Results of the order analysis for the Castelflorite 4, Log 1, Huesca DFS.

Bullfrog 2 Log 5, Metric statistics

A. Log

B. Variation with scale

C. Comparison with synthetic models

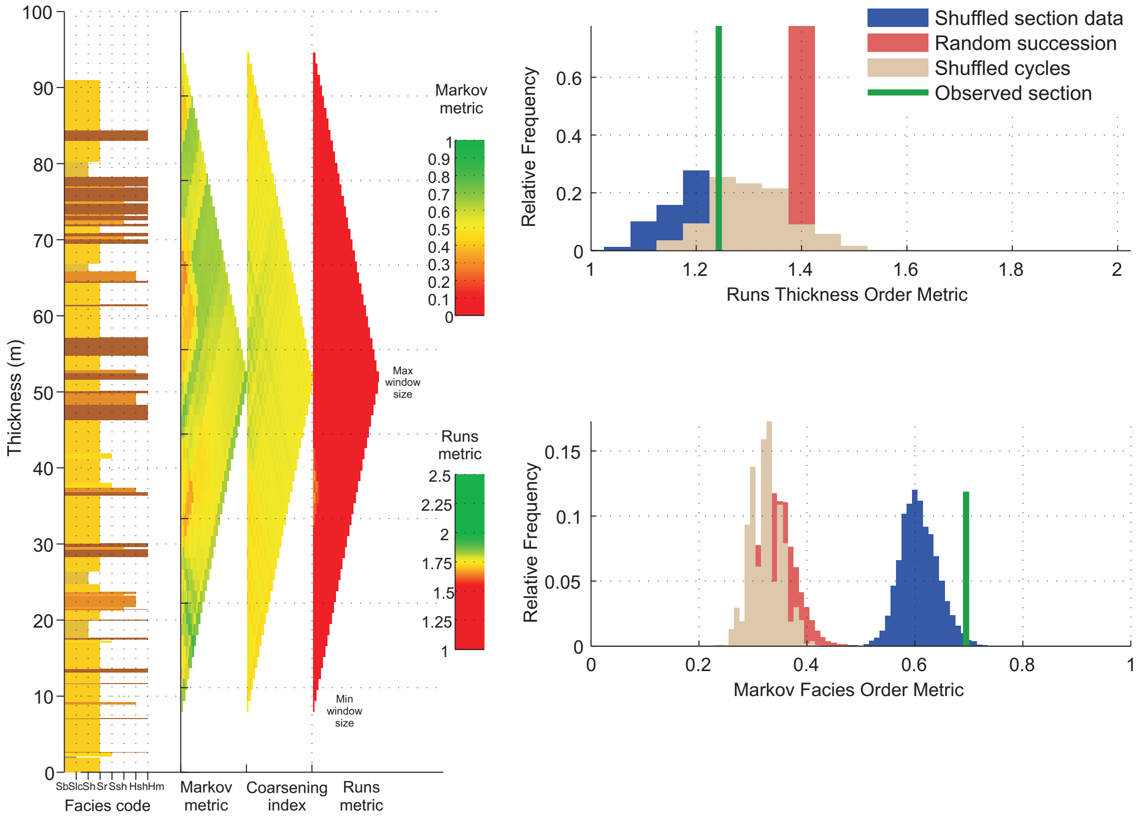

D. Facies distribution

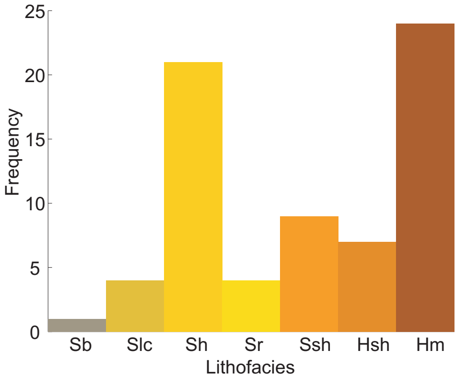

E. Transition probability matrix

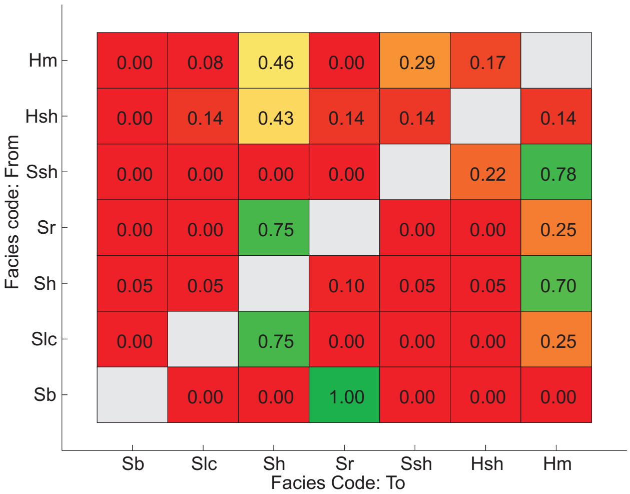

Facies code: From / Facies Code: To	Sb	Slc	Sh	Sr	Ssh	Hsh	Hm
Hm	0.00	0.08	0.46	0.00	0.29	0.17	
Hsh	0.00	0.14	0.43	0.14	0.14		0.14
Ssh	0.00	0.00	0.00	0.00		0.22	0.78
Sr	0.00	0.00	0.75		0.00	0.00	0.25
Sh	0.05	0.05		0.10	0.05	0.05	0.70
Slc	0.00		0.75	0.00	0.00	0.00	0.25
Sb		0.00	0.00	1.00	0.00	0.00	0.00

Appendix 6.3. Results of the order analysis for the Bullfrog 2, Log 5, Salt Wash DFS.

Bullfrog 3 Log 34, Metric statistics

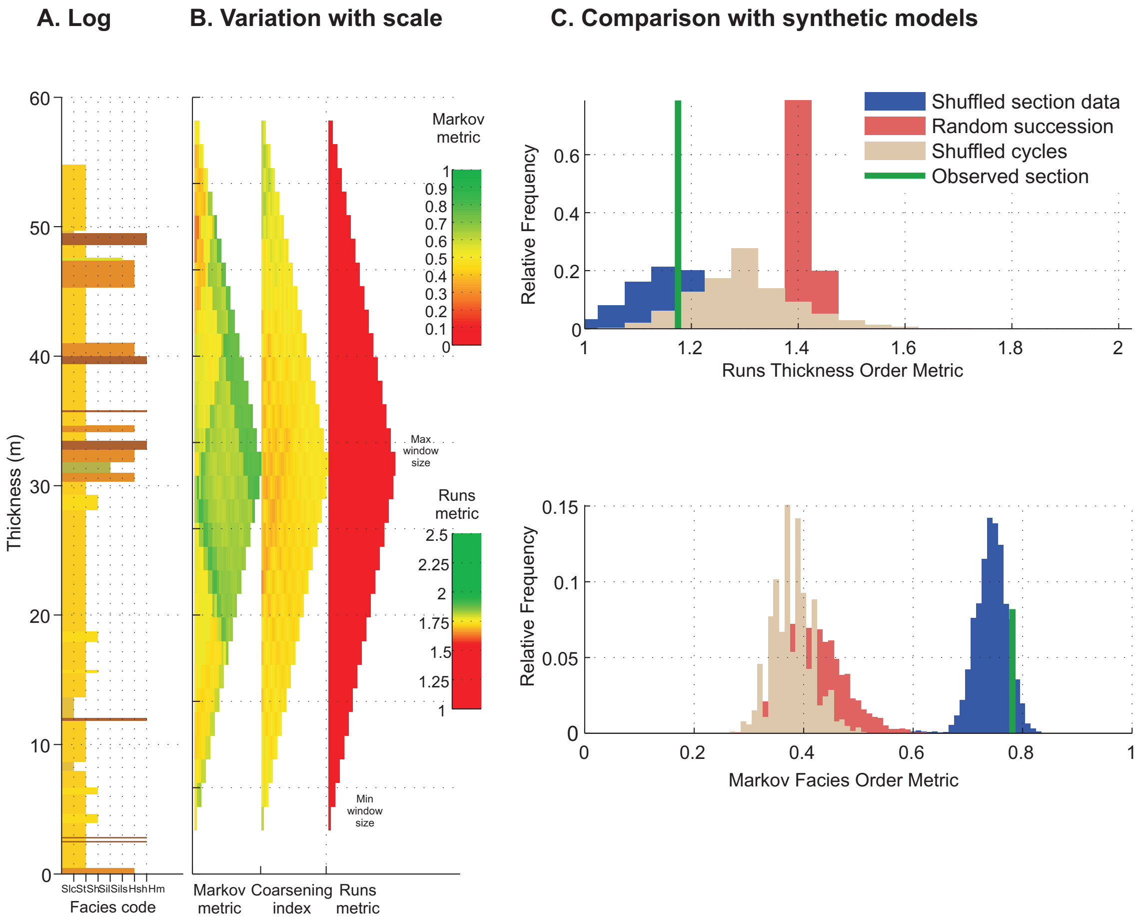

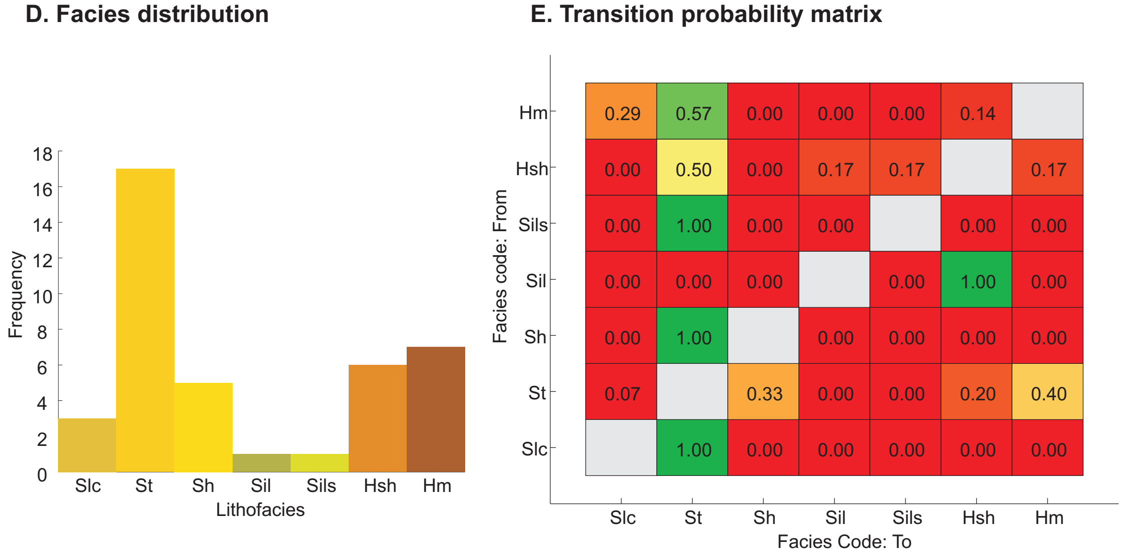

Facies code: From	Slc	St	Sh	Sil	Sils	Hsh	Hm
Hm	0.29	0.57	0.00	0.00	0.00	0.14	
Hsh	0.00	0.50	0.00	0.17	0.17		0.17
Sils	0.00	1.00	0.00	0.00		0.00	0.00
Sil	0.00	0.00	0.00		0.00	1.00	0.00
Sh	0.00	1.00		0.00	0.00	0.00	0.00
St	0.07		0.33	0.00	0.00	0.20	0.40
Slc		1.00	0.00	0.00	0.00	0.00	0.00

Appendix 6.4. Results of the order analysis for the Bullfrog 3, Log 3, 4, Salt Wash DFS.

Monźon 4 Log1, Metric statistics

A. Log B. Variation with scale C. Comparison with synthetic models

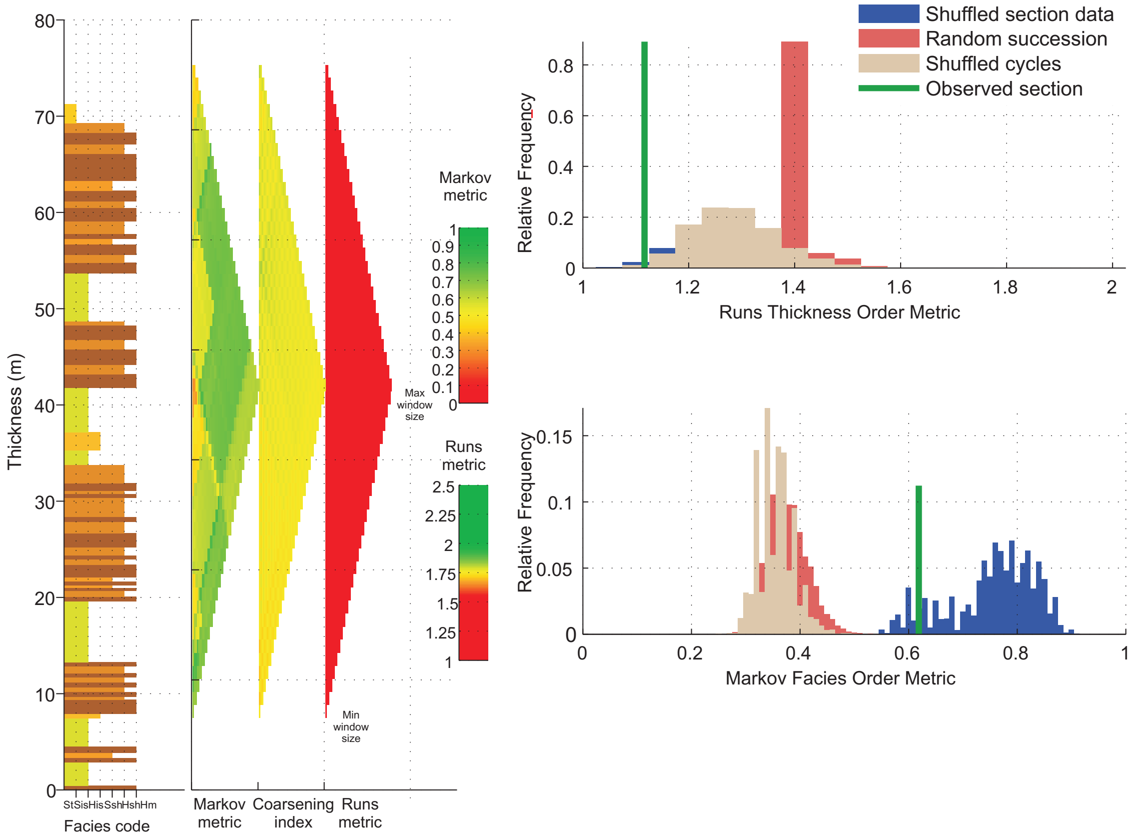

D. Facies distribution E. Transition probability matrix

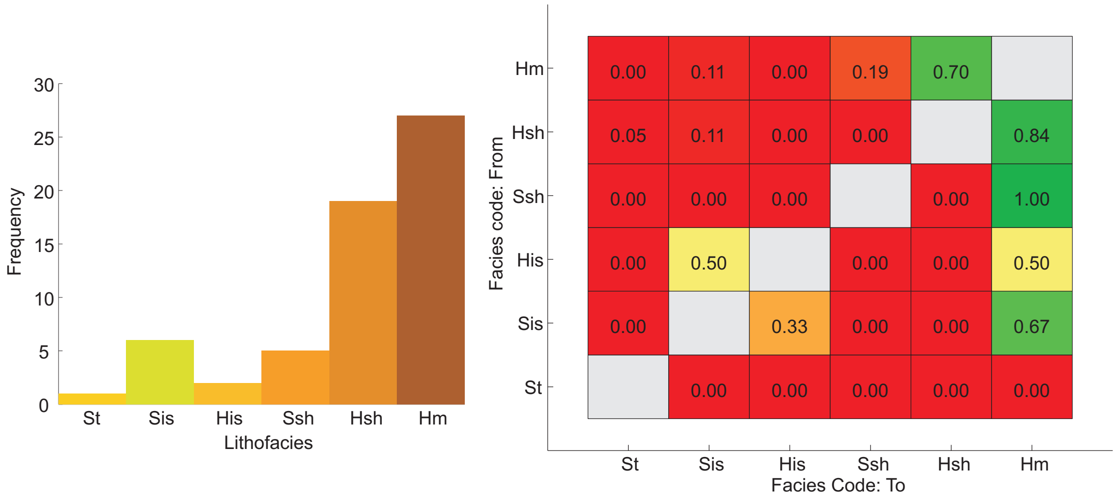

	St	Sis	His	Ssh	Hsh	Hm
Hm	0.00	0.11	0.00	0.19	0.70	
Hsh	0.05	0.11	0.00	0.00		0.84
Ssh	0.00	0.00	0.00		0.00	1.00
His	0.00	0.50		0.00	0.00	0.50
Sis	0.00		0.33	0.00	0.00	0.67
St		0.00	0.00	0.00	0.00	0.00

Appendix 6.5. Results of the order analysis for the Monźon 4, Log1, Huesca DFS.

Little Park 3 Log 7, Metric statistics

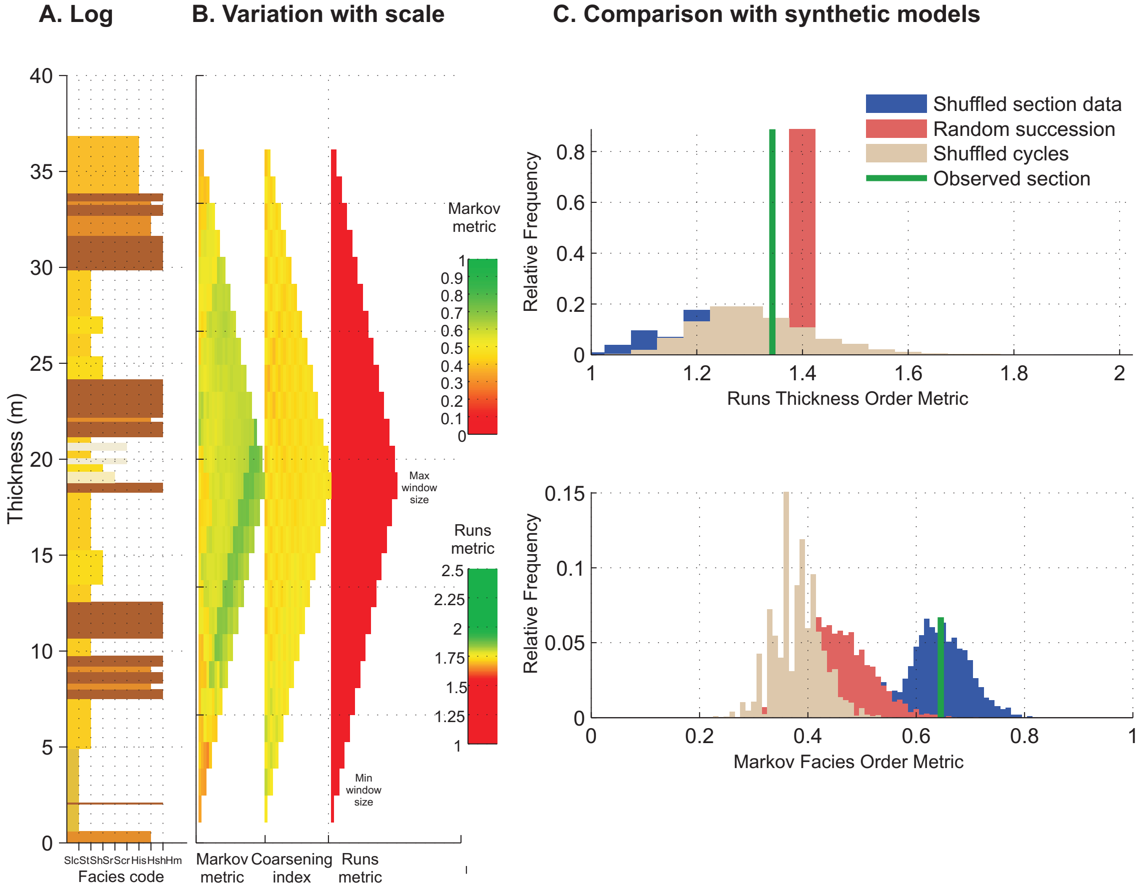
A. Log
B. Variation with scale
C. Comparison with synthetic models

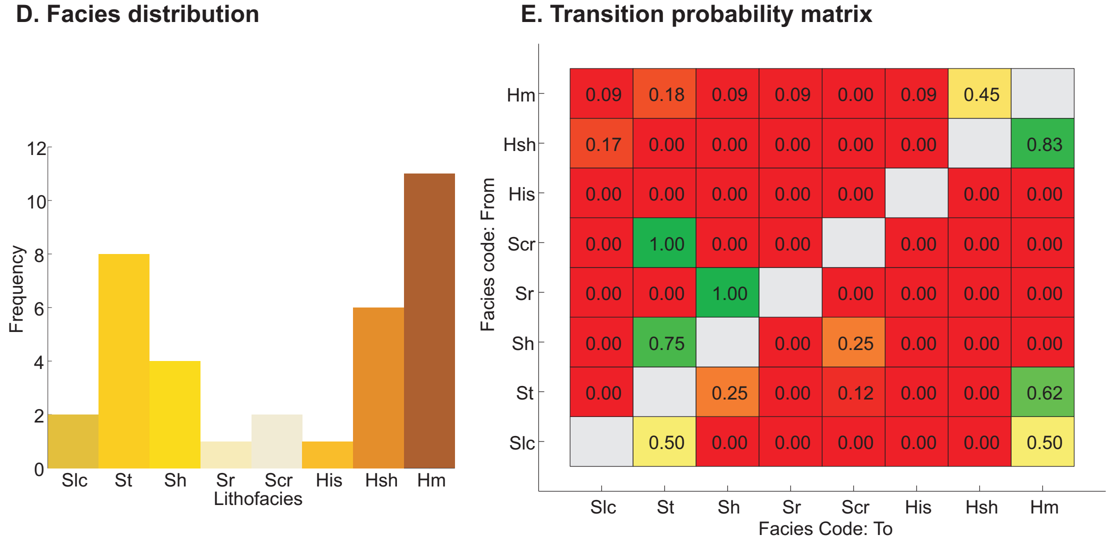
D. Facies distribution
E. Transition probability matrix

Facies code: From	Slc	St	Sh	Sr	Scr	His	Hsh	Hm
Hm	0.09	0.18	0.09	0.09	0.00	0.09	0.45	
Hsh	0.17	0.00	0.00	0.00	0.00	0.00		0.83
His	0.00	0.00	0.00	0.00	0.00		0.00	0.00
Scr	0.00	1.00	0.00	0.00		0.00	0.00	0.00
Sr	0.00	0.00	1.00		0.00	0.00	0.00	0.00
Sh	0.00	0.75		0.00	0.25	0.00	0.00	0.00
St	0.00		0.25	0.00	0.12	0.00	0.00	0.62
Slc		0.50	0.00	0.00	0.00	0.00	0.00	0.50

Appendix 6.6. Results of the order analysis for the Little Park 3, Log 7, Salt Wash DFS.

Slick Rock Log 1, Metric statistics

A. Log **B. Variation with scale** **C. Comparison with synthetic models**

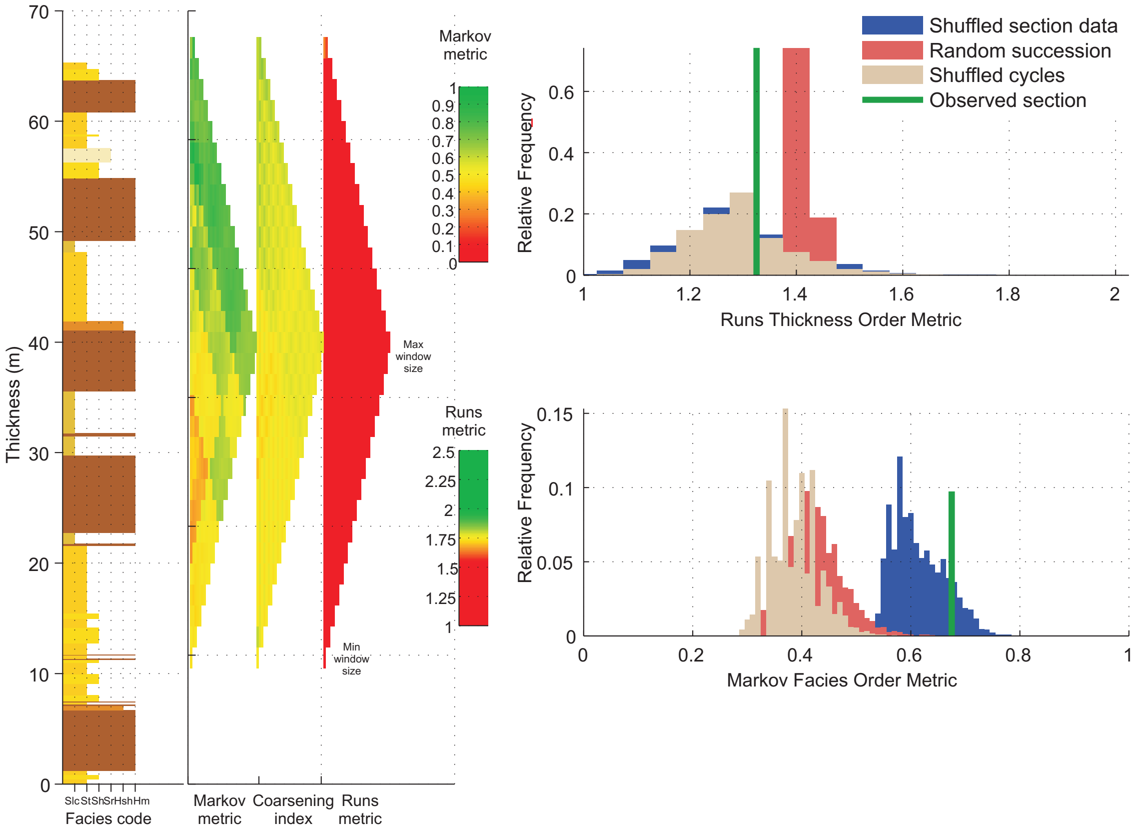

D. Facies distribution

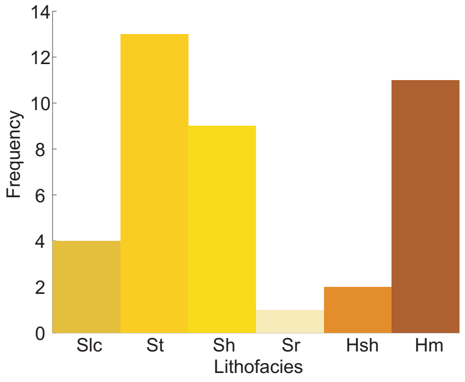

E. Transition probability matrix

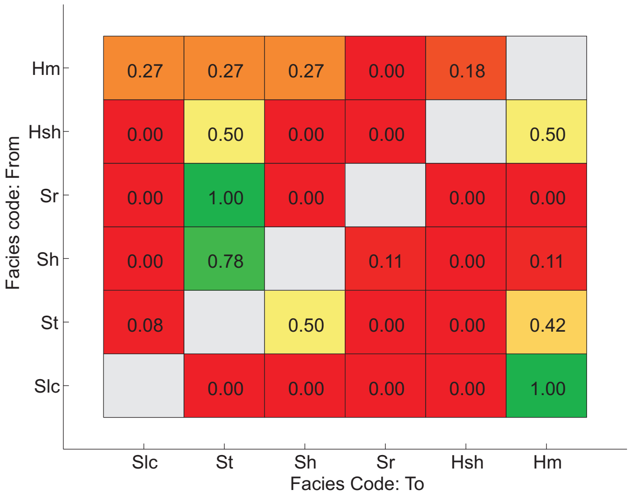

Facies code: From	Slc	St	Sh	Sr	Hsh	Hm
Hm	0.27	0.27	0.27	0.00	0.18	
Hsh	0.00	0.50	0.00	0.00		0.50
Sr	0.00	1.00	0.00		0.00	0.00
Sh	0.00	0.78		0.11	0.00	0.11
St	0.08		0.50	0.00	0.00	0.42
Slc		0.00	0.00	0.00	0.00	1.00

Appendix 6.7. Results of the order analysis for the Slick Rock, Log 1, Salt Wash DFS.

Castelflorite 2&3 Log 2, Metric statistics

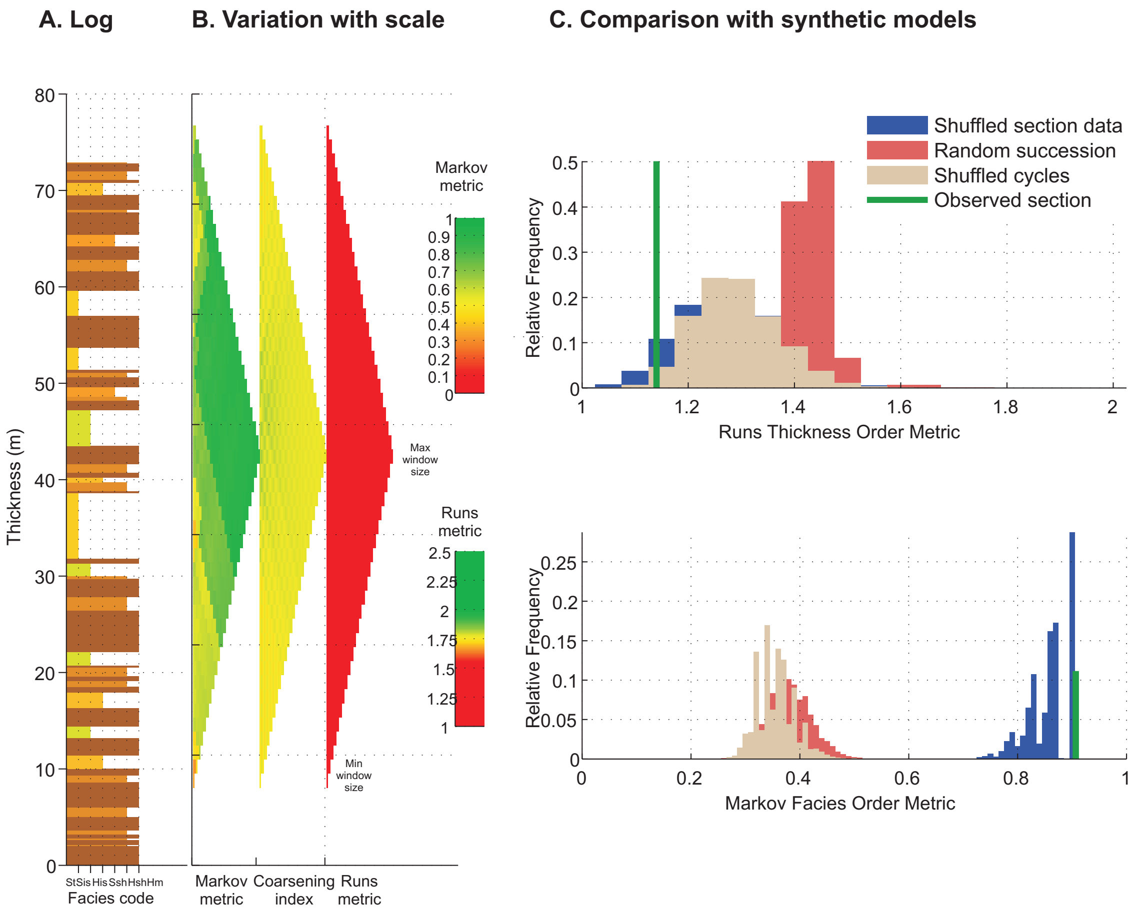

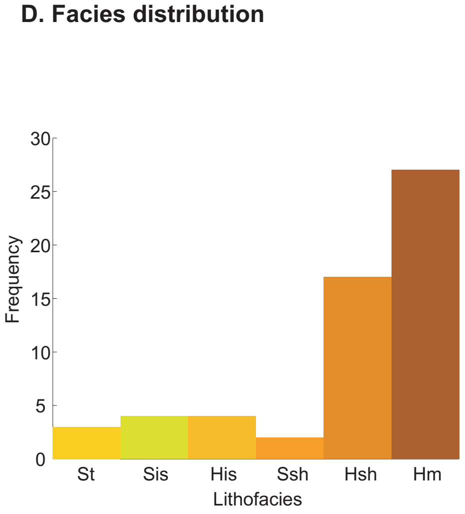

D. Facies distribution

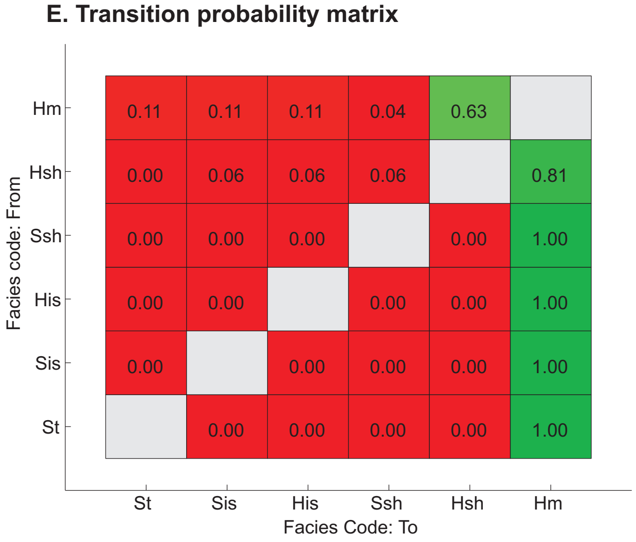

E. Transition probability matrix

Facies code: From \ Facies Code: To	St	Sis	His	Ssh	Hsh	Hm
Hm	0.11	0.11	0.11	0.04	0.63	
Hsh	0.00	0.06	0.06	0.06		0.81
Ssh	0.00	0.00	0.00		0.00	1.00
His	0.00	0.00		0.00	0.00	1.00
Sis	0.00		0.00	0.00	0.00	1.00
St		0.00	0.00	0.00	0.00	1.00

Appendix 6.8. Results of the order analysis for the Castelflorite 2 & 3, Log 2, Huesca DFS.

Little Park 1 Log 456, Metric statistics

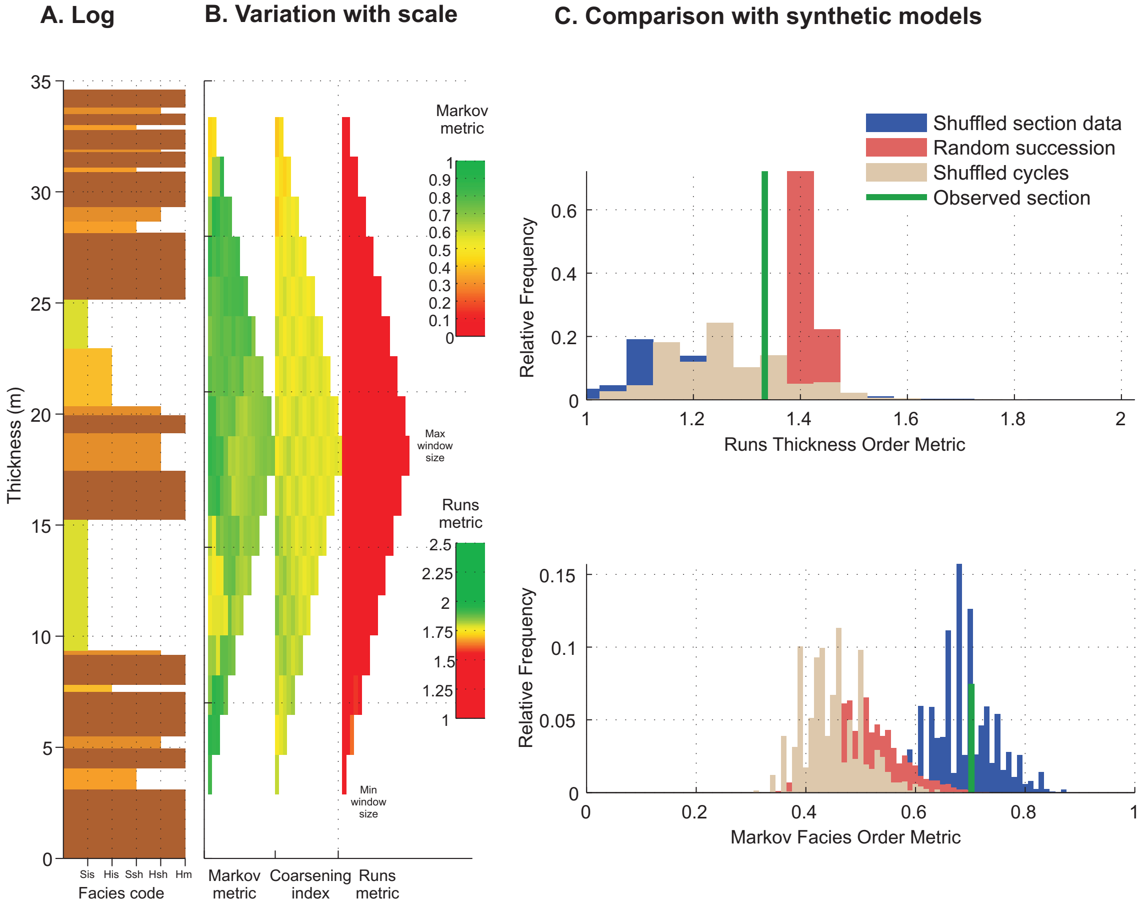
A. Log

B. Variation with scale

C. Comparison with synthetic models

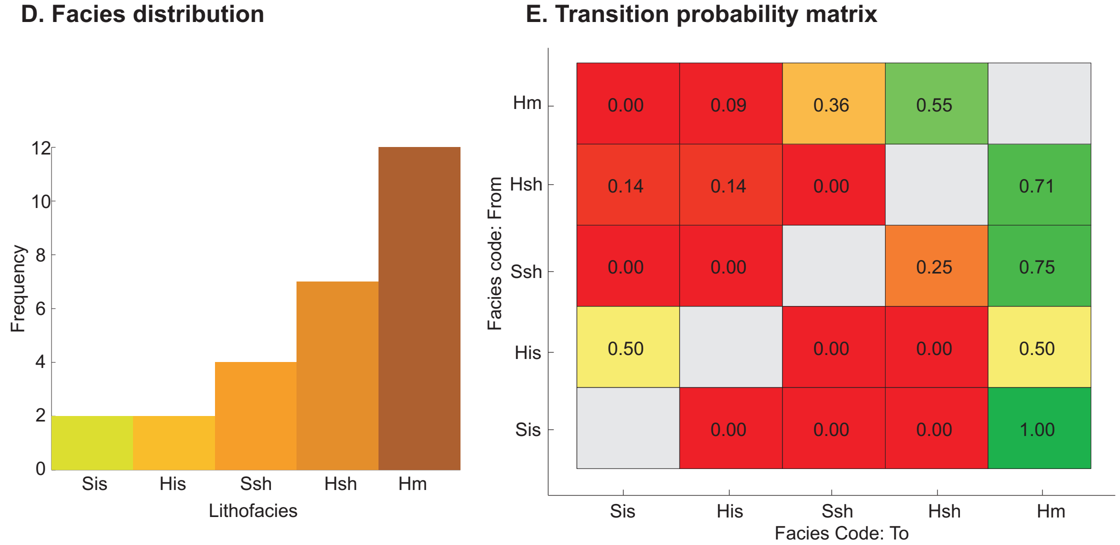
D. Facies distribution

E. Transition probability matrix

Facies code: From \ To	Sis	His	Ssh	Hsh	Hm
Hm	0.00	0.09	0.36	0.55	
Hsh	0.14	0.14	0.00		0.71
Ssh	0.00	0.00		0.25	0.75
His	0.50		0.00	0.00	0.50
Sis		0.00	0.00	0.00	1.00

Appendix 6.9. Results of the order analysis for the Little Park 1, Log 4, 5, 6, Salt Wash DFS.

Monźon 1 Log12, Metric statistics

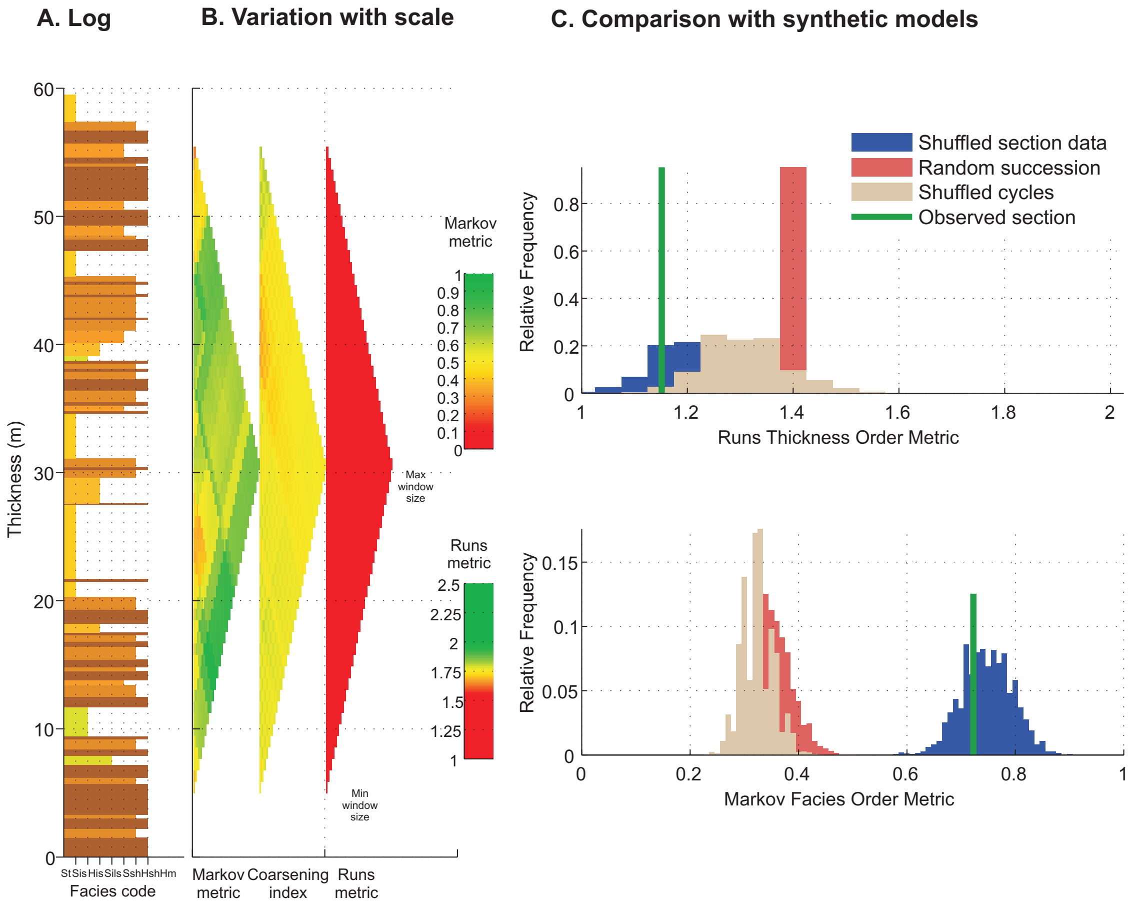

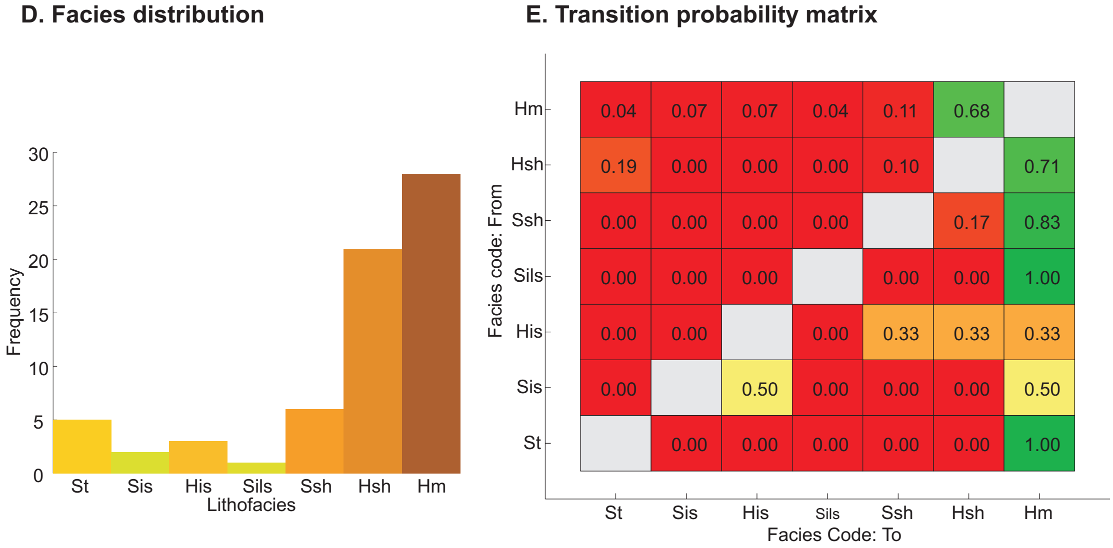

	St	Sis	His	Sils	Ssh	Hsh	Hm
Hm	0.04	0.07	0.07	0.04	0.11	0.68	
Hsh	0.19	0.00	0.00	0.00	0.10		0.71
Ssh	0.00	0.00	0.00	0.00		0.17	0.83
Sils	0.00	0.00	0.00		0.00	0.00	1.00
His	0.00	0.00		0.00	0.33	0.33	0.33
Sis	0.00		0.50	0.00	0.00	0.00	0.50
St		0.00	0.00	0.00	0.00	0.00	1.00

Appendix 6.10. Results of the order analysis for the Monźon 1, Log 1, 2, Huesca DFS.

Monźon, Log4, Metric statistics

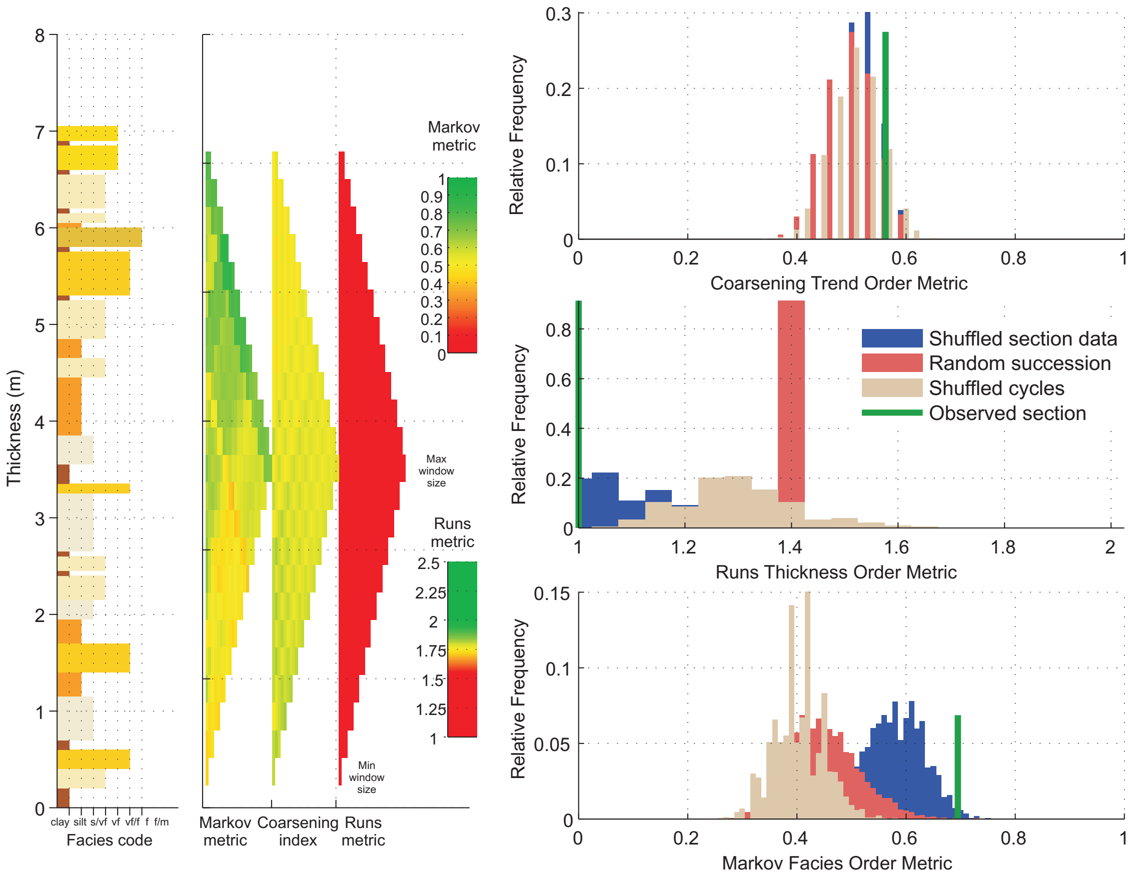

A. Log

B. Variation with scale

C. Comparison with synthetic models

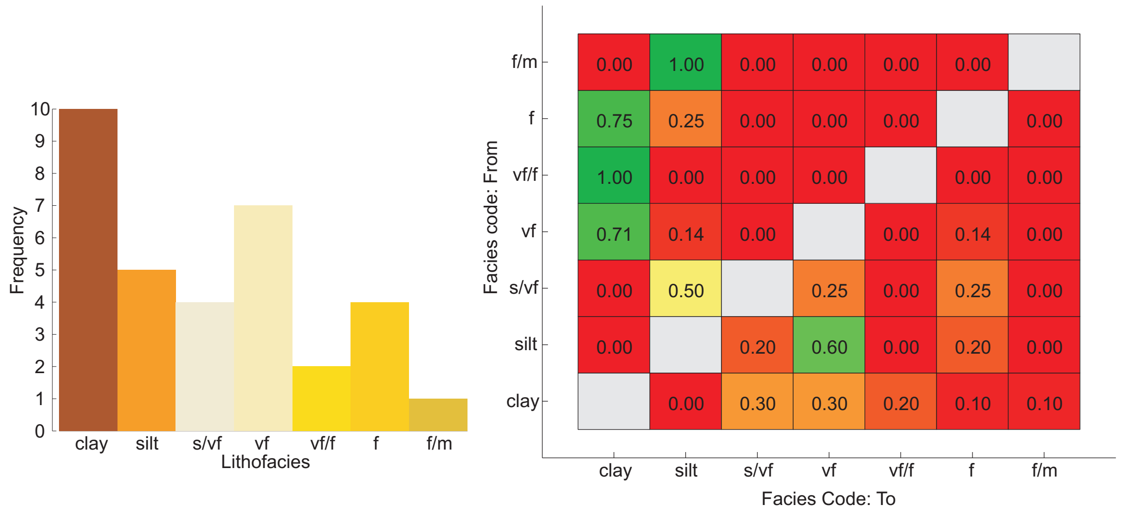

D. Facies distribution

E. Transition probability matrix

Facies code: From \ Facies Code: To	clay	silt	s/vf	vf	vf/f	f	f/m
f/m	0.00	1.00	0.00	0.00	0.00	0.00	
f	0.75	0.25	0.00	0.00	0.00		0.00
vf/f	1.00	0.00	0.00	0.00		0.00	0.00
vf	0.71	0.14	0.00		0.00	0.14	0.00
s/vf	0.00	0.50		0.25	0.00	0.25	0.00
silt	0.00		0.20	0.60	0.00	0.20	0.00
clay		0.00	0.30	0.30	0.20	0.10	0.10

Appendix 6.11. Results of the order analysis for the Monźon, Log 4 of the floodplain deposits, Huesca DFS.

Monte Aragón 4, Metric statistics

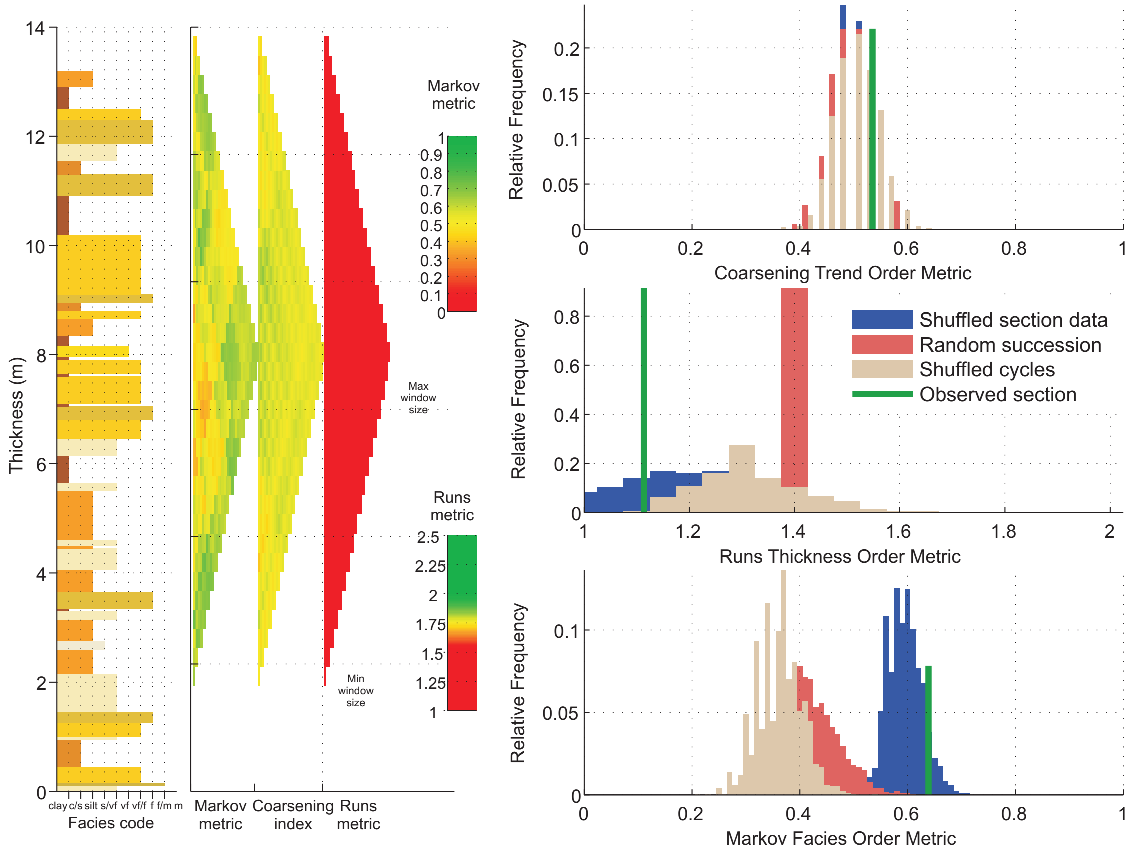

A. Log

B. Variation with scale

C. Comparison with synthetic models

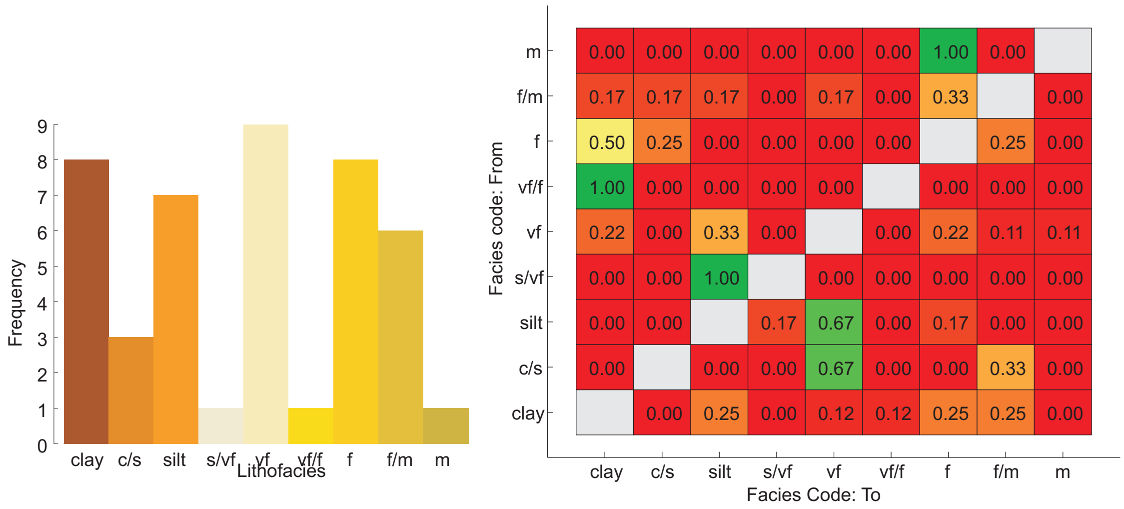

D. Facies distribution

E. Transition probability matrix

Facies code: From	clay	c/s	silt	s/vf	vf	vf/f	f	f/m	m
m	0.00	0.00	0.00	0.00	0.00	0.00	1.00	0.00	
f/m	0.17	0.17	0.17	0.00	0.17	0.00	0.33		0.00
f	0.50	0.25	0.00	0.00	0.00	0.00		0.25	0.00
vf/f	1.00	0.00	0.00	0.00	0.00		0.00	0.00	0.00
vf	0.22	0.00	0.33	0.00		0.00	0.22	0.11	0.11
s/vf	0.00	0.00	1.00		0.00	0.00	0.00	0.00	0.00
silt	0.00	0.00		0.17	0.67	0.00	0.17	0.00	0.00
c/s	0.00		0.00	0.00	0.67	0.00	0.00	0.33	0.00
clay		0.00	0.25	0.00	0.12	0.12	0.25	0.25	0.00

Appendix 6.12. Results of the order analysis for the Monzon Aragón 4 log of the floodplain deposits, Huesca DFS.

Bolea, Log 2, Metric statistics

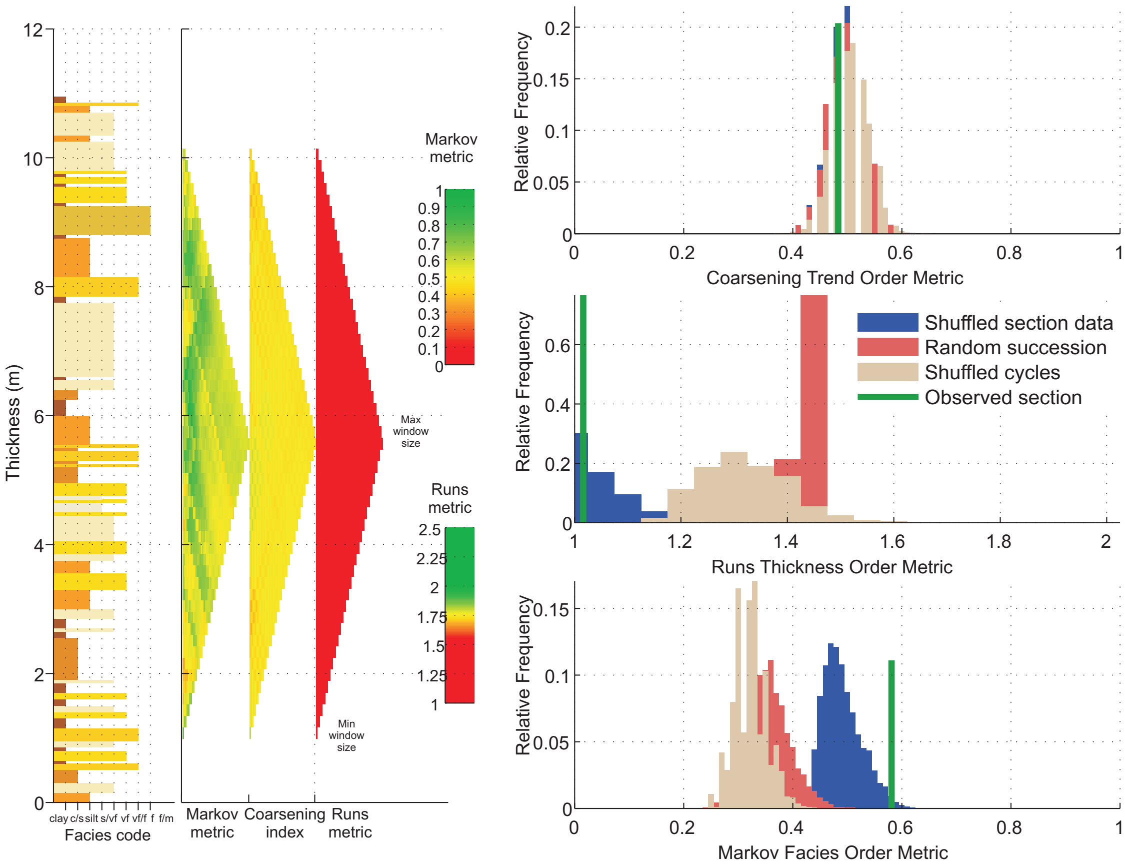
A. Log

B. Variation with scale

C. Comparison with synthetic models

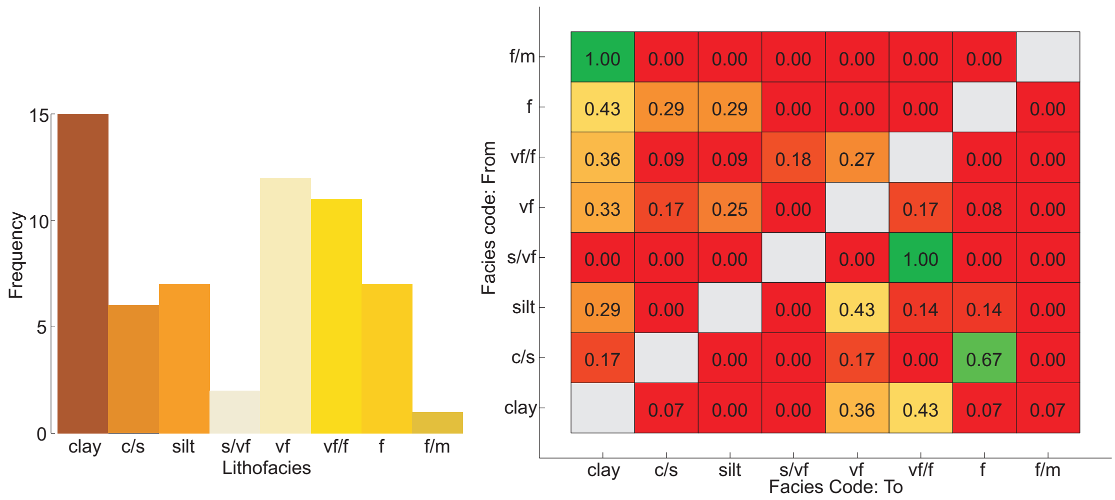
D. Facies distribution

E. Transition probability matrix

	clay	c/s	silt	s/vf	vf	vf/f	f	f/m
f/m	1.00	0.00	0.00	0.00	0.00	0.00	0.00	
f	0.43	0.29	0.29	0.00	0.00	0.00		0.00
vf/f	0.36	0.09	0.09	0.18	0.27		0.00	0.00
vf	0.33	0.17	0.25	0.00		0.17	0.08	0.00
s/vf	0.00	0.00	0.00		0.00	1.00	0.00	0.00
silt	0.29	0.00		0.00	0.43	0.14	0.14	0.00
c/s	0.17		0.00	0.00	0.17	0.00	0.67	0.00
clay		0.07	0.00	0.00	0.36	0.43	0.07	0.07

Appendix 6.13. Results of the order analysis for the Bolea, Log 2 of the floodplain deposits, Huesca DFS.

Castelflorite, Log 1, Metric statistics

A. Log **B. Variation with scale** **C. Comparison with synthetic models**

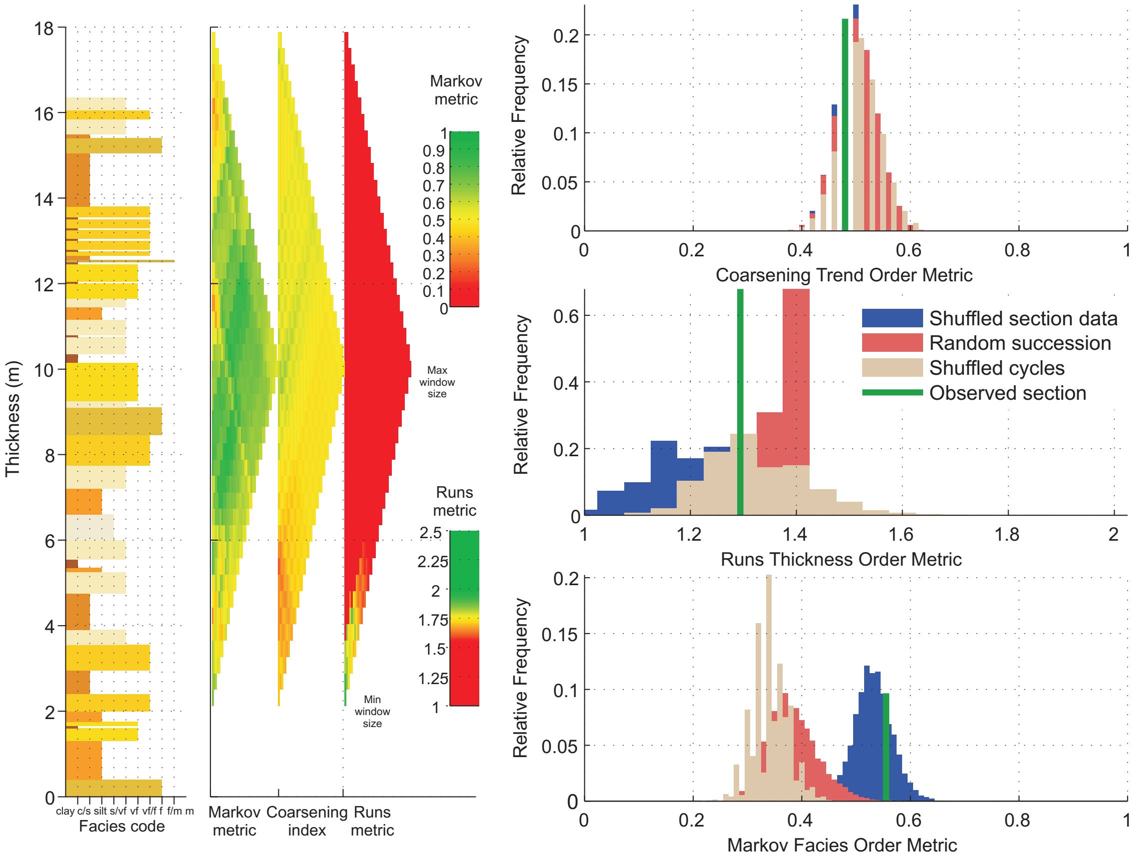

D. Facies distribution

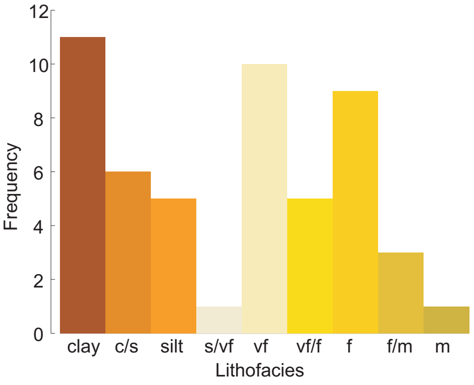

E. Transition probability matrix

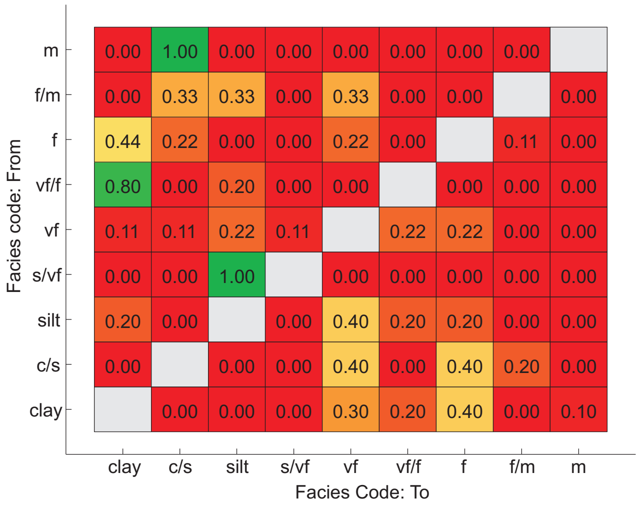

Facies code: From \ Facies Code: To	clay	c/s	silt	s/vf	vf	vf/f	f	f/m	m
m	0.00	1.00	0.00	0.00	0.00	0.00	0.00	0.00	
f/m	0.00	0.33	0.33	0.00	0.33	0.00	0.00		0.00
f	0.44	0.22	0.00	0.00	0.22	0.00		0.11	0.00
vf/f	0.80	0.00	0.20	0.00	0.00		0.00	0.00	0.00
vf	0.11	0.11	0.22	0.11		0.22	0.22	0.00	0.00
s/vf	0.00	0.00	1.00		0.00	0.00	0.00	0.00	0.00
silt	0.20	0.00		0.00	0.40	0.20	0.20	0.00	0.00
c/s	0.00		0.00	0.00	0.40	0.00	0.40	0.20	0.00
clay		0.00	0.00	0.00	0.30	0.20	0.40	0.00	0.10

Appendix 6.14. Results of the order analysis for the Castelflorite, Log 1 of the floodplain deposits, Huesca DFS.

Monte Aragón 2, Metric statistics

A. Log **B. Variation with scale** **C. Comparison with synthetic models**

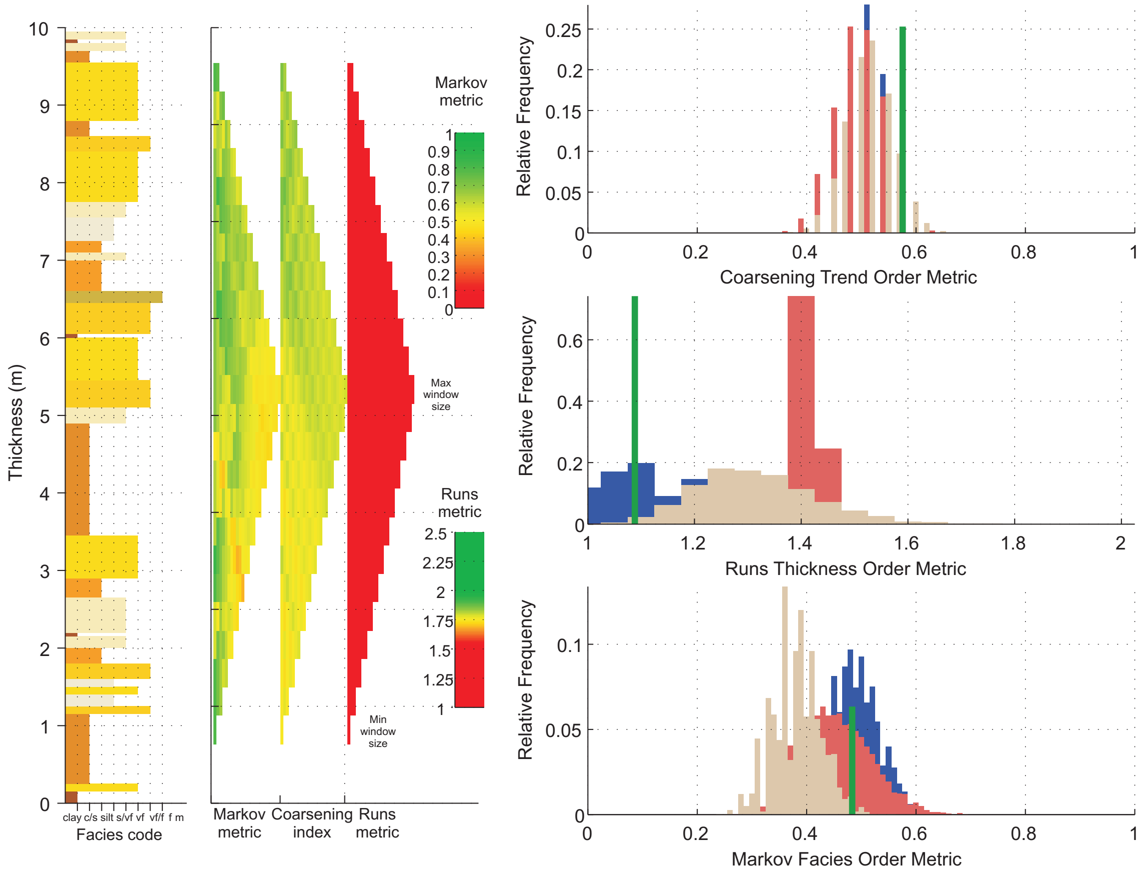

D. Facies distribution

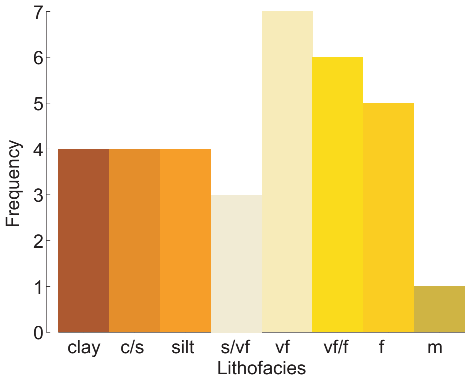

E. Transition probability matrix

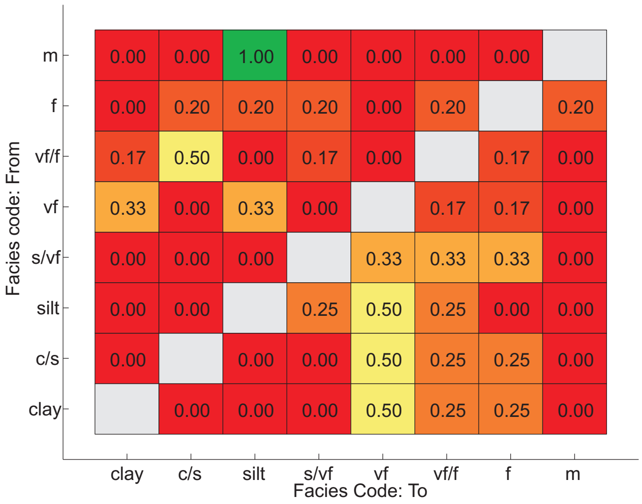

Facies code: From	clay	c/s	silt	s/vf	vf	vf/f	f	m
m	0.00	0.00	1.00	0.00	0.00	0.00	0.00	
f	0.00	0.20	0.20	0.20	0.00	0.20		0.20
vf/f	0.17	0.50	0.00	0.17	0.00		0.17	0.00
vf	0.33	0.00	0.33	0.00		0.17	0.17	0.00
s/vf	0.00	0.00	0.00		0.33	0.33	0.33	0.00
silt	0.00	0.00		0.25	0.50	0.25	0.00	0.00
c/s	0.00		0.00	0.00	0.50	0.25	0.25	0.00
clay		0.00	0.00	0.00	0.50	0.25	0.25	0.00

Appendix 6.15. Results of the order analysis for the Monte Aragón 2 log of the floodplain deposits, Huesca DFS.

Monźon, Log 3, Metric statistics

A. Log **B. Variation with scale** **C. Comparison with synthetic models**

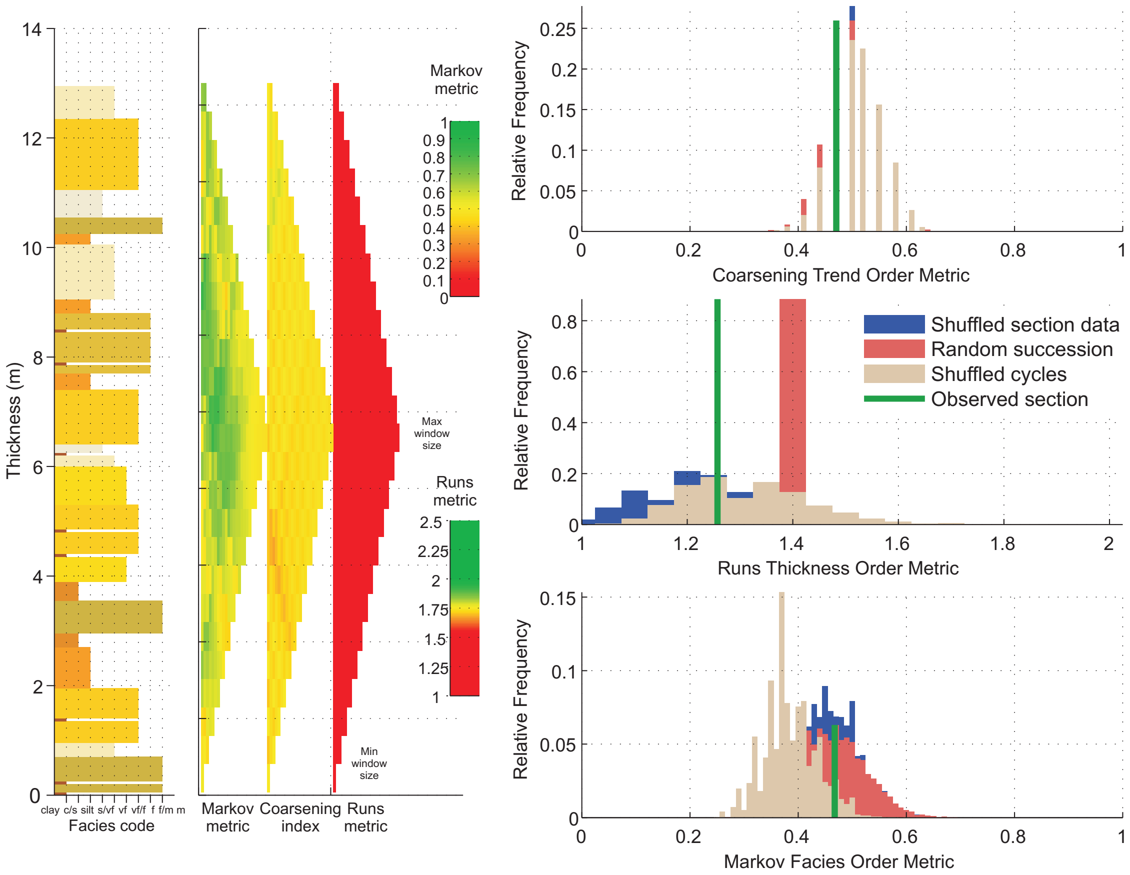

D. Facies distribution **E. Transition probability matrix**

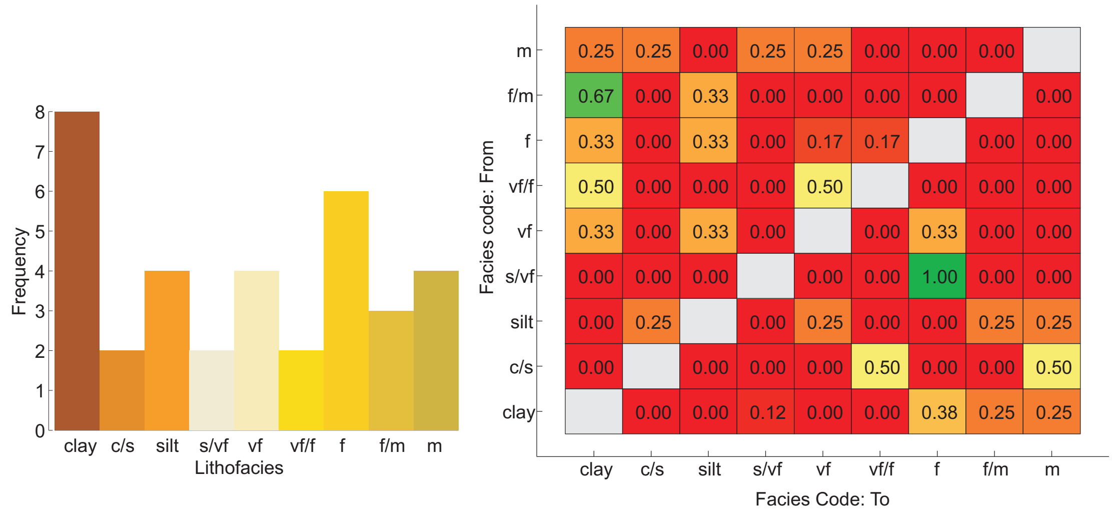

Facies code: From \ Facies Code: To	clay	c/s	silt	s/vf	vf	vf/f	f	f/m	m
m	0.25	0.25	0.00	0.25	0.25	0.00	0.00	0.00	
f/m	0.67	0.00	0.33	0.00	0.00	0.00	0.00		0.00
f	0.33	0.00	0.33	0.00	0.17	0.17		0.00	0.00
vf/f	0.50	0.00	0.00	0.00	0.50		0.00	0.00	0.00
vf	0.33	0.00	0.33	0.00		0.00	0.33	0.00	0.00
s/vf	0.00	0.00	0.00		0.00	0.00	1.00	0.00	0.00
silt	0.00	0.25		0.00	0.25	0.00	0.00	0.25	0.25
c/s	0.00		0.00	0.00	0.00	0.50	0.00	0.00	0.50
clay		0.00	0.00	0.12	0.00	0.00	0.38	0.25	0.25

Appendix 6.16. Results of the order analysis for the Monźon, Log 3 of the floodplain deposits, Huesca DFS.

Pertusa, Log 1, Metric statistics

A. Log **B. Variation with scale** **C. Comparison with synthetic models**

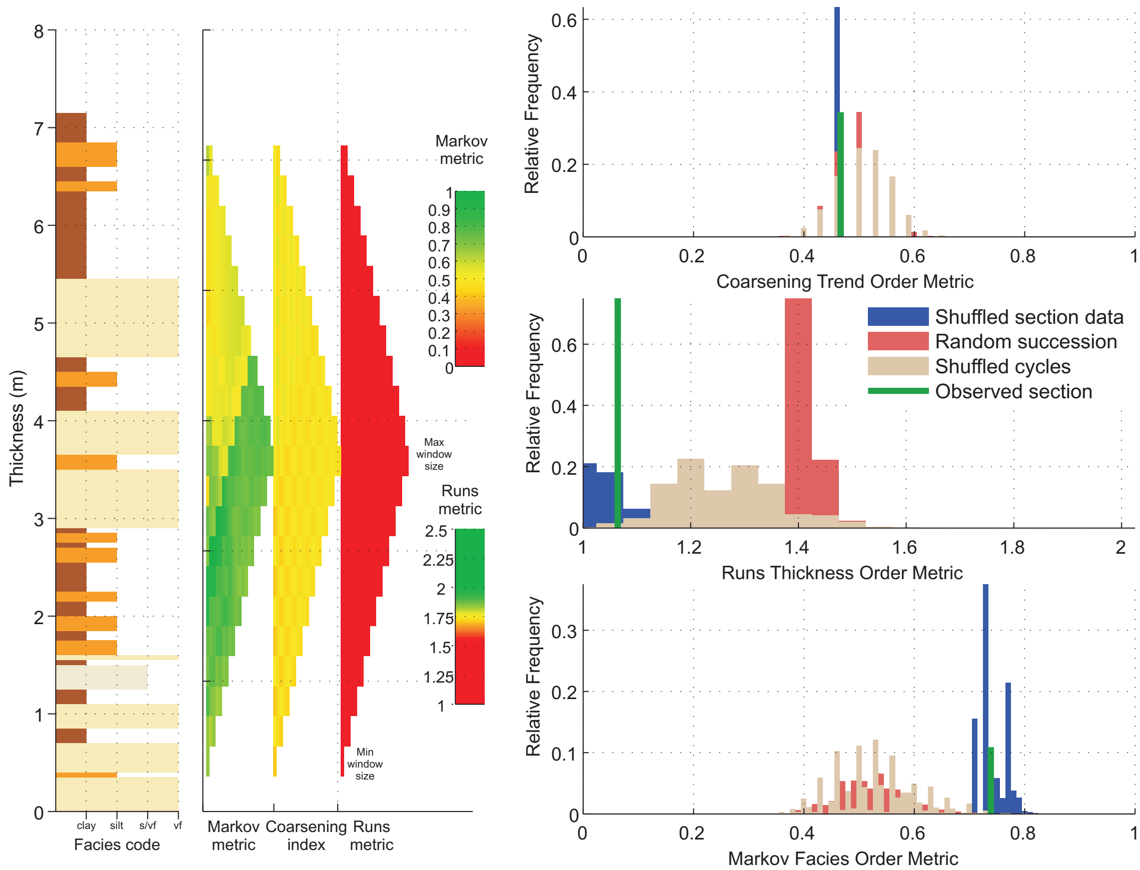

D. Facies distribution **E. Transition probability matrix**

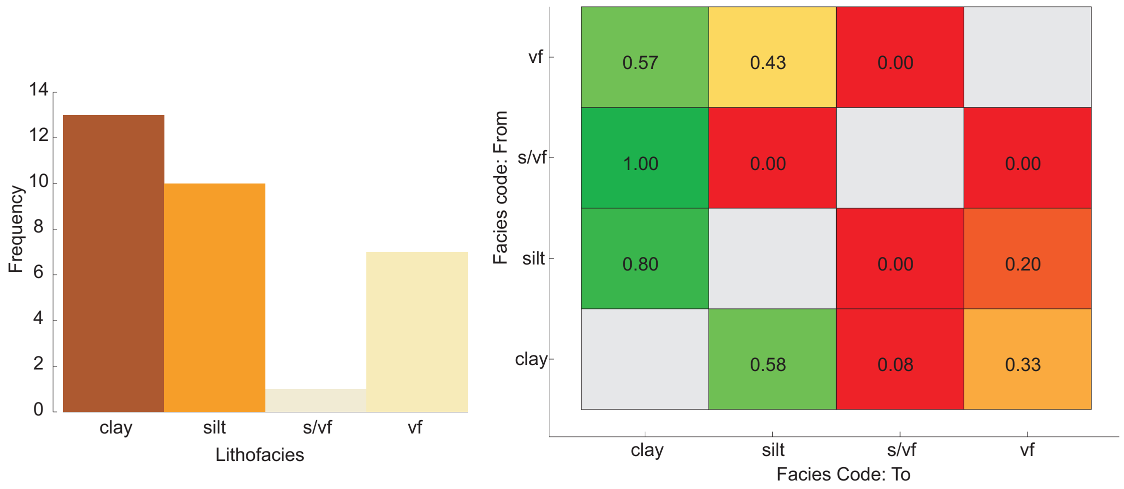

Facies code: From \ Facies Code: To	clay	silt	s/vf	vf
vf	0.57	0.43	0.00	
s/vf	1.00	0.00		0.00
silt	0.80		0.00	0.20
clay		0.58	0.08	0.33

Appendix 6.17. Results of the order analysis for the Pertusa, Log 1 of the floodplain deposits, Huesca DFS.

Piracés, Log 3, Metric statistics

A. Log

B. Variation with scale

C. Comparison with synthetic models

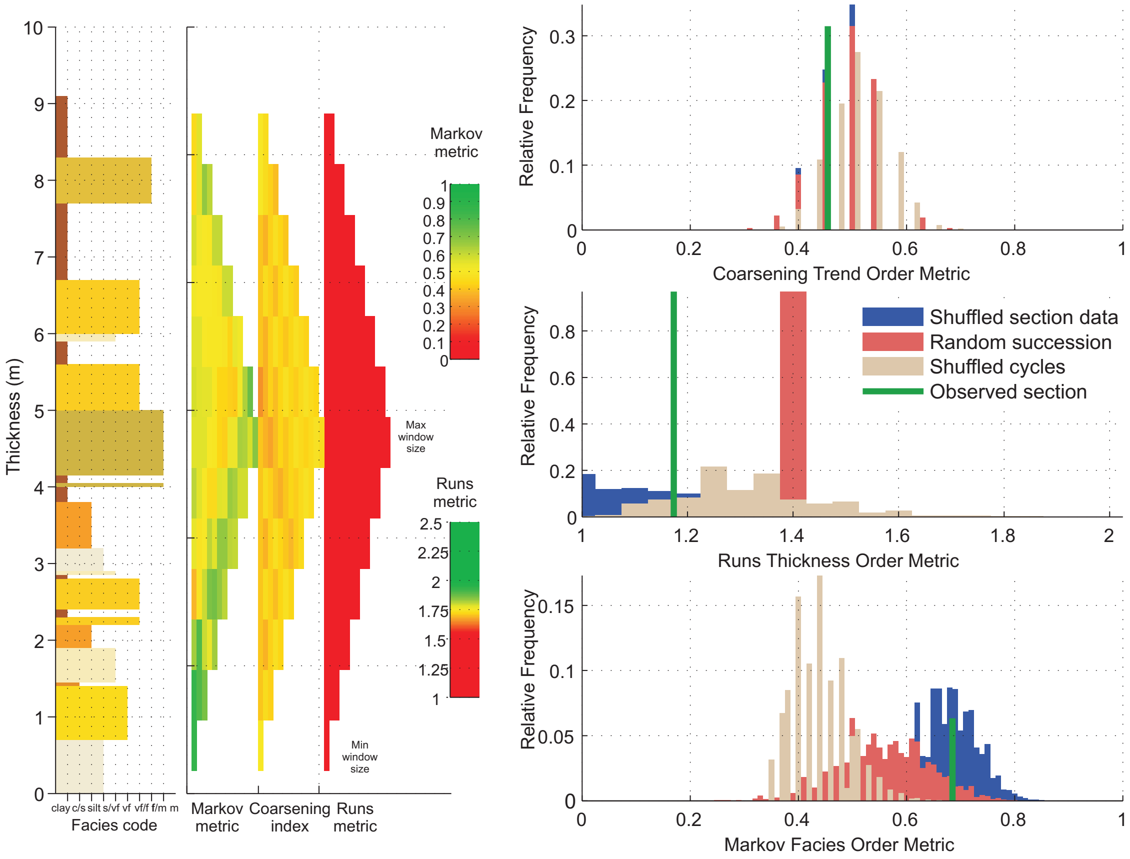

D. Facies distribution

E. Transition probability matrix

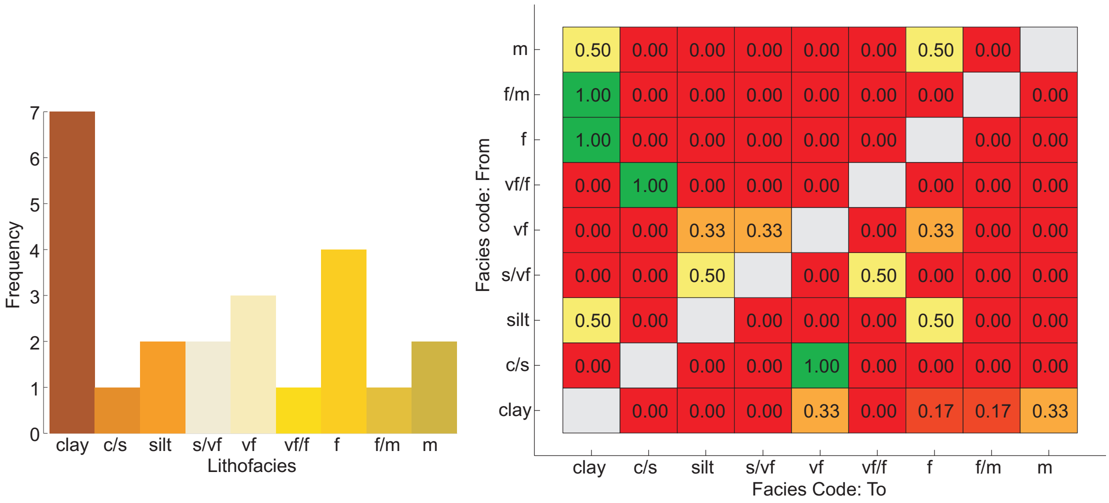

	clay	c/s	silt	s/vf	vf	vf/f	f	f/m	m
m	0.50	0.00	0.00	0.00	0.00	0.00	0.50	0.00	
f/m	1.00	0.00	0.00	0.00	0.00	0.00	0.00		0.00
f	1.00	0.00	0.00	0.00	0.00	0.00		0.00	0.00
vf/f	0.00	1.00	0.00	0.00	0.00		0.00	0.00	0.00
vf	0.00	0.00	0.33	0.33		0.00	0.33	0.00	0.00
s/vf	0.00	0.00	0.50		0.00	0.50	0.00	0.00	0.00
silt	0.50	0.00		0.00	0.00	0.00	0.50	0.00	0.00
c/s	0.00		0.00	0.00	1.00	0.00	0.00	0.00	0.00
clay		0.00	0.00	0.00	0.33	0.00	0.17	0.17	0.33

Appendix 6.18. Results of the order analysis for the Piracés, Log 3 of the floodplain deposits, Huesca DFS.

Piracés, Log 4, Metric statistics

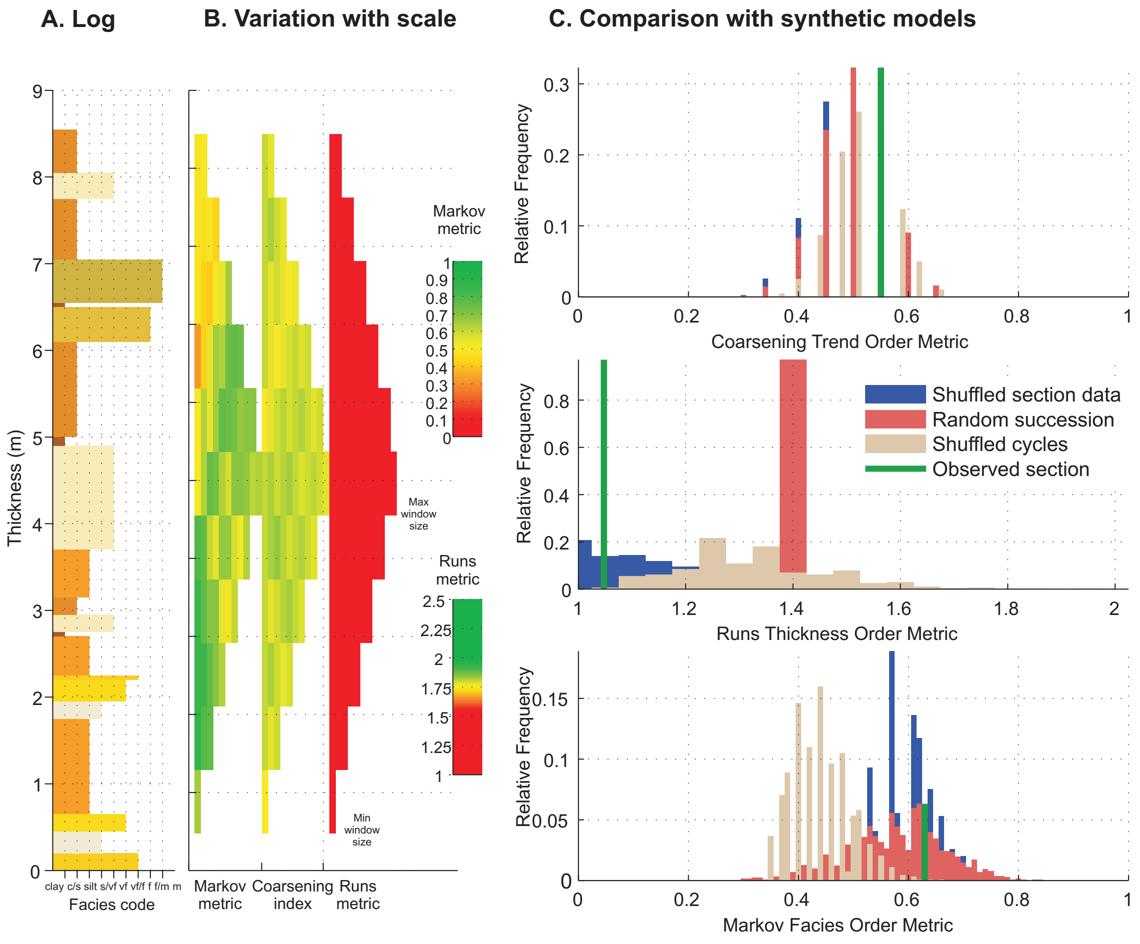

A. Log

B. Variation with scale

C. Comparison with synthetic models

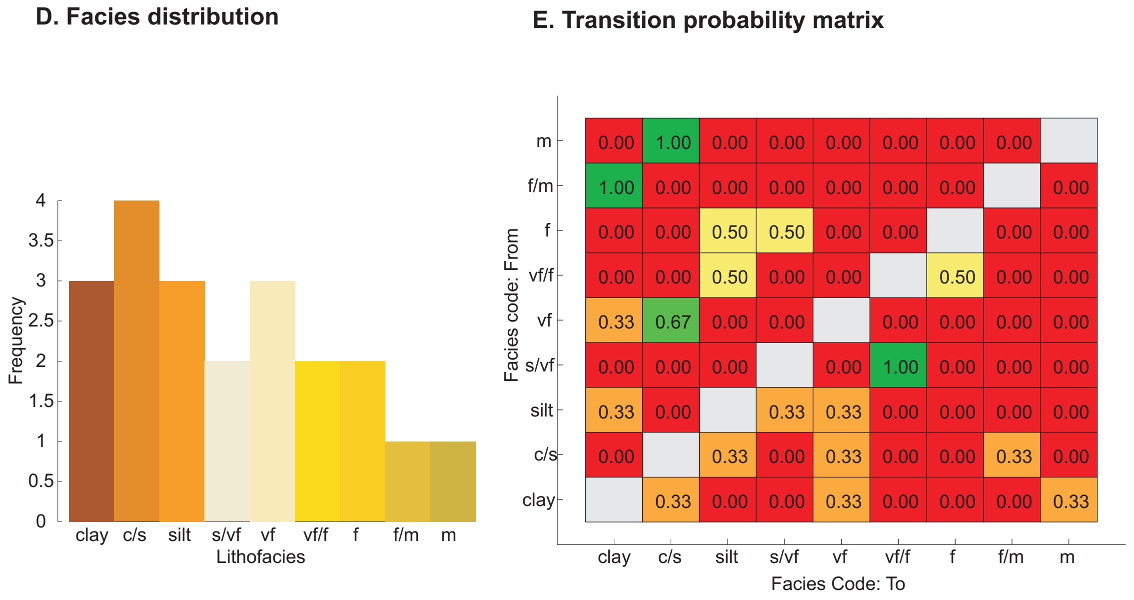

D. Facies distribution

E. Transition probability matrix

	clay	c/s	silt	s/vf	vf	vf/f	f	f/m	m
m	0.00	1.00	0.00	0.00	0.00	0.00	0.00	0.00	
f/m	1.00	0.00	0.00	0.00	0.00	0.00	0.00		0.00
f	0.00	0.00	0.50	0.50	0.00	0.00		0.00	0.00
vf/f	0.00	0.00	0.50	0.00	0.00		0.50	0.00	0.00
vf	0.33	0.67	0.00	0.00		0.00	0.00	0.00	0.00
s/vf	0.00	0.00	0.00		0.00	1.00	0.00	0.00	0.00
silt	0.33	0.00		0.33	0.33	0.00	0.00	0.00	0.00
c/s	0.00		0.33	0.00	0.33	0.00	0.00	0.33	0.00
clay		0.33	0.00	0.00	0.33	0.00	0.00	0.00	0.33

Appendix 6.19. Results of the order analysis for the Piracés, Log 4 of the floodplain deposits, Huesca DFS.

Bolea, Log 1, Metric statistics

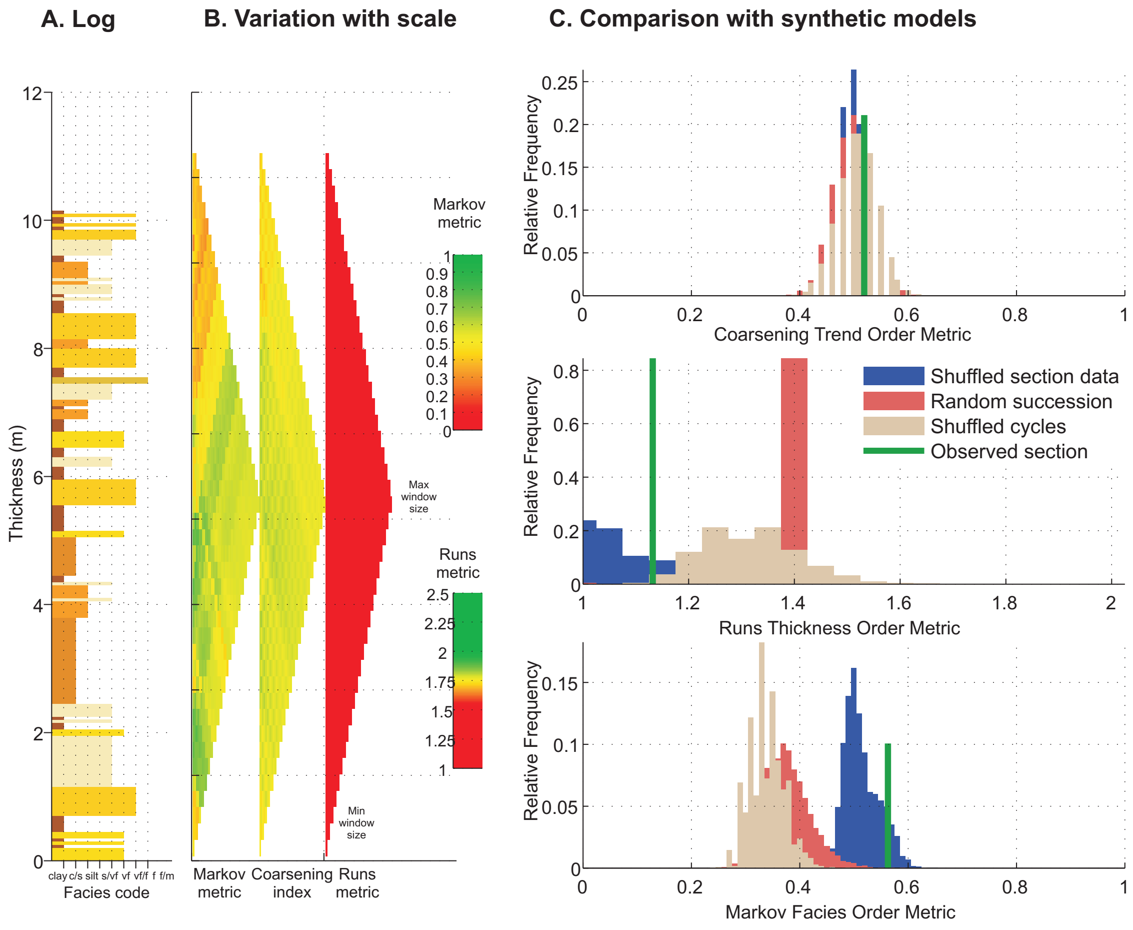
A. Log

B. Variation with scale

C. Comparison with synthetic models

D. Facies distribution

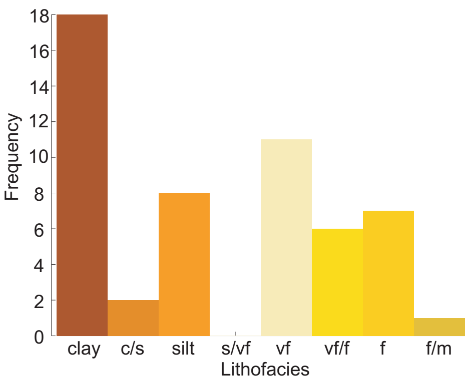

E. Transition probability matrix

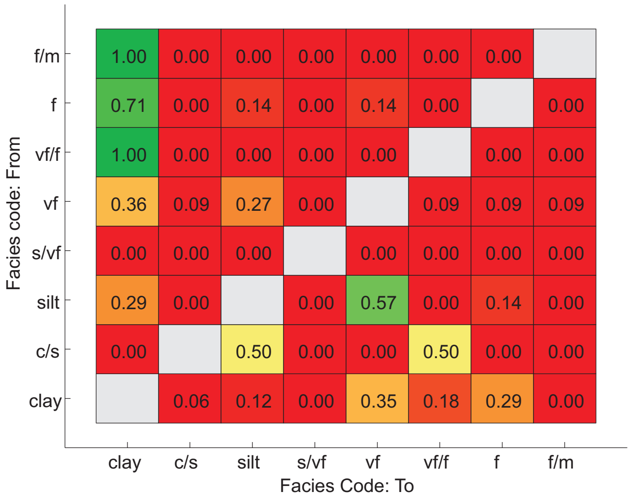

	clay	c/s	silt	s/vf	vf	vf/f	f	f/m
f/m	1.00	0.00	0.00	0.00	0.00	0.00	0.00	
f	0.71	0.00	0.14	0.00	0.14	0.00		0.00
vf/f	1.00	0.00	0.00	0.00	0.00		0.00	0.00
vf	0.36	0.09	0.27	0.00		0.09	0.09	0.09
s/vf	0.00	0.00	0.00		0.00	0.00	0.00	0.00
silt	0.29	0.00		0.00	0.57	0.00	0.14	0.00
c/s	0.00		0.50	0.00	0.00	0.50	0.00	0.00
clay		0.06	0.12	0.00	0.35	0.18	0.29	0.00

Appendix 6.20. Results of the order analysis for the Bolea, Log 1 of the floodplain deposits, Huesca DFS.

Monźon, Log 1, Metric statistics

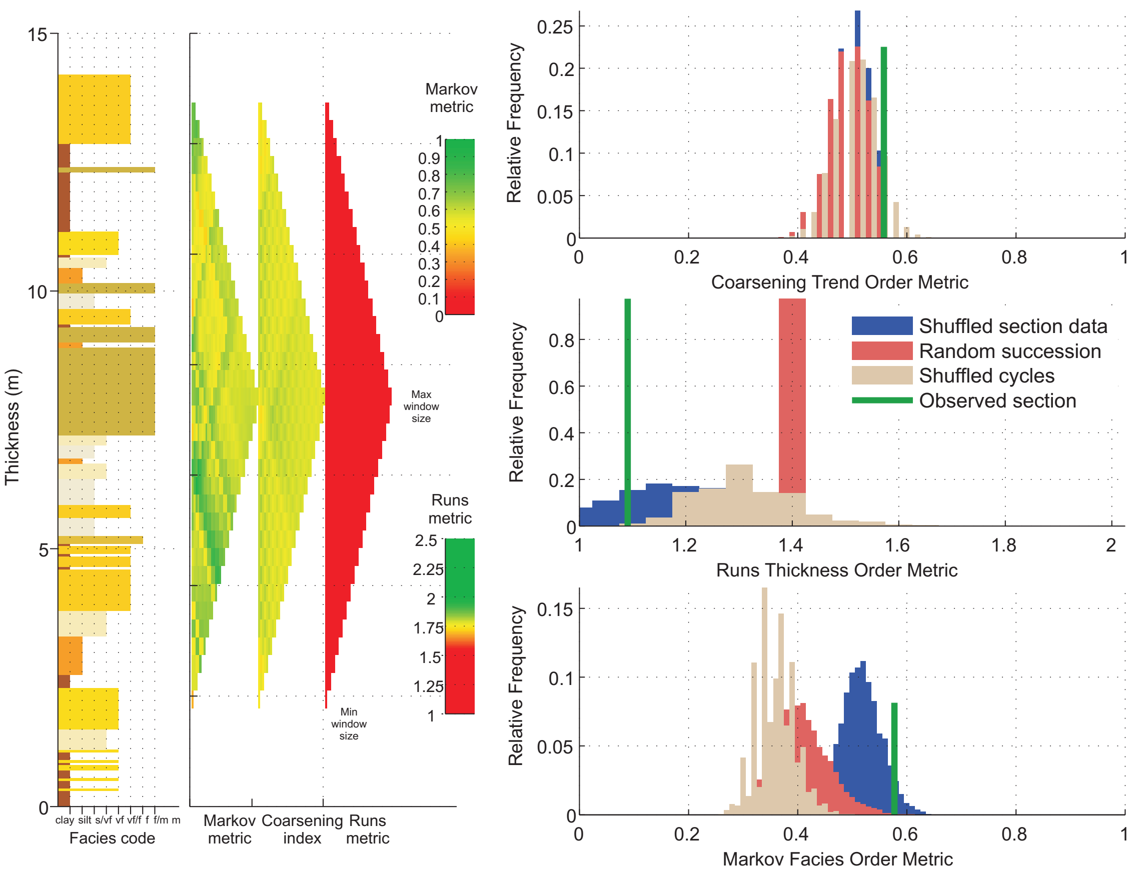

A. Log

B. Variation with scale

C. Comparison with synthetic models

D. Facies distribution

E. Transition probability matrix

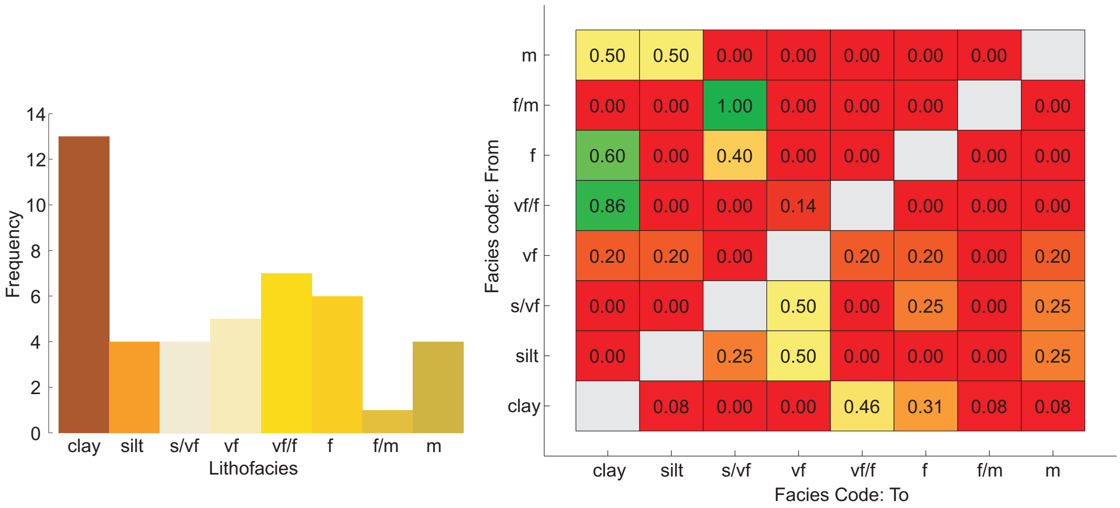

	clay	silt	s/vf	vf	vf/f	f	f/m	m
m	0.50	0.50	0.00	0.00	0.00	0.00	0.00	
f/m	0.00	0.00	1.00	0.00	0.00	0.00		0.00
f	0.60	0.00	0.40	0.00	0.00		0.00	0.00
vf/f	0.86	0.00	0.00	0.14		0.00	0.00	0.00
vf	0.20	0.20	0.00		0.20	0.20	0.00	0.20
s/vf	0.00	0.00		0.50	0.00	0.25	0.00	0.25
silt	0.00		0.25	0.50	0.00	0.00	0.00	0.25
clay		0.08	0.00	0.00	0.46	0.31	0.08	0.08

Appendix 6.21. Results of the order analysis for the Monźon, Log 1 of the floodplain deposits, Huesca DFS.

Piracés, Log 6, Metric statistics

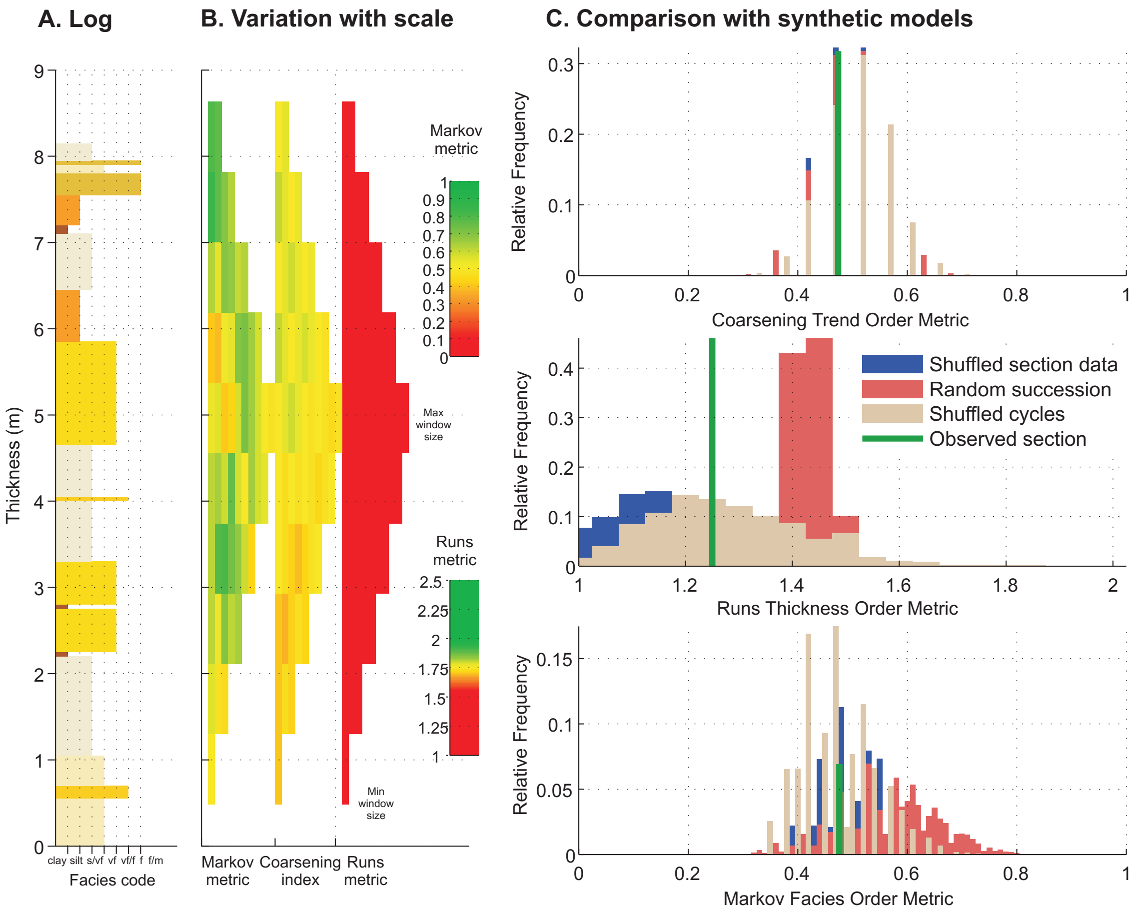

A. Log

B. Variation with scale

C. Comparison with synthetic models

D. Facies distribution

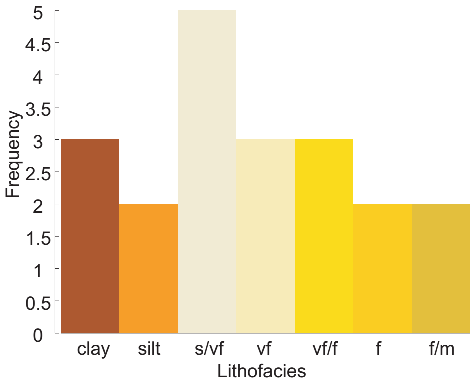

E. Transition probability matrix

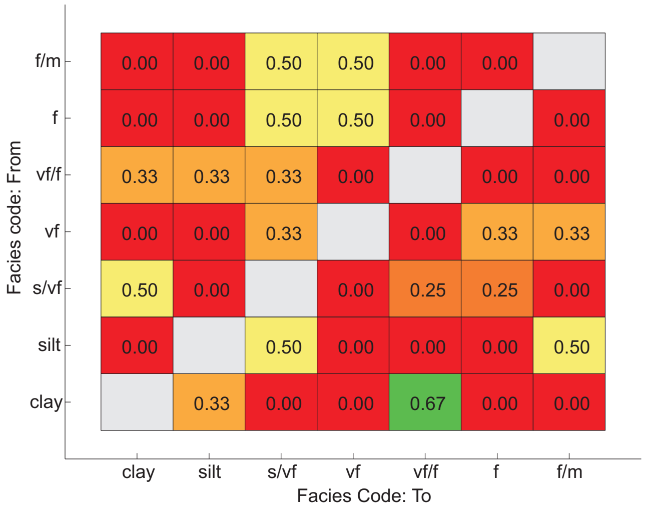

	clay	silt	s/vf	vf	vf/f	f	f/m
f/m	0.00	0.00	0.50	0.50	0.00	0.00	
f	0.00	0.00	0.50	0.50	0.00		0.00
vf/f	0.33	0.33	0.33	0.00		0.00	0.00
vf	0.00	0.00	0.33		0.00	0.33	0.33
s/vf	0.50	0.00		0.00	0.25	0.25	0.00
silt	0.00		0.50	0.00	0.00	0.00	0.50
clay		0.33	0.00	0.00	0.67	0.00	0.00

Appendix 6.22. Results of the order analysis for the Piracés, Log 6 of the floodplain deposits, Huesca DFS.

Appendix 7:
Gamma ray logs and results of preliminary analysis

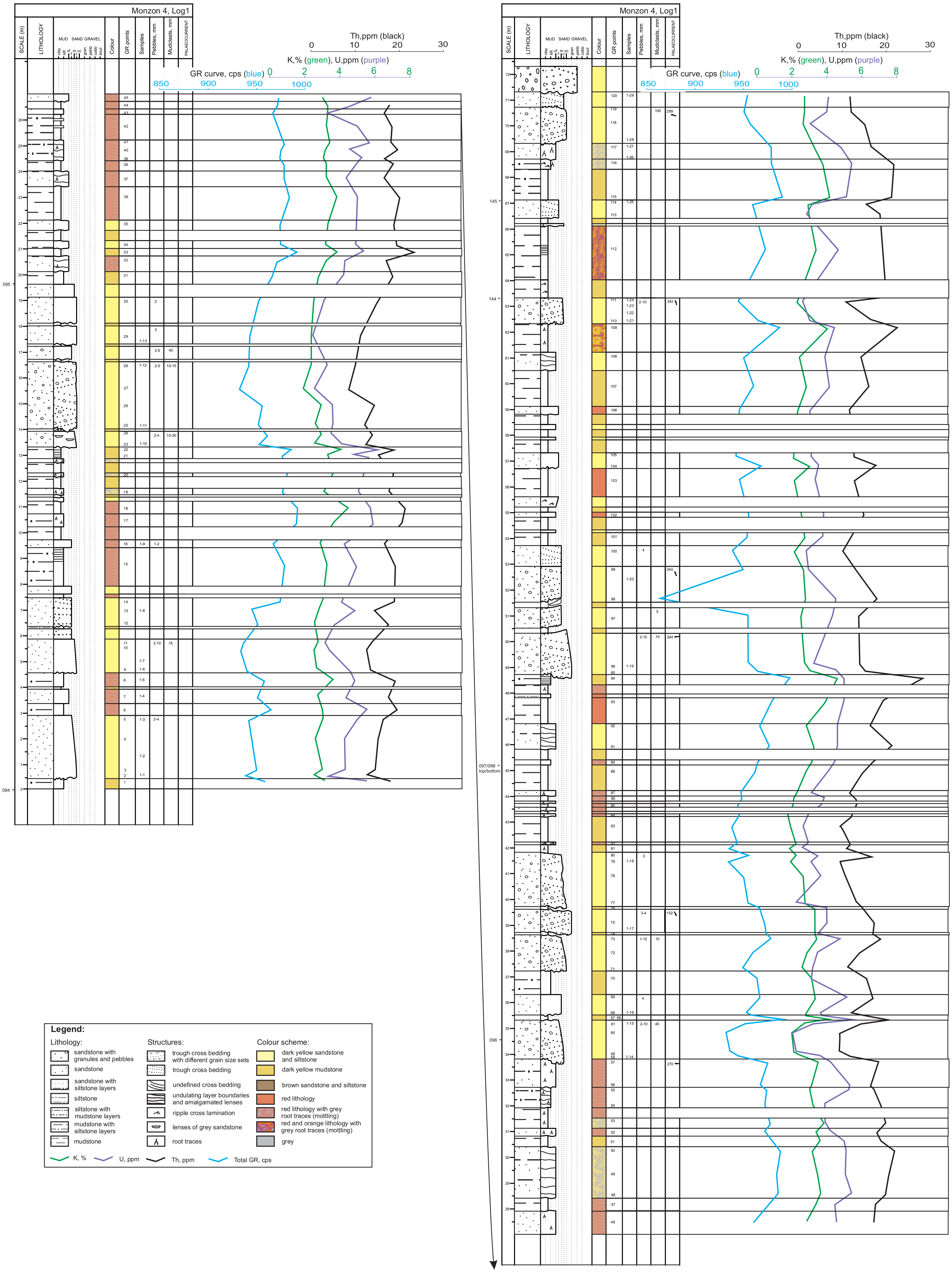

Appendix 7.1. Sedimentary log of the relatively proximal Huesca DFS succession (Monźon 4 outcrop) with total and spectral GR readings.

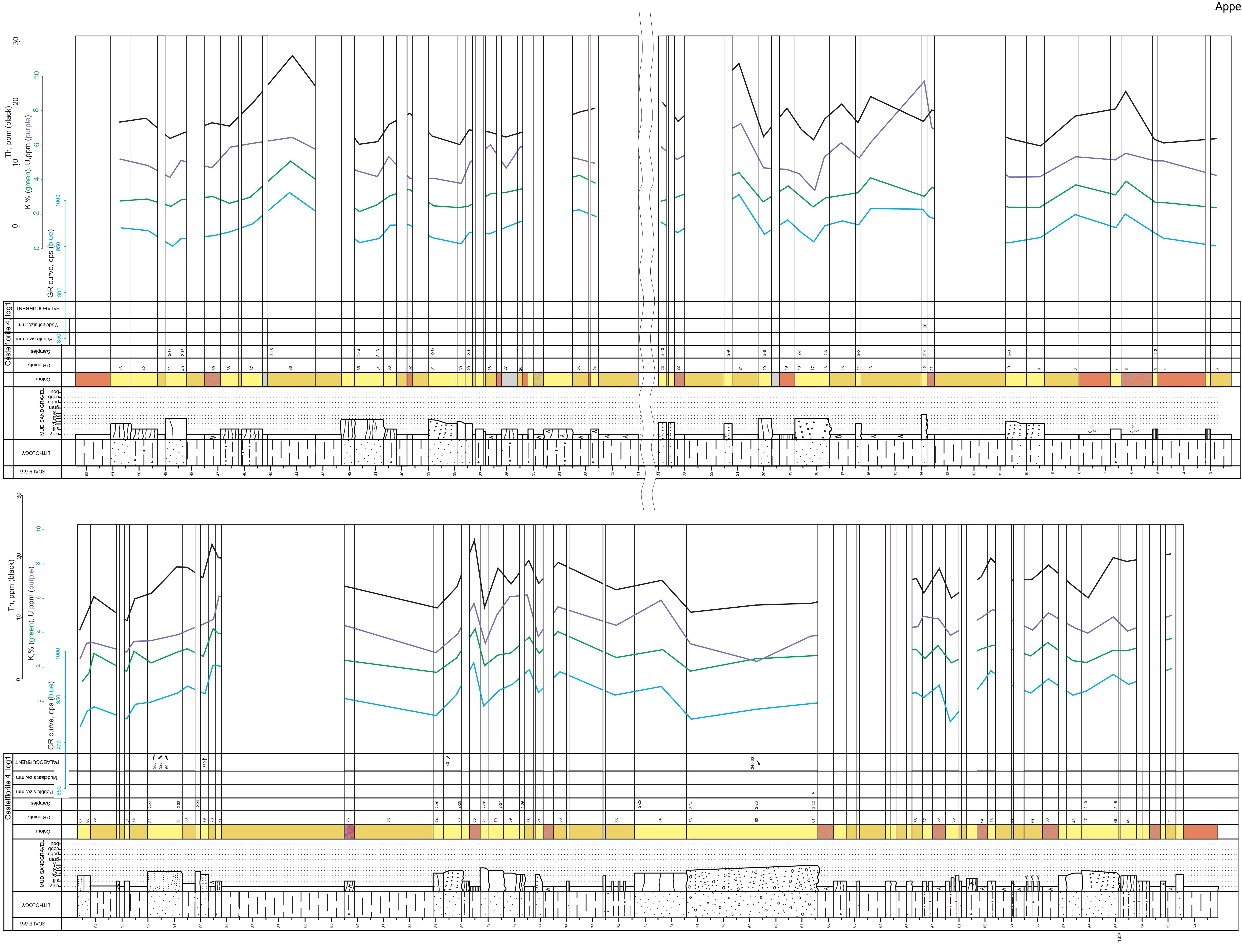

Appendix 7.2. Sedimentary log of the medial Huesca DFS succession (Castelflorite 4 outcrop) with total and spectral GR readings. See Appendix 7.1 for legend.

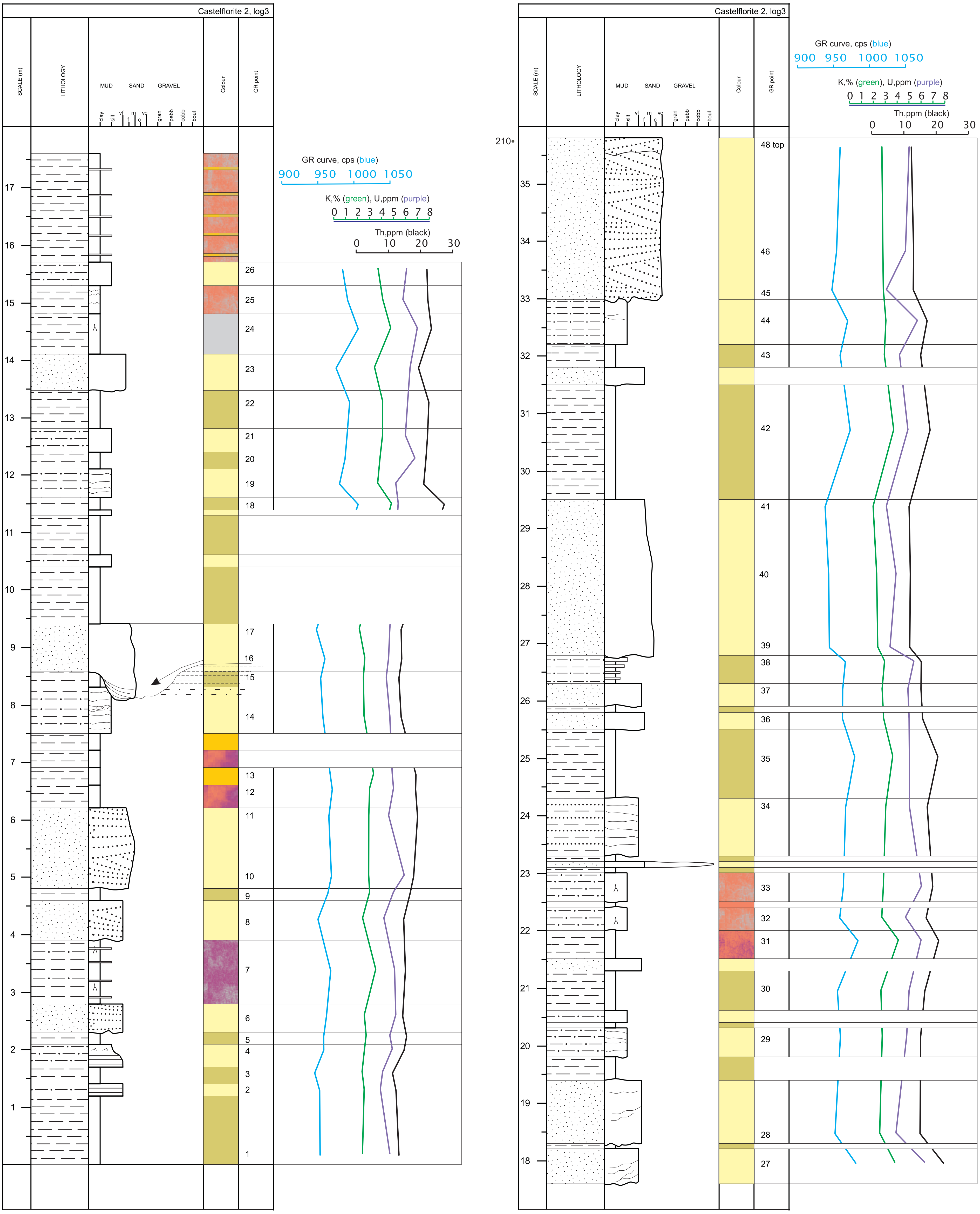

Appendix 7.3. Sedimentary log of the medial Huesca DFS succession (Castelflorite 2 outcrop) with total and spectral GR readings. See Appendix 7.1 for legend.

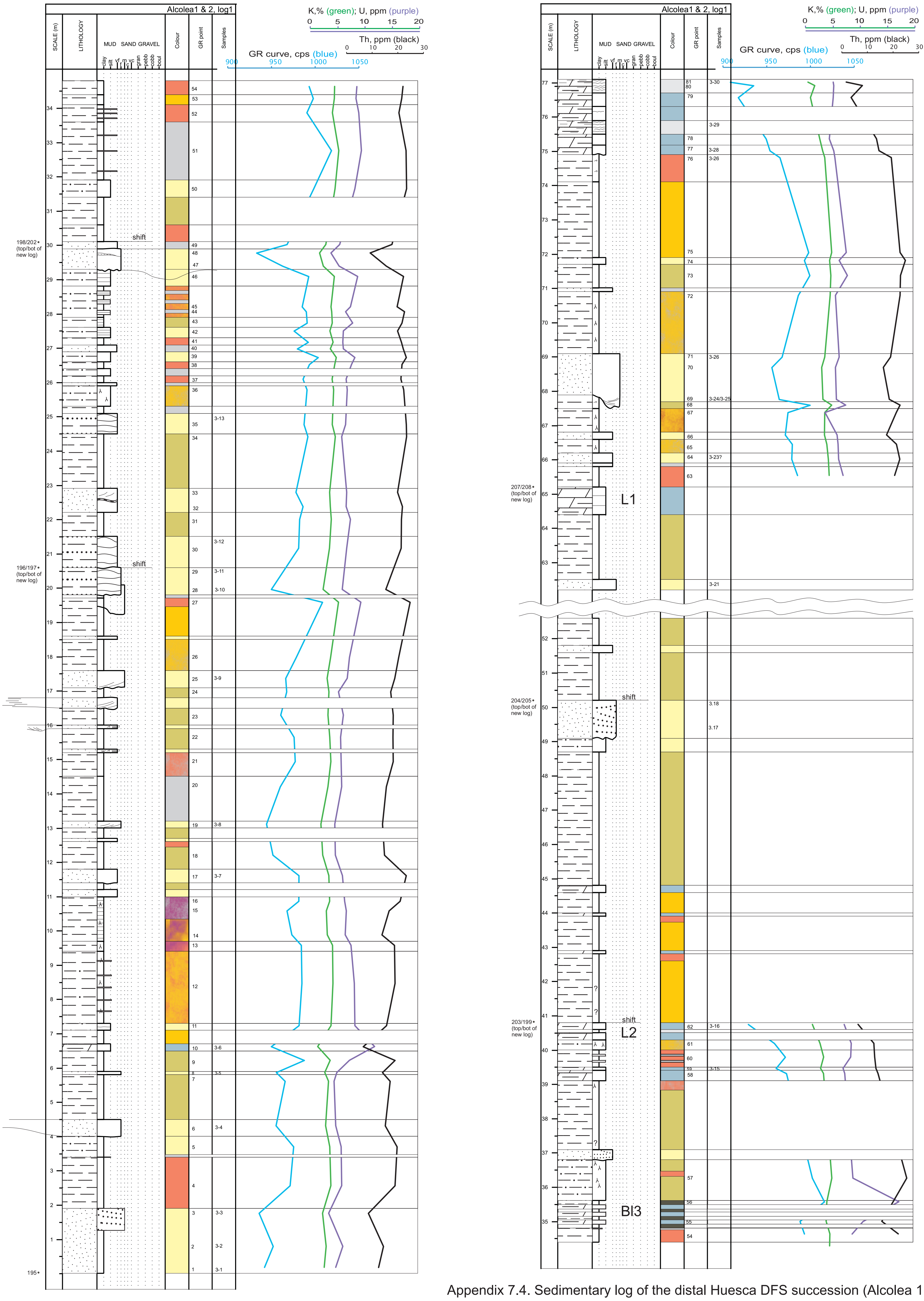

Appendix 7.4. Sedimentary log of the distal Huesca DFS succession (Alcolea 1&2 outcrop) with total and spectral GR readings. See Appendix 7.1 for legend.

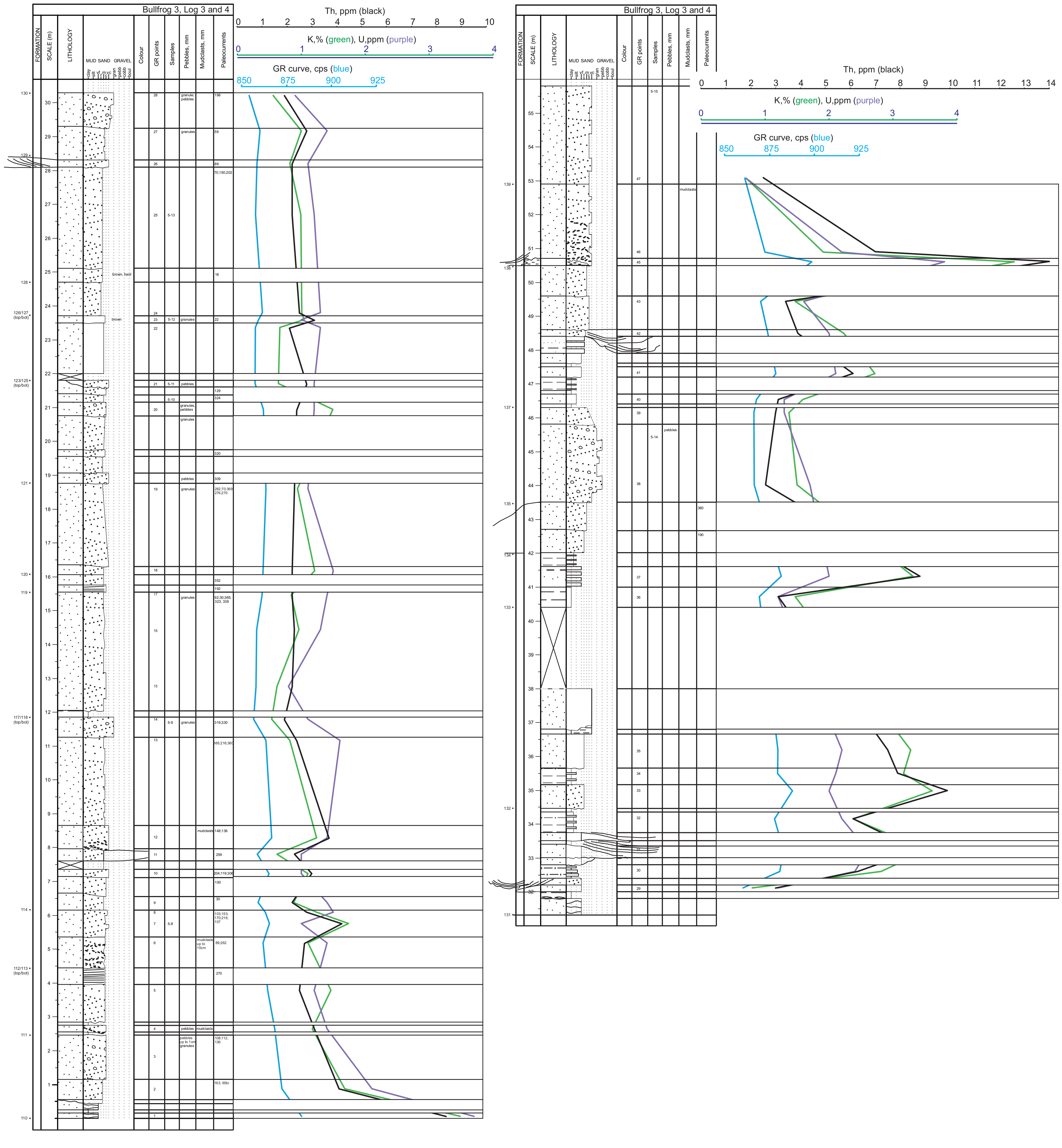

Appendix 7.5. Sedimentary log of the relatively proximal Salt Wash DFS succession (Bullfrog 3 outcrop) with total and spectral GR readings. See Appendix 7.1 for legend.

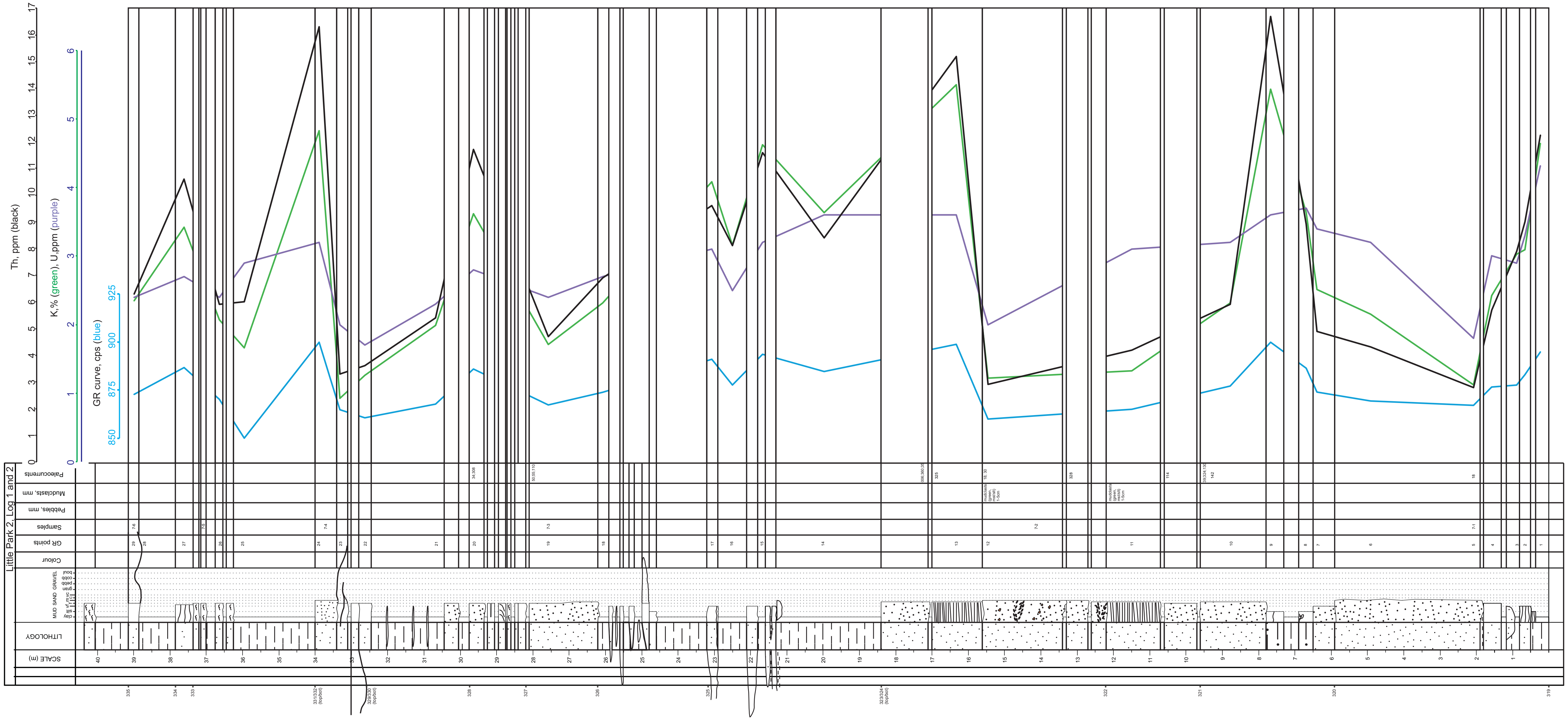

Appendix 7.6. Sedimentary log of the distal Salt Wash DFS succession (Little Park 2 outcrop) with total and spectral GR readings. See Appendix 7.1 for legend.

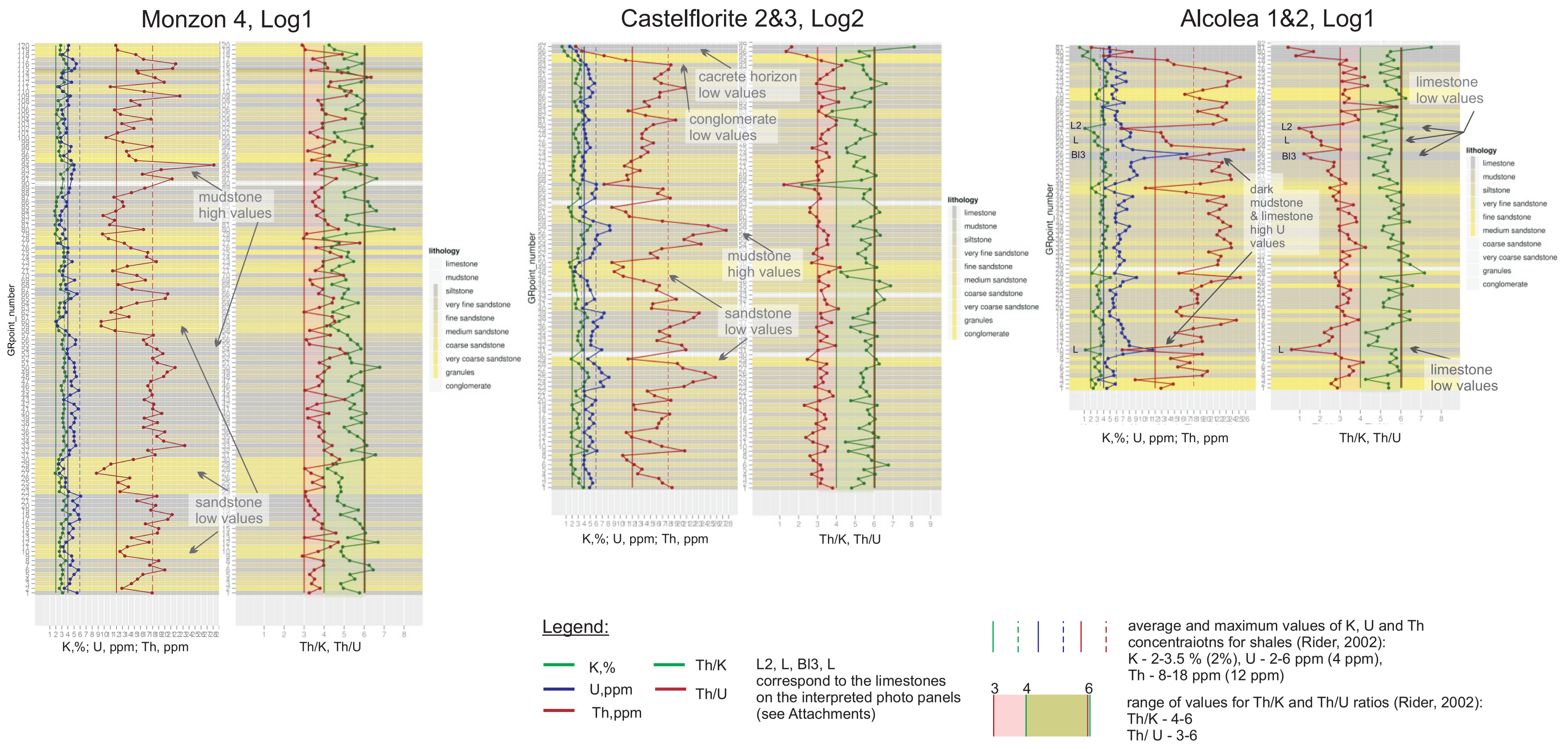

Appendix 7.7. Spectral gamma ray curves for the relatively proximal, medial and distal Huesca DFS deposits including Potassium (K), Thorium (Th) and Uranium (U) concentrations and Th/U and Th/K ratios.

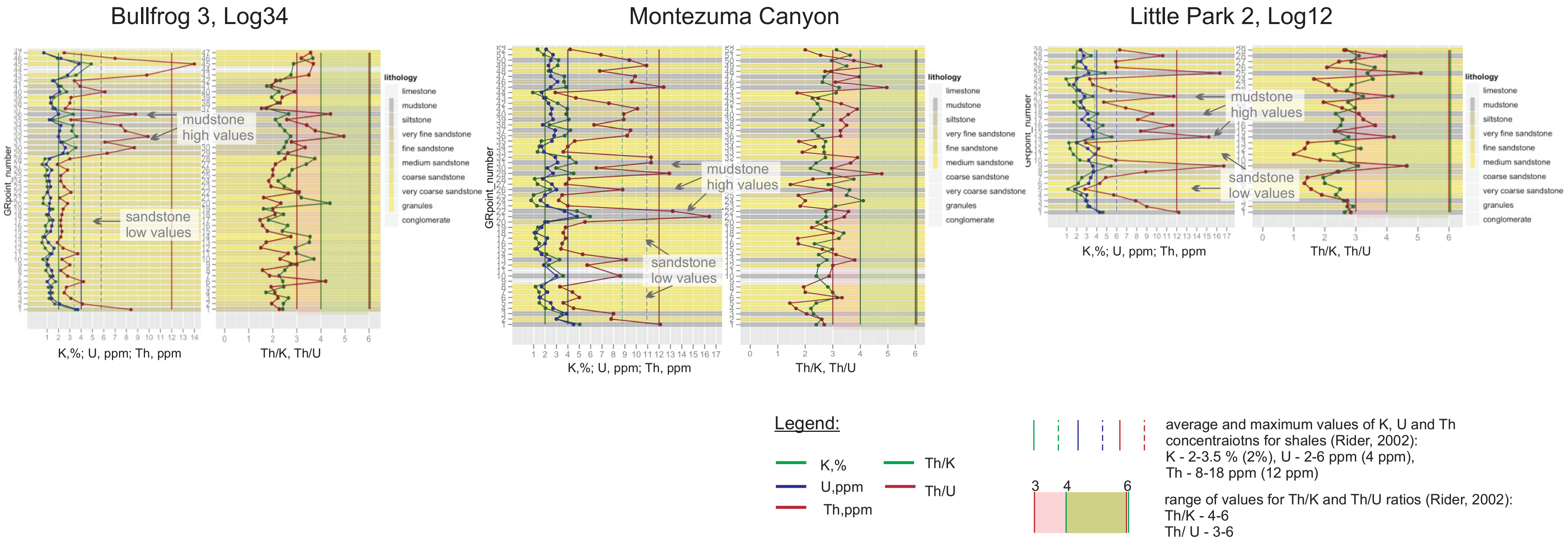

Appendix 7.8. Spectral gamma ray curves for the relatively proximal, medial and distal Salt Wash DFS deposits including Potassium (K), Thorium (Th) and Uranium (U) concentrations and Th/U and Th/K ratios.

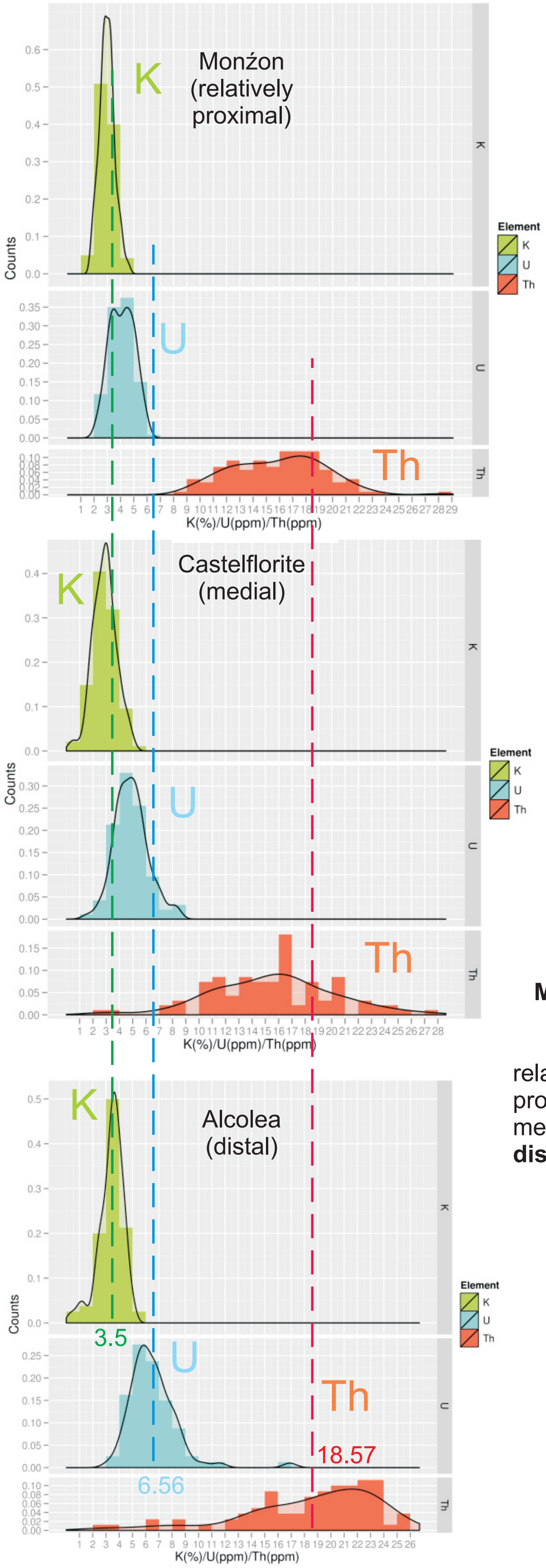

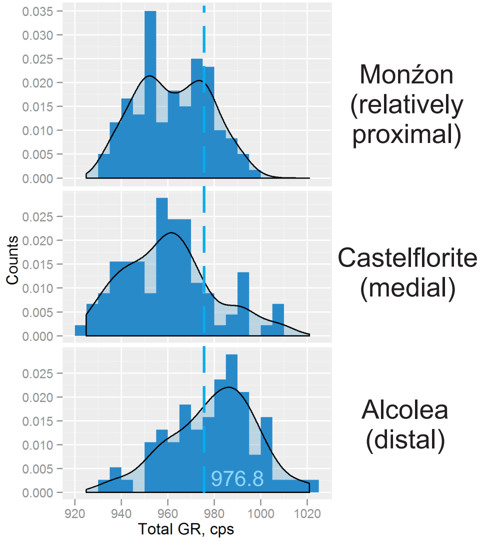

Mean for K, U and Th concentrations and Total GR values

	K	U	Th	Total GR
relatively proximal	2.97	4.11	15.92	961.31
medial	2.85	4.7	15.5	958.66
distal	**3.5**	**6.56**	**18.57**	**976.81**

Appendix 7.9. Downstream variations in Spectral and Total gamma-ray readings in the deposits of the Huesca DFS.

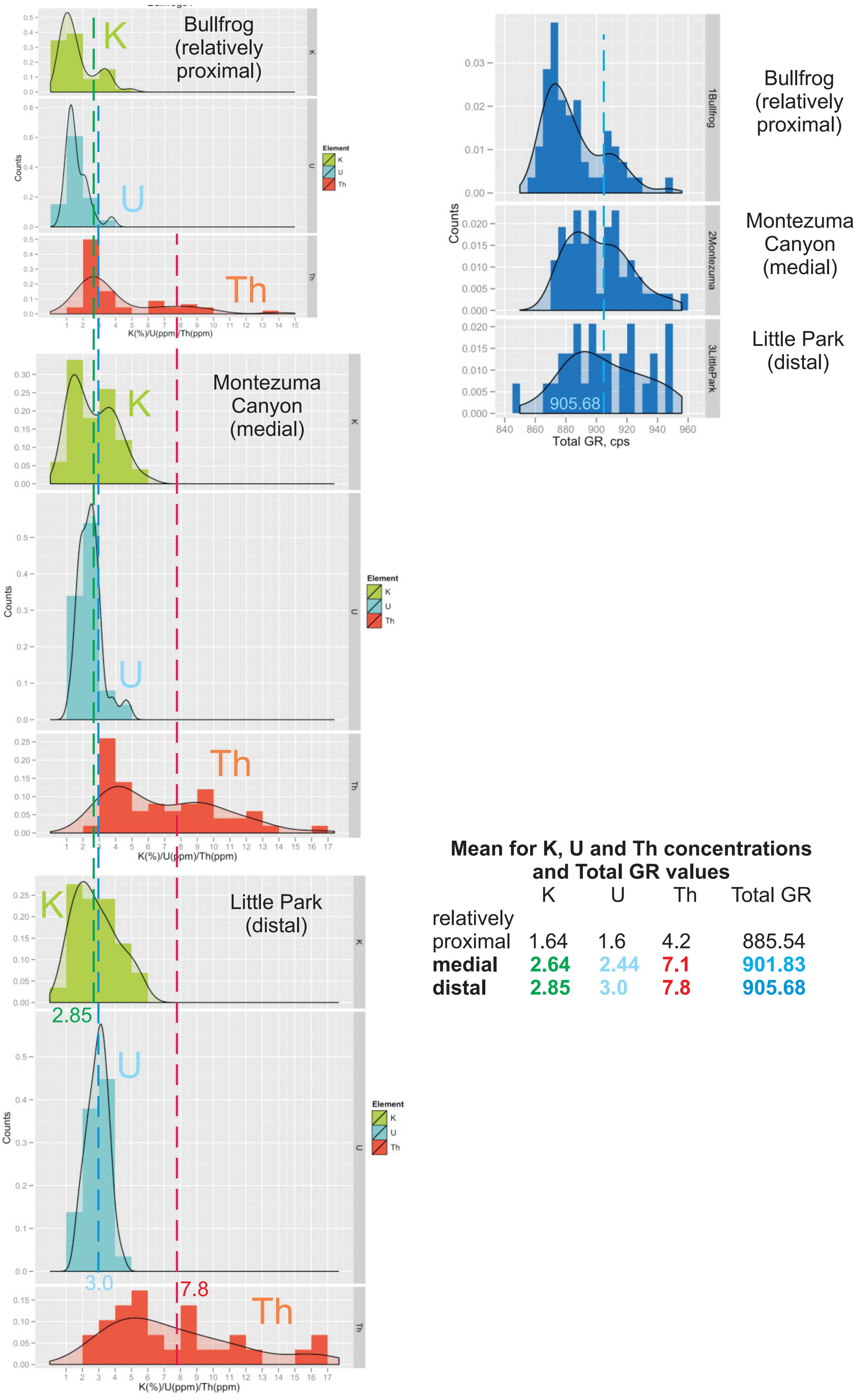

Mean for K, U and Th concentrations and Total GR values

	K	U	Th	Total GR
relatively proximal	1.64	1.6	4.2	885.54
medial	**2.64**	**2.44**	**7.1**	**901.83**
distal	**2.85**	**3.0**	**7.8**	**905.68**

Appendix 7.10. Downstream variations in Spectral and Total gamma-ray readings in the deposits of the Salt Wash DFS.

Monzon 4, Log 1

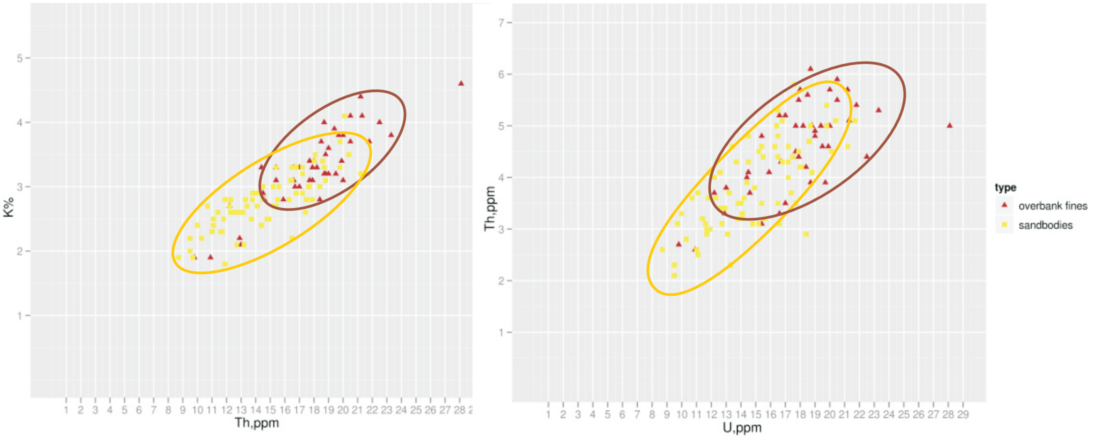

Castelflorite 2&3, Log 2

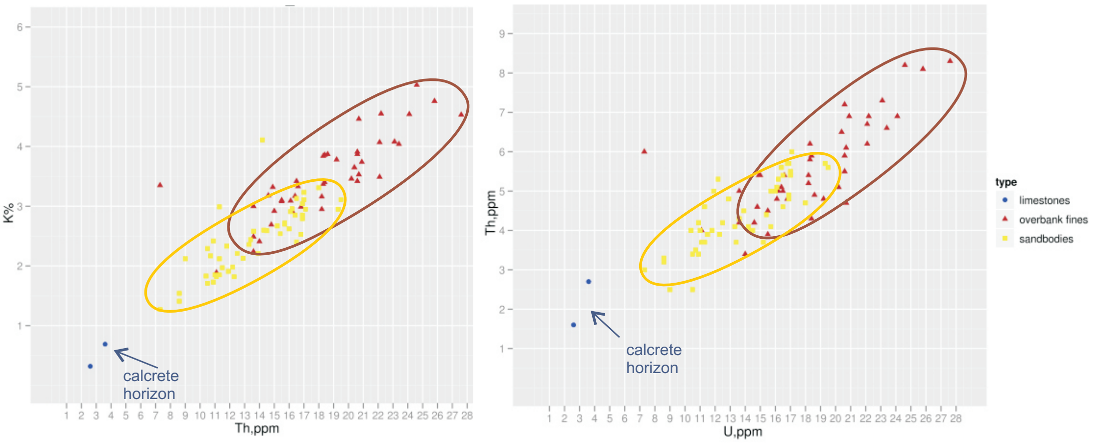

Alcolea 1&2, Log 1

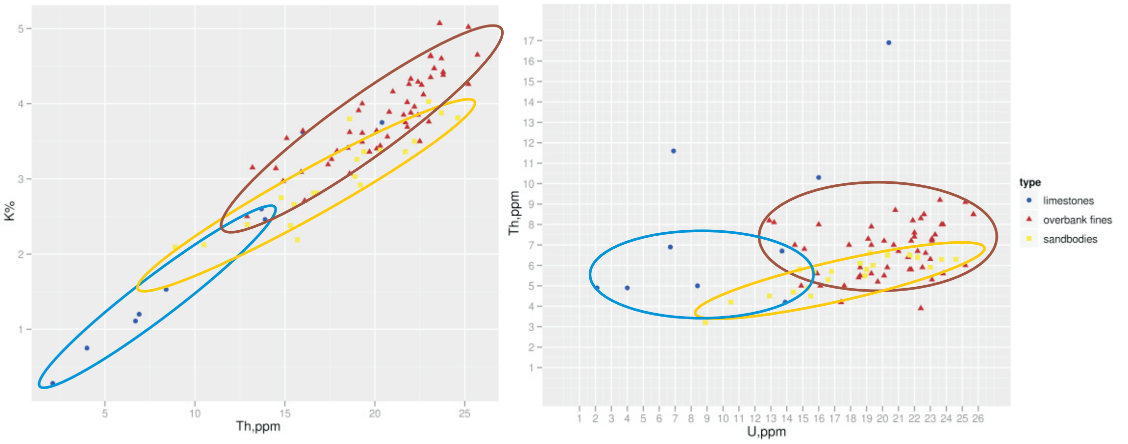

Appendix 7.11. Plots showing difference invalues of Potassium, Thorium and Uranium concentrations in sandstone bodies, fine-grained overbank deposits and lacustrine limestones of the Huesca DFS succession.

Monzon 4, Log 1

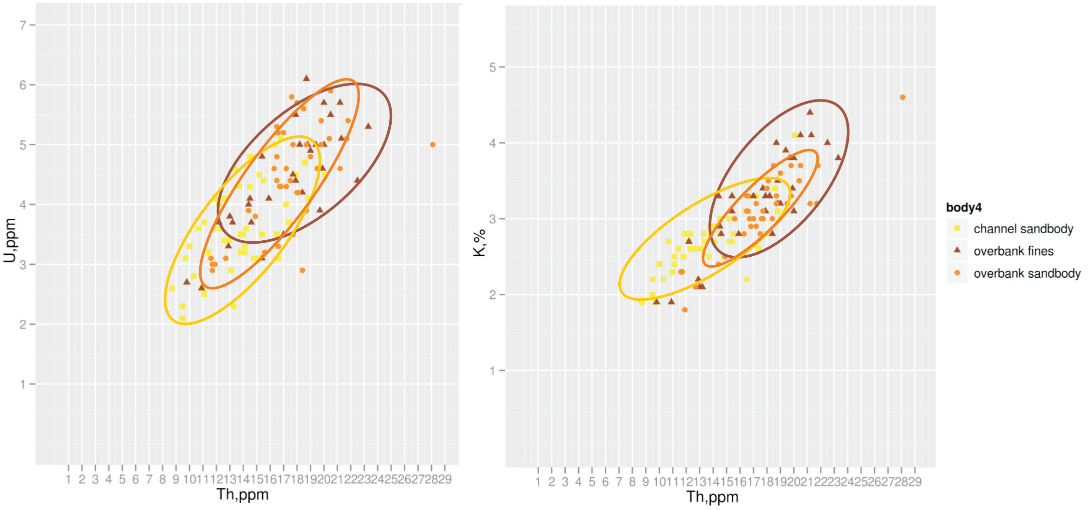

Castelflorite 2&3, Log 2

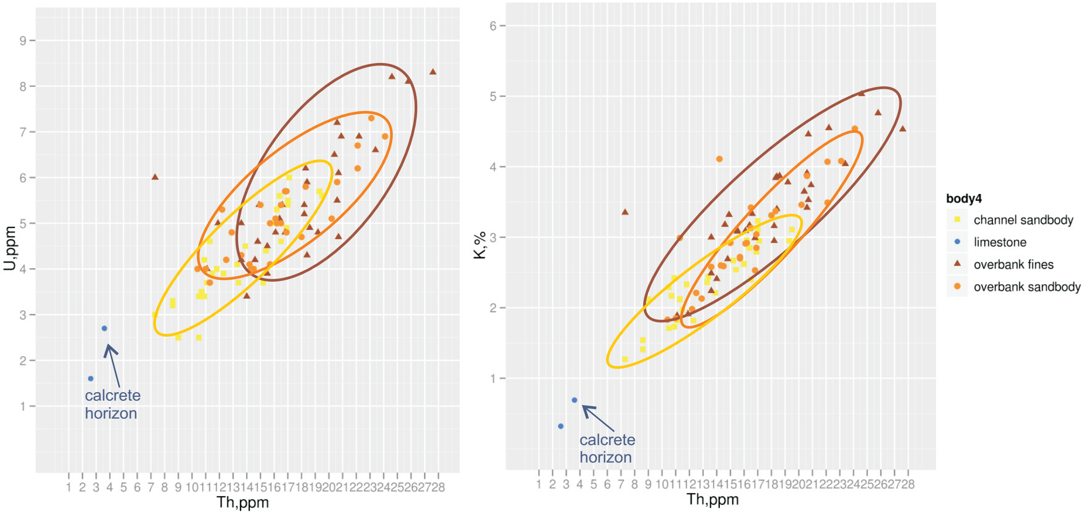

Alcolea 1&2, Log 1

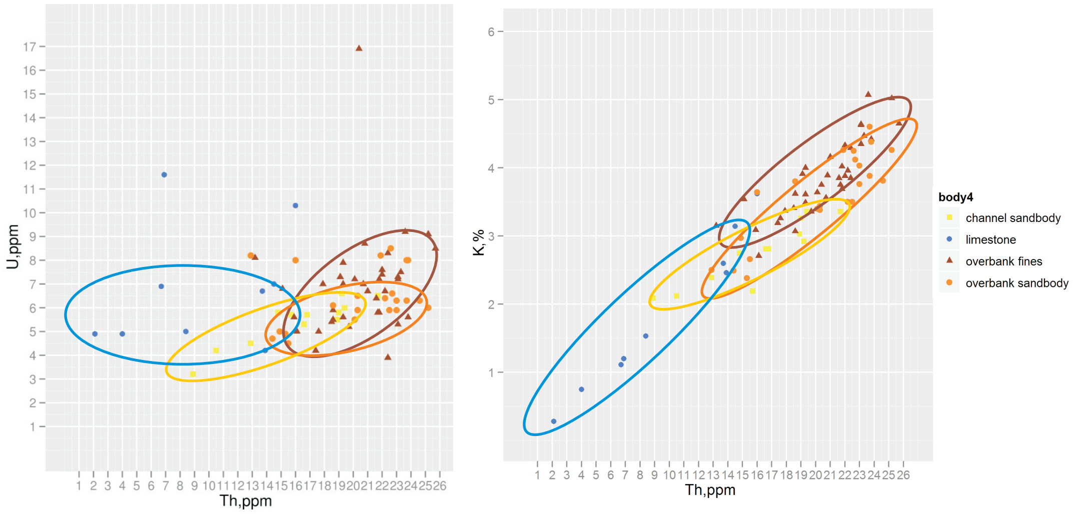

Appendix 7.12. Plots showing difference in values of Potassium, Thorium and Uranium concentrations in channel sandstone bodies, overbank sandstone bodies, fine-grained overbank deposits and lacustrine limestones of the Huesca DFS succession.

Monzon 4, Log 1

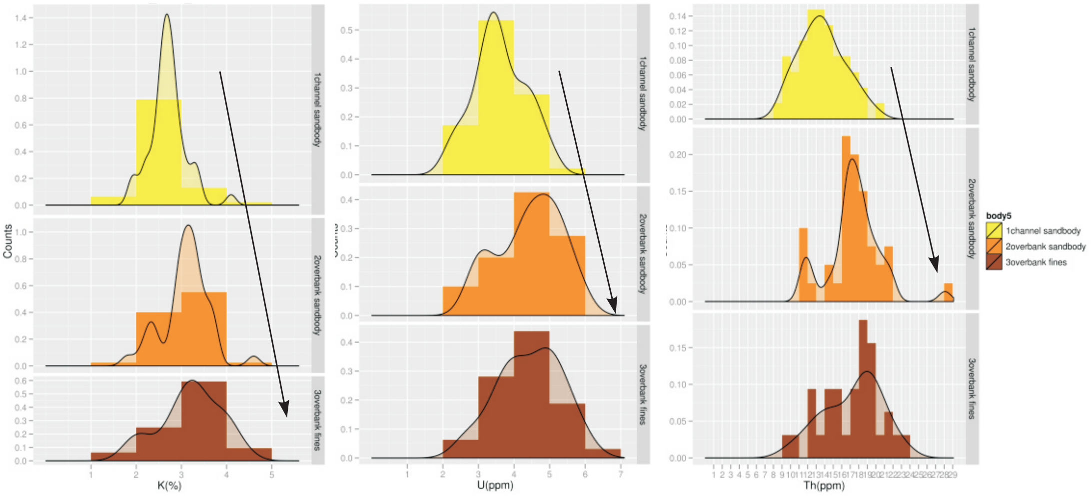

Castelflorite 2&3, Log 2

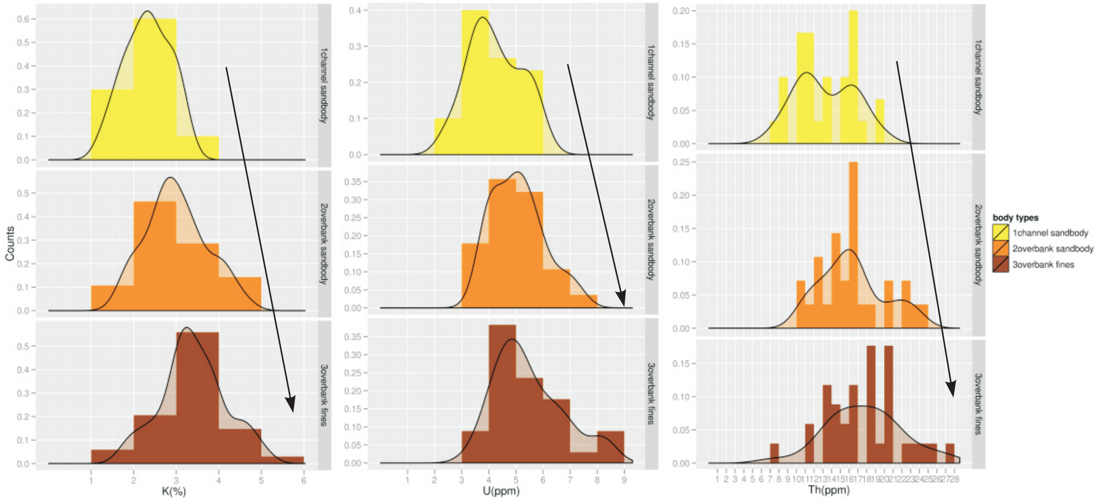

Alcolea 1&2, Log 1

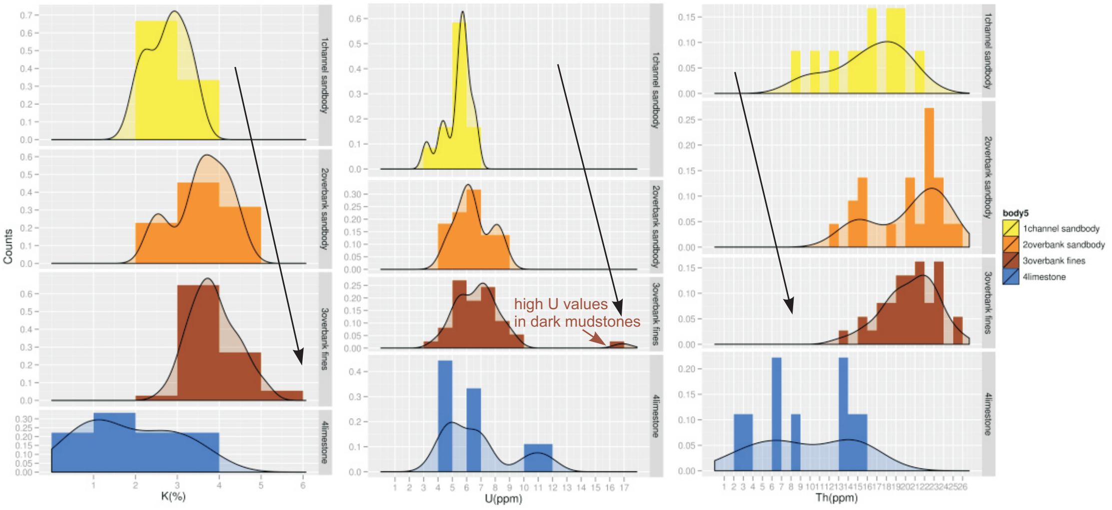

Appendix 7.13. Histograms showing difference in values of Potassium, Thorium and Uranium concentrations in channel sandstone bodies, overbank sandstone bodies, fine-grained overbank deposits and lacustrine limestones of the Huesca DFS succession.